

The University of Hull

**Advanced Nanotechnologies for Overcoming
Antimicrobial Resistance**

Being a Thesis submitted for the Degree of Doctor of Philosophy
in the University of Hull

by

Paul James Weldrick

BSc, PGCert (University of Hull, UK, 2017)

February 2021

Acknowledgements

I want to thank my academic supervisor, Professor Vesselin Paunov. I really appreciate his careful and professional supervision, which allowed me to gain an in-depth understanding of an area that I was not familiar with. It has been a real pleasure having you as a supervisor. I would also like to thank Dr Cheryl Walter and Dr Tommy Horozov for their advice and feedback during my PhD. I am grateful to SEM technician Tim Dunstan, TEM technician Ann Lowry and Dr Leigh Madden for their assistance with SEM/TEM sample preparation, cryostat training and flow cytometry training. I am also grateful to The University of Leeds for allowing me access to the electron microscopy and spectroscopy centre and Dr Mike Draper to complete EDX analysis at Ansell Ltd. I would also like to thank the students in the chemistry and biomedical departments for their help and advice during my time at The University of Hull. Finally, I would like to thank Asher for her support during my project.

Publications, Posters and Presentation

The work contained within this thesis has given rise to the following publications, posters and presentations and qualifications.

The publisher's The Royal Society of Chemistry (RSC), American Chemical Society (ACS) and Wiley-VCH GmbH (Wiley) in which the research in this thesis has been published, allow the full reproduction of articles in a thesis provided the correct acknowledgement is given with the reproduced material. The acknowledgement to these publishers is given at the beginning of the appropriate chapters in this thesis.

Published Research Articles;

- Weldrick, P. J., Iveson, S., Hardman, M. J., & Paunov, V. N. (2019). Breathing new life into old antibiotics: overcoming antibacterial resistance by antibiotic-loaded nanogel carriers with cationic surface functionality. *Nanoscale*, 11(21), 10472–10485.
- Weldrick, P. J., Hardman, M. J., & Paunov, V. N. (2019). Enhanced Clearing of Wound-Related Pathogenic Bacterial Biofilms Using Protease-Functionalized Antibiotic Nanocarriers. *ACS applied materials & interfaces*, 11(47), 43902–43919.
- Weldrick, P. J., Hardman, M. J., & Paunov, V. N. (2021). Smart active antibiotic nanocarriers with protease surface functionality can overcome biofilms of resistant bacteria. *Mater. Chem. Front.*, 5, 961-972.
- Weldrick, P. J., Hardman, M. J., & Paunov, V. N. (2021). Super-Enhanced Removal of Fungal Biofilms by Protease-Functionalized Amphotericin B Nanocarriers. *Adv. Nanobiomed. Res.*, 1, 2000027.
- Weldrick, P. J., San, S., & Paunov, V. N. (2021) Advanced Alcalase-Coated Clindamycin-Loaded Carbopol Nano-gels for Removal of Persistent Bacterial Biofilms. *ACS Appl. Nano Mater.*, 5, 961–972.

Posters;

- Weldrick, P. J., Hardman, M. J., Paunov, V. N. Enhancement of antimicrobial agent chlorhexidine using nanogel carrier and cationic functionality, *Annual Postgraduate Conference 2017/18* - School of Life Sciences, 19th Jan 2018, University of Hull, U.K.
- Weldrick, P., Iveson, S., Hardman, M. & Paunov, V. Overcoming antibacterial resistance by antibiotic-loaded nanogel carriers with cationic surface functionality. *Postgraduate Research Colloquium*, 15th July 2019, University of Hull, U.K.

Oral Presentations;

- Weldrick, P. J., Hardman, M. J., Paunov, V. N. Nanotechnologies in the fight against antimicrobial resistance. *UK-Russia Bio-Inspired Materials conference*, 2nd Feb 2020, University of Lancaster, U.K.
- Weldrick, P. J., Hardman, M. J., Paunov, V. N. Nanotechnologies in the fight against antimicrobial resistance. *Biological & Environmental Science and Engineering division of KAUST*, 18th Nov 2019, King Abdullah University of Science and Technology, Thuwal, Saudi Arabia.

Abstract

Multidrug-resistant pathogens are prevalent in chronic wounds. There is an urgent need to develop novel antimicrobials and formulation strategies to overcome antibiotic resistance and provide a safe alternative to traditional antibiotics. Chapter 2 aims to create a novel nanocarrier for two cationic antibiotics, tetracycline hydrochloride and lincomycin hydrochloride, overcoming antibiotic resistance. In this study, the use of surface-functionalised polyacrylic copolymer nanogels as carriers for cationic antibiotics is investigated. These nanogels can encapsulate small cationic antimicrobial molecules and act as a drug delivery system. They were further functionalised with a biocompatible cationic polyelectrolyte, bPEI, to increase their affinity towards the negatively charged bacterial cell walls. These bPEI-coated nanocarrier-encapsulated antibiotics were assessed against a range of wound isolated pathogens, which had been shown through antimicrobial susceptibility testing (AST) to be resistant to tetracycline and lincomycin. The data reveals that bPEI-coated nanogels with encapsulated tetracycline or lincomycin displayed increased antimicrobial performance against selected wound-derived bacteria, including strains resistant to the free antibiotic in solution.

Next, after experimentation into the use of Carbopol nanogels against antibiotic-resistant wound-derived pathogens, in planktonic form, the work in chapter 3 investigated their use against biofilm-formed pathogens. Biofilms are prevalent in chronic wounds and once formed, are very hard to remove, which is associated with poor outcomes and high mortality rates. Biofilms are comprised of surface-attached bacteria embedded in an extracellular polymeric substance (EPS) matrix, which confers increased antibiotic resistance and host immune evasion. Therefore, disruption of this matrix is essential to tackle the biofilm-embedded bacteria. Novel nanotechnology is applied to do this, based on protease-functionalised nanogel carriers of antibiotics. Such active antibiotic nanocarriers, surface coated with the protease Alcalase, "digest" their way through the biofilm EPS matrix, reach the buried bacteria, and deliver a high dose of antibiotic directly on their cell walls, which overwhelms their defences. This thesis's work demonstrates that they are effective against six wound biofilm-forming bacteria, *Staphylococcus aureus*, *Pseudomonas aeruginosa*, *Staphylococcus epidermidis*, *Klebsiella pneumoniae*, *Escherichia coli*, and *Enterococcus faecalis*. Additionally, it is shown that co-treatments of ciprofloxacin and Alcalase-coated Carbopol nanogels led to a 3-log reduction in viable biofilm-forming cells when compared to ciprofloxacin treatments alone. Encapsulating an equivalent concentration of ciprofloxacin into the Alcalase-coated nanogel particles boosted their antibacterial effect much further, reducing the bacterial cell viability to below detectable amounts after 6 hours of treatment.

Chapter 4 combines the work of chapter 2 (NPs against antibiotic-resistant pathogens) and chapter 3 (NPs against biofilm-forming pathogens). This concept is demonstrated by encapsulating Penicillin G and Oxacillin into shellac nanoparticles, subsequently coated Alcalase. It is shown for the first time that these active nanocarriers can destroy biofilms of *S. aureus* resistant to Penicillin G and are significantly more effective in killing the bacterial cells within compared to an equivalent concentration of free antibiotic. The approach of concentrating the antibiotic by encapsulating it into a nanocarrier allows a localised antibiotic delivery to the anionic cell wall, facilitated by coating the NPs with a cationic protease. This approach allowed the antibiotic to restore its effectiveness against *S. aureus*, characterised as resistant to the same antibiotic and cause rapid bacterial biofilm degradation. This approach could be potentially used to revive old antibiotics which have already limited clinical use due to developed resistance.

Chapter 5 continued investigating the antimicrobial properties of antibiotic-loaded shellac NPs, with a cationic protease surface functionalisation, however this time on a pathogen fungal species, *Candida albicans*. These Amphotericin B (AmpB)-loaded shellac NPs are fabricated by pH-induced nucleation of aqueous solutions of shellac and AmpB in the presence of Poloxamer 407 (P407) as a steric stabiliser (in the same fashion as penicillin G and oxacillin in chapter 4). The AmpB-loaded shellac NPs are surface coated with the cationic protease Alcalase. The AmpB-loaded shellac NPs show a remarkable boost of their antifungal action compared to free AmpB when applied to *C. albicans* in both planktonic and biofilm forms. The surface functionalisation with a cationic protease allows the NPs to adhere to the fungal cell walls, delivering AmpB directly to their membranes. Additionally, the hydrolysing activity of the protease coating degrades the biofilm matrix, thus increasing the effectiveness of the encapsulated AmpB compared to free AmpB at the same concentration.

Additionally, these protease-coated nanocarrier-based antibiotics showed no detectable cytotoxic effect against human keratinocytes. It is envisaged these antibiotic-loaded NPs. Subsequently, surface functionalised with the cationic protease could be potentially used to treat antibiotic-resistant biofilm infections in the clinic, for example, in recalcitrant chronic wounds. Chapter 6 outlines future work which could be performed using these NP formulations.

Contents

Title page.....	1
Acknowledgements.....	2
List of publications, presentations and posters created from this thesis.....	3
Abstract.....	4
Contents.....	6
1.0 Chapter 1 – Introduction.....	10
1.1 Skin structure and function.....	10
1.1.1 Skin microbiology.....	11
1.1.2 Wound healing and microbiology.....	13
1.1.3 Strategies for managing infected wounds.....	15
1.2 Biofilms.....	16
1.3 Antibiotics and antibiotic resistance.....	21
1.4 Nanoparticles as antimicrobials.....	26
1.4.1 Lipid-based.....	30
1.4.2 Inorganic.....	32
1.4.3 Polymeric.....	36
1.4.3.1 Carbopol Aqua SF1.....	39
1.4.3.2 Shellac.....	41
1.4.3.3 Surfactants.....	44
1.4.3.3.1 Poloxamer 407 (P407).....	45
1.5 Functionalisation of NPs.....	45
1.5.1 Polyelectrolytes.....	47
1.5.1.1 Branched polyethylenimine (bPEI).....	48
1.5.2 Proteases.....	49
1.6 Nanocarriers for drug delivery – characteristics and application.....	52
1.6.1 Drug loading/swelling behaviour.....	52
1.6.2 Microgel absorption/swelling technique.....	52
1.6.3 Encapsulation stability.....	53
1.6.4 Drug release from NPs and nanogels.....	53
1.7 Use of NPs in the treatment of infected wounds.....	55
1.7.1 Clinical use of NPs.....	55
1.8 Aims of the thesis.....	60
1.9 Ethical statement.....	61
1.10 Reference list.....	62
2.0 Chapter 2 - Breathing new life into old antibiotics: overcoming antibacterial resistance by antibiotic-loaded nanogel carriers with cationic surface functionality.....	92
2.1 Introduction.....	93
2.2 Materials and methods.....	97
2.2.1 Materials.....	97
2.2.2 Bacterial culture.....	98
2.2.3 HaCaT culture.....	98
2.2.4 Hydrodynamic diameter and zeta potential distributions of Carbopol Aqua SF1 NPs.....	99

2.2.5 Zeta potential of wound bacterial species.....	99
2.2.6 Encapsulation of tetracycline and lincomycin into Carbopol and its effect on stability.....	99
2.2.7 Encapsulation efficiency of tetracycline and lincomycin in Carbopol Aqua SF1.....	100
2.2.8 Release kinetics of tetracycline and lincomycin from Carbopol nanogel formulations.....	100
2.2.9 Functionalisation of ABX–Carbopol Aqua SF1 nanogel with bPEI.....	101
2.2.10 Antimicrobial susceptibility testing (AST) disk diffusion test of wound species.....	101
2.2.11 Cell viability of HaCaT cells treated with free ABX and Carbopol nanogel-ABX.....	101
2.2.12 Minimum inhibitory concentration (MIC).....	102
2.2.13 Time-kill assays.....	103
2.2.14 SEM imaging of the treated cells.....	103
2.2.15 Statistical analysis.....	104
2.3 Results and discussion.....	105
2.3.1 Encapsulation of tetracycline and lincomycin into Carbopol Aqua SF1 nanogel.....	105
2.3.2 Encapsulation efficiency and release kinetics of tetracycline and lincomycin in Carbopol..	109
2.3.3 Zeta potential of wound-relevant bacterial species.....	113
2.3.4 Antimicrobial susceptibility testing (AST) disk diffusion test of wound species.....	114
2.3.5 Viability of HaCaT cells treated with tetracycline/lincomycin and Carbopol.....	116
2.3.6 Antibacterial activity of bPEI-coated tetracycline/lincomycin loaded Carbopol.....	118
2.4 Conclusions.....	125
2.5 Reference list.....	126
3.0 Chapter 3 - Enhanced clearing of wound-related pathogenic bacterial biofilms using protease-functionalised antibiotic nanocarriers.....	128
3.1 Introduction.....	130
3.2 Materials and methods.....	134
3.2.1 Materials.....	134
3.2.2 Synthesis of Alcalase-coated nanogel particles.....	134
3.2.3 Preparation of ciprofloxacin-loaded nanogel.....	135
3.2.4 Characterisation of free Alcalase, Alcalase-nanogel and Alcalase-ciprofloxacin-nanogel...	136
3.2.5 Hydrodynamic diameter, zeta potential, UV-Vis and FTIR spectroscopic studies.....	136
3.2.6 Protease activity of free Alcalase vs nanogel-immobilised Alcalase.....	136
3.2.7 Bacterial culture and biofilm producing assessment.....	137
3.2.8 Zeta potential of bacteria treated with free Alcalase and Alcalase-coated nanogel.....	138
3.2.9 Biofilm staining with Crystal Violet and Congo Red.....	138
3.2.10 Membrane colony biofilm NP and ciprofloxacin treatment.....	139
3.2.11 Antimicrobial susceptibility testing of <i>Staphylococcus aureus</i>	139
3.2.12 Resazurin sodium salt <i>in situ</i> bacterial metabolic activity assay.....	140
3.2.13 Biofilm formation assay on a glass surface.....	140
3.2.14 Atomic force microscopy (AFM).....	140
3.2.15 TEM images of Alcalase-nanogel and SEM images of the treated biofilms.....	141
3.2.16 Cytotoxicity and apoptotic stasis of HaCaT cells after treatment with nanogels.....	141
3.2.17 Statistical analysis.....	142
3.3 Results and discussion.....	143
3.3.1 Coating and immobilisation of Alcalase 2.4 L FG on to Carbopol nanogel particles.....	147
3.3.2 Protease activity of free Alcalase vs Alcalase nanogel.....	150

3.3.3 Qualitative biofilm-producing capability assessment of ATCC bacterial species.....	151
3.3.4 Biofilm disruption by Alcalase-coated nanogel particles.....	153
3.3.5 Resazurin sodium salt <i>in situ</i> bacterial biofilm metabolic activity assay.....	159
3.3.6 <i>S. aureus</i> biofilm cellular viability after treatment with Alcalase-nanogels.....	161
3.3.7 Antibiofilm efficacy of Alcalase-nanogel particles on <i>S. aureus</i> biofilm structure.....	166
3.3.8 Zeta potential of bacteria treated with free Alcalase and Alcalase-nanogel.....	169
3.3.9 Comparison with standard treatments for biofilm-forming bacteria.....	170
3.3.10 Cytotoxicity and apoptosis-inducing sbility of nanogel on human cells.....	172
3.4 Conclusions.....	176
3.5 Reference list.....	177
4.0 Chapter 4 - Smart active antibiotic nanocarriers with protease surface functionality can overcome biofilms of resistant bacteria.....	181
4.1 Introduction.....	182
4.2 Materials and methods.....	187
4.2.1 Materials.....	187
4.2.2 Preparation of PenG/Oxa-loaded P407-stabilised shellac NPs.....	187
4.2.3 Enzyme surface functionalisation of the Shellac- P407-AmpB NPs.....	188
4.2.4 Shellac NPs hydrodynamic diameter, zeta-potential and TEM characterisation.....	188
4.2.5 Encapsulation efficiency and release kinetics of PenG/Oxa from the shellac NPs.....	188
4.2.6 Fourier transform infrared (FTIR) and UV-vis spectroscopy analysis.....	189
4.2.7 Bacterial culture.....	190
4.2.8 Time Kills.....	190
4.2.9 Minimum inhibitory and bactericidal concentration (MIC/MBC).....	190
4.2.10 Antimicrobial susceptibility testing (AST).....	191
4.2.11 SEM imaging of the treated cells.....	191
4.2.12 TEM and EDX imaging of the treated cells.....	192
4.2.13 Beta lactamase activity.....	192
4.2.14 Preparation of microtiter <i>S. aureus</i> biofilms.....	193
4.2.15 Crystal Violet staining, biofilm weight and biofilm protein concentration.....	193
4.2.16 <i>S. aureus</i> cellular viability after PenG/Oxa-NP treatments.....	194
4.2.17 <i>S. aureus</i> fluorescent images, biofilm quantification and CSLM.....	195
4.2.18 Cryostat sectioning of <i>S. aureus</i> biofilm.....	195
4.2.19 Cytotoxicity and of HaCaT and HEP G2 cells after treatment.....	196
4.2.20 Statistical analysis.....	196
4.3 Results and discussion.....	197
4.3.1 NP characterisation.....	197
4.3.2 <i>S. aureus</i> antimicrobial susceptibility screening.....	209
4.3.3 Effectiveness of shellac-P407- PenG/Oxa-Alcalase NPs against planktonic <i>S. aureus</i>	212
4.3.4 Effectiveness of shellac- P407-PenG/Oxa-Alcalase NPs against biofilm-formed <i>S. aureus</i>	219
4.3.5 The structure of biofilm-formed <i>S. aureus</i> when treated with PenG/Oxa-NPs.....	225
4.3.6 Human cell cytotoxicity when treated with PenG/Oxa-NPs.....	228
4.4 Conclusions.....	231
4.5 Reference list.....	232
5.0 Chapter 5 - Enhanced Removal of Fungal Biofilms by Protease-Functionalised Amphotericin B Nanocarriers.....	235

5.1 Introduction	236
5.2 Materials and Methods	241
5.2.1 Materials	241
5.2.2 Preparation of AmpB-Loaded P407-stabilised shellac NPs	242
5.2.3 Enzyme surface functionalisation of the wt% shellac–P407–AmpB NPs	242
5.2.4 Shellac NP hydrodynamic diameter, zeta potential, and SEM/TEM characterisation	242
5.2.5 Surface tension measurements of AmpB solutions at various concentrations	243
5.2.6 Encapsulation efficiency and release kinetics of AmpB from the shellac NPs	243
5.2.7 FTIR, UV–Vis spectroscopy, and XRD studies	244
5.2.8 Time-kill assays for planktonic <i>Candida albicans</i>	244
5.2.9 Preparation of <i>C. albicans</i> biofilms	245
5.2.10 CV staining, biofilm weight, and biofilm protein concentration after treatments	245
4.2.11 Measuring <i>C. albicans</i> biofilm metabolic activity using XTT colorimetric assay	246
4.2.12 Measuring HaCaT metabolic activity using MTT colorimetric Assay	246
4.2.13 SEM imaging of planktonic <i>C. albicans</i> and <i>C. albicans</i> biofilms	247
4.2.14 Statistical analysis	248
5.3 Results and discussion	249
5.3.1 Preparation, encapsulation efficiency, and release kinetics of AmpB-loaded shellac NPs.	249
5.3.2 Surface functionalisation of AmpB-loaded shellac NPs with a cationic protease.....	255
5.3.4 Characterisation of shellac–AmpB–Alcalase NPs.....	257
5.3.5 Time-kill assay for Alcalase-Coated AmpB-shellac NPs against planktonic <i>C. albicans</i>	261
5.3.6 Antibiofilm action of Alcalase-Coated AmpB-shellac NPs against <i>C. albicans</i>	265
5.3.7 HaCaT cell cytotoxicity of shellac–AmpB–Alcalase NPs.....	272
5.4 Conclusions	274
5.5 Reference list	275
6.0 Chapter 6	279
6.1 Summary of thesis	279
6.2 Future work	282
6.3 Reference list	284

1.0 Chapter 1

1.1 Skin structure and function

Skin is commonly regarded as the largest organ in the human body and is essential for an individual's survival and health (Grice & Segre, 2011). One of the primary roles of skin is to act as a physical barrier to the external environment and facilitate the individual's protection from biological and chemical insults (Baroni et al., 2011). Additionally, it mediates tactile interactions between an individual and the external environment via skin embedded afferent neurons and mechanoreceptors and regulating thermal stability (Abraira & Ginty, 2013). Healthy skin is generally a dry, acidic (pH \approx 5.6-6.4), salty environment that is waterproof and creates an impermeable barrier for infection from microorganisms (Kruse et al., 2015). During life, the skin is often damaged, reducing its protective properties and renders the individual vulnerable to infection and colonisation from pathogenic microorganisms (Percival et al., 2015). Non-pathogenic commensal skin microbiota may also enter a cutaneous lesion (Misic et al., 2014). To maintain health and minimise the risk of infection from trauma skin has a highly regulated multi-staged healing mechanism comprising 1) haemostasis 2) inflammation 3) proliferation and 4) remodelling (maturation) (Reinke & Sorg, 2012). Failure to complete this process can result in the development of a chronic wound environment which subsequently requires ongoing treatment and maintenance to prevent the detrimental function of the body area wounded, and possible deleterious infection (Frykberg & Banks, 2015). Antimicrobial agents are often administered in chronic wound treatments. However, these agents' efficiency is often negated due to the prevalence of resistant bacterial species (Rahim et al., 2016). Due to antibiotic discovery's stalled nature and increasing resistance, nanocarrier-mediated delivery of antimicrobials is under investigation to understand if this approach can overcome bacterial resistance mechanisms (Wang et al., 2017).

Skin is divided into three main layers, the outer epidermis, the middle dermis, and the inner subcutaneous tissue layer (Baroni et al., 2011). These regions have unique structural histology pertinent to the role of a particular layer of the skin has (Arda et al., 2014). There is a variation in skin thickness, ranging from 0.5 mm in the eyelids to 4 mm thick on the heels (Farage et al., 2013). This variation in thickness is proportional to the abrasion and pressure the skin is exposed to. For example, fingertips and other areas with high amounts of pressure, i.e. heels are considerably thicker than skin located nearby (Pouradier et al., 2013). Additionally, skin properties are dependent on sex and age, with males on average having thicker skin than females post-puberty, and skin becoming progressively

thicker until adulthood in both genders (Derraik et al., 2014). The functions of the skin are broad and are summarised in **table 1.1**.

Table 1.1 A summary of the functions of human skin.

Function	Description
Physical Protection	UV light is absorbed by melanin, derived from melanocytes, and protects the skin from excessive exposure and potential free radical production (D’Orazio et al., 2013). The elasticity of skin allows flexibility, movement and growth whilst still retaining structural integrity (Pawlaczyk et al., 2013). Keratin forms a strong protective barrier to extracellular insults (Anford et al., 2015).
Immunity	Various cells, such as innate immune Langerhans and phagocytic cells, provide immediate protection from a bacterial infection (Sanford & Gallo, 2013). Secreted host defence peptides (HDPs) include cathelicidins, protegrins and α -defensins and convey a wide array of antimicrobial actions. Some species such as <i>S. aureus</i> display resistance to these agents (Brett & Bradfute, 2015).
Sensation	Somatic sensory receptors situated in the skin allow pressure stimuli to be detected (Park & Kim, 2013).
Thermoregulation	Hair follicles provide limited heat insulation and can be involuntarily controlled by erector pili muscles, straightening the angle of hair can decrease heat loss from the skin’s surface (Romanovsky et al., 2014). Additionally, thermoreceptors can sense external and internal temperatures and stimulate blood vessel dilation to cause superficial blood perfusion and protect against a cold external environment, or constricted to reduce blood perfusion and conserve heat, particularly in extremities (Tansey & Johnson, 2015). Secretions from sweat glands allow evaporation and reduction in skin (and body) temperature (Lu & Fuchs, 2014).
Absorption	Cells in the outermost epidermis (0.25 to 0.40 mm) are primarily supplied by external oxygen, and not the hosts own respiratory system (Stücker et al., 2002).
Storage and synthesis	Vitamin D ₃ is synthesised photochemically from precursor 7-dehydrocholesterol upon exposure to UVB light, allowing an endocrine release of this vitamin (Mostafa & Hegazy, 2015). Triacylglycerols are stored as an energy reserve in adipocytes below the skin’s subcutaneous layer, acting as a layer of insulation (Alexander et al., 2015).
Water resistance	Sebum is secreted to create a hydrophobic barrier on the stratum corneum to prevent water loss via seepage and evaporation (Grice & Segre, 2011).

1.1.1 Skin microbiology

Skin is home to a diverse milieu of microorganisms, with the vast majority commensal to the host (Grice & Segre, 2011). The ecology of the skin surface is highly relevant to microorganisms' ability to colonise, with conditions changing depending on the topographical location of the skin (Cundell, 2016). Additionally, endogenous host factors such as antimicrobial peptides (AMPs), the adhesion and aggregation capability of the microorganism determine its success at skin colonisation (Pfalzgraff et al., 2018). As well as the ability of AMPs to directly kill microorganisms by electrostatic membrane disruption resulting in cell lysis, they can also have a chemotactic function and recruit immunocytes, interacting with Toll-like receptors (TLRs) to help educate the immune and aid in the removal of bacterial products and promote inflammation (Zhang & Gallo, 2016). Skin flora can also have a mutualistic influence on the host by consuming nutrients and occupying space used by transient pathogens (Campbell & Koch, 2017). They can also release molecules to inhibit the growth of and help

prevent colonisation by exogenic pathogens (Nakatsuji et al., 2017). *S. epidermidis* has been shown to secrete phenol-soluble modulins which can inhibit the growth of nearby species such as *S. aureus* (Otto, 2014). Disruption to this microbiome ecosystem has been linked to skin disorders, providing evidence on the importance of the skin habitat, dysbiosis reversion is currently being researched to understand if this can help treat or prevent disease (Williams & Gallo, 2017). Additionally, these symbiotic species may prime and educate T-cells located in the skin, allowing them to respond to pathogenic threats if required (Ali & Rosenblum, 2017). This benefit is not without risk, however, as non-pathogenic species still can cause disease in immunosuppressed individuals, or cause bacteraemia via wounds (Sasson et al., 2017).

Skin, as the largest organ with approximately 1.8 square metres of surface area, is primarily cooler than the internal temperature of 37°C, with the averaging being 34°C (Grice & Segre, 2011). The numerous folds and invagination create changes in temperature in different areas of the body. This is a factor for the variation of microorganism species at other skin sites with the humidity and presence of sebaceous glands influencing the microbiome composition (Li et al., 2017). Facultative anaerobes and lipophiles such as *Propionibacterium acnes* and *Malassezia* spp. can thrive in these areas due to the decreased oxygen content and higher relative humidity (Leheste et al., 2017). This accounts for the increased concentration of these species on the scalp due to the abundance of lipids (Perez et al., 2016). *S. aureus* can grow more effectively in areas such as the groin due to the increased temperature and higher humidity (Albrecht et al., 2015). Areas more open to abrasion with reduced humidity and dryness (hands, arms, and legs) are much less confluent in bacterial populations due to the harsher conditions for bacteria to grow (Grice & Segre, 2011). Selective pressure of the more niche areas of human skin creates a more limited range of species, whereas other sites have a much higher bacterial diversity (Oh et al., 2016). It is suggested skin microbiota is more stable in areas that are occluded than regions in which there are more environmental fluctuations, such as the limbs (Schommer & Gallo et al., 2013). However, host factors are considered more significant than environmental factors, due to the composition of the skin microbiota remaining relatively stable over time, regardless of changes in the environment (Grice & Segre, 2011). The mycobiome is often overlooked when considering skin and wound sites' microbiota, despite evidence they are present in 80% of diabetic foot ulcer samples (Kalan et al., 2016). This could be because the sensitivity of detecting fungi using traditional cell culture methods results in a much lower detection rate, 5% in the Kalan et al., 2016 study. Using molecular methods in this study increased the detection rate to 80%. The study also revealed the presence of the phylum *Ascomycota* in wound sites increased the healing time, providing evidence of the importance of understanding the mycobiome's role in wound healing (Kalan et al., 2016).

Host and environmental factors play a large part in determining the skin microbiota (Grice & Segre, 2011). Age, sex, and location cause variations in the skin microenvironment (Prescott et al., 2017). Age is an essential factor to consider, *in utero* foetal skin is sterile, and the baby is colonised during vaginal birth from the mother, interestingly the profile of bacteria the baby is exposed to differs if caesarean section birth is performed (Mueller et al., 2015). During puberty, there is a change in the skin microbiome of the individual as higher sebum production levels increase the prevalence of lipophilic species, according to samples taken and inoculated in cultured based methods (Kennedy et al., 2017). Gender is also thought to be responsible for differences in individuals' skin profile (Ying et al., 2015). There are conflicting opinions of whether gender is significant in the variations observed in skin profiles, or if it is an artefact created by the increased use of cosmetics and hygienic products used by women (Lee et al., 2018). The environment an individual lives in and their occupation may affect the skin microbiome (Prescott et al., 2017). Hygiene products and cosmetics can change the skin's chemical conditions and may result in different bacterial profiles, but this area is not well understood (Kong et al., 2017). Some hypothesise that overuse of antibacterial products may do more harm than good by disrupting the beneficial resident microorganisms on the host (Kong & Segre, 2012). The climate an individual lives and works in can also affect the skin microbiome, with increased temperature and humidity associated with increased concentrations of bacteria on the back, axilla, and feet (Manus et al., 2017). Additionally, UV light is known to be bactericidal, so areas with increased exposure to the UV light would likely result in reductions in microorganism concentrations (Rosenthal et al., 2011).

1.1.2 Wound healing and microbiology

The wound healing process is vital in maintaining the structural integrity and functionality of skin following injury and negating the negative consequences of pathogens or other external chemical agents (Ganapathy et al., 2012). Depending on the healing process's success, a wound is categorised into either 1) acute wounds or 2) chronic wounds (Martin & Nunan, 2015). Acute wound healing is the successful repair of the wound site via the bodies intrinsic healing processes, comparatively chronic wounds fail to heal correctly (within 3 months), either due to intrinsic metabolic issues or external bacterial infection (Frykberg & Banks, 2015). Wound healing is a coordinated systemic process which is separated into four phases (**Figure 1.1**), these are highly dynamic with a high degree of overlap (Eming et al., 2014). This is especially true in irregularly shaped wounds which may be undergoing different healing phases simultaneously (Shah et al., 2012). The process is generally described as linear, but each phase has varying duration times (Demidova-Rice et al., 2012). The wound healing process is comprised of the following stages 1) haemostasis 2) inflammatory response 3) proliferation and 4)

maturation (Yates et al., 2012). An interruption in one of these phases could lead a wound away from normal healing and into a chronic condition, with chronic inflammation being a driving factor in chronic wounds (Zhao et al., 2016). Age and gender also play a role in wound healing. Older people heal slower than younger, primarily due to a delayed inflammatory response (Guo & DiPietro, 2010) and increased cellular senescence (Wilkinson & Hardman, 2017). Additionally, females' wounds have been shown to physiologically heal faster than male equivalent wounds (Engeland et al., 2009). The role of oestrogen has been investigated in wound healing, with deficiencies in 17β -estradiol shown to increase macrophage migration inhibitory factor (MIF) (Wilkinson & Hardman, 2017), resulting in disruption of the inflammatory healing phase and subsequent slowed healing (Junker et al., 2013). It has been suggested that microorganisms are present and propagating in all chronic wounds (Wolcott et al., 2016). However, these microorganisms' role in chronic wounds and how they influence wound healing is multifaceted (**Table 1.2**) (Zhao et al., 2013a).

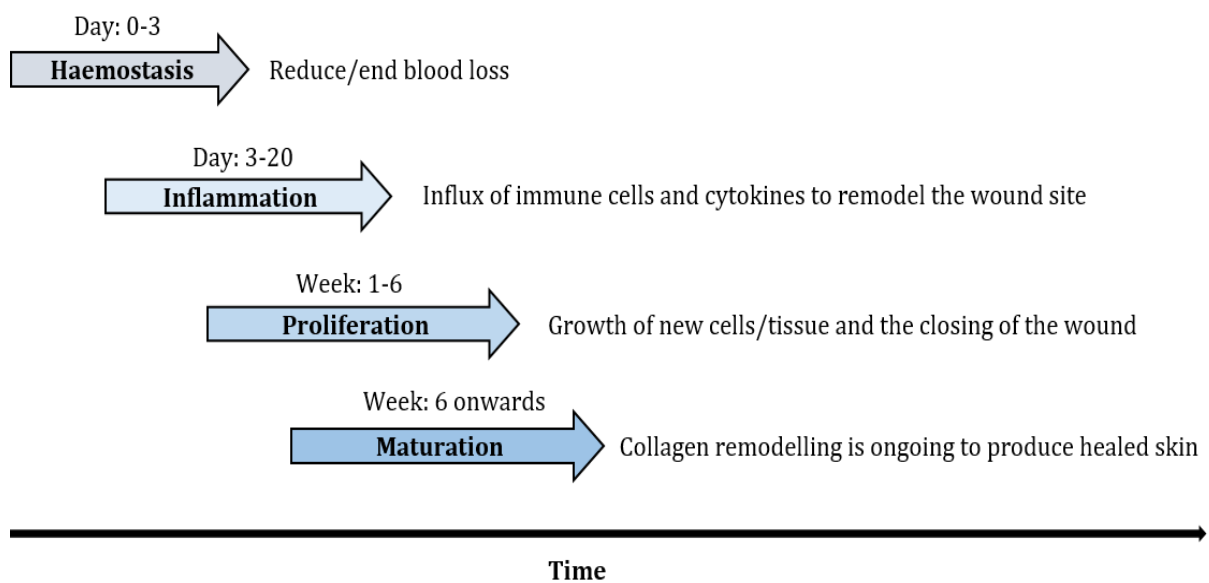


Figure 1.1 The phases of wound healing in the skin. Immediately following injury blood clotting occurs (haemostasis) to reduce and prevent blood loss from the wound site (Golebiewska & Poole, 2015). Inflammation occurs shortly afterwards to begin the process of removing dead cells and potential extrinsic materials via phagocytosis (Landén et al., 2016). New tissue is grown during the proliferation phase to replace dead or missing tissue from the injury (Demidova-Rice et al., 2012). Skin is fully healed and strengthened by collagen production and the formation of scar tissue (Yates et al., 2012). Image adapted from Nauta et al., 2014.

Table 1.2 The potential role of microbiota within wounds and how they may affect wound healing.

Role of microbiota in wounds	Ref
The microbiota in a wound consists of a diverse range of species, most of which are commensal contaminants but within this population, one species may cause problematic infection.	(Scales & Huffnagle, 2013)
The microbiota within a wound form a biofilm, and this presents different challenges for the host, which contributes to persistent infection.	(Percival et al., 2015)
The wound acts as a reservoir for future infection if environmental and host conditions permit growth.	(Misic et al., 2014)
Inflammation is produced persistently due to continuous bacterial presence, and this can influence wound healing.	(Gardiner et al., 2017)
The wound microbiota is not harmful to the host and is controlled by the immune system. However, growth can happen on wound dressings and release toxins which may be detrimental to the hosts wound healing.	(Chen et al., 2018)
Microorganisms are present within the wound but are not shown to be causing any adverse effect on wound healing.	(Williams et al., 2018)

1.1.3 Strategies for managing infected wounds

Currently, there are several strategies for treating biofilm infected wounds. These mostly consist of debridement (biological, ultrasound, enzymatic, mechanical and surgical) and topical treatments alongside systemic antibiotic therapy (Manna et al., 2020; Negut et al., 2018). If the wound bed is not clear of infection, particularly biofilms, and devitalised tissue, wound healing is impaired (Sherman et al., 1997; Liu et al., 2017). Biological debridement consists of using maggots (*Lucilia sericata* (green bottle fly)), grown in sterile conditions. These maggots are applied to the wound bed and confined by a specialised dressing (Bazaliński et al., 2019). This practice is usually reserved for severe chronic infections, such as a diabetic foot ulcer and is becoming less common, although still practised in the NHS (Rafter, 2010). Ultrasound debridement uses a curette to emit ultrasonic sound waves in the wound bed vicinity. This separates necrotic tissues and some biofilms whilst keeping the healthy tissue intact (Bekara et al., 2015). Enzymatic debridement is applying a topical agent that chemically liquifies necrotic tissue (Patry et al., 2017). Autolytic debridement uses the body's own enzymes. The wound must be kept moist for this to be effective, requiring the use of dressings consisting of hydrogels or hydrocolloids (Choo et al., 2019). Mechanical debridement includes hydrotherapy, irrigation and abrasion of the infected wound. It often results in the unintended damage of healthy tissue and is most commonly used in small wounds (Hess et al., 2003). Likewise, surgical debridement by a partitioning using scalpels etc. is often used in the same context (Lebrun et al., 2010). Lastly, topical antibiofilm therapies can be applied. These include; various antiseptics, antibiotics, and other materials with antimicrobial properties, e.g. povidone-iodine (PVP-I), ionic silver, polyhexamethylene biguanide (PHMB) and mupirocin (Cambiaso-Daniel et al., 2018). However, biofilms are known to be tolerant to most antimicrobial agents, which often results in chronic wound infection (Bowler et al., 2018). This project focuses on the creation of novel antibiofilm NPs.

1.2 Biofilms

Biofilms allow bacteria to exist in an environment which helps increase survivability due to the decreased efficacy of antimicrobials which must diffuse through the biofilm matrix (Stewart, 2015). Social cooperation and interspecies interaction (Raghupathi et al., 2017), and resource capture and retention also play a part (Flemming et al., 2016). These properties allow bacteria living within a biofilm to have emergent properties and therefore should be considered separately in regard to planktonic bacteria when investigating their role within wounds. Biofilms are composed of extracellular polymeric substances (EPS). The cells within live in an aggregated form that can contain multiple layers, vastly increasing cell to cell contact cohesion (Aggarwal et al., 2015).

The vast majority of the biofilm is hydrated EPS, making up approximately 90% of the biomass, with the remaining 10% being cells (Briley et al., 2014). Biofilms are commonly surface-attached with one layer of cells in direct contact with the substratum. However, they can be found in flocs in which biofilms are formed around cells without contact with a substratum (Kim et al., 2014). The biofilm is highly influential in the growth and phenotype of bacteria. This means that properties discovered by investigating the planktonic form of the same species are not always replicated in cells living in a biofilm (Levipan & Avendaño-Herrera, 2017). Biofilms are among the most successful and widely distributed forms of life with their presence found in a diverse range of environments that would not support planktonic cells (Høiby et al., 2011). The density of cells within biofilms is high, ranging from 10^8 to 10^{11} cells per gram (Melaugh et al., 2016). It is often made up of a wide range of species making unique biogenic microconsortia habitat (Liu et al., 2016). Biofilms are primarily composed of polysaccharides, proteins, lipids and extracellular DNA (eDNA) (Limoli et al., 2015). Biofilms are commonly found in chronic wounds but rarely in acute wounds (Attinger & Wolcott, 2012), and regularly form on the outer layers, but are capable of inhabiting deeper layers of wound tissue (Ashrafi et al., 2018).

Bacteria can interchange between living in planktonic and biofilms. However, biofilms are the predominant form of bacteria found, likely due to the increased survivability of cells within EPS (Petrova & Sauer, 2016). Biofilms allow cells to avoid being washed away, resist shear forces and physical damage, and limit antimicrobial compounds' diffusion through the EPS (Saur et al., 2017). Additionally, horizontal gene transfer of resistance genes (plasmid derived conjugation) is more easily achieved in EPS due to the decreased bacterial motility and closer cell to cell contact between species (Stalder & Top, 2016).

Biofilm formation (**figure 1.2**) can begin from a single cell which typically lands on a suitable surface (Song et al., 2015). A single planktonic cell can reversibly adhere to a suitable surface (either

biotic or abiotic) either by physical forces of bacterial appendages such as pili or flagella (Xu et al., 2013a), they then can begin to grow into a microcolony (Saini et al., 2011). Forces that allow bacteria to adhere to a substrate include electrostatic interactions, steric interactions, and van der Waals. This adhesion is highly influenced by the substrate's temperature, pressure, and chemical properties (Busscher & van der Mei, 2012). Attachment is irreversible when these forces, often modulated by bacterial appendages, are greater than repulsive forces applied to cells from the environment (Kostakioti et al., 2013). The biofilm then matures into a mushroom-like structure containing exopolymers such as polysaccharides, proteins, and lipids that form a complicated scaffold-like structure that has been suggested to be analogous to the extracellular matrix (ECM) of animal tissues (Ghanbari et al., 2016). Growth within the biofilm is not uniform and channels, or pores, are formed which allow gradients of nutrients and oxygen, creating pockets which are higher in nutrient density compared to other areas of the biofilm (Melaugh et al., 2016). The biofilm microenvironment can also have gradients of oxygen that promote different metabolic activities of the cells within, e.g. low oxygen environments on the interior, leading to anaerobic and higher oxygen content on the exterior leads to aerobic species growing (Wessel et al., 2014). The microenvironment also has pH gradients that influence growth in species sensitive to pH fluctuations (Dige et al., 2016). The substrate the biofilm forms on can also affect the biofilm microenvironment, e.g. a biotic surface such as a plant may be rich in cellulose which is converted into glucose supporting anaerobic bacteria closed to the substrate (Limoli et al., 2015). The microcolony can reach thicknesses of 1000 μm (in extreme cases, see **table 1.3**). Sessile cells within the biofilm can be dispersed and revert to a motile planktonic form with increased expression of flagella proteins allowing them to be released from the biofilm and potentially being able to form a new biofilm (Berlanga & Guerrero et al., 2016).

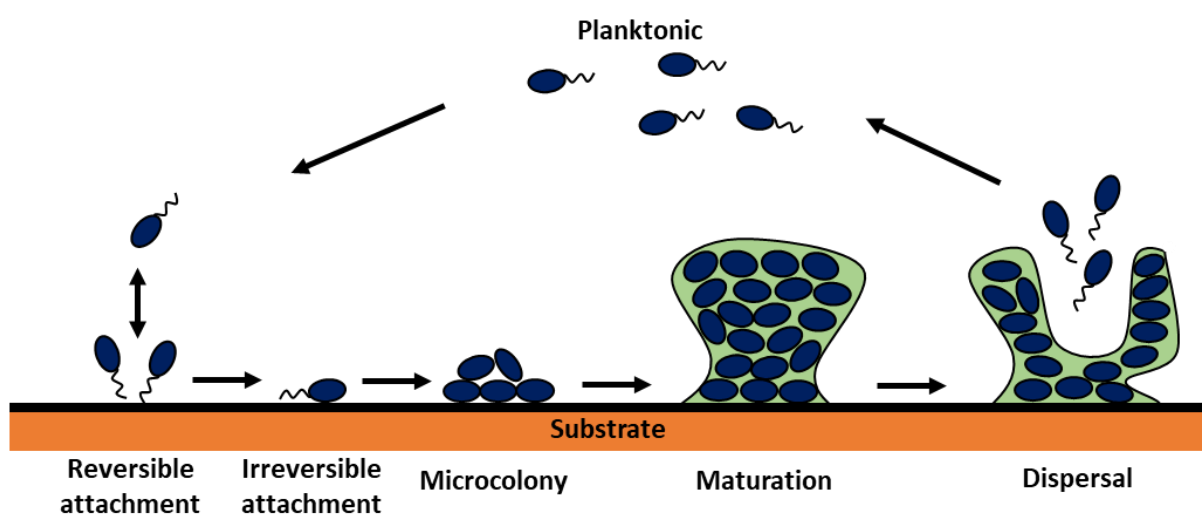


Figure 1.2. Biofilm formation schematic. Image modified from Toyofuku et al., 2015.

Table 1.3. Size characteristics of clinically *in vivo* occurring biofilms, measured as their longest diameter or length [Bjarnsholt et al., 2013].

Clinical location of biofilm	Size / μm
Catheter and shunt associated	5 - 1000
Implant associated	5 - 500
Chronic wounds	35 - 200
Contact lenses	50 - 100
Lung infections	4 - 100
Otitis media (ear)	4 - 80
Chronic osteomyelitis (bone)	5 - 50
Chronic rhinosinusitis (sinuses and nasal cavity)	5 - 30

Quorum sensing (QS) is utilised by bacteria to respond to cell population density and modulate growth by sensing the concentration of QS signalling molecules in the local environment, and regulate gene expression when a threshold concentration of signalling molecules is achieved (Solano et al., 2014). During biofilm formation, the increasing density of cells increases the QS signalling process and alters neighbouring cells' gene expression (Rutherford & Bassler, 2012). An example is an upregulation of genes allowing for fibrous pili production, which increases inter-connectivity between the biofilm microcolonies (Persat et al., 2015). The pili connections allow bacteria within the biofilm to adjust their position using a process called twitching motility, which can influence the biofilm's overall morphology as motile cells 'crawl' over non-motile cells to access faster-growing areas of the biofilm (Anyan et al., 2014). The increased concentration of QS signalling molecules also alters the gene expression of local bacteria to create an EPS-producing phenotype (Jayathilake et al., 2017). These QS signalling molecules are termed autoinducers, Gram-negative species produce acyl-homoserine lactones, and Gram-positive species produce oligo-peptides (Li & Nair, 2012). When they bind to specific receptors, one of the outcomes is increased EPS-producing genes (Tan et al., 2014).

An interesting property of biofilms is the increased ability to process nutrients which contribute to cells within being able to survive. Bacteria often secrete digestive enzymes which can diffuse away in the aqueous environment when the bacteria are in planktonic form but are retained within the biofilm creating a biofilm digestive system which benefits the cells in the biofilm (Bogino et al., 2013). The heterogeneity of cells within a biofilm allows signalling molecules, genetic materials, defensive molecules to be shared by multiple species allowing cooperation between species which would not be possible in planktonic form, further contributing to the benefits of growing within a biofilm (Liu et al., 2016).

As mentioned above, biofilms confer benefits to the cells within in regard to quenching antimicrobial agents which may kill planktonic cells (Algburi et al., 2017). **Figure 1.3** illustrates the

mechanisms and factors involved in conferring drug resistance in pathogenic biofilms. The biofilm itself can decrease the antimicrobial agent's ability to diffuse through the EPS, which in turn reduces the concentration of antimicrobial a cell may be exposed to, thus increasing the resistance of the cells to the chemical (Singh et al., 2017). An example of this is the neutralisation of toxic metals such as copper which can be complexed to the EPS polysaccharides (Nocelli et al., 2016). EPS can act as a sacrificial fodder to many toxic metals by oxidising them to the EPS structure and limiting exposure to cells to sublethal levels (Gupta & Diwan, 2017). However, they can also become resistant to a specific antimicrobial agent such as an antibiotic by continuous low exposure and the potential acquisition of a resistant gene from a cell which is in cohesion within the biofilm (Castaneda et al., 2016). Biofilms are also home to cells which are much more likely to be in a stationary phase as well as dormant non-metabolic active persister cells, and therefore are not susceptible to antimicrobials which rely on disrupting and inhibiting the growing metabolic activity of cells (Spoering et al., 2001; Lewis et al., 2006). As well as the passive defensive benefits of a biofilm, certain species within a biofilm such as *S. aureus* and *Janthinobacterium lividum* have been shown to actively produce a secondary metabolite called violacein which has anti-viral, protozoan, and fungal properties (Bilsland et al., 2018). This purple pigmented molecule could act as a defence against predation from grazing protozoa, particularly in freshwater environments (Im et al., 2017).

EPS can be targeted to cause degradation and allow the cells inside to be vulnerable to antimicrobial agents (Fleming & Rumbaugh, 2017). eDNA can be targeted with DNases to potentially reduce the ability of gene transfer (Brown et al., 2015). The ability to degrade the exopolysaccharides with glycoside hydrolases such as Dispersin B has also been investigated as a potential biofilm treatment option (Garnett & Matthews, 2012). Biofilm adhesion has also been targeted with EPS adhesion-binding antibodies or inhibitors, which have been shown to reduce biofilm's ability to form (Kostakioti et al., 2013). Signalling molecules secreted by bacteria to promote EPS production have also been targeted in an effort to reduce biofilm formation. Cyclic-di-GMP and cyclic-do-AMP are secondary messengers used in signal transduction of EPS products, small-molecule inhibitors of cyclic-di-GMP and cyclic-do-AMP have been identified using *in silico* drug discovery models. They have shown promise in biofilm degradation when applied *in vitro* (Ha & O'Toole, 2015).

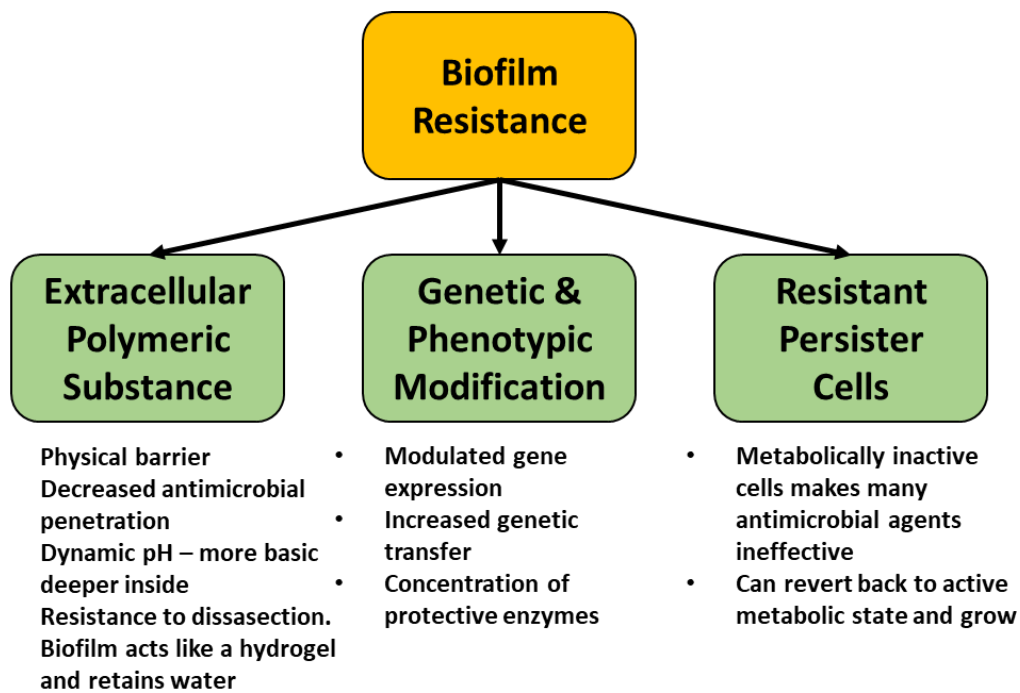


Figure 1.3. Mechanisms and factors involved in conferring drug resistance in pathogenic biofilms. Data from Flemming et al., 2016. Image adapted from Singh et al., 2016.

There is evidence that biofilms are constantly remodelling the EPS, with distinct zones which have different viscosities, allowing the movement of cells within the biofilm (Persat et al., 2005; Billings et al., 2015). This remodelling allows biofilms to adapt to the environment, such as hydrodynamic shear. Additionally, this allows the biofilm's active dispersal, mediated from enzymes produced by the cells within, not just simple passive sloughing of the cells away (Whitfield et al., 2015). There have been many enzymes discovered which confer biofilm remodelling in a wide range of pathogen bacteria. Ones of particular interest are bacterial adhesin proteins that allow the bacteria to attach to host tissues and indwelling medical devices (Pisithkul et al., 2019). This family of proteins are called microbial surface components recognizing adhesive matrix molecules (MSCRAMMs). They have been investigated as a potential therapeutic target to disrupt biofilm remodelling and adhesion abilities (Paterson et al., 2010; Ghasemian et al., 2015; Otto, 2012).

Biofilms can be targeted by interfering with their metabolic requirements. An example is the use of Gallium, which has similar chemical properties to Iron (Kaneko et al., 2007). Iron is an essential nutrient for bacterial growth and is uptaken by siderophores or other iron-chelating molecules (Johnstone & Nolan, 2015). Gallium can be uptaken by these receptors but when internalised does not replication the function of iron in the pathways reasonable for cell growth and EPS production (Kaneko et al., 2007). Silver nanoparticles (AgNPs) have been investigated for their bactericidal anti-biofilm properties (Markowska et al., 2013). AgNPs biological effect is not well understood. However,

it has been suggested AgNPs release Ag⁺ ions in the presence of water interact with the cell membrane modifying the charge and ultimately causing cell death (Salvioni et al., 2017). Silver has also been used in conjunction with bioactive glass and proved an effective antimicrobial and anti-biofilm agent (Wilkinson et al., 2018).

The targeting of QS autoinducers has also been investigated as a potential anti-biofilm agent in *P. aeruginosa* (Smith & Iglewski, 2003) and *S. aureus* (Lonn-Stensrud et al., 2008). Furanones have been used as competitive inhibitors of QS autoinducers (Asif & Acharya, 2012), and autoinducer antibodies such as RS2-1G9 have been used to quench the signalling potential of in *P. aeruginosa* and significantly reduce the biofilm forming capability (Debler et al., 2007).

The mechanism of antibiotic-EPS interaction is not well understood (Fulaz et al., 2019). However, ionic-based interactions between antibiotics and the EPS has been suggested (Davenport et al., 2014). Experimentation showed that by modulating the addition of metal cations (Ca²⁺ and Mg²⁺) to the biofilm treatment area, the penetration of the antibiotic tobramycin could be increased to *P. aeruginosa* biofilms (Tseng et al., 2013). It has hypothesised that the addition of these cations blocks binding sites that would otherwise trap and hinder the antibiotic's penetration. There are many charged groups in biofilm EPS, i.e. glycol proteins and polysaccharides (Speziale et al., 2014).

1.3 Antibiotics and antibiotic resistance

Bacterial infection can be considered one of the largest threats to public health in human history (Prestinaci et al., 2015). Bacterial infection in the pre-antibiotic era was a leading cause of mortality and morbidity (Aminov, 2010). Recent projections indicate that deaths from antibiotic-resistant pathogens could reach 10 million annually in 2050, overtaking cancer death projections (Willyard, 2017). Since the discovery of penicillin by Alexander Fleming in 1928, antibiotic therapy has become ubiquitous in infection treatment (Lobanovska & Pilla, 2017). The potent bactericidal effects, coupled with low mammalian cell toxicity, make them ideal agents for treating infections in humans (Davies & Davies, 2010). Such is the dependence on antibiotics that most routine surgeries require the administration of antibiotics as a preventative measure (Enzler et al., 2011). Unfortunately, the overuse and abuse of antibiotics have led to the development of resistant strains, which ultimately could render most antibiotics useless (Llor & Bjerrum, 2014). The reduced susceptibility of bacteria to antibiotics has been gradually occurring over the last century, leading to the evolution of so-called "superbugs", which are resistant to most or all antibiotics used therapeutically (Aslam et al., 2018).

The World Health Organisation stated that in 2013, the post-antibiotic era had arrived (McKenna, 2013). To confound the situation, the development of new antibiotics is diminishing due

to high development costs, and a low return on the investment (Ardal et al., 2020). The spread or emergence of resistant strains is far outpacing the development of new antibiotics (Aslam et al., 2018). The treatment of resistant strains requires the antibiotic dosage to be increased and treatment time lengthened (Raymond, 2019). Antibiotics target essential bacterial processes such as cell wall synthesis, protein synthesis, DNA, and RNA (Kohanski et al., 2010). However, the ability of bacteria to transfer resistant genes horizontally means resistance can spread quickly, creating multi-drug resistant organisms (MDRO) (Sun et al., 2019).

Antibiotics are molecules which are cytotoxic or cytostatic (bactericidal or bacteriostatic) to microorganisms, removing them from the body, or inhibiting them sufficiently that the host immune system can fight the infection without being outcompeted by fast-growing microorganisms (Leekha et al., 2011). There are many antibiotic classifications, which is often characterised by groups of antibiotics that have a common mode of action or molecular structure (**table 1.4**). Common modes of action include; inhibiting the cell wall synthesis, synthesis of DNA, RNA, and proteins. They can also be internalised by simply diffusing through the cell wall and membrane, or by energy-dependent transport mechanisms (Kohanski et al., 2010). Since the discovery of the first antibiotic in 1928 (Fleming, 1929), a continuous 'golden age' of discovery between the 1950s and 1970s began, and there was an optimistic belief that antibiotics would bring an end to infectious disease by targeting the pathogen whilst having a minimal effect against the host (Gould, 2016). However, antibiotic resistance (the ability of bacteria to grow in the presence of antibiotics) emerged almost immediately after penicillin was first used, and resistance species were discovered before penicillin first began to be administered to patients (Davies & Davies, 2010). This emergence of resistance has been dramatically amplified by the mis- and over-prescription of antibiotics, and their use in animal husbandry (Llor & Bjerrum, 2014). Decades ago, the development of resistance was negated by discovering new antibiotics. However, the antibiotic discovery void beginning in the 1980s has tipped the balance of discovery/resistance towards bacteria with an ever-increasing population of resistant species (Silver, 2011). Teixobactin is a proposed new antibiotic targeting a lipid precursor to peptidoglycan, discovered by the novel isolation of bacterial soil samples (Ling et al., 2015). Like many new drug discoveries, it may never be available to clinicians due to the extremely high costs and regulatory obstacles, 15 of the 18 largest pharmaceutical companies have ceased research into new antibiotics for these reasons (Ventola, 2015). With limited new antibiotic discovery's coming to market for over 30 years, efforts have focused on antimicrobial stewardship and limiting the inappropriate use, particularly in a clinical setting (Doron & Davidson, 2011). However, despite the implementation of stewardship programs, a study between 2012-2017 investigating the effect these

programs had on reducing resistant species showed no significant reduction in hospital settings (Bertollo et al., 2018).

The use of antibiotics has resulted in selective pressure towards species which have developed resistance and increased the prevalence of resistance species in nature, primarily due to antibiotic pollution generated entering the environment through wastewater (Tello et al., 2012). Modes of resistance which bacteria may employ include; expression efflux pumps which create an extracellular gradient reducing the concentration of the antibiotic in the cell, enzymatic inactivation of the antibiotic, increased membrane impermeability, or by modification of the target to remove or reduce the antibiotic affinity towards it (**Figure 1.4**) (Munita & Arias, 2016). *S. aureus* has been studied extensively regarding antibiotic resistance, within six years of aminoglycoside introduction, resistance had already emerged via enzyme modification, with over 50 separate enzymes discovered (Davies & Wright, 1997).

This process can become overlapping, penicillinase-producing *S. aureus* was targeted with a semi-synthetic analogous penicillin drug, methicillin. However, this soon became inhibited, leading to MRSA strains (Harkins et al., 2017). A similar outcome occurred with vancomycin resistance *S. aureus* (VRSA) in 2002 (Gardete et al., 2014), multi-drug resistance is becoming an increasing obstacle to effectivity treat a pathogen (Assis et al., 2017). The spread of resistance is increased due to bacteria's ability to transfer genetic material either by extracellular DNA transformation or by direct bacterial conjunction (Munita & Arias, 2016). This allows species that may have a natural resistance due to a mutated DNA section to spread this gene throughout the bacterial population, increasing the breadth of resistance gene expression (Perron et al., 2012).

Table 1.4 A Brief overview of several antibiotic classes and mode of actions.

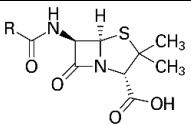
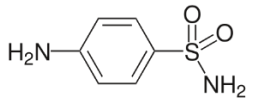
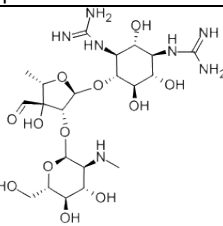
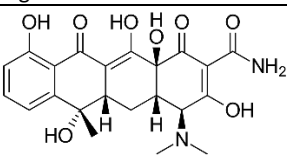
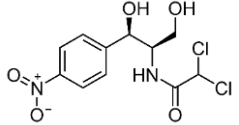
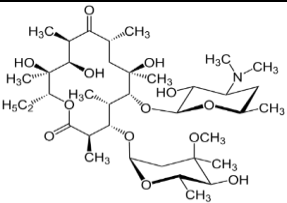
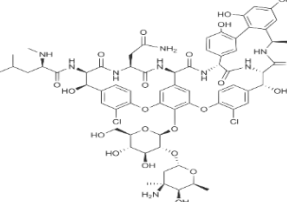
Class	Examples	Molecular Structure	Mode of action	Ref
Beta-lactams	Penicillin, amoxicillin, flucloxacillin	 <p>Beta-lactam ring present in all species</p>	Inhibition of cell wall biosynthesis	(Kong et al., 2010)
Sulfonamides	Sulfanilamide, sulfisoxazole, sulfadiazine, prontosil	 <p>Sulfonamide group present in all species</p>	Folate synthesis inhibitor. Competitive inhibition of dihydropteroate synthase, a vital enzyme in folate production	(Villa-Costa et al., 2017)
Aminoglycosides	Streptomycin, paromycin, kanamycin, neomycin	 <p>All species contain amino-sugar substructures</p>	Inhibition of protein synthesis. Binds to the 30s ribosomal sub-unit causing mis-reading of DNA and subsequent mis-folded structural abnormal proteins	(Kotra et al., 2000)
Tetracyclines	Tetracycline, doxycycline, oxytetracycline, limecycline, tigecycline	 <p>All species contain four adjacent cyclic hydrocarbon rings</p>	Inhibition of protein synthesis. Binds to the 30s ribosomal sub-unit at aminoacyl site prevent tRNA from binding.	(Grossman, 2016)
Chloramphenicol	Chloramphenicol	 <p>No subgrouping, one individual compound</p>	Inhibits protein synthesis. Inhibits peptidyl transferase activity of the 50s ribosome sub-unit and prevents protein chain elongation.	(Wiest et al., 2012)
Macrolides	Erythromycin, azithromycin, clarithromycin	 <p>All species contain 14-, 15-, or 16-membered macrolide ring</p>	Inhibits protein synthesis. Inhibits peptidyl transferase activity of the 50s ribosome sub-unit and prevents protein chain elongation.	(Jelić & Antolović, 2016)
Glycopeptides	Vancomycin, teicoplanin, talavancin, ramoplanin	 <p>Species contain carbohydrates linked to a peptide composed of amino acids</p>	Inhibits cell wall synthesis. Hydrogen bond interactions between the glycopeptide and terminal D-alanyl-D-alanine moieties prevents long polymers of N-acetylmuramic acid (NAM) and N-acetylglucosamine (NAG) forming backbone of Gram-positive species	(Binda et al., 2014)

Table 1.4 continued.

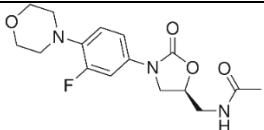
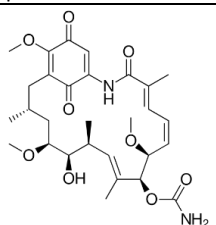
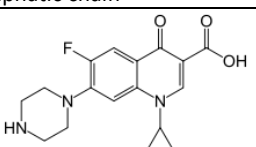
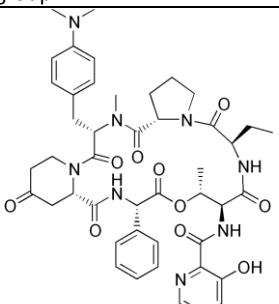
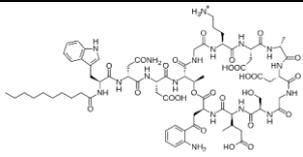
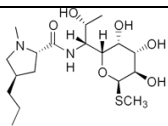
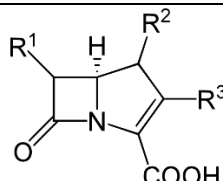
<p>Oxazolidinones</p>	<p>Linezolid, cycloserine, tedizolid, posizolid</p>	 <p>All species contain the structure 2-oxazolidinones somewhere within the compound</p>	<p>Inhibits protein synthesis. Inhibits peptidyl transferase activity of the 50s ribosome sub-unit. Prevents fMet-tRNA binding to the ribosomal P site.</p>	<p>(Douros et al., 2015)</p>
<p>Ansamycins</p>	<p>Geldanamycin, naphthomycin, rifamycin</p>	 <p>All species contain an aromatic ring bridged by an aliphatic chain</p>	<p>Inhibits the synthesis of RNA resulting in cell death. Ansamycins bind to the prokaryotic RNA polymerase</p>	<p>(Wilson et al., 2011)</p>
<p>Quinolones</p>	<p>Ciprofloxacin, levofloxacin, trovafloxacin</p>	 <p>All species contain a double aromatic ring with an attached carboxylic acid group</p>	<p>Inhibition of DNA replication and transcription. Interact with DNA gyrase or topoisomerase IV preventing DNA replication and transcription.</p>	<p>(Aldred et al., 2014)</p>
<p>Streptogramins (Group A and B – distinct compounds which interact to form one antibiotic)</p>	<p>Pristinamycin IA Pristinamycin IIA</p>	 <p>Antibiotic is comprised of two distinct units – unit A is shown above</p>	<p>When group A and B are used in conjunction they have a synergistic effect which results in 50s ribosomal sub-unit protein inhibition</p>	<p>(Johnston et al., 2002)</p>
<p>Lipopeptides</p>	<p>Daptomycin, surfactin</p>	 <p>Species contain a peptide bonded to lipid of varying length</p>	<p>Disrupts the cell membrane of bacteria by aggregating together creating a curvature within the membrane which allows ions to leak resulting in cell lysis. Resistance to this mode of action is rare and therefore Lipopeptides are often reserved for infection with highly resistant species.</p>	<p>(Beiras-Fernandez et al., 2010)</p>
<p>Lincosamides</p>	<p>Lincomycin, clindamycin, pirlimycin</p>	 <p>Species are derivatives of an amino acid and a sulphur containing octose</p>	<p>Inhibits protein synthesis. Inhibits peptidyl transferase activity of the 50s ribosome sub-unit and prevents protein chain elongation.</p>	<p>(Morar et al., 2009)</p>

Table 1.4 continued.

<p>Carbapenems (beta-lactam subclass)</p>	<p>Doripenem, Ertapenem, Imipenem, meropenim</p>	 <p>Structurally similar to beta-lactams (penicillins), however the sulfur atom in position 1 is replaced with a carbon atom</p>	<p>Inhibition of cell wall biosynthesis</p>	<p>(Papp-Wallace et al., 2011)</p>
--	--	---	---	------------------------------------

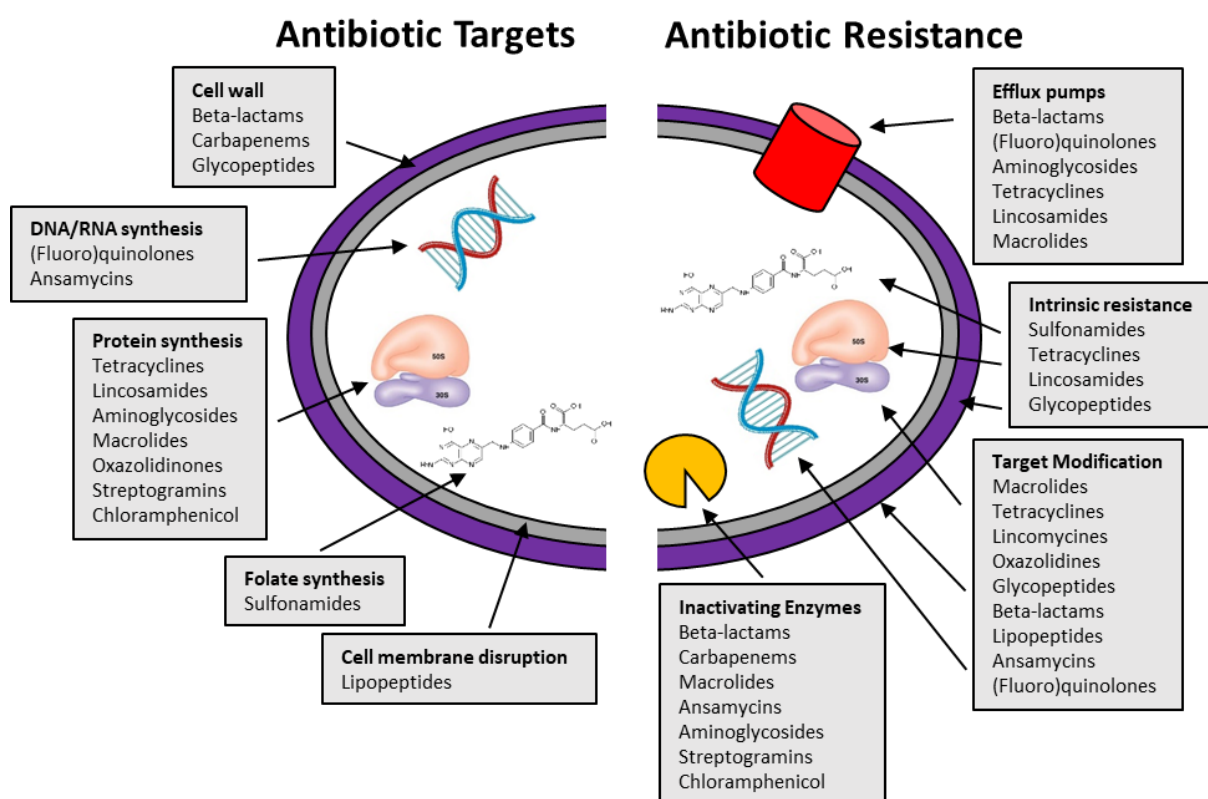


Figure 1.4 Overview of the primary antibiotic targets and the most common resistance mechanisms (Adapted from Zhivich et al., 2017).

1.4 Nanoparticles as antimicrobials

Traditional therapeutic agents are often limited for a variety of reasons. These include; low water solubility, lack of target selectivity, systemic toxicity, drug resistance, physiological degradation, low circulation half-life, aggregation, and low therapeutic index (requiring high drug dose) (Wen et al.,

2015). Nanoparticles (NPs) can be used to negate some of these problems, by targeted delivery and increases localisation, reduction in required dose, improved pharmacokinetics and sustained drug release (either by diffusion- or erosion-controlled release) (Singh & Lillard, 2009). Nanotechnology has been continuously investigated as an alternative to traditional antibiotic therapy, both alone as individual material NPs or nanocarriers (NCs) for antimicrobial agents (Singh et al., 2014; Natan & Banin, 2017; Baptista et al., 2018; Hayat, 2018). They also have a wide range of applications in diseases (Mitchell et al., 2020), see **Table 1.5** for details. Nanomaterials (NMs) are defined as materials with at least one dimension between 1 – 1000 nanometres (nm), but preferably between 1 -100 nm (Jeevanandam et al., 2018). The nanoscale of the material can be limited to one dimension, e.g. nanofilms, two dimensions, e.g. nanotubes or nanowires, or three dimensions termed NPs (Müller et al., 2017). The structure of these materials gives a range of different tunable physical and chemical properties which can have beneficial effects, e.g. vastly increases surface areas, surface charge, increased tensile strength, and unique crystalline or amorphous structures (Gatoo et al., 2014). NPs can be used to interact with a target to cause an effect directly, e.g., silver NP cellular toxicity (Wei et al., 2015), or as a carrier for other chemicals which can chemically interact with the NP (Al-Awady et al., 2017; Al-Awady et al., 2018; Weldrick et al., 2019a; Weldrick et al., 2019b). NM occur in nature, such as viral capsids (Koudelka et al., 2015), and colloid suspensions in blood and milk (Niemi et al., 2010). **Figure 1.5** illustrates different types of NPs.

NPs can be bioactive and have been used to target biofilms either by intrinsic antimicrobial activity or by acting as a vehicle or carrier for antimicrobial agents (Wang et al., 2017). Liposomes represent one of the most physiologically compatible drug delivery nanocarriers and are well tolerated by bacterial species (Gao et al., 2014). They can protect the antimicrobial they are carrying from the biofilm's deleterious environment (such as enzyme inactivation or chemical interaction with EPS) and able to directly deliver the drug to the bacterial cell by fusing to the lipid bilayer of the bacterial cell (Rukavina & Vanić, 2016). An example of liposome encapsulation of ciprofloxacin and amikacin have shown to be effective against *P. aeruginosa* in chronic cystic fibrosis infection (Paranjpe & Müller-Goymann, 2014). There are conflicting reports of the effectiveness of liposome-encapsulated antimicrobials. However, it seems it is dependent on the composition of the biofilm, with microorganism-derived substances such as alginate and mucus inhibiting the liposome-bacteria interactions (Barua & Mitragotri, 2014). Poly(lactic-co-glycolic acid) NPs have shown that when functionalised with EPS degrading enzymes such as DNase they can be effective at degrading the biofilm allowing the bacterial cells within to be more vulnerable to treatment (Baelo et al., 2015).

The pH-triggered release of antimicrobials have been investigated, farnesol (shown to be bactericidal and inhibitory against biofilm formation in *S. aureus* (Unnanuntana et al., 2009)), can be

loaded in a hydrophobic nanoparticle core (2-(dimethylamino)ethyl methacrylate) and remains stable at neutral and basic conditions, but is released at acidic pH as the nanoparticle becomes unstable. This has shown to be effective at degrading biofilms which can have varying acidic microenvironments (Horey et al., 2015). Infections from biofilm-forming pathogens make up to 80% of clinical infections, leading to recalcitrant infections and ultimately increased morbidity and mortality (Potera, 1999).

Recent epidemiological data shows that in the USA approximately 6.5 million people suffer from chronic wounds, with a healthcare financial burden of \$25 billion (Brem et al., 2007; Tomic-Canic et al., 2008), and in the UK the approximately 200,000 people suffer from chronic wounds with an estimated cost of £2 to £3 billion for the NHS (3% of the UK healthcare budget) (Upton et al., 2012; Posnett et al., 2008).

NPs can often be functionalised or modified on the surface to confer a useful property such as targeted delivery or protection from external physiological conditions such as acidic pH (Mout et al., 2012), the ability to encapsulate an active agent prevent inactivation or unwanted targeting (Da Silva et al., 2017a). Stimuli responsiveness of the NPs can also allow a drug to be released when certain conditions are present. This includes thermos-sensitivity, pH-sensitivity, or photo-sensitivity (Tayo, 2017). The use of nanotechnology to increase the efficacy of antibiotics to extend their useful lifespan is an achievable goal (Tyers & Wright, 2019).

Various mechanisms for causing bacterial cell death have been investigated, including; direct interaction with the cell wall, the production of reactive oxygen species and the hindrance of intracellular processes such as DNA and protein synthesis (Wang et al., 2020a; Galbadage et al., 2019; Wang et al., 2016; Al-Awady et al., 2015). NCs that have been used to encapsulate antibiotics have shown an improvement in cell interaction and localised topical concentration (Qayyum & Khan, 2016; Galbadage et al., 2019; Wang et al., 2016; Weldrick et al., 2019a). This ultimately allows the antibiotic to be effective when faced with degradation or efflux pump expulsion. The ability of NCs to concentrate a large amount of antimicrobial agent within or upon the surface, with a targeted and with a controlled and sustained rate of release is a crucial facet of their ability to treat antimicrobial-resistant pathogens (Pissuwan et al., 2011; Gholipourmalebadi et al., 2017). Additionally, nanomaterials can convey protection to the agent encapsulated, allowing application in hostile environments (Hamad et al., 2012a; Hamad et al., 2012b).

Functionalisation of the NPs or NCs with a cationic agent can also allow specific electrostatic interaction with anionic bacterial cell wall due to the presence of peptidoglycan and teichoic acids (Caudill et al., 2020). Silver NPs with antimicrobial function are currently in use in a wide range of broad-scale products (Han et al., 2020; Wilkinson et al., 2018). NPs can also have an advantage over

conventional treatments in that they do not target a pathway which bacteria can circumvent or evolve an alternative mechanism (Graves et al., 2017; Galbadage et al., 2019; Wang et al., 2016). NPs have also been deployed for use in treating biofilms, as both a preventative measure for initial biofilm formation and for treating established biofilms (Iannitelli et al., 2011; Flemming et al., 2000a; Beyth et al., 2008; Roe et al., 2008; Lellouche et al., 2012). NCs have also been demonstrated to protect the antibiotic encapsulated from binding to EPS materials, increasing its effectiveness (Weldrick et al., 2019b). The next section evaluates the latest approaches and developments in classes of NPs and NCs with applications against antibiotic planktonic bacteria and biofilm-forming bacteria.

Table 1.5. List of FDA approved nanomedicines and date of first approval. Data obtained from Mitchell et al., 2020; Anselmo et al., 2019; Fenton et al., 2018; Bobo et al., 2016; Caster et al., 2017.

Drug	Company	Application	Year of first approval
<i>Lipid-based</i>			
Doxil	Janssen	Kaposi's sarcoma, ovarian cancer, multiple myeloma	1995
DaunoXome	Galen	Kaposi's sarcoma	1996
AmBisome	Gilead Sciences	Fungal/protozoal infections	1997
Visudyne	Bausch and Lomb	macular degeneration, myopia, ocular histoplasmosis	2000
Marqibo	Acrotech Biopharma	Acute lymphoblastic leukaemia	2012
Onivyde	Ipsen	Metastatic pancreatic cancer	2015
Vyxeos	Jazz Pharmaceuticals	Acute myeloid leukaemia	2017
Onpattro	Alnylam Pharmaceuticals	Transthyretin-mediated amyloidosis	2018
<i>Polymer-based</i>			
Oncaspar	Servier Pharmaceuticals	Acute lymphoblastic leukaemia	1994
Copaxone	Teva	Multiple sclerosis	1996
PegIntron	Merck	Hepatitis C infection	2001
Eligard	Tolmar	Prostate cancer	2002
Neulasta	Amgen	Neutropenia, chemotherapy induced	2002
Abraxane	Celgene	Lung cancer, metastatic breast cancer, metastatic pancreatic cancer	2005
Cimiza	UCB	Crohn's disease, rheumatoid arthritis, psoriatic arthritis, ankylosing spondylitis	2008
Plegridy	Biogen	Multiple sclerosis	2014
ADYNOVATE	Takeda	Haemophilia	2015
<i>Inorganic</i>			
INFeD	Allergan	Iron-deficient anaemia	1992
DexFerrum	American Regent	Iron-deficient anaemia	1996
Ferrlecit	Sanofi	Iron deficiency in chronic kidney disease	1999
Venofer	American Regent	Iron deficiency in chronic kidney disease	2000
Feraheme	AMAG	Iron deficiency in chronic kidney disease	2009
Injectafer	American Regent	Iron-deficient anaemia	2013

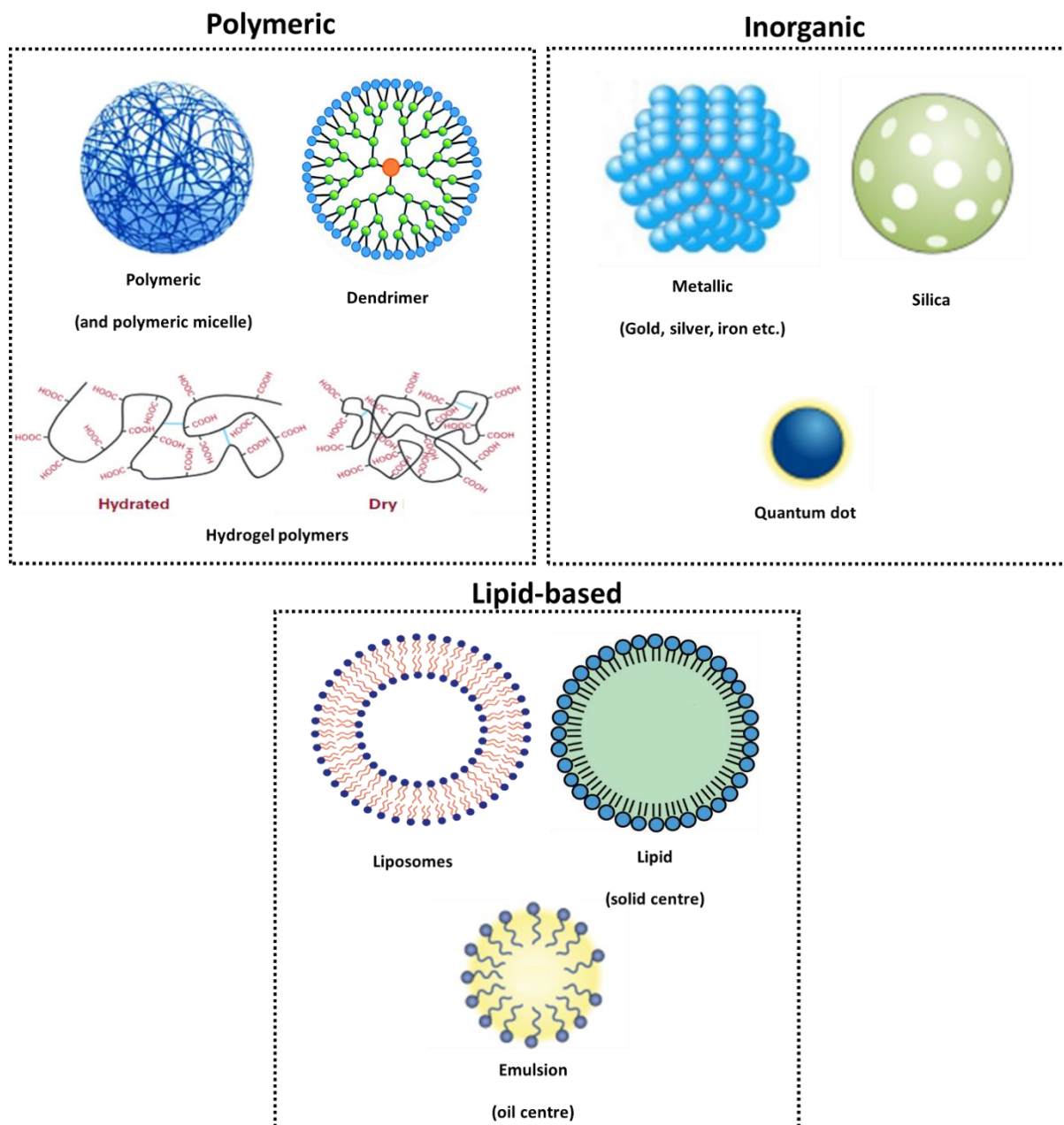


Figure 1.5. Illustration of the different types of nanomaterials used in therapeutics. Image adapted from Mitchell et al., 2020.

1.4.1 Lipid-based

Liposomes are synthetic spherical vesicles with a lipid bilayer (potentially multiple layers) usually composed of phospholipids polymers (Akbarzadeh et al., 2013). They are amphiphilic in nature and have been successfully used in pharmaceutical formulations (Beltrán-Gracia et al., 2019). These structures are non-toxic and biocompatible making them useful in gene therapy molecule delivery to cells due to their ability to fuse with a cells membrane and release the liposome contents into a cell (Balazs & Godbey, 2011; Sachetelli et al., 2000). This can be either a passive non-targeted method for

the use of delivering nutritional or dietary molecules (Shade, 2016), or targeted by functionalising the surface with a specific molecule or ligand (Riaz et al., 2018). This can assist the drug delivery of hydrophobic molecules and prevent early inactivation by encapsulation within the lipid bilayer (Sercombe et al., 2015). They are relatively simple to formulate, which is desirable in biomedical applications (Mitchell et al., 2020). Liposomes are the most common utilised nanomaterial used for antimicrobial drug delivery (Forier et al., 2014; Tamilvanan et al., 2008; Alhariri et al., 2013). They have also been demonstrated to be effective in several different routes, including dermal, pulmonary, ocular and vaginal (Vanić et al., 2015; Aljuffali et al., 2015; Cipolla et al., 2014; Hadinoto et al., 2014; Mishra et al., 2011; Vanić et al., 2014). Benzylpenicillin (penicillin G) has been successfully encapsulated into liposomes of approximately 140 nm. The liposomal penicillin G formulation was shown to reduce the biofilm-forming ability and growth rate of *S. aureus* (Kim et al., 2014). The aminoglycoside antibiotic amikacin (marketed as Arikace™ and passed a phase III clinical trial) has been incorporated into a liposome and shown to improve the antibiotic's effectiveness against cystic fibrosis patients with *P. aeruginosa* infections (Waters et al., 2014). Lipoquin™ is another liposomal formulation (90 nm), in this case, encapsulating ciprofloxacin. This was also proven to reduce the burden of *P. aeruginosa* infections in patients with cystic fibrosis (Cipolla et al., 2016). Arikace™ and Lipoquin™ are both designed as liposomal formulations which are dispersed into droplets for inhalation, see **Figure 1.6A** for an illustration. Liposomal amphotericin B (AmBisome®) is used to encapsulate the poorly soluble drug. It has been shown to reduce the toxicity of amphotericin B whilst maintaining its antifungal effect. However, no demonstration of this on biofilm fungal infection has been demonstrated (Stone et al., 2016). See **Figure 1.6B** for an illustration of the application of liposomal amphotericin B.

Solid lipid nanoparticles (SLNPs) consist of a solid lipid core and are usually 50 to 1000 nm in diameter and dispersed in water or an aqueous surfactant solution. This is facilitated by the surface monolayer of phospholipids (Ghasemiyeh et al., 2018). The lipid core can be made of various materials such as fatty acids, triglycerides and steroids (Patil et al., 2019). They are useful for encapsulating insoluble drugs such as antifungal azoles (Yang et al., 2008). Another example is the insoluble antifungal drug bifonazole used to treat skin infections such as cutaneous candidiasis (Garse et al., 2015). An SLNP encapsulation of bifonazole showed penetration and increased antifungal activity in *ex vivo* and *in vitro* experiments (Pouton et al., 2000).

Antimicrobial agents can also be administered as emulsions, most commonly in cosmetics, but also in biomedical applications (Gupta et al., 2016). These are typically low viscosity lotions and high viscosity creams and have a particle size of 0.1 to 100 µm (Agarwal and Rajesh, 2007). Nanoemulsions (particle size < 100 nm) are a useful application for the of poorly insoluble drugs in topical applications

(Jaiswal et al., 2015). Amphotericin B, fluconazole and terbinafine are examples of poorly soluble antifungal drugs which are dispersed in nanoemulsions for topical and transdermal application (Nastiti et al., 2017).

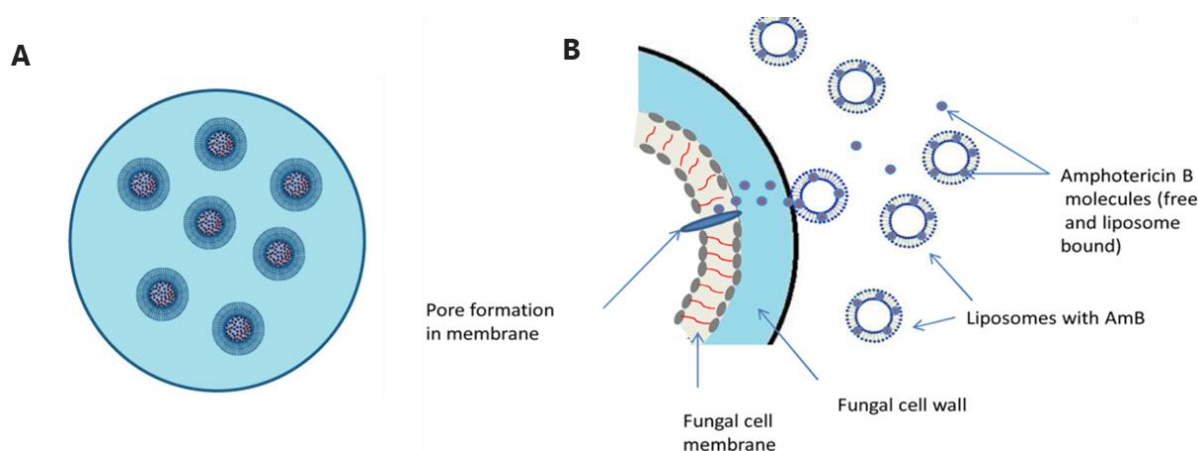


Figure 1.6. (A) Liposomal encapsulated ciprofloxacin (90 nm) dispersed into a 5 to 10-micron droplet ready for inhibition (Image adapted from Cipolla et al., 2014). (B) Schematic representation of the theorised mode of action of liposomal Amphotericin B on a fungal cell membrane (Image adapted from Stone et al., 2016).

1.4.2 Inorganic

The use of inorganic materials is a vast area of research, with NPs having unique electrical, magnetic and optical properties, as well as large variations in size and geometry and theranostic applications (Mitchell et al., 2020). Unique to this NPs class, geometries such as nanorods, nanoshells, nanocages and nanospheres have been fabricated (Yang et al., 2019). Photothermal properties are also possible in metallic NPs such as gold, with free surface electrons oscillating at different frequencies depending on their size and shape (Wang et al., 2020a). Iron oxide one of the most researched inorganic materials for NP synthesis and biomedical application (see **Table 1.5**). Calcium phosphate is another inorganic NP which has been researched and has found useful applications in drug and gene delivery (Huang et al., 2020).

The majority of inorganic NPs have good stability and provide applications in photothermal and diagnostic which other types of NPs cannot, however, clinical application is hampered by low solubility and toxicity concerns of heavy metals (Arias et al., 2020; Manshian et al., 2017). A wide variety of inorganic metal NPs have been studied to understand their potential antimicrobial applications. These include zinc oxide NPs, titanium oxide NPs, magnesium hydroxide NPs, copper NPs, silver NPs, and gold NPs. These NPs have demonstrated potential as antimicrobial agents and have various mechanisms (Halbus et al., 2017). Antimicrobial mechanisms include the release of reactive oxygen species in the presence of UV light (titania oxide NPs) which damages the cells causing death

(Al-Awady et al., 2015). Magnesium oxide and zinc oxide NPs have been shown to disrupt the bacterial cell wall's integrity, increasing permeability, and reactive oxygen species (ROS) generation increasing cell cytotoxicity (He et al., 2016; Halbus et al., 2019a; Halbus et al., 2020).

Copper NPs have been shown to have a potent antimicrobial action due to their proposed interaction and inactivation of vital bacterial enzymes (Beyth et al., 2015). Copper NPs are easily oxidised and therefore are less effective in aerobic conditions but very useful in anaerobic conditions (El Zowalaty et al., 2013). The accumulation of CuO NPs upon the bacterial cell wall can also cause cell death (Halbus et al., 2019b). To enhance this property, CuO NPs have been functionalised with (3-glycidyloxypropyl)-trimethoxysilane (GLYMO) to allow further covalent coupling of 4-hydroxyphenylboronic acid (4-HPBA), which provides a very strong boost of their action as antibacterial, anti-algal and anti-yeast agents. The boronic acid (BA) terminal groups on the surface of the CuONPs/GLYMO/4-HPBA can form reversible covalent bonds with the diol groups of carbohydrates and glycoproteins expressed on the cell surface where they bind and accumulate, which is not based on electrostatic adhesion (Halbus et al., 2019b; Halbus et al., 2019c).

Inorganic NPs have also been researched as co-treatments with antibiotics with the goal of creating a synergistic outcome (Wang et al., 2020a). ZnO NPs and antibiotic co-treatments (ciprofloxacin, erythromycin, methicillin and vancomycin) have been shown to reduce the minimum inhibitory concentration (MIC) required against antibiotic-resistant pathogens, including Vancomycin-resistant Enterococcus (VRE) (Iram et al., 2016). It has been proposed that metallic NPs may increase the membrane permeability (but not disrupt the integrity) in bacteria and enhance passive antibiotic penetration, providing an explanation for the synergistic results with antibiotic-inorganic co-treatments. This was accomplished by measuring the leakage of liposomal encapsulated fluorescence dye calcein when bacterial cells were exposed to metallic NPs (Bellio et al., 2018). Superparamagnetic iron oxide NPs (SPIONs) have been used in conjunction with methicillin to excellent effect against *Staphylococcus epidermidis* biofilms. With the application of an external magnetic field, the NPs were shown to be able to penetrate 20 µm thick biofilms and allow methicillin to be more effective (Geilich et al., 2017). It has been revealed that magnetically modulated iron oxide NPs can be driven into biofilms creating artificial channels, which in turn allows improved antibiotic penetration and bacterial death, as demonstrated in *S. aureus* when treated with gentamicin after magnetic iron oxide NP treatment (Quan et al., 2019).

Silver NPs are one of the most studied metals for antimicrobial potential (Marin et al., 2015). Silver NPs have been shown to disrupt the bacterial cell wall causing pits which causes the cell to fragment and die (Slavin et al., 2017). Silver ions released from the NPs can have several adverse

biological effects on cells, these include binding to DNA and RNA neutralising their function, the chemical interaction with sulphur containing peptides, inactivating them, inactivating enzymes and generating ROS to increase oxidative stress (McShan et al., 2014; Wu et al., 2019; Cui et al., 2013; Choi et al., 2008). **Table 1.6** shows a list of discovered antimicrobial mechanisms of silver NPs.

Table 1.6. Antimicrobial mechanism of silver NPs.

Antimicrobial mechanism of silver NPS	Ref
Electrostatic interaction with lipopolysaccharides (LPS), allowing for permeability alteration, membrane disruption and protein gradient dissipation	(Dakal et al., 2016)
Electron transport chain inhibition by interaction with cytochromes	(Hemeg et al., 2017)
Key biomolecule activity change via interaction with sulfhydryl groups	(Hemeg et al., 2017)
Gram-positive cell wall synthesis disruption	(Pelgrift et al., 2013)
Blockage of DNA replication	(Rai et al., 2012)
Blocking of protein synthesis via interaction with 30S ribosomal subunit	(Dakal et al., 2016)
The generation of reactive oxygen species	(Durán et al., 2016)

Silver NPs have been used in many antiseptic products due to their highly effective antimicrobial action (Marassi et al., 2018). A common feature of silver (and other metal) NPs is the interaction with the anionic bacterial cell wall which increased the NP's concentration and, therefore the accumulation of localised ROS which damage the cell (Quinteros et al., 2016). The various mechanisms silver uses for killing bacteria make it difficult for bacterial to evolve resistance, increasing its popularity in developing biomedical applications (Panáček et al., 2019). It has also been researched in conjunction with antibiotic treatments to determine if a synergistic effect is present (Naqvi et al., 2013; Wypij et al., 2018). Examples include; daptomycin conjugated silver NPs, which when administered to *S. aureus* showed an increased efficacy compared to equivalent concentrations of the free silver NPs and daptomycin. This was attributed to the creation of large pores by the silver NP on the bacterial membrane, increasing antibiotic uptake into the cell (Zheng et al., 2016). The use of silver NP has also been shown to increase the cell membranes' permeability and allowed an increased uptake of chloramphenicol, kanamycin, biapenem, and aztreonam, as demonstrated on species including *S. aureus* and *E. coil* (Vazquez-Muñoz et al., 2019).

Gold NPs have also been extensively studied, primarily because of their bio-inertness and ability to be formulated with antibiotics (Feng et al., 2015; Zhao et al., 2013b). Although gold NPs have not demonstrated antimicrobial activity, they have been shown to increase antibiotics' effectiveness

when applied as a co-treatment and if functionalised with an antibiotic (Fan et al., 2019). Gold NPs have been synthesised with a vancomycin coating which showed enhanced antibacterial against vancomycin-resistant enterococci. This effect was reported to be caused by the polyvalent interaction between the bacteria, and the vancomycin coated gold NP (Gu et al., 2003). Similarly, gentamicin has been coated to gold NPs and increased to efficacy against *S. aureus* and MRSA. It was demonstrated that the gentamicin was released slowly and continuously over 2 days, enabling the antibiotic to be effective over a more extended period (Perni et al., 2014). Amoxicillin surface coated gold NPs demonstrated an increased effect against MRSA in vitro and in vivo compared to an equivalent free amoxicillin concentration (Kalita et al., 2016). A beneficial attribute of gold NP is in photothermal therapy, due to the excellent photothermal conversion capability of gold (Ma et al., 2018).

An example of this is with vancomycin coated gold NPs. After 5 mins of exposure to near-infrared radiation to the sample's temperature was raised by 15°C, causing a significant reduction in the vancomycin-resistant Enterococci viability (Wang et al., 2018; Wang et al., 2019a). The use of photothermal NPs has been further investigated with the synthesis of gold/silica shape-selective anisotropic colloid particles fabricated as negative replicas of the target cells. After the synthesis, these shape-selective colloid antibiotics can bind specifically to a bacterium or yeast cell. Upon the application of laser irradiation, this caused fatal disruption to the cell wall (Borovička et al., 2013a; Borovička et al., 2013b). Antimicrobial phototherapy NPs continue to be researched due to their excellent potential for treating antimicrobial-resistant pathogens (Li et al., 2020).

Graphene oxide is an emerging material which is being investigated for its nanomaterial formulated antimicrobial application, it has unique advantages such as a large surface area, good biocompatibility, disperses in most solvents, and has an abundance of oxygen-containing functional groups making it reactive and therefore easy to interact with other antimicrobial compounds, or microorganism (Liu et al., 2012; Bussy et al., 2017). Graphene oxide NPs are effective alone against bacteria, mostly by physically damaging the cells wall and membrane (Zou et al., 2016; Lu et al., 2017). Like many other inorganic materials, graphene oxide has been investigated as a carrier for antibiotics and has demonstrated a synergistic effect. It has been suggested that graphene oxide sheets could increase the permeability of bacteria by damaging the cell membrane, and therefore increase the effectiveness of antibiotic treatments (Gao et al., 2017). Graphene oxide sheets have also been investigated with a vast amount of NP in an effort to find useful biomedical applications (Díez-Pascual et al., 2020).

Quantum dot NPs (typically < 2 nm) have been used for potential antimicrobial applications (Mitchell et al., 2020). They are often made of a semiconducting material, i.e. silicon, and have found

more use in *in vitro* imaging applications and *in vivo* diagnostics (Wagner et al., 2019; Zhang et al., 2019a). Cadmium telluride quantum dots (CdTe-QDs) have been shown to have an antibacterial effect on bacteria such as *E. coli*. The accumulation of these CdTe-QDs results in cell death; however, the mechanism for this is not proven. A possible cause is the release of heavy metal ions or oxides which occurs as the QD decompose (Lu et al., 2008). CdTe-QDs have also been functionalised with antimicrobial peptides further increasing the antimicrobial ability whilst simultaneously reducing their haemolytic activity. The haemolytic reduction was suggested to be caused by the inability of the QD bound antimicrobial peptide being unable to insert their hydrophobic moieties into the zwitterionic, mammalian membranes. This, in effect, means a higher concentration of antimicrobial peptide CdTe-QDs could be used safely (Williams et al., 2020). Carbon dots (CDots) have recently been synthesised and show promise in antimicrobial applications. When in contact with a bacterial surface they have been shown to generate ROS with the application of visible light (Dong et al., 2020a; Abu Rabe et al., 2019). Nitrogen-doped carbon dots (N@CDs) have been coated with ciprofloxacin via intramolecular hydrogen bonding have shown to be effective at destroying *E. coli* and *S. aureus* cells (Saravanan et al., 2020)

1.4.3 Polymeric

Polymeric (polymer-based) NPs allow precise control of particle characteristics, encapsulation (or payload) variability, allowing hydrophobic or hydrophilic compounds within, depending on the NP's materials, and are easily surface modified. A drawback is a tendency for aggregation at high concentrations (Mitchell et al., 2020). An example is micelles. Micelles are similar to liposomes but contain a solid core that can easily encapsulate hydrophobic molecules (unlike liposomes with a hydrophilic core) (Nishiyama et al., 2016). The hydrophilic surface can be modified to covalently bind targeting molecules such as antibodies or peptides and coated with a polymer coat such as PEG (polyethylene glycol) to increase with stability and longevity of the micelle (Torchilin et al., 2005). They have been investigated extensively as a delivery system of the hydrophobic drug docetaxel in chemotherapy studies (Zhang et al., 2016). Polymer micelles, sometimes referred to as core-shell NPs, are among the most widely studied NP types for biomedical applications (Aliabadi et al., 2005). A self-assembled micelle NP formulation, consisting of cationic and amphiphilic random polyacrylates bearing tertiary amine (N,N-diethylethylenediamine) and hydrophobic catecholic (hydroxytyrosol) side chains have been synthesised. This micelle formulation containing both these moieties was effective against *S. epidermidis* due to the cationic side chain interaction with the anionic bacterial cell wall (Taresco et al., 2015a; Taresco et al., 2015b). Biodegradable polymer micelles have been synthesised from amphiphilic triblock polycarbonates and proven to be effective against Gram-positive bacteria, including *Bacillus subtilis*, *Enterococcus faecalis*, *S. aureus*, MRSA, and *Cryptococcus*

neoformans, a fungal species. The micelles toxicity towards bacterial and fungal cells was shown to be provided by the cells' lysis via interactions between the cell wall and cell membrane (Nederberg et al., 2011).

Dendrimers are tree-like macromolecules composed of branched synthetic polymers containing repeated molecular units (Madaan et al., 2014). The abundance of functionalisable and easily modifiable peripheral groups makes them useful for a drug delivery role through useful chemical properties such as charge or cell receptor binding. The increased internal void space can be used for molecular cargo (Mendes et al., 2017). The hyperbranched nature of these polymer creates a complex 3D architecture in which size and geometry can be controlled. Different types of internal functional groups allow a variety of compounds to be encapsulated. However, they are mostly used to deliver small molecules and nucleic acids (Xu et al., 2013b; Palmerston-Mendes et al., 2017). One of the most commonly used polymers used for dendritic NPs are the charged poly(ethylenimine) (PEI) and poly(amidoamine) (PAMAM), and several there are dendritic-based NP currently in clinical trials as theranostic agents, transfection agents, topical gels and contrast agents (Palmerston-Mendes et al., 2017; Kannan et al., 2014; Menjoge et al., 2010). Dendritic NPs unique structure allows for a release of the encapsulated active agent in a more passive manner. The large surface to volume ratio allows compounds to be localised throughout the NP's tree-like structure (like a unit of the NP) and, therefore, localise these agents and allow a potential highly likelihood of target interaction such as a microorganism (Zhang et al., 2010). Like many other types, dendritic NPs interact with a target microorganism via electrostatic attraction (cationic polymers to anionic bacterial cell walls) (García-Gallego et al., 2017; Rasines et al., 2009).

A drawback of dendritic NPs is their abundance of cationic polyelectrolytes, which make up the vast majority of the NPs branches. They are often toxic to mammalian cells by disrupting the cytoplasmic membrane (Jevprasesphant et al., 2003). Quaternary ammonium salts (QAC) and silver have been functionalised onto the branches of these NPs in an attempt to increase the efficacy of these materials by creating high surface concentrations, these have demonstrated improved antimicrobial activity against *S. aureus*, *P. aeruginosa*, and *E. coli* [Chen et al., 2000; Balogh et al., 2001].

An interesting approach was synthesising a dendritic NPs using the antimicrobial peptide G3KL, which is composed only of lysine and leucine residues. This was effective against *P. aeruginosa* and *A. baumannii* with only a mild effect against mammalian cells (Stach et al., 2014; Pires et al., 2015). Antimicrobial dendrimeric peptides have also been investigated for their antibiofilm properties, have been shown to hinder growth and destroy mature grown biofilms (Hou et al., 2009). The reduction of biofilm formation by *P. aeruginosa* was possible by inhibiting the LecA and LecB (Fucose-binding lectin)

proteins, thereby preventing the cells' attachment onto tissue surfaces. Glycopeptide dendrimers were used as they have a high affinity to lectins (carbohydrate-binding proteins) (Johansson et al., 2008; Reymond et al., 2013). Examples of small molecule encapsulated dendritic NP included the loading of the antibiotic sulfamethoxazole. This insoluble compound showed a 4- to 8- fold increase in antimicrobial activity against *E. coli*, compared to the free antibiotic (Ma et al., 2007).

Dendritic NPs can be useful in concentrating other poorly soluble antibiotics such as nadifloxacin, prulifloxacin and erythromycin and increasing their effectiveness against *S. aureus*, *E. coli*, *P. aeruginosa*, and *P. hauseri* compared to an equivalent concentration of the free antibiotic (Cheng et al., 2007; Winnicka et al., 2013; Felczak et al., 2013). Like other NPs, targeted drug delivery has been employed to increase the active agent's localisation and reduce potential untargeted tissue damage, particularly in poorly perfused tissues such as wounds (Vassallo et al., 2020). Ciprofloxacin-loaded light controlled dendritic NPs have been synthesised, which allows the specific drug delivery to Gram-negative bacteria by utilising bacteria-specific ligands (lipopolysaccharide (LPS)-binding dendrimer G5(Ligand)). This permitted a bacterial cell wall localisation, and stimulus-controlled delivery of the ciprofloxacin to the target that was suggested could be applied in infected wounds using light-based therapy (Wong et al., 2016).

Another type of polymeric NPs are hydrogels, which on the nanosize are called nanogels. Nanogels are a network of polymer chains which can be highly cross-linked and highly absorbent (Ahmed, 2015). They can form stable colloid NPs and can be modulated in NP diameter by pH changes. This is due to the abundance of COOH groups that protonate in basic conditions causing repulsion between COO⁻ groups and the gel's subsequent swelling (Akhtar et al., 2016). They have been shown to be viable drug vehicle agents by interacting with cationic groups of antimicrobial agents, e.g. berberine hydrochloride, chlorhexidine digluconate, tetracycline hydrochloride, lincomycin hydrochloride and ciprofloxacin hydrochloride (Al-Awady et al., 2017; Al-Awady et al., 2018; Weldrick et al., 2019a; Weldrick et al., 2019b). The antibiotic lincomycin was encapsulated into Carbopol nanogels, surface functionalised with a protease. This resulted in an improved ability to degrade *S. aureus* biofilms and reduce the cellular viability within. These lincomycin-Carbopol nanogels were shown to be more effective anti-biofilm agents than common antiseptics such as PVP-I, cetrimide, benzalkonium chloride and chlorohexanol, at both an equivalent and recommended therapeutic concentration (Weldrick et al., 2021).

Nanogels are also responsive to other environmental conditions such as temperature (Ramos et al., 2012). The preparation of nanogels via cross-linking can be accomplished either by covalent or hydrogen bonding, electrostatic and hydrophobic interactions, and nano or microemulsion

polymerisation (Sasaki et al., 2010). Water-soluble drugs, for example, anti-cancer drug doxorubicin, and other bioactive molecules such as proteins and DNA have been successfully encapsulated into nanogels and employed for drug delivery (Sasaki et al., 2010; Oh et al., 2008). An interesting application of nanogels was to use them to coat gold nanorods. These nanogel-gold composites are sensitive to temperature changes, and the nanogel portion could be collapsed under the presence of near-IR laser irradiation, releasing the gold nanorods. *In vitro* experiments showed that an external near-IR laser source could modulate the gold nanorods' release, indicating that the nanogels could be utilised as an antimicrobial control mechanism (Satarkar et al., 2010). Nanogels have also been synthesised to allow hydrophobic drugs to be encapsulated inside, such as the antibacterial molecule triclosan, via binding to hydrophobic domains inside the nanogel. This cationic nanogel was shown to bind to bacterial cell walls electrostatically and allow for a localised and sustained triclosan release, increasing the efficacy significantly compared to the free triclosan (Zu et al., 2020).

In this project, two different polymeric NP systems (Carbopol Aqua SF1 nanogels, and shellac NPs) were synthesised, characterised, and employed as antimicrobial nanocarriers. The targets were antimicrobial-resistant and biofilm-forming pathogens. Background information on these NP materials is given below.

1.4.3.1 Carbopol Aqua SF1

Carbopol compounds are used in medicine, manufacturing and cosmetics due to their excellent biocompatibility and lack of side effects on human cells (Zhang et al., 2020). Carbopol Aqua SF1 used in this study is a lightly cross-linked and hydrophilic acrylic polymer dispersion, which can provide thickening, stabilising and suspending properties to a wide range of materials (Bonacucina et al., 2004; Proniuk et al., 2002; Chakraborti et al., 2014). As supplied by the manufacturer, Lubrizol, it is a milky white liquid with a mild acrylic odour, comprising 30% active polymer in water. It has a low viscosity and is highly miscible, providing applications for suspending and stabilising products into formulations with insoluble and difficult to stabilise ingredients, i.e. silicones (Varges et al., 2019). Carbopol products have cosmetic applications, for example, thickening shampoos and body washes to their desired viscosity and flow characteristics (Chang et al., 2012). It has also been used in surfactant formulations over a wide range of pH (3.5 to 10) to deliver insoluble drugs, i.e. estradiol (Barreiro-Iglesias et al., 2003). It is compatible with anionic, cationic, non-ionic and amphoteric surfactants (Lubrizol, 2006). Carbopol Aqua SF1 is supplied in a protonated form, and the polymer molecules are coiled providing the viscosity and suspension in the liquid. When pH neutralised, the molecules ionise and expand due to the anionic carboxylate's electrostatic repulsion, allowing thickening and suspension properties (Varges et al., 2019). This property, which is also found in

hydrophobic polymers, allows its use is much more therapeutic and cosmetic applications (compared to hydrophobic polymers), such as shampoos, body washes, toothpaste etc. (da Cruz et al., 2018). Another benefit is the lack of any known toxicity towards mammalian cells, tissue and organs, as well as microorganisms (Lubrizol, 2006). **Figure 1.7** shows the Carbopol Aqua SF1 hydrogel polymer used in this project and illustrates the mechanism for swelling.

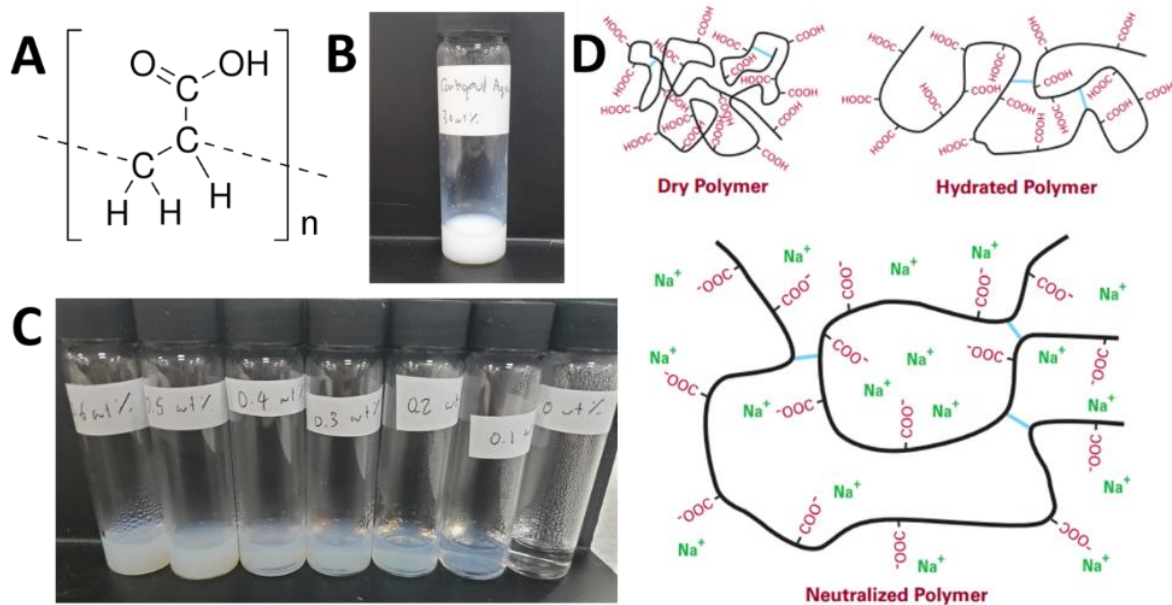


Figure 1.7. (A) Chemical structure of Carbopol Aqua SF1 (Polyacrylic acid). (B) A photograph of the stock 30 wt% Carbopol Aqua SF1 as supplied by the manufacture Lubrizol. (C) Photograph of 0.6 wt% to 0 wt% (deionised water) Carbopol Aqua SF1 dispersions at pH 6. (D) Polymer swelling mechanism illustration in basic pH (Lubrizol, 2006).

Carbopol dispersions have a wide array of therapeutic uses. Enhanced localised delivery of ocular drugs have used Carbopol (974P NF, 980 NF, 1342 NF) as a loading drug formulation. This facilitated an increased absorbance of the therapeutic agent at the treatment site due to the mucoadhesive property of Carbopol (Ludwig, 2005). Carbopol super porous hydrogel composites (SPHCs) have been synthesised using Carbopol 934P and 974P. Carbopol 934P and 974P can swell quickly in water via a cross-linking bond in their chemical structure. This allowed adhesion to intestinal mucus due to the carboxylic acid functional groups in the polymer forming hydrogen bonds to the intestinal mucus allowing interpenetration to the mucus layer. An *in vitro* study confirmed these Carbopol SPHCs had useful bio adhesion properties that increased insulin absorption into the intestines (Tang et al., 2007). Carbopol 980NF was formulated with silver NPs to evaluated wound healing properties. A rat model revealed via histological sections and transdermal examination that Carbopol 980NF-silver NPs provided superior wound healing efficacy compared to commercially available silver ion products (Kaler et al., 2014). A Carbopol (934P) and pluronic solution (F-127) shows

the capability of drug loading (pilocarpine hydrochloride). This Carbopol 394P-pluronic F-127 mixture demonstrated increased bioavailability of the ocular drug improving its performance (Lin et al., 2000). Carbopol 934P was also used with pluronic poloxamer 407/188 to increase mucoadhesive properties. An ocular drug, puerarin, was encapsulated inside the nanogel allowed a more concentrated concentration of the drug at the target site via *in situ* gelling of the Carbopol/poloxamer-puerarin formulation. This resulted in increased bioavailability of the drug at the target site (Qi et al., 2007).

1.4.3.2 Shellac

Shellac is a natural resin which has been investigated by pharmaceutical companies for therapeutic applications (Pearnchob et al., 2003). It is abundant in nature, has a low cost, and is and eco-friendly (Ogaji et al., 2012). Shellac is the refined product of the natural material Lac (resin), secreted by the parasitic insect *kerria lacca* on trees in South-Eastern Asia (Chen et al., 2011). **Figure 1.8A and B** shows shellac resin and the refined shellac material. Refined shellac is a complex mixture of polar and non-polar compounds. These consist of polyhydroxy polycarboxylic esters, lactones and anhydrides, with the main acidic compounds being terpenic and aleuritic acids (Chauhan et al., 2011). **Figure 1.8C and D** shows the shellac structure of shellac and the manufactured SSB® AquaGold aqueous solution of ammonium shellac salt (25 wt%) product used in this project. Shellac is insoluble in acidic to neutral pH, consistent with other carboxylic polymers (Bellan er al., 2012). It is also insoluble in hydrocarbon solvents, glycerol and esters, whilst dissolving in basic aqueous solutions, alcohols, and ketones. This is due to the carboxyl, hydroxyl and carbonyl groups in its chemical structure.

Shellac has an empirical chemical formula of $C_{60}H_{90}O_{15}$ (Rowe et al., 2003). The shellac chemical composition is dependent on its components and constituent acids. These are aliphatic hydroxyl acids (insoluble in water) and terpenic acids (soluble in water), of which shellac is approximately a 1:1 ratio (Sharma et al., 1983). Aleuritic acid ($\approx 35\%$) is the most abundant aliphatic acid, jalaric acid ($\approx 25\%$) is the most abundant terpenic acid. Butolic acid ($\approx 8\%$), laccijalaric acid ($\approx 8\%$) and shellolic acid ($\approx 8\%$) comprise other significant isolated acids (Cockeram et al., 1961). See **Figure 1.9** for chemical structures. Nevertheless, shellac composition is dependent on the original source and purification/manufacturing process (Buch et al., 2009).

Shellac resins are non-toxic, hypoallergenic, hard, and also have good adhesion and electrical properties (Limmatvapirat et al., 2004). Shellac can be degraded over time due to the presence of hydroxyl and carboxyl groups, which allows self-esterification. Esterification causes reduced solubility and a decline in acidity (Farag et al., 2009). Antioxidants, storage at $<5^{\circ}C$ and protection from light increased the shelf-life and shellac stability (Nath et al., 2009). Additionally, shellac stability can be

increased by salt formation with ammonia (Specht et al., 1998). This creates steric hindrance and therefore decreases self-esterification.

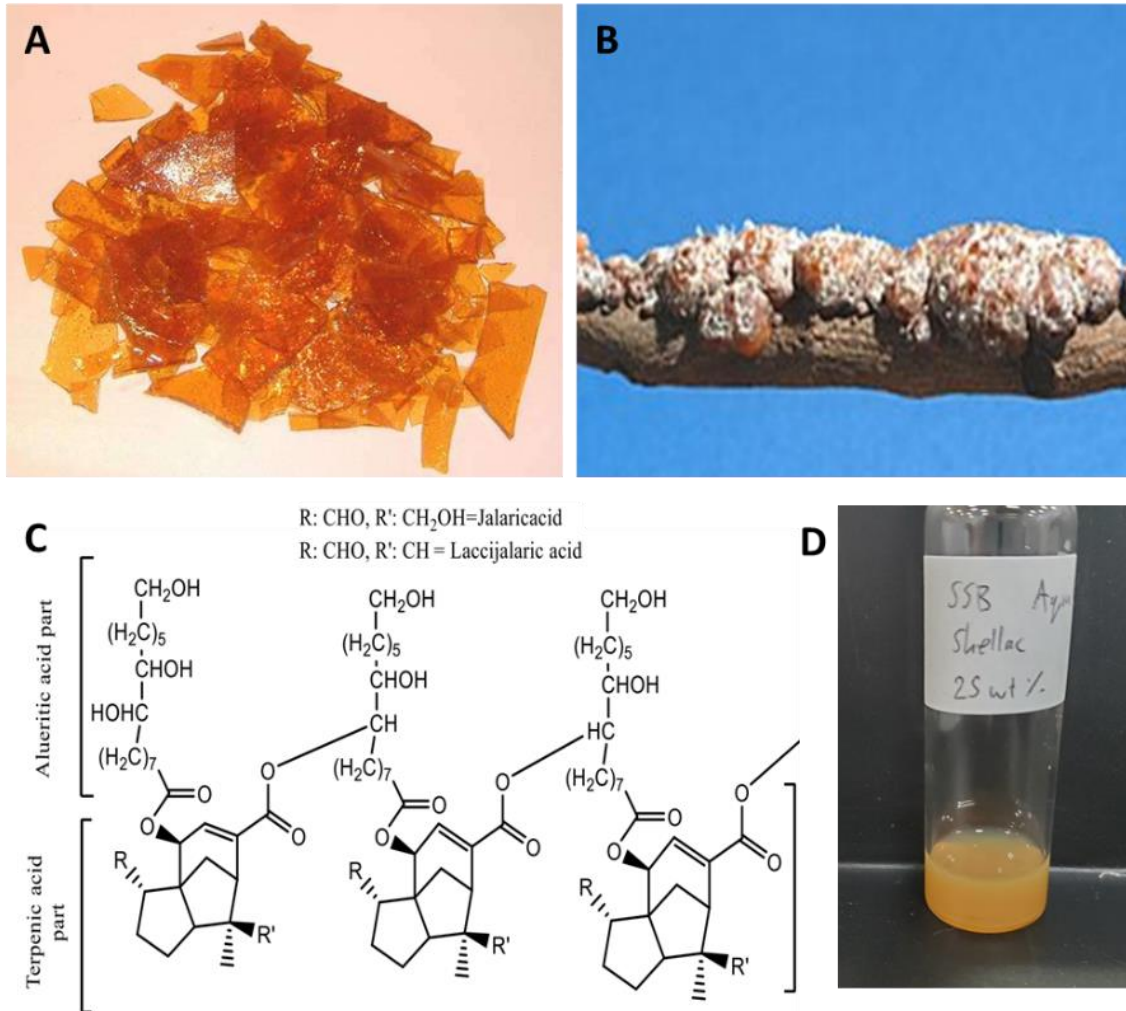


Figure 1.8. (A) An example of purified shellac and (B) shellac resin deposited on a tree branch by *Kerria lacca*. (Common lac insect, 2018; Shellac | resin, 1998). (C) Chemical structure of shellac (Kraisit et al., 2002) and (D) A photograph of the stock 25 wt% AquaGold aqueous solution of ammonium shellac salt as supplied by the manufacture SSB®.

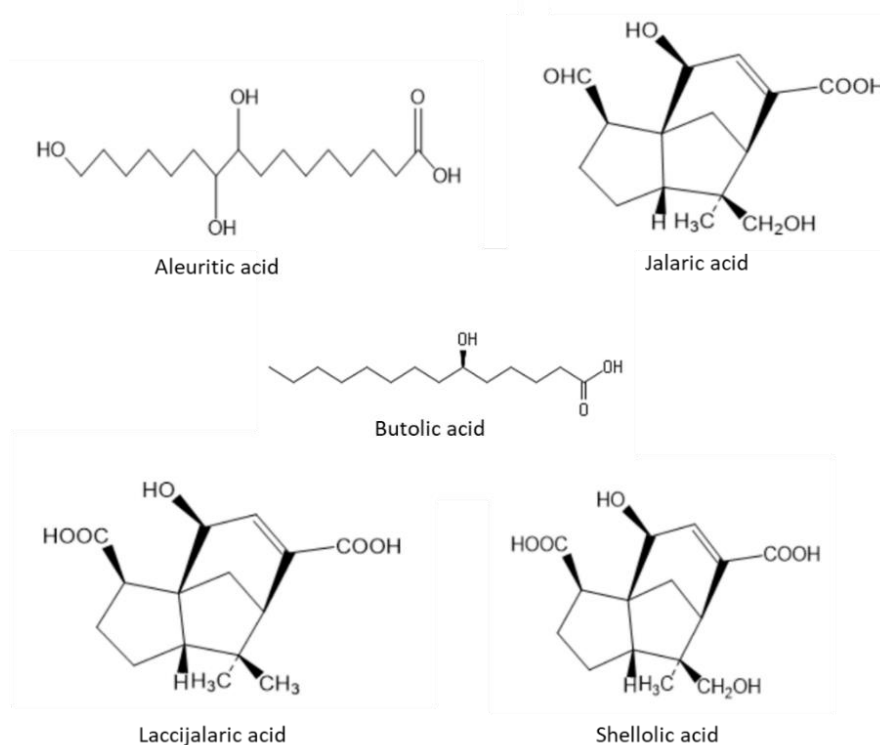


Figure 1.9. The chemical structures of the main components of shellac (Wang et al., 1999). Aleuritic acid, Jalaric acid, Butolic acid, Laccijalaric acid and Shellolic acid.

Shellac has a variety of non-pharmaceutical uses. For example, furniture and instrument lacquers (Ansari et al., 2006; Nevin et al., 2009), and coating materials for shell-like confectionary (E number 904) (lee et al., 2002). It has also been used as a water-repellent coating to prevent fruit and vegetables from premature spoilage (Hagenmaier et al., 1991). It also has uses in dentistry, i.e. the material used to manufacture dental base plates (Azouka et al., 1993). Pharmaceutically, it is commonly used to encapsulate drugs (Leick et al., 2011; Hamad et al., 2012a; Hamad et al., 2013). Microencapsulation is one of the primary uses of shellac (Sheorey et al., 1991; Campbell et al., 2009). It can be used as a coating on gelatine microspheres and modified using esterification to increase encapsulation properties (Labhassetwar et al., 1990). Shellac-calcium microspheres encapsulated with carbamide peroxide is used cosmetically as a tooth whitening agent (Xue et al., 2008). Shellac has been used to form NPs, with xanthan gum used as a stabiliser. These 150-300 nm NPs were used to encapsulate silibinin (an acid unstable compound) for drug delivery to the intestines. The NPs provided protection to the silibinin from the acidic stomach (Patel et al., 2011). Protein encapsulated into shellac NPs has also been demonstrated (Kraisit et al., 2012). Shellac has also been used to encapsulate probiotics such as yeast (*Saccharomyces cerevisiae*), allowing a triggered release at specific pH (Hamed et al., 2012; Hamad et al., 2013).

1.4.3.3 Surfactants

The polymeric surfactant poloxamer 407 (P407) was used in the preparation of shellac NPs in this project. This section gives an overview of surfactants and P407 used in the shellac NPs preparation for this project. Surfactants are amphiphilic compounds which reduce the surface tension of a liquid even at low concentrations. This process is accomplished by adsorbing as a molecular monolayer on the liquid surface. They are also known as surface-active agents (Kunjappu et al., 2013). They have numerous industrial applications, including; industrial processing, food processing, laundry products, adhesions, paints, agrochemicals etc. (Atkins et al., 2010). Surfactants are also useful in pharmaceutical applications and medicine manufacturing (Falk, 2019). Upon saturation at the liquid surface, the surfactant may begin self-assembly into micelles. This concentration is called the critical micelle concentration (CMC). It is still possible for individual surfactant molecules to be in the solution at this time (Atkins et al., 2010). It occurs due to hydrophobic and hydrophilic groups' presence on the surfactant molecule and allows excellent detergency and solubilisation properties to the solution (Cheng et al., 2020; Bala et al., 2006). **Figure 1.10** shows various surfactant types. They are classified based on the charge (or lack of) present in the molecule's hydrophilic part (Kunjappu et al., 2013). Surfactants are classified as ionic if they have either an amphiphilic anion (anionic) or amphiphilic cationic (cationic). Non-ionic surfactants do not ionise in aqueous solution to non-dissociable groups (Atkins et al., 2010). P407 is a non-ionic copolymer surfactant. It was used to sterically stabilise shellac NPs due to the repulsion from the P407 surrounding the shellac core, illustrated and described in chapter 4 and 5 in this project.

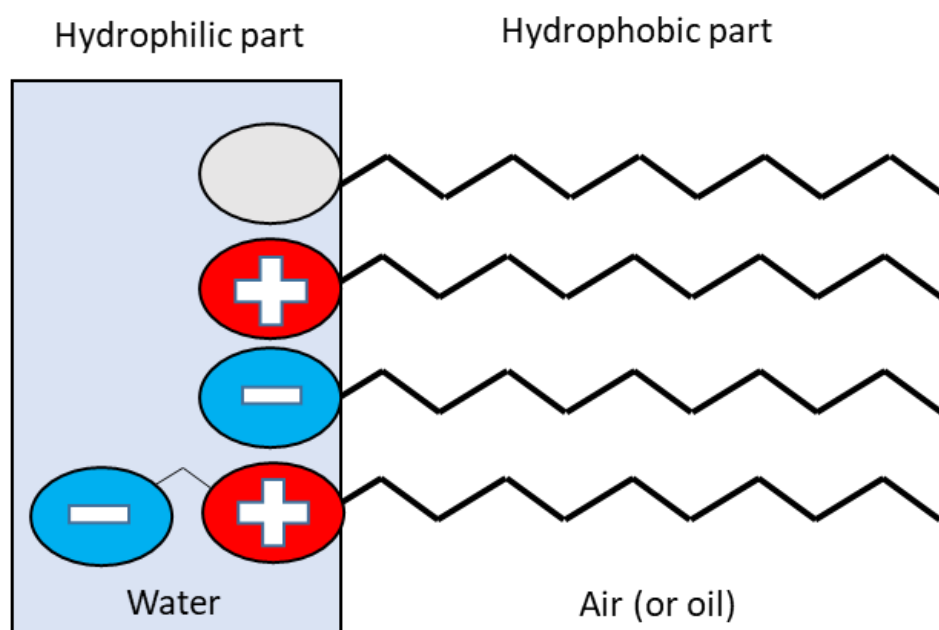


Figure 1.10. A schematic of different types of surfactant.

1.4.3.3.1 Poloxamer 407 (P407)

P407 is an amphiphilic non-ionic block copolymer surfactant with a molecular weight of approximately 12,600 g/mol (Kabanov et al., 2002; Dumortier et al., 2006). The copolymers consist of polyethylene oxide (PEO) and polypropylene oxide (PPO) and are organised in a triblock structure of $(\text{PEO})_a\text{-(PPO)}_b\text{-(PEO)}_a$. It has the chemical formula $\text{HO}[\text{CH}_2\text{-CH}_2\text{O}]_a [\text{CH}(\text{CH}_3)\text{-CH}_2\text{O}]_b [\text{CH}_2\text{-CH}_2\text{O}]_a\text{OH}$, ($a = 101$ and $b = 56$ block lengths), equating to approximately 70% PEO and 30% PPO (Russo et al., 2019). **Figure 1.11A** illustrates the chemical structure of P407, and **Figure 1.11B** shows the proposed micelle formation of P407 in aqueous solution. The Federal Drug Administration (FDA) has classified P407 as an inactive ingredient for different types of oral, topical, inhalation and ophthalmic formulations (McDonnell et al., 2001). P407 has been part of many studies regarding the application of topical/dermal formulations (Miyazaki et al., 1995; Wang et al., 2001; Fang et al., 2002; Shin et al., 2001; Liaw et al., 2000).

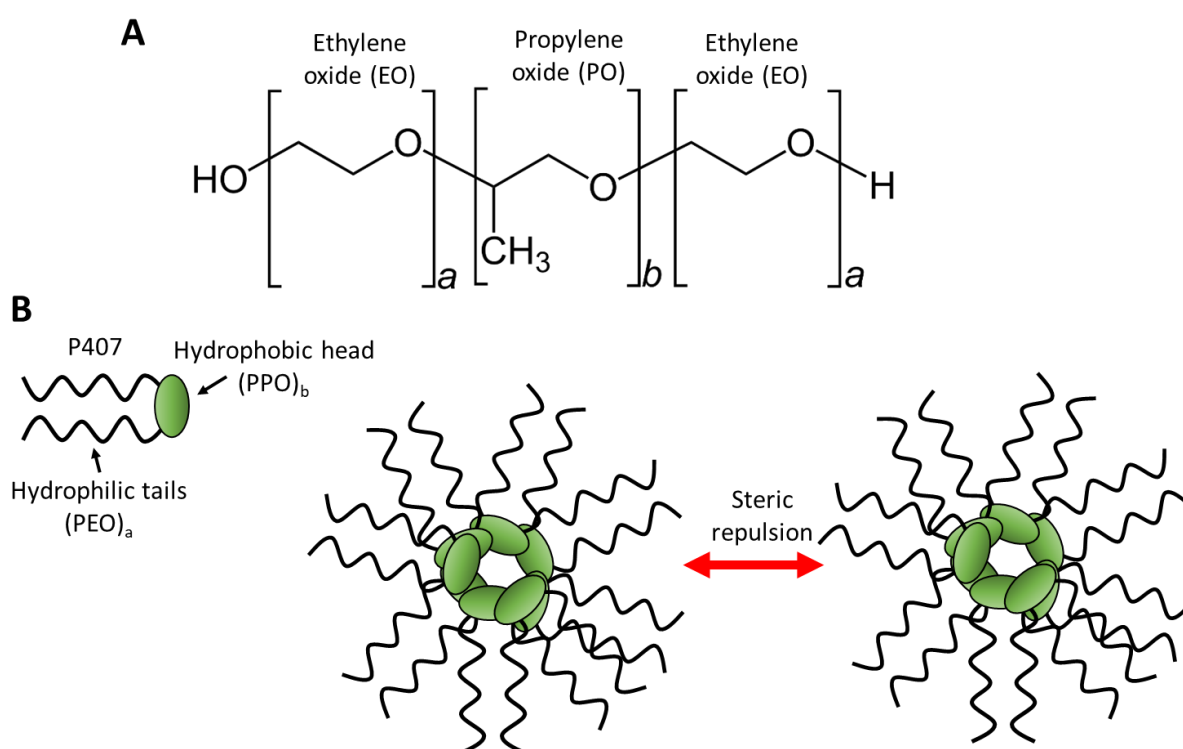


Figure 1.11. (A) The P407 surfactant triblock copolymer chemical structure. (B) Illustration of the formation of micelles formed by P407 in aqueous solution.

1.5 Functionalisation of NPs

For NPs to have the greatest chance of successfully interacting with their target, they must be functionalised in such a way to increase the affinity towards the target (Das et al., 2014; Delfi et al., 2020). There are several ways to this can be accomplished, see **Figure 1.12** for an outline of these mechanisms. Using a specific molecule to functionalise the NP surface, such as an antibody or peptide

ligand is one approach (Farahavar et al., 2019). The conjugation of NPs with aptamers, antibodies and proteins has been used to target specific tumour tissues (Chanphai et al., 2020; Bintang et al., 2020; Munzar et al., 2019). A specific example is the functionalisation of chitosan loaded fluorouracil NPs, which, when surface functionalised with an aptamer, increased the drug's concentration at the cancerous tissues (Rață et al., 2019). The targeting of *S. aureus* using 20 nm silver NPs conjugated with anti-protein A antibody (protein A is cell wall surface protein expressed in bacteria) has been demonstrated to provide a specific technique to kill bacteria by increasing the affinity of the silver NPs to the cell wall (Al-Sharqi et al., 2019). Gold NPs have been functionalised with peptides to increase detection at target tissue and targeted drug delivery and cellular uptake (Zong et al., 2017). An example is the functionalisation of gold NPs with cell-penetrating peptides (CPPs), which increased these NP's uptake into mammalian cells (Chithrani et al., 2007).

Surface modification of an NP with a polyelectrolyte with the intended goal of increasing the electrostatic attraction to the anionic bacterial cell wall or facilitating contact killing is another approach (Delfi et al., 2020; Al-Awady et al., 2015; Al-Awady et al., 2017; Richter et al., 2015). Gram-positive and Gram-negative bacteria, and fungal cells all have anionic cell surfaces (Malanovic et al., 2016; Garcia-Rubio et al., 2020). In the case of Gram-positive bacteria, this is provided by the presence of teichoic acid and lipopolysaccharides (LPS), also known as endotoxins, which the cell wall is comprised off (Gottenbos et al., 2001). Gram-negative contains an abundance of anionic glycoproteins in the thicker peptidoglycan cell wall (Slavin et al., 2017). The anionic charge of fungal cell walls is primarily provided by the presence of the amorphous polymer melanin (Garcia-Rubio et al., 2020). Further details of the interaction between cationic NPs and anionic microorganism cell walls are provided in the later chapters.

NPs have also been functionalised with specific reactive groups to provide beneficial characteristics. An example is the coating of silica NPs with SOCl_2 and *N*-Boc-1,4-butanediamine, creating chlorine and amine groups on the surface. These groups offer fluorescence characteristics to the NP and provided photoluminescent detection of NP interactions with mammalian cells (Natalio et al., 2012). Boronic acid functional groups conjugated to NPs allows a non-electrostatic interaction with cis-diol groups contained with the bacterial cell wall (Halbus et al., 2019b). The post-NP synthesis surface functionalisation is a vast area involving a diverse array of functional groups.

In this project, the NPs were surface functionalised with either the polyelectrolyte, bPEI (Branched polyethyleneimine), or the protease Alcalase 2.4 L FG, with the intention of providing an electrostatic attraction to bacterial cell walls, and in the case of the protease at active agent to degrade the EPS of biofilms. Further details of these materials are discussed below.

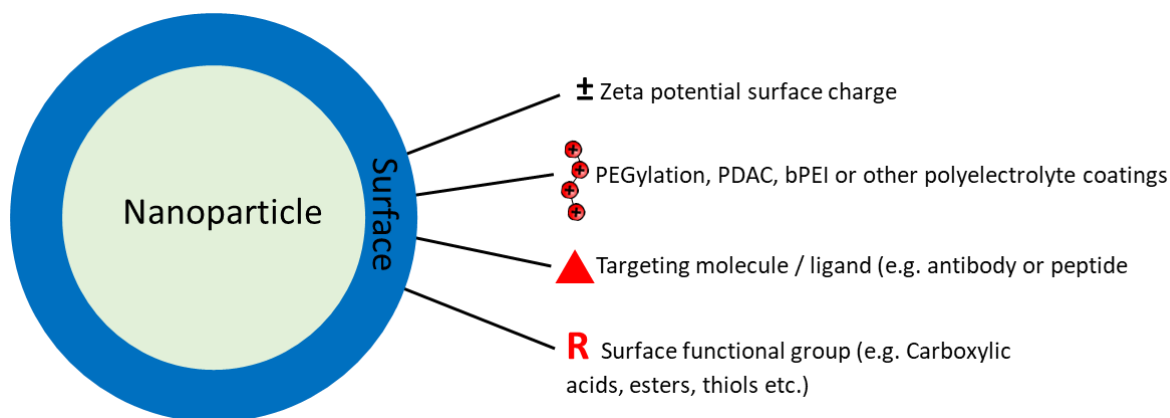


Figure 1.12. Examples of surface modifications to NPs. Image created by Author.

1.5.1 Polyelectrolytes

Polyelectrolytes are polymers with a cationic or anionic functional group, which can dissociate in aqueous solution to create a charged polymer, i.e. polycation or polyanion. They are usually of high molecular weight and create a viscous solution at high concentrations. Like acids which are classified as weak or strong depending on their ability to dissociate a proton, the same is true of polyelectrolytes and their ability to disassociate their electrolyte functional group (Atkins et al., 2010). Polyelectrolytes have many applications, including cosmetically as emulsifiers, thickeners, and conditioners (Hössel et al., 2000). Their use is also common in biomedical applications (Ishihara et al., 2019). They can also be used to apply a surface charge to NPs, which are neutral or charged themselves (Fuller et al., 2019). **Figure 1.13** shows some common polyelectrolytes which have been used in biomedical applications. Poly(diallyldimethylammonium chloride) (PDAC) has been used to apply a cationic charge to NPs, encapsulating antimicrobial agents berberine and chlorhexidine, and increased the efficacy of the antimicrobial agents against pathogens (Al-Awady et al., 2017; Al-Awady et al., 2018). Chitosan, a cationic polysaccharide, has been researched extensively as a drug delivery agent in so-called polyelectrolyte complexes (PEC) (Luo et al., 2014). Sodium alginate has also been used in PECs with potential applications for drug delivery and tissue engineering (Wasupalli et al., 2018, Wang et al., 2020b). In this project, the polycation electrolyte Polyethylenimine, branched (bPEI) was used as a NP surface modification agent to confer a positive charge to the NPs.

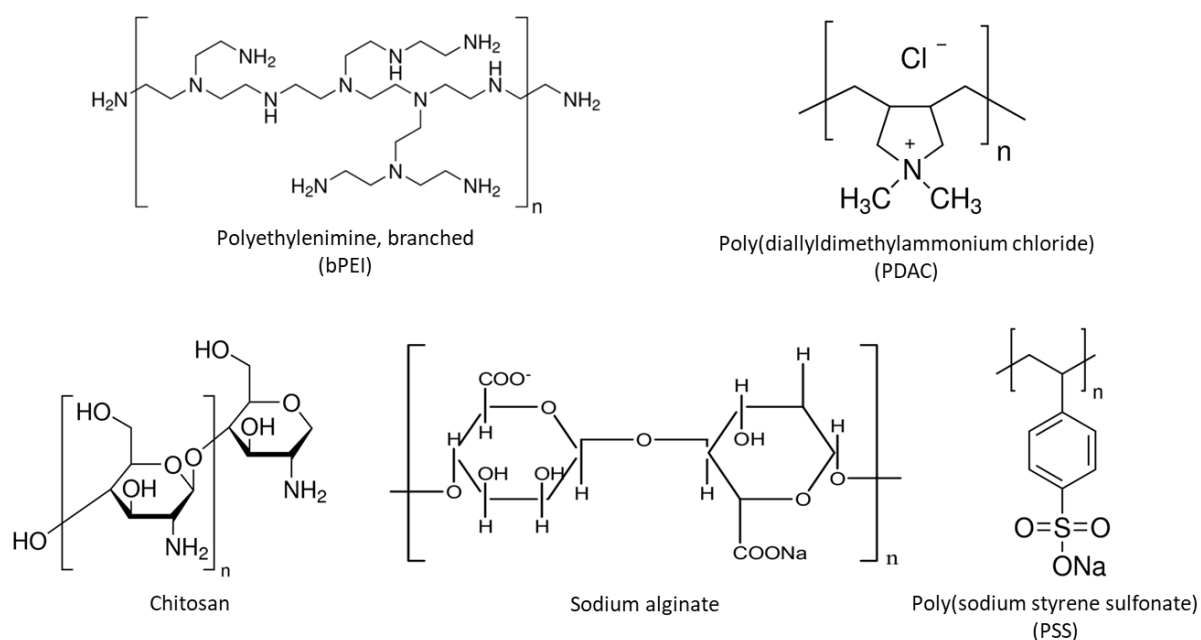


Figure 1.13. Common polyelectrolytes used in biomedical applications (Kulkarni et al., 2016).

1.5.1.1 Branched polyethylenimine (bPEI)

bPEI is a branched polymer which has repeating units of ethylenediamine and is a strong cationic polyelectrolyte. PEIs are polymeric molecules composed of repeating units of amine groups and two aliphatic carbons; a branched PEI, bPEI, may have all types of primary, secondary and tertiary amino groups while a linear PEI, PEI, contains only secondary and primary amino groups (Lungu et al., 2016). It is stable in many polar solvents such as water, ethanol and chloroform. It has a useful application as a surface charge applicator to NPs and retains its cationic charge over a wide pH range. It also has excellent salt stability, a very large saline concentration is needed to shield the charge of a bPEI coated NP (NanoComposix, 2020). There have been numerous applications of PEI in biomedical applications. PEI has been used to transfect DNA to cells, and demonstrates less toxicity than commercially available reagents such as Effectene, LipofectAMINE 2000 and ExGen (Huh et al., 2007). Liposomes have been surface modified with PEI. The liposomes, which had small interfering RNA (siRNA) inside, showed increased efficacy against drug-resistant cancers when the PEI surface coating was applied (Mendes et al., 2019). PEI has been shown to have synergistic properties when administered with antibiotics. PEI, combined with several different antibiotic classes (aminoglycosides, polymyxins and vancomycin's) resulted in 5 to 8-fold log CFU/mL reductions compared to the free antibiotic alone. Likely due to increased permeability bPEI applies to bacteria (Khalil et al., 2008).

Permeabilising of bacteria has also been reported that a possible mechanism for this is interaction with the anionic LPS (Helander et al., 1998). bPEI has also demonstrated usefulness against

antibiotic-resistant pathogens. In methicillin-resistant *staphylococcus epidermidis* and MRSA, which are resistant to beta-lactam antibiotics by expressing penicillin-binding protein 2a (PBP2a). bPEI was shown to interact with teichoic acid, reducing cell wall synthesis, allowing oxacillin to be more effective (Lam et al., 2018). bPEI interactions with PBP2a and subsequent prevention of localisation of this enzyme at the bacteria septum during binary fission is another mechanism for increasing antibiotic susceptibility against resistant pathogens. The abnormal cell wall morphology allowing beta-lactams to be effective against species resistant to them (Hill et al., 2019). bPEI has also been revealed to be a potentiator for beta-lactam antibiotic piperacillin, allowing it to be effective against *Pseudomonas aeruginosa*, which was otherwise resistant. The bPEI again interacted with the bacterial cell wall resulting in abnormal morphology and presumed increase in antibiotic penetration (Lam et al., 2020).

Interestingly, bPEI has also been shown to reduce biofilm formation. The EPS matrix has been revealed to not form in the usual fashion, compared to a control. This provided another useful application of bPEI, as antibiotics are more effective against planktonic bacteria, rather than bacteria within a biofilm (Lam et al., 2019). bPEI has also been investigated for the coating of NPs and microparticles (MPs), which have peptides or DNA inside. This increased the NP/MP content's transfection by endocytosis mediated by the bPEI-coating (Shen et al., 2017). bPEI does confer some cytotoxic effects against mammalian cells, like all polyelectrolytes. However, it is tolerated by cells at low concentrations (Fischer et al., 2003).

1.5.2 Proteases

Proteases are enzymes which catalyse the breakdown of proteins into polypeptides or single amino acids via hydrolyses of the peptide (CO-NH) bond. Proteases are required in all life to for various reasons, such as cell signalling, protein catabolism, wound repair, haemostasis, inflammation, immunity, apoptosis, necrosis, angiogenesis, DNA replication etc. (Lovrić et al., 2012). Proteases were originally grouped into either endopeptidases, which target internal peptide bonds, or exopeptidases, targeting NH₂ and COOH termini. Often proteases can be grouped based on their optimal pH activity, i.e., acid proteases, neutral proteases, or basic proteases (Razzaq et al., 2019). Currently, the mechanism of catalysis is how proteases are grouped (López-Otín et al., 2008). There are seven groups of proteases with a wide array of different specific proteases in that group (Mótyán et al., 2013; López-Otín et al., 2008; Jensen et al., 2010). **Table 1.7** outlines the seven groups of proteases and gives examples of specific proteases in that group. The use of proteases in research is vast, with applications such as laundry and cleaning applications, food technology, medicine manufacturing, and biomedical applications (Nahar et al., 2018).

A serine group protease, tissue plasminogen activator (TPA) is used to treat ischemic strokes. The enzyme can activate plasmin, which cleaves fibrin and reduces blood clotting (Wardlaw et al., 2012). Wounds often contain damaged and necrotic tissue which is proteinaceous in nature. The cysteine group proteases, papain and bromelain, the serine group trypsin, and the metalloproteinase group collagenase have been researched for use as biological debridement agents, able to be effective without causing further tissue damage (Klasen et al., 2000).

Table 1.7. Proteases groups (by proteolytic mechanism) and examples of specific proteases (data obtained from M6ty6n et al., 2013; L6pez-Ot6n et al., 2008; Jensen et al., 2010; da Silva et al., 2017b).

Protease group	Examples of specific proteases	Enzyme class	Nucleophilic agent
Serine	Trypsin Elastase Subtilisin Thrombin	Hydrolase E.C. 3.4.	Serine residue (Ser)
Cysteine	Bromelain Papain Ficin	Hydrolase E.C. 3.4.	Cysteine residue (Cys)
Threonine	Ornithine acetyltransferase Testes-Specific Protease	Hydrolase E.C. 3.4.	Threonine residue (Thr)
Aspartic	Pepsin Cathepsin D	Hydrolase E.C. 3.4.	Water molecule activated by two aspartates
Glutamic	pepG1	Hydrolase E.C. 3.4.	Water molecule associated with glutamate
Metalloproteinase	Collagenase Dispase Thermolysin	Hydrolase E.C. 3.4.	Water molecule activated by metallic ions
Asparagine peptide lyase	Nodavirus coat protein	Lyase E.C. 4.3.2.	Asparagine residue (Asn)

As discussed above, proteins are produced by biofilm-forming bacteria, with the function of facilitating adherence to a substrate and providing the physically protective nature of the EPS. Other than proteases, biofilm degradation/disruption can be created by applying agents such as DNase (hydrolytic DNA cleaving), Dispersin B (glycoside hydrolase) and lysostaphin (antimicrobial peptide agent) (Boles et al., 2011). Regarding proteases, the bacterially derived metalloproteinase serratiopeptidase has been researched for its therapeutic use against *S. epidermidis* biofilms in an animal model. This enzyme's application reduced the biofilm burden and increased the efficacy of antibiotic ofloxacin when applied as a co-treatment (Mecikoglu et al., 2006). Cysteine group ficin has also been investigated for its potential anti-biofilm properties. When applied to *S. aureus* and *S. epidermidis* biofilms a significant reduction in biofilm thickness and adherence was reported (Baidamshina et al., 2017).

A metalloprotease obtained from bacterial sp. SKS10 was purified and revealed to be highly effective in reducing *S. aureus* biofilms (Saggu et al., 2019). Proteases have also been functionalised

on to NPs. Serine group Alcalase 2.4L was immobilised onto chitosan NPs and shown to have increased activity longevity when applied on soy protein isolate compared to the free Alcalase 2.4L (Wang et al., 2014). α -amylase from the *Bacillus* sp. and protease isolated bovine pancreas have been immobilised onto copper NPs. The results indicated that the immobilised enzymes showed an improved pH and temperature stability than free enzymes (Murugappan et al., 2021). Chitosan NP immobilised ficin has also been shown to increase the clearing of wound burdened *S. aureus* biofilms in a murine model. An equivalent concentration of chitosan NP immobilised ficin resulted in an improved wound healing outcome after 15 days (Baidamshina et al., 2020). Proteinase K has been functionalised onto gold and silica NPs and has demonstrated the ability to degrade biofilms and reduce their thickness (Zanono et al., 2015; Habimana et al., 2018). **Table 1.8** shows different groups of enzymes which have been used to target biofilms.

In this study, Alcalase 2.4 L FG was chosen as the protease to be researched for potential NP functionalisation and its antibiofilm potential. Alcalase 2.4 L FG is a serine group subtilisin derived protease with an optimum usage activity between 30-65°C and pH 7-9. Crucially, it has an isoelectric point (IEP) of approximately 9 (as shown later in chapter 3), allowing it to be cationic at neutral and acid pH, facilitating the electrostatic functionalisation to anionic NPs (Strem, 2021). More information on this process is provided in chapter 3.

Table 1.8. Different groups of enzymes which have been used to target the EPS components of biofilms.

Enzyme group	Catalytic activity	Example of enzyme	EPS target	Ref
Hydrolases	Cleaves C-C, C-O and C-N bonds, peptide bonds and enhydride linkages	AiiA, α -amylase, Proteinase K	Quorum-signalling molecules, exopolysarchrides, exoproteins	(Dong et al., 2000; Fagerlund et al., 2016; Kalpana et al., 2012)
Lysases	Cleaves C-C, C-O and C-N bonds	Alginate lyase	Exopolysarchrides	(Lamppa et al., 2013)
Oxidoreductase	Catalyzes reactions of electron transfer from reductant to oxidant	Glucose oxidase, Curvularia haloperoxidase	Bacterial growth by producing H ₂ O ₂ , directly or indirectly	(Ge et al., 2012; Hansen et al., 2003)

1.6 Nanocarriers for drug delivery – characteristics and application

Drug delivery to a specific target is an area commonly researched. With most intravenous administered drugs, only a small amount reaches the target site (Ayyaswamy et al., 2013). The use of nanocarriers can fulfil the goal of targeted delivery, i.e. infected tissues and tumours (i.e., extravasation, whilst also reducing the unwanted accumulation of drugs at healthy tissue (Din et al., 2017). Common drug delivery nanocarriers include polymeric micelles dendrimers, liposomes and biodegradable scaffolds (Singh et al., 2019).

As used in this project, microgels are cross-linked polymeric particles in a sub-micrometre range (Richtering et al., 2014). A microgel which can have therapeutic use must be biocompatible and not induce a metabolic or immune response when administered (Campbell et al., 2019). Additionally, they must be small enough in size not to cause blood clotting or induce cancer (Urakami et al., 2013).

1.6.1 Drug loading / swelling behaviour

A good NP drug delivery system needs to have a high drug loading/encapsulation capacity (Shen et al., 2017). The NP composition determines the drug loading efficiency, as well as the solubility and charge characteristics of the drug and NP itself (Patra et al., 2018). For example, in polymeric NPs, the functional groups, i.e. carboxyl or ester can interact with functional groups of the drug chosen to be encapsulated (Al-Awady et al., 2017; Al-Awady et al., 2018).

There are two ways to encapsulate a drug within a NP.

- Absorption/adsorption technique: The NP is synthesised, and a mixture of the drug is added, and the two combine to create an encapsulated NP (Kumari et al., 2014). This is the method used with the nanogel Carbopol Aqua SF1 and the antibiotics tetracycline, lincomycin and ciprofloxacin described later in chapter 2 and 3.
- Incorporation technique: the drug is encapsulated during the NP preparation/synthesis (Kumari et al., 2014). This is the method used with the shellac/p407 polymeric NP and antibiotics amphotericin B, penicillin G and oxacillin described later in chapter 4 and 5.

1.6.2 Microgel absorption/swelling technique

A nanogels swelling ability is dependant on the aqueous environment the polymer is in. pH, temperature, and ionic strength influence the swelling characteristic (Soni et al., 2016). For example, ionisation of carboxylic groups with the cross-linked matrix causes electrostatic repulsion and subsequent swelling of the nanogel. This is shown with poly(ethylene glycol)-b-poly(methacrylic acid) (PEG-b-PMA) nanogels in which high pH causes swelling (Bontha et al., 2016). This same function is

utilised with Carbopol Aqua SF1 used in this project. Swelling can also be decreased at high pH (the opposite of Carbopol and PEG-b-PMA) depending on the functional groups within the nanogel. For example, poly(ethylene glycol) and polyethyleneimine (PEG-*cl*-PEI) nanogels deswell at high pH due to the protonation of amino groups within the PEI (Tatiana et al., 2001). The incorporation technique was used to load amphotericin B, penicillin G and oxacillin into shellac/P407 NPs in this project.

1.6.3 Encapsulation stability

Cross-linked nanogel polymers can be used to retain the encapsulated drug and prevent its premature release (Li et al., 2016). This allows drugs within the nanogel to be retained and provide the therapeutic purpose of the nanogel, i.e. a concentrated targeted release of the encapsulated drug. The chemistry of the drug loading into the nanogel can be accomplished with several different strategies (**table 1.9**).

Table 1.9. Drug loading into nanogel strategies.

Nanogel drug loading strategy	Ref
Covalent/electrostatic bonding of the drug and nanogel. Examples include copolymerisation of modified enzymes with acrylamide which allowed the formation of drug-loaded nanogels. This technique was used to encapsulated tetracycline, lincomycin and ciprofloxacin into Carbopol Aqua SF1 in this project.	(Ming et al., 2016)
Diffusion based drug loading. Silver has been loaded into dextran-lysozyme nanogels, for example. This is a simple technique in which the drugs and the nanogel are simply mixed with constant mixing/agitation.	(Coll Ferrer et al., 2014; Soltani et al., 2016)
Drug loading by physical encapsulation. Several drugs have been loaded into nanogel using this method, i.e. hydrophobic/ hydrophilic interactions (Wang et al., 2019b). Doxorubicin has been loaded into a nanogel (Missirlis et al., 2006), proteins into cholesterol-modified pullulan nanogels (Tao et al., 2016), and siRNA into hyaluronic nanogels (Serrano-Sevilla et al., 2019).	(Wang et al., 2019b; Missirlis et al., 2006; Tao et al., 2016; Serrano-Sevilla et al., 2019)

1.6.4 Drug release from NPs and nanogels

Drug release is required to happen at the target site, increasing the nanocarrier's therapeutic capability (Eckmann et al., 2014). This allows a high concentration of the drug localised to the target, increasing the efficacy, and reducing the unintended effect on non-target tissues (Kamaly et al., 2012). A lack of drug release at a specific target is why drugs which are successful in cell culture often fail to be useful in complex systems, i.e. the human body (Rawat et al., 2006). Factors that affect drug release include the drug solubility, and the diffusion out of the NP/degradation of the NP matrix itself (Patra

et al., 2018). Size also influences drug release. Larger NPs tend to have a smaller initial burst release with a longer sustained release than small NP alternatives (Lu et al., 2011). Drug-loaded content also affects release. NPs with highly dense drug encapsulations increase the rate of drug release. For example, Poly-lactic acid (PLA) NPs with a high 16.7 wt% savoxepine content release 90% of the drug within 24 hours, compared to a drug loading content of 7.1% savoxepine which release the same 90% over 3 weeks (Leroux et al., 1996). Initial burst release is thought to be due to drugs not just encapsulated but also adsorbed onto the NP's surface (Yoo et al., 2020). Drug release can be achieved using a different mechanism. The drug can be released by diffusion, for example, the release of dexamethasone from dextran lysosome nanogels (Coll Ferrer et al., 2014). The drug release can also be engineered due to the NP itself losing integrity, either because the NP is chemically or biologically unstable (Begines et al., 2020). For example, cross-linked disulphide poly(oligo(ethylene oxide) monomethyl ether methacrylate nanogels could be degraded and release their drug when exposed to glutathione tripeptide, commonly found in cells (Yin et al., 2020). Doxorubicin was released from nanogels due to the pH sensitivity of the nanogel. Acidic conditions accelerated the release increasing usefulness against carcinoma cells with an acid pH microenvironment (Oh et al., 2010).

The localised sustained release of drugs has had successful applications. Cisplatin was encapsulated into multivesicular liposomes and achieved a sustained and localised release of cisplatin over 7 days. This increased its effectiveness against tumour areas in a mouse model, compared to equivalent cisplatin concentrations alone (Xiao et al., 2004). Overall, the success or failure of the drug-loaded NP is dependent on its release kinetics. Optimal drug release should be slow enough to avoid drug loss before the NP reaches its target (Loew et al., 2011; Zeng et al., 2011). Whilst simultaneously controlled and timed to ensure a high localised concentration of the drug is released near or on the target site, allowing it to outperform the free drug (Patra et al., 2018). Streptomycin-loaded chitosan magnetic iron oxide NPs (StrepCS-MNPs) showed controlled release and allowed increased the effectiveness of streptomycin against MRSA (Hussein et al., 2014). The encapsulation of vancomycin into chitosan NPs showed the release could be modulated based on pH. Vancomycin was released more readily at pH 6.5 compared to pH 7.4 due to decreased NP stability in acidic conditions. This allowed the vancomycin-chitosan NPs to be 8-fold more effective in an MRSA burdened mouse model skin infection than equivalent concentrations of free vancomycin (Kalhapure et al., 2017).

Carbon nanotubes covalently functionalised with ciprofloxacin have been demonstrated to release 90% of the loaded drug within 2.5 hours. This allowed it to achieve a 16-fold increase in effectiveness against *S. aureus* and an 8-fold increase against *P. aeruginosa* and *E. coli* compared to free ciprofloxacin, due to accumulation of the carbon nanotubes on the bacteria. (Assali et al., 2017). Vancomycin-loaded aragonite (VANPs) have shown 120 hours of drug release and showed an

increased effectiveness against MRSA, again due to localised release on the bacteria (Saidykhan et al., 2016). Metal-carbenicillin framework-coated mesoporous silica NPs showed an increased effectiveness against MRSA and better biofilm penetration (Duan et al., 2017). These are just some examples of how encapsulation and improved release kinetics can have beneficial antimicrobial performance.

1.7 Use of NPs in the treatment of infected wounds

Pathogenic infection is highly prevalent in chronic wounds, with over 90% presenting with bacteria or fungi living within a biofilm, inside the wound (Attinger & Wolcott, 2012). A wound that has failed to heal is termed chronic (Iqbal et al., 2017). They are most likely to occur in patients already suffering from disease resulting in increased morbidity and mortality, whilst also causing health care providers substantial financial burdens (Darwin & Tomic-Canic, 2018). Chronic wounds are classified into three types; diabetic foot ulcers (DFUs), venous leg ulcers (VLUs) and pressure ulcers (PUs) (Frykberg & Banks, 2015). PUs usually form due to continuous pressure and friction from a bony prominence in the body, therefore are typically found in bedridden patients (Boyko et al., 2018). VLUs are usually caused by poor circulation and localised hypoxia caused by a venous obstruction (Alavi et al., 2016). As the name implies, DFUs are found in patients suffering from diabetes, where hyperglycaemia impairs normal leukocyte function leading to an attenuated inflammatory response and tissue damage, in addition, diabetes causes damage to the microvasculature causing increased hypoxia (Lim et al., 2017). Burns also represent another example of a wound that is vulnerable to infection, in severe cases leading to sepsis (Dvorak et al., 2021). A recent study estimated that 5.5% of the total healthcare spending in the UK was on chronic wounds (Phillips et al., 2016). There is a critical need for innovative treatments for pathogen-infected chronic wounds which can be effective against biofilms and species with antibiotic resistance (Negut et al., 2018).

1.7.1 Clinical use of NPs

As discussed previously, targeting is what is vital to a successful drug-loaded NP treatment. NPs can naturally and passively accumulate at diseased tissue through a phenomenon known as enhanced permeability and retention (EPR) at a specific pathophysiology target (Greish, 2010). For example, increased permeation due to a damaged endothelial layer (Kobayashi et al., 2013). The increased vascular permeability is common in inflammation and allows NP ingress (Torchilin, 2000). Generally, however, current research focuses on active targeting as it is more controllable, precise, and relevant if tissue is not damaged (Muhamad et al., 2018). A variety of surface NP modifications have been used to facilitate active targeting. The molecules used to select for target area must be able

to effectively target this area without demonstrating any deleterious effects on the NP or drug content, either by inhibiting activity or release (Eckmann et al., 2014). An example is the functionalisation of CuONPs with 4-hydroxyphenylboronic acid, which allowed a targeted covalent bond to diol groups of glycoproteins on the bacterial cell surface, resulting in increased concentration of the NP and toxicity to bacteria (Halbus et al., 2019b). See **figure 1.14** for examples of how size, shape and surface functionalisation/coating of NPs influence circulation and clearance in the body. Overall, the increased accumulation of NPs (and therefore the loaded drug) at the target site, and subsequent reduction of the drug at a non-target site, greatly increases the usefulness of drug-loaded NP (Smerkova et al., 2020). In this project, bPEI and Alcalase 2.4 L FG are used as an active targeting / NP surface modification agent for increased electrostatic attraction to bacterial cell walls/antibiofilm properties.

The use of NPs for treating patients has been refocused, in part, to the increasing tendency of precision/personalised medicine and the creation of the Precision Medicine Initiative (PMI) in 2015 (Collins et al., 2015). The application of PMI can use information such as a patient’s genetic profile or comorbidities to develop a specific treatment plan. This allows a more effective treatment than a heterogenetic approach to administering medicines. NPs, and their ability for specific targeting, have been implicated as a useful tool in personalised medicine (Mitchell et al., 2020).

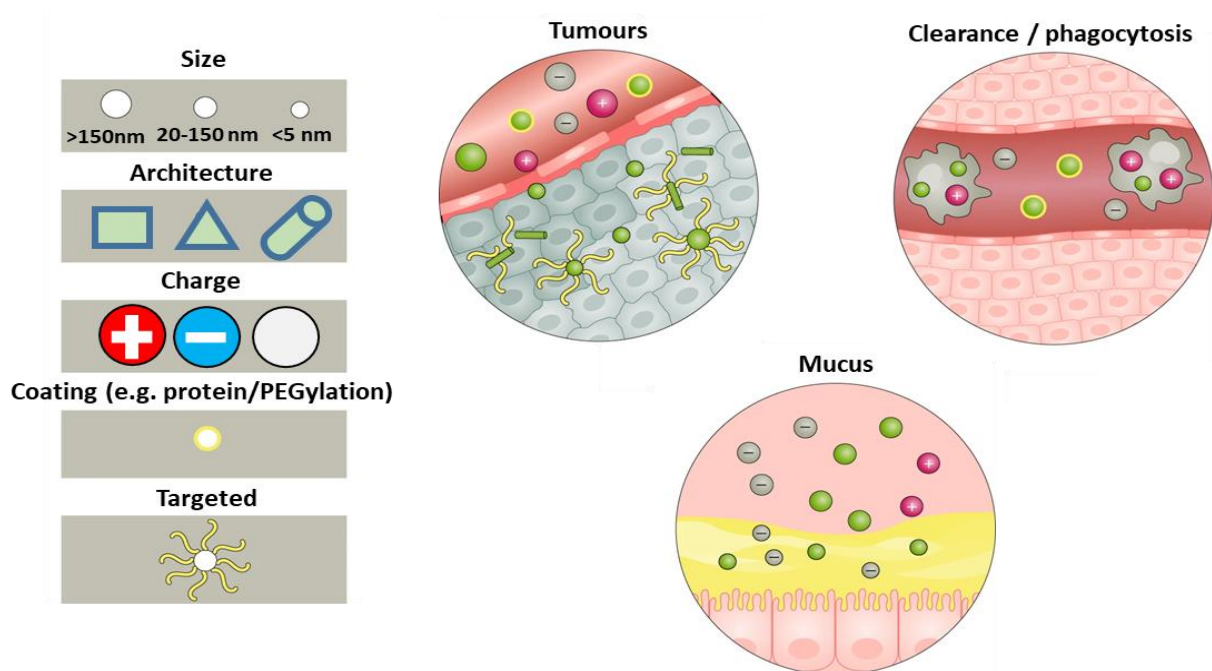


Figure 1.14. Examples of how size, shape and surface functionalisation/coating of NPs influence circulation and clearance in the body. General trends include, spherical and larger NPs marginating more during circulation compared to rod-shaped which are more likely to extravasate. Phagocytosis, for example by macrophages or monocytes, is more likely to occur to cationic/neutral and protein-functionalised NPs. None-spherical, target-specific and neutral NPs are more likely to penetrate tumours. Finally, smaller NPs are more likely to transverse mucosal barriers (Image adapted from Mitchell et al., 2020).

An example of the application of NPs in precision medicine is the use of graphene oxide nanoflakes. These nanoflakes can bind to very low albumin levels in a patient's blood sample, and are subsequently coated in a biomolecular corona of proteins, the analysis of which can provide high-throughput results for the detection of pancreatic cancer biomarkers when the nanoflakes are analysed (Papi et al., 2019). Gold NPs are also used in biomarker detection. They can be functionalised with agents such as thrombin binding aptamers or a celiac specific peptide, and therefore accumulate a key biomarker that can be detected with greater sensitivity (Zhang et al., 2019b; Kaur et al., 2018). There are numerous other biomedical applications in precision medicine (Aguado et al., 2018). A challenge to overcome in the application of NPs is the effective biodistribution if administered systemically in a patient, such as rapid clearance, shear forces in the blood, and protein absorption which may limit their functionality (Wilhelm et al., 2016). NP could potentially be delivered locally to circumvent obstacles of systemic delivery, but that may not also be practical, if for example in an infectious or tumourous site that is not accessible.

For this reason, systemic NP treatments are more common (Gehr et al., 2019). NPs administered systemically, i.e. in blood, face obstacles such as interaction with phagocytic cells (Mitchell et al., 2020). Additionally, NPs under 10 nm are rapidly eliminated by the kidneys, and NP over 200 nm risk activating the complement system, which could lead to unwanted immune response problems (Hoshyar et al., 2016). Polyethylene glycol (PEG), sometimes referred to as macrogol, is commonly used in biopharmaceutical drugs to improve bioavailability by conferring preferable characteristics, such as physiologically pH changes and improved solubility (Veronese et al., 2005). PEGylation coating of NPs is often used as this provides a "stealth" coating and reduces the accumulation of antibodies and enzymes, which may result in the NPs having a longer serum half-life. Anti-PEG antibodies can be present in patients who have been exposed PEG through non-medical means, providing another hurdle of NP application (Wang et al., 2007; McSweeney et al., 2018; Yang et al., 2016; Chen et al., 2015). NP stability in blood circulation is dependant on the materials they are synthesised from, with lipid and polymer-based NP more susceptible to aggregation and colloidal instability, for this reason, surface coating with cross-linking polymers and PEGylation of lipids is often performed (Palanikumar et al., 2020; Tanaka et al., 2020; Sedighi et al., 2018; Cheng et al., 2016).

Variations in blood flow rates have also been shown to induce shear stress on NPs and make resulting stripping of surface coatings and loss of encapsulated cargo prematurely (Jarvis et al., 2018; Hosta-Rigau et al., 2013). Microscale NPs are less susceptible to these forces, and even the shape of the NP is relevant as non-spherical geometries are less inclined to be rolled around the blood from the edges of blood vessels (Cooley et al., 2018; Da Silva-Candal et al., 2019; Uhl et al., 2018). Overall, a NPs haemodynamic performance is an important consideration, e.g. patients with hypertension often

also have stenosis, which affects how the NP is distributed around the blood/body (Malota et al., 2018; Chacón-Lozán et al., 2018). Additionally, biomolecules also flowing in the blood can interact with NP, these can create a corona of proteins on the surface of the NP, and reduce function and stability (Scheetz et al., 2019; Tenzer et al., 2013; Cox et al., 2018; von Roemeling et al., 2017). Although this has been taken advantage of in some therapeutic NP applications as described above. An example of how this can be deleterious is the protein corona NP coating of apolipoprotein E (ApoE), which when it accumulates encourages the NPs to target lipoprotein receptors and localisation to hepatocytes (Chen et al., 2019; Yeo et al., 2019; Dal Magro et al., 2017; Dong et al., 2014). Furthermore, the build-up of opsonin molecules can cause the NP treatment to become a target of phagocyte immune cells (von Roemeling et al., 2017).

The clearance of NPs by phagocyte immune cells is influenced by the apparent charge and physical hardness of the NPs. Cationic and harder NPs tend to be cleared more rapidly than softer neutral or anionic NPs (Key et al., 2015; Hui et al., 2019; Kou et al., 2018; Blanco et al., 2015). NPs in the blood have also been shown to trigger other immune responses such as secretion of interleukins and interferons, potentially causing damaging tissue inflammation (von Roemeling et al., 2017, Nizzero et al., 2018). NP geometry also plays a part in phagocyte clearance, with spherical NPs tending to be less susceptible to phagocytosis than rods or other less smooth shapes (Nishita et al., 2017; Wang et al., 2019c, Garapaty et al., 2019). Overall, the immune response, haemodynamic interactions and biomolecule interactions are all important considerations when designing and eventually potentially administering NPs for biomedical applications (Scheetz et al., 2019, Papi et al., 2019).

Interestingly, where the NPs are injected into the blood can impact how they are distributed eventually, for examples polymeric NPs like poly(lactic-co-glycolic) acid (PLGA) NPs, if injected intravenously, tend to accumulate in the liver and spleen. However, unsurprisingly, an intranodal injection tends to accumulate in the lymph nodes. This is an important consideration depending on the NPs purpose (e.g. anti-cancer) (Zhong et al., 2016; Battaglia et al., 2018; Dölen et al., 2020). An alternative to blood administration is inhalation which increased distribution in the pulmonary system, and potentially avoid nullification of the NP via the mechanism explained previously, however, the mucus-like nature of lung tissue provides a physical barrier (Zhong et al., 2016, Dong et al., 2020b; Cone et al., 2009). Antibody targeting has shown to be on the most successful surface modifications to NP due to their highly specific nature. However, a downside is an affinity for phagocytes to these proteins, regardless of the antibodies intended specificity (Wu et al., 2020, Hoshyar et al., 2016). If the NP is intended to reach tissues deeper within a patient, tight junctions in endothelial cells provide a physical barrier (Schwartz, 2017, von Roemeling et al., 2017; Saraiva et al., 2016). The oral delivery of NP faces challenges when crossing the intestinal endothelium, as they will have to do so by passive

means (Ensign et al., 2012). Some NPs, such as silica-based ones have actually been shown to increase the uptake of encapsulated drugs. They have been shown to open tight junctions (Lamson et al., 2020). Generally, orally administered NPs will have to go through endocytosis and exocytosis, for which NP of approximately 100 nm has shown to be the best (Le et al., 2018; Tian et al., 2018; Banerjee et al., 2016; Yong et al., 2019; Zhang et al., 2019c). Unfortunately, NPs which undergo endocytosis, most do not then go through exocytosis, effectively creating a considerable loss of NPs (Zhuang et al., 2018).

The environment that the NPs will encounter if administered intravenously or orally must also be taken into account. For example, NPs which enter the gastrointestinal tract will encounter a highly acidic environment and high concentrations of proteolytic enzymes which could degrade the NP or a proteinous functional coating (Ensign et al., 2012; Oliva et al., 2015). The differences in pathological environments can be taken advantage of, however. Wounds are often hyperthermic, so a temperature-sensitive NP system could be targeted to these regions. Also, stenosis due to atherosclerosis can be used to provide a target to NPs which have been designed to break down under increased shear stress (Hathaway et al., 2017; Holme et al., 2012). In the context of cancerous tumours, the serpentine nature of the abnormal vasculature can be advantageous towards NPs, as they tend to accumulate in these regions enhancing the EPR (Scheetz et al., 2019, Sindhvani et al., 2020). As discussed earlier in this chapter, and in chapters 3 and 4 later, biofilms provide a potential barrier for NPs (all other small molecule therapeutics) (Ensign et al., 2012; Witten et al., 2017). Any potential endocytosis of NPs is also dependent on how the NP interacts with the cell membrane. Features such as lipid rafts and the distribution and concentration of cell surface proteins effectively change the fluid mosaic properties and charge of various cell membranes, and in turn influence how NPs interact with them (Scheetz et al., 2019; Ho et al., 2019; Behzadi et al., 2017; Kou et al., 2018; Gehr et al., 2019). The size of the NPs required to undergo endocytosis is also a factor. NPs on the very small size, i.e. less than 30 nm, may not be capable of driving membrane wrapping enough to facilitate an endocytic process (Hoshyar et al., 2016). As discussed above, a variety of complex factors must be considered when administering a systemic NP treatment (Mitchell et al., 2020).

1.8 Aims of the thesis

As seen above, the first chapter provides a general introduction overviewing skin microbiology, antibiotics and antibiotic resistance, biofilms and the application of NPs as antimicrobial agents. There is an essential need for improved treatments for antibiotic-resistant species, which is confounded by their ability to form biofilms. The research presented in this thesis explores if polymeric NPs can be used to encapsulate and deliver concentrated antibiotics by subsequent functionalisation of the NP with a cationic coating agent to kill antibiotic-resistant pathogenic planktonic and biofilm-formed bacteria and fungi. Each following chapter provides an introduction and aims, and includes the methods, results, discussion, and conclusions.

The research in chapter 2 investigates nanogel polymeric nanocarriers encapsulated with the antibiotics, tetracycline and lincomycin and subsequently functionalised with a cationic polyelectrolyte (bPEI) to facilitate increased electrostatic interaction between the functionalised particles and the anionic bacterial cell wall. The goal was to synthesis an antibiotic-NP based delivery system which could allow the antibiotics encapsulated inside to be useful again towards pathogens characterised as resistant to these antibiotics.

Chapter 3 advances the nanogel nanocarrier by surface functionalisation with the protease, Alcalase 2.4 L FG. The aim was to prove that functionalisation with the protease could degrade biofilms and allow an increased effect of the antibiotic encapsulated within the NP to in a more complex bacterial phenotype.

Chapter 4 aimed to combine the efforts of utilising concentrated antibiotics into a polymeric NP (chapter 2) and the active surface functionalisation, using Alcalase 2.4 L FG (chapter 3) and prove if this could be effective against an antibiotic-resistant biofilm-formed pathogen. The antimicrobial susceptibility profile of *Staphylococcus aureus* was analysed and found to be resistant to penicillin G. It so was chosen as the pathogen to test the efficacy of the antibiotic encapsulated, protease functionalised NPs. Pathogens of this nature often result in dire outcomes for patients and are very difficult to treat, for example, in infected chronic wounds.

Chapter 5 aimed to prove antibiotic encapsulated NPs, surface functionalised with a protease could also be used against fungal pathogens, broadening their therapeutic potential. Further emphasise on the reduced toxicity of NPs, by way of reducing the overall concentration of the active agent encapsulated whilst simultaneously maintaining the anti-biofilm effect is explored.

The final aim was to examine the cytotoxic effects of these NP formulations against mammalian cells to provide preliminary data regarding their potential application *in vivo*.

The thesis concludes in Chapter 6 with a summary of the project's findings, identifying areas deemed prudent for further study.

1.9 Ethical statement

There are no ethical implications in the project for public health and safety. The human cells used (HaCaT, a spontaneously transformed aneuploid immortal keratinocyte cell line from adult human skin and HEP G2, human liver cancer cell line) in this study are derived from a commercially available and well-characterised depository, AddexBio, T0020001 and the European Collection of Authenticated Cell Cultures (ECACC) at Public Health England, 85011430, respectively. This does not require the cell lines to be regulated by the Human Tissue Act 2004.

The chronic wound bacterial isolates were provided by the Hull Royal Hospital Pathology department and have been fully anonymised with no patient data collected. *Staphylococcus aureus subsp. aureus* Rosenbach (ATCC® 29213™), *Pseudomonas aeruginosa* (Schroeter) Migula (ATCC® 27853™), *Staphylococcus epidermidis* (Winslow and Winslow) Evans (ATCC® 35984™), *Klebsiella pneumoniae subsp. pneumoniae* (Schroeter) Trevisan (ATCC® 35657™), *Escherichia coli* (Migula) Castellani and Chalmers (ATCC® 25922™), *Enterococcus faecalis* (Andrewes and Horder) Schleifer and Kilpper-Balz (ATCC® 51299™) and *Candida albicans* (Robin) Berkhout (ATCC® MYA-2876) were purchased from ATCC and are commercially available from a well-characterised depository.

1.10 Reference list

- Abraira, V. E., & Ginty, D. D. (2013). The Sensory Neurons of Touch. *Neuron*, 79(4), 618-639.
- Abu Rabe, D. I., Al Awak, M. M., Yang, F., Okonjo, P. A., Dong, X., Teisl, L. R., Wang, P., Tang, Y., Pan, N., Sun, Y. P., & Yang, L. (2019). The dominant role of surface functionalization in carbon dots' photo-activated antibacterial activity. *International journal of nanomedicine*, 14, 2655–2665.
- Agarwal SP, Rajesh K (2007). Physical Pharmacy. CBS Publisher, Delhi, India, pp. 177-186.
- Aggarwal, S., Stewart, P. S., & Hozalski, R. M. (2015). Biofilm Cohesive Strength as a Basis for Biofilm Recalcitrance: Are Bacterial Biofilms Overdesigned? *Microbiology Insights*, 8(Suppl 2), 29–32.
- Aguado, B., Grim, J., Rosales, A., Watson-Capps, J. & Anseth, K. (2018) Engineering precision biomaterials for personalized medicine. *Science Translational Medicine*, 10(424), eaam8645.
- Ahmed, E. M. (2015). Hydrogel: Preparation, characterization, and applications: A review. *Journal of Advanced Research*, 6(2), 105–121.
- Akbarzadeh, A., Rezaei-Sadabady, R., Davaran, S., Joo, S. W., Zarghami, N., Hanifehpour, Y., Samiei, M., & Nejati-Koshki, K. (2013). Liposome: classification, preparation, and applications. *Nanoscale Research Letters*, 8(1), 102.
- Akhtar, M. F., Hanif, M., & Ranjha, N. M. (2016). Methods of synthesis of hydrogels ... A review. *Saudi Pharmaceutical Journal : SPJ*, 24(5), 554–559.
- Alavi, A., Sibbald, R., Phillips, T., Miller, O., Margolis, D., Marston, W., Woo, K., Romanelli, M. & Kirsner, R. (2016) What's new: Management of venous leg ulcers. *Journal of the American Academy of Dermatology*, 74(4), 643-664.
- Al-Awady, M., Fauchet, A., Greenway, G. & Paunov, V. (2017) Enhanced antimicrobial effect of berberine in nanogel carriers with cationic surface functionality. *J Mater Chem B*, 5(38), 7885-7897.
- Al-Awady, M., Greenway, G. and Paunov, V. (2015). Nanotoxicity of polyelectrolyte-functionalized titania nanoparticles towards microalgae and yeast: role of the particle concentration, size and surface charge. *RSC Advances*, 5(46), 37044-37059.
- Al-Awady, M., Weldrick, P., Hardman, M., Greenway, G. & Paunov, V. (2018) Amplified antimicrobial action of chlorhexidine encapsulated in PDAC-functionalized acrylate copolymer nanogel carriers. *Materials Chemistry Frontiers*, 2(11), 2032-2044.
- Albrecht, V., Limbago, B., Moran, G., Krishnadasan, A., Gorwitz, R., McDougal, L. and Talan, D. (2015). Staphylococcus aureus Colonization and Strain Type at Various Body Sites among Patients with a Closed Abscess and Uninfected Controls at U.S. Emergency Departments. *Journal of Clinical Microbiology*, 53(11), 3478-3484.
- Alcalase® 2.4 L FG. (2021) Strem.com. Available online: https://www.strem.com/uploads/technical_notes/06-3110tech.pdf [Accessed 10/1/2021].
- Aldred, K. J., Kerns, R. J., & Osheroff, N. (2014). Mechanism of Quinolone Action and Resistance. *Biochemistry*, 53(10), 1565–1574.
- Alexander, C. M., Kasza, I., Yen, C.-L. E., Reeder, S. B., Hernando, D., Gallo, R. L., Johoda, C, A, B., Horsley, V., & MacDougald, O. A. (2015). Dermal white adipose tissue: a new component of the thermogenic response. *Journal of Lipid Research*, 56(11), 2061–2069.
- Algburi, A., Comito, N., Kashtanov, D., Dicks, L. M. T., & Chikindas, M. L. (2017). Control of Biofilm Formation: Antibiotics and Beyond. *Applied and Environmental Microbiology*, 83(3), e02508–16.
- Alhariri, M., Azghani, A., & Omri, A. (2013). Liposomal antibiotics for the treatment of infectious diseases. *Expert opinion on drug delivery*, 10(11), 1515–1532.
- Ali, N. and Rosenblum, M. (2017). Regulatory T cells in skin. *Immunology*, 152(3), 372-381.
- Aliabadi, H. & Lavasanifar, A. (2005) Polymeric micelles for drug delivery. *Expert Opinion on Drug Delivery*, 3(1), 139-162.

- Aljuffali, I. A., Huang, C. H., & Fang, J. Y. (2015). Nanomedical strategies for targeting skin microbiomes. *Current drug metabolism*, 16(4), 255–271.
- Al-Sharqi, A., Apun, K., Vincent, M., Kanakaraju, D., Bilung, L. & Sum, M. (2019) Investigation of the antibacterial activity of Ag-NPs conjugated with a specific antibody against Staphylococcus aureus after photoactivation. *Journal of Applied Microbiology*, 128(1), 102-115.
- Aminov R. I. (2010). A brief history of the antibiotic era: lessons learned and challenges for the future. *Frontiers in microbiology*, 1, 134.
- Ansari, M., & Goswami, D. (2006) Shellac-Acrylic Emulsion Paint For Cementations Surfaces. *Pigment & Resin Technology*, 35 (4), 183-187.
- Anselmo, A. C. & Mitragotri, S. Nanoparticles in the clinic: an update. *Bioeng. Transl. Med.* 4, 1–16 (2019). This review comprehensively examines recent NP systems that are currently clinically approved or under clinical trials.
- Anyan, M. E., Amiri, A., Harvey, C. W., Tierra, G., Morales-Soto, N., Driscoll, C. M., Alber, M, S., & Shrout, J. D. (2014). Type IV pili interactions promote intercellular association and moderate swarming of *Pseudomonas aeruginosa*. *Proceedings of the National Academy of Sciences of the United States of America*, 111(50), 18013–18018.
- Arda, O., Göksügür, N. and Tüzün, Y. (2014). Basic histological structure and functions of facial skin. *Clinics in Dermatology*, 32(1), 3-13.
- Arias, L., Pessan, J., Vieira, A., Lima, T., Delbem, A. & Monteiro, D. (2018) Iron Oxide Nanoparticles for Biomedical Applications: A Perspective on Synthesis, Drugs, Antimicrobial Activity, and Toxicity. *Antibiotics*, 7(2), 46.
- Ashrafi, M., Novak-Frazer, L., Bates, M., Baguneid, M., Alonso-Rasgado, T., Xia, G., Rautemaa-Richardson, R. and Bayat, A. (2018). Validation of biofilm formation on human skin wound models and demonstration of clinically translatable bacteria-specific volatile signatures. *Scientific Reports*, 8(1).
- Asif, M., & Acharya, M. (2012). Quorum sensing: A nobel target for antibacterial agents. *Avicenna Journal of Medicine*, 2(4), 97–99.
- Assali, M., Zaid, A. N., Abdallah, F., Almasri, M., & Khayyat, R. (2017). Single-walled carbon nanotubes-ciprofloxacin nanoantibiotic: strategy to improve ciprofloxacin antibacterial activity. *International journal of nanomedicine*, 12, 6647–6659.
- Assis, L., Nedeljković, M. and Dessen, A. (2017). New strategies for targeting and treatment of multi-drug resistant Staphylococcus aureus. *Drug Resistance Updates*, 31, 1-14.
- Atkins, P., Trapp, C., & De Paula, J. (2010) *Physical chemistry*; Oxford Univ. Press: Oxford.
- Attinger, C., & Wolcott, R. (2012). Clinically Addressing Biofilm in Chronic Wounds. *Advances in Wound Care*, 1(3), 127–132.
- Ayyaswamy, P. S., Muzykantov, V., Eckmann, D. M., & Radhakrishnan, R. (2013). Nanocarrier Hydrodynamics and Binding in Targeted Drug Delivery: Challenges in Numerical Modeling and Experimental Validation. *Journal of nanotechnology in engineering and medicine*, 4(1), 101011–1010115.
- Azouka, A., Huggett, R., & Harrison, A. (1993) The Production Of Shellac And Its General And Dental Uses: A Review. *Journal of Oral Rehabilitation*, 20 (4), 393-400.
- B. Aslam, W. Wang, M. Arshad, M. Khurshid, S. Muzammil, M. Rasool, M. Nisar, R. Alvi, M. Aslam, M. Qamar, M. Salamat and Z. Baloch, *Infection and Drug Resistance*, 2018, Volume 11, 1645-1658.
- B. Raymond, *Evolutionary Applications*, 2019, 12, 1079-1091.
- Baelo, A., Levato, R., Julián, E., Crespo, A., Astola, J., Gavaldà, J., Engel, E., Mateos-Timoneda, M. and Torrents, E. (2015). Disassembling bacterial extracellular matrix with DNase-coated nanoparticles to enhance antibiotic delivery in biofilm infections. *Journal of Controlled Release*, 209, 150-158.
- Baidamshina, D., Koroleva, V., Trizna, E., Pankova, S., Agafonova, M., Chirkova, M., Vasileva, O., Akhmetov, N., Shubina, V., Porfiriyev, A., Semenova, E., Sachenkov, O., Bogachev, M., Artyukhov, V., Baltina, T., Holyavka, M. & Kayumov, A. (2020) Anti-biofilm and wound-healing activity of chitosan-immobilized Ficin. *International Journal of Biological Macromolecules*, 164, 4205-4217.

- Baidamshina, D., Trizna, E., Holyavka, M., Bogachev, M., Artyukhov, V., Akhatova, F., Rozhina, E., Fakhruddin, R. & Kayumov, A. (2017) Targeting microbial biofilms using Ficin, a nonspecific plant protease. *Scientific Reports*, 7(1).
- Bala, I., Bhardwaj, V., Hariharan, S., & Kumar, M. (2006) Analytical Methods For Assay Of Ellagic Acid And Its Solubility Studies. *Journal of Pharmaceutical and Biomedical Analysis*, 40 (1), 206-210.
- Balazs, D. A., & Godbey, W. (2011). Liposomes for Use in Gene Delivery. *Journal of Drug Delivery*, 2011, 326497.
- Balogh, L., Swanson, D., Tomalia, D., Hagnauer, G. & McManus, A. (2001) Dendrimer–Silver Complexes and Nanocomposites as Antimicrobial Agents. *Nano Letters*, 1(1), 18-21.
- Banerjee, A., Qi, J., Gogoi, R., Wong, J., & Mitragotri, S. (2016). Role of nanoparticle size, shape and surface chemistry in oral drug delivery. *Journal of controlled release : official journal of the Controlled Release Society*, 238, 176–185.
- Baptista, P., McCusker, M., Carvalho, A., Ferreira, D., Mohan, N., Martins, M. and Fernandes, A., 2018. Nano-Strategies to Fight Multidrug Resistant Bacteria—“A Battle of the Titans”. *Frontiers in Microbiology*, 9.
- Baroni, A., Buommino, E., De Gregorio, V., Ruocco, E., Ruocco, V., & Wolf, R. (2012). Structure and function of the epidermis related to barrier properties. *Clinics in dermatology*, 30(3), 257-262.
- Barreiro-Iglesias, R., Alvarez-Lorenzo, C., & Concheiro, A. (2003) Controlled Release Of Estradiol Solubilized In Carbopol/Surfactant Aggregates. *Journal of Controlled Release*, 93 (3), 319-330.
- Barua, S., & Mitragotri, S. (2014). Challenges associated with Penetration of Nanoparticles across Cell and Tissue Barriers: A Review of Current Status and Future Prospects. *Nano Today*, 9(2), 223–243.
- Battaglia, L., Panciani, P., Muntoni, E., Capucchio, M., Biasibetti, E., De Bonis, P., Mioletti, S., Fontanella, M. & Swaminathan, S. (2018) Lipid nanoparticles for intranasal administration: application to nose-to-brain delivery. *Expert Opinion on Drug Delivery*, 15(4), 369-378.
- Bazaliński, D., Kózka, M., Karnas, M., & Więch, P. (2019). Effectiveness of Chronic Wound Debridement with the Use of Larvae of *Lucilia Sericata*. *Journal of clinical medicine*, 8(11), 1845.
- Begines, B., Ortiz, T., Pérez-Aranda, M., Martínez, G., Merinero, M., Argüelles-Arias, F., & Alcludia, A. (2020). Polymeric Nanoparticles for Drug Delivery: Recent Developments and Future Prospects. *Nanomaterials (Basel, Switzerland)*, 10(7), 1403.
- Behzadi, S., Serpooshan, V., Tao, W., Hamaly, M. A., Alkawareek, M. Y., Dreaden, E. C., Brown, D., Alkilany, A. M., Farokhzad, O. C., & Mahmoudi, M. (2017). Cellular uptake of nanoparticles: journey inside the cell. *Chemical Society reviews*, 46(14), 4218–4244.
- Beiras-Fernandez, A., Vogt, F., Sodian, R., & Weis, F. (2010). Daptomycin: a novel lipopeptide antibiotic against Gram-positive pathogens. *Infection and Drug Resistance*, 3, 95–101.
- Bellan, L., Pearsall, M., Cropek, D., & Langer, R. (2012) A 3D Interconnected Microchannel Network Formed In Gelatin By Sacrificial Shellac Microfibers. *Advanced Materials*, 24 (38), 5187-5191.
- Bellio, P., Luzi, C., Mancini, A., Cracchiolo, S., Passacantando, M., Di Pietro, L., Perilli, M., Amicosante, G., Santucci, S. & Celenza, G. (2018) Cerium oxide nanoparticles as potential antibiotic adjuvant. Effects of CeO₂ nanoparticles on bacterial outer membrane permeability. *Biochimica et Biophysica Acta (BBA) - Biomembranes*, 1860(11), 2428-2435.
- Beltrán-Gracia, E., López-Camacho, A., Higuera-Ciapara, I., Velázquez-Fernández, J. & Vallejo-Cardona, A. (2019) Nanomedicine review: clinical developments in liposomal applications. *Cancer Nanotechnology*, 10(1).
- Berlanga, M., & Guerrero, R. (2016). Living together in biofilms: the microbial cell factory and its biotechnological implications. *Microbial Cell Factories*, 15, 165.
- Bertollo, L., Lutkemeyer, D. and Levin, A. (2018). Are antimicrobial stewardship programs effective strategies for preventing antibiotic resistance? A systematic review. *American Journal of Infection Control*, 46(7), 824-836.
- Beyth, N., Houry-Haddad, Y., Baraness-Hadar, L., Yudovin-Farber, I., Domb, A. J., & Weiss, E. I. (2008). Surface antimicrobial activity and biocompatibility of incorporated polyethylenimine nanoparticles. *Biomaterials*, 29(31), 4157–4163.
- Beyth, N., Houry-Haddad, Y., Domb, A., Khan, W., & Hazan, R. (2015). Alternative Antimicrobial Approach: Nano-Antimicrobial Materials. *Evidence-Based Complementary and Alternative Medicine : eCAM*, 2015, 246012.

- Billings, N., Birjiniuk, A., Samad, T., Doyle, P., & Ribbeck, K. (2015) Material Properties Of Biofilms—A Review Of Methods For Understanding Permeability And Mechanics. *Reports on Progress in Physics*, 78 (3), 036601.
- Bilsland, E., Tavella, T. A., Krogh, R., Stokes, J. E., Roberts, A., Ajioka, J., Spring, D, R., Andricopulo, A, D., Costa, F, T, M., & Oliver, S. G. (2018). Antiplasmodial and trypanocidal activity of violacein and deoxyviolacein produced from synthetic operons. *BMC Biotechnology*, 18, 22.
- Binda, E., Marinelli, F., & Marcone, G. L. (2014). Old and New Glycopeptide Antibiotics: Action and Resistance. *Antibiotics*, 3(4), 572–594.
- Bintang Ilhami, F., Huang, S., Chen, J., Kao, C. & Cheng, C. (2020) Multifunctional adenine-functionalized supramolecular micelles for highly selective and effective cancer chemotherapy. *Polymer Chemistry*, 11(4), 849-856.
- Bjarnsholt, T., Alhede, M., Alhede, M., Eickhardt-Sørensen, S., Moser, C., Kühl, M., Jensen, P., & Høiby, N. (2013) The In Vivo Biofilm. *Trends in Microbiology*, 21, 466-474.
- Blanco, E., Shen, H. & Ferrari, M. (2015) Principles of nanoparticle design for overcoming biological barriers to drug delivery. *Nature Biotechnology*, 33(9), 941-951.
- Bobo, D., Robinson, K. J., Islam, J., Thurecht, K. J. & Corrie, S. R. (2016) Nanoparticle-based medicines: a review of FDA-approved materials and clinical trials to date. *Pharm. Res.* 33, 2373–2387.
- Bogino, P. C., de las Mercedes Oliva, M., Sorroche, F. G., & Giordano, W. (2013). The Role of Bacterial Biofilms and Surface Components in Plant-Bacterial Associations. *International Journal of Molecular Sciences*, 14(8), 15838–15859.
- Boles, B. & Horswill, A. (2011) Staphylococcal biofilm disassembly. *Trends in Microbiology*, 19(9), 449-455.
- Bonacucina, G., Martelli, S., & Palmieri, G. (2004) Rheological, Mucoadhesive And Release Properties Of Carbopol Gels In Hydrophilic Cosolvents. *International Journal of Pharmaceutics*, 282 (1-2), 115-130.
- Bontha, S., Kabanov, A. V., & Bronich, T. K. (2006). Polymer micelles with cross-linked ionic cores for delivery of anticancer drugs. *Journal of controlled release : official journal of the Controlled Release Society*, 114(2), 163–174.
- Borovička, J., Metheringham, W., Madden, L., Walton, C., Stoyanov, S. & Paunov, V. (2013b) Photothermal Colloid Antibodies for Shape-Selective Recognition and Killing of Microorganisms. *Journal of the American Chemical Society*, 135(14), 5282-5285.
- Borovička, J., Stoyanov, S. & Paunov, V. (2013a) Nanoantibiotic Particles for Shape and Size Recognition of Pathogens. *MRS Proceedings*, 1498, 127-132.
- Bowler, P. G. (2018) Antibiotic resistance and biofilm tolerance: a combined threat in the treatment of chronic infections. *J Wound Care*, 27(5), 273-277.
- Boyko, T. V., Longaker, M. T., & Yang, G. P. (2018). Review of the Current Management of Pressure Ulcers. *Advances in wound care*, 7(2), 57–67.
- Brem, H., Stojadinovic, O., Diegelmann, R. F., Entero, H., Lee, B., Pastar, I., Golinko, M., Rosenberg, H., & Tomic-Canic, M. (2007). Molecular markers in patients with chronic wounds to guide surgical debridement. *Molecular medicine (Cambridge, Mass.)*, 13(1-2), 30–39.
- Brett, M. and Bradfute, S. (2015). Staphylococcus aureus: Current State of Prevalence, Impact, and Vaccine Development. *Current Pharmaceutical Design*, 21(16), 2131-2135.
- Briley, K. A., Camilleri, L. B., Zane, G. M., Wall, J. D., & Fields, M. W. (2014). Biofilm growth mode promotes maximum carrying capacity and community stability during product inhibition syntrophy. *Frontiers in Microbiology*, 5, 693.
- Bronich, T., Vinogradov, S. & Kabanov, A. (2001) Interaction of Nanosized Copolymer Networks with Oppositely Charged Amphiphilic Molecules. *Nano Letters*, 1(10), 535-540.
- Brown, H. L., Reuter, M., Hanman, K., Betts, R. P., & van Vliet, A. H. M. (2015). Prevention of Biofilm Formation and Removal of Existing Biofilms by Extracellular DNases of *Campylobacter jejuni* . *PLoS ONE*, 10(3), e0121680.
- Buch, K., Penning, M., Wächtersbach, E., Maskos, M., & Langguth, P. (2009) Investigation Of Various Shellac Grades: Additional Analysis For Identity. *Drug Development and Industrial Pharmacy*, 35 (6), 694-703.

- Busscher, H. J., & van der Mei, H. C. (2012). How Do Bacteria Know They Are on a Surface and Regulate Their Response to an Adhering State? *PLoS Pathogens*, 8(1), e1002440.
- Bussy, C., Ali-Boucetta, H. & Kostarelos, K. (2012) Safety Considerations for Graphene: Lessons Learnt from Carbon Nanotubes. *Accounts of Chemical Research*, 46(3), 692-701.
- C. Ardal, M. Balasegaram, R. Laxminarayan, D. McAdams, K. Outtersson, J. H. Rex and N. Sumpradit, *Nat. Rev. Microbiol.*, 2020, 18, 267-274.
- Cambiaso-Daniel, J., Boukoulas, S., Bitz, G. H., Branski, L. K., Herndon, D. N., & Culnan, D. M. (2018). Topical Antimicrobials in Burn Care: Part 1-Topical Antiseptics. *Annals of plastic surgery*, 10.1097/SAP.0000000000001297.
- Campbell S., Smeets N. (2019) Drug Delivery: Polymers in the Development of Controlled Release Systems. In: Jafar Mazumder M., Sheardown H., Al-Ahmed A. (eds) *Functional Polymers. Polymers and Polymeric Composites: A Reference Series*. Springer, Cham.
- Campbell, A., Stoyanov, S., & Paunov, V. (2009) Novel Multifunctional Micro-Ampoules For Structuring And Encapsulation. *ChemPhysChem*, 10 (15), 2599-2602.
- Campbell, D. and Koch, M. (2017). Living in Peace: Host-Microbiota Mutualism in the Skin. *Cell Host & Microbe*, 21(4), 419-420.
- Castaneda, P., McLaren, A., Tavaziva, G., & Overstreet, D. (2016). Biofilm Antimicrobial Susceptibility Increases With Antimicrobial Exposure Time. *Clinical Orthopaedics and Related Research*, 474(7), 1659–1664.
- Caster, J. M., Patel, A. N., Zhang, T. & Wang, A. (2017) Investigational nanomedicines in 2016: a review of nanotherapeutics currently undergoing clinical trials. *Wiley Interdiscip. Rev. Nanomed. Nanobiotechnol.* 9, 1416.
- Caudill, E., Hernandez, R., Johnson, K., O'Rourke, J., Zhu, L., Haynes, C., Feng, Z. & Pedersen, J. (2020) Wall teichoic acids govern cationic gold nanoparticle interaction with Gram-positive bacterial cell walls. *Chemical Science*, 11, 4106-4118.
- Chacón-Lozán, F., Rodríguez-Torres, M. & Rojas, R. (2018) A1201 Hemodynamic Management of High Blood Pressure. *Journal of Hypertension*, 36, e116.
- Chakraborti, C., Sahoo, S., & Behera, P. (2014) Role Of Different Biodegradable Polymers On The Permeability Of Ciprofloxacin. *Journal of Advanced Pharmaceutical Technology & Research*, 5 (3), 140.
- Chang, R., Raw, A., Lionberger, R., & Yu, L. (2012) Generic Development Of Topical Dermatologic Products: Formulation Development, Process Development, And Testing Of Topical Dermatologic Products. *The AAPS Journal*, 15 (1), 41-52.
- Chanphai, P., Thomas, T. & Tajmir-Riahi, H. (2020) Application and biomolecular study of functionalized folic acid-dendrimer nanoparticles in drug delivery. *Journal of Biomolecular Structure and Dynamics*, 1-8.
- Chauhan, O., Raju, P., Singh, A., & Bawa, A. (2011) Shellac And Aloe-Gel-Based Surface Coatings For Maintaining Keeping Quality Of Apple Slices. *Food Chemistry*, 126 (3), 961-966.
- Chen, B., Su, Y., Chang, C., Burnouf, P., Chuang, K., Chen, C., Cheng, T., Chen, Y., Wu, J. & Roffler, S. (2016) Measurement of Pre-Existing IgG and IgM Antibodies against Polyethylene Glycol in Healthy Individuals. *Analytical Chemistry*, 88(21), 10661-10666.
- Chen, C., Beck-Tan, N., Dhurjati, P., van Dyk, T., LaRossa, R. & Cooper, S. (2000) Quaternary Ammonium Functionalized Poly(propylene imine) Dendrimers as Effective Antimicrobials: Structure–Activity Studies. *Biomacromolecules*, 1(3), 473-480.
- Chen, D., Parayath, N., Ganesh, S., Wang, W. & Amiji, M. (2019) The role of apolipoprotein- and vitronectin-enriched protein corona on lipid nanoparticles for in vivo targeted delivery and transfection of oligonucleotides in murine tumor models. *Nanoscale*, 11(40), 18806-18824.
- Chen, X., Chen, H., Feng, Y., He, R., & Yang, Z. (2011) Status Of Two Species Of Lac Insects In The Genus *Kerria* From China Based On Morphological, Cellular, And Molecular Evidence. *Journal of Insect Science*, 11 (106), 1-14.
- Cheng, K., Khoo, Z., Lo, N., & Tan, W. (2020) Chemmangattuvalappil, N. Design And Performance Optimisation Of Detergent Product Containing Binary Mixture Of Anionic-Nonionic Surfactants. *Heliyon*, 6 (5), e03861.

- Cheng, X. & Lee, R. (2016) The role of helper lipids in lipid nanoparticles (LNPs) designed for oligonucleotide delivery. *Advanced Drug Delivery Reviews*, 99, 129-137.
- Cheng, Y., Qu, H., Ma, M., Xu, Z., Xu, P., Fang, Y. & Xu, T. (2007) Polyamidoamine (PAMAM) dendrimers as biocompatible carriers of quinolone antimicrobials: An in vitro study. *European Journal of Medicinal Chemistry*, 42(7), 1032-1038.
- Chithrani, B. & Chan, W. (2007) Elucidating the Mechanism of Cellular Uptake and Removal of Protein-Coated Gold Nanoparticles of Different Sizes and Shapes. *Nano Letters*, 7(6), 1542-1550.
- Choi, O. & Hu, Z. (2008) Size Dependent and Reactive Oxygen Species Related Nanosilver Toxicity to Nitrifying Bacteria. *Environmental Science & Technology*, 42(12), 4583-4588.
- Choo, J., Nixon, J., Nelson, A., & McGinnis, E. (2019). Autolytic debridement for pressure ulcers. *The Cochrane Database of Systematic Reviews*, 2019(6), CD011331.
- Cipolla, D., Blanchard, J., & Gonda, I. (2016). Development of Liposomal Ciprofloxacin to Treat Lung Infections. *Pharmaceutics*, 8(1), 6.
- Cipolla, D., Shekunov, B., Blanchard, J., & Hickey, A. (2014). Lipid-based carriers for pulmonary products: preclinical development and case studies in humans. *Advanced drug delivery reviews*, 75, 53–80.
- Cockeram, H. S., & Levine, S. A. (1961) The Physical and Chemical Properties of Shellac. *Journal of the Society of Cosmetic Chemists*, 12, 316-323.
- Coll Ferrer, M. C., Dastgheyb, S., Hickok, N. J., Eckmann, D. M., & Composto, R. J. (2014). Designing nanogel carriers for antibacterial applications. *Acta biomaterialia*, 10(5), 2105–2111.
- Collins, F. & Varmus, H. (2015) A New Initiative on Precision Medicine. *New England Journal of Medicine*, 372(9), 793-795.
- Common lac insect (*Kerria lacca*). (2018) <https://www.forestryimages.org/browse/detail.cfm?imgnum=5385241> [Accessed 16/11/2020].
- Cone R. A. (2009). Barrier properties of mucus. *Advanced drug delivery reviews*, 61(2), 75–85.
- Cooley, M., Sarode, A., Hoore, M., Fedosov, D., Mitragotri, S. & Sen Gupta, A. (2018) Influence of particle size and shape on their margination and wall-adhesion: implications in drug delivery vehicle design across nano-to-micro scale. *Nanoscale*, 10(32), 15350-15364.
- Cox, A., Andreozzi, P., Dal Magro, R., Fiordaliso, F., Corbelli, A., Talamini, L., Chinello, C., Raimondo, F., Magni, F., Tringali, M., Krol, S., Jacob Silva, P., Stellacci, F., Masserini, M. & Re, F. (2018) Evolution of Nanoparticle Protein Corona across the Blood–Brain Barrier. *ACS Nano*, 12(7), 7292-7300.
- Cui, L., Chen, P., Chen, S., Yuan, Z., Yu, C., Ren, B. & Zhang, K. (2013) In Situ Study of the Antibacterial Activity and Mechanism of Action of Silver Nanoparticles by Surface-Enhanced Raman Spectroscopy. *Analytical Chemistry*, 85(11), 5436-5443.
- Cundell, A. (2016). Microbial Ecology of the Human Skin. *Microbial Ecology*.
- D’Orazio, J., Jarrett, S., Amaro-Ortiz, A., & Scott, T. (2013). UV Radiation and the Skin. *International Journal of Molecular Sciences*, 14(6), 12222–12248.
- da Cruz, L., Hill, R., Chen, X., & Gillam, D. (2018) Dentine Tubule Occlusion By Novel Bioactive Glass-Based Toothpastes. *International Journal of Dentistry*, 2018, 1-10.
- Da Silva, C. G., Peters, G. J., Ossendorp, F., & Cruz, L. J. (2017a). The potential of multi-compound nanoparticles to bypass drug resistance in cancer. *Cancer Chemotherapy and Pharmacology*, 80(5), 881–894.
- da Silva, R. (2017b) Bacterial and Fungal Proteolytic Enzymes: Production, Catalysis and Potential Applications. *Applied Biochemistry and Biotechnology*, 183(1), 1-19.
- Da Silva-Candal, A., Brown, T., Krishnan, V., Lopez-Loureiro, I., Ávila-Gómez, P., Pusuluri, A., Pérez-Díaz, A., Correa-Paz, C., Hervella, P., Castillo, J., Mitragotri, S. & Campos, F. (2019) Shape effect in active targeting of nanoparticles to inflamed cerebral endothelium under static and flow conditions. *Journal of Controlled Release*, 309, 94-105.

- Dakal, T., Kumar, A., Majumdar, R. & Yadav, V. (2016) Mechanistic Basis of Antimicrobial Actions of Silver Nanoparticles. *Frontiers in Microbiology*, 7.
- Dal Magro, R., Ornaghi, F., Cambianica, I., Beretta, S., Re, F., Musicanti, C., Rigolio, R., Donzelli, E., Canta, A., Ballarini, E., Cavaletti, G., Gasco, P. & Sancini, G. (2017) ApoE-modified solid lipid nanoparticles: A feasible strategy to cross the blood-brain barrier. *Journal of Controlled Release*, 249, 103-110.
- Darwin, E., & Tomic-Canic, M. (2018). Healing Chronic Wounds: Current Challenges and Potential Solutions. *Current dermatology reports*, 7(4), 296–302.
- Das, A.A.K., & Paunov, V.N. (2014) Synthetic Colloids with Antimicrobial Action, *Microbiologist*, 16–19.
- Davenport, E. K., Call, D. R., & Beyenal, H. (2014). Differential protection from tobramycin by extracellular polymeric substances from *Acinetobacter baumannii* and *Staphylococcus aureus* biofilms. *Antimicrobial agents and chemotherapy*, 58(8), 4755–4761.
- Davies, J., & Davies, D. (2010). Origins and Evolution of Antibiotic Resistance. *Microbiology and Molecular Biology Reviews* : *MMBR*, 74(3), 417–433.
- Davies, J., & Wright, G. (1997) Bacterial Resistance to Aminoglycoside Antibiotics. *Trends in Microbiology*, 5, 234-239.
- Debler, E. W., Kaufmann, G. F., Kirchdoerfer, R. N., Mee, J. M., Janda, K. D., & Wilson, I. A. (2007). Crystal Structures of a Quorum-Quenching Antibody. *Journal of Molecular Biology*, 368(5), 1392–1402.
- Delfi, M., Ghomi, M., Zarrabi, A., Mohammadinejad, R., Taraghdari, Z., Ashrafizadeh, M., Zare, E., Agarwal, T., Padil, V., Mokhtari, B., Rossi, F., Perale, G., Sillanpaa, M., Borzacchiello, A., Kumar Maiti, T. & Makvandi, P. (2020) Functionalization of Polymers and Nanomaterials for Biomedical Applications: Antimicrobial Platforms and Drug Carriers. *Prosthesis*, 2(2), 117-139.
- Demidova-Rice, T. N., Hamblin, M. R., & Herman, I. M. (2012). Acute and Impaired Wound Healing: Pathophysiology and Current Methods for Drug Delivery, Part 1: Normal and Chronic Wounds: Biology, Causes, and Approaches to Care. *Advances in Skin & Wound Care*, 25(7), 304–314.
- Derraik, J. G. B., Rademaker, M., Cutfield, W. S., Pinto, T. E., Tregurtha, S., Faherty, A., Peart, J. M., Drury, P. L., & Hofman, P. L. (2014). Effects of Age, Gender, BMI, and Anatomical Site on Skin Thickness in Children and Adults with Diabetes. *PLoS ONE*, 9(1), e86637.
- Díez-Pascual, A. (2020) Antibacterial Action of Nanoparticle Loaded Nanocomposites Based on Graphene and Its Derivatives: A Mini-Review. *International Journal of Molecular Sciences*, 21(10), 3563. Zou, X., Zhang, L., Wang, Z. & Luo, Y. (2016) Mechanisms of the Antimicrobial Activities of Graphene Materials. *Journal of the American Chemical Society*, 138(7), 2064-2077.
- Dige, I., Baelum, V., Nyvad, B., & Schlafer, S. (2016). Monitoring of extracellular pH in young dental biofilms grown *in vivo* in the presence and absence of sucrose. *Journal of Oral Microbiology*, 8, 10.
- Din, F. U., Aman, W., Ullah, I., Qureshi, O. S., Mustapha, O., Shafique, S., & Zeb, A. (2017). Effective use of nanocarriers as drug delivery systems for the treatment of selected tumors. *International journal of nanomedicine*, 12, 7291–7309.
- Dölen, Y., Valente, M., Tagit, O., Jäger, E., Van Dinther, E., van Riessen, N. K., Hruby, M., Gileadi, U., Cerundolo, V., & Figdor, C. G. (2020). Nanovaccine administration route is critical to obtain pertinent iNKT cell help for robust anti-tumor T and B cell responses. *Oncoimmunology*, 9(1), 1738813.
- Dong, W., Ye, J., Zhou, J., Wang, W., Wang, H., Zheng, X., Yang, Y., Xia, X. & Liu, Y. (2020b) Comparative study of mucoadhesive and mucus-penetrative nanoparticles based on phospholipid complex to overcome the mucus barrier for inhaled delivery of baicalein. *Acta Pharmaceutica Sinica B*, 10(8), 1576-1585.
- Dong, X., Liang, W., Meziari, M. J., Sun, Y. P., & Yang, L. (2020a). Carbon Dots as Potent Antimicrobial Agents. *Theranostics*, 10(2), 671–686.
- Dong, Y. H., Xu, J. L., Li, X. Z., & Zhang, L. H. (2000). AiiA, an enzyme that inactivates the acylhomoserine lactone quorum-sensing signal and attenuates the virulence of *Erwinia carotovora*. *Proceedings of the National Academy of Sciences of the United States of America*, 97(7), 3526–3531.

- Dong, Y., Love, K., Dorkin, J., Sirirungruang, S., Zhang, Y., Chen, D., Bogorad, R., Yin, H., Chen, Y., Vegas, A., Alabi, C., Sahay, G., Olejnik, K., Wang, W., Schroeder, A., Lytton-Jean, A., Siegwart, D., Akinc, A., Barnes, C., Barros, S., Carioto, M., Fitzgerald, K., Hettinger, J., Kumar, V., Novobrantseva, T., Qin, J., Querbes, W., Koteliansky, V., Langer, R. & Anderson, D. (2014) Lipopeptide nanoparticles for potent and selective siRNA delivery in rodents and nonhuman primates. *Proceedings of the National Academy of Sciences*, 111(11), 3955-3960.
- Doron, S., & Davidson, L. E. (2011). Antimicrobial Stewardship. *Mayo Clinic Proceedings*, 86(11), 1113–1123.
- Douros, A., Grabowski, K. and Stahlmann, R. (2015). Drug–drug interactions and safety of linezolid, tedizolid, and other oxazolidinones. *Expert Opinion on Drug Metabolism & Toxicology*, 11(12), 1849-1859.
- Duan, F., Feng, X., Jin, Y., Liu, D., Yang, X., Zhou, G., Liu, D., Li, Z., Liang, X. J., & Zhang, J. (2017). Metal-carbenicillin framework-based nanoantibiotics with enhanced penetration and highly efficient inhibition of MRSA. *Biomaterials*, 144, 155–165.
- Dumortier, G., Grossiord, J., Agnely, F., & Chaumeil, J. (2006) A Review Of Poloxamer 407 Pharmaceutical And Pharmacological Characteristics. *Pharmaceutical Research*, 23 (12), 2709-2728.
- Durán, N., Durán, M., de Jesus, M., Seabra, A., Fávoro, W. & Nakazato, G. (2016) Silver nanoparticles: A new view on mechanistic aspects on antimicrobial activity. *Nanomedicine: Nanotechnology, Biology and Medicine*, 12(3), 789-799.
- Dvorak, J. E., Ladhani, H. A., & Claridge, J. A. (2021). Review of Sepsis in Burn Patients in 2020. *Surgical infections*, 22(1), 37–43.
- Eckmann, D. M., Composto, R. J., Tsourkas, A., & Muzykantov, V. R. (2014). Nanogel Carrier Design for Targeted Drug Delivery. *Journal of materials chemistry. B*, 2(46), 8085–8097.
- El Zowalaty, M., Ibrahim, N., Salama, M., Shamel, K., Usman, M. and Zainuddin, N. (2013). Synthesis, characterization, and antimicrobial properties of copper nanoparticles. *International Journal of Nanomedicine*, 4467.
- Eming, S. A., Martin, P., & Tomic-Canic, M. (2014). Wound repair and regeneration: Mechanisms, signaling, and translation. *Science Translational Medicine*, 6(265), 265.
- Engeland, C. G., Sabzehei, B., & Marucha, P. T. (2009). Sex Hormones and Mucosal Wound Healing. *Brain, Behavior, and Immunity*, 23(5), 629–635.
- Ensign, L., Cone, R. & Hanes, J. (2012) Oral drug delivery with polymeric nanoparticles: The gastrointestinal mucus barriers. *Advanced Drug Delivery Reviews*, 64(6), 557-570.
- Enzler, M. J., Berbari, E., & Osmon, D. R. (2011). Antimicrobial prophylaxis in adults. *Mayo Clinic proceedings*, 86(7), 686–701.
- Fagerlund, A., Langsrud, S., Heir, E., Mikkelsen, M. I., & Møretrø, T. (2016). Biofilm Matrix Composition Affects the Susceptibility of Food Associated Staphylococci to Cleaning and Disinfection Agents. *Frontiers in microbiology*, 7, 856.
- Falk N. A. (2019). Surfactants as Antimicrobials: A Brief Overview of Microbial Interfacial Chemistry and Surfactant Antimicrobial Activity. *Journal of surfactants and detergents*, 22(5), 1119–1127.
- Fan, Y., Pauer, A., Gonzales, A. & Fenniri, H. (2019) Enhanced antibiotic activity of ampicillin conjugated to gold nanoparticles on PEGylated rosette nanotubes. *International Journal of Nanomedicine*, Volume 14, 7281-7289.
- Fang, J., Leu, Y., Wang, Y., & Tsai, Y. (2002) In Vitro Topical Application And In Vivo Pharmacodynamic Evaluation Of Nonivamide Hydrogels Using Wistar Rat As An Animal Model. *European Journal of Pharmaceutical Sciences*, 15 (5), 417-423.
- Farag, Y., & Leopold, C. (2009) Physicochemical Properties Of Various Shellac Types. *Dissolution Technologies*, 16 (2), 33-39.
- Farage, M. A., Miller, K. W., Elsner, P., & Maibach, H. I. (2013). Characteristics of the Aging Skin. *Advances in Wound Care*, 2(1), 5–10.
- Farahavar, G., Abolmaali, S., Gholijani, N. & Nejatollahi, F. (2019) Antibody-guided nanomedicines as novel breakthrough therapeutic, diagnostic and theranostic tools. *Biomaterials Science*, 7(10), 4000-4016.

- Felczak, A., Zawadzka, K., Wrońska, N., Janaszewska, A., Klajnert, B., Bryszewska, M., Appelhans, D., Voit, B. & Lisowska, K. (2013) Enhancement of antimicrobial activity by co-administration of poly(propylene imine) dendrimers and nadifloxacin. *New Journal of Chemistry*, 37(12), 4156.
- Feng, Z., Gunsolus, I., Qiu, T., Hurley, K., Nyberg, L., Frew, H., Johnson, K., Vartanian, A., Jacob, L., Lohse, S., Torelli, M., Hamers, R., Murphy, C. & Haynes, C. (2015) Impacts of gold nanoparticle charge and ligand type on surface binding and toxicity to Gram-negative and Gram-positive bacteria. *Chemical Science*, 6(9), 5186-5196.
- Fenton, O. S., Olafson, K. N., Pillai, P. S., Mitchell, M. J. & Langer, R. (2018) Advances in biomaterials for drug delivery. *Adv. Mater.* 30, 1705328.
- Fischer, D., Li, Y., Ahlemeyer, B., Krieglstein, J., & Kissel, T. (2003) In vitro cytotoxicity testing of polycations: influence of polymer structure on cell viability and hemolysis, *Biomaterials*, (24)7, 1121-1131.
- Fleming, A. (1929). On the Antibacterial Action of Cultures of a Penicillium, with Special Reference to their Use in the Isolation of B. influenzae. *British Journal of Experimental Pathology*, 10(3), 226–236.
- Fleming, D., & Rumbaugh, K. P. (2017). Approaches to Dispersing Medical Biofilms. *Microorganisms*, 5(2), 15.
- Flemming, H., Wingender, J., Szewzyk, U., Steinberg, P., Rice, S. & Kjelleberg, S. (2016) Biofilms: an emergent form of bacterial life. *Nature Reviews Microbiology*, 14(9), 563-575.
- Flemming, R. G., Capelli, C. C., Cooper, S. L., & Proctor, R. A. (2000a). Bacterial colonization of functionalized polyurethanes. *Biomaterials*, 21(3), 273–281.
- Foier, K., Raemdonck, K., De Smedt, S. C., Demeester, J., Coenye, T., & Braeckmans, K. (2014). Lipid and polymer nanoparticles for drug delivery to bacterial biofilms. *Journal of controlled release : official journal of the Controlled Release Society*, 190, 607–623.
- Frykberg, R. G., & Banks, J. (2015). Challenges in the Treatment of Chronic Wounds. *Advances in Wound Care*, 4(9), 560–582.
- Fuller, M., & Köper, I. (2019) Biomedical Applications Of Polyelectrolyte Coated Spherical Gold Nanoparticles. *Nano Convergence*, 6 (1).
- Galbadage, T., Liu, D., Alemany, L. B., Pal, R., Tour, J. M., Gunasekera, R. S., & Cirillo, J. D. (2019). Molecular Nanomachines Disrupt Bacterial Cell Wall, Increasing Sensitivity of Extensively Drug-Resistant *Klebsiella pneumoniae* to Meropenem. *ACS nano*, 13(12), 14377–14387.
- Ganapathy, N., Venkataraman, S. S., Daniel, R., Aravind, R. J., & Kumarakrishnan, V. M. (2012) Molecular biology of wound healing. *Journal of Pharmacy & bioallied sciences*, 23(3), 4(2), 629-635.
- Gao, W., Thamphiwatana, S., Angsantikul, P., & Zhang, L. (2014). Nanoparticle Approaches against Bacterial Infections. *Wiley Interdisciplinary Reviews. Nanomedicine and Nanobiotechnology*, 6(6), 532–547.
- Gao, Y., Wu, J., Ren, X., Tan, X., Hayat, T., Alsaedi, A., Cheng, C. & Chen, C. (2017) Impact of graphene oxide on the antibacterial activity of antibiotics against bacteria. *Environmental Science: Nano*, 4(5), 1016-1024.
- Garapaty, A. & Champion, J. (2019) Shape of ligand immobilized particles dominates and amplifies the macrophage cytokine response to ligands. *PLOS ONE*, 14(5), e0217022.
- García-Gallego, S., Franci, G., Falanga, A., Gómez, R., Folliero, V., Galdiero, S., de la Mata, F. & Galdiero, M. (2017) Function Oriented Molecular Design: Dendrimers as Novel Antimicrobials. *Molecules*, 22(10), 1581.
- Garcia-Rubio, R., de Oliveira, H., Rivera, J. & Trevijano-Contador, N. (2020) The Fungal Cell Wall: Candida, Cryptococcus, and Aspergillus Species. *Frontiers in Microbiology*, 10.
- Gardete, S., & Tomasz, A. (2014). Mechanisms of vancomycin resistance in *Staphylococcus aureus*. *The Journal of Clinical Investigation*, 124(7), 2836–2840.
- Gardiner, M., Vicaretti, M., Sparks, J., Bansal, S., Bush, S., Liu, M., Darling, A., Harry, E., & Burke, C. M. (2017). A longitudinal study of the diabetic skin and wound microbiome. *PeerJ*, 5, e3543.
- Garnett, J. A., & Matthews, S. (2012). Interactions in Bacterial Biofilm Development: A Structural Perspective. *Current Protein & Peptide Science*, 13(8), 739–755.

- Garse H, Jagtap P, Kadam V. (2015) Solid lipid nanoparticles based gel for topical delivery of antifungal agent. *Int J Pharm Sci Res*, 6, 3571e9.
- Gatoo, M. A., Naseem, S., Arfat, M. Y., Mahmood Dar, A., Qasim, K., & Zubair, S. (2014). Physicochemical Properties of Nanomaterials: Implication in Associated Toxic Manifestations. *BioMed Research International*, 2014, 498420.
- Ge, L., Zhao, Y., Mo, T., Li, J. & Li, P. (2012) Immobilization of glucose oxidase in electrospun nanofibrous membranes for food preservation. *Food Control*, 26(1), 188-193.
- Gehr, P. & Zellner, R. (2019) *Biological responses to nanoscale particles*. New York: Springer.
- Geilich, B., Gelfat, I., Sridhar, S., van de Ven, A. & Webster, T. (2017) Superparamagnetic iron oxide-encapsulating polymersome nanocarriers for biofilm eradication. *Biomaterials*, 119, 78-85.
- Ghanbari, A., Dehghany, J., Schweps, T., Müsken, M., Häussler, S. and Meyer-Hermann, M. (2016). Inoculation density and nutrient level determine the formation of mushroom-shaped structures in *Pseudomonas aeruginosa* biofilms. *Scientific Reports*, 6(1).
- Ghasemian A, Najar Peerayeh S, Bakhshi B, & Mirzaee M. (2015) The Microbial Surface Components Recognizing Adhesive Matrix Molecules (MSCRAMMs) Genes among Clinical Isolates of *Staphylococcus aureus* from Hospitalized Children. *Iran J Pathol.*,10(4), 258-264.
- Ghasemiyeh, P., & Mohammadi-Samani, S. (2018). Solid lipid nanoparticles and nanostructured lipid carriers as novel drug delivery systems: applications, advantages and disadvantages. *Research in pharmaceutical sciences*, 13(4), 288–303.
- Gholipourmalekabadi, M., Mobaraki, M., Ghaffari, M., Zarebkohan, A., Omrani, V., Urbanska, A. and Seifalian, A. (2017) Targeted Drug Delivery Based on Gold Nanoparticle Derivatives. *Current Pharmaceutical Design*, 23(20).
- Golebiewska, E. and Poole, A. (2015). Platelet secretion: From haemostasis to wound healing and beyond. *Blood Reviews*, 29(3), 153-162.
- Gottenbos, B. (2001) Antimicrobial effects of positively charged surfaces on adhering Gram-positive and Gram-negative bacteria. *Journal of Antimicrobial Chemotherapy*, 48(1), 7-13.
- Gould, K (2016); Antibiotics: from prehistory to the present day, *Journal of Antimicrobial Chemotherapy*, 71(3), 572–57.
- Graves, J. L., Thomas, M., & Ewunkem, J. A. (2017). Antimicrobial Nanomaterials: Why Evolution Matters. *Nanomaterials (Basel, Switzerland)*, 7(10), 283.
- Greish K. (2010). Enhanced permeability and retention (EPR) effect for anticancer nanomedicine drug targeting. *Methods in molecular biology (Clifton, N.J.)*, 624, 25–37.
- Grice, E. A., & Segre, J. A. (2011). The skin microbiome. *Nature Reviews. Microbiology*, 9(4), 244–253.
- Grossman, T. (2016). Tetracycline Antibiotics and Resistance. *Cold Spring Harbor Perspectives in Medicine*, 6(4), p.a025387.
- Gu, H., Ho, P., Tong, E., Wang, L. & Xu, B. (2003) Presenting Vancomycin on Nanoparticles to Enhance Antimicrobial Activities. *Nano Letters*, 3(9), 1261-1263.
- Guo, S., & DiPietro, L. A. (2010). Factors Affecting Wound Healing. *Journal of Dental Research*, 89(3), 219–229.
- Gupta, A.; Eral, H.; Hatton, T.; Doyle, P. (2016) Nanoemulsions: Formation, Properties And Applications. *Soft Matter.*, 12, 2826-2841.
- Gupta, P., & Diwan, B. (2017). Bacterial Exopolysaccharide mediated heavy metal removal: A Review on biosynthesis, mechanism and remediation strategies. *Biotechnology Reports*, 13, 58–71.
- Ha, D.-G., & O'Toole, G. A. (2015). c-di-GMP and its effects on biofilm formation and dispersion: a *Pseudomonas aeruginosa* review. *Microbiology Spectrum*, 3(2), 10.
- Habimana, O., Zanoni, M., Vitale, S., O'Neill, T., Scholz, D., Xu, B. & Casey, E. (2018) One particle, two targets: A combined action of functionalised gold nanoparticles, against *Pseudomonas fluorescens* biofilms. *Journal of Colloid and Interface Science*, 526, 419-428.
- Hadinoto, K., & Cheow, W. S. (2014). Nano-antibiotics in chronic lung infection therapy against *Pseudomonas aeruginosa*. *Colloids and surfaces. B, Biointerfaces*, 116, 772–785.

- Hagenmaier, R., & Shaw, P. (1991) Permeability Of Shellac Coatings To Gases And Water Vapor. *Journal of Agricultural and Food Chemistry*, 39 (5), 825-829.
- Halbus, A., Horozov, T. & Paunov, V. (2017) Colloid particle formulations for antimicrobial applications. *Advances in Colloid and Interface Science*, 249, 134-148.
- Halbus, A., Horozov, T. & Paunov, V. (2019a) Controlling the Antimicrobial Action of Surface Modified Magnesium Hydroxide Nanoparticles. *Biomimetics*, 4(2), 41.
- Halbus, A., Horozov, T. & Paunov, V. (2019b) Strongly Enhanced Antibacterial Action of Copper Oxide Nanoparticles with Boronic Acid Surface Functionality. *ACS Applied Materials & Interfaces*, 11(13), 12232-12243.
- Halbus, A., Horozov, T. & Paunov, V. (2019c) Self-grafting copper oxide nanoparticles show a strong enhancement of their anti-algal and anti-yeast action. *Nanoscale Advances*, 1(6), 2323-2336.
- Halbus, A., Horozov, T. & Paunov, V. (2020) Surface-Modified Zinc Oxide Nanoparticles for Antialgal and Antiyeast Applications. *ACS Applied Nano Materials*, 3(1), 440-451.
- Hamad, S. A., Stoyanov, S. D., & Paunov, V. N (2013) Triggered Release Kinetics Of Living Cells From Composite Microcapsules. *Physical Chemistry Chemical Physics*, 15 (7), 2337.
- Hamad, S.A., Stoyanov, S.D., Paunov, V.N. (2012a) Triggered cell release from shellac-cell composite microcapsules, *Soft Matter*, 8, 5069–5077.
- Hamad, S.A., Stoyanov, S.D., Paunov, V.N. (2012b) Triggered release kinetics of living cells from composite microcapsules, *Phys. Chem. Chem. Phys.*, 15, 2337–2344.
- Han, H., Hou, Y., Chen, X., Zhang, P., Kang, M., Jin, Q., Ji, J., & Gao, M. (2020). Metformin-Induced Stromal Depletion to Enhance the Penetration of Gemcitabine-Loaded Magnetic Nanoparticles for Pancreatic Cancer Targeted Therapy. *Journal of the American Chemical Society*, 142(10), 4944–4954.
- Hansen, E. H., Albertsen, L., Schäfer, T., Johansen, C., Frisvad, J. C., Molin, S., & Gram, L. (2003). *Curvularia haloperoxidase*: antimicrobial activity and potential application as a surface disinfectant. *Applied and environmental microbiology*, 69(8), 4611–4617.
- Harkins, C. P., Pichon, B., Doumith, M., Parkhill, J., Westh, H., Tomasz, A., De Lencastre, H., Bentley, S. D., Kearns, A. M., & Holden, M. T. G. (2017). Methicillin-resistant *Staphylococcus aureus* emerged long before the introduction of methicillin into clinical practice. *Genome Biology*, 18, 130.
- Hathaway, H., Ajuebor, J., Stephens, L., Coffey, A., Potter, U., Sutton, J. M., & Jenkins, A. T. (2017). Thermally triggered release of the bacteriophage endolysin CHAP_K and the bacteriocin lysostaphin for the control of methicillin resistant *Staphylococcus aureus* (MRSA). *Journal of controlled release : official journal of the Controlled Release Society*, 245, 108–115.
- Hayat, S. (2018) Nanoantibiotics Future nanotechnologies to combat antibiotic resistance. *Frontiers in Bioscience*, 10(2), 352-374.
- He, Y., Ingudam, S., Reed, S., Gehring, A., Strobaugh, T. P., & Irwin, P. (2016). Study on the mechanism of antibacterial action of magnesium oxide nanoparticles against foodborne pathogens. *Journal of Nanobiotechnology*, 14, 54.
- Helander, I., Latva-Kala, K., & Lounatmaa, K. (1998) Permeabilizing Action Of Polyethyleneimine On Salmonella Typhimurium Involves Disruption Of The Outer Membrane And Interactions With Lipopolysaccharide. *Microbiology*, 144 (2), 385-390.
- Hemeg, H. (2017) Nanomaterials for alternative antibacterial therapy. *International Journal of Nanomedicine*, Volume 12, 8211-8225.
- Hess, C. L., Howard, M. A., & Attinger, C. E. (2003). A review of mechanical adjuncts in wound healing: hydrotherapy, ultrasound, negative pressure therapy, hyperbaric oxygen, and electrostimulation. *Annals of plastic surgery*, 51(2), 210–218.
- Hill, M. A., Lam, A. K., Reed, P., Harney, M. C., Wilson, B. A., Moen, E. L., Wright, S. N., Pinho, M. G., & Rice, C. V. (2019). BPEI-Induced Delocalization of PBP4 Potentiates β -Lactams against MRSA. *Biochemistry*, 58(36), 3813–3822.

- Ho, L., Liu, Y., Han, R., Bai, Q., & Choi, C. (2019). Nano-Cell Interactions of Non-Cationic Bionanomaterials. *Accounts of chemical research*, 52(6), 1519–1530.
- Høiby, N., Ciofu, O., Johansen, H. K., Song, Z., Moser, C., Jensen, P. Ø., Molin, S., Givskov, M., Tolker-Nielsen, T., & Bjarnsholt, T. (2011). The clinical impact of bacterial biofilms. *International Journal of Oral Science*, 3(2), 55–65.
- Holme, M. N., Fedotenko, I. A., Abegg, D., Althaus, J., Babel, L., Favarger, F., Reiter, R., Tanasescu, R., Zaffalon, P. L., Ziegler, A., Müller, B., Saxer, T., & Zumbuehl, A. (2012). Shear-stress sensitive lenticular vesicles for targeted drug delivery. *Nature nanotechnology*, 7(8), 536–543.
- Horey, B., Klein, M., Hwang, G., Li, Y., Kim, D., Koo, H. and Benoit, D. (2015). pH-Activated Nanoparticles for Controlled Topical Delivery of Farnesol To Disrupt Oral Biofilm Virulence. *ACS Nano*, 9(3), 2390-2404.
- Hoshyar, N., Gray, S., Han, H. & Bao, G. (2016) The effect of nanoparticle size on in vivo pharmacokinetics and cellular interaction. *Nanomedicine*, 11(6), 673-692.
- Hössel, P., Dieing, R., Nörenberg, R., Pfau, A., & Sander, R. (2000) Conditioning polymers in today's shampoo formulations - efficacy, mechanism and test methods. *Int J Cosmet Sci.*, 22(1), 1-10.
- Hosta-Rigau, L. & Städler, B. (2013) Shear Stress and Its Effect on the Interaction of Myoblast Cells with Nanosized Drug Delivery Vehicles. *Molecular Pharmaceutics*, 10(7), 2707-2712.
- Hou, S., Zhou, C., Liu, Z., Young, A., Shi, Z., Ren, D. & Kallenbach, N. (2009) Antimicrobial dendrimer active against Escherichia coli biofilms. *Bioorganic & Medicinal Chemistry Letters*, 19(18), 5478-5481.
- Huang, K., Hsu, F., Qiu, J., Chern, G., Lee, Y., Chang, C., Huang, Y., Sung, Y., Chiang, C., Huang, R., Lin, C., Dinh, T., Huang, H., Shih, Y., Alson, D., Lin, C., Lin, Y., Chang, P., Lin, S. & Chen, Y. (2020) Highly efficient and tumor-selective nanoparticles for dual-targeted immunogene therapy against cancer. *Science Advances*, 6(3), DOI: 10.1126/sciadv.aax5032.
- Huh, S. H., Do, H. J., Lim, H. Y., Kim, D. K., Choi, S. J., Song, H., Kim, N. H., Park, J. K., Chang, W. K., Chung, H. M., & Kim, J. H. (2007). Optimization of 25 kDa linear polyethylenimine for efficient gene delivery. *Biologicals : journal of the International Association of Biological Standardization*, 35(3), 165–171.
- Hui, Y., Yi, X., Hou, F., Wibowo, D., Zhang, F., Zhao, D., Gao, H. & Zhao, C. (2019) Role of Nanoparticle Mechanical Properties in Cancer Drug Delivery. *ACS Nano*, 13(7), 7410-7424.
- Hussein-Al-Ali, S. H., El Zowalaty, M. E., Hussein, M. Z., Ismail, M., & Webster, T. J. (2014) Synthesis, characterization, controlled release, and antibacterial studies of a novel streptomycin chitosan magnetic nanoantibiotic. *Int J Nanomedicine*, 9, 549-57.
- Iannitelli, A., Grande, R., Di Stefano, A., Di Giulio, M., Sozio, P., Bessa, L. J., Laserra, S., Paolini, C., Protasi, F., & Cellini, L. (2011). Potential antibacterial activity of carvacrol-loaded poly(DL-lactide-co-glycolide) (PLGA) nanoparticles against microbial biofilm. *International journal of molecular sciences*, 12(8), 5039–5051.
- Im, H., Choi, S. Y., Son, S., & Mitchell, R. J. (2017). Combined Application of Bacterial Predation and Violacein to Kill Polymicrobial Pathogenic Communities. *Scientific Reports*, 7, 14415.
- Iqbal, A., Jan, A., Wajid, M. A., & Tariq, S. (2017). Management of Chronic Non-healing Wounds by Hirudotherapy. *World journal of plastic surgery*, 6(1), 9-17.
- Iram, S., Akbar Khan, J., Aman, N., Nadhman, A., Zulfiqar, Z. & Arfat Yameen, M. (2016) Enhancing the Anti-Enterococci Activity of Different Antibiotics by Combining With Metal Oxide Nanoparticles. *Jundishapur Journal of Microbiology*, 9(3).
- Ishihara, M., Kishimoto, S., Nakamura, S., Sato, Y., & Hattori, H. (2019) Polyelectrolyte Complexes Of Natural Polymers And Their Biomedical Applications. *Polymers*, 11 (4), 672.
- Jaiswal, M., Dudhe, R., & Sharma, P. K. (2015). Nanoemulsion: an advanced mode of drug delivery system. *3 Biotech*, 5(2), 123–127. <https://doi.org/10.1007/s13205-014-0214-0>
- Jarvis, M., Arnold, M., Ott, J., Krishnan, V., Pant, K., Prabhakarandian, B. & Mitragotri, S. (2018) Detachment of ligands from nanoparticle surface under flow and endothelial cell contact: Assessment using microfluidic devices. *Bioengineering & Translational Medicine*, 3(2), 148-155.

- Jayathilake, P. G., Jana, S., Rushton, S., Swailes, D., Bridgens, B., Curtis, T., & Chen, J. (2017). Extracellular Polymeric Substance Production and Aggregated Bacteria Colonization Influence the Competition of Microbes in Biofilms. *Frontiers in Microbiology*, *8*, 1865.
- Jeevanandam, J., Barhoum, A., Chan, Y. S., Dufresne, A., & Danquah, M. K. (2018). Review on nanoparticles and nanostructured materials: history, sources, toxicity and regulations. *Beilstein Journal of Nanotechnology*, *9*, 1050–1074.
- Jelić, D., & Antolović, R. (2016). From Erythromycin to Azithromycin and New Potential Ribosome-Binding Antimicrobials. *Antibiotics*, *5*(3), 29.
- Jensen, K., Oestergaard, P., Wilting, R. & Lassen, S. (2010) Identification and characterization of a bacterial glutamic peptidase. *BMC Biochemistry*, *11*(1), 47.
- Jevprasesphant, R. (2003) The influence of surface modification on the cytotoxicity of PAMAM dendrimers. *International Journal of Pharmaceutics*, *252*(1-2), 263-266.
- Johansson, E., Cruz, S., Kolomiets, E., Buts, L., Kadam, R., Cacciarini, M., Bartels, K., Diggie, S., Cámara, M., Williams, P., Loris, R., Nativi, C., Rosenau, F., Jaeger, K., Darbre, T. & Reymond, J. (2008) Inhibition and Dispersion of *Pseudomonas aeruginosa* Biofilms by Glycopeptide Dendrimers Targeting the Fucose-Specific Lectin LecB. *Chemistry & Biology*, *15*(12), 1249-1257.
- Johnston, N. J., Mukhtar, T. A., & Wright, G. D. (2002) Streptogramin antibiotics: Mode of action and resistance. *Curr Drug Targets.*, *3*, 335–44.
- Johnstone, T. C., & Nolan, E. M. (2015). Beyond Iron: Non-Classical Biological Functions of Bacterial Siderophores. *Dalton Transactions (Cambridge, England : 2003)*, *44*(14), 6320–6339.
- Junker, J. P. E., Kamel, R. A., Caterson, E. J., & Eriksson, E. (2013). Clinical Impact Upon Wound Healing and Inflammation in Moist, Wet, and Dry Environments. *Advances in Wound Care*, *2*(7), 348–356.
- Kabanov, A., Batrakova, E., & Alakhov, V. (2002) Pluronic® Block Copolymers As Novel Polymer Therapeutics For Drug And Gene Delivery. *Journal of Controlled Release*, *82* (2-3), 189-212.
- Kalan, L., Loesche, M., Hodgkinson, B., Heilmann, K., Ruthel, G., Gardner, S. and Grice, E. (2016). Redefining the Chronic-Wound Microbiome: Fungal Communities Are Prevalent, Dynamic, and Associated with Delayed Healing. *mBio*, *7*(5), e01058-16.
- Kaler, A., Mittal, A., Katariya, M., Harde, H., Agrawal, A., Jain, S., & Banerjee, U. (2014) An Investigation Of In Vivo Wound Healing Activity Of Biologically Synthesized Silver Nanoparticles. *Journal of Nanoparticle Research*, *16* (9).
- Kalhapure, R. S., Jadhav, M., Rambharose, S. (2017) pH-responsive chitosan nanoparticles from a novel twin-chain anionic amphiphile for controlled and targeted delivery of vancomycin. *Colloids Surf B Biointerfaces*, *158*, 650-657.
- Kalita, S., Kandimalla, R., Sharma, K., Katakai, A., Deka, M. & Kotoky, J. (2016) Amoxicillin functionalized gold nanoparticles reverts MRSA resistance. *Materials Science and Engineering: C*, *61*, 720-727.
- Kalpna, B. J., Aarthy, S., & Pandian, S. K. (2012). Antibiofilm activity of α -amylase from *Bacillus subtilis* S8-18 against biofilm forming human bacterial pathogens. *Applied biochemistry and biotechnology*, *167*(6), 1778–1794.
- Kamaly, N., Xiao, Z., Valencia, P. M., Radovic-Moreno, A. F., & Farokhzad, O. C. (2012). Targeted polymeric therapeutic nanoparticles: design, development and clinical translation. *Chemical Society reviews*, *41*(7), 2971–3010.
- Kaneko, Y., Thoendel, M., Olakanmi, O., Britigan, B. E., & Singh, P. K. (2007). The transition metal gallium disrupts *Pseudomonas aeruginosa* iron metabolism and has antimicrobial and antibiofilm activity. *The Journal of Clinical Investigation*, *117*(4), 877–888.
- Kannan, R., Nance, E., Kannan, S. & Tomalia, D. (2014) Emerging concepts in dendrimer-based nanomedicine: from design principles to clinical applications. *Journal of Internal Medicine*, *276*(6), 579-617.
- Kaur, A., Shimoni, O. & Wallach, M. (2018) Novel screening test for celiac disease using peptide functionalised gold nanoparticles. *World Journal of Gastroenterology*, *24*(47), 5379-5390.
- Kennedy, E. A., Connolly, J., Hourihane, J. O., Fallon, P. G., McLean, W. H. I., Murray, D., Jo, J-H., Segre, J. A., Kong, H. H., & Irvine, A. D. (2017). Skin microbiome before development of atopic dermatitis: Early colonization with commensal

- staphylococci at 2 months is associated with a lower risk of atopic dermatitis at 1 year. *The Journal of Allergy and Clinical Immunology*, 139(1), 166–172.
- Key, J., Palange, A., Gentile, F., Aryal, S., Stigliano, C., Di Mascolo, D., De Rosa, E., Cho, M., Lee, Y., Singh, J. & Decuzzi, P. (2015) Soft Discoidal Polymeric Nanoconstructs Resist Macrophage Uptake and Enhance Vascular Targeting in Tumors. *ACS Nano*, 9(12), 11628-11641.
- Khalil, H., Chen, T., Riffon, R., Wang, R., & Wang, Z. (2008) Synergy Between Polyethylenimine And Different Families Of Antibiotics Against A Resistant Clinical Isolate Of Pseudomonas Aeruginosa. *Antimicrobial Agents and Chemotherapy*, 52 (5), 1635-1641.
- Khavkin, J.; Ellis, D. (2011) Aging Skin: Histology, Physiology, And Pathology. *Facial Plastic Surgery Clinics of North America*, 19 (2), 229-234.
- Kim, H. J., & Jones, M. N. (2004). The delivery of benzyl penicillin to Staphylococcus aureus biofilms by use of liposomes. *Journal of liposome research*, 14(3-4), 123–139.
- Kim, L., Pagaling, E., Zuo, Y. Y., & Yan, T. (2014). Impact of Substratum Surface on Microbial Community Structure and Treatment Performance in Biological Aerated Filters. *Applied and Environmental Microbiology*, 80(1), 177–183.
- Klasen, H. (2000) A review on the nonoperative removal of necrotic tissue from burn wounds. *Burns*, 26(3), 207-222.
- Knöbel, M., O’Toole, E. and Smith, F. (2015). Keratins and skin disease. *Cell and Tissue Research*, 360(3), 583-589.
- Kobayashi, H., Watanabe, R., & Choyke, P. L. (2013). Improving conventional enhanced permeability and retention (EPR) effects; what is the appropriate target?. *Theranostics*, 4(1), 81–89.
- Kohanski, M. A., Dwyer, D. J., & Collins, J. J. (2010). How antibiotics kill bacteria: from targets to networks. *Nature Reviews. Microbiology*, 8(6), 423–435.
- Kong, H. H., & Segre, J. A. (2012). Skin Microbiome: Looking Back to Move Forward. *The Journal of Investigative Dermatology*, 132(3 0 2), 933–939.
- Kong, H. H., Andersson, B., Clavel, T., Common, J. E., Jackson, S. A., Olson, N. D., Segre, J. A., & Traidl-Hoffmann, C. (2017). Performing skin microbiome research: A method to the madness. *The Journal of Investigative Dermatology*, 137(3), 561–568.
- Kong, K.-F., Schnepfer, L., & Mathee, K. (2010). Beta-lactam Antibiotics: From Antibiosis to Resistance and Bacteriology. *APMIS : Acta Pathologica, Microbiologica, et Immunologica Scandinavica*, 118(1), 1–36.
- Kostakioti, M., Hadjifrangiskou, M., & Hultgren, S. J. (2013). Bacterial Biofilms: Development, Dispersal, and Therapeutic Strategies in the Dawn of the Postantibiotic Era. *Cold Spring Harbor Perspectives in Medicine*, 3(4), a010306.
- Kotra, L. P., Haddad, J., & Mobashery, S. (2000). Aminoglycosides: Perspectives on Mechanisms of Action and Resistance and Strategies to Counter Resistance. *Antimicrobial Agents and Chemotherapy*, 44(12), 3249–3256.
- Kou, L., Bhutia, Y., Yao, Q., He, Z., Sun, J. & Ganapathy, V. (2018) Transporter-Guided Delivery of Nanoparticles to Improve Drug Permeation across Cellular Barriers and Drug Exposure to Selective Cell Types. *Frontiers in Pharmacology*, 9.
- Koudelka, K. J., Pitek, A. S., Manchester, M., & Steinmetz, N. F. (2015). Virus-Based Nanoparticles as Versatile Nanomachines. *Annual Review of Virology*, 2(1), 379–401.
- Kraisit, P., Limmatvapirat, S., Nunthanid, J., Sriamornsak, P., & Luangtana-anan, M. (2012) Nanoparticle Formation By Using Shellac And Chitosan For A Protein Delivery System. *Pharmaceutical Development and Technology*, 18 (3), 686-693.
- Kruse, C. R., Nuutila, K., Lee, C. C., Kiwanuka, E., Singh, M., Caterson, E. J., Eriksson, E., & Sørensen, J. A. (2015). The external microenvironment of healing skin wounds. *Wound repair and regeneration*, 23(4), 456-465.
- Kulkarni, A., Vanjari, Y., Sancheti, K., Patel, H., Belgamwar, V., Surana, S. & Pardeshi, C. (2016) Polyelectrolyte complexes: mechanisms, critical experimental aspects, and applications. *Artificial Cells, Nanomedicine, and Biotechnology*, 44(7), 1615-1625.
- Kumari, A., Singla, R., Guliani, A., & Yadav, S. K. (2014). Nanoencapsulation for drug delivery. *EXCLI journal*, 13, 265–286.
- Kunjappu, J., & Rosen, M. (2013) *Surfactants and interfacial phenomena*; Wiley: Hoboken, N.J..

- Labhasetwar, V., Puranik, P., & Dorle, A. (1990) Study Of Shellac-Glycerol Esters As Microencapsulating Materials. II. Quantitative Correlation Between Physico-Chemical Properties And Release Characteristics. *Journal of Microencapsulation*, 7 (4), 553-554.
- Lam, A. K., Panlilio, H., Pusavat, J., Wouters, C. L., Moen, E. L., & Rice, C. V. (2020) Overcoming Multidrug Resistance and Biofilms of *Pseudomonas aeruginosa* with a Single Dual-Function Potentiator of β -Lactams. *CS Infect. Dis.*, 6, 5, 1085–1097
- Lam, A. K., Wouters, C. L., Moen, E. L., Pusavat, J., & Rice, C. V. (2019). Antibiofilm Synergy of β -Lactams and Branched Polyethylenimine against Methicillin-Resistant *Staphylococcus epidermidis*. *Biomacromolecules*, 20(10), 3778–3785.
- Lam, A., Hill, M., Moen, E., Pusavat, J., Wouters, C., & Rice, C. (2018) Cationic Branched Polyethylenimine (BPEI) Disables Antibiotic Resistance In Methicillin-Resistant *Staphylococcus Epidermidis*(MRSE). *ChemMedChem*, 13 (20), 2240-2248.
- Lamppa, J. W., & Griswold, K. E. (2013). Alginate lyase exhibits catalysis-independent biofilm dispersion and antibiotic synergy. *Antimicrobial agents and chemotherapy*, 57(1), 137–145.
- Lamson, N. G., Berger, A., Fein, K. C., & Whitehead, K. A. (2020). Anionic nanoparticles enable the oral delivery of proteins by enhancing intestinal permeability. *Nature biomedical engineering*, 4(1), 84–96.
- Landén, N. X., Li, D., & Ståhle, M. (2016). Transition from inflammation to proliferation: a critical step during wound healing. *Cellular and Molecular Life Sciences*, 73(20), 3861–3885.
- Le, Z., Chen, Y., Han, H., Tian, H., Zhao, P., Yang, C., He, Z., Liu, L., Leong, K. W., Mao, H. Q., Liu, Z., & Chen, Y. (2018). Hydrogen-Bonded Tannic Acid-Based Anticancer Nanoparticle for Enhancement of Oral Chemotherapy. *ACS applied materials & interfaces*, 10(49), 42186–42197.
- Lebrun, E., Tomic-Canic, M., & Kirsner, R. S. (2010). The role of surgical debridement in healing of diabetic foot ulcers. Wound repair and regeneration : official publication of the Wound Healing Society [and] the European Tissue Repair Society, 18(5), 433–438.
- Lee, H. J., Jeong, S. E., Lee, S., Kim, S., Han, H., & Jeon, C. O. (2018). Effects of cosmetics on the skin microbiome of facial cheeks with different hydration levels. *MicrobiologyOpen*, 7(2), e00557.
- Lee, S., Dangaran, K., & Krochta, J. (2002) Gloss Stability Of Whey-Protein/Plasticizer Coating Formulations On Chocolate Surface. *Journal of Food Science*, 67 (3), 1121-1125.
- Leekha, S., Terrell, C. L., & Edson, R. S. (2011). General Principles of Antimicrobial Therapy. *Mayo Clinic Proceedings*, 86(2), 156–167.
- Leheste, J., Ruvoilo, K., Chrostowski, J., Rivera, K., Husko, C., Miceli, A., Selig, M., Brüggemann, H. and Torres, G. (2017). P. acnes-Driven Disease Pathology: Current Knowledge and Future Directions. *Frontiers in Cellular and Infection Microbiology*, 7.
- Leick, S., Kott, M., Degen, P., Henning, S., Päsler, T., Suter, D., & Rehage, H. (2011) Mechanical Properties Of Liquid-Filled Shellac Composite Capsules. *Phys. Chem. Chem. Phys.*, 13 (7), 2765-2773.
- Lellouche, J., Friedman, A., Lahmi, R., Gedanken, A., & Banin, E. (2012). Antibiofilm surface functionalization of catheters by magnesium fluoride nanoparticles. *International journal of nanomedicine*, 7, 1175–1188.
- Leroux, C. J., Allémann, E., De Jaeghere, D., Doelker, E., & Gurny, R. (1996) Biodegradable nanoparticles — From sustained release formulations to improved site specific drug delivery, *Journal of Controlled Release*, 39, 339-350.
- Levipan, H. and Avendaño-Herrera, R. (2017). Different Phenotypes of Mature Biofilm in *Flavobacterium psychrophilum* Share a Potential for Virulence That Differs from Planktonic State. *Frontiers in Cellular and Infection Microbiology*, 7.
- Lewis, K. (2006) Persister cells, dormancy and infectious disease, *Nat. Rev. Microbiol.*, 5 , 48 —56.
- Li, J., & Mooney, D. J. (2016). Designing hydrogels for controlled drug delivery. *Nature reviews. Materials*, 1(12), 16071.
- Li, X., Yuan, C., Xing, L. and Humbert, P. (2017). Topographical diversity of common skin microflora and its association with skin environment type: An observational study in Chinese women. *Scientific Reports*, 7(1).
- Li, Z., & Nair, S. K. (2012). Quorum sensing: How bacteria can coordinate activity and synchronize their response to external signals? *Protein Science : A Publication of the Protein Society*, 21(10), 1403–1417.

- Li, Z., Bai, H., Jia, S., Yuan, H., Gao, L. & Liang, H. (2021) Design of functional polymer nanomaterials for antimicrobial therapy and combatting resistance. *Materials Chemistry Frontiers*
- Liaw, J., & Lin, Y. (2000) Evaluation Of Poly(Ethylene Oxide)–Poly(Propylene Oxide)–Poly(Ethylene Oxide) (PEO–PPO–PEO) Gels As A Release Vehicle For Percutaneous Fentanyl. *Journal of Controlled Release*, 68 (2), 273-282.
- Lim, J. Z., Ng, N. S., & Thomas, C. (2017). Prevention and treatment of diabetic foot ulcers. *Journal of the Royal Society of Medicine*, 110(3), 104–109.
- Limmatvapirat, S., Limmatvapirat, C., Luangtana-anan, M., Nunthanid, J., Oguchi, T., Tozuka, Y., Yamamoto, K., & Puttipipatkachorn, S. (2004) Modification Of Physicochemical And Mechanical Properties Of Shellac By Partial Hydrolysis. *International Journal of Pharmaceutics*, 278 (1), 41-49.
- Limoli, D. H., Jones, C. J., & Wozniak, D. J. (2015). Bacterial Extracellular Polysaccharides in Biofilm Formation and Function. *Microbiology Spectrum*, 3(3), 10.1128/microbiolspec.MB-0011–2014.
- Lin, H., & Sung, K. (2000) Carbopol/Pluronic Phase Change Solutions For Ophthalmic Drug Delivery. *Journal of Controlled Release*, 69 (3), 379-388.
- Ling, L., Schneider, T., Peoples, A., Spoering, A., Engels, I., Conlon, B., Mueller, A., Schäberle, T., Hughes, D., Epstein, S., Jones, M., Lazarides, L., Steadman, V., Cohen, D., Felix, C., Fetterman, K., Millett, W., Nitti, A., Zullo, A., Chen, C. and Lewis, K. (2015). Erratum: A new antibiotic kills pathogens without detectable resistance. *Nature*, 520(7547), 388-388.
- Liu, S., Hu, M., Zeng, T., Wu, R., Jiang, R., Wei, J., Wang, L., Kong, J. & Chen, Y. (2012) Lateral Dimension-Dependent Antibacterial Activity of Graphene Oxide Sheets. *Langmuir*, 28(33), 12364-12372.
- Liu, W., Røder, H. L., Madsen, J. S., Bjarnsholt, T., Sørensen, S. J., & Burmølle, M. (2016). Interspecific Bacterial Interactions are Reflected in Multispecies Biofilm Spatial Organization. *Frontiers in Microbiology*, 7, 1366.
- Llor, C., & Bjerrum, L. (2014). Antimicrobial resistance: risk associated with antibiotic overuse and initiatives to reduce the problem. *Therapeutic Advances in Drug Safety*, 5(6), 229–241.
- Lobanovska, M., & Pilla, G. (2017). Penicillin's Discovery and Antibiotic Resistance: Lessons for the Future?. *The Yale journal of biology and medicine*, 90(1), 135–145.
- Loew, S., Fahr, A., & May, S. (2011). Modeling the release kinetics of poorly water-soluble drug molecules from liposomal nanocarriers. *Journal of drug delivery*, 2011, 376548.
- Lonn-Stensrud, J., Landin, M., Benneche, T., Petersen, F. and Scheie, A. (2008). Furanones, potential agents for preventing Staphylococcus epidermidis biofilm infections?. *Journal of Antimicrobial Chemotherapy*, 63(2), 309-316.
- López-Otín, C. & Bond, J. (2008) Proteases: Multifunctional Enzymes in Life and Disease. *Journal of Biological Chemistry*, 283(45), 30433-30437.
- Lovrić, J. (2012) *Introducing proteomics*. Oxford: Wiley-Blackwell.
- Lu, C., & Fuchs, E. (2014). Sweat Gland Progenitors in Development, Homeostasis, and Wound Repair. *Cold Spring Harbor Perspectives in Medicine*, 4(2),
- Lu, X. Y., Wu, D. C., Li, Z. J., & Chen, G. Q. (2011). Polymer nanoparticles. *Progress in molecular biology and translational science*, 104, 299–323.
- Lu, X., Feng, X., Werber, J., Chu, C., Zucker, I., Kim, J., Osuji, C. & Elimelech, M. (2017) Enhanced antibacterial activity through the controlled alignment of graphene oxide nanosheets. *Proceedings of the National Academy of Sciences*, 114(46), E9793-E9801.
- Lu, Z., Li, C., Bao, H., Qiao, Y., Toh, Y. & Yang, X. (2008) Mechanism of Antimicrobial Activity of CdTe Quantum Dots. *Langmuir*, 24(10), 5445-5452.
- Lubrizol. (2006) Carbopol® Aqua SF-1 Polymer, Product Summary Sheet.
- Ludwig, A. (2005) The Use Of Mucoadhesive Polymers In Ocular Drug Delivery. *Advanced Drug Delivery Reviews*, 57 (11), 1595-1639.

- Lungu, C. N., Diudea, M. V., Putz, M. V., & Grudziński, I. P. (2016). Linear and Branched PEIs (Polyethylenimines) and Their Property Space. *International journal of molecular sciences*, 17(4), 555.
- Luo, Y., & Wang, Q. (2014) Recent Development Of Chitosan-Based Polyelectrolyte Complexes With Natural Polysaccharides For Drug Delivery. *International Journal of Biological Macromolecules*, 64, 353-367.
- Ma, J., Li, P., Wang, W., Wang, S., Pan, X., Zhang, F., Li, S., Liu, S., Wang, H., Gao, G., Xu, B., Yuan, Q., Shen, H. & Liu, H. (2018) Biodegradable Poly(amino acid)–Gold–Magnetic Complex with Efficient Endocytosis for Multimodal Imaging-Guided Chemo-photothermal Therapy. *ACS Nano*, 12(9), 9022-9032.
- Ma, M., Cheng, Y., Xu, Z., Xu, P., Qu, H., Fang, Y., Xu, T. & Wen, L. (2007) Evaluation of polyamidoamine (PAMAM) dendrimers as drug carriers of anti-bacterial drugs using sulfamethoxazole (SMZ) as a model drug. *European Journal of Medicinal Chemistry*, 42(1), 93-98.
- Madaan, K., Kumar, S., Poonia, N., Lather, V., & Pandita, D. (2014). Dendrimers in drug delivery and targeting: Drug-dendrimer interactions and toxicity issues. *Journal of Pharmacy & Bioallied Sciences*, 6(3), 139–150.
- Malanovic, N. & Lohner, K. (2016) Gram-positive bacterial cell envelopes: The impact on the activity of antimicrobial peptides. *Biochimica et Biophysica Acta (BBA) - Biomembranes*, 1858(5), 936-946.
- Malota, Z., Glowacki, J., Sadowski, W. & Kostur, M. (2018) Numerical analysis of the impact of flow rate, heart rate, vessel geometry, and degree of stenosis on coronary hemodynamic indices. *BMC Cardiovascular Disorders*, 18(1).
- Manna, B., Nahirniak, P., & Morrison, C. A. (2020). Wound Debridement. In *StatPearls*. StatPearls Publishing.
- Manshian, B., Jiménez, J., Himmelreich, U. & Soenen, S. (2017) Personalized medicine and follow-up of therapeutic delivery through exploitation of quantum dot toxicity. *Biomaterials*, 127, 1-12.
- Manus, M. B., Yu, J. J., Park, L. P., Mueller, O., Windsor, S. C., Horvath, J. E., & Nunn, C. L. (2017). Environmental influences on the skin microbiome of humans and cattle in rural Madagascar. *Evolution, Medicine, and Public Health*, 2017(1), 144–153.
- Marassi, V., Di Cristo, L., Smith, S. G. J., Ortelli, S., Blosi, M., Costa, A. L., Reschiglian, V., Volkov, Y., & Prina-Mello, A. (2018). Silver nanoparticles as a medical device in healthcare settings: a five-step approach for candidate screening of coating agents. *Royal Society Open Science*, 5(1), 171113.
- Marin, S., Vlasceanu, G., Tiplea, R., Bucur, I., Lemnaru, M., Marin, M. and Grumezescu, A. (2015). Applications and Toxicity of Silver Nanoparticles: A Recent Review. *Current Topics in Medicinal Chemistry*, 15(16), pp.1596-1604.
- Markowska, K., Grudniak, A. M., & Wolska, K. L. (2013) Silver nanoparticles as an alternative strategy against bacterial biofilms. *Acta Biochimica Polonica*, 60(4), 523-530.
- Martin, P., & Nunan, R. (2015). Cellular and molecular mechanisms of repair in acute and chronic wound healing. *The British Journal of Dermatology*, 173(2), 370–378.
- McDonnell, G., & Russell, A. (2001) Antiseptics And Disinfectants: Activity, Action, And Resistance. *Clinical Microbiology Reviews*, 14 (1), 227-227.
- McKenna M. (2013). Antibiotic resistance: the last resort. *Nature*, 499(7459), 394–396.
- McShan, D., Ray, P. C., & Yu, H. (2014). Molecular Toxicity Mechanism of Nanosilver. *Journal of Food and Drug Analysis*, 22(1), 116–127.
- McSweeney, M., Wessler, T., Price, L., Ciociola, E., Herity, L., Piscitelli, J., Zamboni, W., Forest, M., Cao, Y. & Lai, S. (2018) A minimal physiologically based pharmacokinetic model that predicts anti-PEG IgG-mediated clearance of PEGylated drugs in human and mouse. *Journal of Controlled Release*, 284, 171-178.
- Mecikoglu, M., Saygi, B., Yildirim, Y., Karadag-Saygi, E., Ramadan, S. & Esemeli, T. (2006) The Effect of Proteolytic Enzyme Serratiopeptidase in the Treatment of Experimental Implant-Related Infection. *The Journal of Bone & Joint Surgery*, 88(6), 1208-1214.
- Melaugh, G., Hutchison, J., Kragh, K. N., Irie, Y., Roberts, A., Bjarnsholt, T., Diggle, S. P., Gordon, V. D., & Allen, R. J. (2016). Shaping the Growth Behaviour of Biofilms Initiated from Bacterial Aggregates. *PLoS ONE*, 11(3), e0149683.

- Mendes, L. P., Pan, J., & Torchilin, V. P. (2017). Dendrimers as Nanocarriers for Nucleic Acid and Drug Delivery in Cancer Therapy. *Molecules (Basel, Switzerland)*, 22(9), E1401
- Mendes, L., Sarisozen, C., Luther, E., Pan, J., & Torchilin, V. (2019) Surface-Engineered Polyethyleneimine-Modified Liposomes As Novel Carrier Of Sirna And Chemotherapeutics For Combination Treatment Of Drug-Resistant Cancers. *Drug Delivery*, 26 (1), 443-458.
- Menjoge, A., Kannan, R. & Tomalia, D. (2010) Dendrimer-based drug and imaging conjugates: design considerations for nanomedical applications. *Drug Discovery Today*, 15(5-6), 171-185.
- Mishra, G., Bagui, M., Tamboli, V. & Mitra, A. (2011) Recent Applications of Liposomes in Ophthalmic Drug Delivery. *Journal of Drug Delivery*, 2011, 1-14.
- Misic, A. M., Gardner, S. E., & Grice, E. A. (2014). The Wound Microbiome: Modern Approaches to Examining the Role of Microorganisms in Impaired Chronic Wound Healing. *Advances in Wound Care*, 3(7), 502–510.
- Missirlis, D., Kawamura, R., Tirelli, N., & Hubbell, J. A. (2006). Doxorubicin encapsulation and diffusional release from stable, polymeric, hydrogel nanoparticles. *European journal of pharmaceutical sciences : official journal of the European Federation for Pharmaceutical Sciences*, 29(2), 120–129.
- Mitchell, M., Billingsley, M., Haley, R., Wechsler, M., Peppas, N., & Langer, R. (2020) Engineering Precision Nanoparticles For Drug Delivery. *Nature Reviews Drug Discovery*.
- Mitzel, M. & Tufenkji, N. (2014) Transport of Industrial PVP-Stabilized Silver Nanoparticles in Saturated Quartz Sand Coated with *Pseudomonas aeruginosa* PAO1 Biofilm of Variable Age. *Environmental Science & Technology*, 48(5), 2715-2723.
- Miyazaki, S., Tobiyama, T., Takada, M., & Attwood, D. (1995). Percutaneous absorption of indomethacin from pluronic F127 gels in rats. *The Journal of pharmacy and pharmacology*, 47(6), 455–457.
- Morar, M., Bhullar, K., Hughes, D., Junop, M. and Wright, G. (2009). Structure and Mechanism of the Lincosamide Antibiotic Adenyltransferase LinB. *Structure*, 17(12), 1649-1659.
- Mostafa, W. Z., & Hegazy, R. A. (2015). Vitamin D and the skin: Focus on a complex relationship: A review. *Journal of Advanced Research*, 6(6), 793–804.
- Mótyán, J., Tóth, F. & Tózsér, J. (2013) Research Applications of Proteolytic Enzymes in Molecular Biology. *Biomolecules*, 3(4), 923-942.
- Mout, R., Moyano, D. F., Rana, S., & Rotello, V. M. (2012). Surface functionalization of nanoparticles for nanomedicine. *Chemical Society Reviews*, 41(7), 2539–2544.
- Mueller, N. T., Bakacs, E., Combellick, J., Grigoryan, Z., & Dominguez-Bello, M. G. (2015). The infant microbiome development: mom matters. *Trends in Molecular Medicine*, 21(2), 109–117.
- Muhamad, N., Plengsuriyakarn, T., & Na-Bangchang, K. (2018). Application of active targeting nanoparticle delivery system for chemotherapeutic drugs and traditional/herbal medicines in cancer therapy: a systematic review. *International journal of nanomedicine*, 13, 3921–3935.
- Müller, K., Bugnicourt, E., Latorre, M., Jorda, M., Echegoyen Sanz, Y., Lagaron, J. M., Miesbauer, O., Bianchin, A., Hankin, S., Bolz, U., Perez, G., Jesdinszki, M., Lindner, M., Scheuerer, Z., Castello, S., & Schmid, M. (2017). Review on the Processing and Properties of Polymer Nanocomposites and Nanocoatings and Their Applications in the Packaging, Automotive and Solar Energy Fields. *Nanomaterials*, 7(4), 74.
- Munita, J. M., & Arias, C. A. (2016). Mechanisms of Antibiotic Resistance. *Microbiology Spectrum*, 4(2), 10.1128/microbiolspec.VMBF-0016-2015.
- Munzar, J., Ng, A. & Juncker, D. (2019) Duplexed aptamers: history, design, theory, and application to biosensing. *Chemical Society Reviews*, 48(5), 1390-1419.
- Murugappan, G. & Sreeram, K. (2021) Nano-biocatalyst: Bi-functionalization of protease and amylase on copper oxide nanoparticles. *Colloids and Surfaces B: Biointerfaces*, 197, 111386.
- Nakatsuji, T., Chen, T., Narala, S., Chun, K., Two, A., Yun, T., Shafiq, F., Kotol, P., Bouslimani, A., Melnik, A., Latif, H., Kim, J., Lockhart, A., Artis, K., David, G., Taylor, P., Streib, J., Dorrestein, P., Grier, A., Gill, S., Zengler, K., Hata, T., Leung, D. and

- Gallo, R. (2017). Antimicrobials from human skin commensal bacteria protect against *Staphylococcus aureus* and are deficient in atopic dermatitis. *Science Translational Medicine*, 9(378), p.eeah4680.
- NanoComposix. (2020) Branched Polyethylenimine (BPEI) Surface. <https://nanocomposix.com/pages/branched-polyethylenimine-bpei-surface> [Accessed 19/11/2021].
- Naqvi, S., Kiran, U., Ali, Jamal, Hameed, Ahmed & Ali (2013) Combined efficacy of biologically synthesized silver nanoparticles and different antibiotics against multidrug-resistant bacteria. *International Journal of Nanomedicine*, 3187.
- Nastiti, C., Ponto, T., Abd, E., Grice, J. E., Benson, H., & Roberts, M. S. (2017). Topical Nano and Microemulsions for Skin Delivery. *Pharmaceutics*, 9(4), 37.
- Natalio, F., Kashyap, A., Lorenz, S., Kerschbaumer, H., Dietzsch, M., Tahir, M., Duschner, H., Strand, S., Strand, D. & Tremel, W. (2012) Multi-photon imaging of amine-functionalized silica nanoparticles. *Nanoscale*, 4(15), 4680.
- Natan, M., & Banin, E. (2017). From Nano to Micro: using nanotechnology to combat microorganisms and their multidrug resistance. *FEMS microbiology reviews*, 41(3), 302–322.
- Nath Goswami, D., Prasad, N., Baboo, B., Kishore Kumar, K., & Fahim Ansari, M. (2009) Degradation Of Lac With Storage And A Simple Method To Check The Same. *Pigment & Resin Technology*, 38 (4), 211-217.
- Nauta, T. D., van Hinsbergh, V. W. M., & Koolwijk, P. (2014). Hypoxic Signaling During Tissue Repair and Regenerative Medicine. *International Journal of Molecular Sciences*, 15(11), 19791–19815.
- Nederberg, F., Zhang, Y., Tan, J., Xu, K., Wang, H., Yang, C., Gao, S., Guo, X., Fukushima, K., Li, L., Hedrick, J. & Yang, Y. (2011) Biodegradable nanostructures with selective lysis of microbial membranes. *Nature Chemistry*, 3(5), 409-414.
- Negut, I., Grumezescu, V., & Grumezescu, A. M. (2018). Treatment Strategies for Infected Wounds. *Molecules (Basel, Switzerland)*, 23(9), 2392.
- Negut, I., Grumezescu, V., & Grumezescu, A. M. (2018). Treatment Strategies for Infected Wounds. *Molecules (Basel, Switzerland)*, 23(9), 2392.
- Bekara, F., Vitse, J., Fluieraru, S., Masson, R., Runz, A., Georgescu, V., Bressy, G., Labbé, J. L., Chaput, B., & Herlin, C. (2018). New techniques for wound management: A systematic review of their role in the management of chronic wounds. *Archives of plastic surgery*, 45(2), 102–110.
- Nevin, A., Echard, J., Thoury, M., Comelli, D., Valentini, G., & Cubeddu, R. (2009) Excitation Emission And Time-Resolved Fluorescence Spectroscopy Of Selected Varnishes Used In Historical Musical Instruments. *Talanta*, 80 (1), 286-293.
- Niemi, T., Miyashita, R. and Yamakage, M. (2010). Colloid solutions: a clinical update. *Journal of Anesthesia*, 24(6), 913-925.
- Nishita, M., Park, S., Nishio, T., Kamizaki, K., Wang, Z., Tamada, K., Takumi, T., Hashimoto, R., Otani, H., Pazour, G., Hsu, V. & Minami, Y. (2017) Ror2 signaling regulates Golgi structure and transport through IFT20 for tumor invasiveness. *Scientific Reports*, 7(1).
- Nishiyama, N., Matsumura, Y., & Kataoka, K. (2016). Development of polymeric micelles for targeting intractable cancers. *Cancer Science*, 107(7), 867–874.
- Nizzero, S., Ziemys, A. & Ferrari, M. (2018) Transport Barriers and Oncophysics in Cancer Treatment. *Trends in Cancer*, 4(4), 277-280.
- Nocelli, N., Bogino, P. C., Banchio, E., & Giordano, W. (2016). Roles of Extracellular Polysaccharides and Biofilm Formation in Heavy Metal Resistance of Rhizobia. *Materials*, 9(6), 418.
- Ogaji, I., Nep, E., & Audu-Peter, J. (2012) Advances In Natural Polymers As Pharmaceutical Excipients. *Pharmaceutica Analytica Acta*, 03 (01).
- Oh, J., Byrd, A. L., Park, M., NISC Comparative Sequencing Program, Kong, H. H., & Segre, J. A. (2016). Temporal Stability of the Human Skin Microbiome. *Cell*, 165(4), 854–866.
- Oh, J., Drumright, R., Siegwart, D. & Matyjaszewski, K. (2008) The development of microgels/nanogels for drug delivery applications. *Progress in Polymer Science*, 33(4), 448-477.

- Oh, N., Oh, K., Baik, H., Lee, B., Lee, A., Youn, Y., & Lee, E. (2010) A Self-Organized 3-Diethylaminopropyl-Bearing Glycol Chitosan Nanogel For Tumor Acidic Ph Targeting: In Vitro Evaluation. *Colloids and Surfaces B: Biointerfaces*, 78 (1), 120-126.
- Oliva, N., Carcole, M., Beckerman, M., Seliktar, S., Hayward, A., Stanley, J., Parry, N., Edelman, E. & Artzi, N. (2015) Regulation of dendrimer/dextran material performance by altered tissue microenvironment in inflammation and neoplasia. *Science Translational Medicine*, 7(272), 272ra11-272ra11.
- Otto, M. (2014) Staphylococcus epidermidis pathogenesis. *Methods in Molecular Biology*, 1106, 17-31.
- Otto, M. (2012) Targeted Immunotherapy For Staphylococcal Infections. *BioDrugs*, 22 (1), 27-36.
- Palanikumar, L., Al-Hosani, S., Kalmouni, M., Nguyen, V., Ali, L., Pasricha, R., Barrera, F. & Magzoub, M. (2020) pH-responsive high stability polymeric nanoparticles for targeted delivery of anticancer therapeutics. *Communications Biology*, 3(1).
- Palmerston-Mendes, L., Pan, J. & Torchilin, V. (2017) Dendrimers as Nanocarriers for Nucleic Acid and Drug Delivery in Cancer Therapy. *Molecules*, 22(9), 1401.
- Panáček, A., Kvítek, L., Smékalová, M., Večeřová, R., Kolář, M., Röderová, M., Dyčka, F., Šebela, M., Pucek, R., Tomanec, O. & Zbořil, R. (2017) Bacterial resistance to silver nanoparticles and how to overcome it. *Nature Nanotechnology*, 13(1), 65-71.
- Papi, M., Palmieri, V., Digiacomo, L., Giulimondi, F., Palchetti, S., Ciasca, G., Perini, G., Caputo, D., Cartillone, M., Cascone, C., Coppola, R., Capriotti, A., Laganà, A., Pozzi, D. & Caracciolo, G. (2019) Converting the personalized biomolecular corona of graphene oxide nanoflakes into a high-throughput diagnostic test for early cancer detection. *Nanoscale*, 11(32), 15339-15346.
- Papp-Wallace, K. M., Endimiani, A., Taracila, M. A., & Bonomo, R. A. (2011). Carbapenems: Past, Present, and Future . *Antimicrobial Agents and Chemotherapy*, 55(11), 4943–4960.
- Paranjpe, M., & Müller-Goymann, C. C. (2014). Nanoparticle-Mediated Pulmonary Drug Delivery: A Review. *International Journal of Molecular Sciences*, 15(4), 5852–5873.
- Park, B., & Kim, S. J. (2013). Cooling the Skin: Understanding a Specific Cutaneous Thermosensation. *Journal of Lifestyle Medicine*, 3(2), 91–97.
- Patel, A., Heussen, P., Hazekamp, J., & Velikov, K. (2011) Stabilisation And Controlled Release Of Silibinin From Ph Responsive Shellac Colloidal Particles. *Soft Matter*, 7 (18), 8549.
- Paterson, G., & Orihuela, C. (2010) Pneumococcal Microbial Surface Components Recognizing Adhesive Matrix Molecules Targeting Of The Extracellular Matrix. *Molecular Microbiology*, 77 (1), 1-5.
- Patil, J.; Dhadde, S.; Chandakavathe, B. Nanostructure Drug Delivery System Is An Option To Solve Antimicrobial Drug Resistance. *Characterization and Biology of Nanomaterials for Drug Delivery 2019*, 165-197.
- Patra, J. K., Das, G., Fraceto, L. F., Campos, E., Rodriguez-Torres, M., Acosta-Torres, L. S., Diaz-Torres, L. A., Grillo, R., Swamy, M. K., Sharma, S., Habtemariam, S., & Shin, H. S. (2018). Nano based drug delivery systems: recent developments and future prospects. *Journal of nanobiotechnology*, 16(1), 71.
- Patry, J., & Blanchette, V. (2017). Enzymatic debridement with collagenase in wounds and ulcers: a systematic review and meta-analysis. *International wound journal*, 14(6), 1055–1065.
- Pawlaczyk, M., Lelonkiewicz, M., & Wieczorowski, M. (2013). Age-dependent biomechanical properties of the skin. *Advances in Dermatology and Allergology/Postępy Dermatologii i Alergologii*, 30(5), 302–306.
- Pearnchob, N., Siepmann, J., * Bodmeier, R. (2003) Pharmaceutical Applications Of Shellac: Moisture-Protective And Taste-Masking Coatings And Extended-Release Matrix Tablets. *Drug Development and Industrial Pharmacy*, 29 (8), 925-938.
- Pelgrift, R. & Friedman, A. (2013) Nanotechnology as a therapeutic tool to combat microbial resistance. *Advanced Drug Delivery Reviews*, 65(13-14), 1803-1815.
- Percival, S. L., McCarty, S. M., & Lipsky, B. (2015). Biofilms and Wounds: An Overview of the Evidence. *Advances in Wound Care*, 4(7), 373–381.

- Perez, G. I., Gao, Z., Jourdain, R., Ramirez, J., Gany, F., Clavaud, C., Demaude, J., Breton, L. and Blaser, M. (2016). Body Site Is a More Determinant Factor than Human Population Diversity in the Healthy Skin Microbiome. *PLOS ONE*, 11(4), e0151990.
- Perni, S. & Prokopovich, P. (2014) Continuous release of gentamicin from gold nanocarriers. *RSC Adv*, 4(94), 51904-51910.
- Perron, G. G., Lee, A. E. G., Wang, Y., Huang, W. E., & Barraclough, T. G. (2012). Bacterial recombination promotes the evolution of multi-drug-resistance in functionally diverse populations. *Proceedings of the Royal Society B: Biological Sciences*, 279(1733), 1477–1484.
- Persat, A., Inclan, Y. F., Engel, J. N., Stone, H. A., & Gitai, Z. (2015). Type IV pili mechanochemically regulate virulence factors in *Pseudomonas aeruginosa*. *Proceedings of the National Academy of Sciences of the United States of America*, 112(24), 7563–7568.
- Persat, A., Nadell, C., Kim, M., Ingremeau, F., Siryaporn, A., Drescher, K., Wingreen, N., Bassler, B., Gitai, Z., & Stone, H. (2015) The Mechanical World Of Bacteria. *Cell*, 161 (5), 988-997.
- Petrova, O. E., & Sauer, K. (2016). Escaping the biofilm in more than one way: Desorption, detachment or dispersion. *Current Opinion in Microbiology*, 30, 67–78.
- Pfalzgraff, A., Brandenburg, K. and Weindl, G. (2018). Antimicrobial Peptides and Their Therapeutic Potential for Bacterial Skin Infections and Wounds. *Frontiers in Pharmacology*, 9.
- Phillips, C. J., Humphreys, I., Fletcher, J., Harding, K., Chamberlain, G., & Macey, S. (2016). Estimating the costs associated with the management of patients with chronic wounds using linked routine data. *International wound journal*, 13(6), 1193–1197.
- Pires, J., Siriwardena, T., Stach, M., Tinguely, R., Kasraian, S., Luzzaro, F., Leib, S., Darbre, T., Reymond, J. & Endimiani, A. (2015) In Vitro Activity of the Novel Antimicrobial Peptide Dendrimer G3KL against Multidrug-Resistant *Acinetobacter baumannii* and *Pseudomonas aeruginosa*. *Antimicrobial Agents and Chemotherapy*, 59(12), 7915-7918.
- Pisithkul, T., Schroeder, J., Trujillo, E., Yeesin, P., Stevenson, D., Chaiamarit, T., Coon, J., Wang, J., & Amador-Noguez, D. (2019) Metabolic Remodeling During Biofilm Development Of *Bacillus Subtilis*. *mBio*, 10 (3).
- Pissuwan, D., Niidome, T. and Cortie, M. (2011) The forthcoming applications of gold nanoparticles in drug and gene delivery systems. *Journal of Controlled Release*, 149(1), 65-71.
- Posnett, J., Franks, P. J. (2008) The burden of chronic wounds in the UK, *Nurs. Times*, 104(3), 44-45.
- Potera C. (1999). Forging a link between biofilms and disease. *Science (New York, N.Y.)*, 283(5409), 1837–1839.
- Pouradier, F., Céline, C., Marie-Florence, D., Frédéric, F., Ségolène, P., Stéphane, D. and Geneviève, L. (2013). Functional and structural age-related changes in the scalp skin of Caucasian women. *Skin Research and Technology*, 19(4), 384-393.
- Pouton CW. Lipid formulations for oral administration of drugs: non-emulsifying, self-emulsifying and 'self-microemulsifying' drug delivery systems. *Eur J Pharm Sci* 2000;11:93e8.
- Prescott, S. L., Larcombe, D.-L., Logan, A. C., West, C., Burks, W., Caraballo, L., Levin, M., Van Etten, E., Horwitz., Kozyrskyi, A., & Campbell, D. E. (2017). The skin microbiome: impact of modern environments on skin ecology, barrier integrity, and systemic immune programming. *The World Allergy Organization Journal*, 10(1), 29.
- Prestinaci, F., Pezzotti, P., & Pantosti, A. (2015). Antimicrobial resistance: a global multifaceted phenomenon. *Pathogens and global health*, 109(7), 309–318.
- Proniuk, S., & Blanchard, J. (2002) Anhydrous Carbopol® Polymer Gels For The Topical Delivery Of Oxygen/Water Sensitive Compounds. *Pharmaceutical Development and Technology*, 7 (2), 249-255.
- Qayyum, S. & Khan, A. U. (2016) Nanoparticles vs. biofilms: a battle against another paradigm of antibiotic resistance. *MedChemComm*, 7, 1479- 1498.
- Qi, H., Chen, W., Huang, C., Li, L., Chen, C., Li, W., & Wu, C. (2017) Development Of A Poloxamer Analogs/Carbopol-Based In Situ Gelling And Mucoadhesive Ophthalmic Delivery System For Puerarin. *International Journal of Pharmaceutics*, 337 (1-2), 178-187.

- Quan, K., Zhang, Z., Chen, H., Ren, X., Ren, Y., Peterson, B., van der Mei, H. & Busscher, H. (2019) Artificial Channels in an Infectious Biofilm Created by Magnetic Nanoparticles Enhanced Bacterial Killing by Antibiotics. *Small*, 15(39), 1902313.
- Quinteros, M., Cano Aristizábal, V., Dalmasso, P., Paraje, M. and Páez, P. (2016). Oxidative stress generation of silver nanoparticles in three bacterial genera and its relationship with the antimicrobial activity. *Toxicology in Vitro*, 36, 216-223.
- R. Vargas, P., M. Costa, C., S. Fonseca, B., F. Naccache, M., & De Souza Mendes, P. (2019) Rheological Characterization Of Carbopol® Dispersions In Water And In Water/Glycerol Solutions. *Fluids*, 4 (1), 3.
- Rafter, L (2010) Debridement and wound healing using larval therapy, *Wounds*, 6(1), 138-142.
- Raghupathi, P. K., Liu, W., Sabbe, K., Houf, K., Burmølle, M., & Sørensen, S. J. (2017). Synergistic Interactions within a Multispecies Biofilm Enhance Individual Species Protection against Grazing by a Pelagic Protozoan. *Frontiers in Microbiology*, 8, 2649.
- Rahim, K., Qasim, M., Rahman, H., Khan, T. A., Ahmad, I., Khan, N., Ullah, A., Basit, A., & Saleha, S. (2016). Antimicrobial resistance among aerobic biofilm producing bacteria isolated from chronic wounds in the tertiary care hospitals of Peshawar, Pakistan. *Journal of Wound Care*, 25(8), 480-486.
- Rai, M., Deshmukh, S., Ingle, A. & Gade, A. (2012) Silver nanoparticles: the powerful nanoweapon against multidrug-resistant bacteria. *Journal of Applied Microbiology*, 112(5), 841-852.
- Ramos, J., Imaz, A. & Forcada, J. (2012) Temperature-sensitive nanogels: poly(N-vinylcaprolactam) versus poly(N-isopropylacrylamide). *Polym Chem*, 3(4), 852-856.
- Rasines, B., Hernández-Ros, J., de las Cuevas, N., Copa-Patiño, J., Soliveri, J., Muñoz-Fernández, M., Gómez, R. & de la Mata, F. (2009) Water-stable ammonium-terminated carbosilane dendrimers as efficient antibacterial agents. *Dalton Transactions*,(40), 8704.
- Rață, D., Cadinoiu, A., Atanase, L., Bacaita, S., Mihalache, C., Daraba, O., Gherghel, D. & Popa, M. (2019) "In vitro" behaviour of aptamer-functionalized polymeric nanocapsules loaded with 5-fluorouracil for targeted therapy. *Materials Science and Engineering: C*, 103, 109828.
- Rawat, M., Singh, D., Saraf, S., & Saraf, S. (2006). Nanocarriers: promising vehicle for bioactive drugs. *Biological & pharmaceutical bulletin*, 29(9), 1790–1798.
- Razzaq, A., Shamsi, S., Ali, A., Ali, Q., Sajjad, M., Malik, A. & Ashraf, M. (2019) Microbial Proteases Applications. *Frontiers in Bioengineering and Biotechnology*, 7.
- Reinke, J, M., & Sorg, H. (2012) Wound repair and regeneration. *European Surgical Journal*, 49(1), 35-43.
- Reymond, J., Bergmann, M. & Darbre, T. (2013) Glycopeptide dendrimers as *Pseudomonas aeruginosa* biofilm inhibitors. *Chemical Society Reviews*, 42(11), 4814.
- Riaz, M. K., Riaz, M. A., Zhang, X., Lin, C., Wong, K. H., Chen, X., Zhang, G., Lu, A., & Yang, Z. (2018). Surface Functionalization and Targeting Strategies of Liposomes in Solid Tumor Therapy: A Review. *International Journal of Molecular Sciences*, 19(1), 195.
- Richter, A. P., Brown, J. S., Bharti, B., Wang, A., Gangwal, S., Houck, K., Cohen Hubal, E. A., Paunov, V. N., Stoyanov, S. D., & Velev, O. D. (2015). An environmentally benign antimicrobial nanoparticle based on a silver-infused lignin core. *Nature nanotechnology*, 10(9), 817–823.
- Richtering, W., & Saunders, B. R. (2014). Gel architectures and their complexity. *Soft matter*, 10(21), 3695–3702.
- Roe, D., Karandikar, B., Bonn-Savage, N., Gibbins, B. & Roulet, J. (2008) Antimicrobial surface functionalization of plastic catheters by silver nanoparticles. *Journal of Antimicrobial Chemotherapy*, 61(4), 869-876.
- Romanovsky, A. A. (2014). Skin temperature: its role in thermoregulation. *Acta Physiologica (Oxford, England)*, 210(3), 498–507.
- Rosenthal, M., Goldberg, D., Aiello, A., Larson, E., & Foxman, B. (2011). Skin microbiota: Microbial community structure and its potential association with health and disease. *Infection, Genetics and Evolution : Journal of Molecular Epidemiology and Evolutionary Genetics in Infectious Diseases*, 11(5), 839–848.

- Rowe, R. C., Sheskey, P. J., & Weller, P. J. (2003) Handbook of pharmaceutical excipients, London ; Chicago : Washington, DC : Pharmaceutical Press ; American Pharmaceutical Association, England, 4th edn.
- Rukavina, Z. and Vanić, Ž. (2016). Current Trends in Development of Liposomes for Targeting Bacterial Biofilms. *Pharmaceutics*, 8(2), 18.
- Russo, E., & Villa, C. (2019) Poloxamer Hydrogels For Biomedical Applications. *Pharmaceutics*, 11 (12), 671.
- Rutherford, S. T., & Bassler, B. L. (2012). Bacterial Quorum Sensing: Its Role in Virulence and Possibilities for Its Control. *Cold Spring Harbor Perspectives in Medicine*, 2(11), a012427.
- Sachetelli, S., Khalil, H., Chen, T., Beaulac, C., Sénéchal, S., & Lagacé, J. (2000). Demonstration of a fusion mechanism between a fluid bactericidal liposomal formulation and bacterial cells. *Biochimica et biophysica acta*, 1463(2), 254–266.
- Saggu, S., Jha, G. & Mishra, P. (2019) Enzymatic Degradation of Biofilm by Metalloprotease From Microbacterium sp. SKS10. *Frontiers in Bioengineering and Biotechnology*, 7.
- Saidykhan, L., Abu Bakar, M. Z., Rukayadi, Y., Kura, A. U., & Latifah, S. Y. (2016). Development of nanoantibiotic delivery system using cockle shell-derived aragonite nanoparticles for treatment of osteomyelitis. *International journal of nanomedicine*, 11, 661–673.
- Saini, R., Saini, S., & Sharma, S. (2011). Biofilm: A dental microbial infection. *Journal of Natural Science, Biology, and Medicine*, 2(1), 71–75.
- Salvioni, L., Galbiati, E., Collico, V., Alessio, G., Avvakumova, S., Corsi, F., Tortora, P., Prosperi, D., & Colombo, M. (2017). Negatively charged silver nanoparticles with potent antibacterial activity and reduced toxicity for pharmaceutical preparations. *International Journal of Nanomedicine*, 12, 2517–2530.
- Sanford, J. A., & Gallo, R. L. (2013). Functions of the skin microbiota in health and disease. *Seminars in Immunology*, 25(5), 370–377.
- SanMiguel, A., & Grice, E. A. (2015). Interactions between host factors and the skin microbiome. *Cellular and Molecular Life Sciences : CMLS*, 72(8), 1499–1515.
- Saraiva, C., Praça, C., Ferreira, R., Santos, T., Ferreira, L., & Bernardino, L. (2016). Nanoparticle-mediated brain drug delivery: Overcoming blood-brain barrier to treat neurodegenerative diseases. *Journal of controlled release : official journal of the Controlled Release Society*, 235, 34–47.
- Saravanan, A., Maruthapandi, M., Das, P., Ganguly, S., Margel, S., Luong, J. & Gedanken, A. (2020) Applications of N-Doped Carbon Dots as Antimicrobial Agents, Antibiotic Carriers, and Selective Fluorescent Probes for Nitro Explosives. *ACS Applied Bio Materials*, 3(11), 8023-8031.
- Sasaki, Y. & Akiyoshi, K. (2010) Nanogel engineering for new nanobiomaterials: from chaperoning engineering to biomedical applications. *The Chemical Record*, n/a-n/a.
- Sasson, G., Bai, A., Showler, A., Burry, L., Steinberg, M., Ricciuto, D., Fernandes, T., Chiu, A., Raybardhan, S., Science, M., Fernando, E., Morris, A. and Bell, C. (2017). Staphylococcus aureus bacteremia in immunosuppressed patients: a multicenter, retrospective cohort study. *European Journal of Clinical Microbiology & Infectious Diseases*, 36(7), 1231-1241.
- Satarkar, N., Biswal, D. & Hilt, J. (2010) Hydrogel nanocomposites: a review of applications as remote controlled biomaterials. *Soft Matter*, 6(11), 2364.
- Saur, T., Morin, E., Habouzit, F., Bernet, N., & Escudié, R. (2017). Impact of wall shear stress on initial bacterial adhesion in rotating annular reactor. *PLoS ONE*, 12(2), e0172113.
- Scales, B. S., & Huffnagle, G. B. (2013). The Microbiome in Wound Repair and Tissue Fibrosis. *The Journal of Pathology*, 229(2), 323–331.
- Scheetz, L., Park, K., Li, Q., Lowenstein, P., Castro, M., Schwendeman, A. & Moon, J. (2019) Engineering patient-specific cancer immunotherapies. *Nature Biomedical Engineering*, 3(10), 768-782.
- Schommer, N. N., & Gallo, R. L. (2013). Structure and function of the human skin microbiome. *Trends in Microbiology*, 21(12), 660–668.

- Schwartz S., Jr (2017). Unmet needs in developing nanoparticles for precision medicine. *Nanomedicine (London, England)*, 12(4), 271–274.
- Sedighi, M., Sieber, S., Rahimi, F., Shahbazi, M., Rezayan, A., Huwylar, J. & Witzigmann, D. (2018) Rapid optimization of liposome characteristics using a combined microfluidics and design-of-experiment approach. *Drug Delivery and Translational Research*, 9(1), 404-413.
- Sercombe, L., Veerati, T., Moheimani, F., Wu, S. Y., Sood, A. K., & Hua, S. (2015). Advances and Challenges of Liposome Assisted Drug Delivery. *Frontiers in Pharmacology*, 6, 286.
- Serrano-Sevilla, I., Artiga, Á., Mitchell, S. G., De Matteis, L., & de la Fuente, J. M. (2019). Natural Polysaccharides for siRNA Delivery: Nanocarriers Based on Chitosan, Hyaluronic Acid, and Their Derivatives. *Molecules (Basel, Switzerland)*, 24(14), 2570.
- Shade, C. W. (2016). Liposomes as Advanced Delivery Systems for Nutraceuticals. *Integrative Medicine: A Clinician's Journal*, 15(1), 33–36.
- Shah, J. M. Y., Omar, E., Pai, D. R., & Sood, S. (2012). Cellular events and biomarkers of wound healing. *Indian Journal of Plastic Surgery : Official Publication of the Association of Plastic Surgeons of India*, 45(2), 220–228.
- Sharma, S., Shukla, S., & Vaid, D. (1983) Shellac-Structure, Characteristics & Modification. *Defence Science Journal*, 33 (3), 261-271.
- Shellac | resin. (1998) <https://www.britannica.com/topic/shellac> [Accessed 16/11/2020].
- Shen, C., Li, J., Zhang, Y., Li, Y., Shen, G., Zhu, J., & Tao, J. (2017). Polyethylenimine-based micro/nanoparticles as vaccine adjuvants. *International journal of nanomedicine*, 12, 5443–5460.
- Shen, S., Wu, Y., Liu, Y., & Wu, D. (2017). High drug-loading nanomedicines: progress, current status, and prospects. *International journal of nanomedicine*, 12, 4085–4109.
- Sheorey, D., Shastri, A., & Dorle, A. (1991) Effect Of Variables On The Preparation Of Shellac Microcapsules By Solvent Evaporation Technique: Part 1. *International Journal of Pharmaceutics*, 68 (1-3), 19-23.
- Shin, S., Cho, C., & Oh, I. (2001) Effects Of Non-Ionic Surfactants As Permeation Enhancers Towards Piroxicam From The Poloxamer Gel Through Rat Skins. *International Journal of Pharmaceutics*, 222 (2), 199-203.
- Silver, L. L. (2011). Challenges of Antibacterial Discovery. *Clinical Microbiology Reviews*, 24(1), 71–109.
- Sindhvani, S., Syed, A. M., Ngai, J., Kingston, B. R., Maiorino, L., Rothschild, J., MacMillan, P., Zhang, Y., Rajesh, N. U., Hoang, T., Wu, J., Wilhelm, S., Zilman, A., Gadde, S., Sulaiman, A., Ouyang, B., Lin, Z., Wang, L., Egeblad, M., & Chan, W. (2020). The entry of nanoparticles into solid tumours. *Nature materials*, 19(5), 566–575.
- Singh, A. P., Biswas, A., Shukla, A., & Maiti, P. (2019). Targeted therapy in chronic diseases using nanomaterial-based drug delivery vehicles. *Signal transduction and targeted therapy*, 4, 33.
- Singh, R., & Lillard, J. W. (2009). Nanoparticle-based targeted drug delivery. *Experimental and Molecular Pathology*, 86(3), 215–223.
- Singh, R., Nadhe, S., Wadhvani, S., Shedbalkar, U., & Chopade, B. (2016) Nanoparticles For Control Of Biofilms Of Acinetobacter Species. *Materials*, 9 (5), 383.
- Singh, R., Smitha, M. and Singh, S. (2014) The Role of Nanotechnology in Combating Multi-Drug Resistant Bacteria. *Journal of Nanoscience and Nanotechnology*, 14(7), 4745-4756.
- Singh, S., Singh, S. K., Chowdhury, I., & Singh, R. (2017). Understanding the Mechanism of Bacterial Biofilms Resistance to Antimicrobial Agents. *The open microbiology journal*, 11, 53–62.
- Slavin, Y. N., Asnis, J., Häfeli, U. O., & Bach, H. (2017). Metal nanoparticles: understanding the mechanisms behind antibacterial activity. *Journal of Nanobiotechnology*, 15, 65.
- Slavin, Y., Asnis, J., Häfeli, U. & Bach, H. (2017) Metal nanoparticles: understanding the mechanisms behind antibacterial activity. *Journal of Nanobiotechnology*, 15(1).

- Smerkova, K., Dolezelikova, K., Bozdechova, L., Heger, Z., Zurek, L., & Adam, V. (2020). Nanomaterials with active targeting as advanced antimicrobials. *Wiley interdisciplinary reviews. Nanomedicine and nanobiotechnology*, 12(5), e1636.
- Smith, R. S., & Iglewski, B. H. (2003). *Pseudomonas aeruginosa* quorum sensing as a potential antimicrobial target. *Journal of Clinical Investigation*, 112(10), 1460–1465.
- Solano, C., Echeverz, M. and Lasa, I. (2014). Biofilm dispersion and quorum sensing. *Current Opinion in Microbiology*, 18, 96-104.
- Soltani, S., Zakeri-Milani, P., Barzegar-Jalali, M., & Jelvehgari, M. (2016). Design of eudragit RL nanoparticles by nanoemulsion method as carriers for ophthalmic drug delivery of ketotifen fumarate. *Iranian journal of basic medical sciences*, 19(5), 550–560.
- Song, F., Koo, H. and Ren, D. (2015). Effects of Material Properties on Bacterial Adhesion and Biofilm Formation. *Journal of Dental Research*, 94(8), 1027-1034.
- Soni, K. S., Desale, S. S., & Bronich, T. K. (2016). Nanogels: An overview of properties, biomedical applications and obstacles to clinical translation. *Journal of controlled release : official journal of the Controlled Release Society*, 240, 109–126.
- Specht, F., Saugestad, M., Waaler, T., & Muller, B. W. (1998) The application of shellac as an acidic polymer for enteric coating. *Pharm. Technol. Eur.*, 10, 20– 28.
- Speziale, P., Pietrocola, G., Foster, T., & Geoghegan, J. (2014) Protein-based biofilm matrices in Staphylococci. *Front Cell Infect Microbiol.*, 4, 171.
- Spoering, A. L., & Lewis, K. (2001). Biofilms and Planktonic Cells of *Pseudomonas aeruginosa* Have Similar Resistance to Killing by Antimicrobials. *Journal of Bacteriology*, 183(23), 6746–6751.
- Stach, M., Siriwardena, T., Köhler, T., van Delden, C., Darbre, T. & Reymond, J. (2014) Combining Topology and Sequence Design for the Discovery of Potent Antimicrobial Peptide Dendrimers against Multidrug-Resistant *Pseudomonas aeruginosa*. *Angewandte Chemie International Edition*, 53(47), 12827-12831.
- Stalder, T., & Top, E. (2016). Plasmid transfer in biofilms: a perspective on limitations and opportunities. *NPJ Biofilms and Microbiomes*, 2, 16022–.
- Stewart, P. S. (2015). Antimicrobial Tolerance in Biofilms. *Microbiology Spectrum*, 3(3), 10.1128/microbiolspec.MB-0010-2014.
- Stone, N. R., Bicanic, T., Salim, R., & Hope, W. (2016). Liposomal Amphotericin B (AmBisome®): A Review of the Pharmacokinetics, Pharmacodynamics, Clinical Experience and Future Directions. *Drugs*, 76(4), 485–500.
- Stücker, M., Struk, A., Altmeyer, P., Herde, M., Baumgärtl, H., & Lübbers, D. W. (2002). The cutaneous uptake of atmospheric oxygen contributes significantly to the oxygen supply of human dermis and epidermis. *The Journal of Physiology*, 538(Pt 3), 985–994.
- Sun, D., Jeannot, K., Xiao, Y., & Knapp, C. W. (2019). Editorial: Horizontal Gene Transfer Mediated Bacterial Antibiotic Resistance. *Frontiers in microbiology*, 10, 1933.
- Tamilvanan, S., Venkateshan, N., & Ludwig, A. (2008). The potential of lipid- and polymer-based drug delivery carriers for eradicating biofilm consortia on device-related nosocomial infections. *Journal of controlled release : official journal of the Controlled Release Society*, 128(1), 2–22.
- Tan, C. H., Koh, K. S., Xie, C., Tay, M., Zhou, Y., Williams, R., Ng, W. J., Rice, S. A., & Kjelleberg, S. (2014). The role of quorum sensing signalling in EPS production and the assembly of a sludge community into aerobic granules. *The ISME Journal*, 8(6), 1186–1197.
- Tanaka, R., Arai, K., Matsuno, J., Soejima, M., Lee, J., Takahashi, R., Sakurai, K. & Fujii, S. (2020) Furry nanoparticles: synthesis and characterization of nanoemulsion-mediated core crosslinked nanoparticles and their robust stability in vivo. *Polymer Chemistry*, 11(27), 4408-4416.
- Tang, C., Yin, L., Yu, J., Yin, C., & Pei, Y. (2007) Swelling Behavior And Biocompatibility Of Carbopol-Containing Superporous Hydrogel Composites. *Journal of Applied Polymer Science*, 104 (5), 2785-2791.
- Tansey, E. and Johnson, C. (2015). Recent advances in thermoregulation. *Advances in Physiology Education*, 39(3), 139-148.

- Tao, X., Xie, Y., Zhang, Q., Qiu, X., Yuan, L., Wen, Y., Li, M., Yang, X., Tao, T., Xie, M., Lv, Y., Wang, Q., & Feng, X. (2016). Cholesterol-Modified Amino-Pullulan Nanoparticles as a Drug Carrier: Comparative Study of Cholesterol-Modified Carboxyethyl Pullulan and Pullulan Nanoparticles. *Nanomaterials (Basel, Switzerland)*, 6(9), 165.
- Taresco, V., Crisante, F., Francolini, I., Martinelli, A., D'Ilario, L., Ricci-Vitiani, L., Buccarelli, M., Pietrelli, L. & Piozzi, A. (2015a) Antimicrobial and antioxidant amphiphilic random copolymers to address medical device-centered infections. *Acta Biomaterialia*, 22, 131-140.
- Taresco, V., Gontrani, L., Crisante, F., Francolini, I., Martinelli, A., D'Ilario, L., Bordi, F. & Piozzi, A. (2015b) Self-Assembly of Catecholic Moiety-Containing Cationic Random Acrylic Copolymers. *The Journal of Physical Chemistry B*, 119(26), 8369-8379.
- Tayo, L. L. (2017). Stimuli-responsive nanocarriers for intracellular delivery. *Biophysical Reviews*, 9(6), 931-940.
- Tello, A., Austin, B., & Telfer, T. C. (2012). Selective Pressure of Antibiotic Pollution on Bacteria of Importance to Public Health. *Environmental Health Perspectives*, 120(8), 1100–1106.
- Tenzer, S., Docter, D., Kuharev, J., Musyanovych, A., Fetz, V., Hecht, R., Schlenk, F., Fischer, D., Kiouptsi, K., Reinhardt, C., Landfester, K., Schild, H., Maskos, M., Knauer, S. & Stauber, R. (2013) Rapid formation of plasma protein corona critically affects nanoparticle pathophysiology. *Nature Nanotechnology*, 8(10), 772-781.
- Tian, H., He, Z., Sun, C., Yang, C., Zhao, P., Liu, L., Leong, K., Mao, H., Liu, Z. & Chen, Y. (2018) Uniform Core-Shell Nanoparticles with Thiolated Hyaluronic Acid Coating to Enhance Oral Delivery of Insulin. *Advanced Healthcare Materials*, 7(17), 1800285.
- Tomic-Canic, M., Ayello, E. A., Stojadinovic, O., Golinko, M. S., & Brem, H. (2008). Using gene transcription patterns (bar coding scans) to guide wound debridement and healing. *Advances in skin & wound care*, 21(10), 487–494.
- Torchilin V. P. (2000). Drug targeting. *European journal of pharmaceutical sciences : official journal of the European Federation for Pharmaceutical Sciences*, 11 Suppl 2, S81–S91.
- Torchilin, V. (2005). Lipid-Core Micelles for Targeted Drug Delivery. *Current Drug Delivery*, 2(4), 319-327.
- Toyofuku, M., Roschitzki, B., Riedel, K. & Eberl, L. (2012) Identification of Proteins Associated with the Pseudomonas aeruginosa Biofilm Extracellular Matrix. *Journal of Proteome Research*, 11(10), 4906-4915.
- Tseng, B. S., Zhang, W., Harrison, J. J., Quach, T. P., Song, J. L., Penterman, J., Singh, P. K., Chopp, D. L., Packman, A. I., & Parsek, M. R. (2013). The extracellular matrix protects Pseudomonas aeruginosa biofilms by limiting the penetration of tobramycin. *Environmental microbiology*, 15(10), 2865–2878.
- Tyers, M., & Wright, G. D. (2019). Drug combinations: a strategy to extend the life of antibiotics in the 21st century. *Nature reviews. Microbiology*, 17(3), 141–155.
- Uhl, C., Gao, Y., Zhou, S. & Liu, Y. (2018) The shape effect on polymer nanoparticle transport in a blood vessel. *RSC Advances*, 8(15), 8089-8100.
- Unnanuntana, A., Bonsignore, L., Shirliff, M. and Greenfield, E. (2009). The Effects of Farnesol on Staphylococcus aureus Biofilms and Osteoblasts. *The Journal of Bone & Joint Surgery*, 91(11), 2683-2692.
- Upton, D., Hender, C., & Solowiej, K. (2012). Mood disorders in patients with acute and chronic wounds: a health professional perspective. *Journal of wound care*, 21(1), 42–48.
- Urakami, H., Hentschel, J., Seetho, K., Zeng, H., Chawla, K., & Guan, Z. (2013). Surfactant-free synthesis of biodegradable, biocompatible, and stimuli-responsive cationic nanogel particles. *Biomacromolecules*, 14(10), 3682–3688.
- Vanić, Ž., & Škalko-Basnet, N. (2013). Nanopharmaceuticals for improved topical vaginal therapy: can they deliver?. *European journal of pharmaceutical sciences : official journal of the European Federation for Pharmaceutical Sciences*, 50(1), 29–41.
- Vanić, Z., Holæter, A. M., & Skalko-Basnet, N. (2015). (Phospho)lipid-based Nanosystems for Skin Administration. *Current pharmaceutical design*, 21(29), 4174–4192.
- Vanić, Ž., Hurler, J., Ferderber, K., Golja Gašparović, P., Škalko-Basnet, N., & Filipović-Grčić, J. (2014). Novel vaginal drug delivery system: deformable propylene glycol liposomes-in-hydrogel. *Journal of liposome research*, 24(1), 27–36.

- Varges, P. R., Costa, C. M., Fonseca, B. S., Naccache, M. F., & De Souza Mendes, P. R. (2019) Rheological Characterization Of Carbopol® Dispersions In Water And In Water/Glycerol Solutions. *Fluids*, 4 (1), 3.
- Vassallo, A., Silletti, M., Faraone, I. & Milella, L. (2020) Nanoparticulate Antibiotic Systems as Antibacterial Agents and Antibiotic Delivery Platforms to Fight Infections. *Journal of Nanomaterials*, 2020, 1-31.
- Vazquez-Muñoz, R., Meza-Villecas, A., Fournier, P., Soria-Castro, E., Juarez-Moreno, K., Gallego-Hernández, A., Bogdanchikova, N., Vazquez-Duhalt, R. & Huerta-Saquero, A. (2019) Enhancement of antibiotics antimicrobial activity due to the silver nanoparticles impact on the cell membrane. *PLOS ONE*, 14(11), e0224904.
- Ventola, C. L. (2015). The Antibiotic Resistance Crisis: Part 1: Causes and Threats. *Pharmacy and Therapeutics*, 40(4), 277–283.
- Veronese, F. & Pasut, G. (2005) PEGylation, successful approach to drug delivery. *Drug Discovery Today*, 10(21), 1451-1458.
- Villa-Costa, M., Gioia, R., Aceña, J., Pérez, S., Casamayor, E. and Dachs, J. (2017). Degradation of sulfonamides as a microbial resistance mechanism. *Water Research*, 115, 309-317.
- von Roemeling, C., Jiang, W., Chan, C., Weissman, I. & Kim, B. (2017) Breaking Down the Barriers to Precision Cancer Nanomedicine. *Trends in Biotechnology*, 35(2), 159-171.
- Wagner, A., Knipe, J., Orive, G. & Peppas, N. (2019) Quantum dots in biomedical applications. *Acta Biomaterialia*, 94, 44-63.
- Wang, A., Madden, L.A., Paunov, V.N. (2020b) High-throughput fabrication of hepatic cell clusteroids with enhanced growth and functionality for tissue engineering applications, *Materials Advances*, 1, 3022–3032.
- Wang, J., Potocny, A., Rosenthal, J. & Day, E. (2019a) Gold Nanoshell-Linear Tetrapyrrole Conjugates for Near Infrared-Activated Dual Photodynamic and Photothermal Therapies. *ACS Omega*, 5(1), 926-940.
- Wang, L. S., Gupta, A., & Rotello, V. M. (2016). Nanomaterials for the Treatment of Bacterial Biofilms. *ACS infectious diseases*, 2(1), 3–4.
- Wang, L., Hu, C., & Shao, L. (2017). The antimicrobial activity of nanoparticles: present situation and prospects for the future. *International Journal of Nanomedicine*, 12, 1227–1249.
- Wang, L., Ishida, Y., Ohtani, H., Tsuge, S., & Nakayama, T. (1999) Characterization Of Natural Resin Shellac By Reactive Pyrolysis–Gas Chromatography In The Presence Of Organic Alkali. *Analytical Chemistry*, 71 (7), 1316-1322.
- Wang, N., Cheng, X., Li, N., Wang, H., & Chen, H. (2019b). Nanocarriers and Their Loading Strategies. *Advanced healthcare materials*, 8(6), e1801002.
- Wang, S., Chen, Y. & Chen, Y. (2018) Antibacterial gold nanoparticle-based photothermal killing of vancomycin-resistant bacteria. *Nanomedicine*, 13(12), 1405-1416.
- Wang, S., Gao, Y., Jin, Q. & Ji, J. (2020a) Emerging antibacterial nanomedicine for enhanced antibiotic therapy. *Biomaterials Science*, 8(24), 6825-6839.
- Wang, S., Zhang, C., Qi, B., Sui, X., Jiang, L., Li, Y., Wang, Z., Feng, H., Wang, R. & Zhang, Q. (2014) Immobilized alcalase alkaline protease on the magnetic chitosan nanoparticles used for soy protein isolate hydrolysis. *European Food Research and Technology*, 239(6), 1051-1059.
- Wang, W., Gaus, K., Tilley, R. & Gooding, J. (2019c) The impact of nanoparticle shape on cellular internalisation and transport: what do the different analysis methods tell us?. *Materials Horizons*, 6(8), 1538-1547.
- Wang, X., Ishida, T. & Kiwada, H. (2007) Anti-PEG IgM elicited by injection of liposomes is involved in the enhanced blood clearance of a subsequent dose of PEGylated liposomes. *Journal of Controlled Release*, 119(2), 236-244.
- Wang, Y., Hong, C., Chiu, W., & Fang, J. (2001) In Vitro And In Vivo Evaluations Of Topically Applied Capsaicin And Nonivamide From Hydrogels. *International Journal of Pharmaceutics*, 224 (1-2), 89-104.
- Wardlaw, J., Murray, V., Berge, E., del Zoppo, G., Sandercock, P., Lindley, R. & Cohen, G. (2012) Recombinant tissue plasminogen activator for acute ischaemic stroke: an updated systematic review and meta-analysis. *The Lancet*, 379(9834), 2364-2372.

- Wasupalli, G., & Verma, D. (2018) Molecular Interactions In Self-Assembled Nano-Structures Of Chitosan-Sodium Alginate Based Polyelectrolyte Complexes. *International Journal of Biological Macromolecules*, 114, 10-17.
- Waters, V., & Ratjen, F. (2014). Inhaled liposomal amikacin. *Expert review of respiratory medicine*, 8(4), 401–409.
- Wei, L., Lu, J., Xu, H., Patel, A., Chen, Z.-S., & Chen, G. (2015). Silver nanoparticles: synthesis, properties, and therapeutic applications. *Drug Discovery Today*, 20(5), 595–601.
- Weldrick, P. J., San, S., & Paunov, V. N. (2021) Advanced Alcalase-Coated Clindamycin-Loaded Carbopol Nano-gels for Removal of Persistent Bacterial Biofilms. *ACS Appl. Nano Mater.*, Advanced Article, DOI: 10.1021/acsnm.0c02810.
- Weldrick, P.J., Hardman, M.J., & Paunov, V.N. (2019b) Enhanced Clearing of Wound-Related Pathogenic Bacterial Biofilms Using Protease-Functionalized Antibiotic Nanocarriers, *ACS Appl. Mater. Interf.*, 11(43), 43902–43919.
- Weldrick, P.J., Iveson, S., Hardman, M.J., Paunov, V.N. (2019a) Breathing new life into old antibiotics: Overcoming antibacterial resistance by antibiotic-loaded nanogel carriers with cationic surface functionality, *Nanoscale*, 11(21), 10472–10485.
- Wen, H., Jung, H., & Li, X. (2015). Drug Delivery Approaches in Addressing Clinical Pharmacology-Related Issues: Opportunities and Challenges. *The AAPS Journal*, 17(6), 1327–1340.
- Wessel, A. K., Arshad, T. A., Fitzpatrick, M., Connell, J. L., Bonnez, R. T., Shear, J. B., & Whiteley, M. (2014). Oxygen Limitation within a Bacterial Aggregate. *mBio*, 5(2), e00992–14.
- Whitfield, G., Marmont, L., & Howell, P. (2015) Enzymatic Modifications Of Exopolysaccharides Enhance Bacterial Persistence. *Frontiers in Microbiology*, 6.
- Wiest, D. B., Cochran, J. B., & Tecklenburg, F. W. (2012). Chloramphenicol Toxicity Revisited: A 12-Year-Old Patient With a Brain Abscess. *The Journal of Pediatric Pharmacology and Therapeutics : JPPT*, 17(2), 182–188.
- Wilhelm, S., Tavares, A., Dai, Q., Ohta, S., Audet, J., Dvorak, H. & Chan, W. (2016) Analysis of nanoparticle delivery to tumours. *Nature Reviews Materials*, 1(5).
- Wilkinson, H, N., & Hardman, M, J. (2017) The role of estrogen in cutaneous ageing and repair. *Maturitas*, 103, 60-64.
- Wilkinson, H., Iveson, S., Catherall, P. & Hardman, M. (2018). A Novel Silver Bioactive Glass Elicits Antimicrobial Efficacy Against *Pseudomonas aeruginosa* and *Staphylococcus aureus* in an ex Vivo Skin Wound Biofilm Model. *Frontiers in Microbiology*, 9.
- Williams, D., Saar, J., Bleicher, V., Rau, S., Lienkamp, K. & Rosenzweig, Z. (2020) Poly(oxanorbornene)-Coated CdTe Quantum Dots as Antibacterial Agents. *ACS Applied Bio Materials*, 3(2), 1097-1104.
- Williams, H., Campbell, L., Crompton, R., Singh, G., McHugh, B., Davidson, D., McBain, A., Cruickshank, S. and Hardman, M. (2018). Microbial Host Interactions and Impaired Wound Healing in Mice and Humans: Defining a Role for BD14 and NOD2. *Journal of Investigative Dermatology*.
- Williams, M. and Gallo, R. (2017). Evidence that Human Skin Microbiome Dysbiosis Promotes Atopic Dermatitis. *Journal of Investigative Dermatology*, 137(12), 2460-2461.
- Willyard C. (2017). The drug-resistant bacteria that pose the greatest health threats. *Nature*, 543(7643), 15.
- Wilson, M. C., Nam, S.-J., Gulder, T. A. M., Kauffman, C. A., Jensen, P. R., Fenical, W., & Moore, B. S. (2011). Structure and biosynthesis of the marine streptomycete ansamycin ansalactam A and its distinctive branched chain polyketide extender unit. *Journal of the American Chemical Society*, 133(6), 1971–1977.
- Winnicka, K., Wroblewska, M., Wiczorek, P., Sacha, P. & Tryniszewska, E. (2013) The Effect of PAMAM Dendrimers on the Antibacterial Activity of Antibiotics with Different Water Solubility. *Molecules*, 18(7), 8607-8617.
- Witten, J., & Ribbeck, K. (2017). The particle in the spider's web: transport through biological hydrogels. *Nanoscale*, 9(24), 8080–8095.
- Wolcott, R., Sanford, N., Gabriliska, R., Oates, J., Wilkinson, J. and Rumbaugh, K. (2016). Microbiota is a primary cause of pathogenesis of chronic wounds. *Journal of Wound Care*, 25(Sup10), 33-43.

- Wong, P., Tang, S., Mukherjee, J., Tang, K., Gam, K., Isham, D., Murat, C., Sun, R., Baker, J. & Choi, S. (2016) Light-controlled active release of photocaged ciprofloxacin for lipopolysaccharide-targeted drug delivery using dendrimer conjugates. *Chemical Communications*, 52(68), 10357-10360.
- Wu, L., Rodríguez-Rodríguez, C., Cun, D., Yang, M., Saatchi, K. & Häfeli, U. (2020) Quantitative comparison of three widely-used pulmonary administration methods in vivo with radiolabeled inhalable nanoparticles. *European Journal of Pharmaceutics and Biopharmaceutics*, 152, 108-115.
- Wu, S., Li, A., Zhao, X., Zhang, C., Yu, B., Zhao, N. & Xu, F. (2019) Silica-Coated Gold–Silver Nanocages as Photothermal Antibacterial Agents for Combined Anti-Infective Therapy. *ACS Applied Materials & Interfaces*, 11(19), 17177-17183.
- Wypij, M., Świecimska, M., Czarnecka, J., Dahm, H., Rai, M. & Golinska, P. (2018) Antimicrobial and cytotoxic activity of silver nanoparticles synthesized from two haloalkaliphilic actinobacterial strains alone and in combination with antibiotics. *Journal of Applied Microbiology*, 124(6), 1411-1424.
- Xiao, C., Qi, X., Maitani, Y., & Nagai, T. (2004). Sustained release of cisplatin from multivesicular liposomes: potentiation of antitumor efficacy against S180 murine carcinoma. *Journal of pharmaceutical sciences*, 93(7), 1718–1724.
- Xu, H., Murdaugh, A. E., Chen, W., Aidala, K. E., Ferguson, M. A., Spain, E. M., & Núñez, M. E. (2013a). Characterizing Pilus-Mediated Adhesion of Biofilm-Forming *E. coli* to Chemically Diverse Surfaces Using Atomic Force Microscopy. *Langmuir*, 29(9), 3000–3011.
- Xu, L., Zhang, H. & Wu, Y. (2013b) Dendrimer Advances for the Central Nervous System Delivery of Therapeutics. *ACS Chemical Neuroscience*, 5(1), 2-13.
- Xue, J., & Zhang, Z. (2008) Preparation And Characterization Of Calcium-Shellac Spheres As A Carrier Of Carbamide Peroxide. *Journal of Microencapsulation*, 25 (8), 523-530.
- Yan, M., Ge, J., Liu, Z., & Ouyang, P. (2006). Encapsulation of single enzyme in nanogel with enhanced biocatalytic activity and stability. *Journal of the American Chemical Society*, 128(34), 11008–11009.
- Yang, Q., Jacobs, T., McCallen, J., Moore, D., Huckaby, J., Edelstein, J. & Lai, S. (2016) Analysis of Pre-existing IgG and IgM Antibodies against Polyethylene Glycol (PEG) in the General Population. *Analytical Chemistry*, 88(23), 11804-11812.
- Yang, W., Liang, H., Ma, S., Wang, D. & Huang, J. (2019) Gold nanoparticle based photothermal therapy: Development and application for effective cancer treatment. *Sustainable Materials and Technologies*, 22, e00109.
- Yang, W., Wiederhold, N, P., & Williams, R, O. (2008) 3rd Drug delivery strategies for improved azole antifungal action. *Expert Opin Drug Deliv.*, 5, 1199e216.
- Yates, C. C., Hebda, P., & Wells, A. (2012). Skin Wound Healing and Scarring: Fetal Wounds and Regenerative Restitution. *Birth Defects Research. Part C, Embryo Today : Reviews*, 96(4), 325–333.
- Yeo, E., Cheah, J., Thong, P., Soo, K. & Kah, J. (2019) Gold Nanorods Coated with Apolipoprotein E Protein Corona for Drug Delivery. *ACS Applied Nano Materials*, 2(10), 6220-6229.
- Yin, Y., Hu, B., Yuan, X., Cai, L., Gao, H., & Yang, Q. (2020). Nanogel: A Versatile Nano-Delivery System for Biomedical Applications. *Pharmaceutics*, 12(3), 290.
- Ying, S., Zeng, D.-N., Chi, L., Tan, Y., Galzote, C., Cardona, C., Lax, S., Gilbert, J., & Quan, Z.-X. (2015). The Influence of Age and Gender on Skin-Associated Microbial Communities in Urban and Rural Human Populations. *PLoS ONE*, 10(10), e0141842.
- Yong, J. M., Mantaj, J., Cheng, Y., & Vllasaliu, D. (2019). Delivery of Nanoparticles across the Intestinal Epithelium via the Transferrin Transport Pathway. *Pharmaceutics*, 11(7), 298.
- Yoo, J. & Won, Y. (2020) Phenomenology of the Initial Burst Release of Drugs from PLGA Microparticles. *ACS Biomaterials Science & Engineering*, 6(11), 6053-6062.
- Zanoni, M., Habimana, O., Amadio, J. & Casey, E. (2015) Antifouling activity of enzyme-functionalized silica nanobeads. *Biotechnology and Bioengineering*, 113(3), 501-512.
- Zeng, L., An, L., & Wu, X. (2011). Modeling drug-carrier interaction in the drug release from nanocarriers. *Journal of drug delivery*, 370308.

- Zhang, L., Huang, T., Bi, J., Zheng, Y., Lu, C., Hui, Q., Wang, X., & Lin, X. (2020) Long-Term Toxicity Study Of Topical Administration Of A Highly-Stable Rh-Afgf Carbomer 940 Hydrogel In A Rabbit Skin Wound Model. *Frontiers in Pharmacology*, 11.
- Zhang, L., Pornpattananankul, D., Hu, C. & Huang, C. (2010) Development of Nanoparticles for Antimicrobial Drug Delivery. *Current Medicinal Chemistry*, 17(6), 585-594.
- Zhang, L., Tan, L., Chen, L., Chen, X., Long, C., Peng, J., & Qian, Z. (2016). A simple method to improve the stability of docetaxel micelles. *Scientific Reports*, 6, 36957.
- Zhang, L.-J., & Gallo, R. L. (2016) Antimicrobial peptides. *Current Biology*, 1(11), 14-19.
- Zhang, S., Asghar, S., Yu, F., Chen, Z., Hu, Z., Ping, Q., Shao, F., & Xiao, Y. (2019c). BSA Nanoparticles Modified with *N*-Acetylcysteine for Improving the Stability and Mucoadhesion of Curcumin in the Gastrointestinal Tract. *Journal of agricultural and food chemistry*, 67(33), 9371–9381.
- Zhang, T., Song, Y., Xing, Y., Gu, Y., Yan, X., Liu, H., Lu, N., Xu, H., Xu, Z., Zhang, Z. & Yang, M. (2019b) The synergistic effect of Au-COF nanosheets and artificial peroxidase Au@ZIF-8(NiPd) rhombic dodecahedra for signal amplification for biomarker detection. *Nanoscale*, 11(42), 20221-20227.
- Zhang, Y., Meng, S., Ding, J., Peng, Q. & Yu, Y. (2019a) Transition metal-coordinated graphitic carbon nitride dots as a sensitive and facile fluorescent probe for β -amyloid peptide detection. *The Analyst*, 144(2), 504-511.
- Zhao, G., Usui, M. L., Lippman, S. I., James, G. A., Stewart, P. S., Fleckman, P., & Olerud, J. E. (2013a). Biofilms and Inflammation in Chronic Wounds. *Advances in Wound Care*, 2(7), 389–399.
- Zhao, R., Liang, H., Clarke, E., Jackson, C., & Xue, M. (2016). Inflammation in Chronic Wounds. *International Journal of Molecular Sciences*, 17(12), 2085.
- Zhao, Y., Chen, Z., Chen, Y., Xu, J., Li, J. & Jiang, X. (2013b) Synergy of Non-antibiotic Drugs and Pyrimidinethiol on Gold Nanoparticles against Superbugs. *Journal of the American Chemical Society*, 135(35), 12940-12943.
- Zheng, K., Setyawati, M., Lim, T., Leong, D. & Xie, J. (2016) Antimicrobial Cluster Bombs: Silver Nanoclusters Packed with Daptomycin. *ACS Nano*, 10(8), 7934-7942.
- Zhivich, A. (2017). Fighting bacterial resistance: approaches, challenges, and opportunities in the search for new antibiotics. Part 1. Antibiotics used in clinical practice: mechanisms of action and the development of bacterial resistance. *Microbiology Independent Research*, 4(1), 31-5.
- Zhong, Q., Merkel, O. M., Reineke, J. J., & da Rocha, S. R. (2016). Effect of the Route of Administration and PEGylation of Poly(amidoamine) Dendrimers on Their Systemic and Lung Cellular Biodistribution. *Molecular pharmaceutics*, 13(6), 1866–1878.
- Zhuang, J., Wang, D., Li, D., Yang, W., Lu, Y., Wu, W., Wu, W., & Qi, J. (2018) The influence of nanoparticle shape on bilateral exocytosis from Caco-2 cells, *Chinese Chemical Letters*, (29)12, 1815-1818,
- Zong, J., Cobb, S. & Cameron, N. (2017) Peptide-functionalized gold nanoparticles: versatile biomaterials for diagnostic and therapeutic applications. *Biomaterials Science*, 5(5), 872-886.
- Zu, G., Steinmüller, M., Keskin, D., van der Mei, H., Mergel, O. & van Rijn, P. (2020) Antimicrobial Nanogels with Nanoinjection Capabilities for Delivery of the Hydrophobic Antibacterial Agent Triclosan. *ACS Applied Polymer Materials*, 2(12), 5779-5789.

2.0 Chapter 2

Breathing new life into old antibiotics: overcoming antibacterial resistance by antibiotic-loaded nanogel carriers with cationic surface functionality

Weldrick, P. J., Iveson, S., Hardman, M. J., & Paunov, V. N. (2019). Breathing new life into old antibiotics: overcoming antibacterial resistance by antibiotic-loaded nanogel carriers with cationic surface functionality. *Nanoscale*, 11(21), 10472–10485. Reproduced by permission of The Royal Society of Chemistry. Conceptualisation, V.N.P. All experiments were performed by P.J.W under V.N.P. supervision. S.I provided the clinical pathogen isolates used in this study. P.J.W prepared the figures and wrote the manuscript, V.N.P and M.J.H. co-edited the manuscript. All authors have given approval to the final version of the manuscript.

Multidrug-resistant pathogens are prevalent in chronic wounds. There is an urgent need to develop novel antimicrobials and formulation strategies that can overcome antibiotic resistance and provide a safe alternative to traditional antibiotics. This work aimed to develop a novel nanocarrier for two cationic antibiotics, tetracycline hydrochloride and lincomycin hydrochloride which can potentially overcome antibiotic resistance. In this study, the use of surface functionalised polyacrylic copolymer nanogels as carriers for cationic antibiotics is reported. These nanogels can encapsulate small cationic antimicrobial molecules and act as a drug delivery system. They were further functionalised with a biocompatible cationic polyelectrolyte, bPEI, to increase their affinity towards the negatively charged bacterial cell walls. These bPEI-coated nanocarrier-encapsulated antibiotics were assessed against a range of wound isolated pathogens, which had been shown through antimicrobial susceptibility testing (AST) to be resistant to tetracycline and lincomycin. This data revealed that bPEI-coated nanogels with encapsulated tetracycline or lincomycin displayed increased antimicrobial performance against selected wound-derived bacteria, including strains highly resistant to the free antibiotic in solution. Additionally, these nanocarrier-based antibiotics showed no detectable cytotoxic effect against human keratinocytes. The increase in the antimicrobial activity is attributed to the cationically functionalised antibiotic-loaded nanogel carriers' specific electrostatic adhesion to the microbial cell wall delivering a higher local antibiotic concentration. This was confirmed by scanning electron microscopy. Such a nanotechnology-based approach may enhance the effectiveness of a wide variety of existing antibiotics, offering a potentially new mechanism to overcome antibiotic resistance.

2.1 Introduction

Antibiotics are bactericidal or bacteriostatic to microorganisms, and remove them from the body or inhibit them sufficiently that the host immune system can fight infection without being outcompeted by fast-growing microorganisms (Leekha et al., 2011). Antibiotics can function by inhibiting the synthesis of the cell wall and the synthesis of DNA, RNA, or proteins. They enter the cell by diffusing through the cell wall/membrane or by energy dependent transport mechanisms (Peach et al., 2013; Kohanski et al., 2010). However, antibiotic resistance emerged almost immediately after penicillin was used, and resistant species were already discovered before penicillin was first administered to patients (Davies & Davies, 2010). This emergence of resistance has been greatly amplified by the mis- and over-prescription of antibiotics (Llor & Bjerrum, 2014). The lack of recent antibiotic discovery has tipped the balance of discovery/resistance towards bacteria, with an ever-increasing population of resistant species (Silver, 2011; Doron & Davidson, 2011).

Modes of resistance which bacteria may employ include: expression efflux pumps which create an extracellular gradient reducing the concentration of the antibiotic in the cell; enzymatic inactivation of the antibiotic; decreased membrane permeability; or modification of the target to reduce antibiotic affinity (Munita & Arias, 2016). *S. aureus* has been studied extensively regarding antibiotic resistance, within six years of aminoglycoside introduction, the resistance had already emerged *via* enzyme modification, with over 50 separate enzymes discovered (Davies & Wright, 1997). When penicillinase-producing *S. aureus* was targeted with a semi-synthetic analogous penicillin drug, methicillin, this soon became inhibited leading to MRSA strains (Harkins et al., 2017). A similar pattern occurred with vancomycin resistance (VRSA) in 2002, with multi-drug resistance becoming an increasing obstacle (Gardete & Tomasz, 2014; Assis et al., 2017). The spread of resistance has increased by the bacterial ability to exchange genetic material (Perron et al., 2011).

Tetracycline is a broad-spectrum antibiotic, active against many clinically relevant pathogens (Chopra & Roberts, 2001). There are species such as *P. aeruginosa*, which have an intrinsic resistance due to the presence of multi-drug efflux transporters and endogenous antimicrobial inactivation (Poole, 2011). Tetracycline inhibits protein synthesis by blocking the ribosomal site A, reducing the ability of charged aminoacyl-tRNA to enter the active site (Markley & Wencewicz, 2018). Bacteria can commonly become resistant to tetracycline by the horizontal gene transfer of efflux pumps (Li et al., 2013). Lincomycin is a member of the lincosamide antibiotic group and was first used clinically in 1964 (MacLeod et al., 1964). It demonstrates strong activity against Gram-positive species, but weaker activity against some Gram-negative species (Matzov et al., 2017). Similar to tetracycline, lincomycin prevents protein synthesis (Spížek

& Řezanka, 2004). However, lincomycin binds to the 23S portion of the 50S subunit of bacterial ribosomes causing the dissociation of peptidyl-tRNA (Hong et al., 2014). Bacteria can resist lincomycin by the use of multi-drug efflux pumps (Leclercq & Courvalin, 2002).²²

Attempts have been made previously to utilise antibiotics in a way which reduces the development of resistant strains (Webster & Seil, 2012). Sequential regimens alternating between two or more antibiotic doses at sub-lethal concentrations have been shown to reduce collateral sensitivity and help preserve antimicrobial susceptibility to secondary antibiotic treatments, helping to limit the emergence of resistant species (Fuentes-Hernandez et al., 2015; Li et al., 2017; Geilich et al., 2015). Synergistic antibiotic paired treatments are often more effective than single treatments. Novel synergistic combinations are rare but have been found using high-throughput genetic dataset analysis of bacteria exposed to different antibiotics (Ayhan et al., 2016). Efforts have also been made in inhibiting the mRNA encoding for efflux pumps expressed in resistant bacteria. Anti-sense oligonucleotides have been shown to inhibit mRNA translation resulting in the reduced expression of efflux pumps, enabling once resisted antibiotics to be effective again (Din et al., 2017). Recently, Geilich et al. reported a polymerosome based carrier of silver nanoparticles encapsulating ampicillin which show promising results against antibiotic resistant *Escherichia coli*. Despite progress in previous research, there still remains an urgent need for overcoming resistance in pathogens by using a method which is non-invasive and simple to use in antimicrobial formulations.

Nanocarriers have previously been used to deliver drugs in a way which is target specific, increasing the concentration of the drug at the desired location (Din et al., 2017). This can also reduce the unwanted interaction of the drug in healthy tissue, facilitating a general reduced toxic effect (Yu et al., 2016). They can also protect the encapsulated active agent from possible degradation or inactivation within a biological system (Kumari et al., 2014). Nanocarriers must be biocompatible, biodegradable, non-immunogenic, and not intrinsically toxic (Jahangirian et al., 2017). Various strategies for using nanomaterials as antimicrobials and for delivery of antibiotics have been recently reviewed (Halbus et al., 2017; Gupta et al., 2019; Halbus et al., 2019). Tetracycline itself, being a cationic antibiotic, has previously been encapsulated into poly(acrylic acid) based interpenetrating polymer gels (IPNs), however, these are not nanocarriers and did not include any bacterial targeting strategy (Bajpai et al., 2015).

Nanogels are lightly crosslinked ionisable polymer chains that can swell in aqueous solutions when mediated by pH changes. Commonly, polymers with carboxyl group functionality are used to swell the nanogel cross-linked scaffold, but other groups such as sulphate and hydroxyl can also be used (Soni et al., 2016). Polyacrylic nanogels have previously been used to encapsulate and deliver cationic antimicrobial molecules such as berberine hydrochloride and chlorhexidine di-gluconate (Al-Awady et al., 2017; Al-Awady

et al., 2018). Dual-functionalised shellac nanoparticles showed a boost in the berberine and vancomycin antimicrobial effect (Al-Obaidy et al., 2019a; Al-Obaidy et al., 2019b).

In this chapter a novel method for delivery of tetracycline and lincomycin is tested, it is designed to significantly enhance their antibiotic action on resistant bacteria. Specifically, these cationic antibiotics were encapsulated into the cores of a commercially available polyacrylic acid copolymer based nanogel, Carbopol Aqua SF1. The surface of the nanogel particles was further functionalised with a mid-molecular weight ($M_w \sim 25,000$) biocompatible polyelectrolyte, branched polyethylenimine (bPEI; outlined in **Figure 2.1A**). **Figure 2.1B** shows the chemical structure of the nanogel and the individual components. This report studied the antimicrobial efficacy of these antibiotic delivery vehicles against validated tetracycline and lincomycin resistant wound derived clinical isolates. The cationic antibiotic is encapsulated within the interior of the nanocarrier where it electrostatically interacts with partially dissociated COOH groups of the polyacrylic acid-based nanogel. Due to the cationic nature of the bPEI coating, the modified nanogel particles can adhere electrostatically to the negatively charged bacterial cell walls which allows the encapsulated antibiotic to be released in a very close proximity to the targeted bacteria with the purpose of amplifying its antimicrobial effect.

Gram-positive bacteria contain an abundance of teichoic acids, which are linked to either the peptidoglycan or the cell membrane directly. These teichoic acids facilitate a negative charge due to the presence of phosphate in their molecular structure. Similarly, Gram-negative bacteria contain an outer layer of lipopolysaccharides and phospholipids, which confers a negative charge to the bacteria (Silhavy et al., 2010). This process is illustrated in **Figure 2.1C**. This strategy can potentially deliver much higher dose of antibiotic directly on the bacteria cell wall that can be achieved through oral intake and could temporarily overwhelm the bacteria efflux transporters. Additionally, targeted nanocarrier-based antibiotic delivery could avoid cytotoxicity by reducing the overall concentration of the antibiotic in the wound required for efficacy. Here, for the first time, this concept is tested on a range of resistant and susceptible bacterial species clinically isolated from wound samples, in an attempt to overcome antibiotic resistance without increasing the overall concentration of the antibiotic treatment.

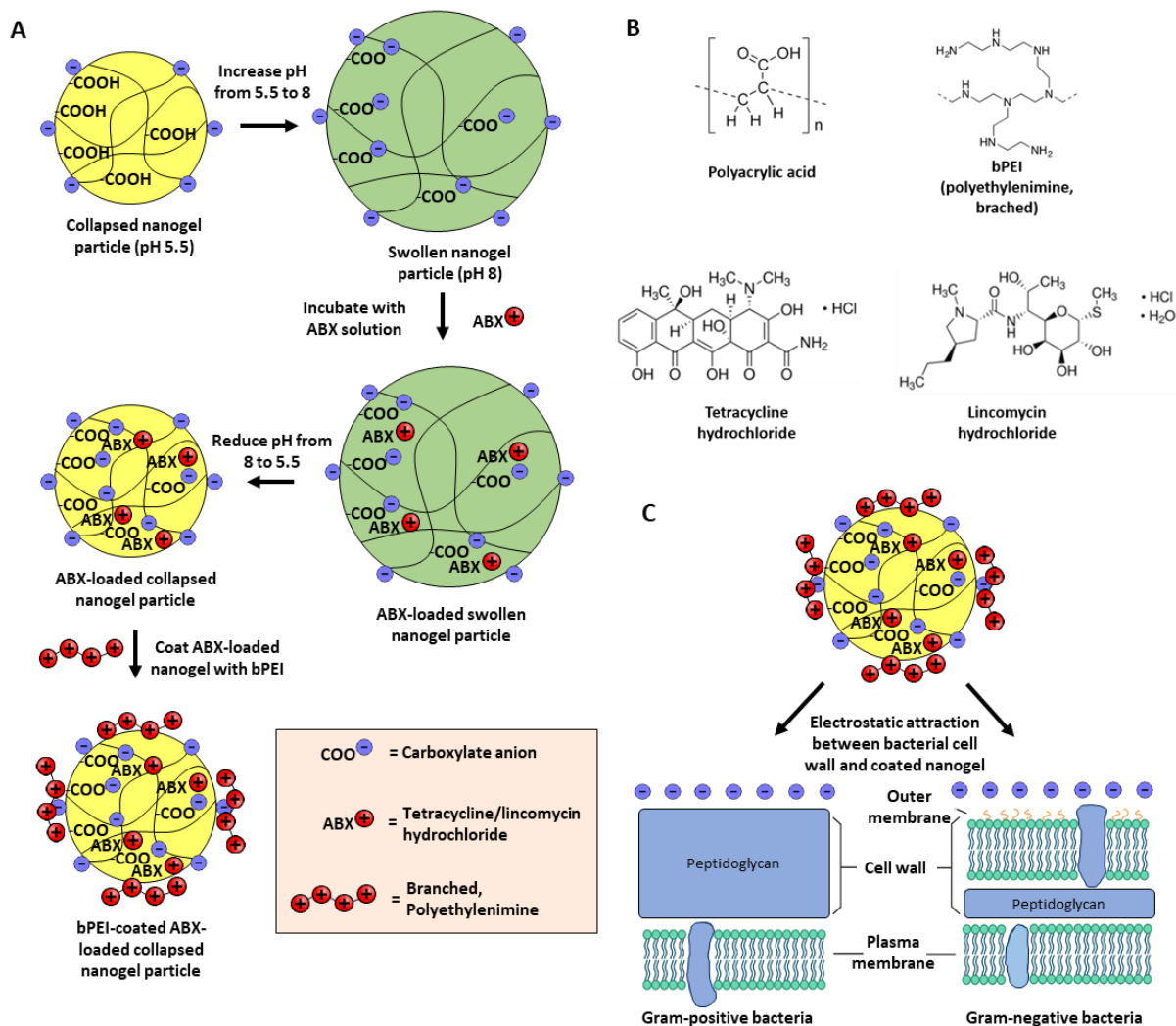


Fig. 2.1. (A) A schematic diagram of the swelling (pH 8) and deswelling (pH 5.5) method used to encapsulate tetracycline and lincomycin hydrochlorides into a polyacrylic acid nanogel carrier (Carbopol Aqua SF1). A biocompatible cationic polyelectrolyte (bPEI) was used to functionalise the nanocarrier surface which makes it non-toxic for mammalian cells, **(B)** the chemical formulas of polyacrylic acid (in the nanogel – partially cross-linked), bPEI, tetracycline hydrochloride, and lincomycin hydrochloride. **(C)** The mechanism for the delivery of antibiotics to the surface of bacteria. The positive charge of the nanoparticle due to ionisation of the bPEI coating binds to the negatively charged surface groups of the bacterial cell wall. The nanogel particle acts as a drug delivery vehicle for cationic antibiotics allowing a localised and continuously release, which can potentially overwhelm the microorganism resistance mechanisms.

2.2 Materials and methods

In this section, the materials and experimental methods used throughout this chapter are described.

2.2.1 Materials

Carbopol Aqua SF1 nanogel was supplied by Lubrizol, USA, as an aqueous suspension (30 wt%). Polyethylenimine, branched (bPEI) was supplied by Sigma-Aldrich (99%), Germany. Resazurin sodium salt (75%, Sigma-Aldrich, UK) was used for cell metabolic activity assays and diluted in Dulbecco's Phosphate Buffered Saline (DPBS) (Gibco, Fisher Scientific, UK) at a concentration of 15 mg mL⁻¹. CellTiter 96® AQueous One Solution Reagent was purchased from Promega, UK, and used to measure the metabolic activity of HaCaT cells. Tetracycline hydrochloride and lincomycin hydrochloride were supplied by Sigma-Aldrich, UK. Mueller-Hilton Broth (MHB), Mueller-Hilton Agar (MHA), tetracycline (30 µg) and lincomycin (15 µg) Antimicrobial Susceptibility Disk were supplied by Oxoid, UK. Dey-Engley neutralising broth was provided by Sigma-Aldrich, UK. Dubecco's Modified Eagle Medium, heated activated Foetal Bovine Serum (FBS), and L-glutamine were delivered by Gibco (Fisher Scientific, UK). Trypsin (10×) was purchased from Sigma-Aldrich, UK, and Trypan Blue Solution (0.4% phosphate buffered saline) was supplied by HyClone™ (GE Healthcare Sciences, UK). *Staphylococcus aureus* subsp. *aureus* Rosenbach (ATCC® 29213™) and *Pseudomonas aeruginosa* (Schroeter) Migula (ATCC® 27853™) were purchased from ATCC. Wound isolated bacterial species (**Table 2.1**) were obtained from Hull Royal Infirmary, inoculated on bijoux slopes. Microbank bead cryovials (Pro-Lab Diagnostics, Canada) were used to store all species for a long term at -80 °C according to the manufacturer's protocol. Deionised water purified by reverse osmosis and ion exchange from a Milli-Q water system (Millipore, UK or PUR1TE SELECT, UK) was used in all studies. Consumable plasticwares used in the study were purchased from Sarstedt (UK), Thermo Scientific (UK), or CytoOne (UK) unless otherwise stated.

Table 2.1. Clinical isolate bacteria used in this study.

Hull Royal Infirmary Code	Genus/Species	Origin
CN1	<i>Staphylococcus epidermidis</i>	Leg ulcer
MR1	Methicillin-resistant <i>Staphylococcus aureus</i>	Leg ulcer
MS1	<i>Staphylococcus aureus</i>	Sebaceous cyst
PS2	<i>Pseudomonas aeruginosa</i>	Leg ulcer
EF7	<i>Enterococcus faecalis</i>	Ulcer
CN10	<i>Staphylococcus pseudointermedius</i>	Burn swab

2.2.2 Bacterial culture

Bacterial stock plates were prepared by streaking one Microbank bead onto an MHA plate and incubating for 24 hours at 37 °C to produce viable colonies. Overnight (O/N) cultures were prepared by incubating a single colony scraped from the MHA stock plates into 10 mL of MHB for 16 hours at 37 °C with 140 rpm (Labnet 211DS shaking incubator, Labnet International). For all bacterial assays, O/N cultures were adjusted to 0.5 McFarland standard by diluting the O/N culture into 0.85 w/v% sterile saline until an optical density of 0.08–0.12 at 625 nm was obtained using a spectrophotometer (Jenway 7310, Cole-Parmer). These adjusted bacterial saline suspensions were then diluted 1:150 into MHB to yield starting concentrations between 5×10^5 and 1×10^6 colony forming units per mL (CFU mL⁻¹).

2.2.3 HaCaT culture

HaCat cells were cultured in DMEM supplemented with 10% FBS and 1% L-Glutamine in humidified conditions at 37°C 5% CO₂ in T75 flasks until a confluency of 80% was achieved, determined by visualisation with a light microscope. Passaging was done at 80% confluency to ensure the cells remained in the exponential phase for experimentation. Passaging was performed by removing spent media and washing in DPBS and incubating with Trypsin (1X) at 37°C 5% CO₂ for 5 minutes until the cells were detached and in suspension. The trypsin was then neutralised with using 1:1 volumetric ratio of fresh DMEM and gently centrifuged at 1000 g for 5 minutes, the supernatant was aspirated, and the pellet resuspended in DMEM (supplemented as above) at a 1:6 ratio and transferred into a fresh T75 flask. Surplus cells were retained for experimentation or frozen at -80°C for long-term storage.

2.2.4 Hydrodynamic diameter and zeta potential distributions of Carbopol Aqua SF1 nanoparticles

67 μL of the 30 wt% Carbopol Aqua SF1 solution was aliquoted and diluted to a final volume of 100 mL in deionised water yielding a 0.02 wt% Carbopol Aqua SF1 solution. Separate aliquots of the 0.02 wt% Carbopol Aqua SF1 solution was adjusted to a pH of 4-12 using droplets 0.25 M NaOH or 0.25 M HCl whilst been stirred on a magnetic plate. The particle size distribution was measured with a Zetasizer Nano ZS (Malvern Instruments, UK) for each pH measurement. 1 mL of each aliquot was placed into a quartz cuvette prior to measurement. At pH 4-7 the refractive index was 1.450 and at pH 8- 12 the refractive index of the swollen nanogel was 1.336, as determined by Al-Awady et al., 2017. The absorption was 1.000 and the temperature was 25°C in both refractive index measurements. A zeta potential dipstick was added to the cuvette to measure the zeta potential distribution.

2.2.5 Zeta potential of wound bacterial species

Bacterial species were cultured as described in as described in the main article. The bacterial suspension was then centrifuged for 10 minutes at 5000 *g* and the supernatant discarded. The pellet was washed twice with deionised water and finally resuspended into 45 mL of deionised water. An1 mL aliquot of this suspension was then added to a quartz cuvette and the mean zeta potential distribution was measured using the Dipstick probe and a Zetasizer Nano ZS (Malvern Instruments, UK). The refractive index was 1.384, the absorption 1.000, and the temperature was 25°C for all measurements.

2.2.6 Encapsulation of tetracycline and lincomycin into Carbopol Aqua SF1 nanogel and its effect on Carbopol stability

The principle of encapsulating a cationic antibiotic (as a hydrochloride salt) is based on the swelling and deswelling cycle of the Carbopol Aqua SF1 at different pH. Briefly, a 0.2 wt% aqueous dispersion of the nanogel was prepared by adding 66.6 μL of the 30 wt% stock solution to a beaker and diluting in 10 mL of deionised water. This was then adjusted to pH 8 by adding droplets of 0.25 M NaOH whilst been stirred. The dispersion was then warmed to 37 °C. An aliquot of 0.2 wt% tetracycline/lincomycin aqueous dispersion was prepared by weighing 20 mg of the antibiotic (ABX = tetracycline or lincomycin) powder, diluting into 10 mL of de-ionized water and then warming to 37 °C. The 10 mL ABX solution was then added to the pH 8 nanogel dispersion and shaken for 30 minutes at 37°C to allow the antibiotic cations to diffuse into and electrostatically bind to the swollen Carbopol nanogel. The pH of the ABX–Carbopol solution was then reduced to pH 5 using droplets of 0.25 M HCl whilst being stirred for another 30 minutes. The ABX–Carbopol solution was then centrifuged at 4000

rpm for 15 minutes, and the supernatant was removed and retained for encapsulation efficiency analysis. The pellet was washed twice with deionised water and re-dispersed into 10 mL of deionised water. The pH was then increased to 8 by gradually adding droplets of 0.25 M NaOH and the solution was gently stirred overnight. The final ABX–Carbopol nanogel solution was reduced to pH 5.5 using acetate buffer solution. The particle size and zeta potential distribution of the ATX–Carbopol dispersion were measured using a Malvern Zetasizer as described above.

2.2.7 Encapsulation efficiency of tetracycline and lincomycin in Carbopol Aqua SF1

The encapsulation efficiency of ABX was measured by analysing the supernatant collected from the centrifugation of ABX-Carbopol dispersion. The absorbance of the supernatant was measured at 625 nm using a spectrophotometer (Jenway 7310, Cole-Parmer). Calibration curves of both tetracycline and lincomycin were produced by diluting different weights of the anti-biotic into 10 mL of deionised water to create a range of aqueous solutions of ABX of concentration in the range of 0–0.2 wt%. A calibration graph was prepared for the absorbance as a function of the ABX concentration. A linear regression was used to determine to the unknown concentration of the un-encapsulated ABX in the supernatant. The encapsulation efficiency of the antibiotic loaded into the Carbopol Aqua SF1 was calculated as follows;

$$\text{Encapsulation efficiency (\%)} = \frac{\text{total antibiotic} - \text{unencapsulated antibiotic}}{\text{total antibiotic}} \times 100$$

2.2.8 Release kinetics of tetracycline and lincomycin from Carbopol Aqua SF1 nanogel formulations

The release kinetics of the ABX from the Carbopol Aqua SF1 was measured by placing the 10 mL 0.2 wt% ABX–Carbopol solution into 12–14 kDa dialysis tubing (Serva, Germany) and sealed with plastic clips. The filled dialysis tubing was then placed into 500 mL of (i) an acetate buffer solution at pH 5.5 or (ii) a phosphate buffer at pH 7.5 in order to monitor the amount of released ABX at a specific pH over 24 hours at room temperature. 1 mL aliquots of the acetate or phosphate buffer solution were removed at specific time points and the absorbance was measured at 625 nm using a spectrophotometer (Jenway 7310, Cole-Parmer). 1 mL of either acetate or phosphate buffer solution was added to the respective solution to retain the volume at 500 mL. Calibration curves of both tetracycline and lincomycin were constructed by diluting different weights of the ABX into 500 mL of either acetate or phosphate buffer solutions to create a range of buffered solutions of ABX of concentrations between 0 and 0.2 wt%. The amount of ABX released from the Carbopol Aqua SF1 nanogel which has transferred into the buffer solution through the dialysis

membrane pores was determined from the calibration curves. The percentage released ABX leaching from the nanogel was calculated by the equation;

$$\text{Antibiotic release (\%)} = \frac{\text{amount of antibiotic in the buffer solution at a specific time}}{\text{amount of antibiotic loaded in to the nanogel}} \times 100$$

2.2.9 Functionalisation of ABX–Carbopol Aqua SF1 nanogel with bPEI

bPEI is a branched cationic polyelectrolyte which was used to reverse the surface charge of the ABX–Carbopol Aqua SF1 nanogel particles from negative to positive. A 0.005 wt% bPEI aqueous solution was produced by weighing a 0.5 mg aliquot of bPEI and placing into a beaker and dispersing in a total volume of 10 mL of deionised water whilst stirring. 10 mL of 0.005 wt% bPEI aliquot was rapidly added to 10 mL of 0.2 wt% ABX–0.2 wt% Carbopol dispersion with vigorous shaking for 5 minutes. The resulting mixture was then centrifuged at 4000 *g* for 15 minutes. The supernatant was discarded, and the pellet was re-dispersed into 10 mL of deionised water yielding a 0.005 wt% bPEI–0.2 wt% ABX–0.2 wt% Carbopol Aqua SF1 dispersion which was used as a stock for antimicrobial testing against wound associated bacterial pathogens.

2.2.10 Antimicrobial susceptibility testing (AST) disk diffusion test of wound species

A single colony of each species was isolated and placed into 10 mL of MHB and grown overnight at 37 °C. The bacteria suspension was then diluted to a 0.5 McFarland standard in MHB by measuring the turbidity at 625 nm yielding $1\text{--}2 \times 10^8$ CFU mL⁻¹. A cotton swab was used to streak a MHA plate lawn. 4 ± 0.5 mm deep MHA plates were prepared by adding 25 mL of molten MHA to a 9 cm round plate and left to solidify at room temperature. Tetracycline (30 µg) and lincomycin (15 µg) antibiotic disks (both Oxoid, UK) were applied to the MHA plates using a disk dispenser (Oxoid, UK), and the plates were incubated for 18 hours at 35 ± 1 °C following EUCAST guidelines. The zone of inhibition diameters were illuminated using a lightbox and the images were measured in mm using a ruler; the diameter was measured across 3 lines and the mean was determined to be the zone of inhibition.

2.2.11 Cell viability of HaCaT cells treated with free ABX and Carbopol nanogel-formulated ABX

HaCaT cells (an immortalised human keratinocyte cell line, sourced from AddexBio, San Diego, Cat. number T0020001) were cultured in DMEM supplemented with 10% FBS and 1% L-glutamine under humidified conditions at 37 °C, 5% CO₂ in T75 flasks until a confluency of 80% was achieved, determined by visualisation with an optical microscope. Passaging was done at 80% confluency to ensure that the cells

remained in the exponential phase for experimentation. Passaging was performed by removing spent media, washing in DPBS and incubating with 1× trypsin at 37 °C 5% CO₂ for 5 min until the cells were detached in suspension. The trypsin was then neutralised with a 1 : 1 volumetric ratio of fresh DMEM and gently centrifuged at 1000 *g* for 5 min, the supernatant was aspirated, and the pellet was resuspended in DMEM (supplemented as above) at a 1 : 6 ratio and transferred into a fresh T75 flask. Surplus cells were diluted and 1 × 10⁴ HaCaT cells were seeded in 50 mL of DMEM (ABX free) supplemented with 2 wt% FBS (foetal bovine calf serum) into a 96-well plate and incubated for 24 hours at 37 °C 5% CO₂. The medium was then removed and replaced with treatment infused media (free ABX or the formulated nanogel-encapsulated ABX) and incubated for 24 hours after which it was replaced with fresh DMEM and 20 µL of CellTiter 96® Aqueous One Solution Reagent™ (Promega, UK) where it was incubated for 3 hours under the same conditions. The absorbance was then read at 492 nm. These data were calculated into cell count data via interpolation from the standard curve (absorbance values from a fixed number of cells in media (see **Figure 2.23A**). The data was represented as viability percentage of the control which was normalised to 100%. The HaCaT cell viability assay was repeated in three independent experiments.

2.2.12 Minimum inhibitory concentration (MIC)

The bacteriostatic properties of the bPEI-coated ABX-loaded Carbopol nanogel particles and its spectrum of activity were measured in comparison to equivalent concentrations of free tetracycline or lincomycin. The antimicrobial activity was tested against each of the strains described in **Table 2.1**. Briefly, O/N cultures of each strain were prepared as described above. 100 µL of each strain suspension was added to the wells of a 96-well microtiter plate yielding 5 × 10⁴–1 × 10⁵ cell per well. An aliquot of bPEI-coated-0.2 wt% ABX–0.2 wt% Carbopol suspension was prepared. This was centrifuged at 4000 *g* for 5 minutes and re-suspended into 10 mL of MHB. 2-Fold dilutions of this suspension were prepared in separate aliquots and 50 µL added to descending rows of bacteria on the microtiter plate. Equivalent 2-fold dilutions of the free ABX were added to separate columns for comparison (50 µL per well). The plates were incubated for 20 hours at 37 °C. 20 µL of resazurin sodium salt (0.15 mg mL⁻¹ in DPBS) was added to each well and incubated at 35 °C for 2 hours. The absorbance was recorded using a spectrophotometer (Jenway 7310, Cole-Parmer). The resazurin in the presence of viable cells is reduced to resorufin by the bacterial co-enzyme NAHD, indicating that the cells remain metabolically active and viable (see **Figure 2.2**). The MIC was determined to be the lowest concentration of active antimicrobial agent which inhibited the growth of each strain. The MIC assay was repeated in three independent experiments.

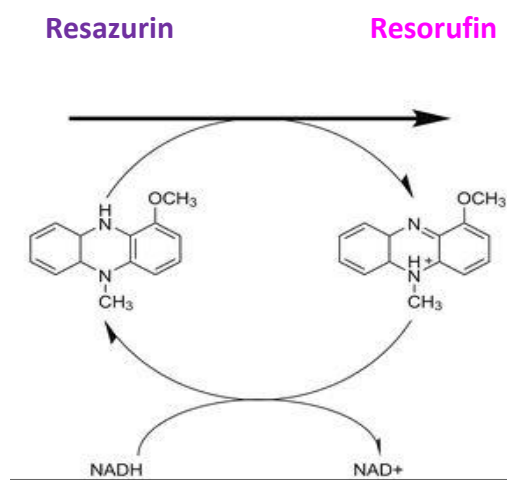


Figure 2.2. Resazurin reduction reaction. Resazurin in the presence of metabolically active cells is reduced to the resorufin product, a blue colour indicates cells are inhibited and unable to reduce the resazurin. Pink indicated the cells are metabolically active and can produce the pink resorufin product.

2.2.13 Time-kill assays

Killing curves were constructed against each representative strain to determine the time taken for the active agent in influencing total bacterial cell populations. O/N cultures were prepared yielding 10 mL of MHB aliquots with 5×10^5 – 1×10^6 cells per mL. 10 mL of 0.005 wt% bPEI-coated–0.2 wt% ABX–0.2 wt% Carbopol nanogel was added to each tube and incubated for 24 hours at 37 °C with 140 rpm. At time points 0, 1, 2, 3, 4, 6, and 24 hours, a 100 μ L sample was removed from each treatment tube and added to 900 μ L of Dey-Engley Neutralising broth. 100 μ L aliquots from each serial dilution tube were plated onto MHA plates and incubated for 24 hours at 37 °C and enumerated. The time-kill assay was repeated in three independent experiments.

2.2.14 SEM imaging of the treated cells

Cells were removed from their media by centrifugation at 2000 *g* for 5 min and washed and resuspended in PBS buffer. The washing process was performed three times to remove excess media peptone. The cells were then fixed in a 1 wt% glutaraldehyde PBS buffer solution for 1 hour at room temperature, the cells were then centrifuged at 2000 *g* and the pellet was washed with deionised water three times to remove excess glutaraldehyde; the cell samples were then re-suspended and dehydrated in 50%/75%/90% and absolute ethanol solutions for 30 minutes per each ethanol concentration. Cells were then swabbed onto a glass slide and submerged into absolute ethanol and dried using liquid CO₂ at its critical point using an E3000 Critical Point Dryer (Quorum Technologies, UK) and then coated in 10 nm Carbon. The samples were imaged using an Ultra-High-Resolution Scanning Electron Microscope using cold field emission (Hitachi SU8230, Japan).

2.2.15 Statistical analysis

Data were expressed as average values \pm standard deviations of the mean. *P*-Values of less than 0.05 were considered significant. All One-Way ANOVAs and Tukey's post-test statistical analysis were performed in GraphPad v7.0.4.

2.3 Results and discussion

2.3.1 Encapsulation of tetracycline and lincomycin into Carbopol Aqua SF1 nanogel

The particle size and zeta potential of Carbopol SF-1 were measured using a Malvern Zetasizer Nano ZS at 25 °C using a refractive index of 1.450. A 30 wt% stock solution was diluted to 0.02 wt% in deionised water. The Carbopol nanogel suspension has an average particle diameter of 100 nm and a zeta potential of -30 ± 1.82 mV (see **Figure 2.3A and 2.3B**, respectively). **Figure 2.3C** shows the useful swelling effect of the Carbopol Aqua SF1 nanogel and how pH changes in the solution can be used to mediate this. There is a change in the nanogel particle diameter from approximately 100 nm to 300 nm when adjusting the pH from 6 to 8, which is due to the COOH groups of the Carbopol undergoing de-protonation to COO⁻ in a basic solution. The electrostatic repulsion of these negatively charged –COO⁻ groups causes the particle swelling effect and facilitates the subsequent electrostatic binding of cationic compounds. The negative zeta potential of the swollen nanogel, which remains between –25 mV and –29 mV in a pH range of 4 to 12 (**Figure 2.3D**), shows the anionic nature of the Carbopol SF1 nanogel. This was exploited to bind the cationic antibiotics (ABX), tetracycline hydrochloride and lincomycin hydrochloride to the cores of the nanogel particles. The particle size of the de-swelled nanogel with encapsulated ABX is dependent on the ABX concentration with which the nanogel has been incubated.

Figure 2.4A and 2.4C shows the relationship between the ABX concentration and the nanogel colloid stability which must be maintained. This requires the ABX concentration to be proportional to the nanogel concentration within a certain range. For both the tetracycline and the lincomycin solutions loaded in the 0.2 wt% Carbopol–0.2 wt% ABX allows a nanogel particle shrink to approximately 110 ± 2 nm. However, for increased ABX concentrations and lower concentrations of the nanogel, the particle may undergo aggregation and the formation of less stable nanogel, approximately 160 ± 5 nm and 220 ± 5.12 nm for tetracycline and lincomycin, respectively. The optimal combination of 0.2 wt% ABX–0.2 wt% Carbopol Aqua SF1 nanogel formulation was chosen as this allowed the highest encapsulation efficiency of ABX without compromising the nanocarrier colloidal stability. The zeta potential of the collapsed ABX-loaded nanogel was unaffected by the concentration of the encapsulated ABX. **Figure 2.4B and 2.4D** (for tetracycline and lincomycin, respectively) show that the zeta potential of 0.2 wt% Carbopol remains stable at approximately -39 ± 1 mV whether loaded with lower or higher concentrations of ABX, indicating that the ABX concentration does not impact the overall surface charge of the collapsed nanogel particles. The purpose of encapsulating the antibiotic was to provide a targeted delivery system which would release it in close proximity to the microbial cell wall. To achieve this, the 0.2 wt%–0.2 wt% ABX formations were mixed with very low concentrations (0.005 wt%) of the cationic polyelectrolyte bPEI (branched polyethyleneimine)

to reverse the surface charge of the collapsed nanogel particles and induce electrostatic attraction to the negative bacterial cell wall. 0.005 wt% bPEI was chosen as it was the optimal concentration that can reverse the surface charge of the nanogel particles and maintain the optimal colloidal stability of the nanocarrier.

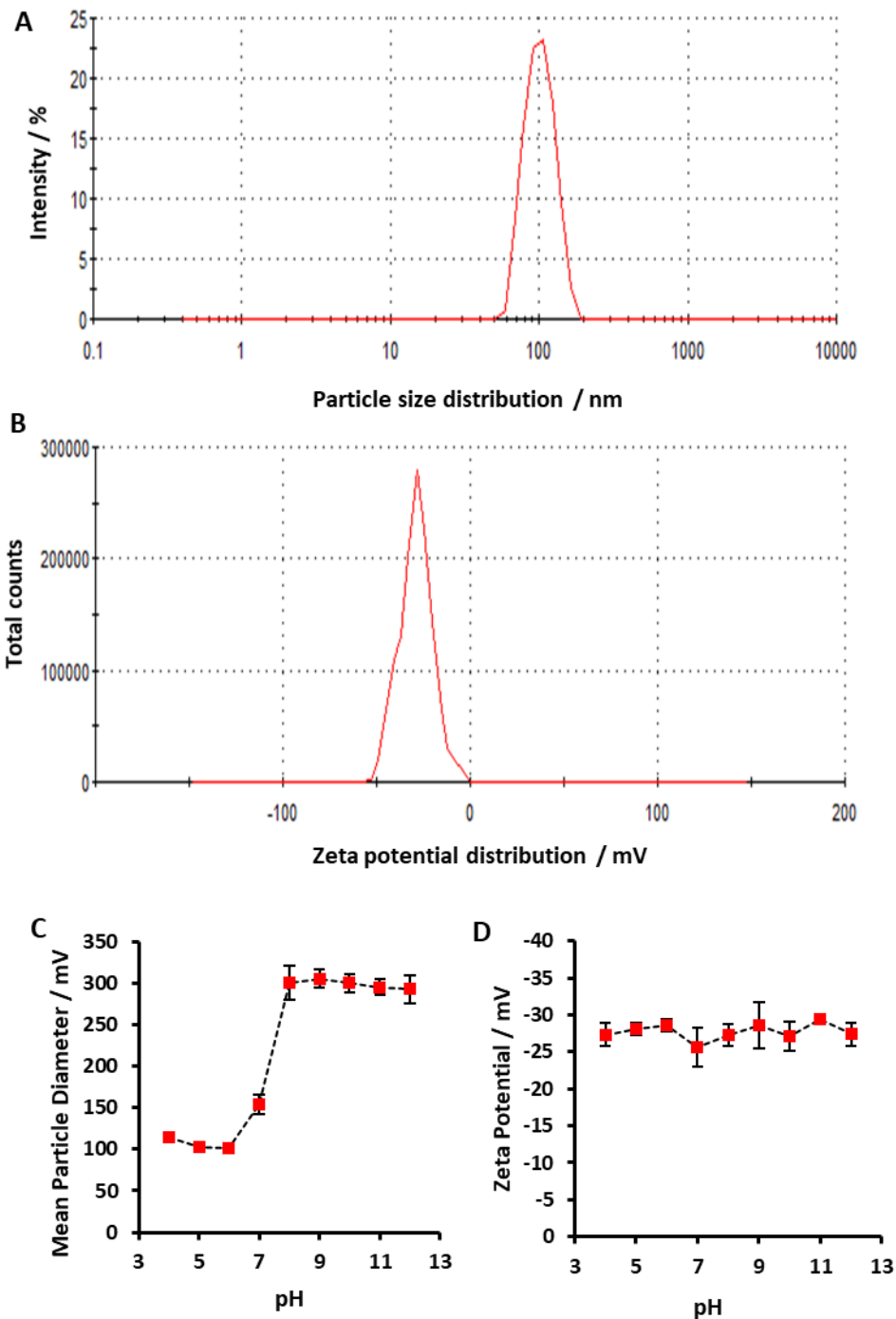


Fig. 2.3. The nanogel particle size (A) and the zeta potential (B) distribution of 0.02 wt% Carbopol Aqua SF-1 suspension measured at pH 5 with a Zetasizer. (C) The 0.02 wt% Carbopol Aqua SF1 nanogel mean particle hydrodynamic diameter and (D) mean zeta potential at varying pH. The particle size and zeta potential are measured using a DLS. Carbopol Aqua SF-1 was diluted from a 30 wt% stock with two refractive indexes (RI). pH 4–7 (collapsed nanogel) is measured with RI 1.450 and pH 8–12 (swollen nanogel) with RI 1.336 at 25 °C. Each value represents a triple replicate with \pm S.D. The lines are guides to the eye.

Figure 2.5 shows that increased concentrations of bPEI-induced aggregation of the nanogel particles with no detectable further increase in their zeta potential. Figure 2.6 shows that the zeta potential of the ABX-loaded nanogel particles was reversed from approximately -39 mV to $+(25\text{--}28)$ mV for both tetracycline and lincomycin loaded in Carbopol Aqua SF1 after coating with bPEI. The measurements showed that the zeta potential of the bPEI-coated nanogel particles remained very stable and positive for more than 24 hours indicating that the bPEI has coated the particle surface, conferring a long-lasting positive surface charge.

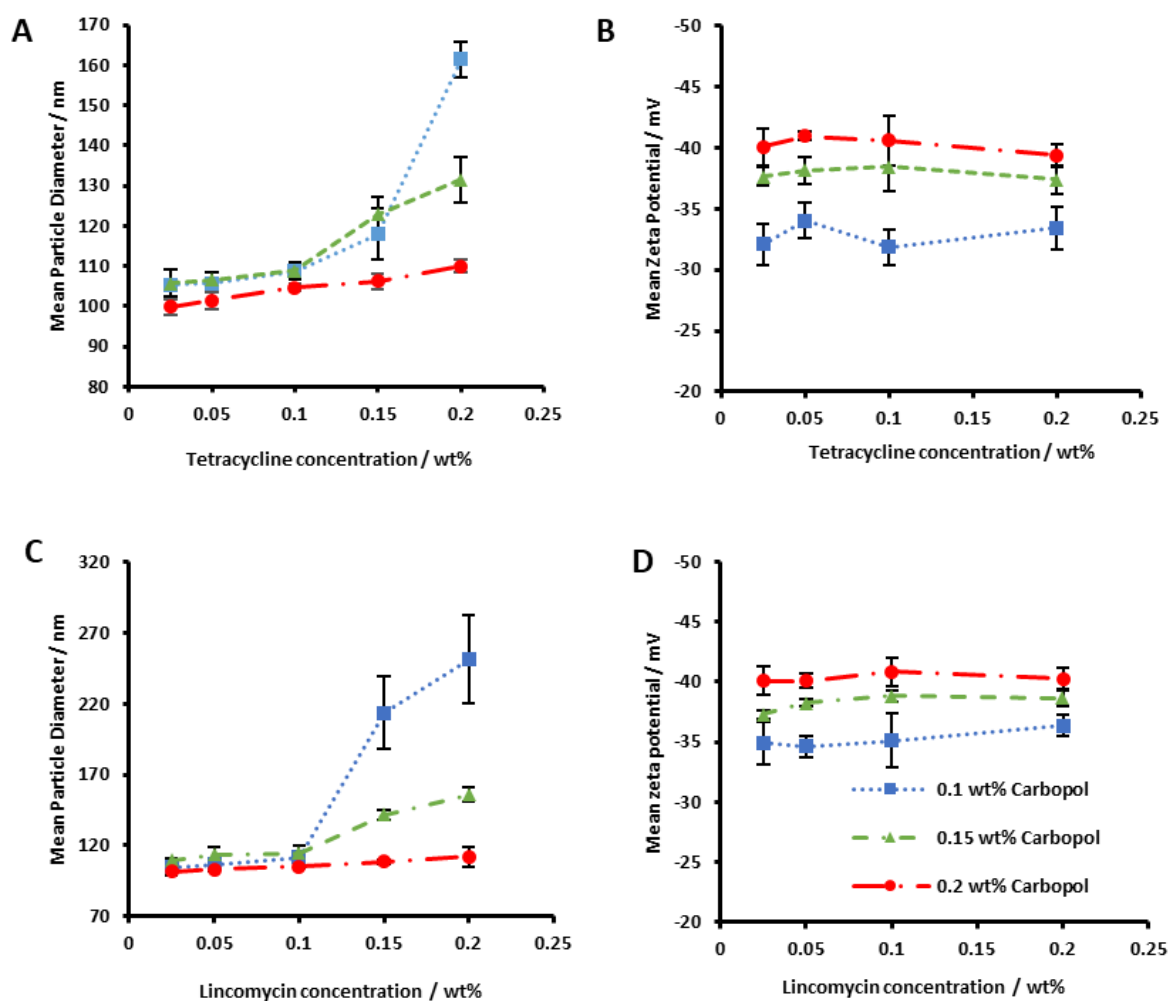


Fig. 2.4. (A) The mean particle diameter and (B) zeta potential of 0.1, 0.15, and 0.2 wt% Carbopol Aqua SF1 nanogel after encapsulation of tetracycline at various concentrations and (C) the particle diameter and (D) zeta potential of 0.1, 0.15, and 0.2 wt% Carbopol Aqua SF1 nanogel after encapsulation of lincomycin at various concentrations at pH 6. 0.1, and 0.15, and 0.2 wt% Carbopol Aqua SF1 nanogel suspensions were prepared and mixed with tetracycline/lincomycin hydrochloride at varying concentrations. Each value represents a triple replicate with \pm S.D. The lines are guides to the eye. The legend is representative of all A, B, C, and D.

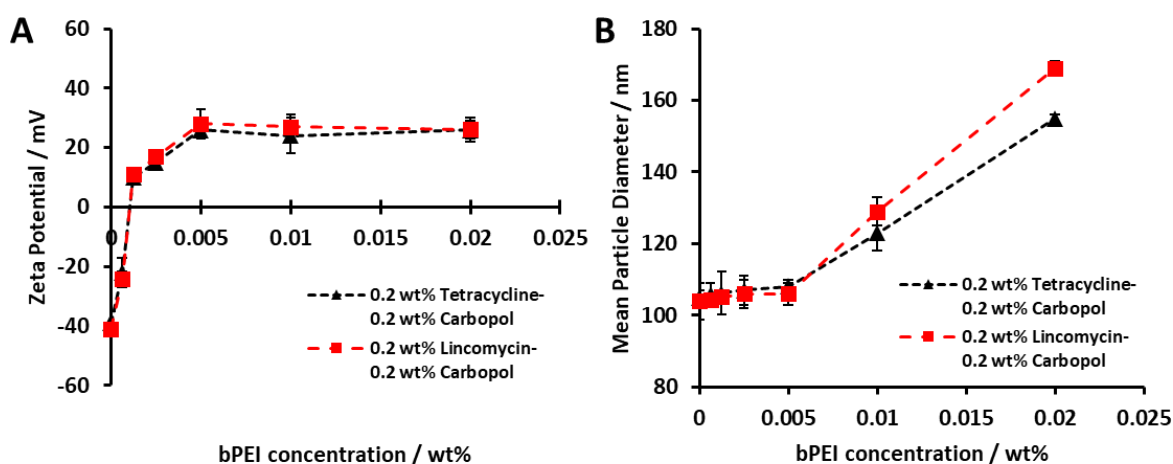


Figure 2.5. (A) The zeta potential of 0.2 wt% tetracycline-0.2 wt% Carbopol and 0.2 wt% lincomycin-0.2 wt% Carbopol NPs coated with various concentrations of bPEI and (B) the mean particle diameter of 0.2 wt% tetracycline-0.2 wt% Carbopol and 0.2 wt% lincomycin-0.2 wt% Carbopol NPs coated with various concentrations of bPEI. Each value represents a triple replicate with \pm S.D. The lines are guides to the eye.

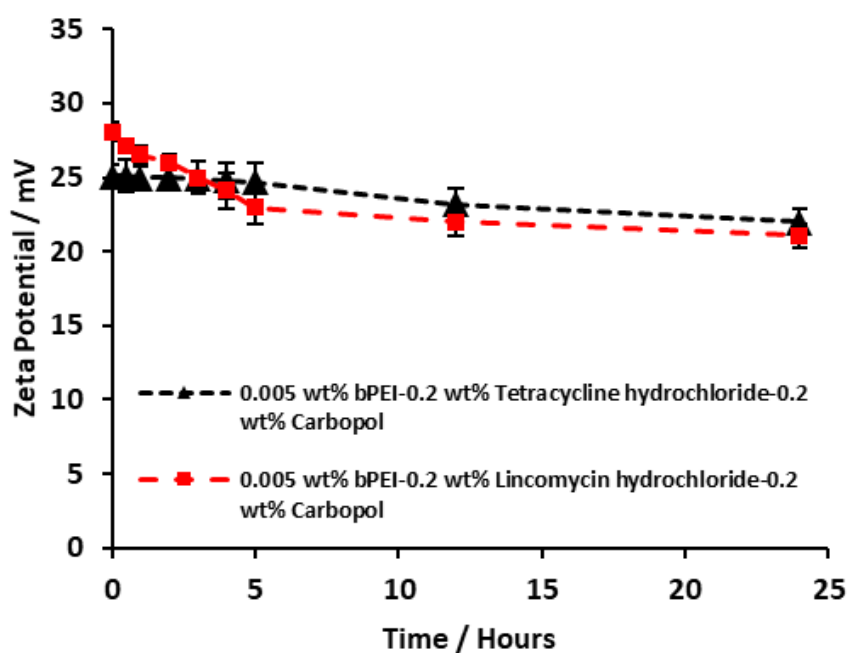


Fig. 2.6. The zeta potential of bPEI coated antibiotic-Carbopol particles at pH 5.5 measured at time intervals after preparation. A Malvern Zetasizer was used to measure the particle diameter and zeta potentials at a refractive index of either 1.450 (below pH 7) or 1.336 (above pH 7). Each value represents average triplicate measurements with error bars representing the \pm S.D. The lines are guides to the eye.

2.3.2 Encapsulation efficiency and release kinetics of tetracycline and lincomycin in Carbopol Aqua SF1

The supernatant of the ABX-nanogel formation was retained after centrifuging to determine how much ABX the nanogel has been encapsulated in the swelling and de-swelling process. **Figure 2.7A** and **2.7B** show the absorbance of the tetracycline and lincomycin in deionised water reduced to pH 5 using 0.25 M HCl. This calibration curve was used to compare the absorbance readings obtained from the supernatant obtained during the centrifugal process used in forming the ABX-loaded nanogel particles. A linear regression equation was used to determine the ABX concentration in the supernatant and from this the ABX concentration retained within the nanogel. **Tables 2.2** and **2.3** show that increasing the temperature to 37 °C while incubating the Carbopol nanogel and the ABX solutions prior to mixing and the duration of the mixing both affect the ABX amount being successfully encapsulated. In both the tetracycline and lincomycin formulations, the 30 min/37 °C mixing conditions yielded the highest encapsulation efficiency, with 89.9% for tetracycline and 79.5% for lincomycin, respectively. The release kinetics of ABX from the ABX-loaded nanogel formations was tested to examine how the ABX release is affected by the pH of the solution.

The experiments indicated that 30 min at 37°C was the optimum time to incubate the antibiotic solution with the swollen Carbopol nanogel in order to gain the maximum encapsulation efficiency. Incubation times greater than this showed no increase in encapsulation efficiency. This is demonstrated by using EDX data from lincomycin encapsulated Carbopol. Lincomycin was chosen as it contains a sulphur atom which can be detected on the EDX spectra. It can be seen that the sulphur-related peak in **Figure 2.8B** (60 min incubation) did not yield a significant increase compared with the sulphur-related peak on **Figure 2.8A** (30 incubation). Hence it is concluded that no further lincomycin was encapsulated into the nanocarrier after the 30 minutes incubation with lincomycin solution at identical conditions.

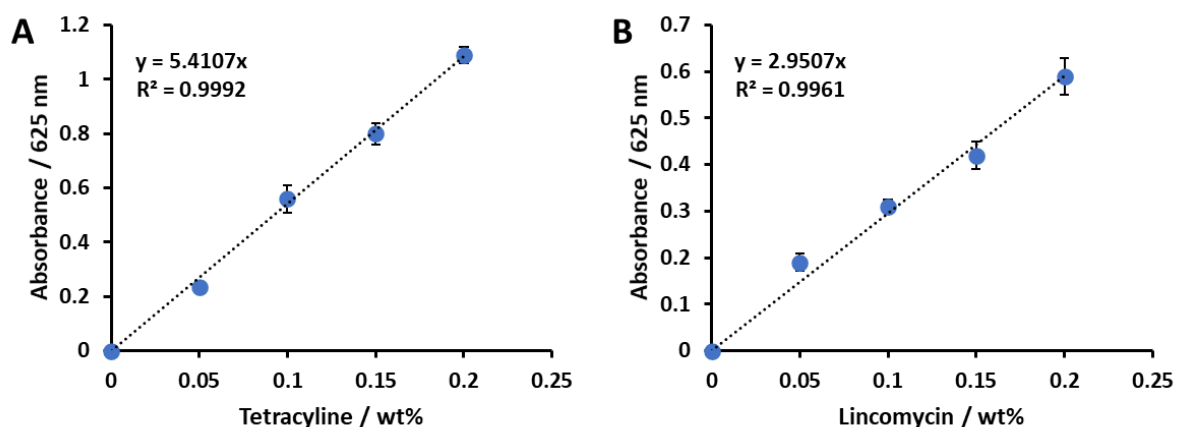


Figure 2.7. Standard calibration graphs of the absorption vs concentrations of **(A)** tetracycline and **(B)** lincomycin hydrochloride. Absorbance was measured at 625 nm. Aliquots were prepared by adding antibiotic hydrochlorides to deionised water at specific concentrations.

Table 2.2. The concentration of tetracycline encapsulated into 0.2 wt% Carbopol Aqua SF1 nanogel.

Carbopol-antibiotic mixture environment	Total tetracycline conc. attempted to encapsulate / wt%	Tetracycline in supernatant / wt%	Tetracycline encapsulated / wt%	Encapsulation efficiency / wt%
15 mins, 20°C	0.2	0.042	0.158	78.9
15 mins, 37°C	0.2	0.026	0.174	86.9
30 mins, 20°C	0.2	0.032	0.168	84
30 mins, 37°C	0.2	0.02	0.18	89.9

Table 2.3. The concentration of lincomycin encapsulated into 0.2 wt% Carbopol Aqua SF1 nanogel.

Carbopol-antibiotic mixture environment	Total lincomycin conc. attempted to encapsulate / wt%	Lincomycin in supernatant / wt%	Lincomycin encapsulated / wt%	Encapsulation efficiency / wt%
15 mins, 20°C	0.2	0.095	0.105	52.4
15 mins, 37°C	0.2	0.078	0.122	61
30 mins, 20°C	0.2	0.081	0.119	59.5
30 mins, 37°C	0.2	0.041	0.159	79.5

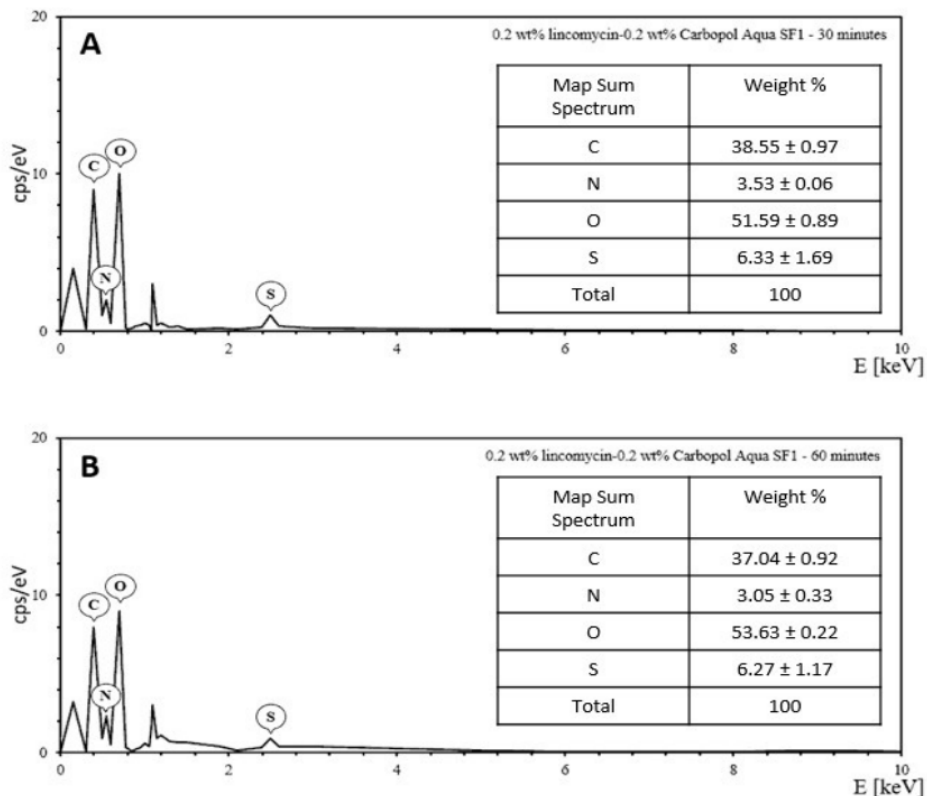


Figure 2.8. EDX spectra of Carbopol Aqua SF-1 NPs after 30 and 60 minutes incubation with lincomycin. **(A)** shows the EDX spectra of a sample of 0.2 wt% lincomycin-0.2 wt% Carbopol Aqua SF1 after 30 min loading time with the antibiotic at 37°C, **(B)** shows 0.2 wt% Lincomycin-0.2 wt%-0.2 wt% Carbopol Aqua SF1 after 60 min loading time with the antibiotic at 37°C. The measurement was taken in the centre of the nanocarrier NPs. Oxford Laboratories micF+ X-stream-2 EHX was used to take measurements, the results were analysed in Aztec One v.3.3.

Figure 2.9A and **2.9B** show that tetracycline and lincomycin are slowly released from the interior of the nanogel particles over a period of 24 hours. In both the tetracycline and lincomycin loaded nanogel-formulations, their release from the nanogel is higher in the PBS (pH 7.5) compared to the acetate buffer (pH 5.5). In both the acetate and phosphate saline buffers, there is a large release of both tetracycline and lincomycin within the first 5 hours between 30% and 70% for the acetate buffer and PBS, respectively. Further release of the antibiotic is much slower and gradual for the remaining time. The increased ABX release rates in the phosphate buffer solutions can be explained by the partial swelling of the nanogel at the higher pH, which will allow ABX to diffuse faster from its interior. The continued release of ABX from the nanogel particles over a long period of time could also potentially be highly beneficial in an antimicrobial context, as the ABX will be delivered locally on the surface of the bacterial cell continuously for a long period of time.

There are not currently any previous studies in which these antibiotics were encapsulated into nanogel particles of the same nanocarrier chemistry. These results allow comparison with typical

encapsulation efficiencies with other cationic antimicrobial molecules such as berberine hydrochloride (Al-Awady et al., 2017) and chlorhexidine digluconate (Fuentes-Hernandez et al., 2015; Al-Awady et al., 2018). These studies show that encapsulation of these cationic antimicrobials has proven successful within anionic microgels and dual functionalised shellac nanocarriers with comparable encapsulation efficiency.

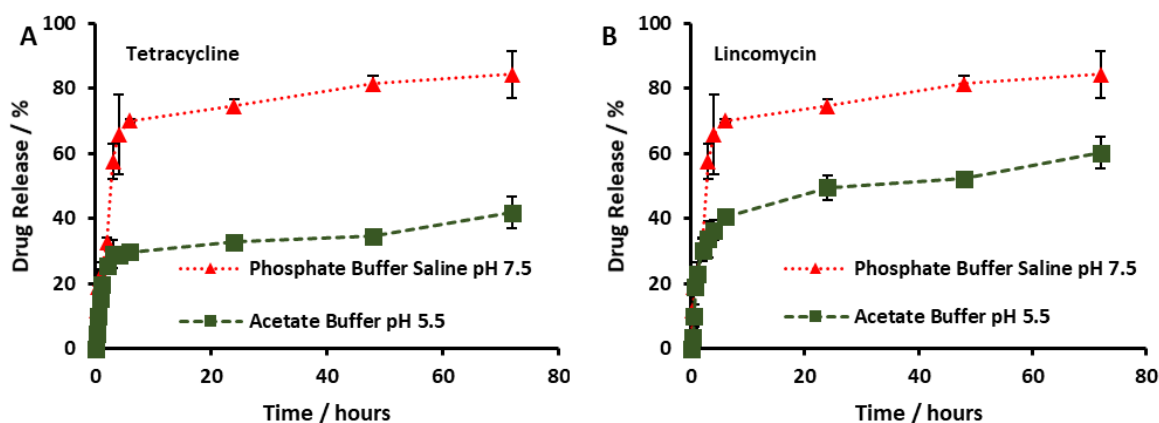


Fig. 2.9 (A) Tetracycline and **(B)** lincomycin release kinetics in different pH solutions. 10 mL of 0.2 wt% ABX–0.2 wt% Carbopol suspension was placed in a 10–12 kDa MWKO dialysis bag. The dialysis bag was submerged into either 250 mL of phosphate or acetate buffer (pH 7.5 and 5.5, respectively) whilst stirred. 1 mL aliquots were taken at specific time points on the absorbance of the aliquot equated into the concentration of ABX in the buffer using a standard calibration curve. Absorption was measured at 625 nm.

Figure 2.10 shows SEM images acquired of **(A)** a sample of 0.2 wt% Carbopol loaded with 0.2 wt% lincomycin, **(B)** 0.005 wt% bPEI–0.2 wt% lincomycin–0.2 wt% Carbopol, and **(C)** 0.2 wt% Carbopol nanogel (empty nanocarrier). Lincomycin was chosen for the characterisation due to the presence of a sulphur in the molecular structure. It can be seen from the EDX spectra the presence of sulphur in the lincomycin-loaded Carbopol nanogel particles after the particles have been washed from the excess of lincomycin. This spectra peak is not present in the unloaded nanocarrier (**Figure 2.10C**). It is concluded from this result that lincomycin has been successfully loaded into the nanogel particles, also in agreement with the dynamic light scattering results presented in **Figure 2.4**. SEM images were acquired of the showing 0.2 wt% Carbopol loaded with 0.2 wt% lincomycin, 0.005 wt% bPEI–0.2 wt% lincomycin–0.2 wt% Carbopol, and 0.2 wt% Carbopol (empty nanocarrier). Lincomycin was chosen for the characterisation due to the presence of a sulphur atom in the molecular structure. EDX spectra shows the presence of sulphur in the lincomycin loaded Carbopol NPs (see **Figure 2.10**). This spectra peak is not present in the unloaded nanogel carrier. As the source of the sulphur is the loaded lincomycin, this additionally confirms that it has been successfully loaded into the nanocarrier, agreeing with the dynamic light scattering results (**Figures 2.4A, 2.4C**) showing the nanocarrier size increase upon loading) and release curves (**Figure 2.9**).

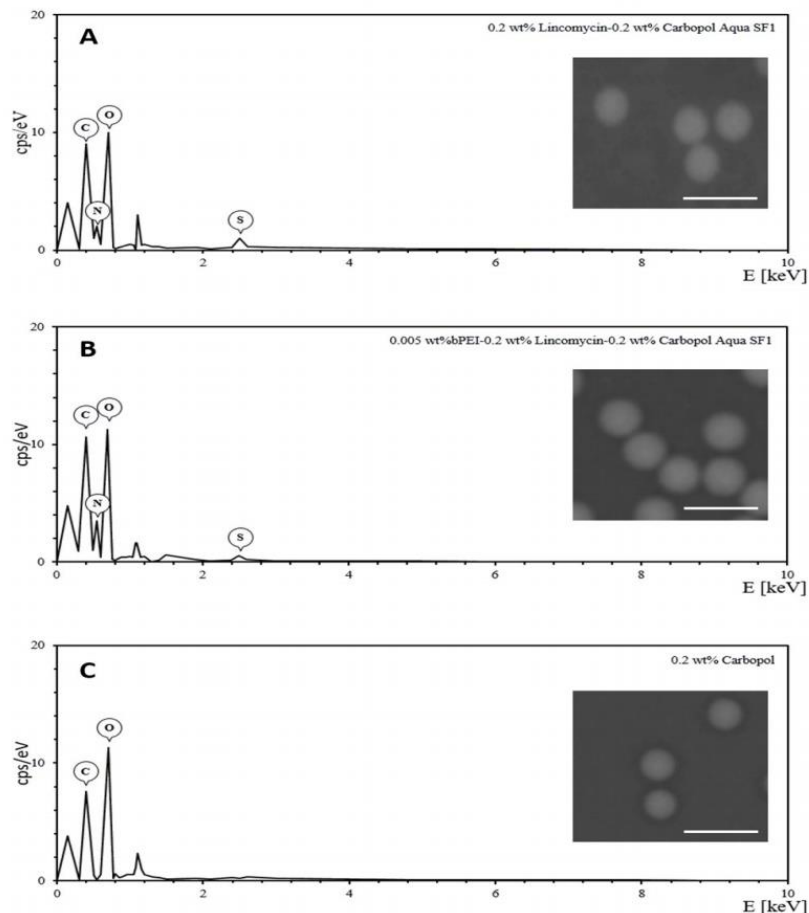


Figure 2.10. SEM images and EDX spectra of Carbopol Aqua SF-1 NPs. **(A)** shows spectra of 0.2 wt% lincomycin-0.2 wt% Carbopol Aqua SF1, **(B)** shows 0.005 wt% bPEI-0.2 wt% Lincomycin-0.2 wt%-0.2 wt% Carbopol Aqua SF1, and **(C)** 0.2 wt% empty Carbopol Aqua SF1. The measurement was taken in the centre of the NPs. Oxford Laboratories micF+ X-stream-2 EHX was used to take measurements, the results were analysed in Aztec One v.3.3. Images were acquired using a TM3030 Plus SEM. Scale bars represent 200 nm.

2.3.3 Zeta potential of wound-relevant bacterial species

The action of the Carbopol encapsulated ABX, functionalised with bPEI to yield a positive surface charge, is to facilitate a sustained and targeted ABX delivery platform, which is based on the electrostatic adhesion between the nanogel particles and the bacterial cell wall. Seven wound-associated bacterial pathogens, along with a *S. aureus* reference strain (ATCC – 21213) and *P. aeruginosa* reference strain (ATCC – 27853), were cultured overnight and centrifuged for 10 minutes at 5000 *g*. The pellet was re-dispersed into deionised water for the zeta potential measurement. The zeta potential for Gram-negative species was between -30 mV and -37 mV, while the six Gram-positive species had a very similar zeta potential of -20 ± 2 mV (**Figure 2.11**). As expected, the additional negatively charged lipopolysaccharide (LPS) confers higher negative surface charge for the Gram-negative species. Crucially, all bacteria tested displayed a negative charge which should allow electrostatic adhesion between the bacterial cell wall and the cationic nanogel formulations.

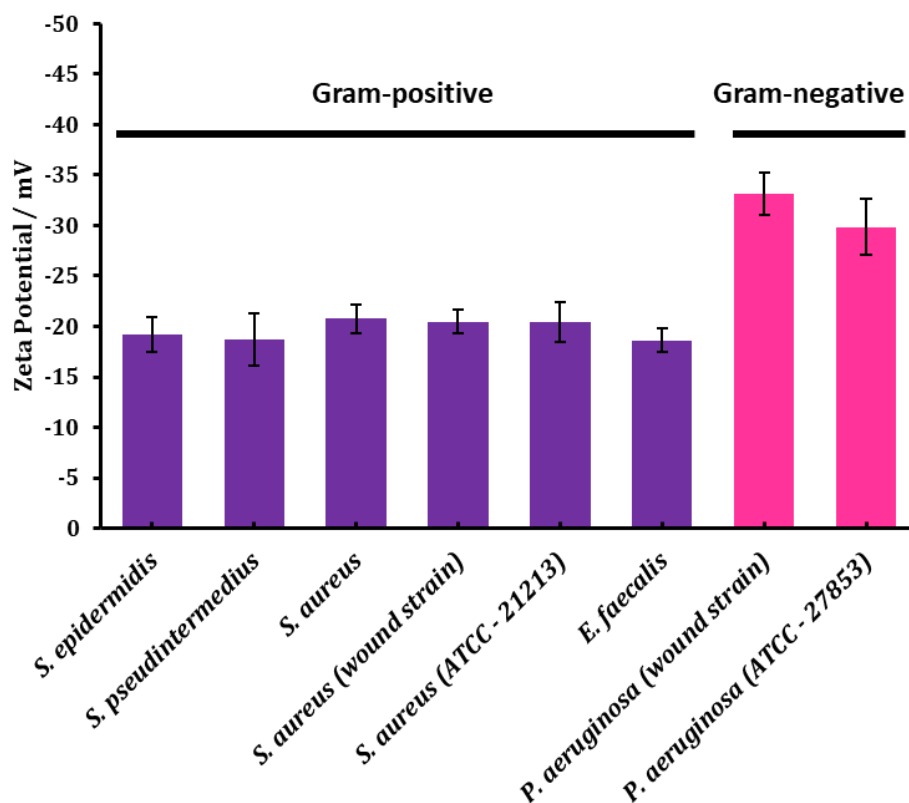


Fig. 2.11. Zeta potential of bacterial wound species. A colony of each species was inoculated into 10 ml of MHB and grown overnight at 37 °C with constant shaking. The bacterial suspension was centrifuged for 10 min at 5000 *g*. The supernatant was discarded, and the pellet was washed twice with deionised water. The pellet was resuspended in 45 ml of deionised water. 1 mL of this suspension was placed in a quartz cuvette and zeta potential was measured using the Dipstick probe and Malvern Zetasizer nano ZS. The refractive index was 1.384 and the absorption was 1.000. N = 3 with \pm S.D.

2.3.4 Antimicrobial susceptibility testing (AST) disk diffusion test of wound species

Tetracycline and lincomycin disks were placed on bacterial lawns of the eight selected bacterial species to confirm antibiotic resistance (**Figure 2.12**). The zone of inhibition surrounding the disk was measured in mm using a ruler and compared to reference values from the European committee of antimicrobial susceptibility testing (EUCAST, 2018). **Table 2.4** shows the results from the antimicrobial susceptibility disk diffusion testing. *S. aureus* (both strains), *S. epidermidis*, MRSA, and *S. pseudointermedius* were susceptible to both tetracycline and lincomycin. *P. aeruginosa* (both strains) and *E. faecalis* were resistant to both tetracycline and lincomycin. **Figure 2.12** shows the clear zones of inhibition which surround the species which confer resistance to either antibiotic.

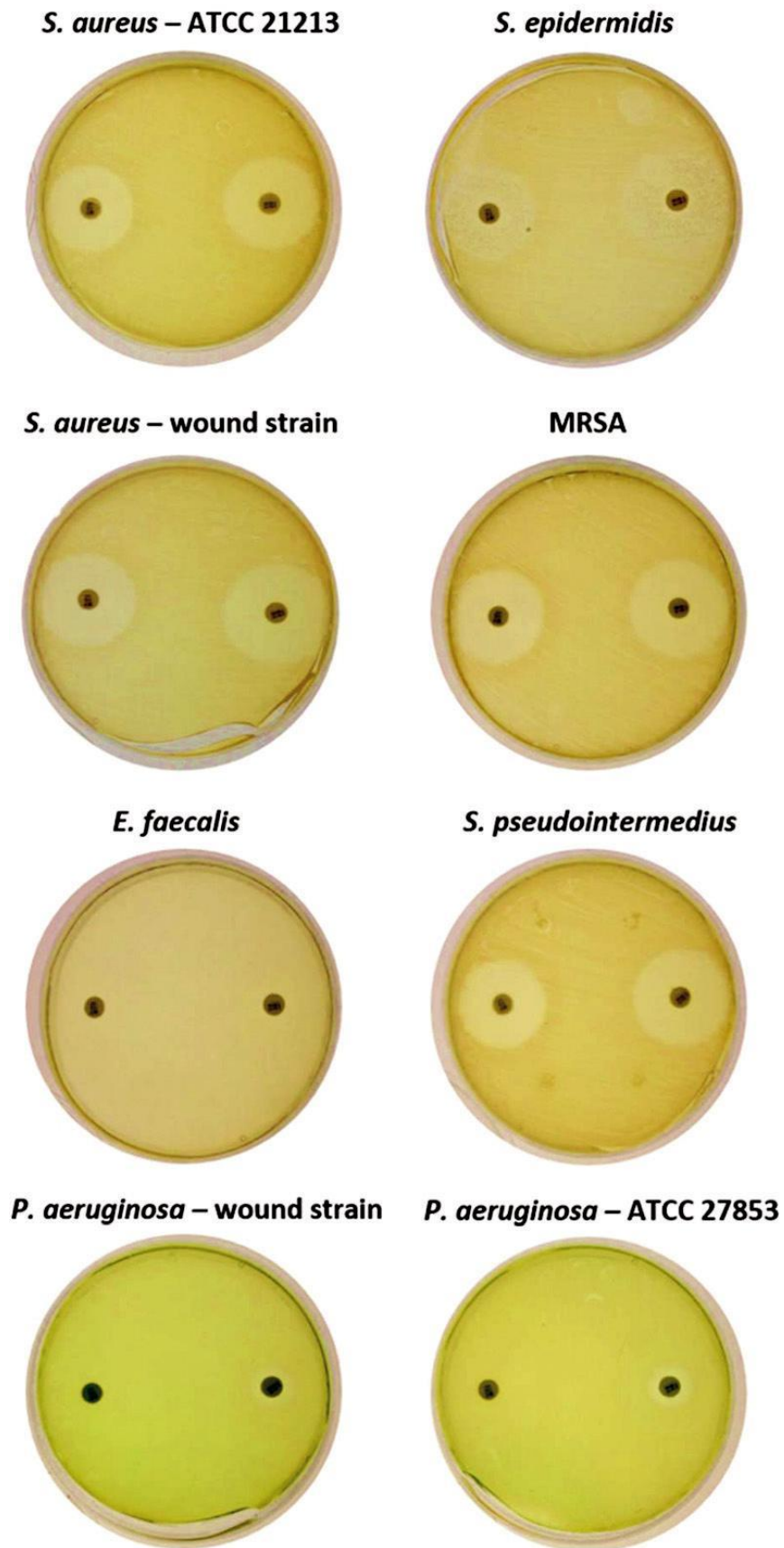


Fig. 2.12 Zones of inhibition (AST disk diffusion test) for wound isolates and reference strains. 15 µg lincomycin disks (left) and 30 µg tetracycline disks (right).

Table 2.4. Antimicrobial resistance tests of tetracycline and lincomycin by disk diffusion method for wound species.

Bacterial strains		Antibiotic disk	
Species	Origin	Tetracycline (30 µg) zone diameter (mm)	Lincomycin (15 µg) zone diameter (mm)
<i>S. aureus</i> N=3	Reference strain 21213	32 (S, 3/3)	30 (S, 3/3)
<i>S. epidermidis</i> N=3	Leg ulcer	34 (S, 3/3)	24 (S, 3/3)
<i>MRSA</i> N=3	Leg ulcer	32 (S, 3/3)	26 (S, 3/3)
<i>S. aureus</i> N=3	Sebaceous cyst	26 (S, 3/3)	26 (S, 3/3)
<i>P. aeruginosa</i> N=3	Leg ulcer	2 (R, 3/3)	2 (R, 3/3)
<i>E. faecalis</i> N=3	Ulcer	1 (R, 3/3)	1 (R, 3/3)
<i>S. pseudointermedius</i> N=3	Burn swab	28 (S, 3/3)	30 (S, 3/3)
<i>P. aeruginosa</i> N=3	Reference strain 27853	2 (R, 3/3)	2 (R, 3/3)

Results of zone of inhibition repeats are in brackets i.e., S=susceptible, R=resistant, for zone diameter interpretation (EUCAST 8.1 (16 May 2018)) standards were used where available.

2.3.5 Viability of HaCaT cells treated with tetracycline/lincomycin and Carbopol encapsulated tetracycline/lincomycin and its individual constituents

A preliminary human cell cytotoxicity experiment was performed on HaCaT cells to assess if the Carbopol Aqua SF1 nanogel formulations (and individual constituents) were toxic to human cells compared to the free antibiotics. Interestingly, **Figure 2.13B** shows that after 24 hours of incubation, 0.2 wt% Carbopol nanogel, 0.005 wt% bPEI, and 0.2 wt% bPEI–0.2 wt% Carbopol (empty carrier) showed no toxic effect compared to the untreated cell controls. This indicates that the individual components of the nanogel formulation did not lead to a reduction in the viable cell number after 24 hours. Treatments with free tetracycline and lincomycin were used at concentrations 0.2, 0.3, and 0.4 wt% and showed a slight reduction in total cell counts when compared to the control, approximately 20% to 25% for lincomycin and tetracycline at 0.4 wt%, respectively. The 0.2 wt% Carbopol–0.2 wt% ABX–0.005 wt% bPEI formulation showed toxicity in line with 0.2% free antibiotic. This indicates that the nanogel-loaded antibiotics confer no increased toxicity to HaCaT cells, both when encapsulating an antibiotic and as an empty nanocarrier. This formulation could have a potential topical application to treat infected wounds. HaCaT cells represent a good proxy for

a typical skin keratinocyte which would be exposed to the ABX-loaded nanocarrier formulation during the wound treatment.

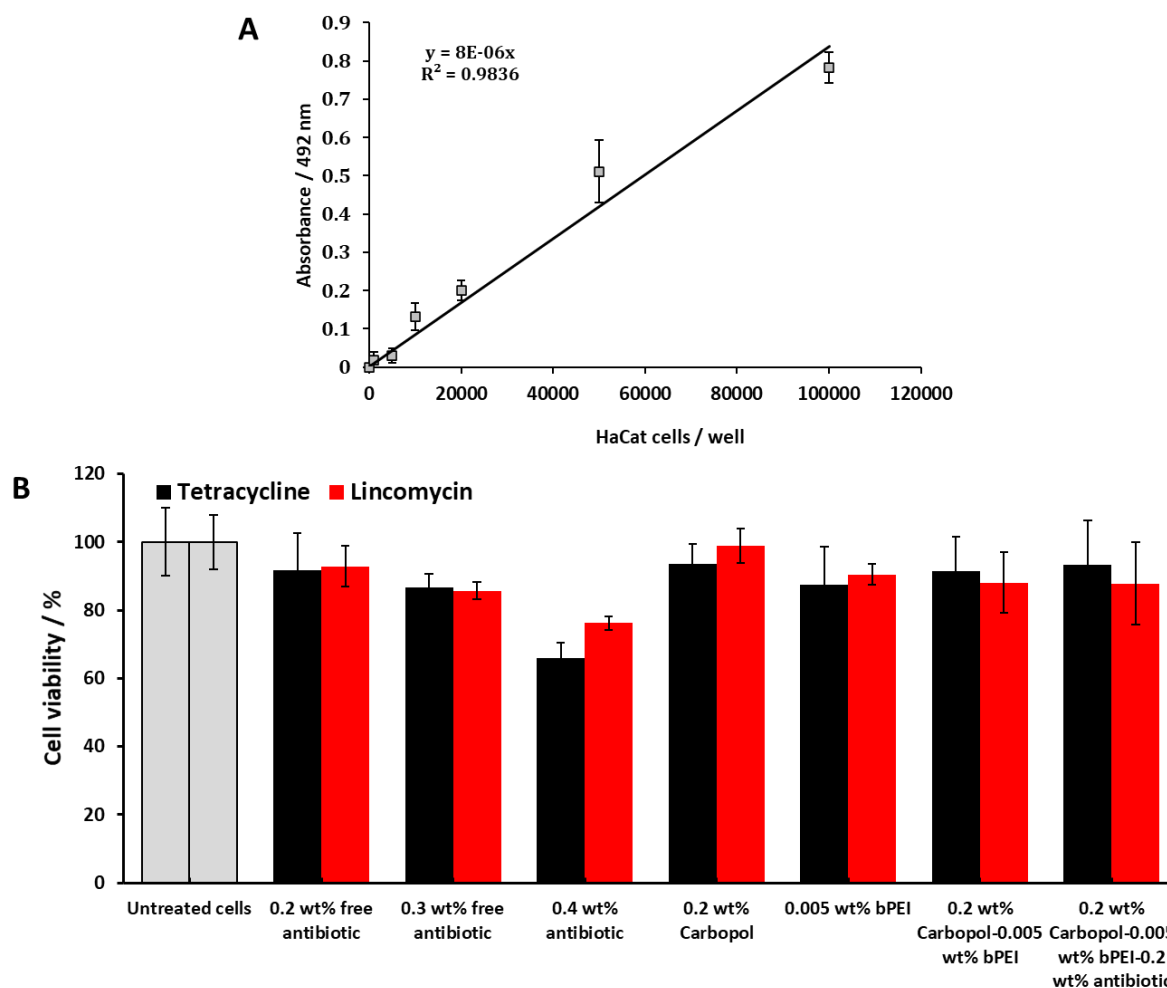


Figure 2.13. (A) Calibration curve of HaCaT cells. Various cell concentrations were seeded in DMEM medium and absorption values obtained at 492 nm. These data were used to calculate the number of cells in parallel treatment / untreated wells. N=3 with \pm S.D. **(B)** HaCat viability after treatment with tetracycline concentrations and Carbopol formulated tetracycline/lincomycin and individual formulation constituents. 1×10^4 HaCat cells were seeded in 50 mL of DMEM (antibiotic free) supplemented with 2 wt% FBS (foetal bovine calf serum) into a 96-well plate and incubated for 24 hours at 37°C 5% CO₂. The medium was then removed and replaced with treatment infused media and incubated for 24 hours in the same conditions. The treatment media was then removed and replaced with fresh DMEM and 20 μ L of CellTiter 96® Aqueous One Solution Reagent added to each well and incubated for 3 hours in the same conditions. The absorbance was then read at 492 nm. These data were calculated into cell count data via interpolation for the standard curve cell count data from (A). N = 3 with \pm S.D.

2.3.6 Antibacterial activity of bPEI-coated tetracycline/lincomycin loaded Carbopol Aqua SF1 on clinical wound isolates

Figures 2.14 and 2.15 show time kill evaluation of 0.005 wt% bPEI–0.2 wt% Carbopol–0.2 wt% ABX (tetracycline and lincomycin, respectively). The uncoated Carbopol nanogel and bPEI coated nanogel were included as unloaded controls. Exponential growth was observed over 24 hours for the eight wound-relevant bacteria under no treatment conditions and in the presence of each control component (0.2 wt% nanogel, 0.005 wt% bPEI, and the 0.005 wt% coated 0.2 wt% nanogel). *S. aureus* (clinical isolate and reference strain), *S. epidermidis*, MRSA, and *S. pseudointermedius* showed after 24 hours that both tetracycline and lincomycin had a bacteriostatic effect on growth, with a small reduction in bacteria number over the 24 hours. By contrast, *P. aeruginosa* (clinical isolate and reference strain) and *E. faecalis* showed no reduction in cell population when treated with 0.2 wt% free tetracycline and lincomycin compared to the untreated growth control. These results are in agreement with the AST disk diffusion results shown in Figure 2.12.

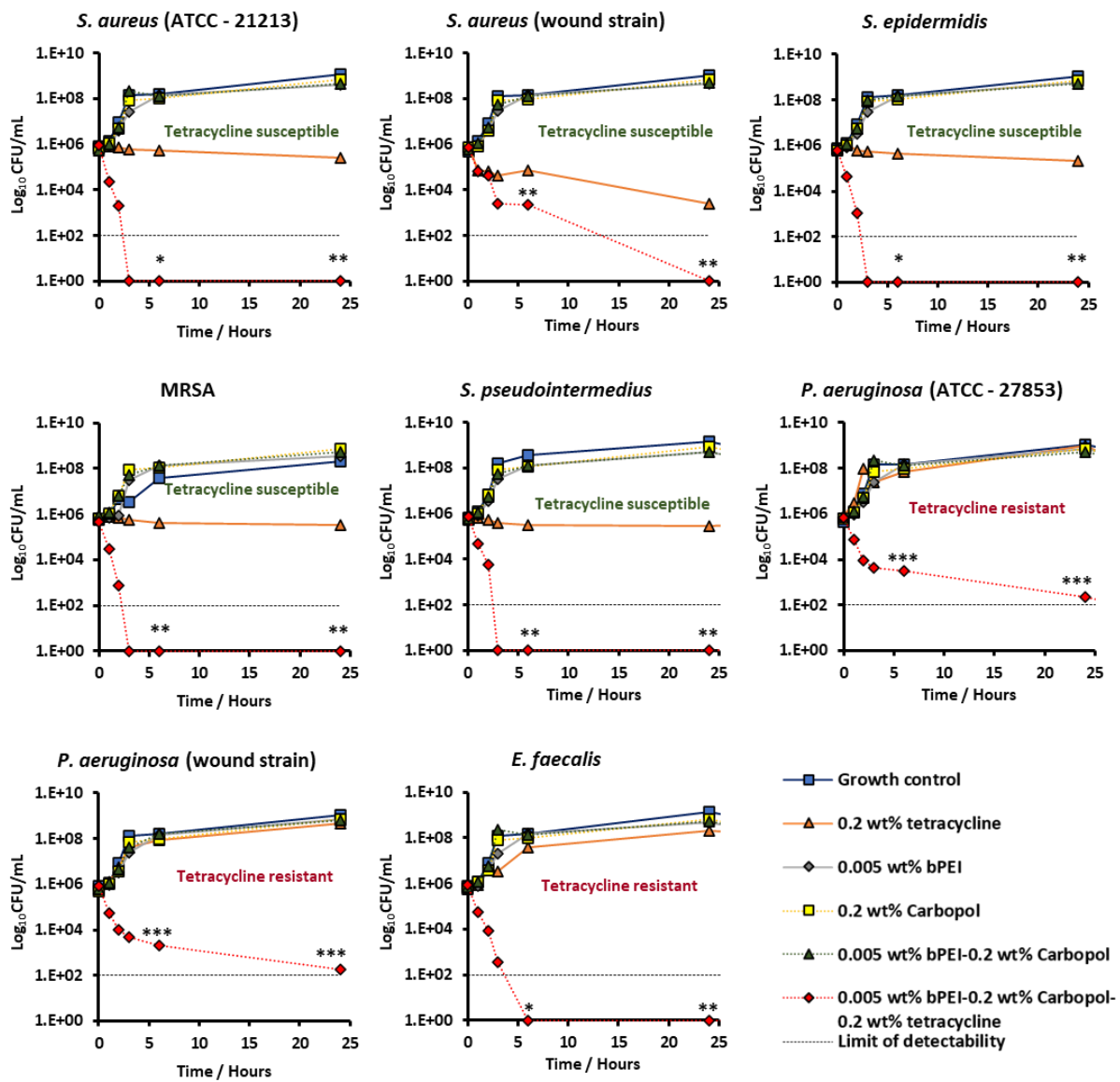


Fig. 2.14. Time kill assays against clinical wound isolates and selected reference species. Tetracycline (0.2 wt%) and 0.005 wt% bPEI-coated 0.2 wt% tetracycline loaded in 0.2 wt% Carbopol (CLC), 0.005 wt% free bPEI and 0.005 wt% bPEI-coated 0.2% Carbopol (empty nanocarrier) tested against several clinical isolate wound bacteria. The results are presented as means ($n = 3$). The lines are guides to the eye. <0.05 is considered significant. * $P < 0.05$, ** $P < 0.01$, *** $P < 0.001$ compared to the free tetracycline.

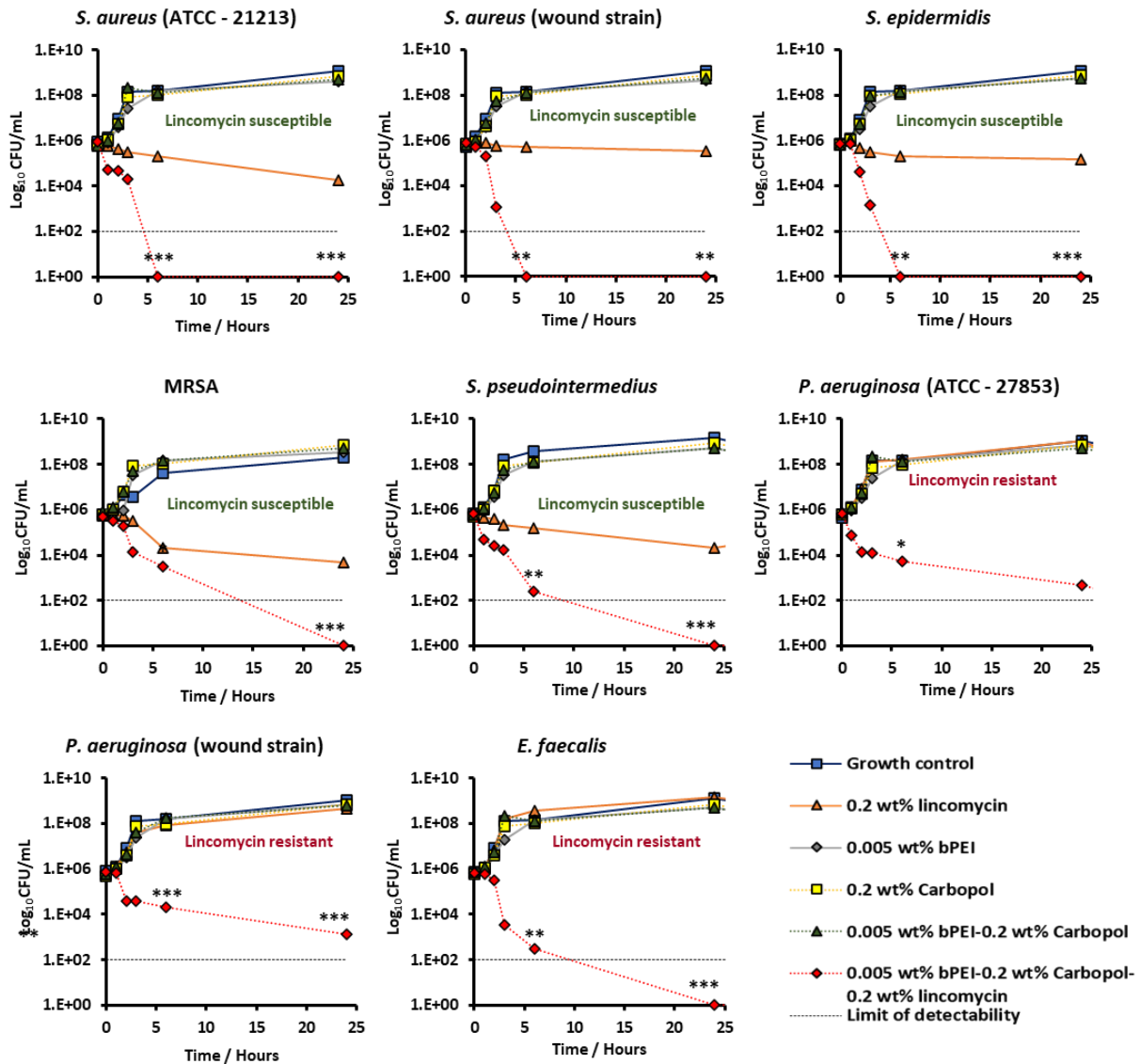


Fig. 2.15. Time kill assays against clinical wound isolates and selected reference species. Lincomycin and 0.005 wt% bPEI-coated 0.2 wt% lincomycin loaded in 0.2 wt% Carbopol (CLC), 0.005 wt% free bPEI and 0.005 wt% bPEI-coated 0.2% Carbopol (empty nanocarrier) tested against several clinical isolate wound bacteria. The results are presented as means ($n = 3$). The lines are guides to the eye. <0.05 is considered significant. * $P < 0.05$, ** $P < 0.01$, *** $P < 0.001$ compared to free lincomycin.

The bPEI-coated nanogel encapsulated tetracycline and lincomycin were highly effective against *S. aureus* (reference strain) and *S. epidermidis* causing a >5 log reduction in cell population after approximately 3 hours. A similar result is observed in MRSA, *S. pseudointermedius* and *E. faecalis* with a >5 log reduction observed with the nanogel-encapsulated tetracycline at 3 hours, and after 24 hours with lincomycin. After 24 hours the wound isolated *S. aureus* has shown a >5 log reduction with encapsulated tetracycline and a >1 log reduction with encapsulated lincomycin. *P. aeruginosa* (ATCC and clinical isolate) showed an approximate >4 log reduction with the nanogel-encapsulated tetracycline and lincomycin compared to equivalent concentrations of the free antibiotic. Collectively, these data show that the cationic antibiotic delivery system enhances the antimicrobial action of tetracycline and lincomycin, across all eight bacteria evaluated in this study. Crucially, cationic nanocarrier-based antibiotic delivery was able to overcome antimicrobial resistance across several isolates, conferring > 5 log reduction within 24 hours (Tables 2.5 and 2.6 show the significance between free and nanogel encapsulated antibiotics).

Table 2.5. Time-Kill assay statistical analysis between free tetracycline and encapsulated tetracycline at 6 and 24-hour time points. Data were expressed as average values \pm standard deviations of the mean. P values of less than 0.05 were considered significant. All One-Way ANOVAs and Tukey's post-test statistical analysis were performed in GraphPad v7.0.4.

Species	Multiple Comparison	P-value	Significance
<i>S. aureus</i> (ATCC - 21213)	6 hour tetracycline vs 6 hour formulated tetracycline	0.02270416	*
	24 hour tetracycline vs 24 hour formulated tetracycline	0.00401855	**
<i>S. epidermidis</i>	6 hour tetracycline vs 6 hour formulated tetracycline	0.03562452	*
	24 hour tetracycline vs 24 hour formulated tetracycline	0.00145661	**
MRSA	6 hour tetracycline vs 6 hour formulated tetracycline	0.00238776	**
	24 hour tetracycline vs 24 hour formulated tetracycline	0.00165489	**
<i>S. aureus</i> (wound strain)	6 hour tetracycline vs 6 hour formulated tetracycline	0.00215412	**
	24 hour tetracycline vs 24 hour formulated tetracycline	0.00545155	**
<i>P. aeruginosa</i> (wound strain)	6 hour tetracycline vs 6 hour formulated tetracycline	0.00025125	***
	24 hour tetracycline vs 24 hour formulated tetracycline	0.00014587	***
<i>E. faecalis</i>	6 hour tetracycline vs 6 hour formulated tetracycline	0.03454452	*
	24 hour tetracycline vs 24 hour formulated tetracycline	0.00654552	**
<i>S. pseudointermedius</i>	6 hour tetracycline vs 6 hour formulated tetracycline	0.00245125	**
	24 hour tetracycline vs 24 hour formulated tetracycline	0.00004412	**
<i>P. aeruginosa</i> (ATCC - 27853)	6 hour tetracycline vs 6 hour formulated tetracycline	0.00021451	***
	24 hour tetracycline vs 24 hour formulated tetracycline	0.00019857	***

Table 2.6. Time-Kill assay statistical analysis between free lincomycin and encapsulated lincomycin at 6 and 24-hour time points. Data were expressed as average values \pm standard deviations of the mean. P values of less than 0.05 were considered significant. All One-Way ANOVAs and Tukey's post-test statistical analysis were performed in GraphPad v7.0.4.

Species	Multiple Comparison	P-value	Significance
<i>S. aureus</i> (ATCC - 21213)	6 hour lincomycin vs 6 hour formulated lincomycin	0.00021545	***
	24 hour tetracycline vs 24 hour formulated lincomycin	0.00025453	***
<i>S. epidermidis</i>	6 hour lincomycin vs 6 hour formulated lincomycin	0.00157455	**
	24 hour tetracycline vs 24 hour formulated lincomycin	0.00068546	***
MRSA	6 hour lincomycin vs 6 hour formulated lincomycin	0.01589456	*
	24 hour tetracycline vs 24 hour formulated lincomycin	0.00259874	**
<i>S. aureus</i> (wound strain)	6 hour lincomycin vs 6 hour formulated lincomycin	0.00486549	**
	24 hour tetracycline vs 24 hour formulated lincomycin	0.00845212	**
<i>P. aeruginosa</i> (wound strain)	6 hour lincomycin vs 6 hour formulated lincomycin	0.00095455	***
	24 hour tetracycline vs 24 hour formulated lincomycin	0.00026845	***
<i>E. faecalis</i>	6 hour lincomycin vs 6 hour formulated lincomycin	0.00985454	**
	24 hour tetracycline vs 24 hour formulated lincomycin	0.00061795	***
<i>S. pseudointermedius</i>	6 hour lincomycin vs 6 hour formulated lincomycin	0.00245214	**
	24 hour tetracycline vs 24 hour formulated lincomycin	0.00079878	***
<i>P. aeruginosa</i> (ATCC - 27853)	6 hour lincomycin vs 6 hour formulated lincomycin	0.02458651	*
	24 hour tetracycline vs 24 hour formulated lincomycin	0.00751254	**

The minimum inhibitory concentrations (MIC) for tetracycline and lincomycin are shown in **Figure 2.16**, and the data are also shown in **Tables 2.7** and **2.8**. The ability of the nanogel-encapsulated tetracycline to inhibit growth was demonstrated through all eight species with up to $8 \times$ MIC reductions shown. The *P. aeruginosa* strains also showed much reduced MIC concentrations when compared to free tetracycline, both $8 \times$ MIC. This effect was also mirrored with the nanogel-encapsulated lincomycin when compared to free lincomycin. Similar to nanogel-encapsulated tetracycline, there were reductions in the MIC of nanogel-encapsulated lincomycin compared to free lincomycin in solution. This was seen across all eight species, ranging from $8 \times$ MIC to $2 \times$ MIC. Interestingly, in the *P. aeruginosa* (ATCC strain and clinical isolate) and *E. faecalis* there was $8 \times$ MIC compared to free lincomycin, providing evidence that the nanogel-encapsulated lincomycin also facilitates an improved inhibitory effect. The increased antimicrobial efficiency of the nanogel-encapsulated antibiotics would also be advantageous in the case of susceptible bacteria as a reduced concentration of antibiotic is required to achieve a comparable result to that of the free antibiotic. This has potential benefits in reducing possible toxicities associated with antibiotic use, and a potential reduction in cost, as the antibiotic is considerably more expensive than the Carbopol nanogel Aqua SF1 and bPEI.

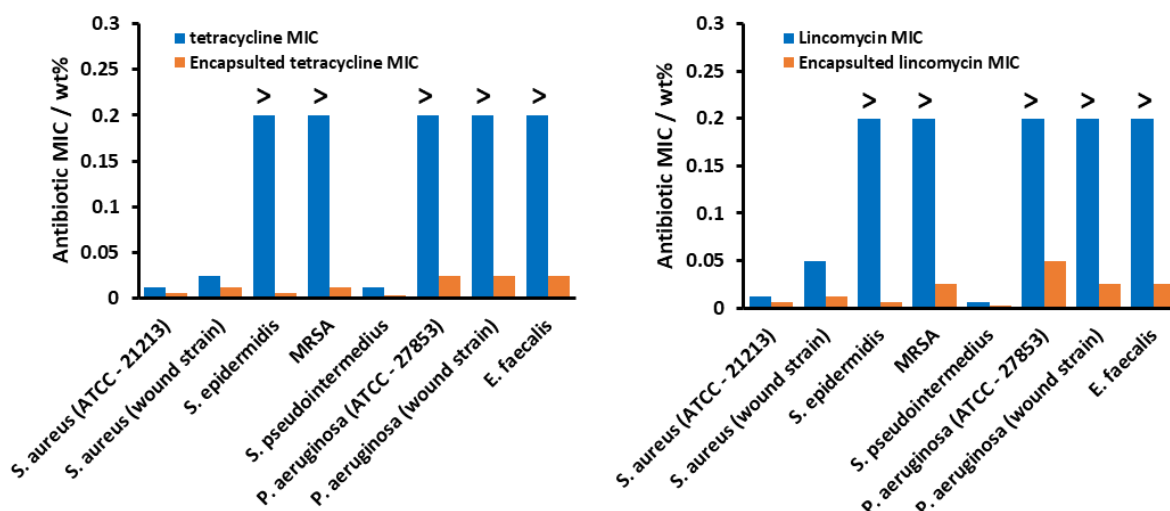


Fig. 2.16 (A) MIC of tetracycline and nanogel-encapsulated tetracycline, **(B)** MIC of lincomycin and nanogel-encapsulated lincomycin. All nanogel particles were coated with bPEI. “>” indicates that a concentration greater than 0.2 wt% is needed to inhibit bacterial growth.

Table 2.7. Minimum inhibitory concentration (MIC) of free tetracycline and bPEI-coated nanogel loaded with the same concentration of tetracycline against several wound species clinical isolates. The lowest concentration of antimicrobial agent inhibiting growth was considered the MIC. > indicates that a concentration greater than 0.2 wt% is needed to inhibit growth.

	Tetracycline MIC (wt%)	Encapsulated tetracycline MIC (wt%)
<i>S. aureus</i> (ATCC - 21213)	0.0125	0.00625
<i>S. aureus</i> (wound strain)	0.025	0.0125
<i>S. epidermidis</i>	> 0.2	0.00625
MRSA	> 0.2	0.0125
<i>S. pseudointermedius</i>	0.0125	0.003125
<i>P. aeruginosa</i> (ATCC - 27853)	> 0.2	0.025
<i>P. aeruginosa</i> (wound strain)	> 0.2	0.025
<i>E. faecalis</i>	> 0.2	0.025

The most important benefit of the nanogel-encapsulated tetracycline and lincomycin formulations is their ability to be effective against species which have demonstrated resistance to these antibiotics. It is envisaged that this could be due to the sustained high concentration of the antibiotic localised to the cell wall of the bacteria being able to overwhelm efflux pumps, which are able to actively remove free antibiotic. **Figure 2.17** shows SEM images of *P. aeruginosa* after treatment with bPEI-coated tetracycline loaded Carbopol nanogel which demonstrates the accumulation of the surface functionalised nanogel particles on the surface of the anionic bacterial cell wall (described and illustrated above).

Table 2.8. Minimum inhibitory concentration (MIC) of free lincomycin and bPEI-coated nanogel loaded with the same concentration of lincomycin against several wound species clinical isolates. The lowest concentration of antimicrobial agent inhibiting growth was considered the MIC. > indicates that a concentration greater than 0.2 wt% is needed to inhibit growth.

	Lincomycin MIC (wt%)	Encapsulated lincomycin MIC (wt%)
<i>S. aureus</i> (ATCC - 21213)	0.0125	0.00625
<i>S. aureus</i> (wound strain)	0.05	0.0125
<i>S. epidermidis</i>	> 0.2	0.00625
MRSA	> 0.2	0.025
<i>S. pseudointermedius</i>	0.00625	0.003125
<i>P. aeruginosa</i> (ATCC - 27853)	> 0.2	0.05
<i>P. aeruginosa</i> (wound strain)	> 0.2	0.025
<i>E. faecalis</i>	> 0.2	0.025

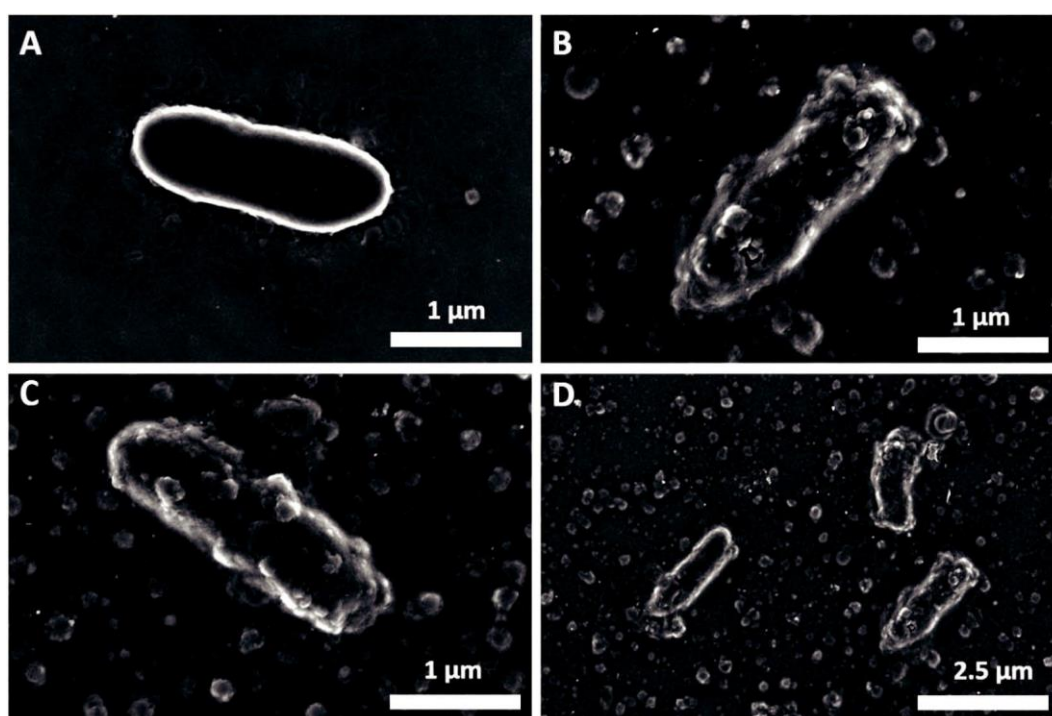


Fig. 2.17. SEM images of *P. aeruginosa* before and after treatment. **(A)** The control sample of non-treated *P. aeruginosa* after 24 hours of growth. **(B–D)** *P. aeruginosa* after 24 hours treatment with 0.005 wt% bPEI–0.2 wt% tetracycline–0.2 wt% Carbopol.

2.4 Conclusions

This chapter shows the development of a novel surface functionalised nanocarrier for tetracycline and lincomycin by using lightly cross-linked polyacrylic acid-based nanogels (Carbopol Aqua SF1) coated with a biocompatible cationic polyelectrolyte (bPEI). It is shown that this approach significantly enhanced the antimicrobial action against a range of wound isolated pathogens. Crucially, the bPEI surface coated nanogel with encapsulated antibiotics had an enhanced effect on several bacterial species which were validated to be resistant to either tetracycline or lincomycin. This enhanced antibiotic efficacy is likely due to favourable electrostatic attraction between the positively charged bPEI-coated antibiotic-loaded nanogel particles and the negatively charged bacterial cell wall. This is mediated by the attachment of the nanocarrier particles which then locally release the encapsulated antibiotic in much higher local concentrations than the free antibiotic at the same overall concentration. The results also show that the cytotoxicity of the antibiotics loaded in these nanocarriers on human keratinocyte cells is practically negligible in the range of concentrations which kill both resistant and susceptible bacteria. Antimicrobial resistance is a growing clinical epidemic. This novel method for bacteria-targeted topical antibiotic applications offers an important new opportunity to extend the clinically useful life-span of existing antibiotics, using inexpensive materials, while reducing future bacterial antibiotic resistance.

2.5 Reference list

- Al-Awady, M., Fauchet, A., Greenway, G. & Paunov, V. (2017) Enhanced antimicrobial effect of berberine in nanogel carriers with cationic surface functionality. *J Mater Chem B*, 5(38), 7885-7897.
- Al-Awady, M., Weldrick, P., Hardman, M., Greenway, G. & Paunov, V. (2018) Amplified antimicrobial action of chlorhexidine encapsulated in PDAC-functionalized acrylate copolymer nanogel carriers. *Materials Chemistry Frontiers*, 2(11), 2032-2044.
- Al-Obaidy, S., Greenway, G. & Paunov, V. (2019a) Dual-functionalised shellac nanocarriers give a super-boost of the antimicrobial action of berberine. *Nanoscale Advances*, 1(2), 858-872.
- Al-Obaidy, S., Halbus, A., Greenway, G. & Paunov, V. (2019b) Boosting the antimicrobial action of vancomycin formulated in shellac nanoparticles of dual-surface functionality. *Journal of Materials Chemistry B*, 7(19), 3119-3133.
- Assis, L., Nedeljković, M. & Dessen, A. (2017) New strategies for targeting and treatment of multi-drug resistant *Staphylococcus aureus*. *Drug Resistance Updates*, 31, 1-14.
- Ayhan, D., Tamer, Y., Akbar, M., Bailey, S., Wong, M., Daly, S., Greenberg, D. & Toprak, E. (2016) Sequence-Specific Targeting of Bacterial Resistance Genes Increases Antibiotic Efficacy. *PLoS Biology*, 14(9), e1002552.
- Bajpai, A. & Mishra, A. (2005) Preparation and characterization of tetracycline-loaded interpenetrating polymer networks of carboxymethyl cellulose and poly(acrylic acid): water sorption and drug release study. *Polymer International*, 54(10), 1347-1356.
- Chopra, I. & Roberts, M. (2001) Tetracycline Antibiotics: Mode of Action, Applications, Molecular Biology, and Epidemiology of Bacterial Resistance. *Microbiology and Molecular Biology Reviews*, 65(2), 232-260.
- Davies, J. & Davies, A. (2010) Origins and evolution of antibiotic resistance. *Mol. Biol. Rev*, 74, 417-433.
- Davies, J. & Wright, G. (1997) Bacterial resistance to aminoglycoside antibiotics. *Trends in Microbiology*, 5(6), 234-240.
- Din, F., Aman, W., Ullah, I., Qureshi, O., Mustapha, O., Shafique, S. & Zeb, A. (2017) Effective use of nanocarriers as drug delivery systems for the treatment of selected tumors. *International Journal of Nanomedicine*, Volume 12, 7291-7309.
- Doron, S. & Davidson, L. (2011) Antimicrobial Stewardship. *Mayo Clinic Proceedings*, 86(11), 1113-1123.
- EUCAST (2018) Breakpoint Tables v 8.0 & v 8.1. Available online: http://www.eucast.org/clinical_breakpoints/ [Accessed 10/5/2018]
- Fuentes-Hernandez, A., Pluain, J., Gori, F., Pena-Miller, R., Reding, C., Jansen, G., Schulenburg, H., Gudelj, I. & Beardmore, R. (2015) Using a Sequential Regimen to Eliminate Bacteria at Sublethal Antibiotic Dosages. *PLoS Biology*, 13(4), e1002104.
- Gardete, S. & Tomasz, A. (2014) Mechanisms of vancomycin resistance in *Staphylococcus aureus*. *Journal of Clinical Investigation*, 124(7), 2836-2840.
- Geilich, B., van de Ven, A., Singleton, G., Sepúlveda, L., Sridhar, S. & Webster, T. (2015) Silver nanoparticle-embedded polymersome nanocarriers for the treatment of antibiotic-resistant infections. *Nanoscale*, 7(8), 3511-3519.
- Gupta, A., Mumtaz, S., Li, C., Hussain, I. & Rotello, V. (2019) Combatting antibiotic-resistant bacteria using nanomaterials. *Chemical Society Reviews*, 48(2), 415-427.
- Halbus, A., Horozov, T. & Paunov, V. (2017) Colloid particle formulations for antimicrobial applications. *Advances in Colloid and Interface Science*, 249, 134-148.
- Halbus, A., Horozov, T. & Paunov, V. (2019) Strongly Enhanced Antibacterial Action of Copper Oxide Nanoparticles with Boronic Acid Surface Functionality. *ACS Applied Materials & Interfaces*, 11(13), 12232-12243.
- Harkins, C., Pichon, B., Doumith, M., Parkhill, J., Westh, H., Tomasz, A., de Lencastre, H., Bentley, S., Kearns, A. & Holden, M. (2017) Methicillin-resistant *Staphylococcus aureus* emerged long before the introduction of methicillin into clinical practice. *Genome Biology*, 18(1), 130.
- Hong, W., Zeng, J. & Xie, J. (2014) Antibiotic drugs targeting bacterial RNAs. *Acta Pharmaceutica Sinica B*, 4(4), 258-265.

- Jahangirian, H., Ghasemian lemraski, E., Webster, T., Rafiee-Moghaddam, R. & Abdollahi, Y. (2017) A review of drug delivery systems based on nanotechnology and green chemistry: green nanomedicine. *International Journal of Nanomedicine*, Volume 12, 2957-2978.
- Kohanski, M., Dwyer, D. & Collins, J. (2010) How antibiotics kill bacteria: from targets to networks. *Nature Reviews Microbiology*, 8(6), 423-435.
- Kumari, A., Singla, R., Guliani, A., & Yadav, S. K. (2014). Nanoencapsulation for drug delivery. *EXCLI journal*, 13, 265–286.
- Leclercq, R. & Courvalin, P. (2002) Resistance to Macrolides and Related Antibiotics in *Streptococcus pneumoniae*. *Antimicrobial Agents and Chemotherapy*, 46(9), 2727-2734.
- Leekha, S., Terrell, C. & Edson, R. (2011) General Principles of Antimicrobial Therapy. *Mayo Clinic Proceedings*, 86(2), 156-167.
- Li, B. & Webster, T. (2017) Bacteria antibiotic resistance: New challenges and opportunities for implant-associated orthopedic infections. *Journal of Orthopaedic Research*, 36, 22-32.
- Li, W., Atkinson, G., Thakor, N., Allas, Ü., Lu, C., Chan, K., Tenson, T., Schulten, K., Wilson, K., Haurlyiuk, V. & Frank, J. (2013) Mechanism of tetracycline resistance by ribosomal protection protein Tet(O). *Nature Communications*, 4(1), 1477.
- Llor, C. & Bjerrum, L. (2014) Antimicrobial resistance: risk associated with antibiotic overuse and initiatives to reduce the problem. *Therapeutic Advances in Drug Safety*, 5(6), 229-241.
- MacLeod, A. J., Ross, H. B., Ozere, R. L., Digout, G., & van Rooyen, C. E. (1964) Lincomycin: A new antibiotic active against staphylococci and other Gram-positive cocci: clinical and laboratory studies. *Can. Med. Association*, 91, 1056-2060.
- Markley, J. & Wencewicz, T. (2018) Tetracycline-Inactivating Enzymes. *Frontiers in Microbiology*, 9, 1058.
- Matzov, D., Eyal, Z., Benhamou, R., Shalev-Benami, M., Halfon, Y., Krupkin, M., Zimmerman, E., Rozenberg, H., Bashan, A., Fridman, M. & Yonath, A. (2017) Structural insights of lincosamides targeting the ribosome of *Staphylococcus aureus*. *Nucleic Acids Research*, 45(17), 10284-10292.
- Munita, J. & Arias, C. (2016) Mechanisms of Antibiotic Resistance. *Virulence Mechanisms of Bacterial Pathogens, Fifth Edition*, 481-511.
- Peach, K., Bray, W., Winslow, D., Linington, P. & Linington, R. (2013) Mechanism of action-based classification of antibiotics using high-content bacterial image analysis. *Molecular BioSystems*, 9(7), 1837.
- Perron, G., Lee, A., Wang, Y., Huang, W. & Barraclough, T. (2011) Bacterial recombination promotes the evolution of multi-drug-resistance in functionally diverse populations. *Proceedings of the Royal Society B: Biological Sciences*, 279(1733), 1477-1484.
- Poole, K. (2011) *Pseudomonas Aeruginosa*: Resistance to the Max. *Frontiers in Microbiology*, 2, 65.
- Silhavy, T., Kahne, D. & Walker, S. (2010) The Bacterial Cell Envelope. *Cold Spring Harbor Perspectives in Biology*, 2(5), a000414-a000414.
- Silver, L. (2011) Challenges of Antibacterial Discovery. *Clinical Microbiology Reviews*, 24(1), 71-109.
- Soni, K., Desale, S. & Bronich, T. (2016) Nanogels: An overview of properties, biomedical applications and obstacles to clinical translation. *Journal of Controlled Release*, 240, 109-126.
- Spížek, J. & Řezanka, T. (2004) Lincomycin, clindamycin and their applications. *Applied Microbiology and Biotechnology*, 64(4), 455-464.
- Webster, T. & Seil, I. (2012) Antimicrobial applications of nanotechnology: methods and literature. *International Journal of Nanomedicine*, 7, 2767-2781.
- Yu, X., Trase, I., Ren, M., Duval, K., Guo, X. & Chen, Z. (2016) Design of Nanoparticle-Based Carriers for Targeted Drug Delivery. *Journal of Nanomaterials*, 2016, 1-15.

3.0 Chapter 3

Enhanced clearing of wound-related pathogenic bacterial biofilms using protease-functionalised antibiotic nanocarriers

Weldrick, P. J., Hardman, M. J., & Paunov, V. N. (2019). Enhanced Clearing of Wound-Related Pathogenic Bacterial Biofilms Using Protease-Functionalized Antibiotic Nanocarriers. *ACS Applied Materials & Interfaces*, 11(47), 43902–43919. Reproduced by permission of The American Chemical Society. Copyright © 2019. Conceptualisation, V.N.P. All experiments were performed by P.J.W under V.N.P. supervision. P.J.W prepared the figures and wrote the manuscript, V.N.P and M.J.H. co-edited the manuscript. All authors have given approval to the final version of the manuscript.

Biofilms are prevalent in chronic wounds and once formed are very hard to remove, which is associated with poor outcomes and high mortality rates. Biofilms are comprised of surface-attached bacteria embedded in an extracellular polymeric substance (EPS) matrix, which confers increased antibiotic resistance and host immune evasion. Therefore, disruption of this matrix is essential to tackle the biofilm-embedded bacteria. Here is proposed a novel nanotechnology to do this, based on protease-functionalised nanogel carriers of antibiotics. Such active antibiotic nanocarriers, surface coated with the protease Alcalase 2.4 L FG, “digest” their way through the biofilm EPS matrix, reach the buried bacteria, and deliver a high dose of antibiotic directly on their cell walls, which overwhelms their defences. The effectiveness was demonstrated against six wound biofilm-forming bacteria, *Staphylococcus aureus*, *Pseudomonas aeruginosa*, *Staphylococcus epidermidis*, *Klebsiella pneumoniae*, *Escherichia coli*, and *Enterococcus faecalis*. The results confirmed a 6-fold decrease in the biofilm mass and a substantial reduction in bacterial cell density using fluorescence, atomic force, and scanning electron microscopy. Additionally, it was showed that co-treatments of ciprofloxacin and Alcalase-coated Carbopol nanogels led to a 3-log reduction in viable biofilm-forming cells when compared to ciprofloxacin treatments alone. Encapsulating an equivalent concentration of ciprofloxacin into the Alcalase-coated nanogel particles boosted their antibacterial effect much further, reducing the bacterial cell viability to below detectable amounts after 6 h of treatment. The Alcalase-coated nanogel particles were noncytotoxic to human adult keratinocyte cells (HaCaT), inducing a very low apoptotic response in these cells. Overall, it is demonstrated that the Alcalase-coated nanogels loaded with a cationic antibiotic elicit very strong biofilm-clearing effects against wound-associated biofilm-

forming pathogenic bacteria. This nanotechnology approach has the potential to become a very powerful treatment of chronically infected wounds with biofilm forming bacteria.

3.1 Introduction

Biofilms are microbial communities surrounded by a structure referred to as extracellular polymeric substance (EPS), composed of biopolymers such as exopolysaccharides, nucleic acids, lipids, and proteins (Leroy et al., 2008). The EPS matrix is highly hydrated, with occasional hydrophobic regions, such as areas containing cellulose (Choong et al., 2016). Combined, these substances form a structured matrix, allowing bacteria to effectively adhere to a range of surfaces (Kostakioti et al., 2013). The formation of biofilms begins when surface attached bacterial cells secrete EPS, which allows complex communal tertiary microcolony structures to form (Richards & Melander, 2009). Biofilms are commonly surface attached with one layer of cells in direct contact with the substratum, however, they can be found in flocs in which biofilms are formed around cells without contact with a substratum (Kim et al., 2014). The EPS matrix provides effective protection of the bacteria within the bio film to a wide array of environmental factors, such as antimicrobial agents and a host immune response molecule (Algburi et al., 2017; Domenech et al., 2013). Biofilms confer benefits to the cells within, in quenching antimicrobial agents, which would kill planktonic cells (Sharma et al., 2019). The biofilm is able to impair the diffusion of antimicrobial agents through the EPS and lower local concentration, thus increasing the tolerance of the cells to the most chemicals (Singh et al., 2017). An example of tolerance is the neutralisation of toxic metal ions such as copper, which is complexed to the polysaccharides of the EPS (Nocelli et al., 2016; Gupta et al., 2017). Biofilm infections in humans with species, which show high resistance to treatment, may result in chronic infections (Yang et al., 2012).

Opportunistic pathogens such as *Staphylococcus*, *Pseudomonas*, and *Klebsiella* genus' can form biofilms on acute and chronic dermal wounds, impairing wound healing, and potentially leading to sepsis (Donlan, 2002). This effect can lead to increased patient mortality and morbidity in regard to biofilm infection (Costerton et al., 1999; Rogers et al., 2010). Nanoparticles (NPs) have been investigated for their antibiofilm properties. Ag–Au nanocomposite particles, CuONPs, Mg(OH)₂ NPs, silica NPs, and Au NPs, have shown high efficacy in this regard (Halbus et al., 2019a; Halbus et al., 2019b; Newase et al., 2017; Markowska et al., 2013; Halbus et al., 2019c). Borovička et al., 2015 developed photo thermal colloid antibodies based on bioimprints that can selectively kill microbial cells by cell shape recognition. Au NPs in conjunction with heat produced with laser irradiation can effectively disrupt biofilms (Pastore, 2018). Taking advantage of the antimicrobial effect of Ag has led to the novel use of bioglass, which incorporates surface-reacted Ag and has been shown to have effective antibiofilm use (Wilkinson et al., 2018). Enzymatic biofilm degradation has also been investigated, e.g., the use of hydrolases, amylases, and proteases (Singh et al., 2016). The principle of disrupting the biofilm network using enzymatic lysis, rather than directly attacking the cells

themselves, has the advantage of not relying on the biocidal action of traditional antimicrobials and as such does not place a direct evolutionary pressure on the bacteria to develop resistance (Blackledge et al., 2013). All components of the EPS matrix have been investigated for the removal of biofilms, these include DNases, glycosidases, and proteases (Kaplan et al., 2010). An example of a glycosidase is dispersin B produced by *Aggregatibacter actinomycetemcomitans* and has been demonstrated as being effective against *Staphylococcus epidermidis* and *Staphylococcus aureus* biofilms (Donelli et al., 2007; Darouiche et al., 2009). Glycoside hydrolase alginate lyase and DNase NucB have also proved effective against *Pseudomonas aeruginosa* and *Escherichia coli* biofilms, respectively (Alkawash et al., 2006; Nijland et al., 2010).

Proteases (EC 3.4) are present in all life forms, providing a wide variety of metabolic and physiological functions, including signal transduction, apoptosis, cell division, blood pressure regulation, and many more (Theron & Divol, 2014). Proteases have previously been investigated for their antibiofilm potential, both as small molecules (e.g., ficin) and bacterial-derived *Bacillus* proteases (AprBp and GseBp) (Baidamshina et al., 2017; Mitrofanova et al., 2017). Ironically, bacteria have become a useful source of antibiofilm proteases (Singh et al., 2015; Singh et al., 2016). Proteases have two unique properties, which make them an excellent enzyme choice for degrading biofilms. Their ability to hydrolyse EPS matrix proteins and adhesins (allowing a biofilm to attach to a solid surface and bacteria–bacteria adhesion) gives them a distinct advantage over other antibiofilm enzymes (Leroy et al., 2018). Additionally, they may disrupt intercellular communication by lysis of type I signal peptidase, as shown in *S. aureus* (Schallenberger et al., 2012). Proteases have also been shown to have potential in improving wound healing by degrading the biofilm EPS, which may be interfering with the normal wound-healing process (Thallinger et al., 2013; Ramasamy et al., 2016). Serine Esp-based protease obtained from *S. epidermidis* and elastase LasB from *P. aeruginosa* have been shown to reduce bio film formation in *S. aureus*, providing further evidence of their efficacy and usefulness in biofilm treatment options (Park et al., 2012; Lequette et al., 2010).

In addition to the evidence that exogenous protease degrades bio films, it has been shown that in the natural self-induced disassembly of biofilms, bacteria induce expression of extracellular proteases to cleave matrix proteins (Boles & Horswill, 2011). Some of these extracellular proteases include sigB and sarA, which have all been shown to reduce bio film capacity in *S. aureus* (Tsang et al., 2008). Novozymes (Denmark) produce a wide array of enzymes produced by *Bacillus* spp. (Gram-positive, rod-shaped, spore forming bacteria), which have applications in industry and biopharmaceutical ingredients, many with useful activity properties, as mentioned above (Jisha et al., 2013). It has been demonstrated that immobilisation of proteases can increase their stability, reusability, and increase their tolerance of environmental stresses (Mateo et al., 2007). Covalent

bonding, ionic interactions, entrapment/encapsulation in polymer or inorganic matrices, and hydrophobic adsorption have previously been demonstrated as methods to immobilise enzymes (Coríci et al., 2011). Although immobilisation can improve the enzyme activity, stability, and storage life, there is also the possibility of enzyme rigidification, particularly in strong covalent techniques, which reduce the effective activity of the enzyme (Rodrigues et al., 2013). Nanoparticle carriers such as chitosan beads and soybean fibres have been shown to be useful biocompatible carriers for proteins and also increase the activity of Alcalase (Tang et al., 2006; Wang et al., 2014).

In this study, the use of Carbopol Aqua SF1 nanogels was investigated as a substrate to immobilise a serine endo-peptidase protease, namely, Alcalase 2.4 L FG (**Figure 3.1** illustrates the process). Polyacrylic acid co-polymer nanogels have crosslinked polymer chains, which due to the abundance of COOH groups confer an anionic charge upon their surface and interior (Al-Awady et al., 2017). These nanogel particles have shown good biocompatibility and have been found to be effective in encapsulating cationic antimicrobials such as chlorhexidine digluconate, tetracycline and lincomycin hydrochloride (Al-Awady et al., 2018 ; Weldrick et al., 2019). Nanocarrier-based antibiotic delivery provides an opportunity to increase the effectiveness of therapeutic agents by specifically targeting bacteria due to their anionic cell wall (e.g., utilising cationic coatings of the nanogel such as poly(diallyldimethylammonium chloride) and branched polyethyleneimine), localising the drug while reducing the unintended damaging effect on neighbouring tissues. Since Alcalase 2.4 L FG has a very high isoelectric point, it is positively charged at neutral pH. The study took advantage of the negative surface charge of Carbopol Aqua SF1 nanogel particles to electrostatically immobilise Alcalase 2.4 L FG on their surface. The study investigated the stability of Alcalase 2.4 L FG coated Carbopol Aqua SF1 nanoparticles and evaluated their potential antibiofilm use on skin-associated pathogens, which are known to produce biofilms. Additionally, there was an investigating the potential synergistic effect of antibiotic co-treatments and encapsulations within the nanogel using ciprofloxacin hydrochloride, combined with a further surface coating of the loaded nanogel with Alcalase 2.4 L FG. This study demonstrates that there is a strong synergistic clearing effect of these novel dual functionalised nanogels on biofilms of a range of pathogenic bacteria.

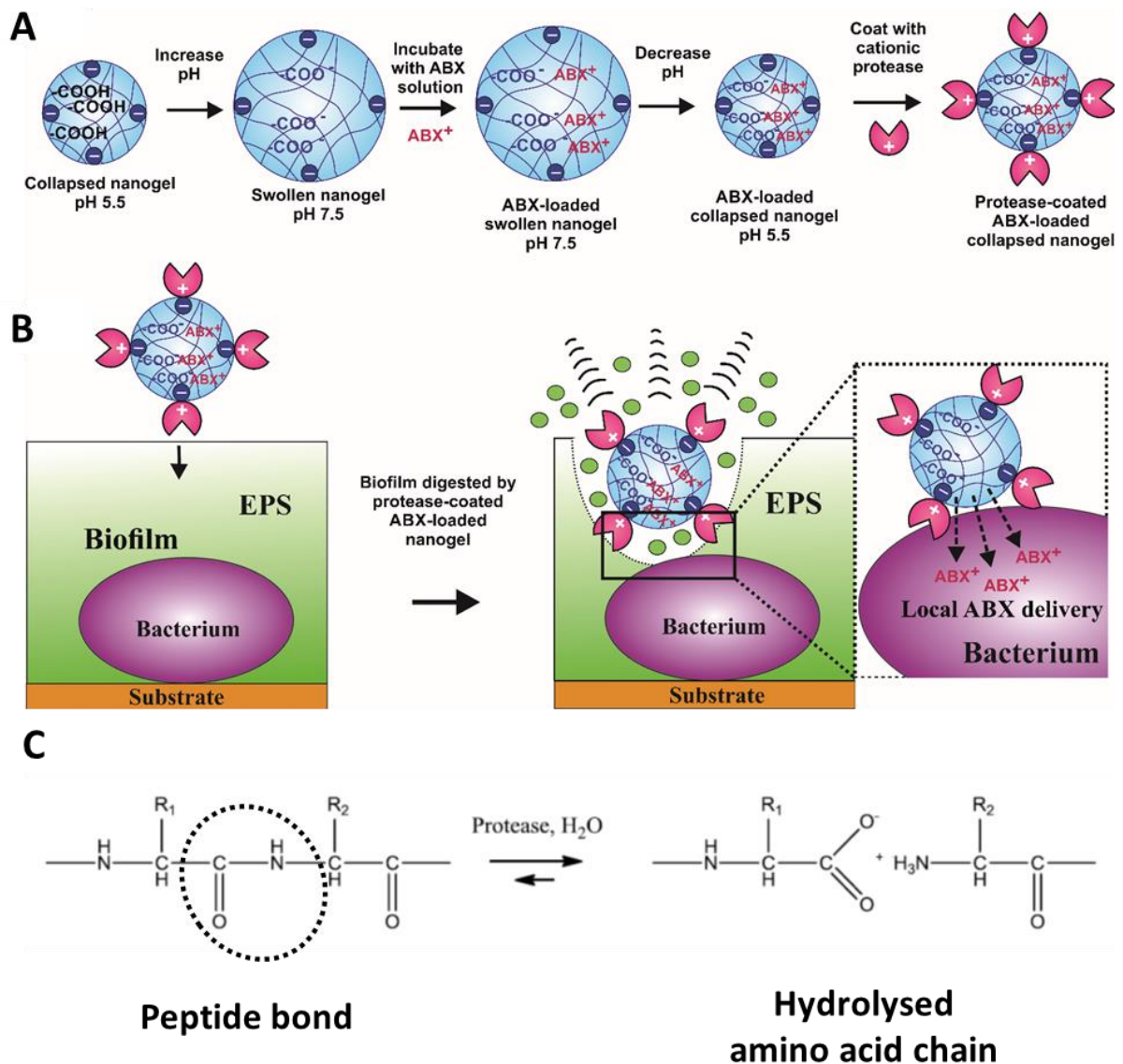


Figure 3.1. (A) Schematic for the loading of the Carbopol Aqua SF1 nanogel with antibiotic (ABX+) followed by surface coating with protease (Alcalase 2.4 L FG). **(B)** Diagram of the mechanism of action of the Carbopol Aqua SF1-Alcalase 2.4 L FG nanogel particles on biofilms adhered to a substrate. Alcalase 2.4 L FG acts as a hydrolase cleaving peptide chains. It also acts as esterase, enabling it to catalyse stereo-selective hydrolysis of some esters including carboxylic esters and amino esters. **(C)** Schematic of the enzymatic degradation of peptide bonds in proteins by Alcalase 2.4 L FG. Alcalase 2.4 L FG acts as a hydrolase cleaving peptide chains. It also acts as esterase, enabling it to catalyse stereo-selective hydrolysis of some esters including carboxylic esters and amino esters.

3.2 Materials and methods

In this section, the materials and experimental methods used throughout this chapter are described.

3.2.1 Materials

Carbopol Aqua SF1 nanogel (30 wt% aqueous suspension) was provided by Lubrizol, USA. Six American Type Culture Collection (ATCC) bacterial species were used in this study. *Staphylococcus aureus subsp. aureus* Rosenbach (ATCC® 29213™), *Pseudomonas aeruginosa* (Schroeter) Migula (ATCC® 27853™), *Staphylococcus epidermidis* (Winslow and Winslow) Evans (ATCC® 35984™), *Klebsiella pneumoniae subsp. pneumoniae* (Schroeter) Trevisan (ATCC® 35657™), *Escherichia coli* (Migula) Castellani and Chalmers (ATCC® 25922™), and *Enterococcus faecalis* (Andrewes and Horder) Schleifer and Kilpper-Balz (ATCC® 51299™). Mueller-Hilton Broth (MHB), Mueller-Hilton Agar (MHA) were supplied by Oxoid, UK. Alcalase 2.4 L FG EC number; 3.4.21.62 was kindly provided by Novozymes, Denmark. Alcalase 2.4 L FG is a Serine endopeptidase (mainly subtilisin A) which performs Stereo selective hydrolysis of amino esters and selective esters. Alcalase also efficiently hydrolyses amino esters which include heterocyclic amino esters. Optimal conditions for usage are 30–65°C and pH 7–9. Its enzymatic activity is 2.4 AU-A/g. The protein concentration of Alcalase 2.4 L FG was 55 mg/mL was determined by a NanoDrop™ Lite Spectrophotometer (Thermo Scientific, UK). Millipore Express PLUS Membrane Filter paper (0.22 µm pore size, hydrophilic polyethersulfone, 47 mm diameter), Ciprofloxacin hydrochloride (≥98.0%), Acridine Orange base (75%) and Resazurin Sodium salt (75%) were purchased from Sigma-Aldrich, UK. Resazurin Sodium salt was used for cell metabolic *in situ* assays and diluted in Dulbecco's Phosphate Buffered Saline (DPBS) (Gibco, Fisher Scientific, UK) at a concentration of 0.015 wt/vol%. HaCaT cells were obtained from AddexBio, T0020001, USA. DMEM and FBS were obtained from Gibco, UK, L-Glutamine and Trypsin EDTA by BioWhittaker, UK. A Pierce™ Protease Assay Kit (Thermo Scientific, USA) was used to characterise the Alcalase 2.4 L FG activity. An MTT colorimetric survival and proliferation kit (Millipore Corp., USA), was used for HaCaT cell viability experiments and an ANNEXIN V apoptosis detection Kit I (BD Pharmogen, USA) was used to measure apoptosis after treatments. Deionised water purified by reverse osmosis and ion exchange with a Milli-Q water system (Millipore, USA) was used in all studies. Its surface tension was 71.9 mN m⁻¹ at 25 °C, with measured resistivity more than 18 MΩ cm⁻¹. Consumable plasticware used in the study were purchased from Sarstedt (UK), Thermo Scientific (UK), or CytoOne (UK) unless otherwise stated.

3.2.2 Synthesis of Alcalase-coated nanogel particles

Carbopol Aqua SF1 (30 wt%) was diluted into 0.6 wt% by pipetting 2 mL of the stock suspension (30 wt%) and diluting with Milli-Q water to a final volume of 100 mL. This suspension was sonicated for 15 min with 2 second on/off pulsing using an ultrasonic bath (Ultrawave, U.K.) to allow effective

dispersion. Droplets 0.25 M HCl was added to the suspension to reduce the pH to 5.5. A 0.6 wt% solution of Alcalase L FG 2.4 was created by diluting 0.6 mL of the stock liquid enzyme solution and diluting with Milli-Q water to a final volume of 100 mL. The 0.6 wt% Alcalase solution was sonicated for 15 minutes to prevent aggregation. 25 mL of the 0.6 wt% Carbopol Aqua SF1 suspension and 25 mL of the 0.6 wt% Alcalase L FG 2.4 solution were mixed together for 30 min at pH 5.5 with constant stirring to allow the enzyme to electrostatically bind to the Carbopol NPs. After mixing the suspension was centrifuged at 4000 *g* for 15 min and the pellet was washed trice with deionised water and then dispersed into 50 mL of fresh deionised water. Droplets of acetate buffer solution were added to maintain the dispersion at 5.5 pH. The supernatant was retained for analysis to determine the surface functionalisation efficiency by UV-Vis absorption measurement. The particle size and zeta potential distribution of the Carbopol-Alcalase NPs were measured using a Malvern Zetasizer as described below. Prior to measurement, and the use of the nanogels in treatments, the 0.6 wt% Carbopol-0.6 wt% Alcalase dispersion was sonicated for 5 minutes to remove aggregation and diluted into deionised water to the appropriate concentration.

3.2.3 Preparation of ciprofloxacin-loaded nanogel

The principle of encapsulating a cationic antibiotic (as a hydrochloride salt) is based on the swelling and deswelling cycle of the Carbopol Aqua SF1 at different pH.⁴⁹ Briefly, a 100 mL of 0.6 wt% aqueous dispersion of the nanogel was prepared, this was then adjusted to pH 7.5 by adding droplets of 0.25 M NaOH whilst been stirred. The dispersion was then warmed to 37 °C. An aliquot of 0.0032 wt% ciprofloxacin hydrochloride aqueous dispersion was prepared by weighing 3.2 mg of the antibiotic (ABX = ciprofloxacin) powder, diluting into 100 mL of deionised water and then warming to 37 °C. The 100 mL ABX solution was then added to the pH 7.5 nanogel dispersion and shaken for 30 min at 37 °C to allow the antibiotic cations to diffuse into and electrostatically bind in the cores of the swollen nanogel particles. The pH of the ABX–Carbopol solution was then reduced to pH 5.5 using droplets of 0.25 M HCl whilst being stirred for another 30 min. The ABX–Carbopol suspension was then centrifuged at 4000 *g* for 15 min, and the supernatant was removed and retained for encapsulation efficiency analysis. The pellet was washed twice with deionised water and re-dispersed into 100 mL of deionised water. The pH was then increased to 7.5 by gradually adding droplets of 0.25 M NaOH and the solution was gently stirred overnight. The final ABX–Carbopol nanogel solution was reduced to pH 5.5 using acetate buffer solution. The particle size and zeta potential distribution of the ATX–Carbopol dispersion were measured using a Malvern Zetasizer Nano ZS as described above. Coating of the ciprofloxacin encapsulated Carbopol NPs with Alcalase 2.4 L FG was performed as described above.

3.2.4 Characterisation of free Alcalase, Alcalase-nanogel and Alcalase-coated ciprofloxacin-loaded nanogel

All hydrodynamic diameter and zeta potential measurements were performed using a Malvern Zetasizer Nano ZS. The isoelectric point of Alcalase L FG 2.4; 10 mL of 0.02 wt% aqueous solution Alcalase aliquots were created at a range of pH 5 to 12 using droplets of either 0.25 M HCl or 0.25 M NaOH. Afterwards, the aliquots were sonicated for 15 min. 1 mL of each aliquot was added to a quartz cuvette and the zeta potential measured using a ZEN1002 dip cell at a refractive index of 1.45 and absorption of 0.001 as per Malvern Instruments protein refractive index manual. Measurements were performed at 25°C and data represented as the mean of 3 repeats.

3.2.5 Hydrodynamic diameter, zeta potential, UV-Vis and FTIR spectroscopic study of Alcalase-nanogel and Alcalase-nanogel loaded with ciprofloxacin

50 mL of pH 5.5 0.6 wt% Carbopol-0.6 wt% Alcalase L FG 2.4 NPs and 0.6 wt% Carbopol-0.0032 wt% ciprofloxacin-0.6 wt% Alcalase-nanogel dispersions were prepared as described above. Aliquots of 0.6 wt% Carbopol were mixed with varying concentrations of Alcalase L FG 2.4 (range; 0.000625 wt% to 0.6 wt%). The hydrodynamic diameter and zeta potential were measured at 25°C using a quartz cuvette at a RI of 1.336 and absorbance of 1.000 as determined by Al-Awady et al.⁴⁹ Each measurement was repeated 3 times and data presented as the mean. The UV-Visible spectrum of 0.05 wt% Carbopol, 0.05wt% Alcalase 2.5 L FG and 0.05 wt% Carbopol with 0.05 wt% Alcalase 2.4 L FG coating; Samples were measured at pH 5.5 by adjustment with acetate buffer solution. The absorbance was measured between 220 nm and 1000 nm using a FLUOstar Omega spectrophotometer, BMP Labtech. The Alcalase coating efficiency of the Carbopol NPs was examined by UV-Vis analysis of the supernatant produced during the synthesis as described above. The absorbance of the supernatant was measured at 500 nm using a spectrophotometer (FLUOstar Omega spectrophotometer, BMP Labtech). Fourier transform infra-red (FTIR) spectra of Carbopol Aqua SF1, Alcalase 2.4 L FG, Ciprofloxacin and Carbopol encapsulated Ciprofloxacin coated with Alcalase NPs; Samples were prepared by removing water using a Silica gel desiccant by in vacuum chamber for 1 day, then dried at 60°C for 2 days. The spectra was measured between 4000-600 cm⁻¹ using PIKE ATR diamond settings. A spectrum was obtained with a blank of just air to reduce transmittance interference with the samples.

3.2.6 Protease activity of free Alcalase vs nanogel-immobilised Alcalase

The activity of free Alcalase 2.4 L FG vs Alcalase 2.4 L FG-Carbopol Aqua SF1 NPs was investigated by measuring the cleavage of succinylated casein in the presence of 0.2 wt% Alcalase, or 0.2 wt% Alcalase-0.2 wt% Carbopol NPs at varying pH, temperature, and over time. 10 mg of lyophilised succinylated was dissolved in 1 mL of acetate buffer (pH 5.5), PBS (pH 7.5), or BupH Borate buffer (pH 8.5). For the purpose of the temperature and time experiments acetate buffer was used

for all measurements, mimicking the buffer used in the NP preparation. 100 μ L of this solution was added to a 96-well plate, and 100 μ L of buffer added creating a total volume of 200 μ L in each well. 100 μ L of plane buffer was used as a blank. 50 μ L of either free Alcalase 2.4 L FG vs Alcalase 2.4 L FG-Carbopol Aqua SF1 NPs was added to the wells. The activity of the samples was measured at different pH (using buffers above) for 30 min at room temperature, over time (30 mins to 24 hr) at room temperature, or at different temperatures (30°C, 37°C, anF1982d 45°C) for 30 min. 100 μ L of trinitrobenzenesulfonic acid was dissolved in 14.9 mL of appropriate buffer to create a TNBSA working solution. Succinylated casein in the presence of proteases is cleaved at the peptide bonds revealing primary amine groups. TNBSA reacts with these groups to produce an orange-yellow product of which the absorbance can be measured at 450 nm informing of protease activity of the samples. The protease activity of the free protease vs nanogel-coated protease were measured at specific time points by adding 50 μ L of the TNBSA solution to the wells and incubating for 20 min. Then, the absorbance of the wells was measured at 450 nm subtracting the absorbance from the blank wells. This data was plotted to assess the relative protease activity of the free Alcalase 2.4 L FG vs Alcalase 2.4 L FG-Carbopol Aqua SF1 nanogels at different experimental conditions.

3.2.7 Bacterial culture and biofilm producing assessment

Frozen ATCC species were prepared onto MHA plates according to manufacturer's instructions. Overnight (O/N) cultures were prepared by incubating a single colony scraped from the MHA stock plates into 10 mL of MHB for 16 hr at 37°C with 140 rpm shaking (Stuart Orbital Incubator S1500). For biofilm assays, O/N cultures were adjusted to 0.5 McFarland standard by diluting the O/N culture into 0.85 w/v% sterile saline until an optical density of 0.08-0.12 at 625 nm ($1-2 \times 10^8$ CFU/mL) was obtained using a spectrophotometer (FLUOstar Omega spectrophotometer, BMP Labtech). These adjusted bacterial saline suspensions were then diluted 1:150 into MHB to yield starting concentrations between $5 \times 10^5 - 1 \times 10^6$ colony forming units per mL (CFU mL⁻¹). All six ATCC species used in this study have previously been confirmed as biofilm producers, however, to validate this a simple qualitative biofilm formation assessment was performed. 2 mL of MHB was placed into glass test tubes and inoculated with a single colony of bacteria from culture plates. The test tubes were incubated for 24 hr at 37°C. Afterward, the culture media was decanted, and the test tubes washed with PBS (pH 7.4), and left to dry for 30 min. 0.1 wt% Crystal Violet was used to stain cells adhered to the glass tubes for 5 min, before being washed away with deionised water. The test tubes were then left to dry in an inverted position for 2 hr. Biofilm formation was considered positive when a visible film lined the wall and bottom of the tube. Ring formation at the liquid interface was not indicative of biofilm formation. The formation of biofilm by staining of adhered cells was scored as either 0-absent, 1-weak, 2-moderate or 3-strong, as first performed by Christensen et al., 1982.

3.2.8 Zeta potential of bacteria treated with free Alcalase and Alcalase-coated nanogel

Bacterial species were cultured as described in as described above. The bacterial suspension was then centrifuged for 10 min at 5000 *g* and the supernatant discarded. The pellet was washed twice with Milli-Q water and finally resuspended into 10 mL of 0.2 wt% Alcalase or 0.2 wt% Alcalase-0.2 wt% Carbopol Aqua SF1 in deionised water. The samples were incubated at room temperature with gentle mixing for 10 minutes or 1 hrs. Afterwards, a 1 mL aliquot of this suspension was then added to a quartz cuvette and the mean zeta potential distribution was measured using the Dipstick probe and a Malvern Zetasizer Nano ZS (Malvern Instruments, UK). The refractive index was 1.384, the absorption 1.000, and the temperature was 25°C for all measurements.

3.2.9 Biofilm staining with Crystal Violet and Congo Red

A standard 96-well microtiter biofilm formation plate assay was performed using Crystal Violet and Congo Red dyes (modified from O'Toole, 2011). Crystal Violet staining. 1 mL of 5×10^5 – 1×10^6 CFU / mL of O/N bacterial culture was pipetted into 48-well TC-treated plates and incubated at 37°C for 24 hrs in static conditions. After incubation, the plates were washed twice by submerging in deionised water to remove any remaining media and suspended cells. The plate was then shaken dry and left to air dry for 15 mins at room temperature. 1 mL of MHB supplemented with Carbopol-Alcalase synthesised NP treatment was added to the wells and incubated for 24 hrs at 37°C in static conditions. The plates were then washed vigorously by submersion in deionised water to remove excess treated media and suspended cells. The plate was then shaken to remove liquid droplets and left to dry for 15 mins at room temperature. 1 mL of 0.1 wt% Crystal Violet solution was added to each well and incubated at room temperature for 15 mins. The plates were then washed thoroughly by submersion in deionised water and blotted with paper towels to remove excess dye and water. The plate was left to dry for 2 hrs at room temperature. 1 mL of 30% acetic acid was added to each well for 15 minutes to solubilise to the Crystal Violet. 125 µL of this solution was transferred to a fresh 96-well plate and the absorbance measured at 570 nm with 30% acetic acid used as a blank measurement. Congo Red staining. As described above, 48-well plate biofilms were formed and treated with 1 mL of MHB supplemented Carbopol-Alcalase nanogel suspension. After the treatment, the enzyme-infused MHB media was removed and the 48-well plate washed thoroughly by submerging in water. The plate was then shaken to remove liquid droplets and left to dry for 15 mins at room temperature. 125 µL of 0.005 wt% Congo Red was added to each well and left to dye the amyloid protein complexes for 15 mins. The 96-well plate was then washed thoroughly again by submersion in deionised water and blotted with paper towels to remove excess Congo Red dye and water. The plate was left to dry for 2 hrs at room temperature. 125 µL of 30% ethanol was added to each well for 15 mins to solubilise to

the Congo Red dye. 125 μL of this solution was transferred to a fresh 96-well plate and the absorbance measured at 550 nm with 30% ethanol used as a blank measurement.

3.2.10 Membrane Colony Biofilm NP and ciprofloxacin treatment

To test the effects of Alcalase-Carbopol nanogel and ciprofloxacin co-treatments on biofilms a filter membrane method was employed. 2 cm^2 Millipore Express PLUS Membrane Filter paper sections were placed on to MHA. An overnight culture was adjusted to 1×10^5 CFU/mL in saline and 20 μL of this culture added as a droplet to the centre of the filter paper. The sample was then incubated for 24 hours at 37°C to allow a colony biofilm to form. After 24 hours the membranes were placed onto fresh agar plates (3mm deep) into a 6-well plate and 1 mL of treatment added to each well. The plate was gently shaken in the incubator during treatment. 1 mL of Milli-Q water was considered the growth control. 0.6 wt% Carbopol, 0.6 wt% Alcalase 2.4 L FG (diluted in Milli-Q water), and 0.6 wt% Carbopol-0.6 wt% Alcalase 2.4 L FG NPs were used as treatments to measure their effect on cell viability. Additionally, ciprofloxacin hydrochloride was added separately and as a co-treatment with the Carbopol-Alcalase NPs at a range of 0 to 32 $\mu\text{g}/\text{mL}$ (0.0032 wt%). Equivalent concentrations of encapsulated ciprofloxacin tested as a comparison. Common standard antimicrobial agents for treating biofilm-forming bacteria on skin (chlorhexidine digluconate, iodine and poly(vinylpyrrolidone)-iodine (PVP-I)) were diluted in deionised water for a comparison assessment. After 24 hrs of treatment the membrane filter paper was peeled from the agar wells and placed into sample tube with 1 mL of fresh MHB and 2 cm of sterile glass beads, enough to cover the sample. Each sample was vortexed for 30 secs at high speed to disintegrate the biofilm and inoculated the MHB with cells. The drop plate enumeration method was used to measure cell viability in CFU/mL. To measure the viability of cells within the biofilms, 10-fold dilutions were made in fresh MHB, 10 μL droplets were placed on to MHA plates and grown for 24 hours at 37°C. CFUs were counted from the last two droplets which contained a countable number of colonies (3 to 30 colonies per 10 μL drop) and averaged.

3.2.11 Antimicrobial susceptibility testing of *Staphylococcus aureus* using minimum inhibitory concentration evaluator (M.I.C.E. TEST®) strips

A single colony of *S. aureus* was isolated and placed into 10 mL of MHB and grown overnight at 37 °C. The bacteria suspension was then diluted to a 0.5 McFarland standard in MHB by measuring the turbidity at 625 nm yielding $1-2 \times 10^8$ CFU mL^{-1} . A cotton swab was used to streak a MHA plate lawn. 4 \pm 0.5 mm deep MHA plates were prepared by adding 25 mL of molten MHA to a 9 cm round plate and left to solidify at room temperature. Within 15 minutes of plate inoculation, sterile forceps were used to place a ciprofloxacin 32 $\mu\text{g}/\text{mL}$ – 0.002 $\mu\text{g}/\text{mL}$ gradient strip onto the plate with the 0.002 $\mu\text{g}/\text{mL}$ side touching the plate first, ensuring only the top section is touched with the forceps and it is placed logo side facing upwards.

The plate was incubated for 24 hours at 37°C in an inverted position, following manufactures instructions. After incubation the MIC is the point in which growth touches the strip nearest the white concentration value.

3.2.12 Resazurin sodium salt *in situ* bacterial metabolic activity assay

After the 24-hr membrane colony biofilm NP treatment, as described above, each membrane biofilm was carefully removed from the agar plate using sterile tweezers at the corner of the membrane. The membrane biofilm was allowed to air dry in sterile conditions for 15 minutes and then placed onto a dry sterile Petri dish. 20 µl of 0.015 wt% Resazurin Sodium Salt was added and incubated for 30 minutes at 37°C to visual metabolically active cells within the biofilm (modified from Wilkinson et al., 2016). Images were captured using an 8MP digital camera and the percentage of cell metabolic activity calculated using ImageJ v1.52d.

3.2.13 Biofilm formation assay on a glass surface

An overnight culture of each species was adjusted to 0.5 McFarland standard. 10 µL of the adjusted culture was placed into a Petri plate containing a glass slide and 10 mL of MHB. The Petri plate was incubated for 48 hrs at 37°C allowing the bacterial species to form a glass slide adhered biofilm. After 24 hr the glass slide was washed with deionised water to remove any remaining planktonic cells, and the media was replaced with 10 mL of fresh MHB supplemented with 0.6 wt% Carbopol, 0.6 wt% Alcalase L FG, and 0.6 wt% Carbopol-0.6 wt% Alcalase 2.4 L FG. Un-supplemented media was considered the control. The glass biofilms were incubated for a further 24 hr at 37°C. Post treatment, the glass slides were washed with deionised water. 100 µL 0.2 wt% Acridine Orange (AO) was added to the Petri dish and incubated at room temperature for 5 mins in darkness with gentle shaking to reduce photobleaching. After incubation the slides were washed three times with deionised water and allowed to air dry for 15 mins. The slides were examined using an Olympus DP70 fluorescent microscope.

3.2.14 Atomic force microscopy (AFM)

AFM images of the air-dried biofilms were obtained using a Dimension Icon scanning probe microscope (Bruker, USA) using tapping mode. The biofilms were prepared and treated as described above in the glass surface biofilm formation assay. Post treatment, the glass slide biofilms were washed gently with deionised water, and the biofilm fixed in 1 wt% aqueous glutaraldehyde for 2 hrs by submersion. After fixation, the slide was washed three times with deionised water and left to air dry inside an enclosed container. TESPA-V2 probes (Bruker, USA) with a nominal length of 127 µm and a tip radius of 7 nm were used, the images obtained at 512 lines/scan at a 0.25 Hz scan rate. Images were acquired in height (topography) and the analyzed using Nanoscope Analysis v.1.7. (Bruker).

3.2.15 TEM images of Alcalase-nanogel and SEM images of the treated biofilms

SEM images of membrane colony biofilms were obtained. Post treatment the membrane was gently removed from the agar using sterile tweezers and placed onto a 7 mm diameter circular glass slide and adhered using Carbon discs. The excess membrane was trimmed from the edges of the glass slide using sterile scissors. The biofilm was gently washed with deionised water from remove excess media and treatment. The biofilms were then fixed in a 1 wt% glutaraldehyde PBS buffer solution for 1 hr at room temperature. After fixation, the biofilms were washed 3 times gently with deionised water to remove excess glutaraldehyde. The samples were then dehydrated in 50%/75%/90% and absolute ethanol solutions for 30 minutes per each ethanol concentration. The absolute ethanol was dried using liquid CO₂ at its critical point using an E3000 Critical Point Dryer (Quorum Technologies, UK) and then coated in 10 nm Carbon. Samples were imaged with variable pressure 100-micron aperture at 40 Pa. EHT = 20 kV, probe current 100 pA. Images captured with Zeiss smartSEM software (Zeiss Evo-60 SEM, Germany). TEM images of bare Carbopol Aqua NPs, free Alcalase 2.4 L FG protease, and Alcalase 2.4 L FG coated Carbopol Aqua SF1 nanogels were obtained by placing a droplet of the suspended sample onto Carbon coated Copper grids (EM Solutions, UK) and allowed to adhere for 2 minutes. The grid was quickly rinsed with deionised water and negatively stained with 1 wt% aqueous uranyl acetate. This was again quickly rinsed with deionised water and allowed to dry in air. The sample was then imaged with a Gatan Ultrascan 4000 digital camera attached to the Jeol 2010 TEM 2010 electron microscope (Jeol, Japan) running at 120kV. EDX data was collected via an Oxford Instruments Nanoanalysis X-Max 65-T detector and INCA software.

3.2.16 Cytotoxicity and apoptotic stasis of HaCaT spontaneously transformed keratinocytes from histological normal skin after treatment with nanogel, Alcalase and Alcalase-nanogels

HaCaT cells were cultured in T75 flask using DMEM supplemented with 10% FBS and 1% L-glutamine under humidified conditions at 37°C, 5% CO₂. When a confluency of 80% was achieved, determined by visualisation with an optical microscope, passaging was performed to ensure that the cells remained in the exponential phase for experimentation. Passaging was performed by removing spent media, washing in DPBS and incubating with 1 × trypsin EDTA at 37°C 5% CO₂ for 5 min until the cells were detached in suspension. The trypsin EDTA was then neutralised with a 1 : 1 volumetric ratio of fresh DMEM and gently centrifuged at 400 *g* for 4 min, the supernatant was aspirated, and the pellet was re-suspended in DMEM (supplemented as above) at a 1 : 6 ratio and transferred into a fresh T75 flask. Surplus cells used for experimentation were diluted in fresh DMEM, supplemented with 2% FBS and 1% L-glutamine and seeded at 5 × 10⁴ in 100 µL media, were placed into 96-well plate wells and incubated for 24 hours at 37 °C 5% CO₂. The medium was then removed and the cells and replaced with 100 µL of treatment infused DPBS. The treatments with only DPBS were used as a control, 0.6

wt% Carbopol, 0.6 wt% free Alcalase, and 0.6 wt% Alcalase – 0.6 wt% Carbopol nanogel were used as treatments. DPBS was used so DMEM peptones did not interfere with the true activity of the Alcalase. Treatments were performed for 1, 6, and 24 hr time points. A colorimetric (MTT) cell survival and proliferation assay kit was used to measure cell viability. Treatment culture was aspirated away, and the cells washed for 2 mins with fresh DPBS. 100 μ L of fresh DMEM was added after which 100 μ L of MTT reagent (50% 3-(4,5-dimethylthiazol-2-yl)2,5-diphenyl tetrasodium bromide and 50% PBS) was added. This was incubated in the same conditions for 2 hrs until intracellular purple formazan crystals were visible under a light microscope. After 2 hrs 100 μ L of colour development reagent isopropanol with 0.04 N HCl was added for 1 hr, allowing the cells to lyse and the formazan crystal to be solubilised to a homogenous blue solution. The absorbance of the blue solution was read at 570 nm on a plate reader and subtracted from a blank of media only. These data were calculated into cell count data via interpolation from the standard curve (absorbance values from a fixed number of cells in media (see **Figure 3.28**). The data was represented as viability percentage of the control which was normalised to 100%. The HaCaT cell viability assay was repeated in three independent experiments. The induction apoptosis was investigated using a FITC Annexin V staining kit according to manufacturer instructions. Apoptosis was measured after 24 hours exposure to 0.6 wt% Alcalase-0.6 wt% Carbopol nanogel. Briefly, post treatment the cells were washed twice with DPBS and detached from the 96-well surface using a mini-cell scraper and re-suspended in 1X binding buffer at a concentration of 1×10^6 cells mL⁻¹. 5 μ L of FITC Annexin V and 5 μ L of Propidium Iodide (PI) solution to 100 μ L of the cell suspension. The cells were then incubated at room temperature for 15 mins in darkness with gentle shaking. After incubating, 400 μ L of 1X binding buffer was added to the cell samples which were then placed quantified by flow cytometry (BD FACSCalibur, USA). Annexin V was measured using a FITC-FL1 detector, and PI measured using a FL2 phycoerythrin signal detector. The experiment was ended after 10,000 cells were counted, the data was analysed by a dot plot scatter and percentages of live, dead, and apoptotic cells determined by cell quadrating.

3.2.17 Statistical analysis

Data were expressed as average values \pm standard deviations of the mean. P-values of less than 0.05 were considered significant. All Student's T-tests were performed in GraphPad v7.0.4.

3.3 Results and discussion

3.3.1 Coating and immobilisation of Alcalase 2.4 L FG on to Carbopol Aqua SF1 nanogel particles

A colloidal suspension of Carbopol Aqua SF1 was chosen as an appropriate nanocarrier for investigating the immobilisation of Alcalase 2.4 L FG protease on its surface. The lightly crosslinked carboxylic groups confer a net anionic surface charge corresponding to a zeta potential of approximately -30 mV at a pH of 5.5. This allows it to be used as a substrate to immobilise the cationic protein on its surface. The suspension was limited to 0.6 wt% to prevent the aggregation of the nanogel particles. Alcalase 2.4 L FG has a diameter of ~ 8 nm, as shown from the dynamic light scattering (DLS) size distribution and TEM micrographs (see **Figures 3.2A** and **3.3A and B**, respectively). Data in **Figure 3.2D** show that Alcalase 2.4 L FG has an isoelectric point of ~ 9 and a pH 5.5 has a zeta potential of $\sim +18$ mV. This allows a successful ionic interaction between the anionic Carbopol NPs and the cationic Alcalase 2.4 L FG. **Figure 3.2C** shows that the bare 0.6 wt% Carbopol NPs have a hydrodynamic diameter of approximately 110 nm, however, when coated with 0.6 wt% Alcalase 2.4 L FG (**Figure 3.2D**), the particle's mean diameter is increased to approximately 120 nm. **Figure 3.2B** confirms this through the measurement of the hydrodynamic diameter of the Alcalase-coated collapsed nanogel particles. **Figure 3.4** shows a comparison between the bare Carbopol and Alcalase coated Carbopol nanogels. It can be seen that by increasing the concentration of the Alcalase, the coated Carbopol NP's average particle size also increases. This can be seen in the TEM images in **Figure 3.3D**, where the corona of the collapsed nanogel particles can be seen coated with a "halo" of the Alcalase protein molecules. The successful coating of the Alcalase on the Carbopol NPs was also confirmed using UV-vis spectrophotometry. **Figure 3.2F** shows that Alcalase has a distinct absorption peak at ~ 245 nm; however, the bare Carbopol shows no such peak. When the Alcalase has coated the Carbopol particles, a small peak also at ~ 245 nm can be seen, indicating that the Carbopol and Alcalase have ionically interacted and formed composite Alcalase-coated Carbopol particles. **Figure 3.5** shows each of the formulations visually. The stability of the Alcalase-coated Carbopol nanogel particles was also investigated.

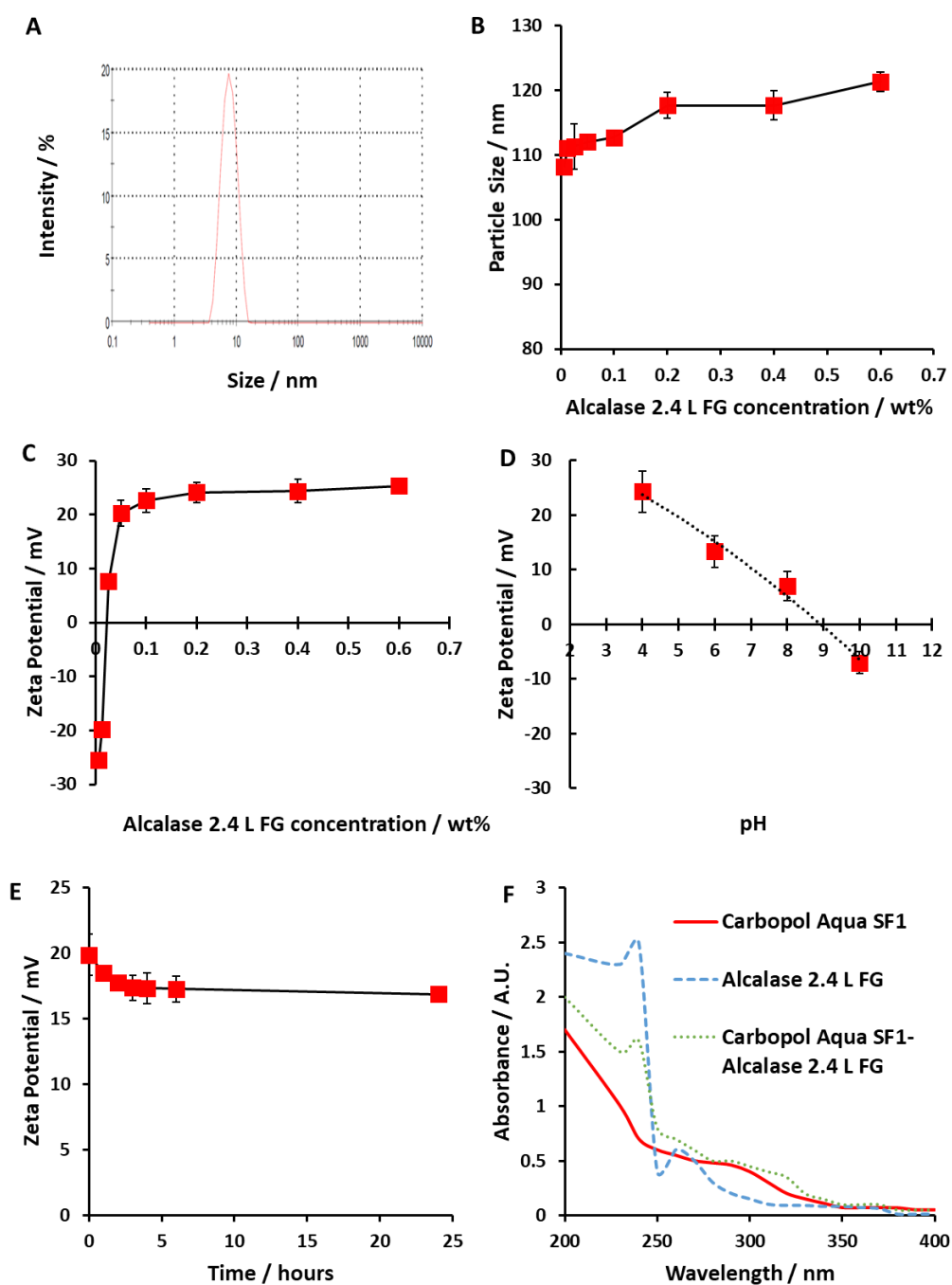


Figure 3.2. (A) Hydrodynamic diameter and (D) isoelectric point of 0.6 wt% Alcalase 2.4 L FG measured using a Malvern zetasizer Nano ZS at 25°C. Each value represents a triple replicate with \pm S.D. (B) The mean particle diameter and (C) mean zeta potential of Alcalase 2.4 L FG coated Carbopol particles measured at pH 5.5 (acetate buffered saline) with various concentrations of Alcalase 2.4 L FG non-specific protease mixed with an equal wt% of Carbopol Aqua NPs. (E) The zeta potential of 0.6 wt% Alcalase 2.4 L FG coated empty 0.6 wt% Carbopol nanogel particles at pH 5.5 (adjusted with acetate buffered saline) measured at time intervals after preparation. The refractive index of either particles was taken as 1.336. Each value represents average triplicate measurements with error bars representing the \pm S.D. The lines are guides to the eye. (F) The UV-Visible spectrum of 0.05 wt% Carbopol (red line), 0.05 wt% Alcalase 2.5 L FG (Blue line) and 0.05 wt% Carbopol with 0.05 wt% Alcalase 2.4 L FG coating (green line). Samples were measured at pH 5.5 adjusted by acetate buffer. The absorbance was measured between 220 and 1000 nm using a FLUOstar Omega spectrophotometer.

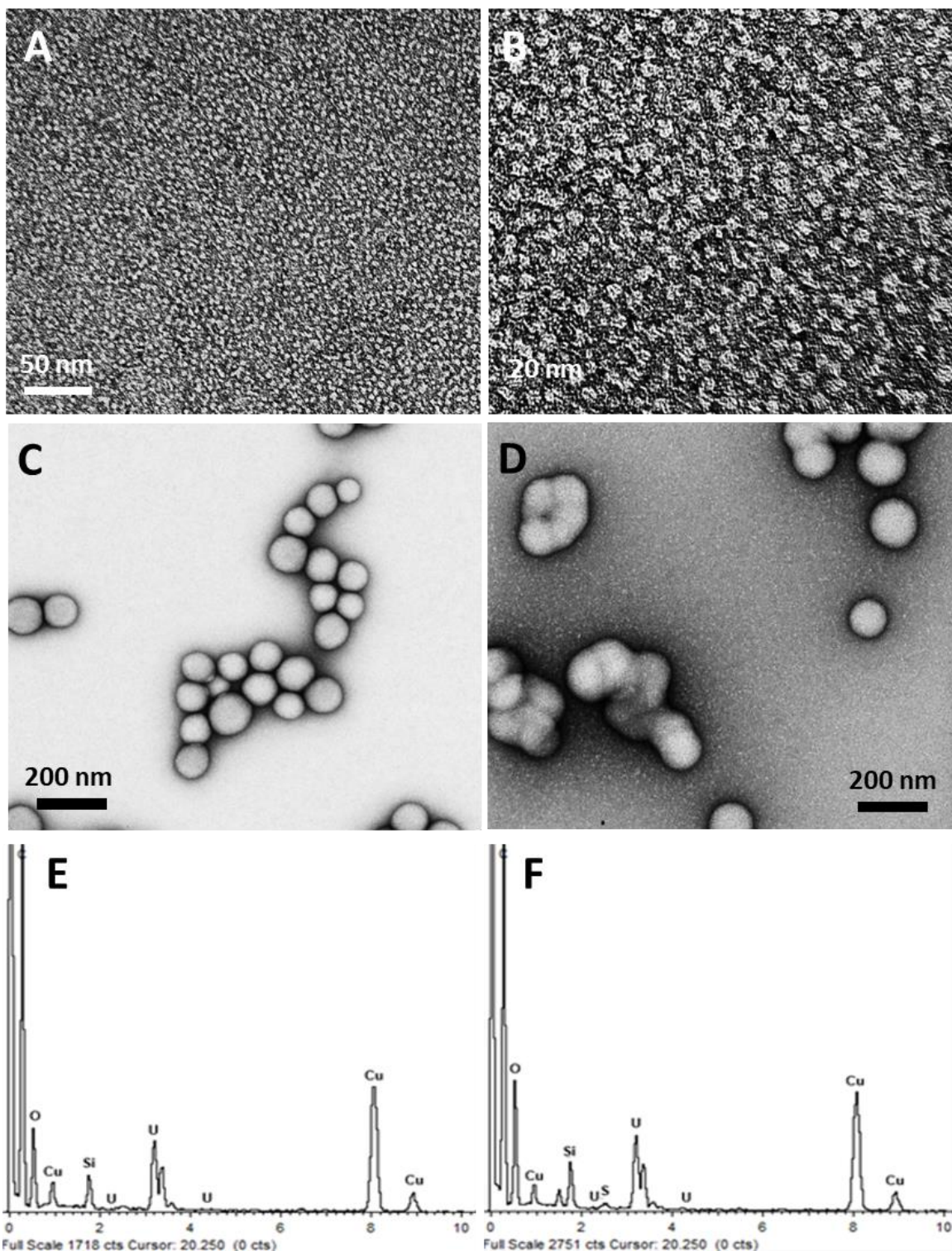


Figure 3.3. (A-B) TEM images of 0.6 wt% Alcalase 2.4 L FG samples counterstained in 1 wt% Uranyl acetate for 1 min during preparation. (C) TEM images of 0.6 wt% empty Carbopol Aqua SF1 nanoparticles; (D) TEM images of the nanoparticles after coating with 0.6 wt% Alcalase 2.5 L FG. Aggregation has occurred during the sample evaporation. All samples were counterstained in 1 wt% Uranyl acetate for 1 minute during preparation. TEM images were obtained using a JEM 2010 (JOEL, Japan) at 120kV, and a Gatan Ultrascan 4000 digital camera. (E) EDX spectra of 0.6 wt% Carbopol Aqua SF1 nanoparticles and (F) 0.6 wt% Carbopol Aqua SF1 nanogel particles coated with 0.6 wt% Alcalase 2.4 L FG. A Nanoanalysis X-Max 65-T detector and INCA software were used to produce the elemental analysis spectra.

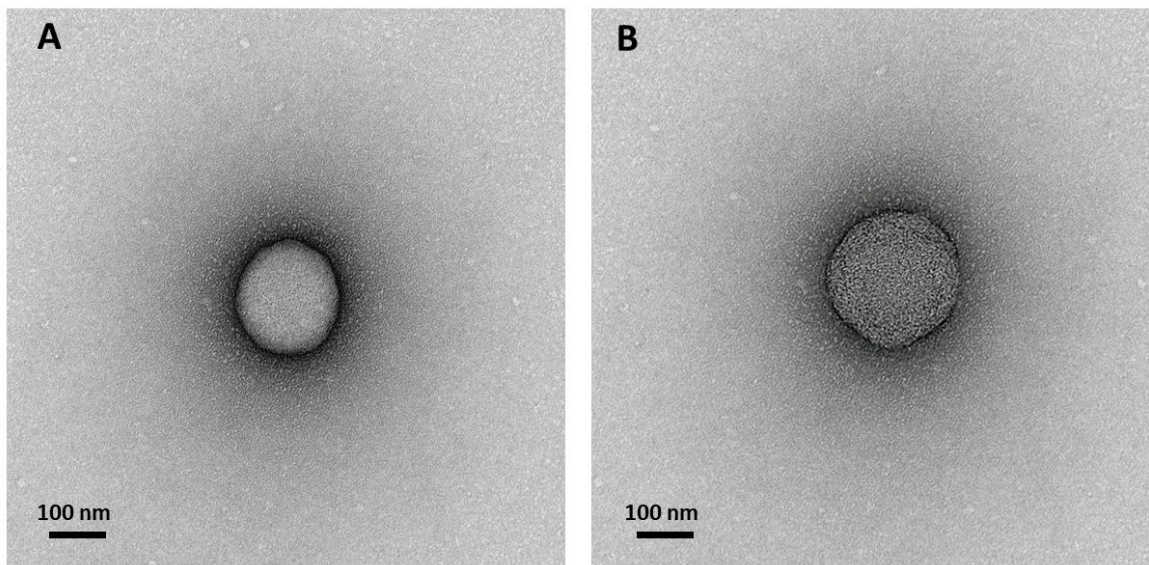


Figure 3.4. TEM images showing the comparison between **(A)** bare Carbopol Aqua SF1 nanogel particles and **(B)** Alcalase 2.4 L FG-coated Carbopol Aqua SF1 nanogel particles. As shown in the images, the coated NPs have a slight grainy and irregular surface texture caused by the coating with the protease. The coated NPs are also slight larger which is consistence with measurement taken by the Zetasizer Nano ZS.

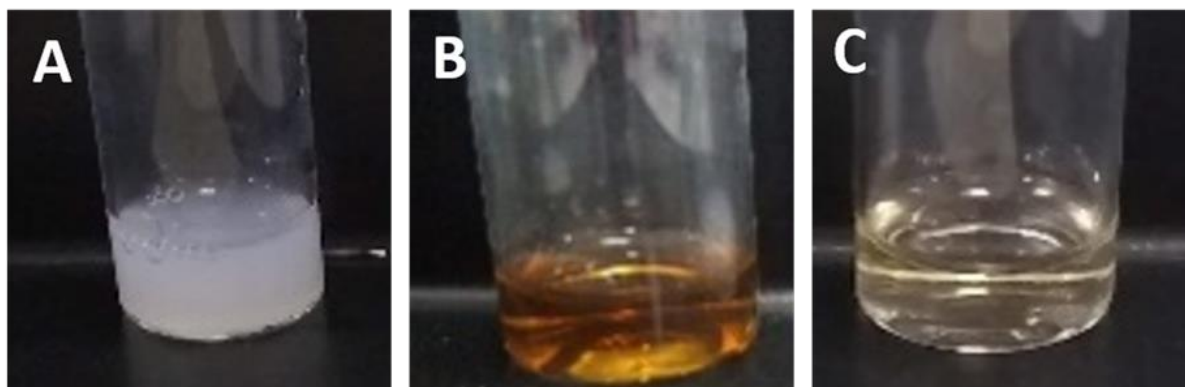


Figure 3.5. Photographs of **(A)** 0.6 wt Carbopol Aqua SF1, **(B)** 0.6 wt% Alcalase 2.4 L FG, and **(C)** 0.6 wt% Carbopol Aqua SF1-0.6 wt% Alcalase 2.4 L FG NPs.

Figure 3.2E shows that over 24 h, the zeta potential was stable in the range between 16 and 20 mV. This indicates that the Alcalase remains electrostatically deposited on the nanogel particles over 24 h, indicating that it is a stable carrier for immobilisation of the enzyme during treatment. Additionally, an EDX spectra investigation of the bare and coated Alcalase-nanogels was performed using samples prepared for TEM (see **Figure 3.3E and F**). The EDX spectra are similar, however, a sulphur peak can be seen in the coated sample spectra, which is not present in the uncoated nanogel. The bare nanogel formulation contains only C, O, and N, so the presence of S, an element commonly found in protein, indicates that the protein has electrostatically bound to the Carbopol nanogel

particles. Fourier transform infrared (FTIR) spectroscopy was used to investigate the composition of the Carbopol/Alcalase/ciprofloxacin NPs at a range of 600–4000 cm^{-1} (**Figure 3.6**). Carbopol Aqua SF1 shows a strong peak at 3350 cm^{-1} . This indicates stretching vibrations of O–H and intermolecular hydrogen bonding. Strong peaks are also seen at 3005 and 1698 cm^{-1} correlating to strong stretching of aliphatic C–H and strong vibration of carbonyl (C=O) bonds. Peaks at 1000 and 1195 cm^{-1} indicate a coupling between in-plane O–H bending and C–O stretching of neighbouring carboxyl groups. Alcalase 2.4 L FG shows weak peaks at 2950 and 3001 cm^{-1} , which are characteristic of amino acid with aromatic side chains, e.g., tyrosine, tryptophan, and phenylalanine. The peak at 1753 cm^{-1} indicates strong C=O stretching, attributed to C=O bond adjacent to secondary amide (peptide) bond. The peak at 1156 cm^{-1} shows strong C–O–H group stretching, present in the amino acids serine and tyrosine. Ciprofloxacin hydrochloride shows a peak at 1451 cm^{-1} attributed to the strong vibration of C–H bonds. The peak 1255 cm^{-1} is associated with the aromatic C–F group present on ciprofloxacin. Peak 801 cm^{-1} is interpreted as tetrasubstituted benzene ring derivatives, present on the ciprofloxacin chemical structure. The tightly packed range of peaks between 600 and 1450 cm^{-1} indicates an array of substituted groups associated with the ciprofloxacin chemical structure. Ciprofloxacin encapsulated Carbopol, coated with Alcalase contains peaks associated with the individual components. The peak at 3358 cm^{-1} shows stretching vibrations of O–H and intermolecular hydrogen bonding, this is analogous to Carbopol alone. The peak at 1721 cm^{-1} provides evidence of strong C=O stretching, attributed to C=O bond adjacent to the secondary amide (peptide) bond, present in this formulation due to the coating effect on the Carbopol surface. High-density peaks at 600–1000 cm^{-1} again are similar to ciprofloxacin alone, which indicates that a variety of substituted groups associated with the ciprofloxacin being present within the Carbopol. The elemental analysis of Carbopol Aqua SF1, Alcalase 2.4 L FG and ciprofloxacin alone, and ciprofloxacin-loaded Carbopol nanogel coated with Alcalase 2.4 L FG was performed using a CHN Analyser (Carlo Erba 1108) (**Table 3.1**). The formulated nanogel particles were centrifuged for 15 min at 8000 *g*. The supernatant was discarded, and the pellet washed three times with deionised water. The precipitate was further dried overnight at room temperature under vacuum. The data show the % value of C, H, N, and S for the above materials. Carbopol alone contained only C and H, which is consistent with polyacrylic acid polymers. Oxygen is present in all samples but not analysed. Alcalase contained C, H, and N, present in all amino acids, and additionally it contained 0.48% S, which is present in the amino acids methionine and cysteine. This is confirmed by the EDX results in **Figure 3.3F**. Ciprofloxacin contains C, H, and N.

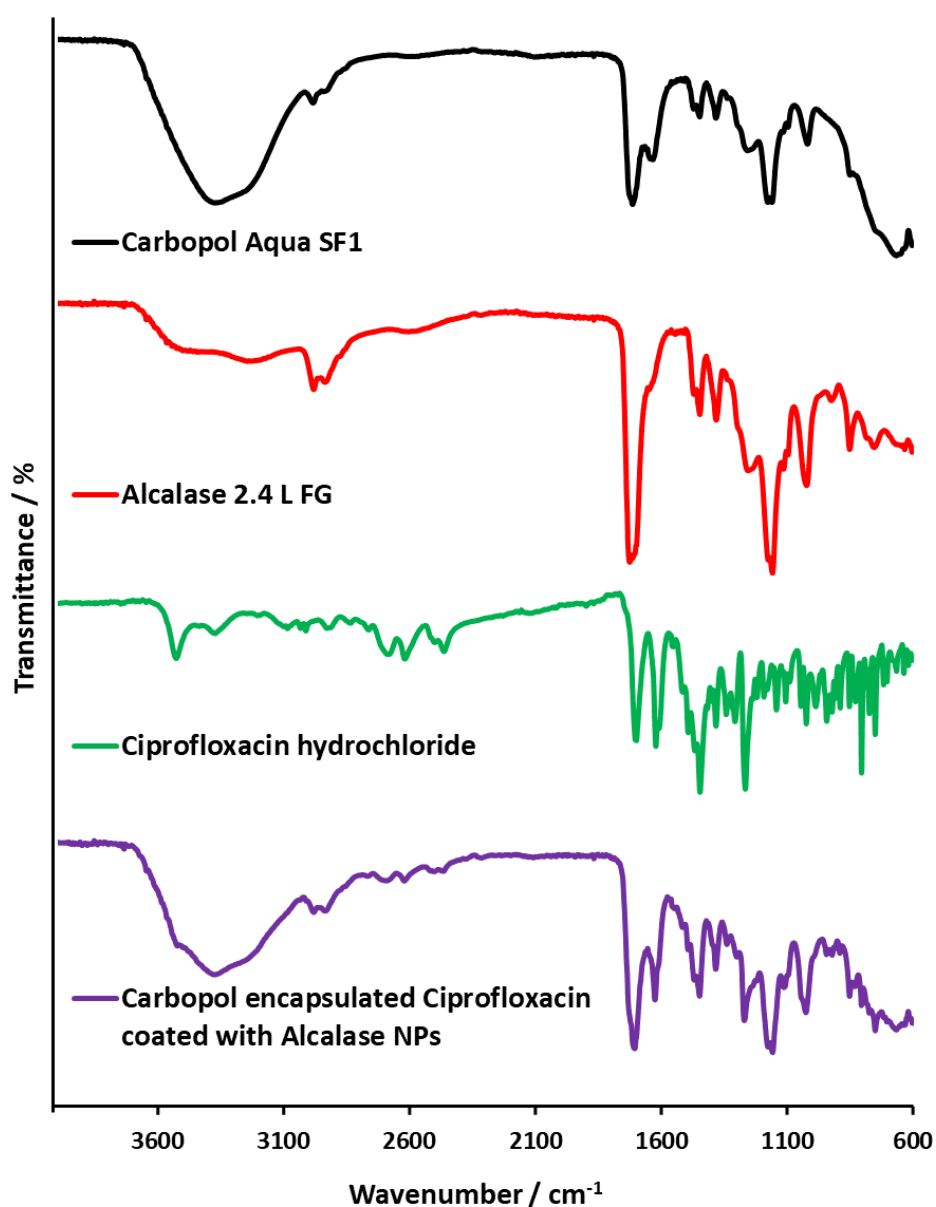


Figure 3.6. Fourier transform infra-red (FTIR) spectra of Carbopol Aqua SF1, Alcalase 2.4 L FG, Ciprofloxacin and Carbopol encapsulated Ciprofloxacin coated with Alcalase NPs. Samples were prepared by removing water using a Silica gel desiccant by in vacuum chamber for 1 day, then dried at 60°C for 2 days. The spectra was measured between 4000-600 cm^{-1} using PIKE ATR diamond settings. A spectrum was obtained with a blank of just air to reduce transmittance interference with the samples.

Table 3.1. The elemental analysis of Carbopol Aqua SF1, Alcalase 2.4 L FG, Ciprofloxacin, and Ciprofloxacin-loaded Carbopol nanogel coated with Alcalase 2.4 L FG.

Element	0.6 wt% Carbopol Aqua SF1 / %	0.6 wt% Alcalase 2.4 L FG / %	0.0032 wt% Ciprofloxacin / %	0.6 wt% Carbopol Aqua SF-1-0.0032 wt% Ciprofloxacin-0.6 wt% Alcalase 2.4 L FG / %
C	35.93	47.60	51.08	41.19
H	5.83	6.59	6.00	5.71
N	0.0	16.58	10.60	7.57
S	0.0	0.48	0.0	0.26

The formulation of 0.6 wt% Carbopol Aqua SF1–0.0032 wt% ciprofloxacin–0.6 wt% Alcalase 2.4 L FG nanogel contained all elements analysed, confirming that the Alcalase had been successfully retained on the Carbopol during preparation. EDX spectra of the 0.6 wt% Carbopol–0.0032 wt% ciprofloxacin– 0.6 wt% Alcalase nanogel and the individual components were performed on SEM-prepared samples (**Figure 3.7**). It can be seen that the formulation contains both sulphur and fluorine peaks, characteristic of Alcalase and ciprofloxacin, respectively. This provides evidence that the formulated nanogel has successfully encapsulated ciprofloxacin and is coated with Alcalase. Alcalase 2.4 L FG was chosen as a potential protease to degrade biofilms due to its favourable activities (see **Figure 3.9**). It is highly active and stable between pH 6 and 9 in the wide-temperature range between 30 and 65 °C. **Table 3.2** also shows that its optimal usage conditions are between 30 and 65 °C and pH 7–9 (Novozymes data). These properties make it an ideal choice for disrupting bacterial biofilms, which are grown at 37 °C and can grow at either acidic or basic conditions (Hořtacká et al., 2010).

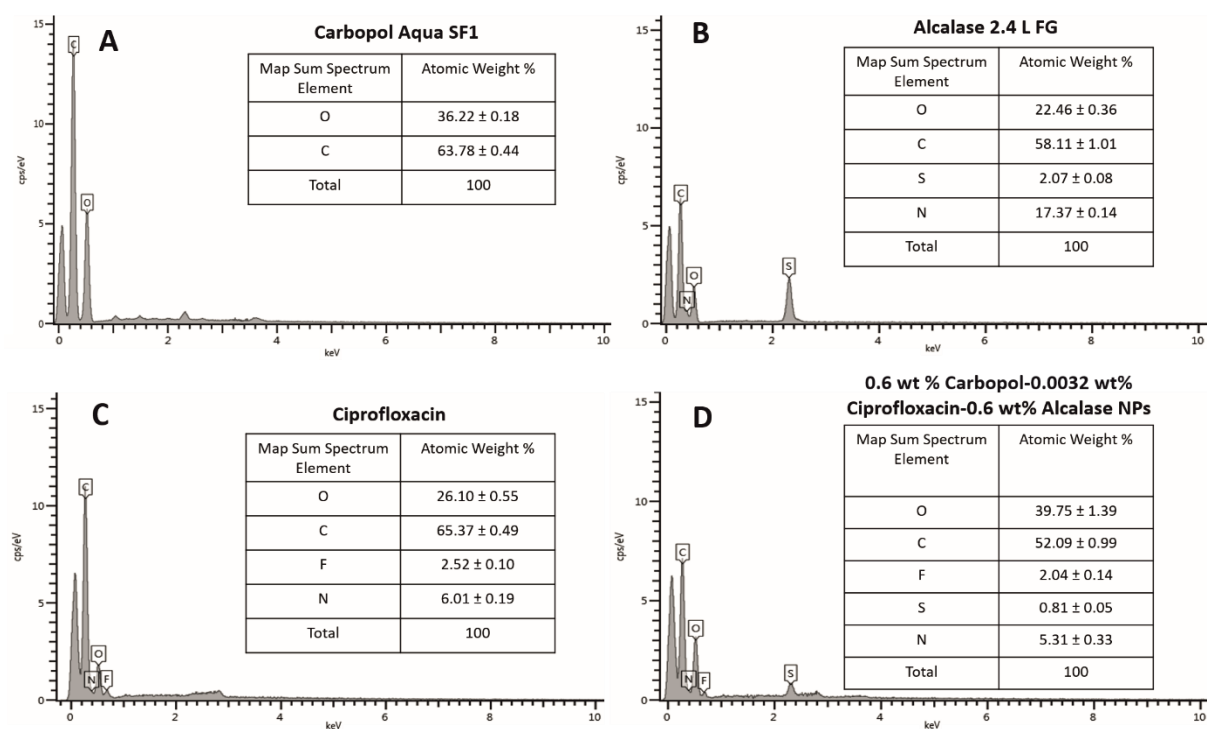


Figure 3.7. EDX spectra of **(A)** 0.6 wt% Carbopol Aqua SF1, **(B)** 0.6 wt% Alcalase 2.4 L FG, **(C)** 0.0032 wt% Ciprofloxacin and **(D)** 0.6 wt% Carbopol-0.0032 wt% Ciprofloxacin-0.6 wt% Alcalase NPs. The measurement for Carbopol, Alcalase and Ciprofloxacin was taken three separate locations and the data averaged. The measurement for the NP was taken in the centres of three separate NPs and averaged. A Hitachi TM3030Plus and Oxford Laboratories micF+ X-stream-2 EHX was used, and the data analysed using Aztec One v.3.3.

Table 3.2. Enzymatic characteristics of Alcalase 2.4 L FG. (Data obtained from Novozymes®).

Product name	EC Number	Type	Form	Optimal Usage Conditions	Activity	Applications
Alcalase 2.4 L FG	3.4.21.62	Serine endo-peptidase (mainly subtilisin A)	Liquid	30–65°C	pH 7–9	2.4 AU-A/g

3.3.2 Protease activity of free Alcalase vs Alcalase nanogel

Enzyme catalytic potential is affected by several factors. The effect of pH, temperature, and time on the free enzyme and the surface-immobilised Alcalase on the Carbopol nanogel particles was investigated (**Figure 3.8**). The effect of pH was investigated at 5.5, 7.5, and 8.5. As seen in **Figure 3.8A**, a higher pH increases the activity of the free Alcalase and Alcalase-nanogel substantially. There is only a marginal difference between the protease performances of each sample, which is likely due to the gentle electrostatic attraction between the anionic Carbopol nanogel particles, and the cationic protease in this pH range, having little effect on the enzyme's tertiary structure. Covalent enzyme immobilisation methods have been shown to cause a decrease in protease activity for this reason (Mendes et al., 2011). A similar trend is observed when measuring the effect of temperature (**Figure 3.8B**) on the activity of the free and immobilised Alcalase. Its activity broadly increased at physiological and higher temperatures, a common feature of biologically derived enzymes, but there is a very little difference in performance between the samples. This data are in agreement with the enzyme activity data provided by Novozymes (see **Figure 3.9**). This provides further evidence that the Carbopol nanogel immobilisation technique is exerting little influence on the enzyme activity. **Figure 3.8C** examines the effect time has on the activity of the free and immobilised samples. As for the effect of pH and temperature, there is only a small difference in the activity, particularly up until 6 h. At the 24 h time point, the immobilised Alcalase– Carbopol nanogel shows increased activity compared to the free counterpart. This indicated that over time, the Alcalase-nanogel can outperform the free Alcalase at an equivalent concentration. However, it is concluded from this data that the immobilisation process is not allowing the enzyme-functionalised nanogel to perform better due to any intrinsic property the Carbopol is inferring, but rather the nanogel allows the enzyme to concentrate and localise at key anionic structures of the biofilm, such as the cell wall, or biofilm surface adherence proteins (Lister & Horswill, 2014).

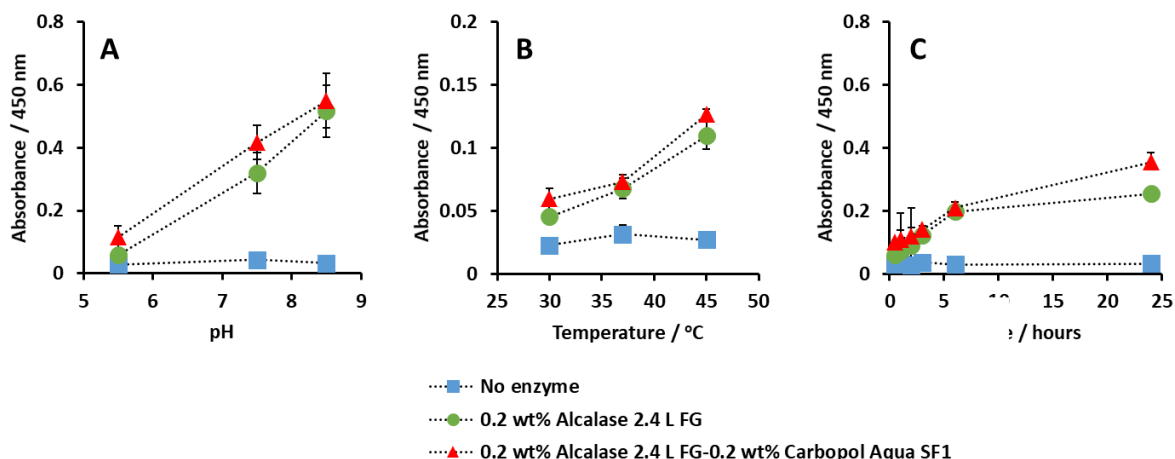


Figure 3.8. Relative activity of 0.2 wt% free Alcalase 2.4 L FG vs 0.2 wt% Alcalase 2.4 L FG- 0.2 wt% Carbopol Aqua SF1 NPs. **(A)** Shows the effect of pH, **(B)** temperature, and **(C)** time. Each value represents a triple replicate with \pm S. D. The lines are guides to the eye.

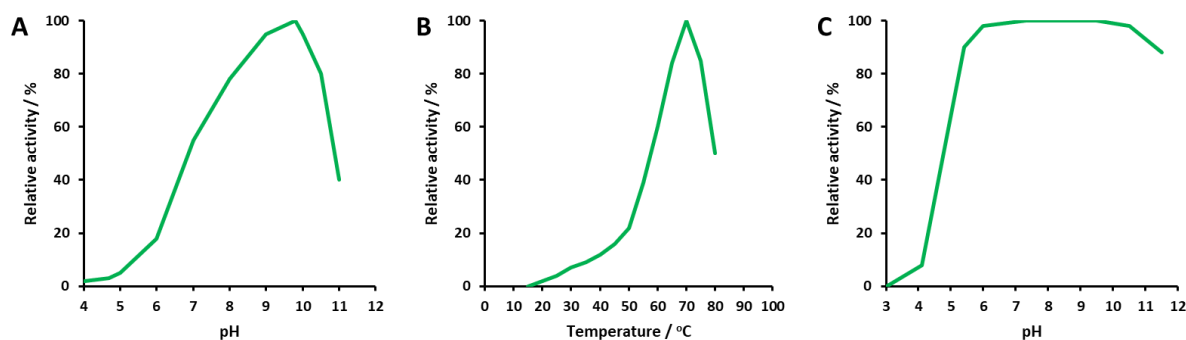


Figure 3.9. Alcalase 2.4 L FG enzymatic characteristics. **(A)** Effect of pH on Alcalase activity, **(B)** effect of temperature on Alcalase activity, **(C)** effect of pH on Alcalase stability. (Data obtained from Novozymes®).

3.3.3 Qualitative biofilm-producing capability assessment of representative ATCC bacterial species

Before the assessment of the Alcalase 2.4 L FG-coated Carbopol NPs on biofilms, the ability of the six types of bacteria to produce biofilms was investigated. A simple glass tube Crystal Violet staining assay was used to assess their adherence to a smooth glass surface after 24 h of growth. **Table 3.4** shows that all six species were able to adhere to the glass tube. The adhered cells and biofilm were relatively scored based on the concentration of Crystal Violet dye retained after washing with deionised water. **Figure 3.10** shows the blue/purple coating of the glass over the area in which the bacterial cells were cultivated and adhered to the glass wall in a biofilm. *S. aureus*, *P. aeruginosa*, and *S. epidermidis* were shown to have strong adherence. *K. pneumoniae* and *E. coli* showed moderate adherence, and, finally, *E. faecalis* was shown to have a weaker adherence. *Staphylococcal*, *Pseudomonas*, *Escherichia*, and *Enterococcus* species have all

been previously shown to form biofilms. A Congo Red agar (CRA) culture method, first demonstrated by Freeman et al., 1989 was also performed (see **Figure 3.11**). This uses a highly nutritional agar supplemented with sucrose, encouraging the production of exopolysaccharides. Biofilm-producing species produce black colonies, which can be seen on the *S. aureus*, *P. aeruginosa*, and *S. epidermidis* species. However, this was not expressed so well on the *K. pneumoniae*, *E. coli*, and *E. faecalis* species, although there was some darkening of the colonies. The sensitivity and the exact mechanism of the production of the black colonies are not well understood, and as it has been suggested by Freeman et al., 1989 that it may be due to the presence of secondary metabolites. Due to this, the study referred to the crystal violet tube method which shows all six species are biofilm producers.

Table 3.4. Biofilm formation visual score (ATCC species).

Bacteria Species	Biofilm score
<i>S. aureus</i>	3-strong
<i>P. aeruginosa</i>	3-strong
<i>S. epidermidis</i>	3-strong
<i>K. pneumoniae</i>	2-moderate
<i>E. coli</i>	2-moderate
<i>E. faecalis</i>	1-weak

The formation of biofilm by staining of adhered cells was scored as either 0-absent, 1-weak, 2-moderate or 3-strong.

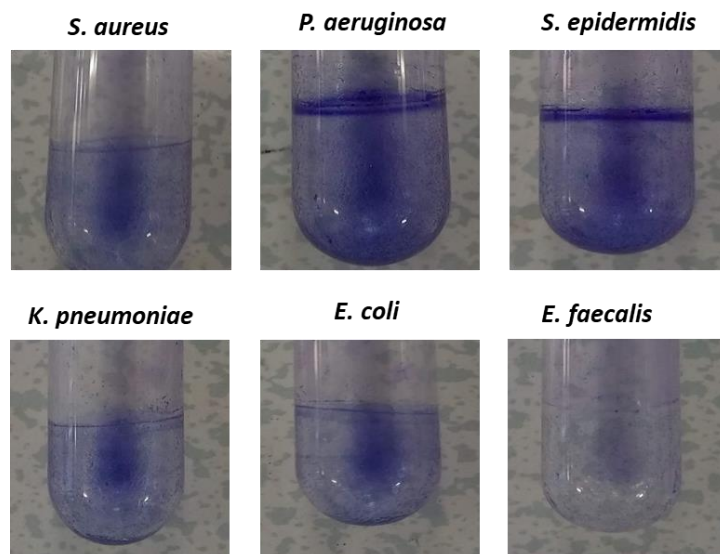


Figure 3.10. Qualitative tube method of biofilm formation detection photographs. Cells and biofilm mass are stained blue/purple by the Crystal Violet dye.

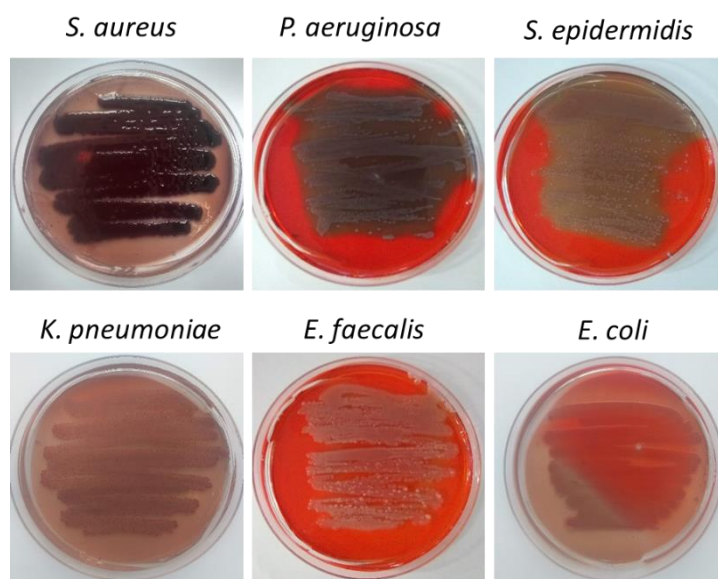


Figure 3.11. Congo Red Agar (CRA) biofilm detection method photographs. Black colonies indicated the species is a biofilm producer. Agar formulated using 37 g/L Brain Heart Infusion agar, 0.8 g/L Congo Red, and 6 g/L sucrose. CRA has a very low sensitivity compared to other biofilm detection methods such as TM.

3.3.4 Biofilm disruption by Alcalase-coated nanogel particles

Proteolytic enzymes have previously been used, particularly in wound-healing applications, as agents to remove the necrotic tissue and cell debris (Baidamshina et al., 2017; Lequette et al., 2010 ; Pavlukhina et al., 2012 ; Thallinger et al., 2013). It was investigated if Alcalase 2.4 L FG-coated Carbopol nanogels were able to disrupt the biofilms formed by the species described above. Biofilms were formed by culturing the bacterial species in TC-coated 48-well plates for 24 h at 37 °C in static conditions. After 24 h, the media was removed and the biofilms adhered to the well plates were washed to remove any remaining planktonic cells. Fresh culture media was supplemented with 0.2 wt% Carbopol, 0.2 wt% Alcalase, and 0.2 wt% Alcalase coated Carbopol nanogel, unsupplemented media was used as a control. Crystal Violet (0.1 wt%) was used to stain the adhered cells and biofilm matrix, before being solubilised in 30% acetic acid. The absorbance was taken to quantify the residual biofilm mass. **Figure 3.12** shows that bare 0.2 wt% Carbopol nanogel showed very little biofilm disruption capability, approximately a 5% reduction in biofilm mass. Free Alcalase (0.2 wt%) showed a marked improvement in biofilm mass reduction. This ranged from around 80 to 40% residual biofilm mass, with *P. aeruginosa* and *K. pneumoniae* showing the least and most reduction in biofilm mass, respectively. Interestingly, across all six species, the 0.2 wt% Alcalase-coated 0.2 wt% Carbopol nanogel showed a much greater reduction in biofilm mass compared to the free Alcalase enzyme. This ranged from around 35 to 15% residual biofilm mass compared to the control. In *S. aureus*, *P. aeruginosa*, *S. epidermidis*, *E. coli*, and *E. faecalis*, there was an over 50% decrease in the biofilm mass

compared to the free Alcalase alone. *K. pneumoniae* showed a 20% decrease in the biofilm mass compared to the free Alcalase. **Figure 3.13** shows visually the reduction in Crystal Violet staining on the biofilms after treatment. To test the hydrolysis of the biofilm matrix, particularly the protein content, the same experiment was performed using 0.005 wt% Congo Red to stain the biofilm. This was solubilised in 30% ethanol and the absorbance taken to quantify the intensity of the staining of the biofilms after treatment. Congo Red has previously been used to stain amyloidosis, an accumulation of proteins, in histology sections. Increased concentrations of protein result in a more intense red staining. **Figure 3.14** shows a similar correlation between the reduction of the biofilm mass observed by Crystal Violet staining. Carbopol nanogel (0.2 wt%) showed no reduction to very little reduction of the protein content (see **Figure 3.15** for visual images of Congo Red biofilm stains). Free 0.2 wt% Alcalase showed between 40 and 60% residual protein content within the biofilms. However, 0.2 wt% Alcalase-coated 0.2 wt% Carbopol shows a much more impressive reduction in protein content within the biofilm, between 25 and 15% residual protein compared to the control. This shows that the Alcalase-coated nanogels are causing the degradation of the protein backbone of the biofilm. The immobilised Alcalase on Carbopol nanogel particles is likely resulting in an increase in enzyme stability and reduction in aggregation, allowing them to outperform their free enzyme counterparts.

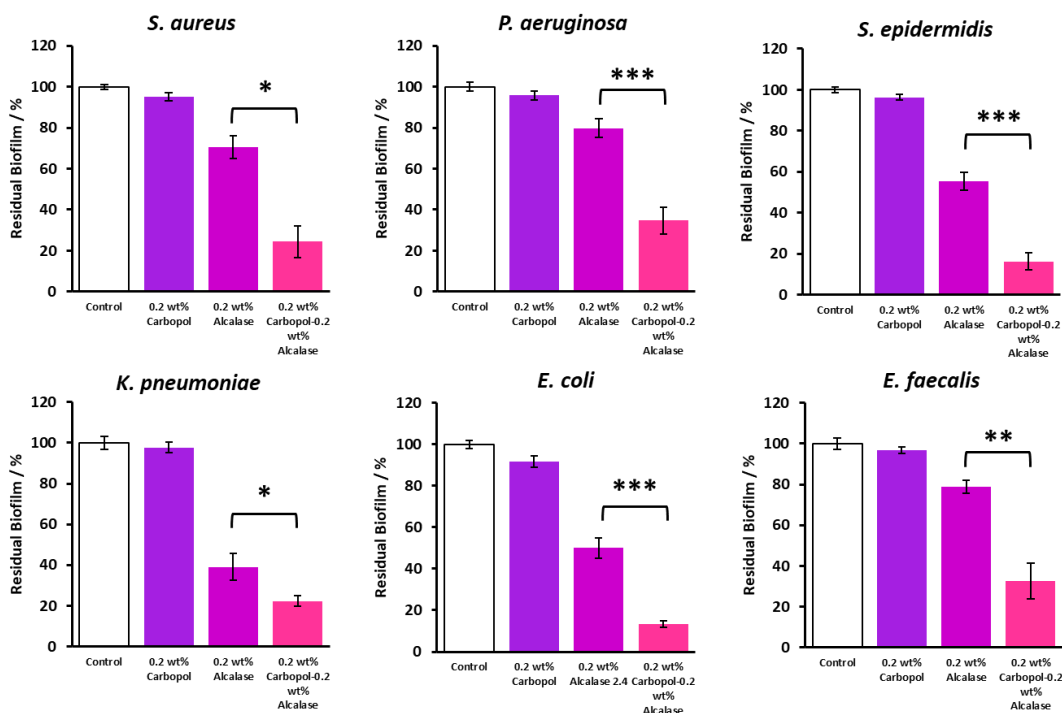


Figure 3.12. The ability of 0.2 wt% Alcalase 2.4 L FG and 0.2 wt% Carbopol-0.2 wt% Alcalase 2.4 I FG to disrupt biofilms. Bacteria were cultured in MHB broth for 24 hours at 37°C to form a biofilm. The excess media and suspended cells were washed away and the remaining mature biofilm incubated for 24 hr in supplemented MHB. After the treatment, the residual biofilms were quantified using Crystal Violet staining. Tests were performed in triplicates (N=3 with \pm S.D). Statistical analysis shown in **Table 3.5**. <0.05 is considered significant. * $P < 0.05$, ** $P < 0.01$, *** $P < 0.001$.

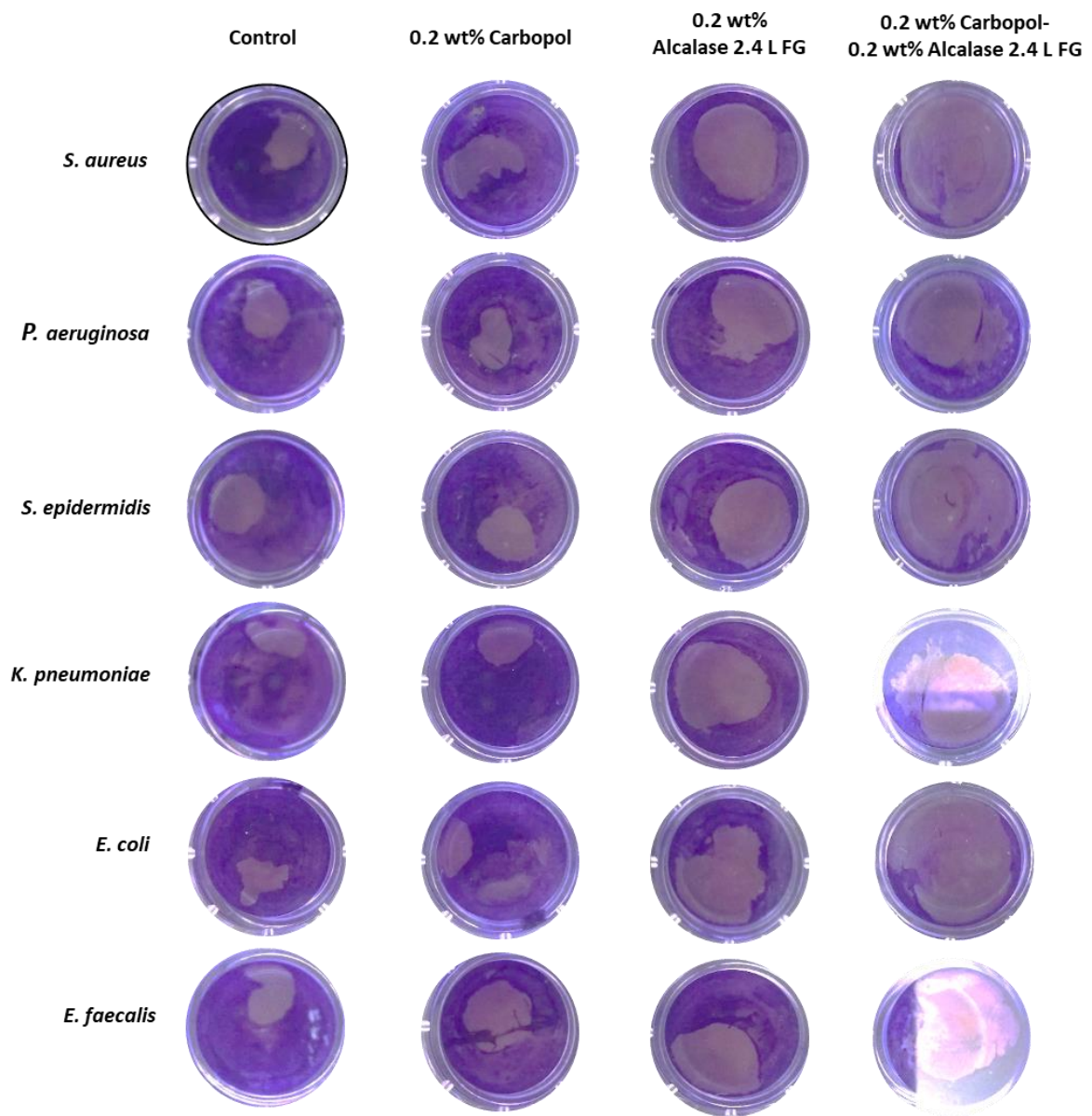


Figure 3.13. Photographs of 48-well plate biofilms after Crystal Violet staining and washing/drying.

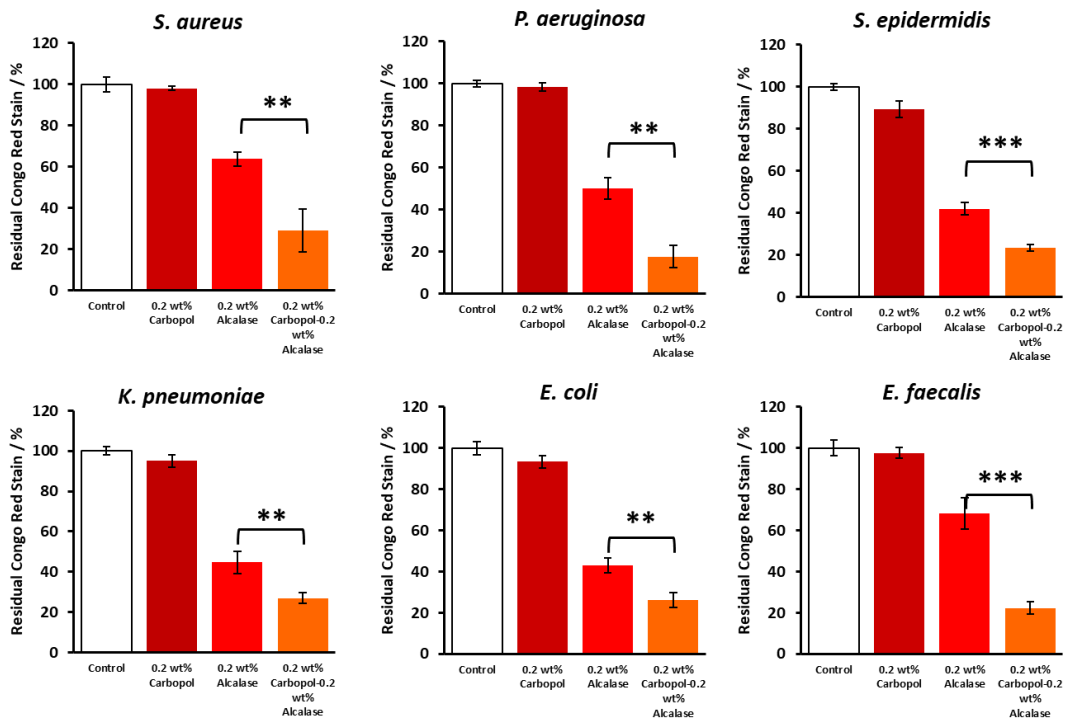


Figure 3.14. The ability of 0.2 wt% Alcalase 2.4 L FG and 0.2 wt% Carbopol Aqua SF1-0.2 wt% Alcalase 2.4 l FG to disrupt matrix protein by hydrolysis. Bacteria were cultured in MHB broth for 24 hr at 37°C to form a biofilm. The excess media and suspended cells were washed away and the remaining mature biofilm incubated for 24 hr in supplemented MHB. After treatment, the residual biofilms were quantified using Congo Red staining. Tests were performed in triplicates (N=3 with \pm S.D). Statistical analysis shown in **Table 3.6**. <0.05 is considered significant. * $P < 0.05$, ** $P < 0.01$, *** $P < 0.001$.

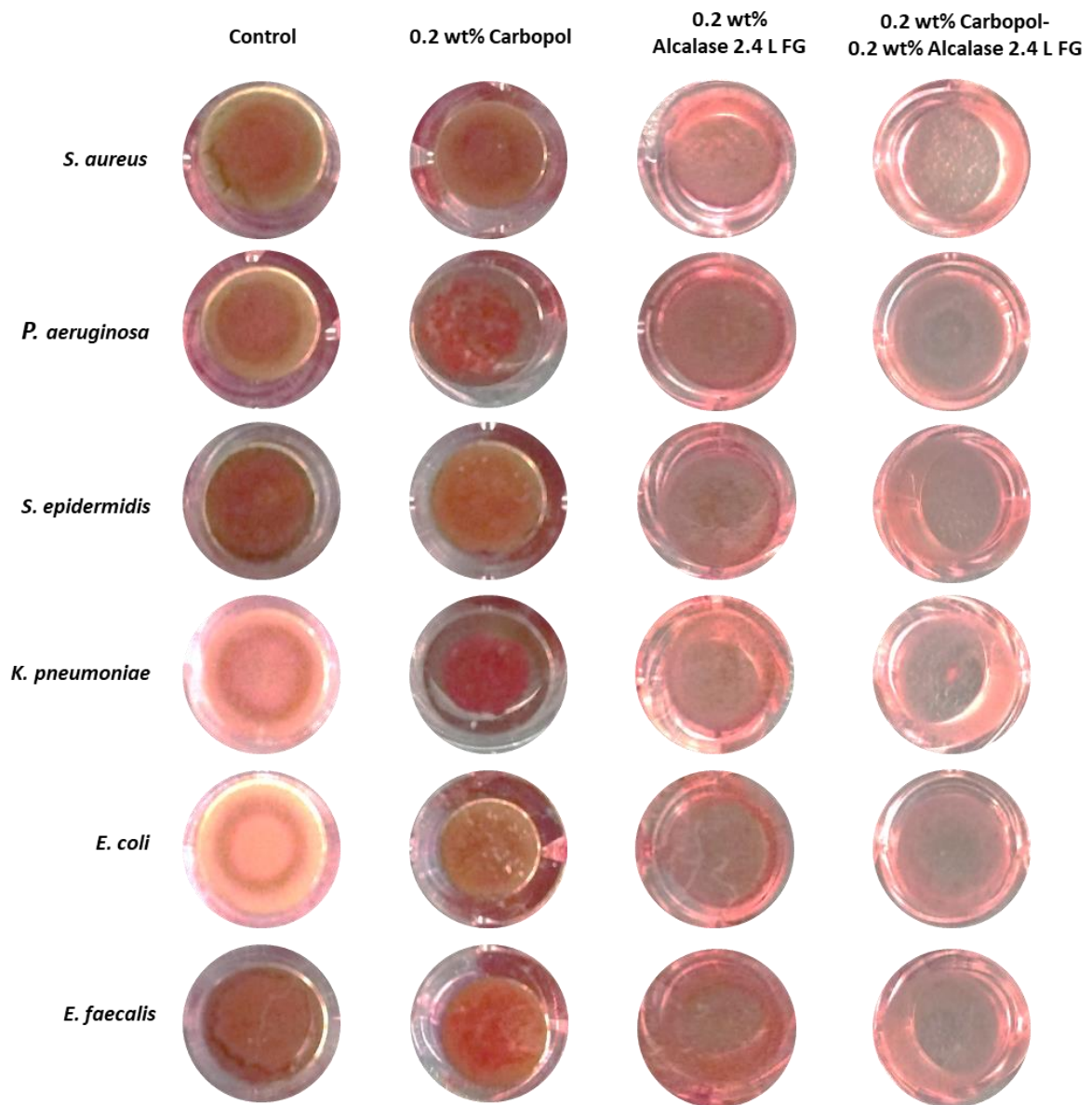


Figure 3.15. Photographs of 48-well plate biofilms after Congo Red staining and washing/drying.

Table 3.5. Crystal Violet staining statistical analysis between 0.2 wt% Alcalase 2.4 L FG and 0.2 wt% Alcalase 2.4. L FG-0.2 wt% Carbopol Aqua SF1. Data were expressed as average values \pm standard deviations of the mean. *P*-values of less than 0.05 were considered significant. All Student's T-tests were performed in GraphPad v7.0.4.

Species	Multiple Comparison	P-value	Significance
<i>S. aureus</i>	0.2 wt% Alcalase vs 0.2 wt% Alcalase-0.2 wt% Carbopol	0.015841	*
<i>P. aeruginosa</i>	0.2 wt% Alcalase vs 0.2 wt% Alcalase-0.2 wt% Carbopol	0.000579	***
<i>S. epidermidis</i>	0.2 wt% Alcalase vs 0.2 wt% Alcalase-0.2 wt% Carbopol	0.000387	***
<i>K. pneumoniae</i>	0.2 wt% Alcalase vs 0.2 wt% Alcalase-0.2 wt% Carbopol	0.014732	*
<i>E. coli</i>	0.2 wt% Alcalase vs 0.2 wt% Alcalase-0.2 wt% Carbopol	0.000264	***
<i>E. faecalis</i>	0.2 wt% Alcalase vs 0.2 wt% Alcalase-0.2 wt% Carbopol	0.001023	**

< 0.05 is considered significant. *P <0.05, **P <0.01, ***P <0.001

Table 3.6. Congo Red staining statistical analysis between 0.2 wt% Alcalase 2.4 L FG and 0.2 wt% Alcalase 2.4. L FG-0.2 wt% Carbopol Aqua SF1. Data were expressed as average values \pm standard deviations of the mean. *P*-values of less than 0.05 were considered significant. All Student's T-tests were performed in GraphPad v7.0.4.

Species	Multiple Comparison	P-value	Significance
<i>S. aureus</i>	0.2 wt% Alcalase vs 0.2 wt% Alcalase-0.2 wt% Carbopol	0.00526	**
<i>P. aeruginosa</i>	0.2 wt% Alcalase vs 0.2 wt% Alcalase-0.2 wt% Carbopol	0.001446	**
<i>S. epidermidis</i>	0.2 wt% Alcalase vs 0.2 wt% Alcalase-0.2 wt% Carbopol	0.000657	***
<i>K. pneumoniae</i>	0.2 wt% Alcalase vs 0.2 wt% Alcalase-0.2 wt% Carbopol	0.007448	**
<i>E. coli</i>	0.2 wt% Alcalase vs 0.2 wt% Alcalase-0.2 wt% Carbopol	0.004157	**
<i>E. faecalis</i>	0.2 wt% Alcalase vs 0.2 wt% Alcalase-0.2 wt% Carbopol	0.000636	***

< 0.05 is considered significant. *P <0.05, **P <0.01, ***P <0.001.

3.3.5 Resazurin sodium salt *in situ* bacterial biofilm metabolic activity assay

Resazurin sodium salt assay was used to measure the metabolic activity of the bacterial cells within the biofilm. Biofilms of the six species were grown for 24 h on membrane filter paper sections placed on to MHA. After 24 h of growth, a biofilm was formed on the filter paper. The membrane biofilm was then transferred onto fresh MHA in a six-well plate and submerged into treatment-infused deionised water (unsupplemented deionised water was used as the control). Treatments were increased to 0.4 and 0.6 wt% Alcalase to investigate if higher concentrations of free Alcalase enzyme and Alcalase-coated Carbopol nanogels would affect the viability of the cells within the biofilm after 24 h. 0.015 wt% resazurin sodium salt was used to measure the metabolic activity of the cells within the biofilm by applying evenly to the surface of the biofilm. Resazurin sodium salt can be used as a metabolic activity assay by measuring the production of resorufin (fluorescent pink) created in the presence of cellular reduced nicotinamide adenine dinucleotide (Markland & Smith, 1971). Only metabolically active cells are able to reduce resazurin to resorufin. The development of resorufin on the biofilm was quantified to measure the metabolic activity of the biofilm after treatments. **Figure 3.16** shows that 0.6 wt% Carbopol has no effect on the metabolic activity of the bacterial cells. Free Alcalase (0.4 and 0.6 wt%) was able to reduce the metabolic activity of cells within the biofilm by on average 60–40% across the six species. *S. epidermidis* showed by far the most decreased metabolic activity, 30–20% viability with 0.4 and 0.6 wt% free Alcalase treatment. *P. aeruginosa* and *E. faecalis* were able to tolerate the free enzyme treatments much better, reducing to approximately 60–50% after treatment with 0.4 and 0.6 wt% free Alcalase, respectively. In agreement with the 48-well biofilms described above, the Alcalase-coated Carbopol nanogel performed much better than the equivalent concentration of the free Alcalase enzyme. In all six species, the 0.6 wt% Alcalase–0.6 wt% Carbopol nanogel was able to reduce the viability of the biofilms to approximately 4%. **Figure 3.17** shows the intensity of the purple colour of biofilm after treatment with 0.6 wt% Alcalase–0.6 wt% Carbopol. This contrasts the control image, which shows a pink colour indicating that the biofilm contains metabolically active cells.

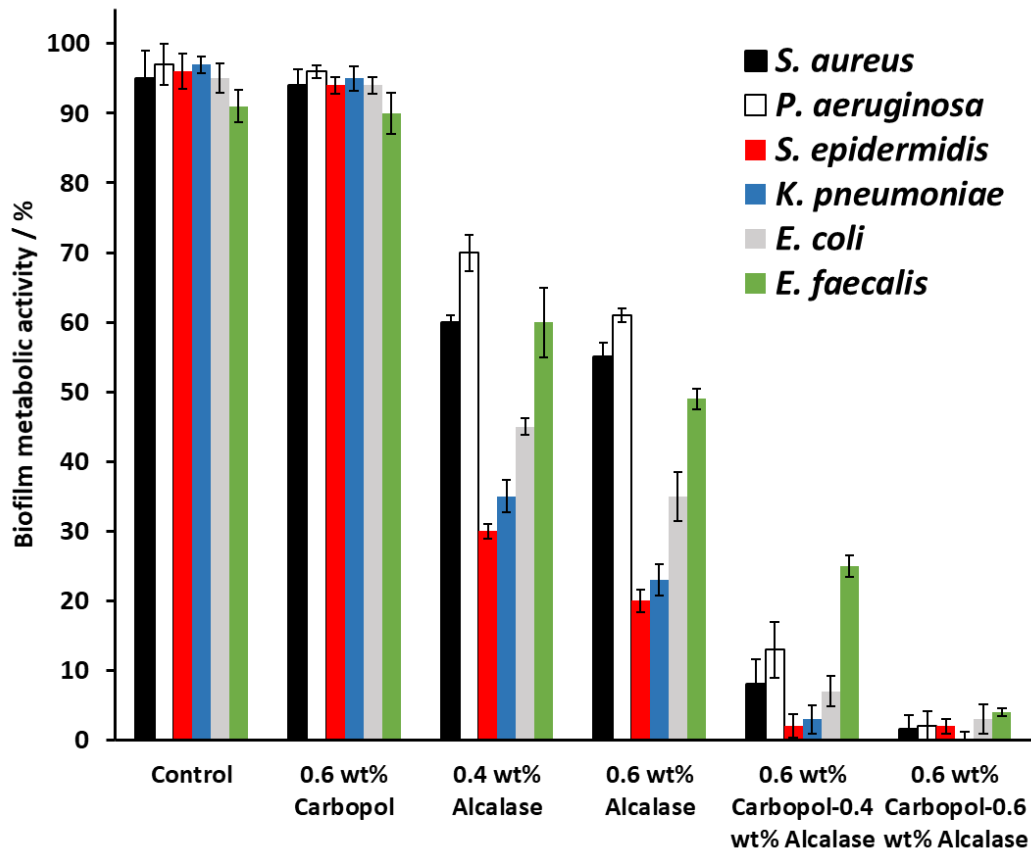


Figure 3.16. Resazurin sodium salt *in situ* bacterial biofilm assay. Membrane biofilms were grown for 24 hr at 37°C. 20 µL of treatment was applied as a droplet to the surface of the biofilm and left to incubate for 24 hr. 20 µL of 0.015 wt% Resazurin sodium salt was added and incubated for 30 minutes. Images were captured using an 8MP digital camera and the percentage of biofilm showing metabolic activity calculated using ImageJ v1.52d.

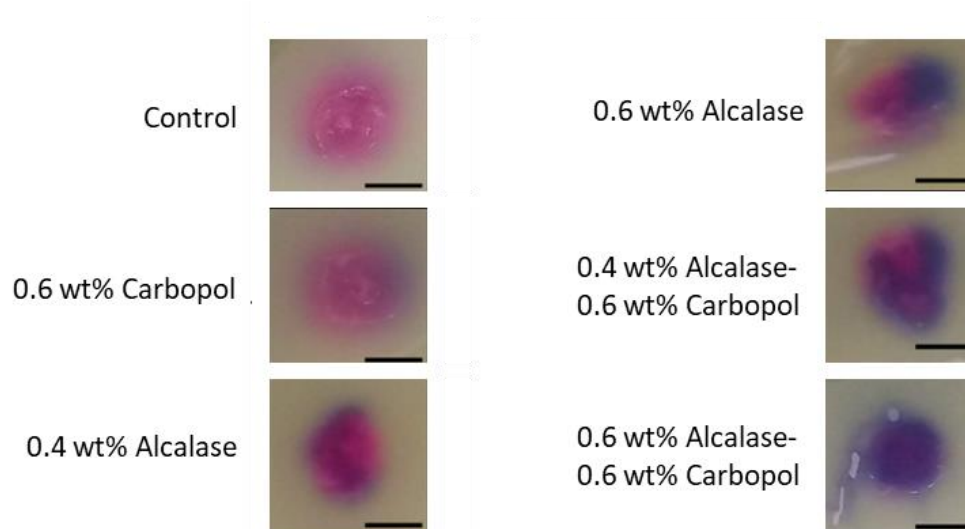


Figure 3.17. Photographs of *S. aureus* biofilms surface after treated with Resazurin Sodium Salt reagent. Pink indicates metabolising cells, purple non-metabolising cells. Black scale bar represents 1 cm.

3.3.6 *S. aureus* biofilm cellular viability after treatment with Alcalase-nanogel particles and co-treatment with free ciprofloxacin hydrochloride.

Alcalase-coated Carbopol nanogel has been shown to reduce the biofilm mass, the protein concentration of biofilm matrix, and the biofilm metabolic activity. The viability of the cells within the biofilms after treatment by CFU enumeration was investigated. *S. aureus* was chosen as the proxy biofilm-producing bacterium for these experiments. *S. aureus* is considered one of the most prevalent pathogens in wound infection (Omar et al., 2017), and has been widely studied making it a good choice for further investigation. Biofilms were grown on the filter membrane atop MHA and treated with 0.6 wt% bare Carbopol, 0.6 wt% free Alcalase, and 0.6 wt% Alcalase-coated 0.6 wt% Carbopol in the same fashion as above. Additionally, the effect of cotreatment with the antibiotic ciprofloxacin was investigated as a free agent and equivalent concentrations of ciprofloxacin encapsulated into Carbopol. It has previously been demonstrated that antibiotics can be encapsulated into Carbopol and this confers an increased efficacy of the antimicrobials against target cells.⁵¹ **Table 3.7** shows that 75% of the ciprofloxacin encapsulated with the Carbopol was retained. The encapsulation efficiency was measured by analysing the supernatant of the formulation immediately after centrifugation; the encapsulation efficiency was calculated using a standard calibration curve of absorption vs known concentrations of ciprofloxacin (**Figure 3.18**).

Post-encapsulation, the mean particle diameter was marginally increased by approximately 1 nm post-encapsulation and there was no detectable change in zeta potential of the nanogel particles (**Figure 3.19**). Previously, polyelectrolytes have been used to reverse the charge of the nanogel and allowed an electrostatic adhesion to the anionic surface of the bacteria (Al-Obaidy et al., 2019a; Halbus et al., 2019d; Al-Obaidy et al., 2019b). In this study, Alcalase was used to accomplish this goal to create a dual-purpose nanocarrier able to effectively degrade the biofilm and simultaneously deliver concentrated doses of the antibiotic localised directly on the cell wall. This strategy is known to work extremely well for planktonic bacteria, but so far this has never been tried for bacteria in a biofilm. The release kinetics of the nanogel-loaded ciprofloxacin hydrochloride was measured over 24 h (**Figure 3.20**), and, as in previous studies, the antibiotic was released slowly over a period of 24 h after dilution of the stock suspension. This facilitated the release of ciprofloxacin in close proximity to the *S. aureus*. Cell enumeration was performed after 1, 6, and 24 h of treatment. The treated biofilms were glass bead beaten and enumerated using the drop plate method. Ciprofloxacin was chosen as an appropriate co-treatment as it can be administered topically, orally, and intravenously. **Figure 3.21** shows that the *S. aureus* strain used in this study was susceptible to ciprofloxacin and had a minimum inhibitory concentration (MIC) of $0.08 \mu\text{g mL}^{-1}$ (0.000008 wt%). 0.0032 wt% was chosen as this is the maximum concentration measured to be effective against *S. aureus* using the ETEST strips. This allowed a fair comparison of nanogel-formulated vs free ciprofloxacin at concentrations shown

to be effective against *S. aureus*. Additionally, this concentration allows the nanocarrier colloidal stability to be maintained due to ciprofloxacin's low water solubility.

Table 3.7. The concentration of ciprofloxacin encapsulated into 0.6 wt% Carbopol Aqua SF1 nanogel.

Carbopol-ciprofloxacin mixture environment	Total ciprofloxacin conc. attempted to encapsulate / wt%	Ciprofloxacin in supernatant / wt%	Ciprofloxacin encapsulated / wt%	Encapsulation efficiency / wt%
30 minutes 37°C pH 7.5	0.0032	0.0008	0.0024	75

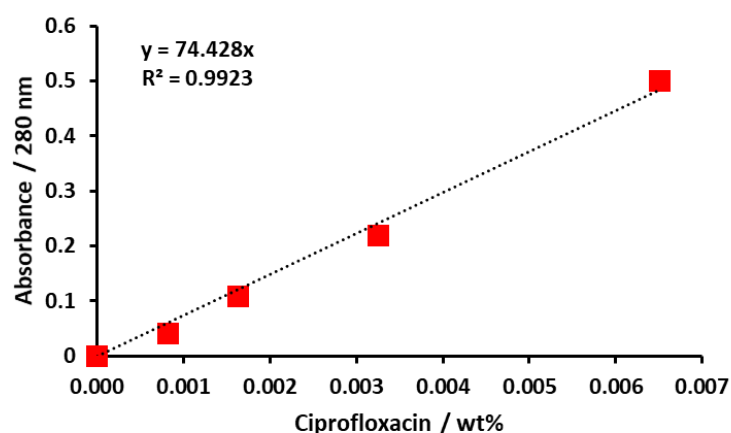


Figure 3.18. Standard calibration graph of the absorption vs concentrations of ciprofloxacin hydrochloride. Absorbance was measured at 280 nm. Aliquots were prepared by adding ciprofloxacin hydrochloride to 250 mL Milli-Q water (adjusted to pH 5.5 using acetate buffer) at specific concentrations. Error bars are within the symbol size.

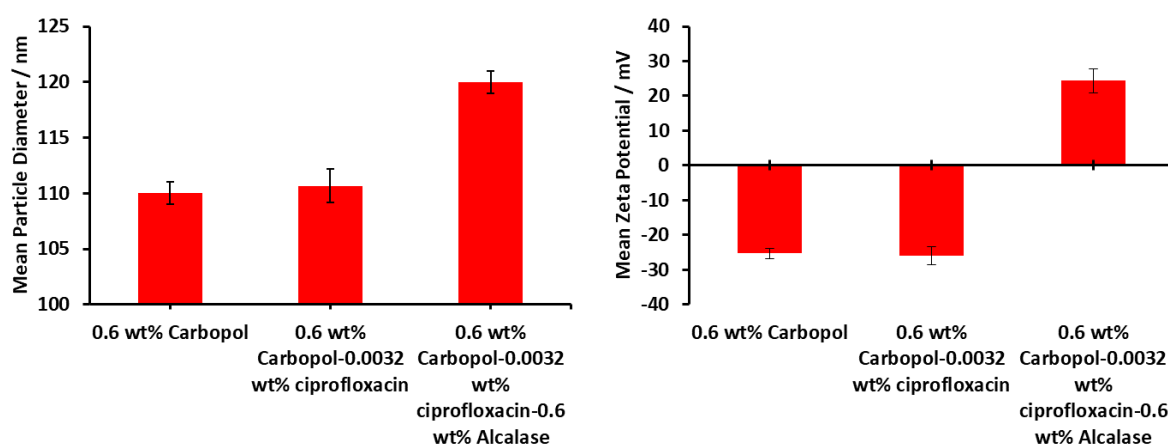


Figure 3.19. The (A) size and (B) zeta potential of 0.6 wt% Carbopol, 0.6 wt% Carbopol encapsulating 0.0032 wt% ciprofloxacin and 0.6 wt% Carbopol encapsulating 0.0032 wt% ciprofloxacin with 0.6 wt% Alcalase coating. All measurements were taken at pH 5.5 (acetate buffer solution) with a RI of 1.450 at 25°C. Each value represents a triple replicate with \pm S.D.

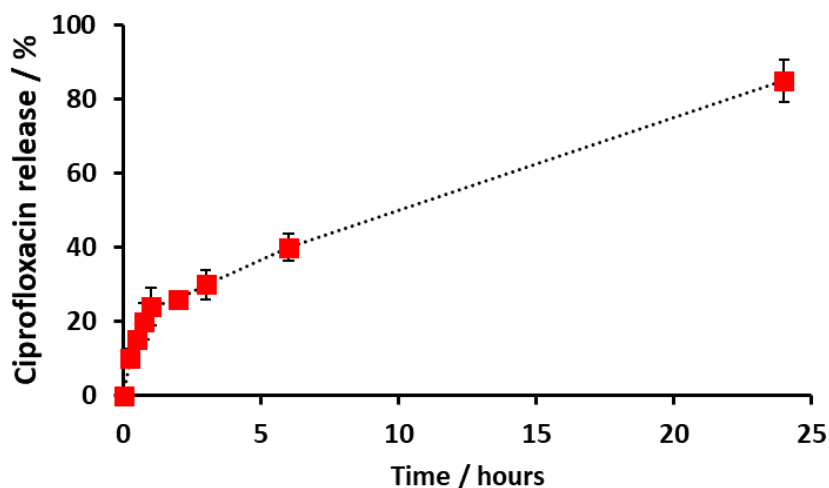


Figure 3.20. Ciprofloxacin release kinetics at pH 5.5. 10 mL of 0.0032 wt% ciprofloxacin-0.6 wt% Carbopol suspension was placed into a 10-12 kDa MWKO dialysis bag. The dialysis bag was submerged into 250 mL of pH 5.5 acetate buffer at 37°C whilst shaken at 100 rpm shaking. 1 mL aliquots were taken at specific time points on the absorbance of the aliquot equated into the concentration of ciprofloxacin in the acetate buffer using a standard calibration curve. Absorption was measured at 280 nm. Each value represents average triplicate measurements with error bars representing the \pm S.D. The lines are guides to the eye.

S. aureus

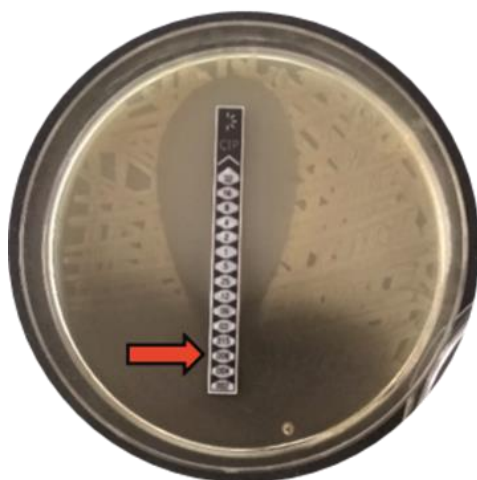


Figure 3.21. Ciprofloxacin M.I.C.E. TEST® Evaluator strips 32-0.002 $\mu\text{g}/\text{mL}$ tested against *S. aureus*. Susceptibility is shown to be 0.08 $\mu\text{g}/\text{mL}$ (0.000008 wt%).

Figure 3.22A shows that after seeding a membrane with 1×10^5 CFU mL^{-1} for 24 h at 37 °C, the growth control continued to increase in cell density after a further 1, 6, and 24 h of growth. Treatment with 0.6 wt% bare Carbopol showed little change in the CFU mL^{-1} of biofilm. After treatment with 0.6 wt% free Alcalase, there was a reduction in viable cells within the *S. aureus* biofilm. There was a little difference after 1 h, but after 24 h, the viable cell count was reduced to just under 1×10^5 CFU mL^{-1} , very close to the

concentration of cells the original membrane was seeded with. Surprisingly, after treatment with 0.6 wt% Alcalase–0.6 wt% Carbopol NPs, there was a very little difference in the number of viable cells after each treatment time point. This is likely due to the Alcalase– Carbopol nanogel degrading the biofilm but having very little effect on the bacterial cell viability, as there is no antibiotic in this treatment to act on the released bacteria. Treatment with 0.0032 wt% ciprofloxacin (higher than the MIC of 0.00008 wt%) was used to measure the number of viable cells, after 24 h of treatment, the viable cells in the *S. aureus* biofilm had reduced from approximately 1×10^6 to 1×10^3 . The cells within the biofilm are much less susceptible to antibiotics due to their poor penetration through the biofilm matrix. There was no real improvement when 0.0032 wt% ciprofloxacin is treated with 0.6 wt% Carbopol. This result is unsurprising due to the Carbopol nanogel alone demonstrating no ability to degrade the biofilm matrix. Again with 0.00032 wt% ciprofloxacin and 0.6 wt% free Alcalase, there was no difference between the CFU mL⁻¹ compared to the antibiotic alone. However, when the antibiotic is administered as a cotreatment with 0.6 wt% Alcalase-coated 0.6 wt% Carbopol NPs, there was a reduction to 1×10^1 . This indicates that the cells in the biofilm have been destroyed due to the degradation of the biofilm matrix by the Alcalase–Carbopol nanogel allowing the ciprofloxacin to reach and penetrate the bacterial cells. This synergistic effect was enhanced further when the ciprofloxacin was delivered to the *S. aureus* encapsulated in the nanogel, rather than as a separate cotreatment. After 6 and 24 h of treatment with 0.0032 wt% ciprofloxacin encapsulated in 0.6 wt% Carbopol with 0.6 wt% Alcalase coating, there were no viable bacteria found in the samples. This provides evidence that the dual functionality of the Alcalase-nanogel mediates biofilm degradation and the localised delivery of ciprofloxacin of this formulation is able to effectively clear the biofilms and kill all released bacterial cells.

Figure 3.22B shows that there is a correlation between the increase of the concentration of free ciprofloxacin in the presence of an equivalent amount of Alcalase–Carbopol NPs and the residual bacterial cell viability after treatment. Different dilutions of the treatments were prepared to measure this effect. A very low treatment concentration, 0.075 wt% Alcalase–0.075 wt% Carbopol + 0.0004 wt% ciprofloxacin, showed very little effect after 1, 6, or 24 h. This is due to the likely ineffective degradation of the biofilm. However, as the concentration of the Alcalase–Carbopol NPs increased alongside the increased concentration of ciprofloxacin, CFU mL⁻¹ was reduced to almost no viable cells. After 24 h at the higher concentration of the formulation, there was a very little difference in the CFU at the 1, 6, and 24 h time points, this indicates that the Alcalase-coated nanogel particles are very fast acting, enabling the ciprofloxacin access to the cells quickly. Interestingly, at the mid-treatment concentrations, CFU mL⁻¹ increased between 1 and 6 h; however, at 24 h, it had fallen below the first time point. This indicates that the lower concentrations of Alcalase–Carbopol NPs are slower to effect the biofilms. Within a biofilm, 0.6 wt% Alcalase–0.6 wt% Carbopol nanogel was found to be the most effective concentration to kill cells when combined with the synergistic effect of ciprofloxacin. **Figure 3.22C** shows the results on the concentration

dependence of the cell viability on the antibiotic treatment in experiments where the ciprofloxacin was encapsulated within the Carbopol nanogel, rather than being delivered separately as a co-treatment. The results demonstrate that there was a significant decrease in cell viability after 1, 6, and 24 h compared to when ciprofloxacin was administered separately at the same concentration. This is attributed to the highly localised release of ciprofloxacin from the adhered nanogel enhancing the effect of the antibiotic. Alcalase functionalised Carbopol nanogel particles can be seen attached to the bacterial cell after the biofilm has been cleared away (**Figure 3.24D**) providing evidence of their ability of local delivery of the antibiotic directly to the bacterial cell wall.

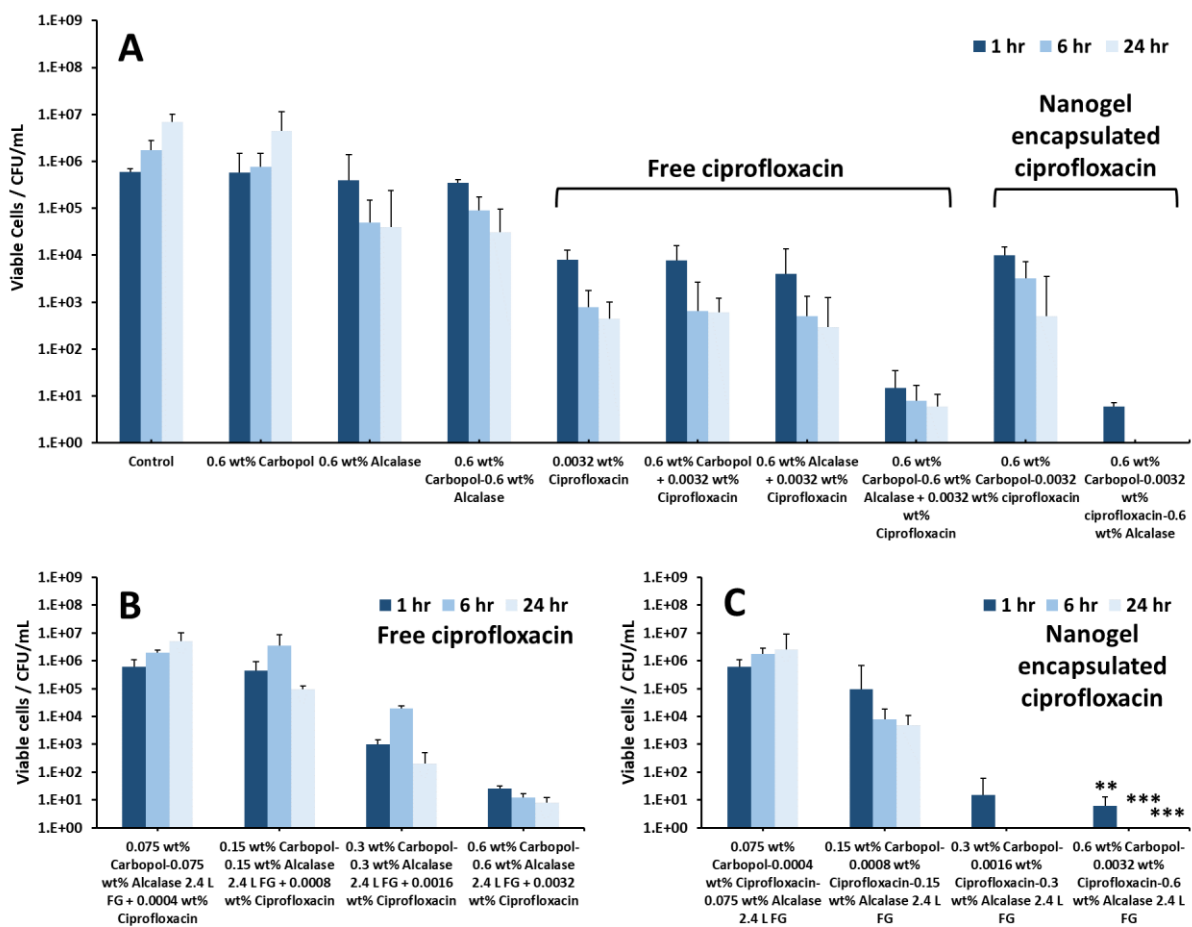


Figure 3.22. (A) *S. aureus* biofilm cellular viability after anti-biofilm treatments. CFU/mL of colony biofilms after timed exposure (1, 6, 24 hr) with a variety of Carbopol Aqua SF1, Alcalase 2.4 L FG, and ciprofloxacin formulations (co-treatment and encapsulated in Carbopol nanogel particles). The cell viability of *S. aureus* from the biofilm culture with **(B)** co treatments of ciprofloxacin and **(C)** treatments with encapsulated ciprofloxacin within Alcalase-coated Carbopol formulations at different dilutions at 1, 6 and 24 hr time-points. The treatment solutions were diluted 2-fold from a starting concentration of 0.6 wt% Carbopol-0.6 wt% Alcalase-0.0032 wt% ciprofloxacin (co-treatment or nanogel-encapsulated). Post-treatment, the colony biofilms were glass bead beaten in 1 mL of MHB with serial dilutions. The agar drop plate method was used to elucidate the CFU/mL. Statistical analysis shown in **Table 3.8**. <0.05 is considered significant. * $P < 0.05$, ** $P < 0.01$, *** $P < 0.001$.

Table 3.8. Statistical analysis of free ciprofloxacin vs encapsulated ciprofloxacin (0.6 wt% Alcalase-0.6 wt% Carbopol formulation) at 1, 6 and 24-hour time points. Data were expressed as average values \pm standard deviations of the mean. *P*-values of less than 0.05 were considered significant. All Student's *T*-tests were performed in GraphPad v7.0.4.

Multiple comparison	P-value	Significance
1 hour free ciprofloxacin VS 1 hour encapsulated ciprofloxacin (0.6 wt% Carbopol-0.6 wt% Alcalase NP)	0.001952	**
6 hour free ciprofloxacin VS 1 hour encapsulated ciprofloxacin (0.6 wt% Carbopol-0.6 wt% Alcalase NP)	0.000314	***
24 hour free ciprofloxacin VS 1 hour encapsulated ciprofloxacin (0.6 wt% Carbopol-0.6 wt% Alcalase NP)	0.000499	***

< 0.05 is considered significant. **P* < 0.05, ***P* < 0.01, ****P* < 0.001.

3.3.7 Antibiofilm efficacy of Alcalase-nanogel particles on *S. aureus* biofilm structure.

An investigation of how 0.6 wt% Alcalase-coated 0.6 wt% Carbopol nanogel affects the biofilm structure of *S. aureus* using fluorescence microscopy was performed. *S. aureus* was allowed to adhere to a glass slide, which has been submerged in this culture for 24 h at 37 °C. After 24 h, the media was removed and the glass slides washed to remove non-sessile cells. Supplemented fresh media containing 0.6 wt% Carbopol, 0.6 wt% free Alcalase, and 0.6 wt% Alcalase–0.6 wt% Carbopol NPs was incubated for a further 24 h covering the slides. Acridine Orange (AO) was used to visualise the remaining cells after treatment. AO is a cell-permeable nucleic acid selective fluorochrome dye. It can emit green light at 520 nm when intercalated with dsDNA. **Figure 3.23A** shows that the growth control has a highly congested biofilm structure, and the cells are highly packed, which is consistent with biofilm formation. There is very little difference to the biofilm structure after treatment with 0.6 wt% bare Carbopol and 0.6 wt% free Alcalase (**Figure 3.23B and C**). The cells remain packed densely together, although there is a moderate reduction in the cell density when treated with free Alcalase. However, in **Figure 3.23D**, there is a marked reduction in the intensity of the AO fluorescence and a reduction in the cell density. The cells have much lower surface density. This suggests that the disruption of the biofilm matrix by the Alcalase–Carbopol nanogel particles has allowed many of the cells to detach from the biofilm during treatment or during the followed washing. For a better understanding of the *S. aureus* biofilm structure, the same samples used for fluorescent analysis were imaged using AFM (**Figure 3.23E–H**). The AFM images again show how the 0.6 wt% Alcalase–0.6 wt% Carbopol NPs effectively remove the biofilm from the glass slide.

Figure 3.23E shows the tightly packed biofilm with staphylococcal cells of thickness approximately 1 μm ; the cells appear to be in a multilayer due to the height sensor recording a maximum height of 2.2 μm . There were no clear differences in structure between the treatments of 0.6 wt% bare Carbopol nanogel and 0.6 wt% free Alcalase treatments (**Figure 3.23F and G**, respectively). There is only a very small reduction in

the average thickness of the biofilm of 0.1 μm , which is insignificant. The AFM scans again show *staphylococcal* layer of approximately 1 μm in a tightly packed fashion. In the control, 0.6 wt% bare Carbopol nanogel and 0.6 wt% free Alcalase showed no discernible difference in cellular morphology. The image in **Figure 3.23H**, however, shows that the biofilm structure has largely been removed, in the scanned region, there were no obvious signs of cell adherence and the peak height was 0.5 μm , which is half the average diameter of an *S. aureus* cell. This result indicates that the cells have been removed during the Alcalase–Carbopol nanogel treatment and washed away after treatment during the preparation of the glass slides for AFM microscopy. This correlates with the data obtained in the AO fluorescence microscopy images. Finally, an investigation of the structure of the *S. aureus* biofilm using scanning electron microscopy (SEM) was carried out. In this case, biofilms grown in filter membranes were used as this allowed feasible samples to be obtained for SEM analysis. The samples were prepared in the same manner as described in the cellular viability assays of biofilm-grown *S. aureus* reported above. The biofilms were treated with 0.6 wt% bare Carbopol nanogel, 0.6 wt% free Alcalase, and 0.6 wt% Alcalase-coated 0.6 wt% Carbopol nanogel particles. Unsupplemented media was considered the growth control. After the treatment, the biofilm membranes were gently removed from the agar using serial tweezers; however, instead of enumeration, the membrane was washed in deionised water, fixed for 1 h in 1 wt% glutaraldehyde, dehydrated in ethanol, and dried in liquid CO_2 at critical point, as described in the methods section 3.2.15. Carbon coating (10 nm) was used to create a conductive layer over the biofilm and reduce thermal damage during SEM imaging.

Figure 3.24 shows the SEM images after the treatments. The control sample shows the highly congested *S. aureus* biofilm. At higher magnification, the EPS within the matrix can also be seen adhered to the surface of the coccus cells and linked to other cells around, consistent with biofilm formation. This morphology is similar in the samples with 0.6 wt% free Carbopol nanogel treatments. The cell density remains highly analogous to the control sample and EPS matrix (dry residue) can be observed around the cells. The cells appear to also be in multilayer with cells atop one and other. Interestingly, in the sample treated with free 0.6 wt% Alcalase, the cellular morphology and density remain largely unchanged; however, there appears to be a distinct lack of EPS matrix coating and surrounding the cells. This indicates that the Alcalase may have digested the biofilm matrix but left the cells largely untouched. Finally, for the sample treated with the Alcalase–Carbopol NPs, there is a clear reduction of the cell density and additionally the biofilm EPS matrix has been degraded. The Alcalase–Carbopol nanogel particles can also be seen adhered to the surface of the *S. aureus* cells, due to the cationic protease molecules on the nanogel surface due to the electrostatic attraction to the anionic surface of the bacterial cell wall. This data correlates with the images obtained using fluorescence and atomic force microscopy and confirms that the Alcalase–Carbopol nanogel particles are degrading the biofilm glycoprotein network.

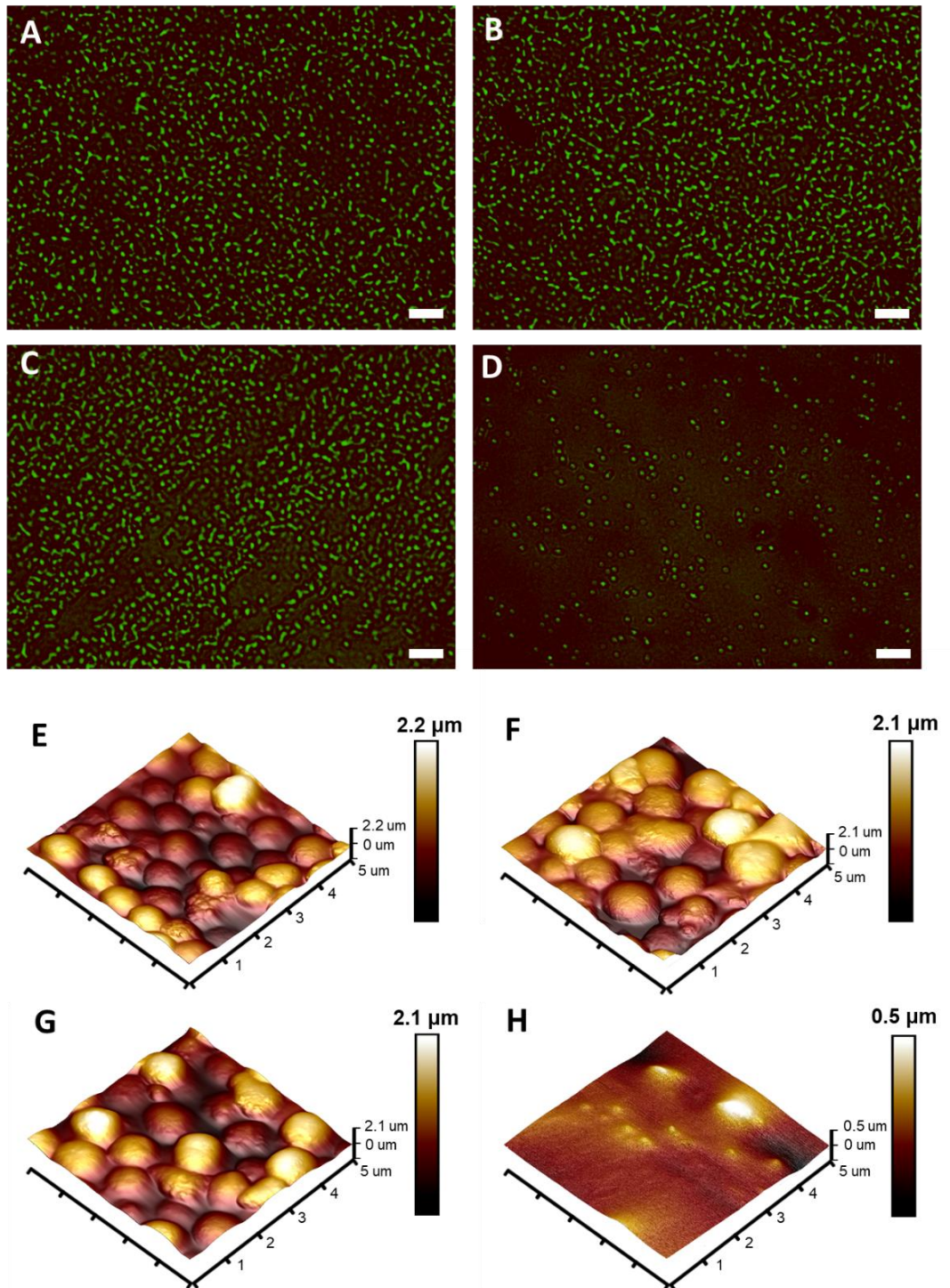


Figure 3.23. Representative fluorescent images of *S. aureus* biofilm formation. **(A)** represents an untreated control sample, **(B)** treatment with 0.6 wt% Carbopol, **(C)** 0.6 wt% Alcalase 2.4 L FG, and **(D)** 0.6wt% Carbopol-0.6 wt% Alcalase 2.4 L FG nanogel particles. Samples were stained with AO. White insert bar represents 5 μm. Tapping Mode Atomic force microscopy of 24-hr growth *S. aureus* biofilms cultured on glass slides. **(E)** Shows biofilm growth control, **(F)** treatment with 0.6 wt% Carbopol, **(G)** 0.6 wt% Alcalase 2.4 L FG and **(H)** 0.6 wt% Carbopol-0.6 wt% Alcalase 2.4 L FG nanogel particles. Images were acquired in height (topography) and then analysed using Nanoscope Analysis v.1.7. (Bruker). The area scanned is 5 μm² per image.

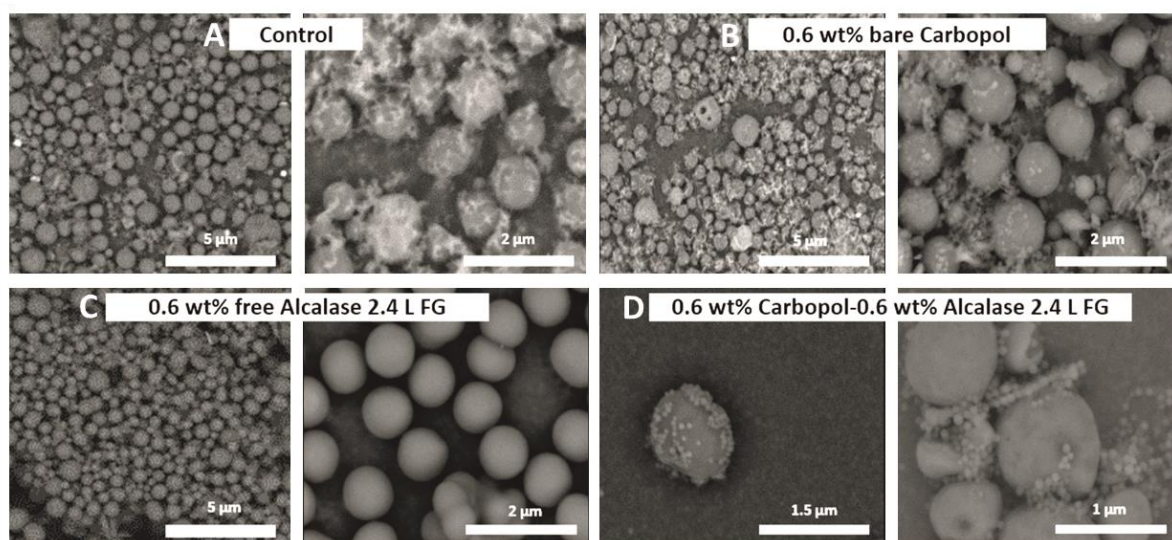


Figure 3.24. SEM images of *S. aureus* before (A) and after treatment with (B) 0.6 wt% bare Carbopol nanogel, (C) 0.6 wt% free Alcalase 2.4 FG and (D) 0.6 wt% Alcalase 2.4G coated 0.6 wt% Carbopol nanogel. All samples were prepared for SEM imaging by drying and coated with ~10 nm carbon layer. Samples were imaged using a Carl Zeiss Evo-60 (Germany) with a variable pressure 100 micron aperture at 40 Pa. EHT was 20 kV with probe current of 100 pA. Images were captured with Zeiss smartSEM software.

3.3.8 Zeta potential of bacteria treated with free Alcalase and Alcalase-nanogel.

An investigation into the effect of the free Alcalase and the immobilized Alcalase on-Carbopol nanogel on the zeta potential of the bacterial species was performed. The experiments on the cells were performed in suspension to allow zeta potential measurements by DLS. **Figure 3.25** indicates that all six species conferred a negative charge on their cell walls, with the Gram negative generally having a stronger charge than the Gram positive. Across all six species, the free Alcalase showed a marginal reduction in the negative zeta potential after 10 min and 1 h. This was likely due to the accumulation of protease on the cell wall. The charge difference was only slight between 10 min and 1 h, indicating that the Alcalase protease had not built up and saturated the surface of the cells. In contrast, the Alcalase- Carbopol nanogel particles showed an increased reduction of the negative charge of the bacterial cells. On average, the zeta potential was reduced by approximately 7–10 mV across the six species. This indicated a build-up of the cationic protease-coated nanogel carriers on the surface of the bacterial cells. The SEM images of *S. aureus* in **Figure 3.24** also support this data, showing that the Alcalase-Carbopol particles adhered to the bacterial cell wall. The experiments were stopped after 1 h due to the aggregation of the cells causing unreliable zeta potential measurements. While these experiments are not indicative of the behaviour of the cells in a biofilm, which will have a much more complex EPS matrix surrounding them, it does provide a valuable insight into the increased attraction of the Alcalase-Carbopol nanogel to the exposed bacterial cells and, therefore, the likely increased affinity of these particles to protein structures within the biofilm matrix.

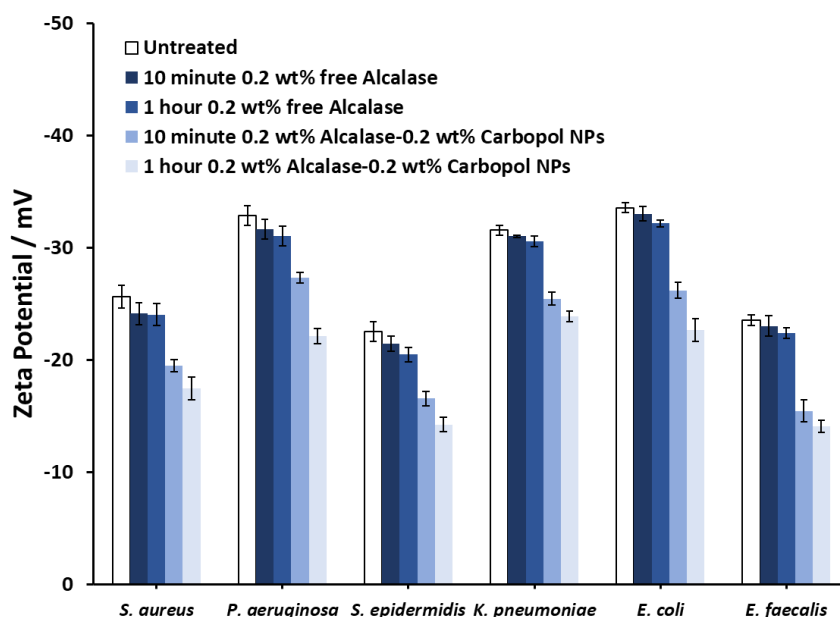


Figure 3.25. The zeta potential of bacterial cells treated with either 0.2 wt% free Alcalase or 0.2 wt% Alcalase-0.2 wt% Carbopol NPs. The bacteria / treatment suspension was placed in a quartz cuvette and zeta potential was measured using the Dipstick probe and Malvern Zetasizer nano ZS. The refractive index was 1.384 and the absorption was 1.000. N = 3 with \pm S.D.

3.3.9 Comparison with standard treatments for biofilm-forming bacteria.

Currently, there is no ‘gold standard’ when it comes to topically treating wound biofilms. There is universal agreement that mechanical debridement is the most effective way to remove biofilm infection, but this is not always possible and often results in regrowth of the biofilm creating a chronic infection (Metcalf et al., 2013; Schultz et al., 2018; Omar et al., 2017). Long-term antibiotic treatment and topical antimicrobial treatments are other common options in treating biofilms. After decades of use, iodophore-based formulations such as poly(vinylpyrrolidone)–iodine (PVP–I) remain prevalent in wound biofilm treatments (Johani et al., 2018). Iodine-based agents are effective antimicrobial agents, which are tolerated well by the body and offer a broad spectrum of activity (Vermeulen et al., 2010). Additionally, they are able to penetrate biofilms, and no clinical evidence presently shows that they have a negative effect on wound healing (Bigliardi et al., 2017). Chlorhexidine is also often used as a disinfectant on patients and is commonly found in formulations designed to reduce infection. However, it is not known to be effective against cells within biofilms (Percival et al., 2914). **Figure 3.26** shows a comparison between 0.6 wt% Carbopol–0.0032 wt% ciprofloxacin–0.6 wt% Alcalase nanogels against iodine, PVP–I and chlorhexidine using the membrane biofilm model. The results show that at the concentrations similar to active agents in the formulation, ciprofloxacin, the alternative treatments are ineffective. This is likely due to the requirement of higher concentrations needed to be effective and the lack of penetration into the biofilm. The quenching effect of the EPS is paramount in preserving cell viability within a biofilm. Additionally, the effect of 0.2 wt%

chlorhexidine and 10 wt% PVP-I concentrations were tested, these are commonly used clinically in wound cleaning and sterilisation (Percival et al., 2914; Edmiston et al., 2013). Again, the results follow the same trend as the low concentrations, with neither agent able to fully eliminate the biofilm bacteria viability.

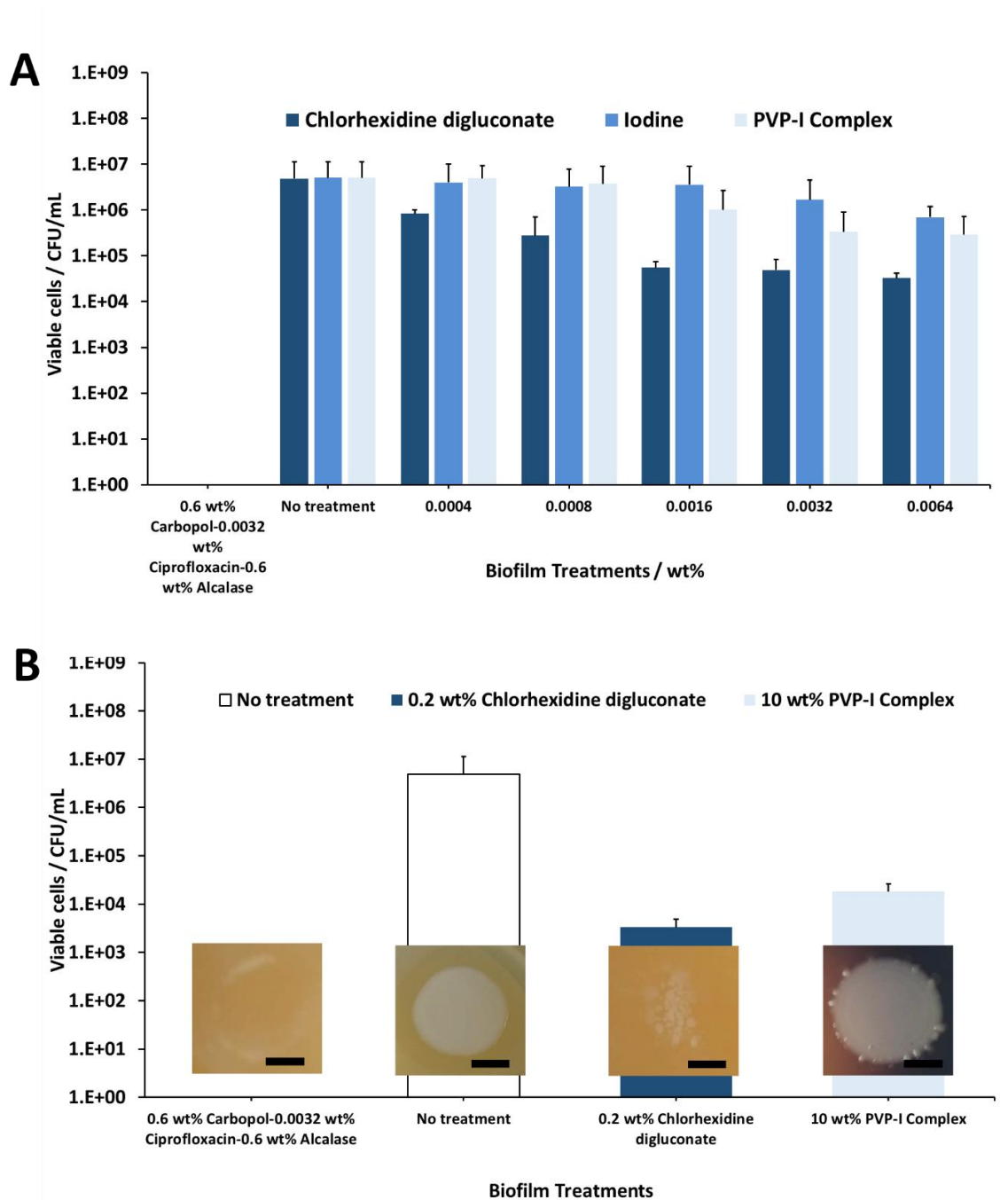


Figure 3.26. *S. aureus* biofilm cellular viability after 24 hours at different concentrations of alternative treatments. **(A)** Shows alternative biofilm treatments at 0 to 0.0062 wt% to compare to the active concentration of ciprofloxacin in the Carbopol-Alcalase formulation. **(B)** Shows a comparison of the alternative biofilm treatments at concentrations used clinically. Biofilm treatments were 0.6 wt% Carbopol-0.0032 wt% Ciprofloxacin-0.6 Alcalase, Chlorhexidine di-gluconate, Iodine and Poly(vinylpyrrolidone)-Iodine (PVP-I). Post-treatment, the membrane biofilms were washed thrice and then glass bead beaten in 1 mL of MHB with serial dilutions. The agar drop plate method was used to elucidate the CFU/mL. Black scale bar in the biofilm pictures is 0.5 cm.

3.3.10 Cytotoxicity and apoptosis-Inducing ability of bare nanogel, free Alcalase, and Alcalase-nanogel on human cells.

A preliminary human cell cytotoxicity experiment was performed on HaCaT cells to investigate if the bare Carbopol Aqua SF1, the free Alcalase 2.4 L FG, and the Alcalase 2.4 L FG-coated Carbopol Aqua SF1 nanogel particles were toxic to human cells. HaCaT cells are very good proxy for studying cytotoxicity of the treatment as they are human keratinocytes, which are the same type of cells likely to be exposed to the formulation in chronic wound cells. **Figure 3.27A** shows that 0.6 wt% Carbopol showed only a marginal reduction in viable cells over 1, 6, and 24 h. This was also the case with 0.6 wt% free Alcalase 2.4 L FG, and Alcalase 2.4 L FG-coated 0.6 wt% Carbopol Aqua SF1 nanogels, the same formulations used in the antibiofilm experiments. This indicates that the Alcalase-coated Carbopol nanogels confer only a slight increase in cytotoxicity toward the HaCaT cells, compared with the free enzyme and the bare nanogel. The data indicate that the enzyme concentration, which provided effect antibiofilm effect, had a very little impact on cell viability, providing evidence that they may be appropriate for in vivo use in surface chronic wounds. Additionally, an investigation into the effect of the 0.6 wt% Alcalase–0.6 wt% Carbopol nanogel particles on inducing apoptosis after 24 h treatment was performed. An Annexin V–FITC staining kit was used to measure the induction of apoptosis using fluorescence-activated cell sorting (FACS). **Figure 3.27B** shows that after 24 h exposure to the Alcalase-coated Carbopol nanogel, there was approximately 10% residual viable cells compared to untreated cells, which correlates well with the MTT viability data shown in **Figure 3.27A**. There is only a marginal difference in induced apoptosis (cells staining positive for Annexin and negative for PI). This indicates that the Alcalase 2.4 FG protease is not triggering apoptosis by way of the caspases cascade apoptosis pathway.

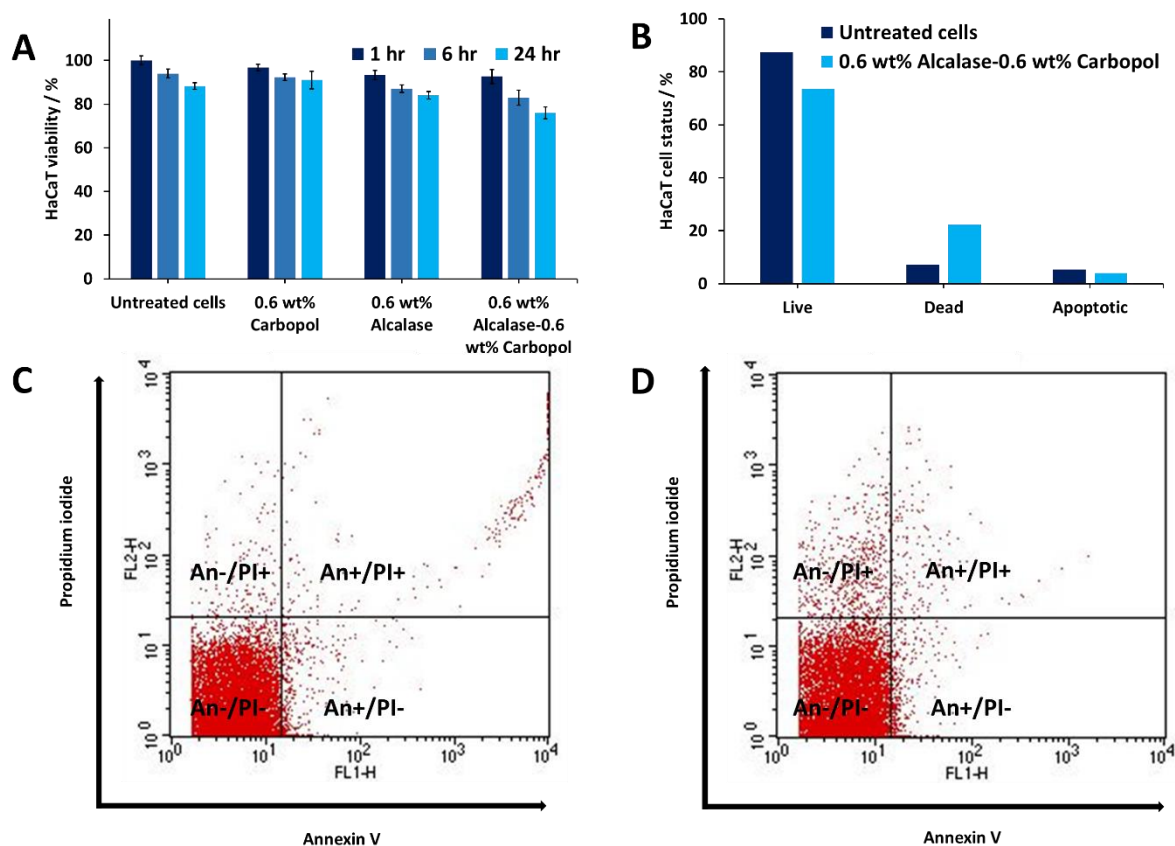


Figure 3.27. (A) HaCaT cell viability after comparative treatment with 0.6 wt% Carbopol Aqua SF1 nanogel, 0.6 wt% Alcalase 2.4 L FG, and -0.6 wt% Alcalase-coated 0.6 wt% Carbopol nanogel particles. Viability counts were performed at 1, 6, and 24 hr. Cell viability % was interpolated from a HaCaT cell calibration curve (**Figure 3.28**) **(B)** HaCaT cell status after 24 hr untreated or 24 hr of 0.6 wt% Alcalase-0.6 wt% Carbopol treatment. **(C)** shows the dot plot distribution for untreated cells after 24 hr and **(D)** shows the dot-plot distribution for 0.6 wt% Alcalase-0.6 wt% Carbopol treatment after 24 hr. The experimental was ended after 10^4 cells were counted after staining using a FITC Annexin staining kit. **Figure 3.29** shows the results for the 0.6 wt% Carbopol and 0.6 wt% Alcalase which were considered controls. **Figure 3.30** shows photographs of the cells after 24 hr treatment and **Table 3.9** shows the cell status after 24 hr of treatment.

Table 3.9. Cell status of HaCaT cells measured using FITC Annexin staining kit and FACS.

Treatment	Cell status		
	Viable cells	Dead cells	Apoptotic cells
Untreated cells	87.4%	7.2%	5.4%
0.6 wt% Carbopol-0.6 wt% Alcalase NPs	73.6%	22.3%	4.1%
0.6 wt% Carbopol	86.2%	7.6%	6.2%
0.6 wt% Alcalase	75.1%	20.4%	4.5%

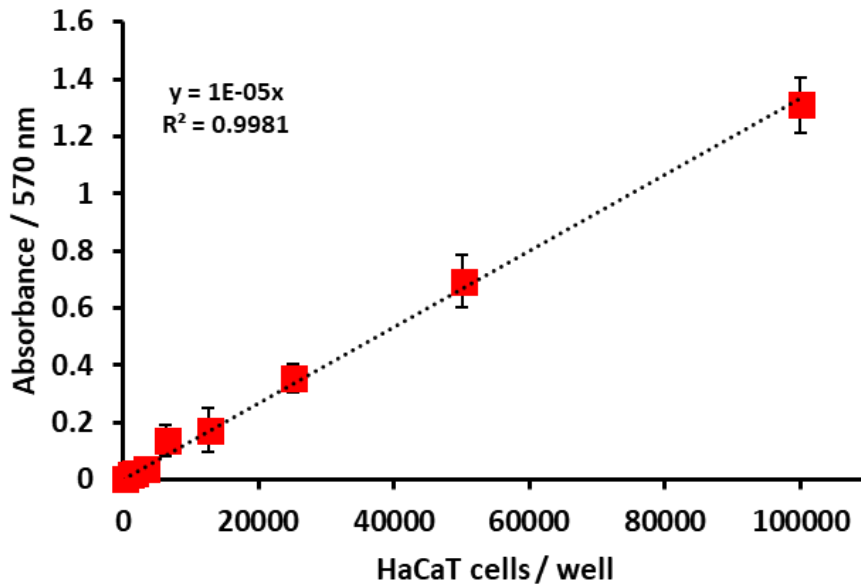


Figure 3.28. Calibration curve of HaCaT cells. Various cell concentrations were seeded in DMEM medium and absorption values obtained at 570 nm. These data were used to calculate the number of cells in parallel treatment / untreated wells. N=3 with \pm S.D.

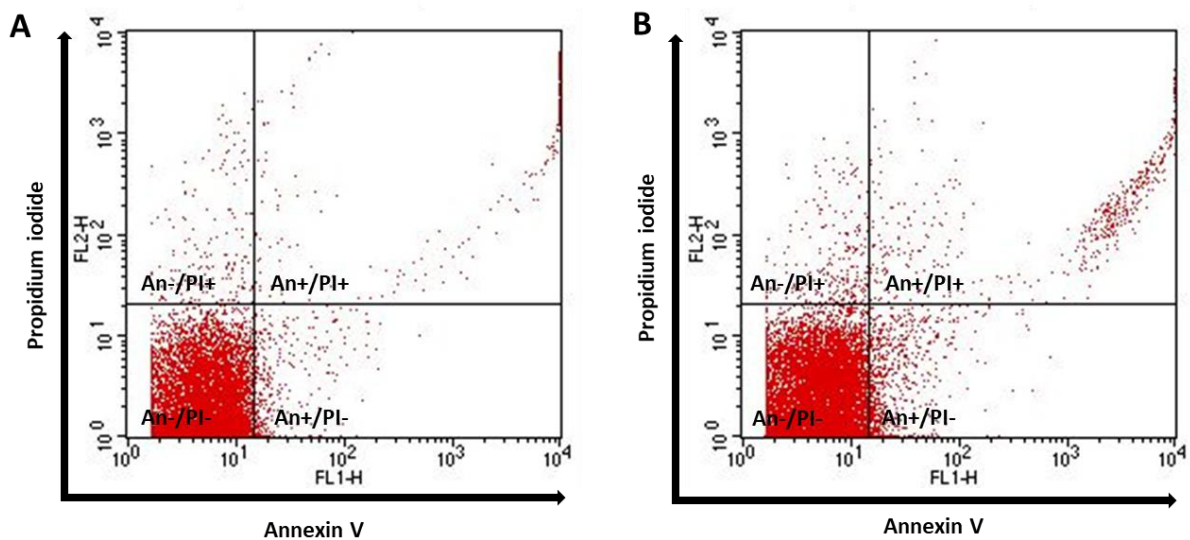


Figure 3.29. HaCaT cell status after 24 hours of treatment with **(A)** 0.6 wt% Carbopol and **(B)** 0.6 wt% Alcalase. FACS dot plots of 10000 cells counted after 24-hour treatment using a FITC Annexin staining kit.

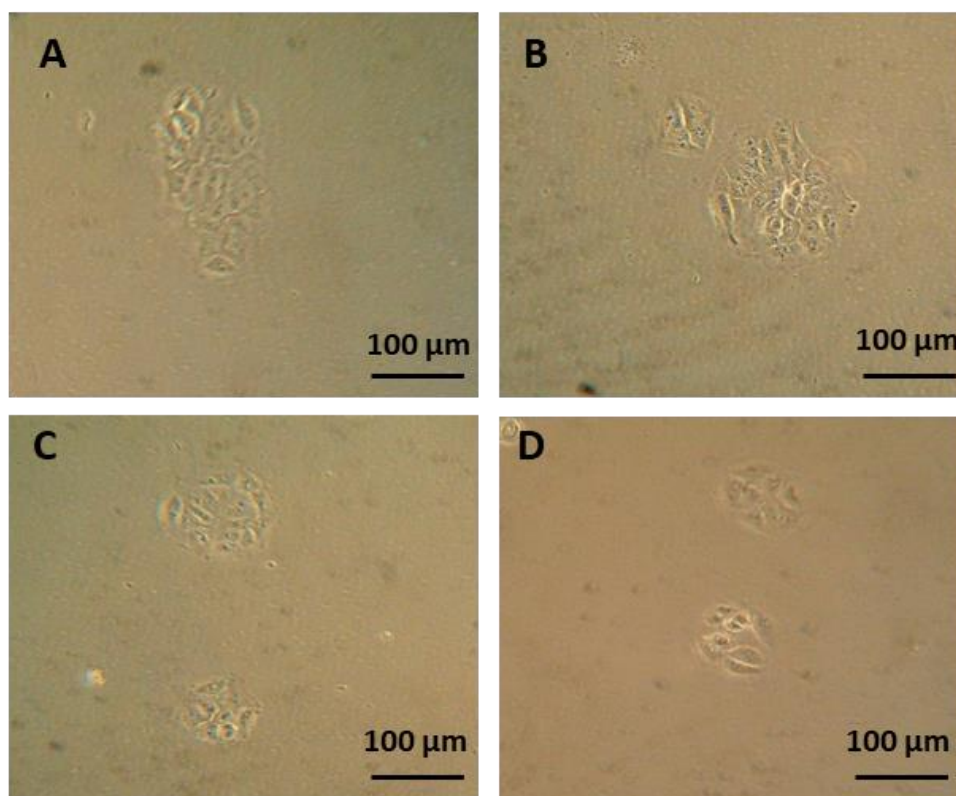


Figure 3.30. Photographs of HaCaT cells in 96-well plates after 24-hour treatment of **(A)** untreated control, **(B)** 0.6 wt% Alcalase-0.6 wt% Carbopol NPs, **(C)** 0.6 wt% bare Carbopol and **(D)** 0.6 wt% free Alcalase. Photographs were taken immediately after treatment and before treatment infused DPBS was aspirated out.

3.4 Conclusions

These results confirm that protease Alcalase 2.4 L FG can disrupt the bacterial biofilm EPS matrix and reduce its biomass. The surface functionalisation of Carbopol Aqua SF1 nanogels with this enzyme further boosts this effect on six wound biofilm associated pathogens reducing the biomass 6-fold compared to untreated biofilms. The efficacy of the Alcalase-coated Carbopol nanogel particles was confirmed using fluorescence, atomic force, and scanning electron microscopy. Additionally, the application of Alcalase–Carbopol nanogels in a co-treatment with ciprofloxacin resulted in a 3-log reduction in viable cell counts compared to using of an equivalent concentration of ciprofloxacin alone. When ciprofloxacin was encapsulated within Alcalase-functionalised Carbopol nanogel at equivalent concentrations to the free ciprofloxacin, there was a very significant further boost to the effectiveness of the antibiotic in this dual-functionalised nanocarrier. These dual purpose Alcalase-coated antibiotic-loaded nanogel particles provided effective treatment against *S. aureus* biofilms, with no detectable CFU after 6 and 24 h treatment times. The Alcalase–Carbopol nanogels also showed negligible cytotoxicity and apoptosis-inducing influence toward adult human keratinocytes. It is concluded that the Alcalase-coated and ciprofloxacin-loaded Carbopol nanogel carriers are very effective and apparently safe antibiofilm formulation, which could provide an alternative approach to the treatment of external wound biofilms. This suggested that further investigation of the practical administration of Alcalase-coated Carbopol nanogels loaded with antibiotics on biofilm-infected wounds is required, where these nanogels could provide an advantageous tool for therapeutic antibiofilm treatments and fight against antimicrobial resistance.

3.5 Reference list

- Al-Awady, M., Fauchet, A., Greenway, G. & Paunov, V. (2017) Enhanced Antimicrobial Effect Of Berberine In Nanogel Carriers With Cationic Surface Functionality. *J. Mater. Chem. B*, 5, 7885–7897.
- Al-Awady, M., Weldrick, P., Hardman, M., Greenway, G. & Paunov, V. (2018) Amplified Antimicrobial Action Of Chlorhexidine Encapsulated In PDAC-Functionalized Acrylate Copolymer Nanogel Carriers. *Mater. Chem. Front.*, 2, 2032–2044.
- Algburi, A., Comito, N., Kashtanov, D., Dicks, L. & Chikindas, M. (2017) Erratum For Algburi Et Al., Control Of Biofilm Formation: Antibiotics And Beyond. *Appl. Environ. Microbiol.*, 83, 2508–2516.
- Alkawash, M., Soothill, J., & Sshiller, N. (2006) Alginate Lyase Enhances Antibiotic Killing Of Mucoïd Pseudomonas aeruginosa In Biofilms. *APMIS*, 114, 131–138.
- Al-Obaidy, S., Greenway, G. & Paunov, V. (2019b) Dual-Functionalised Shellac Nanocarriers Give A Super-Boost Of The Antimicrobial Action Of Berberine. *Nanoscale Adv.*, 1, 858–872.
- Al-Obaidy, S., Halbus, A., Greenway, G. & Paunov, V. (2019a) Boosting The Antimicrobial Action Of Vancomycin Formulated In Shellac Nanoparticles Of Dual-Surface Functionality. *J. Mater. Chem. B*, 7, 3119–3133.
- Baidamshina, D. R., Trizna, E. Y., Holyavka, M. G., Bogachev, M. I., Artyukhov, V. G., Akhatova, F. S., Rozhina, E. V., Fakhrullin, R. F. & Kayumov, A. R. (2017) Targeting Microbial Biofilms Using Ficin, A Nonspecific Plant Protease. *Sci. Rep.*, 7, 46068.
- Bigliardi, P. L., Alsagoff, S. A. L., El-Kafrawi, H. Y., Pyon, J., Wa, C. T. C. & Villa, M. A. (2017) Povidone Iodine In Wound Healing: A Review Of Current Concepts And Practices. *Int. J. Surg.*, 44, 260–268.
- Blackledge, M., Worthington, R. & Melander, C. (2013) Biologically Inspired Strategies For Combating Bacterial Biofilms. *Curr. Opin. Pharmacol.*, 13, 699–706.
- Boles, B. & Horswill, A. (2011) Staphylococcal Biofilm Disassembly. *Trends Microbiol.*, 19, 449–455.
- Borovička, J., Stoyanov, S. D. & Paunov, V. N. (2015) Cell Shape Recognition By Colloidal Cell Imprints: Energy Of The Cell-Imprint Interaction. *Phys. Rev. E*, 92, 032730.
- Choong, F., Bäck, M., Fahlén, S., Johansson, L., Melican, K., Rhen, M., Nilsson, K. & Richter-Dahlfors, A. (2016) Real-Time Optotracing Of Curli And Cellulose In Live Salmonella Biofilms Using Luminescent Oligothiophenes. *npj Biofilms Microbiomes*, 2, 16024.
- Christensen, G. D., Simpson, W. A., Bisno, A. L. & Beachey, E. H. (1982) Adherence of Slime-Producing Strains of Staphylococcus epidermidis to Smooth Surfaces. *Infect. Immun.*, 37, 318–326.
- Coríci, L., Frissen, A., van Zoelen, D., Eggen, I., Peter, F., Davidescu, C. & Boeriu, C. (2011) Sol–Gel Immobilization Of Alcalase From Bacillus licheniformis For Application In The Synthesis Of C-Terminal Peptide Amides. *J. Mol. Catal.*, B, 73, 90–97.
- Costerton, J. W., Stewart, P. S. & Greenberg, E. P. (1999) Bacterial Biofilms: A Common Cause Of Persistent Infections. *Science*, 284, 1318–1322.
- Darouiche, R., Mansouri, M., Gawande, P. & Madhyastha, S. (2009) Antimicrobial And Antibiofilm Efficacy Of Triclosan And Dispersinb(R) Combination. *J. Antimicrob. Chemother.*, 64, 88–93.
- Domenech, M., Ramos-Sevillano, E., García, E., Moscoso, M. & Yuste, J. (2013) Biofilm Formation Avoids Complement Immunity And Phagocytosis Of Streptococcus pneumoniae. *Infect. Immun.*, 81, 2606–2615.
- Donelli, G., Francolini, I., Romoli, D., Guaglianone, E., Piozzi, A., Ragnath, C. & Kaplan, J. (2007) Synergistic Activity Of Dispersin B And Cefamandole Nafate In Inhibition Of Staphylococcal Biofilm Growth On Polyurethanes. *Antimicrob. Agents Chemother.*, 51, 2733–2740.
- Donlan, R. (2002) Biofilms: Microbial Life On Surfaces. *Emerging Infect. Dis.*, 8, 881–890.
- Edmiston, C., Bruden, B., Rucinski, M., Henen, C., Graham, M. & Lewis, B. (2013) Reducing the risk of surgical site infections: Does chlorhexidine gluconate provide a risk reduction benefit? *Am. J. Infect. Control*, 41, S49–S55.
- Freeman, D. J., Falkiner, F. R. & Keane, C. T. (1989) New Method For Detecting Slime Production By Coagulase Negative Staphylococci. *J. Clin. Pathol.*, 42, 872–874.

- Gupta, P. & Diwan, B. (2017) Bacterial Exopolysaccharide Mediated Heavy Metal Removal: A Review On Biosynthesis, Mechanism And Remediation Strategies. *Biotechnology Reports*, 13, 58–71.
- Halbus, A., Horozov, T. & Paunov, V. (2019a) Controlling The Antimicrobial Action Of Surface Modified Magnesium Hydroxide Nanoparticles. *Biomimetics*, 4, 41.
- Halbus, A., Horozov, T. & Paunov, V. (2019b) Self-Grafting Copper Oxide Nanoparticles Show A Strong Enhancement Of Their AntiAlgal And Anti-Yeast Action. *Nanoscale Adv.*, 1, 2323–2336.
- Halbus, A., Horozov, T. & Paunov, V. (2019c) “Ghost” Silica Nanoparticles Of “Host”-Inherited Antibacterial Action. *ACS Appl. Mater. Interfaces*, 11, 38519–38530.
- Halbus, A., Horozov, T. & Paunov, V. (2019d) Strongly Enhanced Antibacterial Action Of Copper Oxide Nanoparticles With Boronic Acid Surface Functionality. *ACS Appl. Mater. Interfaces*, 11, 12232–12243.
- Hošťacká, A., Čížnár, I. & Štefkovičová, M. (2010) Temperature and pH Affect the Production of Bacterial Biofilm. *Folia Microbiol.*, 55, 75–78.
- Jisha, V. N., Smitha, R. B., Pradeep, S., Sreedevi, S., Unni, K. N., Sajith, S., Priji, P., Josh, M. S. & Benjamin, S. (2013) Versatility Of Microbial Proteases. *Adv. Enzyme Res.*, 1, 39–51.
- Johani, K., Malone, M., Jensen, S., Dickson, H., Gosbell, I., Hu, H., Yang, Q., Schultz, G. & Vickery, K. (2018) Evaluation Of Short Exposure Times Of Antimicrobial Wound Solutions Against Microbial Biofilms: From In Vitro To In Vivo. *J. Antimicrob. Chemother.*, 73, 494– 502.
- Kaplan, J. (2010) Biofilm Dispersal: Mechanisms, Clinical Implications, And Potential Therapeutic Uses. *J. Dent. Res.*, 89, 205–218.
- Kim, L., Pagaling, E., Zuo, Y. & Yan, T. (2014) Impact Of Substratum Surface On Microbial Community Structure And Treatment Performance In Biological Aerated Filters. *Appl. Environ. Microbiol.*, 80, 177–183.
- Kostakioti, M., Hadjifrangiskou, M. & Hultgren, S. J. (2013) Bacterial Biofilms: Development, Dispersal, And Therapeutic Strategies In The Dawn Of The Postantibiotic Era. *Cold Spring Harbor Perspect. Med.*, 3, a010306.
- Lequette, Y., Boels, G., Clarisse, M. & Faille, C. (2010) Using Enzymes To Remove Biofilms Of Bacterial Isolates Sampled In The Food Industry. *Biofouling*, 26, 421–431.
- Leroy, C., Delbarre, C., Ghillebaert, F., Compere, C. & Combes, D. (2008) Effects Of Commercial Enzymes On The Adhesion Of A Marine Biofilm-Forming Bacterium. *Biofouling*, 24, 11–22.
- Lister, J. & Horswill, A. (2014) Staphylococcus aureus Biofilms: Recent Developments In Biofilm Dispersal. *Front. Cell. Infect. Microbiol.*, 4, 178.
- Markland, F. S., Jr. & Smith, E. L. (1971) Subtilisins: Primary Structure, Chemical and Physical Properties. *Enzymes*, 3, 561–608.
- Markowska, K., Grudniak, A. & Wolska, K. (2013) Silver Nanoparticles As An Alternative Strategy Against Bacterial Biofilms. *Acta Biochim. Pol.*, 60, 523–530.
- Mateo, C., Palomo, J., Fernandez-Lorente, G., Guisan, J. & Fernandez-Lafuente, R. (2007) Improvement Of Enzyme Activity, Stability And Selectivity Via Immobilization Techniques. *Enzyme Microb. Technol.*, 40, 1451–1463.
- Mendes, A. A., de Castro, H. F., Rodrigues, D. d. S., Adriano, W. S., Tardioli, P. W., Mammarella, E. J., Giordano, R. d. C. & Giordano, R. d. L. C. (2011) Multipoint Covalent Immobilization Of Lipase On Chitosan Hybrid Hydrogels: Influence Of The Polyelectrolyte Complex Type And Chemical Modification On The Catalytic Properties Of The Biocatalysts. *J. Ind. Microbiol. Biotechnol.*, 38, 1055–1066.
- Metcalf, D. G. & Bowler, P. G. (2013) Biofilm Delays Wound Healing: A Review Of The Evidence. *Burns Trauma*, 1, 5.
- Mitrofanova, O., Mardanova, A., Evtugyn, V., Bogomolnaya, L. & Sharipova, M. (2017) Effects Of Bacillus Serine Proteases On The Bacterial Biofilms. *BioMed Res. Int.*, 2017,1–10.
- Newase, S. & Bankar, A. (2017) Synthesis Of Bio-Inspired Ag–Au Nanocomposite And Its Anti-Biofilm Efficacy. *Bull. Mater. Sci.*, 40, 157–162.
- Nijland, R., Hall, M. & Burgess, J. (2010) Dispersal Of Biofilms By Secreted, Matrix Degrading, Bacterial Dnase. *PLoS One*, 5, e15668.

- Nocelli, N., Bogino, P., Banchio, E. & Giordano, W. (2016) Roles Of Extracellular Polysaccharides And Biofilm Formation In Heavy Metal Resistance Of Rhizobia. *Materials*, 9, 418.
- O'Toole, G. (2011) Microtiter Dish Biofilm Formation Assay. *J. Visualized Exp.*, 47, 2437.
- Omar, A., Wright, J., Schultz, G., Burrell, R. & Nadworny, P. (2017) Microbial Biofilms And Chronic Wounds. *Microorganisms*, 5, 9.
- Park, J. H., Lee, J. H., Cho, M. H. & Herzberg, M.; Lee, J. (2012) Acceleration Of Protease Effect On Staphylococcus aureus Biofilm Dispersal. *FEMS Microbiol. Lett.*, 335, 31–38.
- Pastore, C. (2018) Piercing The Biofilm. *Nat. Nanotechnol.*, 13, 1092.
- Pavlukhina, S., Kaplan, J., Xu, L., Chang, W., Yu, X., Madhyastha, S., Yakandawala, N., Mentbayeva, A., Khan, B. & Sukhishvili, S. (2012) Noneluting Enzymatic Antibiofilm Coatings. *ACS Appl. Mater. Interfaces*, 4, 4708–4716.
- Percival, S., Finnegan, S., Donelli, G., Vuotto, C., Rimmer, S. & Lipsky, B. (2014) Antiseptics For Treating Infected Wounds: Efficacy On Biofilms And Effect Of pH. *Crit. Rev. Microbiol.*, 42, 293–309.
- Ramasamy, M. & Lee, J. (2016) Recent Nanotechnology Approaches For Prevention And Treatment Of Biofilm-Associated Infections On Medical Devices. *BioMed Res. Int.*, 1–17.
- Richards, J. & Melander, C. (2009) Controlling Bacterial Biofilms. *ChemBioChem*, 10, 2287–2294.
- Rodrigues, R., Ortiz, C., Berenguer-Murcia, Á., Torres, R. & Fernández-Lafuente, R. (2013) Modifying Enzyme Activity And Selectivity By Immobilization. *Chem. Soc. Rev.*, 42, 6290–6307.
- Rogers, S. A., Huigens, R. W., Cavanagh, J. & Melander, C. (2010) Synergistic Effects Between Conventional Antibiotics And 2-Aminoimidazole-Derived Antibiofilm Agents. *Antimicrob. Agents Chemother.*, 54, 2112–2118.
- Schallenger, M., Niessen, S., Shao, C., Fowler, B. & Romesberg, F. (2012) Type I Signal Peptidase And Protein Secretion In Staphylococcus aureus. *J. Bacteriol.*, 194, 2677–2686.
- Schultz, G. S., Woo, K., Weir, D. & Yang, Q. (2018) Effectiveness Of A Monofilament Wound Debridement Pad At Removing Biofilm And Slough: Ex Vivo And Clinical Performance. *J. Wound Care*, 27, 80–90.
- Sharma, D., Misba, L. & Khan, A. (2019) Antibiotics Versus Biofilm: An Emerging Battleground In Microbial Communities. *Antimicrob. Resist. Infect. Control*, 8, 76.
- Singh, R., Kumar, M., Mittal, A. & Mehta, P. (2016) Microbial Enzymes: Industrial Progress In 21st Century. *3 Biotech*, 6, 174.
- Singh, S. & Bajaj, B. (2015) Medium Optimization For Enhanced Production Of Protease With Industrially Desirable Attributes From Bacillus Subtilis-1. *Chem. Eng. Commun.*, 202, 1051–1060.
- Singh, S. & Bajaj, B. (2016) Bioprocess Optimization For Production Of Thermoalkali-Stable Protease From Bacillus Subtilis-1 Under Solid State Fermentation. *Prep. Biochem. Biotechnol.*, 46, 717–724.
- Singh, S., Singh, S., Chowdhury, I. & Singh, R. (2017) Understanding The Mechanism Of Bacterial Biofilms Resistance To Antimicrobial Agents. *Open Microbiol. J.*, 11, 53–62.
- Tang, Z., Qian, J. & Shi, L. (2006) Characterizations Of Immobilized Neutral Proteinase On Chitosan Nano-Particles. *Process Biochem.*, 41, 1193–1197.
- Thallinger, B., Prasetyo, E., Nyanhongo, G. & Guebitz, G. (2013) Antimicrobial Enzymes: An Emerging Strategy To Fight Microbes And Microbial Biofilms. *Biotechnol. J.*, 8, 97–109.
- Theron, L. & Divol, B. (2014) Microbial Aspartic Proteases: Current And Potential Applications In Industry. *Appl. Microbiol. Biotechnol.*, 98, 8853–8868.
- Tsang, L., Cassat, J., Shaw, L., Beenken, K. & Smeltzer, M. (2008) Factors Contributing To The Biofilm-Deficient Phenotype Of Staphylococcus aureus Sara Mutants. *PLoS One*, 3, e3361.
- Vermeulen, H., Westerbos, S. & Ubbink, D. (2010) Benefit And Harm Of Iodine In Wound Care: A Systematic Review. *J. Hosp. Infect.*, 76, 191–199.
- Wang, S., Zhang, C., Qi, B., Sui, X., Jiang, L., Li, Y., Wang, Z., Feng, H., Wang, R. & Zhang, Q. (2014) Immobilized Alcalase Alkaline Protease On The Magnetic Chitosan Nanoparticles Used For Soy Protein Isolate Hydrolysis. *Eur. Food Res. Technol.*, 239, 1051–1059.

Weldrick, P. J., Iveson, S., Hardman, M. J. & Paunov, V. N. (2019) Breathing New Life Into Old Antibiotics: Overcoming Antibacterial Resistance By Antibiotic-Loaded Nanogel Carriers With Cationic Surface Functionality. *Nanoscale*, 11, 10472–10485.

Wilkinson, H., Iveson, S., Catherall, P. & Hardman, M. (2018) A Novel Silver Bioactive Glass Elicits Antimicrobial Efficacy Against *Pseudomonas aeruginosa* And *Staphylococcus aureus* In An Ex Vivo Skin Wound Biofilm Model. *Front. Microbiol.*, 9, No. 1450.

Wilkinson, H., McBain, A., Stephenson, C. & Hardman, M. (2016) Comparing the Effectiveness of Polymer Debriding Devices Using a Porcine Wound Biofilm Model. *Adv. Wound Care*, 5, 475–485.

Yang, L., Liu, Y., Wu, H., Song, Z., Høiby, N., Molin, S. & Givskov, M. (2012) Combating Biofilms. *FEMS Immunol. Med. Microbiol.*, 65, 146–157.

4.0 Chapter 4

Smart active antibiotic nanocarriers with protease surface functionality can overcome biofilms of resistant bacteria

Weldrick, P. J., Hardman, M. J., & Paunov, V. N. (2021). Smart active antibiotic nanocarriers with protease surface functionality can overcome biofilms of resistant bacteria. *Mater. Chem. Front.*, 5, 961-972. Reproduced by permission of The Royal Society of Chemistry. Attribution-NonCommercial 3.0 Unported (CC BY-NC 3.0). <https://creativecommons.org/licenses/by-nc/3.0/>. Minor changes made to presentation of the material. Conceptualisation, V.N.P. All experiments were performed by P.J.W under V.N.P. supervision. P.J.W prepared the figures and wrote the manuscript, V.N.P and M.J.H. co-edited the manuscript. All authors have given approval to the final version of the manuscript.

Treating bacterial infections with species demonstrating antibiotic resistance to the chosen antibiotic is often hindered due to the ability of certain bacteria to grow biofilms where they can effectively hide and resist the antibiotic action. This chapter reports an innovative solution for overcoming both antibiotic resistance and biofilm formation by designing active antibiotic nanocarriers with protease surface functionality. The data reveals that this active nanocarrier of common antibiotics can efficiently degrade biofilms of resistant bacteria and bypass their defences. The cationic protease coating, whilst allowing electrostatic adhesion of the nanoparticle to the cell, simultaneously also degrades the biofilm and helps the active nanocarriers to reach the entrapped bacterial cells. This concept is demonstrated by encapsulating Penicillin G and Oxacillin into shellac nanoparticles, subsequently coated with a serine endo-peptidase protease, Alcalase 2.4 L FG. It is shown for the first time that these active nanocarriers can destroy biofilms of *S. aureus* resistant to Penicillin G and are significantly more effective in killing the bacterial cells within compared to an equivalent concentration of free antibiotic. The approach of concentrating the antibiotic by encapsulating it into a nanocarrier allows a localised delivery of the antibiotic to the anionic cell wall, facilitated by coating the NPs with a cationic protease. This approach allowed the antibiotic to restore its effectiveness against *S. aureus*, characterised as resistant to the same antibiotic as well as to cause a rapid degradation of the bacterial biofilm. This approach could be potentially used to revive old antibiotics which have already limited clinical use due to developed resistance.

4.1 Introduction

Penicillin is a commonly administered antibiotic used to treat staphylococci and streptococci infections (Creech et al., 2015). Penicillin is part of the beta-lactam cyclic amine antibiotic family, and all antibiotics in the family used the same bacterial cell wall growth inhibition to kill bacteria (Kapoor et al., 2017). There is a range of resistance mechanisms that bacteria have evolved against such antibiotics (Irazoki et al., 2019; Mihelič et al., 2017; Yadav et al., 2018; Yılmaz et al., 2017; Smith et al., 2005). Penicillin's all contain a thiazolidine ring (sulphur-containing with a carbonyl group), a beta-lactam ring (cleaved by beta-lactamases at C-N bond) and a variable side chain attached through an amide linkage (Soares et al., 2012). Penicillin G (benzylpenicillin) is part of a first-generation fermentation-derived family, oxacillin is a second-generation semi-synthetic antibiotic with beta-lactam resistance (Lobanovska et al., 2017). Additional ring structures on the variable group of semi-synthetic penicillin's acts as a steric hindrance and inhibits beta-lactamase (penicillinase) activity, i.e. the isoxazolyl antibiotic oxacillin (Munita et al., 2016).

Bacteria can quickly become resistant to antibiotics due to genetic mutations, formed from environmental pressures such as antibiotic treatments, partially at sub-lethal concentrations (Knudsen et al., 2016). Horizontal gene transfer can allow the creation of resistance strains which can then only be killed with alternative antibiotics are at much higher concentrations (Sun et al., 2019). However, methicillin-resistant *S. aureus* (MRSA) is resistant to all second-generation penicillin's due to the production of a low-affinity penicillin PBP2a (Smith et al., 2005). MRSA is a considerable public health risk due to this mechanism (Goetghebeur et al., 2007). Beta lactamase inhibitors such as clavulanic acid and sulbactam are commonly administered synergistically with penicillin antibiotics for their ability to bind to beta lactamase broadening the effectiveness of the antibiotic (Ba et al., 2015). Gram-positive cell walls are primarily made of peptidoglycan monomer comprised of two covalently joined amino sugars, N-acetylmuramic acid (NAM) and N-acetylglucosamine (NAG), bound using transpeptidases enzymes called penicillin binding proteins (PBPs) (Irazoki et al., 2019). To maintain the rigidity and support this cross-linked NAM-NAG matrix is constantly remodelled to allowed cell growth and replication (Mihelič et al., 2017). Penicillin antibiotics bind to PBPs serine residues in the active site via acetylation and inhibit their peptide bridge cross-linking function preventing new cell wall formation (Yadav et al., 2018). A lack of cell wall quickly results in cell death, leaving humans cells unharmed due to a lack of peptidoglycan in their cellular structure (Yılmaz, & Özcengiz, 2017). Bacteria have also evolved modified PBPs which have a low penicillin binding affinity and therefore can evade inactivation (Sun et al., 2019).

The production of beta-lactamase (which hydrolyses penicillin into penicilloic acid) is common in *Staphylococcus aureus*, a pathogen that can cause infection in skin, lungs and blood (Llarrull et al., 2009). Most strains of *S. aureus* are now resistant to first-generation penicillin's and so second-generation penicillin's such as oxacillin, nafcillin and methicillin are administered (Bæk et al., 2014). A report by the World Health Organisation in 2014 stated that antibiotic resistance is a growing worldwide threat to public health, driven largely by the lack of new therapeutic agents for treating bacterial infections (WHO, 2014). Overcoming resistance to beta-lactam antibiotics is most commonly achieved by using a beta-lactamase inhibitor such as clavulanic acid, which can bind to the active site of beta-lactamases and provide form a stable acyl enzyme complex, thereby inhibiting the enzyme (Worthington & Melander, 2013a). Another approach is to target the pathways of Gram-positive cell wall production. Tunicamycin and ticlopidine have been shown to inhibit the enzymatic pathway for teichoic acid, a key component of the Gram-positive cell wall (Worthington & Melander, 2013b).

The ability of bacteria to form biofilms further complicates their treatment (Gebreyohannes et al., 2019). A biofilm is an extracellular polymeric substance (EPS) which is secreted by bacterial communities and surrounds them in a protective layer (Verderosa et al., 2019). EPS is a structured matrix of exopolysaccharides, lipids, nucleic acids and protein (Limoli et al., 2015). Biofilms protect the bacterial cells within and allow them to tolerate treatments due to the quenching of antimicrobial agents at concentrations that would otherwise kill planktonic cells (Sharma et al., 2019). Impaired diffusion of antimicrobial agents through the EPS increases the tolerance to treatments (Singh et al., 2017). Opportunistic pathogens, such as *S. aureus*, can cause chronic infection in dermal wounds, potentially caused by a combination of biofilm production and antimicrobial resistance (Lister & Horswill, 2014; Richards & Melander, 2009).

Nanoparticles (NPs) have been investigated for their anti-biofilm action and ability to overcome antimicrobial resistance. A variety of different NPs such as Au NPs, silica NPs, Mg(OH)₂ NPs and CuONPs have all been shown to demonstrate increased toxicity towards bacteria (Newase & Bankar, 2017; Markowska et al., 2013; Halbus et al., 2019a; Halbus et al., 2019b; Halbus et al., 2019c; Al-Awady et al., 2015). AgNPs have been researched in anti-biofilm treatments due to the silver ions intrinsic antimicrobial property (Wilkinson et al., 2018; Richter et al., 2016). Nanocarriers for antimicrobial agents have also been shown to increase their efficacy against a wide range of microorganisms, including resistant species (Al-Awady et al., 2018; Weldrick et al., 2019a; Weldrick et al., 2019b; Al-Obaidy et al., 2019a), and deliver drugs specifically to a bacterial target (Din et al., 2017; Al-Obaidy et al., 2019b; Richter et al., 2016; Al-Awady et al., 2017). This can potentially reduce unwanted drug interaction in healthy tissue and lower general toxicity (Yu et al., 2016). They can also

protect the antimicrobial agent from premature degradation and inactivation (Kumari et al., 2014; Jahangirian et al., 2017).

Biofilm degradation has been investigated using a range of biologically inspired hydrolases, amylases and proteases (Singh et al., 2016; Blackledge et al., 2013). The disruption of the biofilm formation by NPs can improve the ability of antimicrobial agents to kill the cells within (Weldrick et al., 2019b). Proteases can be particularly useful for degrading biofilms due to their ability to hydrolyse ESP matrix proteins and bacterial adhesins (Baidamshina et al., 2017; Mitrofanova et al., 2017; Leroy et al., 2008). Disruption of the synthesis of biofilm formation using small molecules to inhibit key signalling pathways such as c-di-GMP and indole has also been investigated (Melander & Melander, 2015).

In this study, a novel concept for an active nanocarrier delivery of Penicillin G and Oxacillin to biofilms by their encapsulation into a protease-functionalised shellac NPs is presented. The NPs surface coating of a cationic protease, Alcalase 2.4 L FG, performs a dual purpose to both degrade the biofilms and increase the electrostatic interaction between the cationic NPs and the anionic cell walls of the entrapped bacteria. **Figure 4.1A** illustrates the scheme for fabrication of the composite shellac NPs, and **figure 4.1B** shows their mechanism of action. **Figure 4.2** provides a detailed information about the individual components of the NP and the chemical structure of the antibiotics. *S. aureus* was chosen as the model pathogen for its ability to form a biofilm. This *S. aureus* strain (ATCC® 29213™) was selected due to its resistance to Penicillin G (PenG) and its sensitivity to oxacillin (Oxa). The gene *blaZ* which produces the protein product beta-lactamase (EC number: 3.5.2.6) was shown to be in the genome of this strain, as confirmed by the ATCC One Codex depository (ATCC Genome Portal, 2020). Additionally, this strain does not carry the *mecA* gene which encodes an altered penicillin-binding protein (PBP2a) which confers resistance to oxacillin due to reduced beta-lactamase affinity (Lowy, 2003).

Here the aim is to prove that its antimicrobial resistance can be overcome by using highly concentrated antibiotics loaded inside the shellac NPs, both in planktonic cells and biofilm treatment experiments.

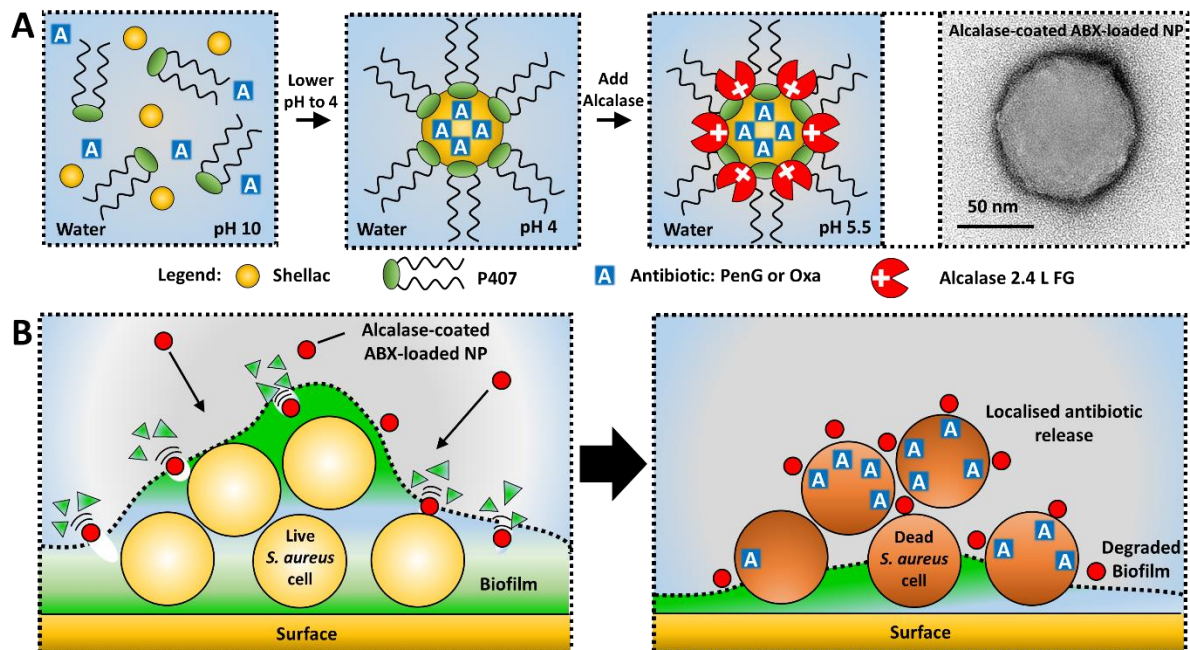


Figure 4.1. (A) Schematic for the synthesis of functionalised shellac NPs as nanocarriers for Benzylpenicillin or Oxacillin (PenG or Oxa). The PenG/Oxa-loaded shellac NPs are sterically stabilised with Poloxamer 407 (P407) and have cationic surface functionality achieved by coating with the cationic protease Alcalase 2.4. L FG. (B) Diagram of the mechanism of action for PenG/Oxa-loaded Alcalase functionalised shellac NPs. Alcalase coating degrades the biofilm exposing the cells and allowing the cationic NPs to adhere to the cell surface. Gradual release of antibiotic is highly localised and results in rapid cell death.

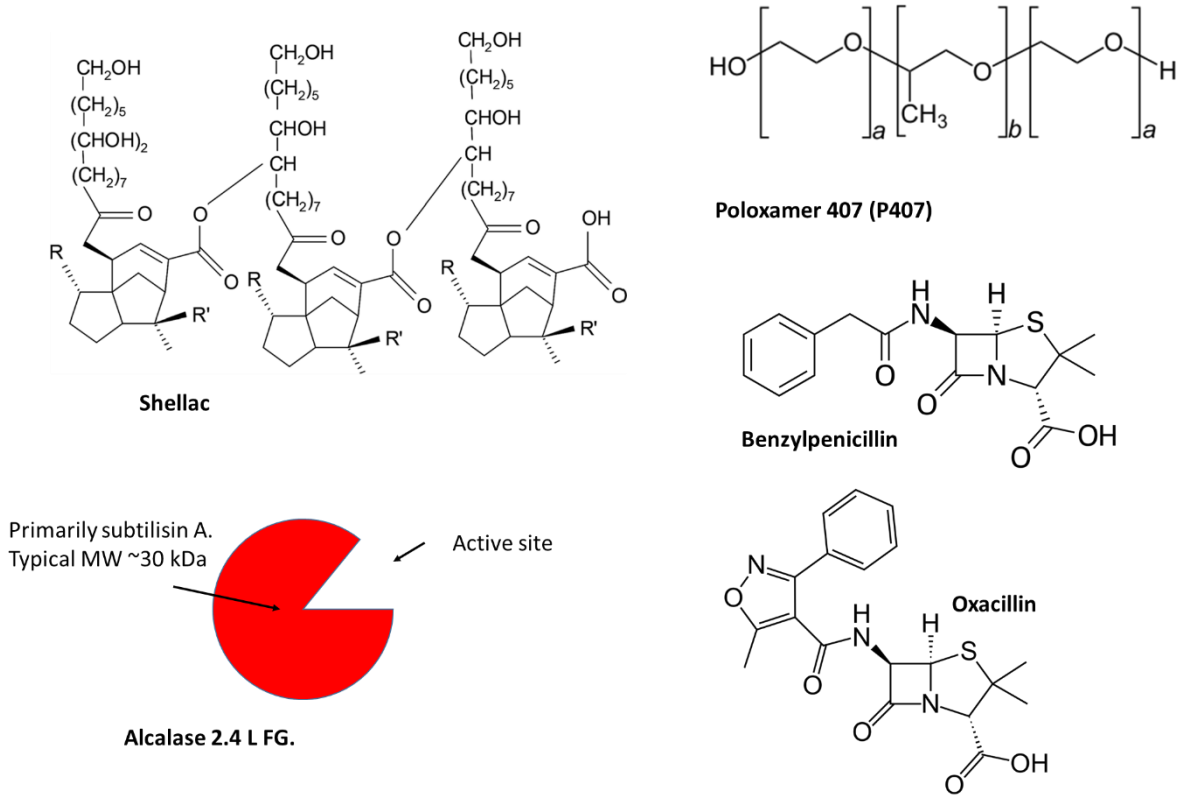


Figure 4.2. Individual components and molecular structures of materials used in the preparation of shellac-P407-PenG/Oxa-Alcalase nanoparticles. Shellac (SSB® Aquagold ammonia salt) R=CHO/COOH, R'=CH₂OH/CH₃, Poloxamer 407 (P407) is a triblock copolymer; consisting of a central hydrophobic block of (b) polypropylene glycol and two hydrophilic blocks of (a) polyethylene glycol. Block lengths; a = ~101 and b = ~56. Alcalase 2.4 L FG is a Serine endo-peptidase with an Isoelectric point ~pH 9 and is cationic below pH 9.

4.2 Materials and methods

4.2.1 Materials

The shellac formulation was kindly provided as a gift by Stroeever Schellack Bremen (SSB) and is commercially available as SSB® AquaGold, an aqueous solution of ammonium shellac salt (25 wt%). Poloxamer 407 (P407) (>99%) was purchased from Sigma-Aldrich, UK. Alcalase 2.4 L FG EC number; 3.4.21.62 was kindly provided as a sample by Novozymes, Denmark. Alcalase 2.4 L FG is a serine endopeptidase (mainly subtilisin A), which performs stereo-selective hydrolysis of amino esters and selective esters. Alcalase also efficiently hydrolyses amino esters, which include heterocyclic amino esters. Optimal conditions for usage are 30–65 °C and pH 7–9. Its enzymatic activity was 2.4 AU A g⁻¹. The protein concentration of Alcalase 2.4 L FG was 55 mg mL⁻¹, determined by a NanoDrop Lite Spectrophotometer (Thermo Scientific, U.K.). *Staphylococcus aureus* subsp. *aureus* Rosenbach (sensitive to Oxacillin) - ATCC® 29213™ was purchased from ATCC. Benzylpenicillin and Oxacillin were supplied by Sigma-Aldrich, UK. Mueller-Hilton Broth (MHB), Mueller-Hilton Agar (MHA), benzylpenicillin (10 U) and oxacillin (5 µg) Antimicrobial Susceptibility Disk were supplied by Oxoid, UK. Dey-Engley neutralising broth was provided by Sigma-Aldrich, UK. A Pierce™ BCA protein assay kit was used to determine protein concentration. Crystal Violet (CV), dye content, ≥ 90% and Acridine Orange (AO) base (≥ 75%) and resazurin sodium salt (75%) were purchased from SigmaAldrich, U.K. Concanavalin A, Alexa Fluor™ 488 Conjugate was purchased from ThermoFisher Scientific, UK. The Beta lactamase Activity Assay Kit (Colorimetric) was purchased from Abcam, UK. HaCaT cells were obtained from AddexBio, T0020001 and HEP G2 cells from the European Collection of Authenticated Cell Cultures (ECACC) at Public Health England, 85011430. Dulbecco's modified Eagle's medium (DMEM), Eagle's minimal essential medium (EMEM) and foetal bovine serum (FBS) were obtained from Gibco, U.K. L-glutamine and trypsin ethylenediaminetetraacetic acid (EDTA) by BioWhittaker, U.K. A 3-(4,5-dimethylthiazol2-yl)-2,5-diphenyltetrazolium bromide (MTT) colorimetric survival and proliferation kit (Millipore Corp., USA) was used for HaCaT and HEP G2 cell viability experiments. Deionised water purified by reverse osmosis and ion exchange with a Milli-Q water system (Millipore, UK) was used in all these studies. Its surface tension was 71.9 mN m⁻¹ at 25 °C, with measured resistivity higher than 18 MΩ cm⁻¹. Consumable plasticware used in the study was purchased from Sarstedt (U.K.), Thermo Scientific (U.K.), or CytoOne (U.K.), unless otherwise stated.

4.2.2 Preparation of PenG/Oxa-loaded P407-stabilised shellac NPs

A stock solution of 25 wt% shellac-ammonia salt was diluted to 0.2 wt% and made up to a volume 50 mL in deionised water, the pH was then raised to 10 using droplets of 0.25 M NaOH and chilled to 4°C for 1 hour. P407 and PenG/Oxa powders were added at various concentrations and

mixed for 30 seconds. Afterwards, the pH was quickly reduced to 4 using 0.25 M HCl to allow the components to precipitate into NPs (temperature kept at 4°C). The final concentration of 0.2 wt% Shellac-0.25 wt% P407-0.1 wt% PenG/Oxa NPs (pH 5.5) was used as a stock preparation and used for further experimentation.

4.2.3 Enzyme surface functionalisation of the 0.2 wt% Shellac-0.25 wt% P407-0.02 wt% AmpB NPs

The stock NP formulation was functionalised with Alcalase 2.4 L FG to create a coating of immobilised protease on the corona of the NPs. The stock solution of Alcalase 2.4 L FG was diluted in deionised water to 0.2 wt% to a volume of 50 mL and sonicated for 15 min to prevent aggregation. 25 mL of this solution was added to 25 mL of AmpB-loaded P407-stabilized shellac NPs dispersion mixed for 30 mins at pH 5.5 to allow an effective coating of the NPs with the cationic protease. Afterwards, the mixture was centrifuged at 8000 *g* for 30 mins to pelletise the NPs. The supernatant was retained for analysis spectroscopic analysis. The pellet was redispersed into 25 mL of deionised water buffered to pH 5.5 (acetate buffer) yielding a stock solution of 0.2 wt% Shellac-0.25 wt% P407-0.02 wt% AmpB-0.2 wt% Alcalase NPs which were used further for NPs characterisation and antimicrobial experimentation.

4.2.4 Shellac NPs hydrodynamic diameter, zeta-potential and TEM characterisation

Particle size distribution and zeta potential were measured using Malvern Zetasizer Nano ZS. The refractive index (RI) of shellac was found to be 1.512 as measured by an Abbe 60 refractometer, and this index and absorbance of 1.000 was used for all measurements. Measurements were repeated three times at 25°C using a quartz cuvette and data represented as the mean. The size of the NPs was examined by TEM. TEM photographs of 0.2 wt% Shellac-0.25 wt% P407-0.02 wt% AmpB-0.2 wt% Alcalase NPs; Particles were prepared and redispersed in deionised water at pH 6. A droplet of the suspended sample was pipetted onto Carbon coated Copper grids (EM Solutions, UK) and allowed to adhere for 2 min. The grid was quickly rinsed with deionised water and negatively stained with 1 wt% aqueous uranyl acetate. This was quickly rinsed with deionised water and allowed to dry in air. The sample was then imaged with a Gatan Ultrascan 4000 digital camera attached to a Jeol 2010 TEM 2010 electron microscope running at 120kV.

4.2.5 Encapsulation efficiency and release kinetics of PenG/Oxa from the shellac NPs

The encapsulation efficiency of PenG/Oxa (formulated as 0.1 wt% PenG/Oxa into 0.25 wt% shellac-0.2 wt% P407 NPs) was examined as a function of concentration. The nanoparticles were centrifuged for 30 min at 8500 *g* to pelletise leaving the supernatant with unencapsulated PenG/Oxa. The absorbance of the supernatant was measured using a spectrophotometer to determine

encapsulation efficiency. The absorbance of the supernatant was compared to a standard curve of PenG/Oxa to calculate the PenG/Oxa retained in the NPs pellet. The supernatant sample and standard curve samples were read at 250 nm, pH 5.5 and room temperature.

Elemental analysis of the NPs pellet was performed using CHN Analyser (Carlo Erba 1108). The pellet was washed with deionised water three times and dried overnight at 60°C to remove any remaining water. This was compared with samples of dried individual components of the NPs (shellac, P407 and PenG/Oxa).

HPLC chromatograms of 0.2 wt% Shellac, 0.25 wt% P407, 0.2 wt% Shellac-0.25 wt% P407-0.1 PenG/Oxa NPs, and 0.1 wt% PenG/Oxa (at various concentrations) were obtained. Data were interpolated from PenG/Oxa peaks in the NP samples compared to PenG/Oxa calibration curves. 20 mL of 0.25 wt% Shellac-0.2 wt% P407-0.1 wt% PenG/Oxa NPs was pelleted and dissolved into 20 mL of acetate buffer (0.1 M, pH 5.5). The supernatant was discarded. 2-fold serial dilutions were made into acetate buffer (0.1 – 0 wt% PenG/Oxa). The samples were sonicated for 5 mins. 20 µL of each sample was injected into a 5 µm C18 column (Phenomenex, UK) and pumped at 1300 psi, 1 mL/min. The mobile phase was ammonium acetate (10 mM, pH 4.5) and acetonitrile in the ratio 75:25 (V:V) under isocratic elution. UV-absorbance at 220 nm was used for sample detection (Perkin-Elmer 785 A UV/VIS Detector, UK). The peak area was measured using Azur software. The same process was used to in PenG/Oxa antibiotic calibration curves.

Release kinetics were also performed as a function of time and temperature over 24 h using the same formulation. 10 mL of the 0.25 wt% Shellac-0.2 wt% P407-0.1 wt% PenG/Oxa NP formulation was placed into a 10-12 kDa MWKO dialysis bag. The dialysis bag was placed into 250 mL of pH 5.5 acetate buffer. 1 mL aliquots were taken at specific time points on the absorbance of the aliquot equated into the concentration of PenG/Oxa in the buffer using a standard calibration curve. Absorption was measured at 250 nm.

4.2.6 Fourier transform infrared (FTIR) and UV-vis spectroscopy analysis

Fourier transform infra-red (FTIR) spectra were taken of Shellac, P407, 0.25 wt% Shellac-0.2 wt% P407 NPs, free PenG/Oxa, and 0.25 wt% Shellac-0.2 wt% P407-0.1 wt% PenG/Oxa NPs. Samples were prepared by removing water using a silica gel desiccant in a vacuum chamber for 1 day, then dried at 60°C for 2 days. The spectra were measured between 4000-600 cm⁻¹ using PIKE ATR diamond settings. A spectrum was obtained with a blank of just air to reduce transmittance interference with the samples. Absorbance spectra of 0.1 wt% PenG and 0.1 wt% Oxa measured between 220 and 1000 nm. Absorbance measurements were taken 250 nm, pH 5.5 and room temperature using a quartz cuvette. Measurements were taken using a PerkinElmer Lambda 25 UV-Vis spectrophotometer.

4.2.7 Bacterial culture

Overnight (O/N) cultures were prepared by incubating a single colony scraped from the MHA stock plates into 10 mL of MHB for 16 hours at 37 °C with 140 rpm (Stuart Orbital Incubator S1500). For all bacterial assays, O/N cultures were adjusted to 0.5 McFarland standard by diluting the O/N culture into 0.85 w/v% sterile saline until an optical density of 0.08–0.12 at 625 nm was obtained using a spectrophotometer (FLUOstar Omega spectrophotometer, BMG Labtech). These adjusted bacterial saline suspensions were then diluted 1:150 into MHB to yield starting concentrations between 5×10^5 and 1×10^6 colony forming units per mL (CFU mL⁻¹).

4.2.8 Time Kills

Killing curves were constructed against planktonic *S. aureus* to determine the time taken for the active agent in influencing total bacterial cell populations. O/N cultures were prepared yielding 10 mL of MHB aliquots with 5×10^5 – 1×10^6 cells per mL. 10 mL of 0.25 wt% Shellac-0.2 wt% P407-0.1 wt% PenG/Oxa-0.2 wt% Alcalase NPs were added to each tube and incubated for 24 hours at 37 °C with 140 rpm. Experiments with other constituents of the NPs and free PenG/Oxa antibiotics at equivalent concentrations were performed for comparison. At time points 0, 0.5, 1, 2, 3, 4, 6, and 24 hours, a 100 µL sample was removed from each treatment tube and added to 900 µL of Dey-Engley Neutralising broth. 100 µL aliquots from each serial dilution tube were plated onto MHA plates and incubated for 24 hours at 37 °C and enumerated. The time-kill assay was repeated in three independent experiments.

4.2.9 Minimum inhibitory and bactericidal concentration (MIC/MBC)

The bacteriostatic and bactericidal properties of the 0.25 wt% Shellac-0.2 wt% P407-0.1 wt% PenG/Oxa-0.2 wt% Alcalase NPs and its spectrum of activity were measured in comparison to equivalent concentrations of free PenG and Oxa. Briefly, O/N cultures of *S. aureus* were prepared as described above. 100 µL of each strain suspension was added to the wells of a 96-well microtiter plate yielding 5×10^4 – 1×10^5 cells per well. Aliquots of 0.25 wt% Shellac-0.2 wt%P407-0.1 wt% PenG/Oxa-0.2 wt% Alcalase NPs were prepared. This was centrifuged at 8000 *g* for 5 minutes and re-suspended into 10 mL of MHB. 2-Fold dilutions of this suspension were prepared in separate aliquots and 50 µL added to descending rows of bacteria on the microtiter plate. Equivalent 2-fold dilutions of the free ABX were added to separate columns for comparison (50 µL per well). The plates were incubated for 24 hours at 37 °C. 20 µL of resazurin sodium salt (0.15 mg mL⁻¹ in DPBS) was added to each well and incubated at 35 °C for 2 hours. The absorbance was recorded using a spectrophotometer (FLUOstar Omega spectrophotometer, BMG Labtech). The resazurin in the presence of viable cells is reduced to resorufin by the bacterial co-enzyme NAHD, indicating that the cells remain metabolically active and viable. The

MIC was determined to be the lowest concentration of active antimicrobial agent which inhibited the growth of each strain. The same procedure was performed to obtain the MBC, minus the addition of resazurin. Instead, 100 μ L from each well was streaked onto MHA and incubated for 24 hours at 37 °C. The MBC concentration was determined from samples in which no CFU was detected. The MIC/MBC assay was repeated in three independent experiments.

4.2.10 Antimicrobial susceptibility testing (AST)

A VITEK[®] 2 (bioMérieux, FRA) microbial identification system was used to profile the susceptibility and resistance of *S. aureus* against a range of antibiotics. VITEK 2 GP (21342) and VITEK 2 ASTP635 (416911) Gram-positive identification and AST cards were used. A suspension of *S. aureus* was created by placing a single colony into 3 mL of 0.45 wt% saline and briefly vortexed. A DensiCHECK[™] was used to measure the optical density of the suspension, the suspension was adjusted with 0.45 wt% saline until a 0.5 McFarland was obtained (in accordance with the VITEK2 protocol). The adjusted suspension was placed into the machine and a capillary tube inserted. The analysis was left to run overnight (typical analysis time of 6 to 12 h). The procedure was performed on 3 separate occasions to confirm the results. Post analysis, the isolates were subcultured on to Columbia blood agar plates to check purity. For further confirmation of the susceptibility and resistance results of PenG and Oxa specifically, disk diffusion AST was performed. Briefly, a single colony of *S. aureus* was isolated and placed into 10 mL of MHB and grown overnight at 37 °C. The bacteria suspension was then diluted to a 0.5 McFarland standard in MHB by measuring the turbidity at 625 nm yielding $1-2 \times 10^8$ CFU mL⁻¹. A cotton swab was used to streak an MHA plate lawn. 4 ± 0.5 mm deep MHA plates were prepared by adding 25 mL of molten MHA to a 9 cm round plate and left to solidify at room temperature. PenG (10 U) and Oxa (5 μ g) antibiotic disks (both Oxoid, UK) were applied to the MHA plates using a disk dispenser (Oxoid, UK), and the plates were incubated for 18 hours at 35 ± 1 °C, following EUCAST guidelines. The zone of inhibition diameters were illuminated using a lightbox and the images were measured in mm using a ruler; the diameter was measured across 3 lines and the mean was determined to be the zone of inhibition.

4.2.11 SEM imaging of the treated cells

S. aureus cells were removed from their media by centrifugation at 2000 *g* for 5 mins. The Cells were then washed thrice and resuspended in PBS buffer. A 1 wt% glutaraldehyde PBS buffer solution, applied for 1 hour, was used to fix the cells. The centrifugation and washing process was repeated to remove excess glutaraldehyde. The cells were dehydrated in 50%/75%/90% and absolute ethanol solutions for 30 mins per ethanol concentration. A sterile swab was used to transfer cell to a glass slide and place into absolute ethanol and dried using liquid CO₂ at its critical point using an E3000

Critical Point Dryer (Quorum Technologies, UK) and then coated in 10 nm Carbon. The samples were imaged using an Ultra-High-Resolution Scanning Electron Microscope using cold field emission (Hitachi SU8230, Japan).

4.2.12 TEM and EDX imaging of the treated cells

TEM images of untreated *S. aureus*, and *S. aureus* treated with 0.1 wt% PenG and 0.1 wt% PenG-NPs for 1 hour were obtained by placing a droplet of the suspended sample onto carbon-coated copper grids (EM Solutions, U.K.) and allowed to adhere for 2 min. The grid was quickly rinsed with deionised water. Negative staining was omitted to reduce interference during EDX analysis. The sample was left to dry in air then imaged with a Gatan UltraScan 4000 digital camera attached to the Jeol 2010 TEM 2010 electron microscope (Jeol, Japan) running at 120 kV. Energy-dispersive X-ray (EDX) data was collected via an Oxford Instruments Nanoanalysis X-Max 65-T detector and the INCA software.

4.2.13 Beta lactamase activity

The ability of *S. aureus* to produce beta lactamase was first verified. Beta lactamase strips were used for acidimetric detection of penicilloic acid, produced when benzylpenicillin (PenG) is hydrolysed by beta lactamase enzymes. The plastic strip contains an active zone saturated with penicillin G and an acid-basic indicator. Three colonies of *S. aureus* and *S. epidermidis* (positive control) were placed into 1 mL of moistening solution (from the kit) and a test strip was added. The bacterial suspension was incubated at room temperature for 10 minutes with shaking. A colour change from pink to yellow indicates the presence of penicilloic acid. A beta lactamase activity kit was used to analyse *S. aureus* after treatments. *S. aureus* samples were obtained after no treatment, or after treatment with either 0.1 wt% PenG, 0.25 wt% shellac-0.2 wt% P407-0.1 wt% PenG-0.2 wt% Alcalase NPs, or 0.2 wt% Alcalase at 1, 2 and 3 hour time points. No treatment was used as a control (3 hours). The experiment was capped at 3 hours due to lack of remaining cells to analyse. Treatments were administered at 37°C to planktonic *S. aureus* with constant shaking. Post treatment, *S. aureus* samples were obtained by centrifugation at 10000 g for 10 mins in a pre-weighed centrifuge tube. The supernatant was removed (used as contaminated media measurements) and the pellet weighed. The pellet was resuspended into beta lactamase buffer using 5 µL of buffer per mg of bacteria. The resuspended bacteria were sonicated for 5 mins and the sample kept chilled on ice. Further insoluble material was removed by centrifugation at 16000 g at 4°C for 20 mins. The supernatant (typically 5 µL) was added to the wells and adjusted to a final volume of 50 µL/well using beta lactamase assay buffer. A positive control was made by 5-fold dilution of 2 µL of positive control to 8 µL of beta lactamase buffer. 5 µL was added to the well and adjusted to a volume of 50 µL/well using beta lactamase assay

buffer. To measure the beta lactamase activity of the contaminated media, 30 μL of the bacterial supernatant was added to a well and adjusted to a volume of 50 μL using beta lactamase buffer. All assays were performed using a reaction mix comprised of 2 μL nitrocefin and 48 μL beta lactamase assay buffer. 50 μL of the reaction mix was added to each well, including the positive control and gentle mixed with the pipette tip. This yielded a final volume of 100 μL /well for all samples. The absorbance of the samples was taken kinetically from 0 to 60 mins and room temperature protected from light (within the spectrophotometer) at 490 nm and calibration graphs plotted showing absorbance over time. The beta lactamase activity of *S. aureus* (PenG, PenG-NPs, or Alcalase after 1 h, 2 h or 3 h treatment, or untreated after 3 hours) was expressed as mg of protein and calculated as;

$$\text{Beta Lactamase Acitivity} = \frac{B}{T2 - T1 * V} * D$$

= nmol/min/mL = mU/mL

where:

B = Amount of hydrolysed nitrocefin from calibration curve

T1 = Time of first absorbance reading in mins

T2 = Time of second absorbance reading in mins

V = Volume added into the reaction well (mL)

D = Sample dilution factor

Unit definition: 1 Unit Beta Lactamase activity = amount of enzyme that generates 1 μmol of nitrocefin per minute at pH 7 at 25°C

4.2.14 Preparation of microtiter *S. aureus* biofilms

100 μL of (5×10^5) - (1×10) CFU mL^{-1} O/N *S. aureus* culture (MHB) was pipetted into 96-well tissue culture (TC)-treated plates and incubated at 37 °C for 24 h in static conditions to allow biofilm formation. Afterwards, the media was aspirated away by pipetting from the side of the well so reduce potential damage from the pipette tip. The biofilms were washed three times using 300 μL of sterile PBS to remove any detached planktonic cells (leaving only sessile cells behind).

4.2.15 Crystal Violet staining, biofilm weight and biofilm protein concentration after treatments

Samples of *S. aureus* biofilms grown for 24 h at 37°C were treated with 0.25 wt% Shellac-0.2 wt% P407-0.1 wt% PenG/Oxa-0.2 wt% Alcalase NPs and their individual components for a further 24

h. Three 96-well plate techniques were used to assess biofilm degradation after treatment; Crystal Violet (CV) staining of the biofilm mass, dry biofilm mass weight and protein concentration. Biofilms were prepared as described above. 100 μL of the stock treatment was added to the wells and incubated at 37°C for 24 h. Afterwards, the treatment was aspirated away, and the plate washed twice by submersion in deionised water. The plate was gently shaken to remove water and left to air dry for 15 mins in an inverted position. For CV staining 125 μL of 0.1 wt% CV solution was added to each well and incubated at room temperature for 15 mins. The plates were then again washed by water submersion to remove excess dye and then left to air dry for 2 h. 30 wt% acetic acid was used to solubilise the CV and 100 μL of this solution was transferred to a new plate and the absorbance read at 570 nm. The readings were blanked against 30 wt% acetic acid and the results compared to normalised controls. For biofilm dry mass measurements, the treatment was again aspirated away. The plates were then left to dry overnight at 60°C. After drying the plate was weighed on a balance and the weight subtracted from the empty plate weight to give a measurement of dry mass biofilm remaining. A Protein Assay Kit (Pierce, USA) was used to determine sample protein content. The treatment was aspirated away and the biofilm was three times in deionised water. The biofilm was scrapped from the wells and placed into a glass test tube with 1 mL of deionised water. The mixture was sonicated in a water bath for 30 min then vortexed with glass beads for 2 min to completely disperse the biofilm. 25 μL of the sample was placed into a 96-well plate. 200 μL of the protein concentration determination working reagent (reagent A: reagent B. 50:1) was added to the wells and incubated for 30 min at 37°C with constant shaking. Absorbance was measured at 572 nm. Results were compared to a calibration curve of fixed protein concentrations prepared as per manufacturer's instructions. All tests were performed in triplicates (N = 3 with \pm S.D.).

4.2.16 *S. aureus* cellular viability after PenG/Oxa-NP treatments

To measure *S. aureus* cellular viability after treatment with PenG/Oxa-NPs and free ABX treatments on biofilms, a filter membrane method was employed. Millipore Express PLUS membrane filter paper sections (2 cm^2) were placed on to MHA. An overnight culture was adjusted to 1×10^5 CFU mL^{-1} in saline, and 20 μL of this culture added as a droplet to the centre of the filter paper. The sample was then incubated for 24 h at 37 °C to allow a colony biofilm to form. After 24 hours, the membranes were placed onto fresh agar plates (3 mm deep) into a six-well plate and 1 mL of treatment added to each well. The plate was gently shaken in the incubator during treatment. Deionised water (1 mL) was considered the growth control. After 24 h of treatment, the membrane filter paper was peeled from the agar wells and placed into the sample tube with 1 mL of fresh MHB and 2 cm of sterile glass beads, enough to cover the sample. Each sample was vortexed for 30 s at high speed to disintegrate the biofilm and inoculated the MHB with cells. 1 mL of the treatment media was retained for viability

analysis. The drop plate enumeration method was used to measure cell viability in CFU mL⁻¹. To measure the viability of cells within the biofilms, 10-fold dilutions were made in fresh MHB, 10 µL droplets were placed on to MHA plates and grown for 24 h at 37 °C. CFUs were counted from the last two droplets, which contained a countable number of colonies (3–30 colonies per 10 µL drop), and averaged.

4.2.17 *S. aureus* fluorescent images, biofilm quantification and confocal scanning laser microscopy

Acridine Orange (AO) was used to stain *S. aureus* biofilms, treated with PenG-Oxa-NPs and individual constituents. Biofilms were formed and treated as described above (CV staining method). The cleaned treated samples were stained with 100 µL of 0.2 wt%, AO in darkness for 5 minutes with gentle shaking. After incubation, the plate was washed three times with deionised water and allowed to air dry for 15 min. The samples were examined using an Olympus BX51 fluorescent microscope with a DP70 digital camera. The percentage of biofilm stained with OA was quantified using ImageJ v1.52d. For 3D visualisation, filter paper membrane biofilms were gently placed onto a glass slide using sterile forceps, and stained with AO as described above for the CV biofilms. Confocal laser scanning microscopy images (CLSM) were obtained with a Carl Zeiss LSM 710 confocal microscope with Z-series images taken in 1-µm slices.

4.2.18 Cryostat sectioning of *S. aureus* biofilm

Membrane biofilms were prepared and treated as described above. Post treatment the membrane was carefully removed from the agar and gently washed with DPBS. A small amount of OCT embedding matrix (CellPath, UK) was placed into a plastic cassette and allowed to settle into a flat viscous liquid. Afterwards, using forceps the membrane paper with the treated biofilm on top was placed onto the OCT and then submerged in more OCT. The cassette was then snap frozen in liquid nitrogen for 5 minutes. The samples stored at -80°C until sectioning. OCT embedded samples were cryosectioned at 10 µm (CM9900, Leica Biosystems) and placed onto positively charge microscope slides (CellPath, UK). Before imaging, the slides were fixed with cold acetone (-20°C) for 2 mins and left to evaporate at room temperature (15 mins). Finally, the slide was washed gently in PBS to remove any residual OCT and left to evaporate at room temperature (15 mins). The samples on the slides were stained with ConcanavalinA (ConA) for 30 minutes in darkness before gently washing excess dye away with deionised water. ConA was prepared to a 5 mg/mL concentration in deionised water and centrifuged at 5000 g for 5 mins before used to remove any aggregated proteins in the solution, only the supernatant was used to stain the samples. Bright-field and fluorescence microscopy of the section biofilms was performed on an Olympus BX51 (Japan).

4.2.19 Cytotoxicity and of HaCaT and HEP G2 cells after treatment with shellac, P407, free Alcalase, free PenG/Oxa and PenG/Oxa-NPs

HaCaT and HEP G2 cells were cultured in a T75 flask using DMEM (HaCaT) or EMEM (HEP G2) supplemented with 10% FBS and 1% L-glutamine under humidified conditions at 37 °C, 5% CO₂. When a confluency of 80% was achieved, determined by visualisation with an optical microscope, passaging was performed to ensure that the cells remained in the exponential phase for experimentation. Passaging was performed by removing spent media, washing in DPBS, and incubating with 1× trypsin EDTA at 37 °C 5% CO₂ for 5 min until the cells were detached in suspension. The trypsin EDTA was then neutralised with a 1:1 volumetric ratio of fresh DMEM and gently centrifuged at 400 g for 4 min, the supernatant was aspirated, and the pellet was resuspended in DMEM (supplemented as above) at a 1:6 ratio and transferred into a fresh T75 flask. Surplus cells used for experimentation were diluted in fresh DMEM or EMEM, supplemented with 2% FBS and 1% L-glutamine, seeded at 5×10^4 in 100 µL of media, placed into a 96-well plate, and incubated for 24 h at 37 °C 5% CO₂. The medium was then removed, and the cells are replaced with 100 µL of treatment-infused DPBS. DPBS was used so DMEM/EMEM peptones did not interfere with the true activity of the Alcalase. The treatments with only DPBS were used as a control, 0.25 wt% shellac, 0.2 wt% P407, 0.2 wt% Alcalase, 0.1 wt% free PenG/Oxa and 0.1 wt% PenG/Oxa-NPs treatments were performed for 1 h, 6 h, and 24 h time points.

A colorimetric (MTT) cell survival and proliferation assay kit was used to measure cell viability. Treatment culture was aspirated away, and the cells washed for 2 min with fresh DPBS. Fresh DMEM/EMEM (100 µL) was added after which 100 µL of MTT reagent (50% 3-(4,5-dimethylthiazol2-yl)-2,5-diphenyltetrazolium bromide and 50% PBS) was added. This was incubated in the same conditions for 2 h until intracellular purple formazan crystals were visible under a light microscope. After 2 h, 100 µL of the colour development reagent in isopropanol with 0.04 M HCl was added for 1 h, allowing the cells to lyse and the formazan crystal to be solubilised to a homogenous blue solution. The absorbance of the blue solution was read at 570 nm on a plate reader and subtracted from a blank of media only. These data were calculated into cell count data via interpolation from the standard curve (absorbance values from a fixed number of cells in media (see **Figure 4.35**). The data was represented as viability percentage of the control which was normalised to 100%. The HaCaT/HEP G2 cell viability assay was repeated in three independent experiments.

4.2.20 Statistical analysis

Data were expressed as average values \pm standard deviations of the mean. P-Values of less than 0.05 were considered significant. All One-Way ANOVAs, Tukey's post-test and Student T-tests statistical analysis were performed in GraphPad v7.0.4.

4.3 Results and discussion

4.3.1 NP characterisation: Preparation, encapsulation efficiency, release kinetics and Alcalase functionalisation of PenG/Oxa-loaded shellac NPs

Figure 4.3A and B shows the particle size and zeta potential of 0.25 wt% shellac-0.2 wt% P407 NPs precipitated at pH 5.5 with various concentrations of PenG (0 to 0.1 wt%). The mean hydrodynamic diameter with no PenG was ~70 nm, increasing slightly up to 80 nm when synthesised with 0.1 wt% PenG. The zeta potential ranged from -19 mV to -15 mV when prepared with 0 to 0.1 wt% PenG. This is due to the residual -COOH groups within shellac which deprotonate in acid conditions yielding a negative zeta potential. **Figure 4.3C and D** shows the same hydrodynamic diameter and zeta potential of the same 0.25 wt% shellac-0.2 wt% P407 NP precipitated with oxacillin. Similar to the penicillin NP size, a range of between 70-80 nm was observed, increasing with higher concentrations of oxacillin, up to 0.1 wt%. The same is true of the zeta potential which is ranges -20 to -10 mV as the oxacillin concentration is increased. The 0.25 wt% shellac-0.2 wt% P407 was chosen as the optimum ratio for antibiotic encapsulation, as this yielded NPs with a size and zeta potential of 70 nm and -20 mV, typical of P407 sterically stabilised NPs.³³ Higher concentrations of P407 have previously shown that the size does not increase, however, the zeta potential is reduced, likely due to offsetting of the shear plane position by the accumulation of PEO chains from the P407, which is covering the COO⁻ groups negative surface charge. This would deleteriously affect the subsequent surface functionalisation of the NPs with the cationic protease Alcalase 2.4 L FG. **Figure 4.4B** shows a 0.25 wt% shellac-0.2 wt% P407 NP TEM image which is approximately 70 nm. **Figure 4.22C and D** show the same NP composition formulated with 0.1 wt% PenG or Oxacillin, with the size increased to 80 nm. These images are in agreement with the DLS data. The encapsulation of PenG and oxacillin was accomplished by mixing the materials at pH 10 and quickly reducing the pH to 4, allowing the rapid precipitation of the compounds. **Figure 4.5** shows when this procedure is carried out at 4°C there is an increased encapsulation efficiency of both PenG and oxacillin across a concentration range of 0.01 to 0.1 wt%, compared to preparation at 23°C (room temperature). At 4°C the encapsulation efficiency of PenG and oxacillin was ~75%, however, the same preparation at 23°C was ~50%. This is likely due to the decreased tendency for the particles to aggregate and agglomerate at room temperature during preparation. Additionally, lowering the temperature decreases the dissociation constant of the -COOH groups of both shellac acid (of which shellac is made) and the PenG & Oxa. At 4°C and pH 4 all these species are less dissociated than at 23°C. At pH 10 they are all charged. Encapsulation efficiency is increased when the pH is dropped to 4 (at 4°C) as the species are less charged and therefore have a reduced tendency to repel at short distances, than they would if the shellac acid, PenG and Oxa had a higher fraction that was ionised.

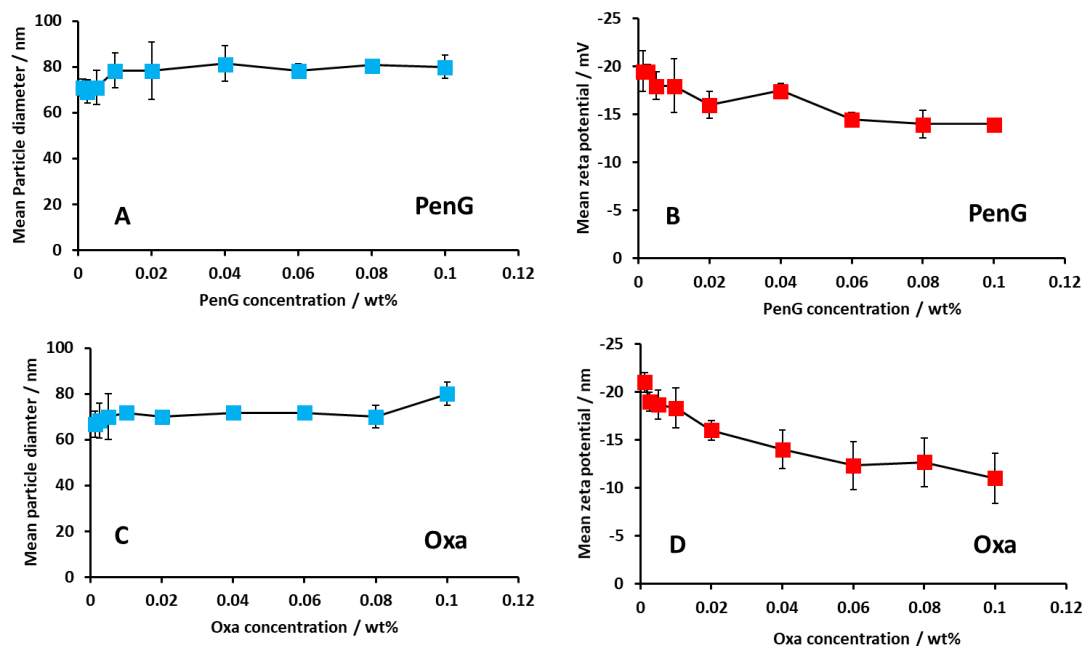


Figure 4.3. Size and zeta potential of different concentrations of penicillin G or oxacillin into 0.25 wt% shellac-0.2 wt% P407 NPs. **(A)** Shows size and **(B)** zeta potential of different concentrations of Penicillin G, **(C)** shows size and **(D)** zeta potential of different concentrations of Oxacillin. Measurements were taken at pH 5.5, 25°C, RI 1.516, Abs 1.000 using a Malvern Zetasizer Nano ZS. Each value represents a triple replicate with \pm S.D.

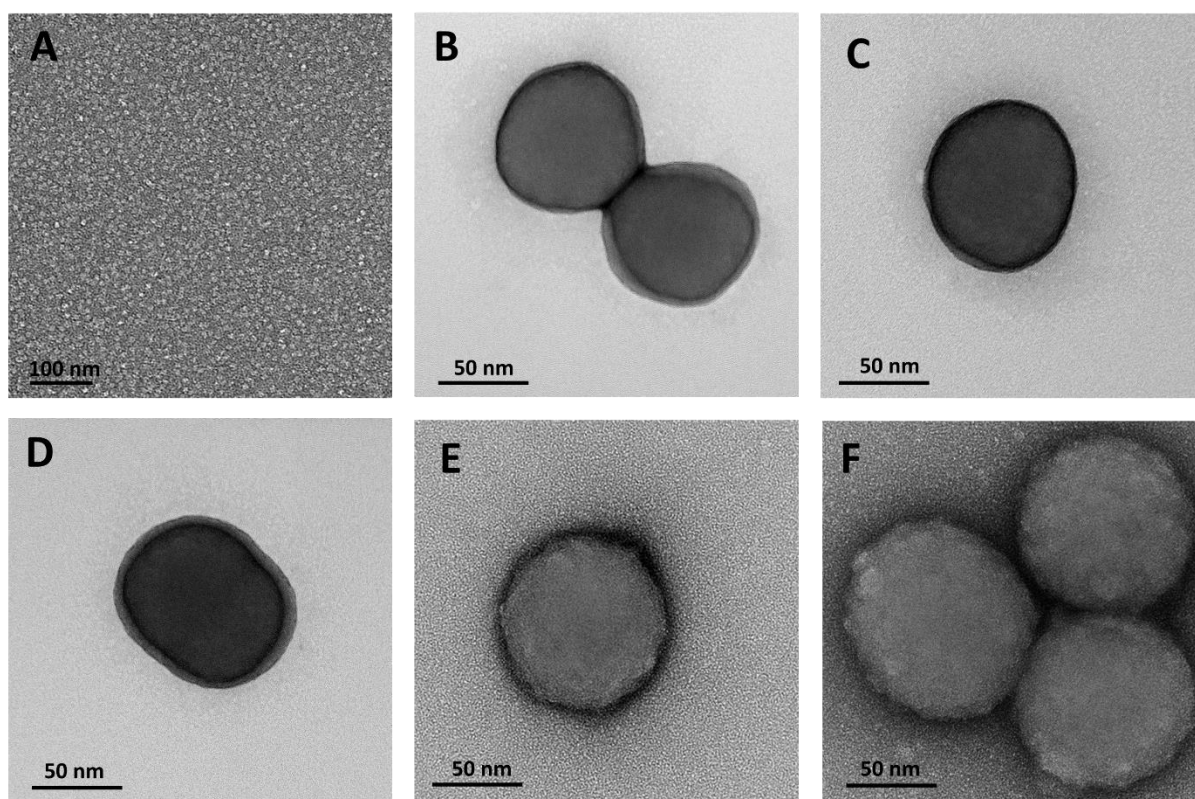


Figure 4.4. TEM photographs of **(A)** Alcalase 2.4 L FG, **(B)** 0.25 wt% Shellac-0.2 wt% P407 NPs, **(C)** 0.25 wt% Shellac-0.2 wt% P407-0.1 wt% PenG NPs, **(D)** 0.25 wt% Shellac-0.2 wt% P407-0.1 wt% Oxa NPs, **(E)** 0.25 wt% Shellac-0.2 wt% P407-0.1 wt% PenG-0.2 wt% Alcalase NPs and **(F)** 0.25 wt% Shellac-0.2 wt% P407-0.1 wt% Oxa-0.2 wt% Alcalase NPs.

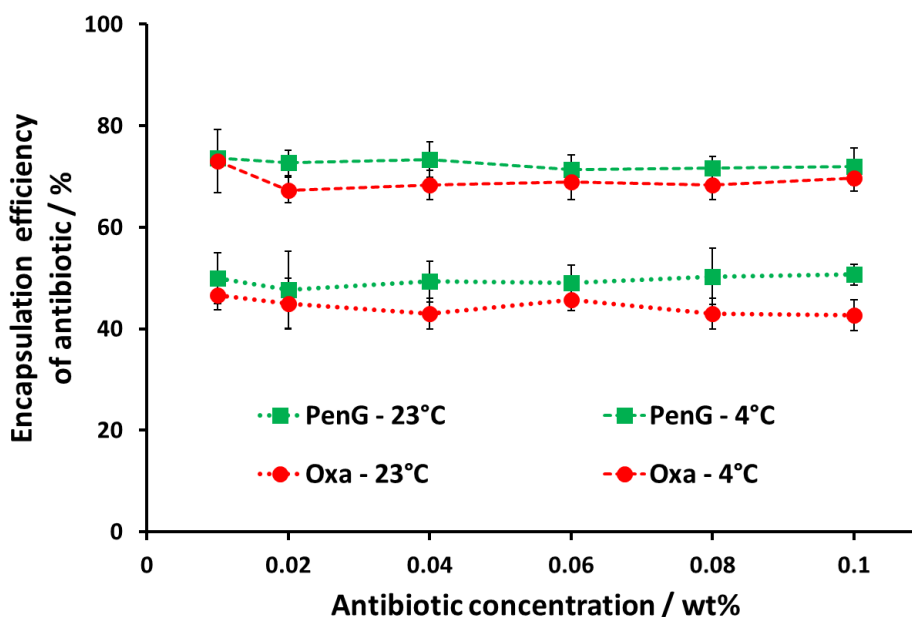


Figure 4.5. Encapsulation efficiency of varied concentrations of penicillin G and oxacillin into 0.25 wt% shellac-0.2 wt% P407 NPs. The shellac solution was adjusted to pH 10 and incubated at 23°C and 4°C for 1 hour to reach temperature. The P407 and antibiotic was then added, and the solution quickly reduced to pH 4. The mixture was then incubated at either 23°C or 4°C for 5 mins. Afterwards, the precipitated NP dispersion was increased to pH 5.5. pH adjustments were made using drops of 0.25 M HCl or 0.25 M NaOH. The nanoparticles were centrifuged for 30 minutes at 8500 g to pelletise leaving the supernatant with unencapsulated AmpB. Absorbance (250 nm) of the supernatant was measured using a spectrophotometer to determine encapsulation efficiency. The follow equation was used to calculate the encapsulation efficiency;

$$\text{Encapsulation efficiency} = \frac{\text{total antibiotic} - \text{unencapsulated antibiotic}}{\text{total antibiotic}} * 100$$

The encapsulation efficiency was measured by analysing the supernatant after the NPs were pelletised and comparing the absorbance vs a calibration curve created with solutions of PenG and oxacillin (**Figure 4.6A and B** respectively). **Figure 4.7** shows the absorbance spectra of PenG and oxacillin had a λ_{max} of ~250 nm, typical of colourless organic solutions. HPLC was used to provide further evidence of the encapsulation efficiency of PenG and oxacillin to shellac-P407 NPs. This was performed by directly measuring the concentration of antibiotic within the NP, rather than indirectly measuring the concentration not encapsulated in the supernatant (absorbance measurements). The supernatant was discarded from the antibiotic NPs and the NP re-dissolved into acetate buffer and the antibiotic allowed to fully defuse out of the NP. **Figure 4.8A and B** show the chromatographs of 0.1 wt% PenG and 0.1 wt% oxacillin NP formulations, which had a retention time of 4 and 5.5 minutes respectively. **Figure 4.9A and B** show HPLC peak area calibration curves created using PenG and oxacillin solutions (0 to 0.1 wt%). **Figure 4.9C** shows an encapsulation efficiency of ~75% was achieved

by comparing the 0.1 wt% PenG/Oxa-NP formulation against the antibiotic solutions and is in agreement with encapsulation data obtained using absorbance measurements. **Table 4.1** shows the elemental ratios of carbon, hydrogen, nitrogen and sulphur in 0.25 wt% shellac-0.2 wt% P407-0.1 wt% PenG/Oxa NPs and compared to the elemental ratios of the individual components. PenG and oxacillin show a sulphur content of 8.67 and 6.72%. Shellac showed sulphur content of 0.12%, likely from the chemical isolation of the compound from resin the product is derived from, as the chemical structure contains no sulphur. However, when analysing the sulphur content of the 0.25 wt% shellac-0.2 wt% P407-0.1 wt% PenG/Oxa NPs it was shown to be 1.44 and 1.11%, with the additional sulphur coming from the antibiotics. Unfortunately, due to the sulphur content in the shellac sample alone a quantitative concentration of antibiotic encapsulation cannot be obtained, however, this data does indicate the presence of PenG and oxacillin in the NP qualitatively. **Figure 4.10** shows the FTIR spectra of shellac, P407, PenG, oxacillin and 0.25 shellac-0.2 wt% P407-0.1 wt% PenG/Oxa NPs. The shellac and P407 samples show an abundance of peaks in the range between 1600-1000 cm^{-1} due to the presence of C-O bonds within the compounds. The PenG and oxacillin samples also show an abundance of peaks between the 1600-1000 cm^{-1} range. P407 has strong peak at 1100 cm^{-1} from the $\text{CH}_2\text{-O-CH}_2$ ether groups. This prominent peak is present in the shellac-P407-antibiotic NP formulation, however it is small likely due to the central hydrophobic polypropylene glycol block absorption on the shellac NP surface. The complexity of the shellac and P407 chemical structures makes unique peaks from the antibiotic encapsulated within the NPs difficult to detect. However, it does show that shellac and P407 have complexed into a NP. For additional NP characterisation an investigation into the elemental composition of the antibiotic encapsulated NPs, and the individual components that the NPs are comprised of was performed. Sulphur was chosen as the element of interest as it is present in the chemical structures of PenG and Oxa, but not the chemical structures of shellac and P407 (see **figure S1** for chemical structures). CHN(S) elemental analysis of shellac showed negligible amounts of sulphur, likely derived from the manufacturing process, however, this was not detected by Energy-dispersive X-ray spectroscopy (EDX) analysis.

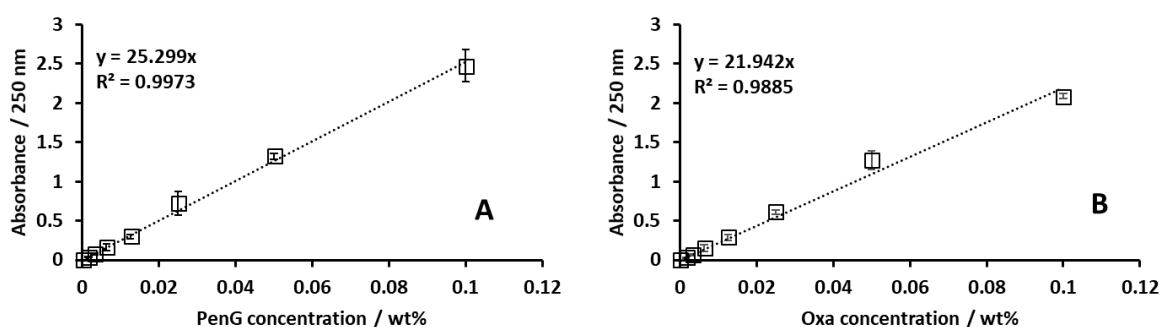


Figure 4.6. Standard calibration curves of difference concentrations of **(A)** Penicillin G and **(B)** Oxacillin. Absorbance measurements were taken 250 nm, pH 5.5 and room temperature.

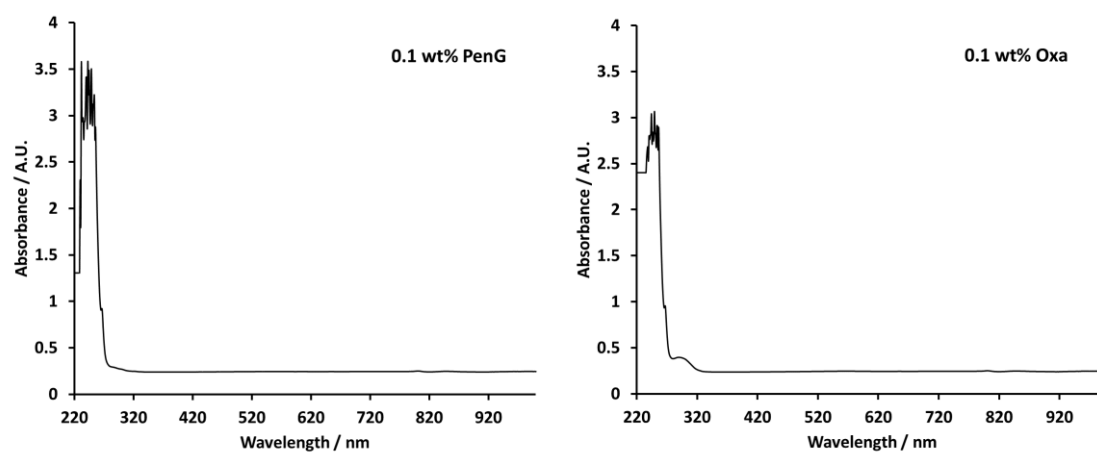


Figure 4.7. Absorbance spectra of PenG and Oxa measured between 220 and 1000 nm. Absorbance measurements were taken 250 nm, pH 5.5 and room temperature using a quartz cuvette. Measurements were taken using a PerkinElmer lambda 25 UV-Vis spectrophotometer.

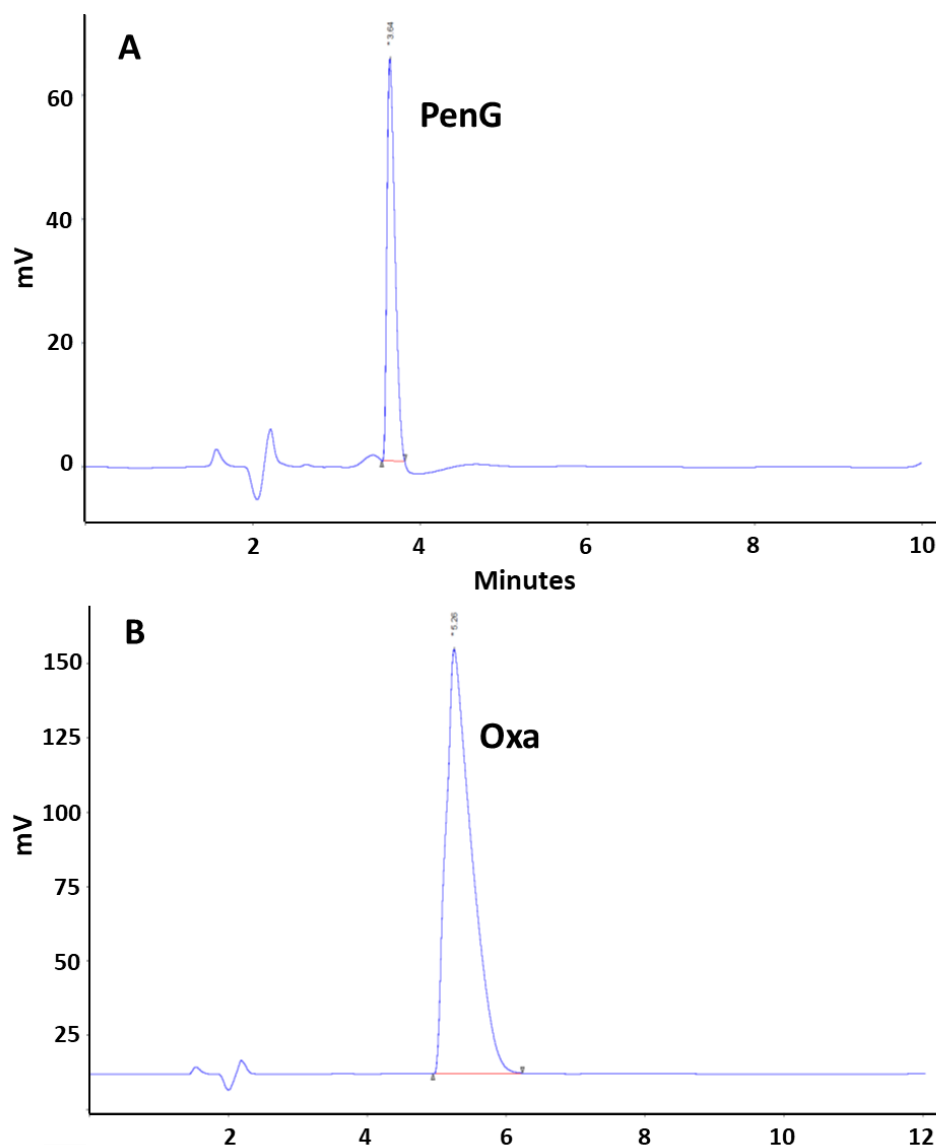


Figure 4.8. HPLC chromatograms of (A) PenG - 1mg/mL (0.1 wt%) and (B) oxacillin - 1mg/mL (0.1 wt%) shown for illustrative purpose.

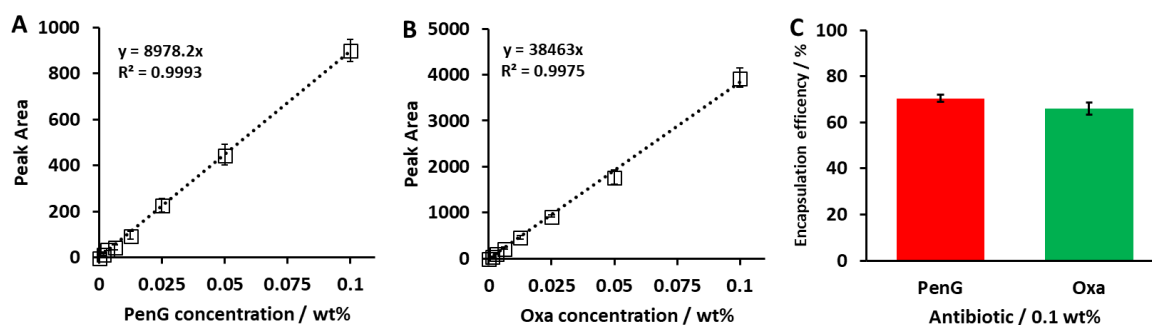


Figure 4.9. PenG (A) and Oxacillin (B) HPLC calibration curves. Calibration curves were obtained from 0 to 0.1 wt% PenG/Oxa dissolved into acetate buffer. (C) Shows the encapsulation efficiency of 0.25 Shellac-0.2 wt% P407-0.1 wt% PenG/Oxa NPs. Data was interpolated from PenG/Oxa peaks in the NP samples compared to PenG/Oxa calibration curves. 20 mL of 0.25 wt% Shellac-0.2 wt% P407- 0.1 wt% PenG/Oxa NPs were pelleted and dissolved into 20 mL of acetate buffer (0.1 M, pH 5.5). The supernatant was discarded. 2-fold serial dilutions were made into acetate buffer (0.1 – 0 wt% PenG/Oxa). The samples were sonicated for 5 mins. 20 μ L of each sample was injected into a 5 μ m C18 column (Phenomenex, UK) and pumped at 1300 psi, 1 mL/min. The mobile phase was ammonium acetate (10 mM, pH 4.5) and acetonitrile in the ratio 75:25 (V:V) under isocratic elution. UV absorbance at 220 nm was used for sample detection (Perkin-Elmer 785 A UV/VIS Detector, UK). The peak area was measured using Azur software. The same process was used to in PenG/Oxa antibiotic calibration curves.

Table 4.1. Elemental analysis of 0.25 wt% shellac-0.2 wt% P407-0.1 wt% PenG/Oxa NPs, and the individual components. The PenG/Oxa content in the nanoparticle is calculated based on the sulphur (32.065 m_a) content of PenG/Oxa. NP samples were prepared and pelleted, and dried overnight under vacuum at room temperature to leave the dry mass of the encapsulated NP.

Element	Shellac / %	P407 / %	PenG* / %	Oxa** / %	0.25 wt% shellac-0.2 wt% P407-0.1 wt% PenG / %	0.25 wt% shellac-0.2 wt% P407-0.1 wt% Oxa / %
C	27.42	56.01	53.62	51.61	45.11	42.66
H	9.09	10.57	4.95	4.74	8.56	8.79
N	0.97	0.22	7.95	9.54	6.55	7.06
S	0.12	0	8.67	6.72	1.44	1.11
% PenG content in shellac-P407 NPs						15.04%
% Oxa content in shellac-P407 NPs						13.92%

*Penicillin G – 334.4 g/mol, $C_{16}H_{18}N_2O_4S$, **Oxacillin – 401.4 g/mol, $C_{19}H_{19}N_4O_5S$

PenG calculation; $(1.44/32)*334.4 = 15.048$

Oxa calculation; $(1.11/32)*401.4 = 13.923$

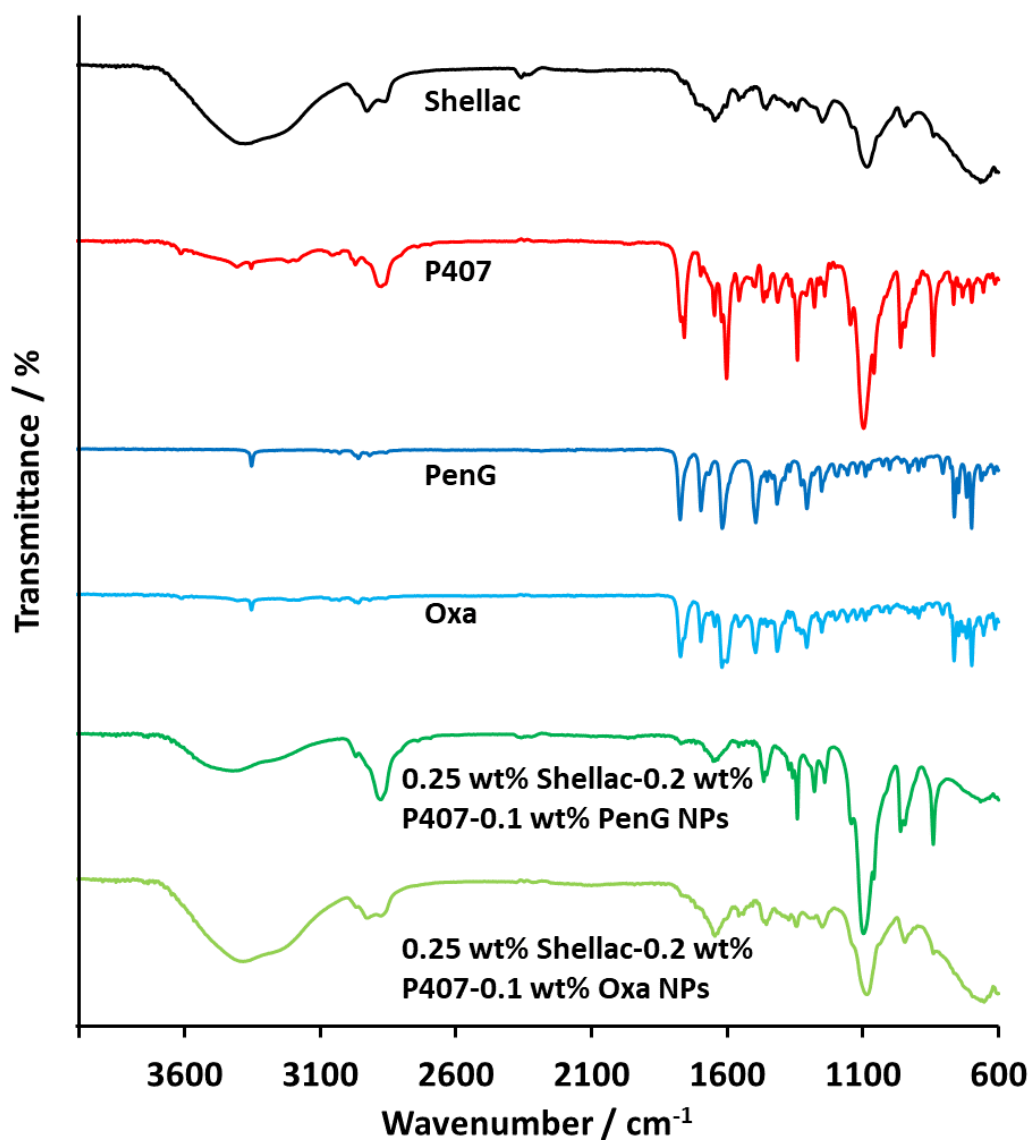


Figure 4.10. Fourier transform infra-red (FTIR) spectra of Shellac, P407, 0.25 wt%, free PenG, free Oxa, 0.25 wt% Shellac-0.2 wt% P407-0.1 wt% PenG NPs and 0.25 wt% Shellac-0.2 wt% P407-0.1 wt% Oxa NPs. Samples were prepared by removing water using a Silica gel desiccant by in vacuum chamber for 1 day, then dried at 60°C for 2 days. The spectra were measured between 4000-600 cm^{-1} using PIKE ATR diamond settings. A spectrum was obtained with a blank of just air to reduce transmittance interference with the samples.

Figure 4.11 shows the EDX elemental spectra for encapsulated NPs and their individual components. Shellac and P407 (**figure 4.11A and B**) show no sulphur peak, which is consistent with their chemical structure. Samples of free PenG and Oxa (**figure 4.11C and D**) show small sulphur peaks of 11.13% and 10.55% atomic weigh, which is correct for the elemental composition of the compounds. Elemental analysis of the PenG-NPs and Oxa-NPs, formulated as 0.25 wt% shellac-0.2 wt% P407-0.1 wt% PenG-NPs, and 0.25 wt% shellac-0.2 wt% P407-0.1 wt% Oxa-NPs (**figure 4.11E and F**) shows peaks

of 3.82% and 3.81% for sulphur, indicating that PenG and Oxa have been successfully encapsulated into the NP in roughly the same composition.

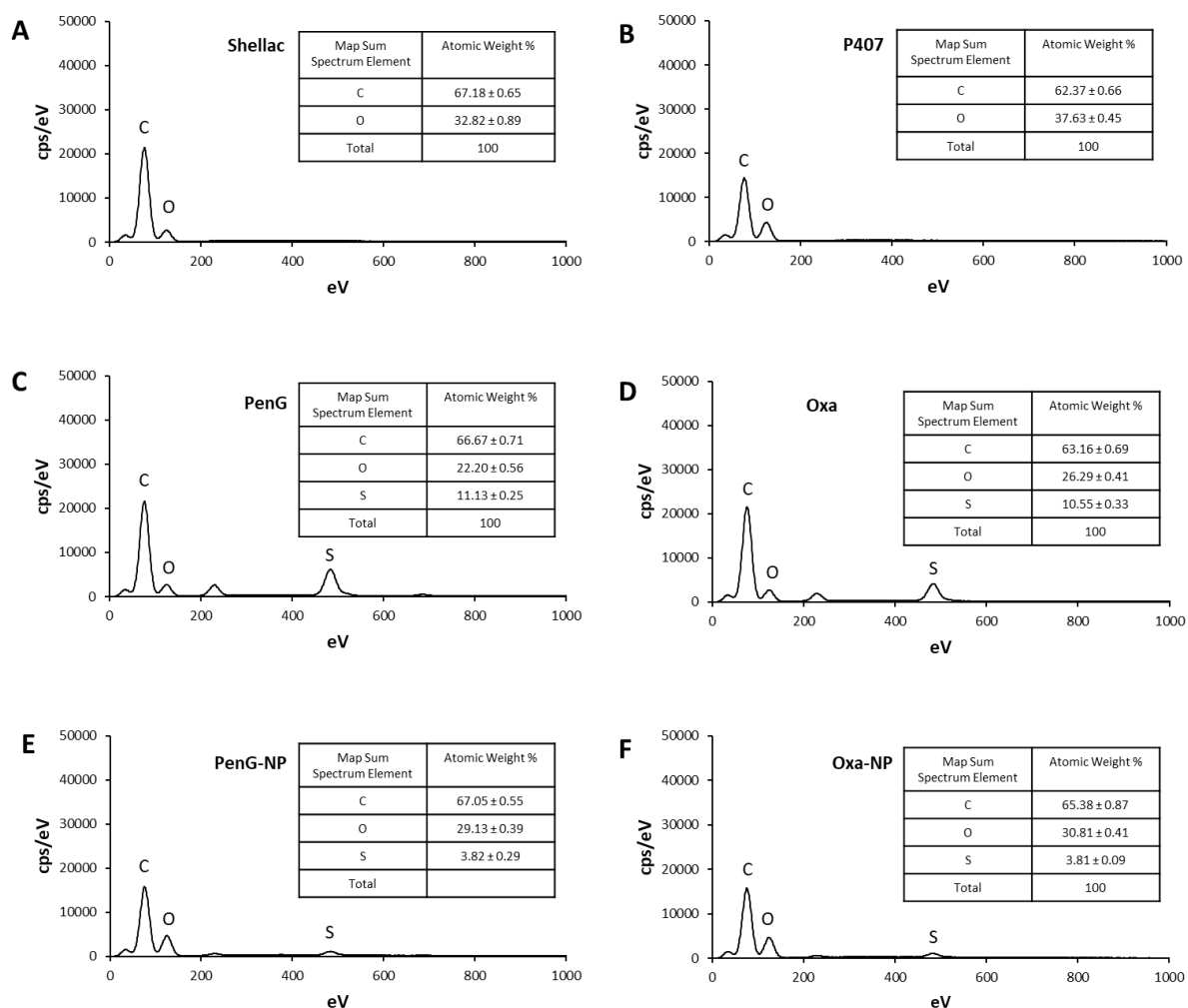


Figure 4.11. EDX spectra of (A) shellac, (B) P407, (C) PenG, (D) Oxa, (E) 0.25 wt% shellac-0.2 wt% P407-0.1 wt% PenG-NPs, and (F) 0.25 wt% shellac-0.2 wt% P407-0.1 wt% Oxa-NPs. The measurement for shellac, P407, PenG and Oxacillin was taken three separate locations and the data averaged. The measurement for the NP was taken in the centres of three separate NPs and averaged. A Nanoanalysis X-Max 65-T detector and the INCA software were used to produce the elemental analysis spectra.

Figure 4.12 shows the release kinetics of 0.1 wt% PenG and 0.1 wt% oxacillin from 0.25 wt% shellac-0.2 wt% P407 NPs was investigated as a function of pH and temperature over time. PenG and oxacillin is slowly released over 24 hours in a similar fashion. At pH 7.5 the release is more rapid, cumulating at 60% and 90% for PenG and oxacillin, compared to 40% and 50% at pH 5.5. This is due to the partial solubilisation of shellac above pH 7 allowing for a more rapid diffusion of the antibiotic from the core. The temperature was also shown to influence the release of the antibiotics from the shellac-P407 NPs. In a similar trend to the increased pH, a higher temperature of 37 °C showed that at

24 hours 65% of PenG had been release compared to 40% at 23°C. For oxacillin 90% was release at 37°C after 24 hours, 50% at 23°C. The higher temperature will increase the diffusion rate in which PenG and oxacillin are released from the NP core indicating that at higher a pH and temperature the antibiotics are released more rapidly, however, in all cases it is still a gradual process. The increased rate of release of the antibiotics at pH is explained by the partial dissolving of the shellac which would increase the rate in which the antibiotics can leach from the NP interior. The 0.1 wt% PenG and 0.1 wt% oxacillin into 0.25 wt% shellac-0.2 wt% was chosen as the NP formulation to be functionalised with a coating of cationic protease 2.4 L FG. The purpose of which was to convey a positive zeta potential to the NP, increased the electrostatic attraction to the anionic bacterial cell wall, and to digest the biofilm EPS.

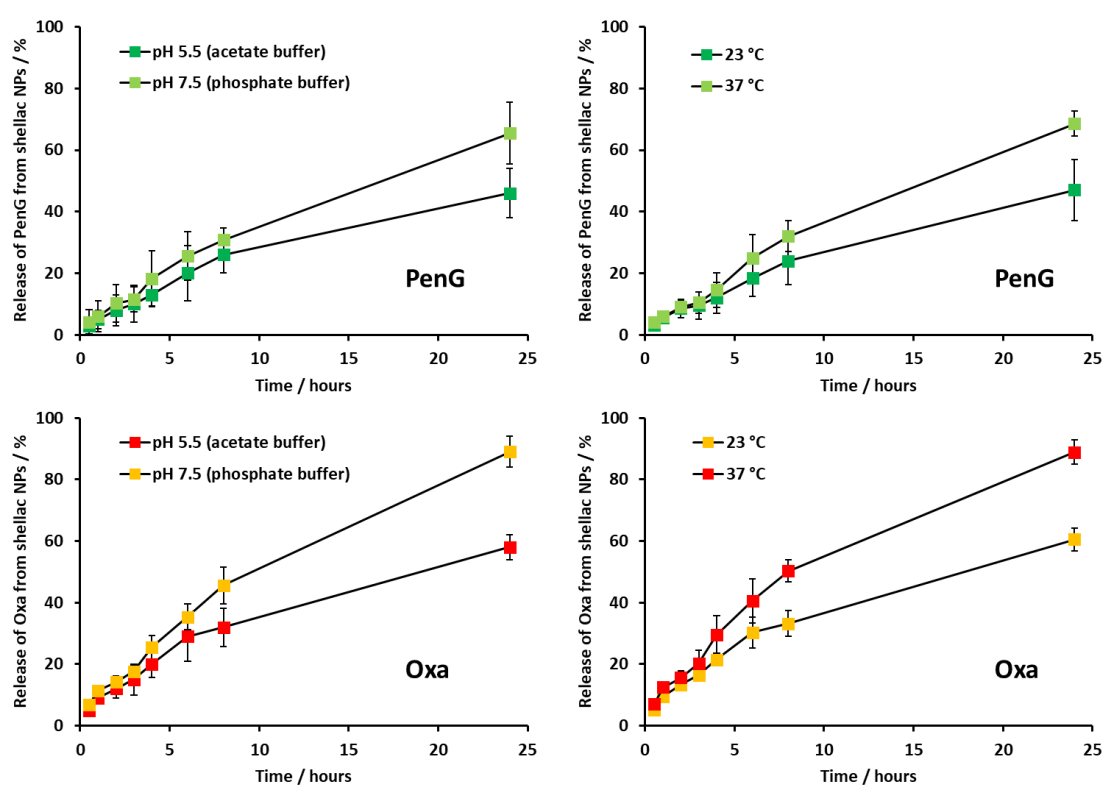


Figure 4.12. Release percentage of PenG and Oxa from 0.25 wt% Shellac-0.2 wt% P407-0.1 wt% PenG/Oxa NPs as a function of pH and temperature. The release percentage of the temperature experiments were performed at pH 5.5, buffered with acetate buffer. For both experiments 50 mL of the 0.25 wt% Shellac-0.2 wt% P407-0.1 wt% ABX NP formulation was placed in to a 10-12 kDa MWKO dialysis bag. The dialysis bag was placed into 500 mL of the specific buffered and at a specific temperature. 1 mL aliquots were taken at specific time points on the absorbance of the aliquot equated into the concentration of PenG/Oxa in the buffer using a standard calibration curve. Absorption was measured at 250 nm. The follow equation was used to calculate the release kinetics;

$$\text{Antibiotic release (\%)} = \frac{\text{amount of antibiotic in the buffer solution at a specific time}}{\text{amount of antibiotic encapsulated into the shellac NP}} * 100$$

Figure 4.13A and B shows the hydrodynamic diameter and the zeta potential after coating with concentrations of Alcalase ranging from 0 to 0.6 wt%. There is an increase in size from ~80 to 90 nm which occurs up to 0.2 wt% Alcalase coating and plateaus afterwards between 0.2 – 0.6 wt%. The zeta potential is shown to flip from -15 mV to 20 mV after a coating of 0.1 wt% Alcalase with only minimal increases thereafter. Similar results are seen when the same concentrations of Alcalase are added to NPs which have encapsulated oxacillin (**figure 4.13C and D**) rather than penicillin. This is due to there being no likely difference between the NP whether encapsulating PenG or oxacillin. **Figure 4.4A** shows a TEM image of a dispersion of globular Alcalase protease, which has a diameter of ~8 to 10 nm, typical of a subtilisin A protease with a MW of ~30 kDa. A coating concentration of 0.2 wt% was chosen as this provided a good zeta potential reversal to 20 mV, increased concentrations showed no such increase indicating the surface was likely saturated with protease. **Figure 4.4E and F** shows TEM images 0.25 wt% shellac-0.2 wt% P407-0.1 wt% PenG/Oxa-0.2 wt% Alcalase NPs, which have a ~10 nm larger diameter and a rough-textured surface indicating the presence of an Alcalase coating, and is consistent with data obtained with DLS. **Figure 4.4C and D** show 0.25 wt% shellac-0.2 wt% P407-0.1 wt% PenG/Oxa NPs without the Alcalase coating. The NPs are approximately 10 nm smaller in diameter and do not have the textured rough coating seen when coating with Alcalase.

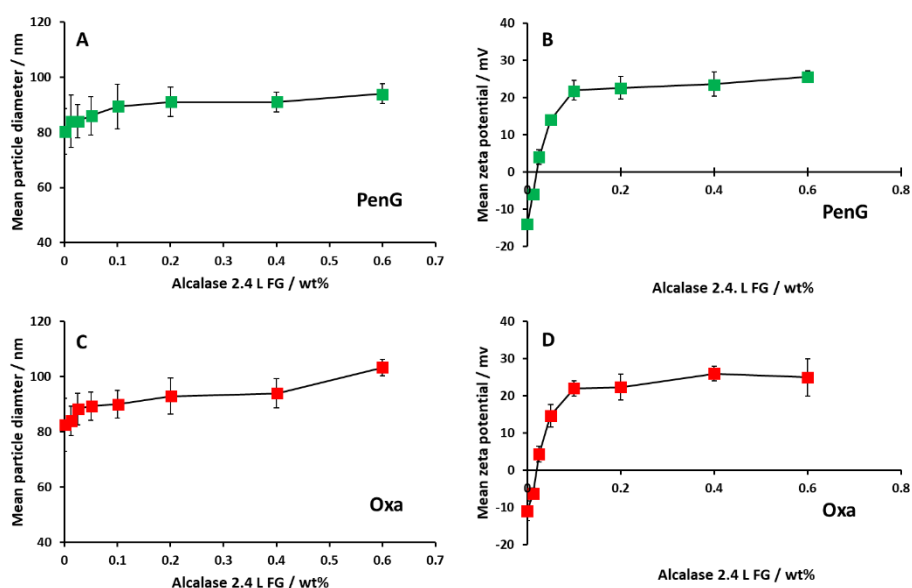


Figure 4.13. The (A) mean particle diameter and (B) zeta potential of 0.25 wt% shellac-0.2 wt% P407-0.1 wt% PenG NPs coated with various concentrations of Alcalase 2.4 L FG. The (C) mean particle diameter and (D) zeta potential of 0.25 wt% shellac-0.2 wt% P407-0.1 wt% Oxa NPs coated with various concentrations of Alcalase 2.4 L FG. Various concentrations of Alcalase were prepared in 25 mL solution and mixed for 30 min at room temperature with an 25 mL of 0.25 wt% shellac-0.2 wt% P407-0.1 wt% PenG/Oxa NPs suspensions at pH 5.5. Afterwards the mixture was centrifuged at 8000 *g* for 30 mins to pelletise the NPs. The pellet was redispersed into 25 mL of deionised water buffered to pH 5.5 (acetate buffer) yielding a stock solution of 0.25 wt% Shellac-0.20 wt% P407-0.1 wt% PenG/Oxa-0.2 wt% Alcalase NPs. Measurements were taken at pH 5.5, 25°C, RI 1.516, Abs 1.000 using a Malvern Zetasizer Nano ZS. Each value represents a triple replicate with \pm S.D.

Figure 4.14 shows the zeta potential of 0.25 wt% shellac-0.2 wt% P407- 0.1 wt% PenG/Oxa-0.2 wt% Alcalase NPs change over time as a measure of the surface coating stability. The positive charge is retained in both formulations over 24 hours, dropping by ~ 10 mV. This shows the protease is retained electrostatically on the anionic shellac NP with only a minimal release over 24 hours. For short-term storage the NP suspension was pelletised and the supernatant removed. The semi-wet NP was then stored at 5°C and individual aliquots removed and left to return to room temperature afterwards. The size and zeta potential were measured to evaluate the NP after storage. Additionally, the encapsulation efficiency of the NPs after storage was measured, to determine if any antibiotic had leached out. **Figure 4.15A** shows that after resuspending the NP, after 24 hours of storage, the size is approximately 87 nm and 88 nm for 0.1 wt% PenG-NPs and 0.1 wt% Oxa-NPs respectively. There is only a negligible difference with an additional 24 hours of storage for each NP sample. This indicates that storage at 5°C does reduce the size of the NP. The same is true of the zeta potential (**figure 4.15B**) which was measured after the same storage time and conditions. Upon redispersion and sonication the NP retained their positive zeta potential with no reduction depending on the length of time storage. Crucially, the concentration of either PenG or Oxa is required to remain high after storage, otherwise storing the NP is not viable. An investigation into the encapsulation efficiency of the 0.1 wt% PenG-NPs and 0.1 wt% Oxa-NPs by supernatant absorbance was completed. After the NP pellets were redispersed into the deionised water (buffered to pH 5 using acetate buffer), the NP suspension was again pelletised on the supernatant examined to determine the antibiotic concentration within. **Figure 4.16** shows that after 1 day storage in a semi-wet pellet that approximately 1% of the encapsulated antibiotic is lost out of the NP, 69% for PenG and 68% for Oxa, compared to 0.1 wt PenG/Oxa encapsulation for fresh NPs (**figure 4.5**). This very small amount is due to the very low amount of water on the pellet. The antibiotic can only diffuse out of the NPs if the concentration in the surrounding solution goes below its equilibrium concentration of partitioning between particle and solution. The small amount of antibiotic that leaches out of the pelletised NPs will quickly saturate the small amount of liquid surrounding the pellet.

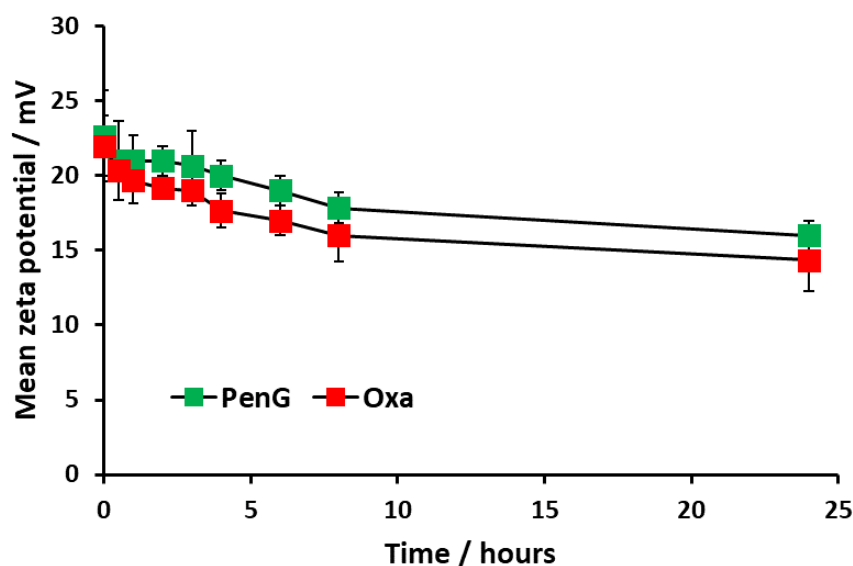


Figure 4.14. The zeta potential of 0.25 wt% Shellac-0.2 wt% P407-0.1 wt% PenG/Oxa NPs coated with 0.2 wt% Alcalase 2.4 L FG over time. After coating with Alcalase 2.4 L FG the NPs were centrifuged at 8000 *g* and the pellet washed three times in deionised water. The pellet was redispersed into deionised water adjusted to pH 5.5 using acetate buffer. Zeta potential measurements were taken at different time points up to 24 hours to investigate the stability of the Alcalase coating.

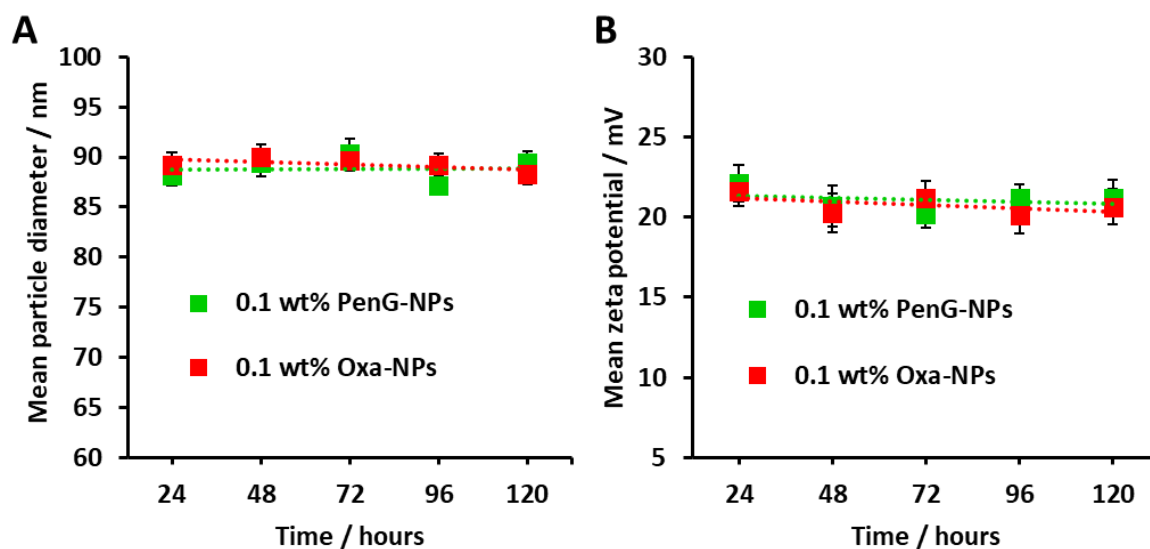


Figure 4.15. The (A) mean particle diameter and (B) zeta potential of 0.25 wt% shellac-0.2 wt% P407-0.1 wt% PenG/Oxa NPs coated with 0.2 wt% Alcalase 2.4 L FG. After NP synthesis the NP suspension was pelleted by centrifugation at 8000 *g* for 30 mins. Afterwards the supernatant was discarded and the semi-wet pellet frozen and stored at -20°C. After storage, the pellet was resuspended into deionised water buffered to pH 5.5 (acetate buffer) to the same volume as synthesised with constant shaking. The samples were then sonicated for 5 minutes in a water bath. Measurements were taken at pH 5.5, 25°C, RI 1.516, Abs 1.000 using a Malvern Zetasizer Nano ZS. Each value represents a triple replicate with \pm S.D.

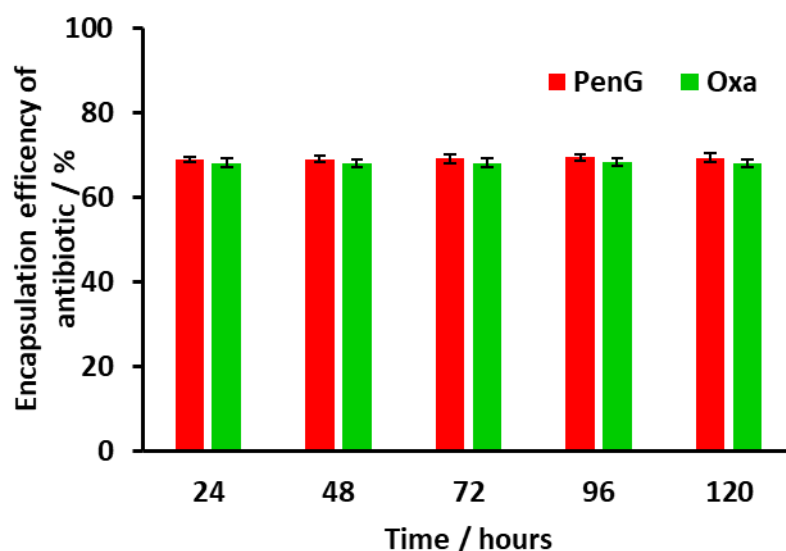


Figure 4.16. Encapsulation efficiency of varied concentrations of penicillin G and oxacillin into 0.25 wt% shellac-0.2 wt% P407-0.2 wt% Alcalase NPs. Absorbance (250 nm) of the supernatant was measured using a spectrophotometer to determine encapsulation efficiency. The following equation was used to calculate the encapsulation efficiency;

$$\text{Encapsulation efficiency} = \frac{\text{total antibiotic} - \text{unencapsulated antibiotic}}{\text{total antibiotic}} * 100$$

4.3.2 *S. aureus* antimicrobial susceptibility screening

A formulation of 0.25 wt% shellac NPs loaded with 0.1 wt% PenG/Oxa and coated with 0.2 wt% P407 and subsequently with 0.2 wt% Alcalase was chosen as the stock treatment for testing against *S. aureus*. Here, it is shown that PenG and Oxacillin encapsulated in the shellac NPs, functionalised with a surface coating of a cationic protease, are significantly more effective than the free antibiotics administered at equivalent concentration. The aim is to demonstrate that antibiotics encapsulated into such active NPs have an increased efficacy that can overwhelm the enzymatic inhibition of the antibiotic (specifically PenG). This is investigated on *S. aureus* in planktonic and biofilm forms.

Firstly, it was confirmed that *S. aureus* was a suitable candidate by performing an antimicrobial susceptibility screen using VITEK®2 ID and AST microwell cards (**Figure 4.17**). **Table 4.2** shows the range of antibiotics tested for susceptibility and their interpretation as resistant or susceptible. This *S. aureus* strain was confirmed to be susceptible to Oxa and resistant to PenG. This was verified using antimicrobial disk diffusion for both Oxa and PenG (**Figure 4.18**). The zone diameter breakpoint for PenG is <26 mm, as stated by the European Committee on Antimicrobial Susceptibility Testing (EUCAST) testing breakpoint tables (EUCAST Breakpoint Tables v 10.0., 2020). There is a clear zone of inhibition diameter around the oxacillin disk (27 mm) confirming its susceptibility to that antibiotic. Most *staphylococci* are now beta-lactamase producers and this is the mechanism of

resistance to penicillin antibiotics, requiring treatment with isoxazolympenicillins (*e.g.* oxacillin). To confirm this a simple beta-lactamase detection strip was used on a *S. aureus* suspension (**Figure 4.19**). This test is based on beta-lactamase hydrolysing the beta lactam ring (present in PenG and all penicillin antibiotics) into penicillioic acid. A yellow solution was generated after 10 min indicating the presence of an acid in the solution (acid–base indicator), and therefore beta-lactamase produced by *S. aureus*.

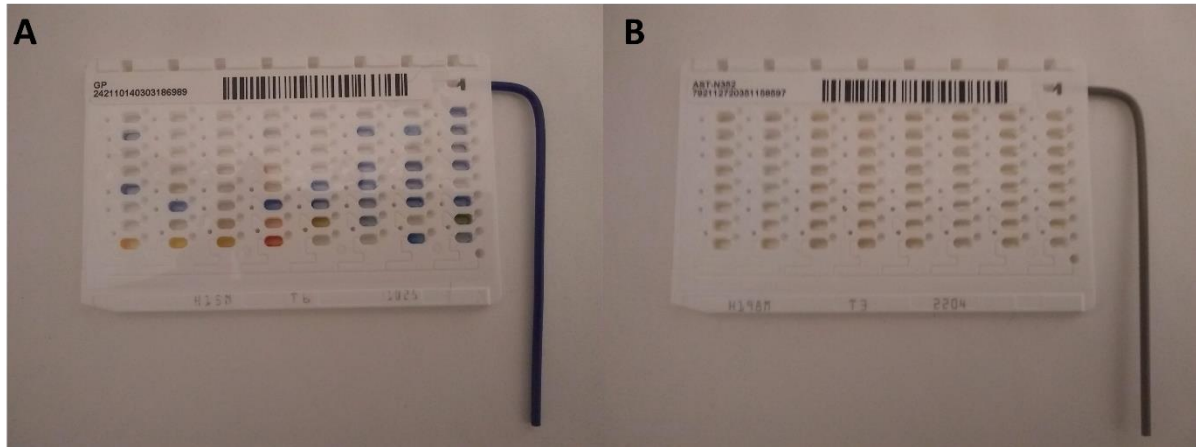


Figure 4.17. Photographs of **(A)** VITEK 2 GP (21342) and **(B)** VITEK 2 AST-P635 (416911) Gram-positive identification and AST cards.



Figure 4.18. Zones of growth inhibition for right oxacillin (1 μ g concentration) and left penicillin G (10iu). Inoculum was at 0.5 McFarland incubated at $35 \pm 1^\circ\text{C}$ for 18 hours.

Table 4.2. VITEK2 *Staphylococcus aureus* Antimicrobial Susceptibility Screen.

Selected Organism: <i>Staphylococcus aureus</i>					
Comments: Rule 5: Chloramphenicol not used for food animals. (Source: CLSI 2015, VET01S, 3 rd edition). Rule 6: tetracycline tested as the class representative for susceptibility to chlortetracycline, doxycycline, minocycline and oxytetracycline. Organisms that are susceptible to tetracycline are also considered susceptible to doxycycline and minocycline. However, some organisms that are intermediate or resistant to tetracycline may be susceptible to doxycycline or minocycline or both. (Source: CLSI 2015, VET01S, 3 rd edition). Rule 8: Cefoxitin is used as a surrogate for oxacillin, report oxacillin susceptible or resistant based on the cefoxitin result. (Source: CLSI 2015, VET01S, 3 rd edition). Rule 11: Clindamycin is also used to test for susceptibility to lincomycin. Clindamycin is more active than lincomycin against most staphylococcal strains. (Source: CLSI 2015, VET01S, 3 rd edition).					
Identification Information	Card: GP		Lot Number: 2420469403		Analysis time: 7.85 hours
Organism Origin	VITEK 2				
Selected Organism	99% Probability <i>Staphylococcus aureus</i>				
	Bionumber: 030412067763271		Confidence: Low discrimination		
Susceptibility Information	Card: AST-P635		Lot Number: 7350480103		Analysis time: 8.41 hours
Antimicrobial	MIC	Interpretation	Antimicrobial	MIC	Interpretation
Cefoxitin Screen	POS	+	Teicoplanin	<= 0.5	S
Benzylpenicillin	>= 0.5	R	Vancomycin	1	S
Oxacillin	>= 4	S	Tetracycline	<= 1	S
Gentamicin	<= 0.5	S	Tigecycline	<= 0.12	S
Inducible Clindamycin Resistance	NEG	-	Fusidic Acid	<= 0.5	S
Erythromycin			Mupirocin	<= 2	
Clindamycin	0.25	S	Chloramphenicol	8	S
Linezolid	2	S	Rifampicin	<= 0.03	S
Daptomycin	0.25	S	Trimethoprim	1	S

+ = Deduced drug * = AES modified ** User modified. Parameter Set: Global CLSI-based+Natural Resistance V2 17 NOV2017.

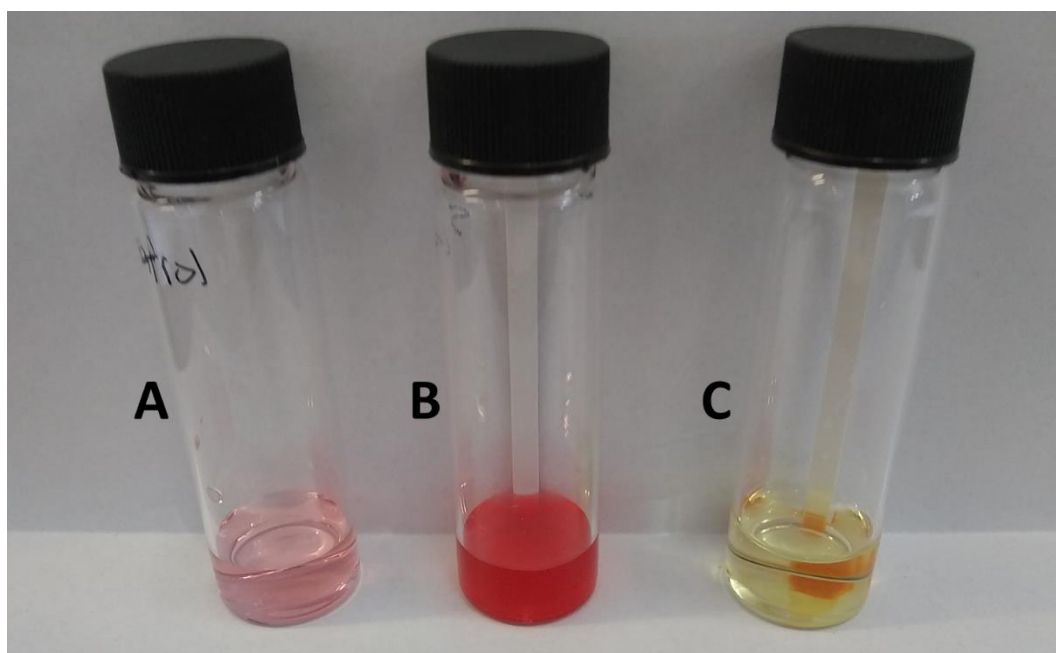


Figure 4.19. Beta-lactamase detection. The plastic strip contains an active zone saturated with penicillin G and an acid-basic indicator. The process is based on the hydrolysis of the beta-lactam ring in penicillin G producing penicilloic acid. This caused acidification of the bacterial suspension (yellow indicated the presence of penicilloic acid and thus beta-lactamase. 3 colonies of *S. aureus* and *S. epidermidis* (positive control) were placed into 1 mL of moistening solution and a test strip was added. The bacterial suspension was incubated at room temperature for 10 minutes with shaking. **(A)** Shows the pink coloured moistening solution with no bacteria, **(B)** shows the *S. epidermidis* suspension and **(C)** shows the *S. aureus* suspension. Red indicates negative and yellow positive for beta-lactamase.

4.3.3 Effectiveness of 0.25 wt% shellac–0.2 wt% P407–0.1 wt% PenG/Oxa–0.2 wt% Alcalase NPs against planktonic *S. aureus*

The effectiveness of the base formulation of 0.25 wt% shellac–0.2 wt% P407–0.1 wt% PenG/Oxa–0.2 wt% Alcalase NPs (0.1 wt% PenG-NPs or 0.1 wt% Oxa-NPs) was tested against the equivalent concentration of free PenG or Oxa (0.1 wt%) using a time-kill assay. **Figure 4.20A and B** show that *S. aureus* starting at a concentration of 1×10^6 cells per mL increased to approximately 1×10^9 cells per mL when untreated. Treatment with 0.1 wt% free PenG had a minimal effect on bacterial growth, with 1×10^7 cells after a 24 h incubation time, confirming the resistance of the cells to this treatment (**Figure 4.20A**). However, when treated with 0.1 wt% PenG-NPs there were no viable cells after 4 h, a 4 log+ reduction from the free PenG sample. This confirms the PenG-loaded NPs are overcoming the resistance and restoring the effectiveness of the antibiotic. This is due to the high concentration of the agent within the NPs cores, which is localised onto the bacterial cell wall due to the electrostatic attraction of the cationic NPs to the anionic surface of the bacterial cell. **Figure 4.20B** shows the same time kill assay performed against *S. aureus*, this time with 0.1 wt% free Oxa and 0.1 wt% Oxa-NPs. As described earlier, this strain of *S. aureus* is susceptible to Oxa and so after 6 h

treatment with 0.1 wt% Oxa (free) there were no viable cells detected. However, the 0.1 wt% Oxa-NPs were faster-acting, killing the cells within 4 h, providing further evidence of their ability to increase the effectiveness of the encapsulated antibiotic. **Figure 4.21** shows the time-kill results for all the individual components of the NP. The 0.25 wt% shellac and 0.2 wt% Alcalase NP components alone had only a mild effect on reducing the viable cell count after 24 h ($\sim 1 \times 10^8$ and 1×10^7 CFU per mL, respectively). The free 0.2 wt% P407 alone reduced the cell viability concentration to $\sim 1 \times 10^5$ CFU per mL after 24 h, however, when combined with 0.25 wt% shellac (0.25 wt% shellac–0.2 wt% P407) empty NPs, the toxicity was reduced, with $\sim 1 \times 10^8$ viable cells per mL detected after 24 h of treatment. This indicates that the complexing of P407 onto shellac cores reduces the toxicity of this Pluronic surfactant and that the shellac-NPs are a safer antibiotic delivery vehicle. Surfactants are intrinsically toxic to life due to their amphipathic nature which can dissolve lipids in water. The free P407 demonstrates a bacteriostatic effect against *S. aureus* by disrupting the cell membrane, however, the lack of cell specificity makes them unsuitable for use in a therapeutic context.

A further investigation into the wt% PenG/Oxa-NPs (2-fold serial dilutions of the stock treatment) was performed to elucidate the MIC/MBC of *S. aureus* after 24 h of treatment. **Figure 4.20C** shows that PenG-NPs had a minimal inhibitory concentration (MIC) of 0.015 wt%, a 5-fold improvement of 0.05 wt% for free PenG. The minimal bactericidal concentration (MBC) for PenG-NPs was less than 0.0003 wt%, an 8-fold decreased from free PenG showing >0.1 wt% (due to its resistance). Oxa-NP and free oxacillin had both MIC and MBC values of <0.0003 wt% after 24 h (oxacillin sensitive), however as described above the Oxa-NP showed increased efficacy by the faster killing of the bacteria. Shellac, P407, shellac–P407 NPs all had MIC and MBC of >0.25 wt%, 0.2 wt% and 0.25 wt% respectively (stock NP concentrations). Alcalase showed a MIC of 0.1 wt% and an MBC of >0.1 wt%, this agrees with the time-kill results which show that the free protease did not have a meaningful impact on cell viability. **Table 4.4** shows tabulated data for the MIC/MBC results.

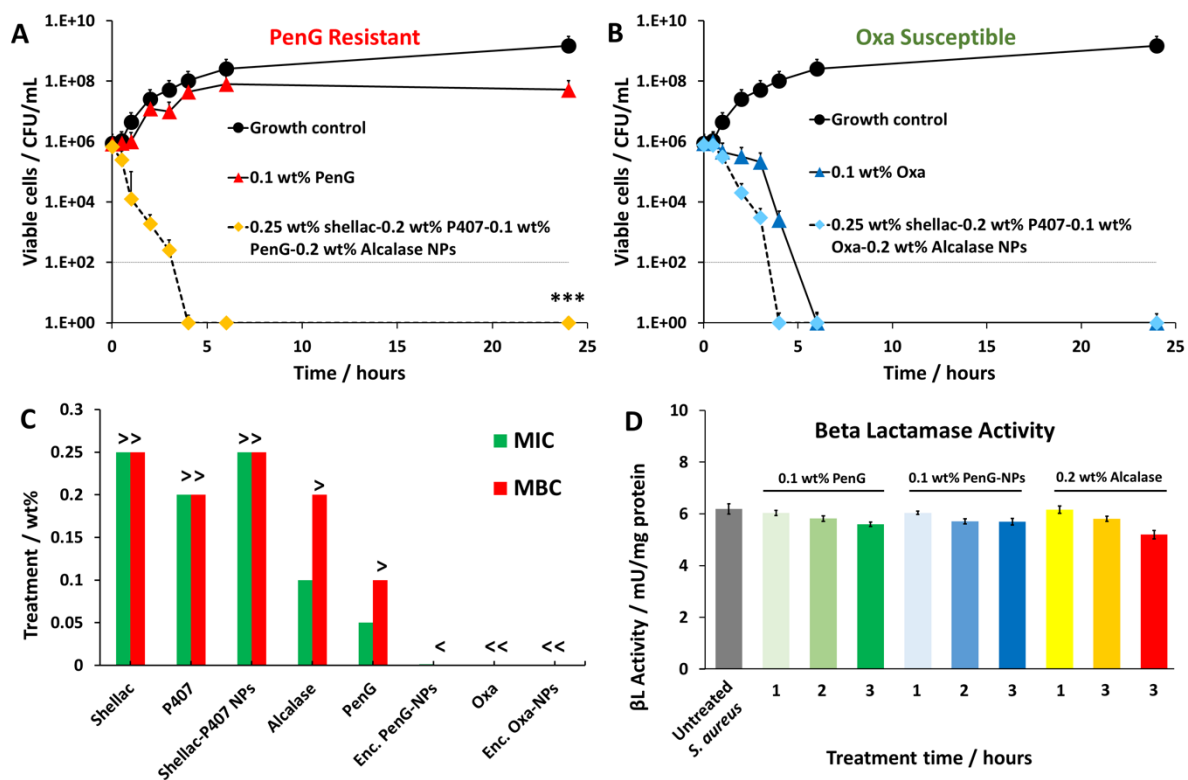


Figure 4.20 Time kill assays against *S. aureus*. Growth control (untreated). **(A)** 0.1 wt% free PenG (Penicillin G) **(B)** and 0.1 wt% Oxa (Oxacillin) were compared to the same antibiotic concentration encapsulated into Alcalase-coated shellac NPs. * $P < 0.05$, ** $P < 0.01$, *** $P < 0.001$ compared to the free antibiotic. **Table 4.3** shows the statistical analysis P -values. **(C)** *S. aureus* MIC and MBC of free PenG/Oxa, encapsulated PenG/Oxa NPs and individual constituents of the NP. 0.25 wt% shellac–0.2 wt% P407–0.1 wt% PenG/Oxa–0.2 wt% Alcalase was the stock treatment solution. Treatment concentrations lower than this were 2-fold dilutions from the stock. “>” indicates that a greater and “<” a lower concentration is needed to either inhibit or kill *S. aureus*. The MIC was determined to be the lowest concentration of active antimicrobial agent which inhibited the growth of each strain. The MBC was the lowest concentration in which no viable cells were detected after streaking the contents onto fresh MHA plates. **(D)** Beta lactamase activity of *S. aureus* after 1 to 3 h PenG, PenG-NP and Alcalase treatments expressed per mg of protein. Experiment was capped at 3 hours due to lack of remaining cells to analyse. Unit definition: 1 Unit Beta lactamase activity = amount of enzyme that generates 1 μmol of nitrocefin per minute at pH 7 at 25 °C.

Table 4.3. Time-Kill assay statistical analysis between free PenG and encapsulated PenG at 24-hour time point. Data were expressed as average values \pm standard deviations of the mean. P -values of less than 0.05 were considered significant. All One-Way ANOVAs and Tukey’s post-test statistical analysis were performed in GraphPad v7.0.4.

Multiple Comparison	P-value	Significance
Free PenG vs PenG NPs	0.00000306	***

Table 4.4. *S. aureus* MIC and MBC tabulated data.

	MIC	MBC
Shellac	> 0.25 wt% (2500 µg/mL)	> 0.25 wt% (2500 µg/mL)
P407	> 0.2 wt% (2000 µg/mL)	> 0.2 wt% (2000 µg/mL)
Shellac-P407 NPs	> 0.25 wt% (2500 µg/mL)	> 0.25 wt% (2500 µg/mL)
Alcalase	0.1 wt% (1000 µg/mL)	> 0.2 wt% (2000 µg/mL)
PenG	0.05 wt% (500 µg/mL)	> 0.1 wt% (1000 µg/mL)
Encapsulated PenG-NPs	0.0015 wt% (15 µg/mL)	< 0.0003 wt% (03 µg/mL)
Oxa	< 0.0003 wt% (3 µg/mL)	< 0.0003 wt% (3 µg/mL)
Encapsulated Oxa-NPs	< 0.0003 wt% (3 µg/mL)	< 0.0003 wt% (3 µg/mL)

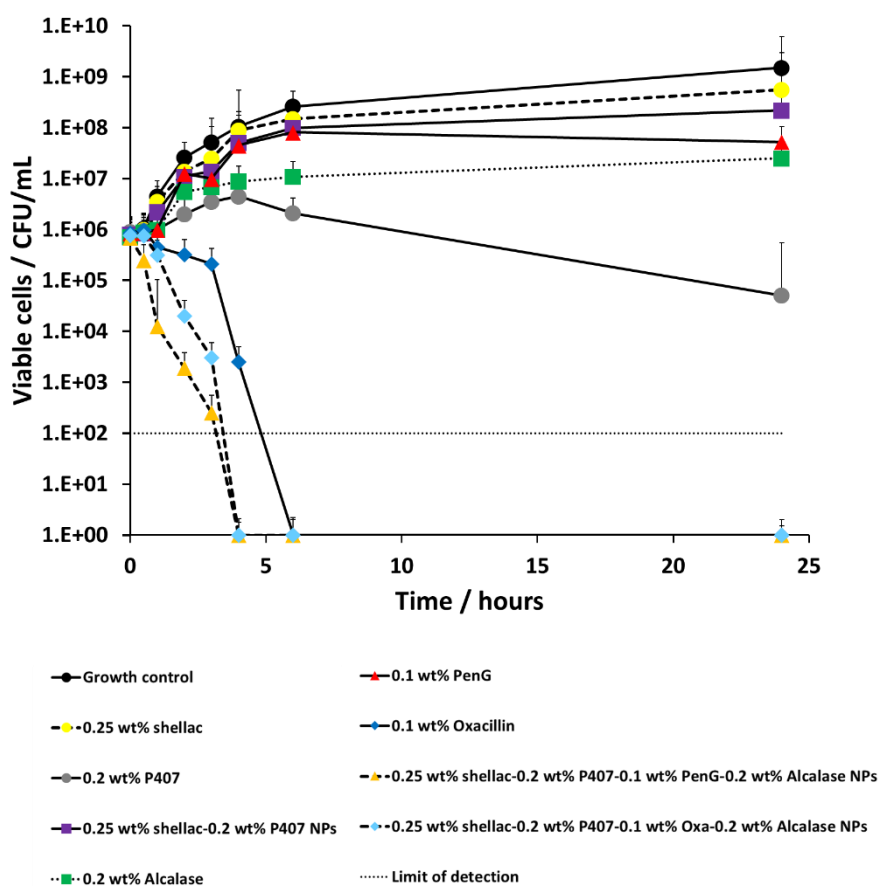


Figure 4.21. Time kill assays against *S. aureus*. Growth control (untreated), 0.25 wt% shellac, 0.2 wt% P407, 0.25 wt% shellac-0.2 wt% P407 NPs and 0.2 wt% Alcalase are considered controls. 0.1 wt% free PenG and 0.1 wt% Oxacillin were compared to the same antibiotic concentration encapsulated into Alcalase-coated shellac NPs. The results are presented as means (N=3).

Figure 4.22A and B shows SEM images of untreated planktonic *S. aureus* which appear to have good morphology with no visible NPs on their surface. When compared to **Figure 4.22C and D** in which planktonic *S. aureus* was treated for 1 hour with 0.1 wt% PenG-NPs, there is a clear coating of NPs on the surface of the bacteria. This provides further evidence of the cationic NPs adhering to the anionic bacterial cell *via* electrostatic interactions. This highly localised concentration of antibiotic encapsulated NPs is apparently able to overcome the enzymatic resistance mechanism of the *S. aureus*. An investigation into *S. aureus* using TEM and EDX (Energy-dispersive X-ray spectroscopy) elemental mapping was performed. **Figure 4.23** shows the elemental distribution of carbon, oxygen, nitrogen and sulphur in *S. aureus*. When treated with 0.1 wt% free PenG there is an increased concentration of sulphur compared to the natural sulphur concentration contained in the untreated sample. This indicates the presence of PenG, which contains the element sulphur in its thiazolidine ring. The sample treated with 0.1 wt% PenG-NPs contains a further increase in sulphur, with small pockets located where the NP has adhered to the bacterial cell wall. This further supports the increased concentration of PenG, highly localised on the cell wall.

The beta-lactamase activity of *S. aureus* after treatment with either 0.1 wt% PenG, 0.1 wt% PenG-NPs and 0.2 wt% Alcalase was investigated. **Figure 4.20D** shows the beta-lactamase activity measured in *S. aureus* cells after 1, 2 and 3 h treatments (compared to a 3 h *S. aureus* sample which was untreated). The activity was obtained from the hydrolysis of nitrocefin (a beta-lactamase substrate). **Figure 4.24** shows the nitrocefin calibration curve. The untreated *S. aureus* had beta-lactamase of an enzyme activity of 6 mU per mg protein per min. Interestingly, there was only a marginal decrease in activity in the free PenG and PenG-NPs over 3 h, and no discernible difference between free PenG and PenG-NPs. This indicates that *S. aureus* is not actively increasing the production and secretion of the beta-lactamase during treatment. This lack of PenG defence activity may explain a mechanism for why PenG-loaded NPs can be effective against *S. aureus*, when an equivalent concentration of free PenG is not. The bacterial cell is not able to produce enough beta-lactamase enzyme activity to inhibit the PenG, which is locally delivered and highly concentrated on the cell surface, leached by the adhered PenG-NPs. **Figure 4.25** shows the beta-lactamase activity *S. aureus* cell and the culture media (containing any secreted enzyme). There is no notable difference in beta-lactamase activity of *S. aureus* when treated with either free PenG or PenG-NPs (both 0.1 wt%) between 1 h and 3 h. The effect of 0.2 wt% Alcalase was also investigated. There is a marginal decrease in beta-lactamase activity after 3 h, compared to the control, 0.1 wt% PenG and 0.1 wt% PenG-NPs, which are almost identical. This is likely due to the Alcalase hydrolysing a small amount of beta-lactamase produced by the bacteria, and therefore lowering the detected enzymatic activity. This

provides evidence that the Alcalase itself can confer benefits in the context of reducing a beta-lactamase producing bacteria's resistance mechanism.

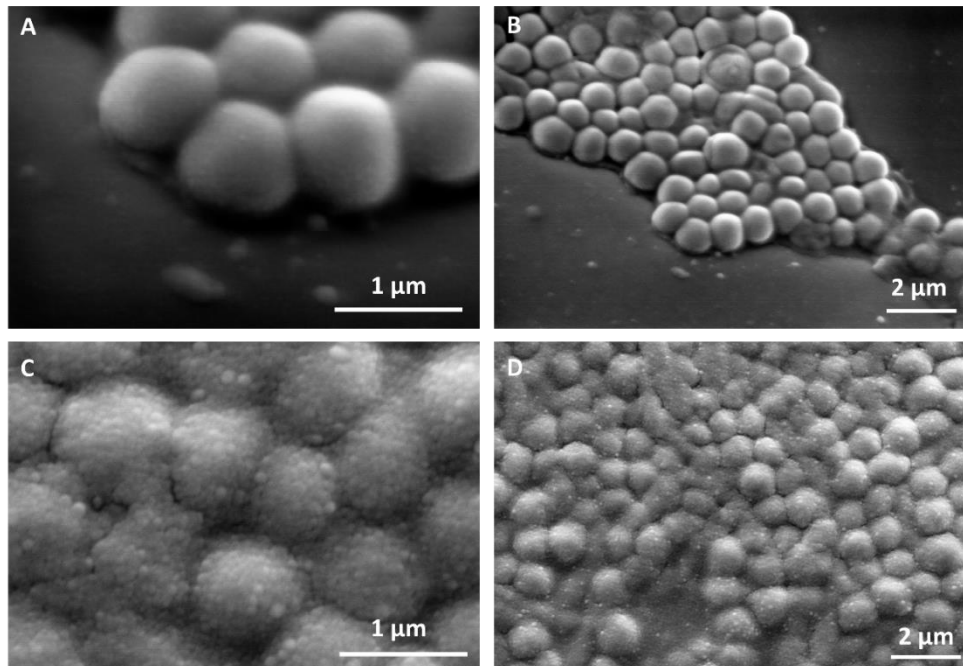


Figure 4.22. (A) and (B) SEM images of planktonic *S. aureus* after 24 hours growth (no treatment) and (C) and (D) SEM images of *S. aureus* after 24 hours growth (0.1 wt% PenG-NPs, 1 hour treatment). 10 nm gold coating. Samples were imaged using a Carl Zeiss Evo-60 (Germany) with a variable pressure 100-micron aperture at 40 Pa. EHT was 20 kV with probe current of 100 pA. Images were captured with Zeiss smartSEM software.

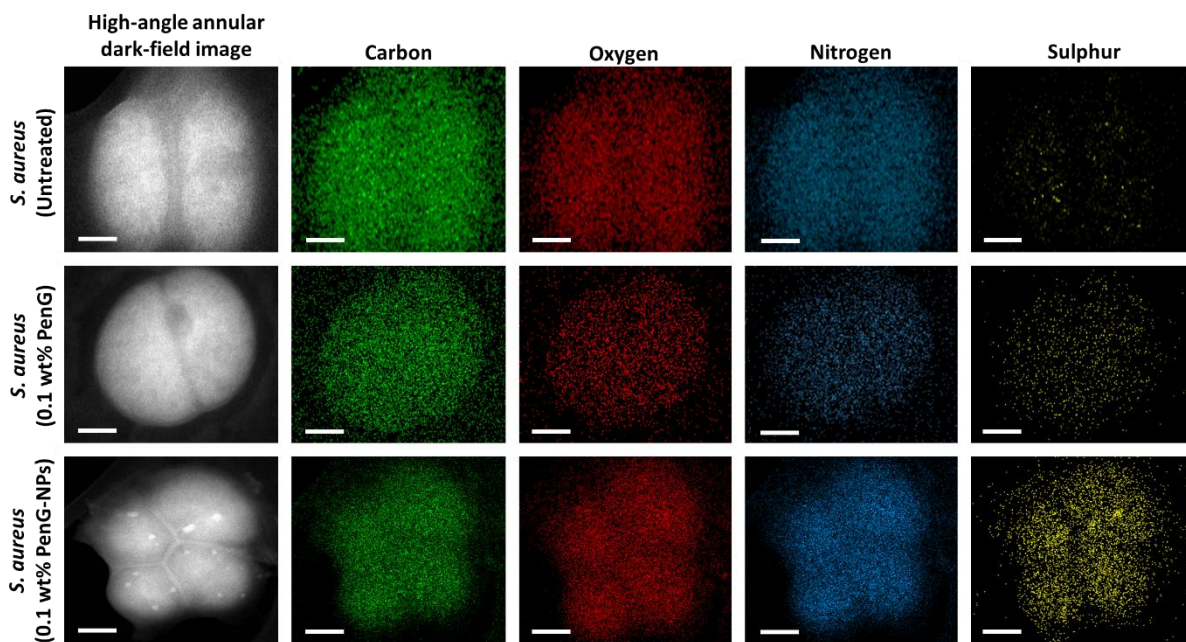


Figure 4.23. TEM/EDX images/scans of *S. aureus* after 24-hour treatment with either 0.1 wt% PenG or 0.1 wt% PenG-NPs. TEM images were obtained using a JEM 2010 (JOEL, Japan) at 120 kV and a Gatan Ultrascan 4000 digital camera. A nanoanalysis X-Max 65-T detector and the INCA software were used to produce the elemental analysis maps. White scale bar = 250 nm.

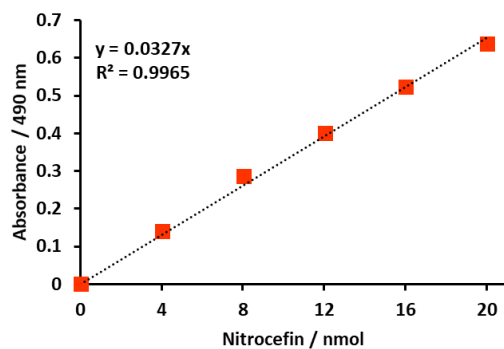


Figure 4.24. Nitrocefin standard calibration curve. The nitrocefin stock solution was hydrolysed by adding 8 μL of nitrocefin to 8 μL of Beta Lactamase Hydrolysis Buffer and 28 μL of DMSO (ratio 1:2:7) into an Eppendorf tube. The mixture was reacted at 60°C for 10 minutes before cooling to room temperature (23°C) and centrifuged at 1000 g for 1 minute. 0, 2, 4, 6, 8 & 10 μL of the hydrolysed Nitrocefin Standard (2 mM) was added into a series of wells in a 96-well plate to generate 0, 4, 8, 12, 16 & 20 nmol/well of Nitrocefin Standard. The final volume of each well was adjusted to 100 μL /well using Beta Lactamase Buffer solution. Absorbance was read at 490 nm, 0 nmol nitrocefin was used as a blank. Error bars are within the symbol size.

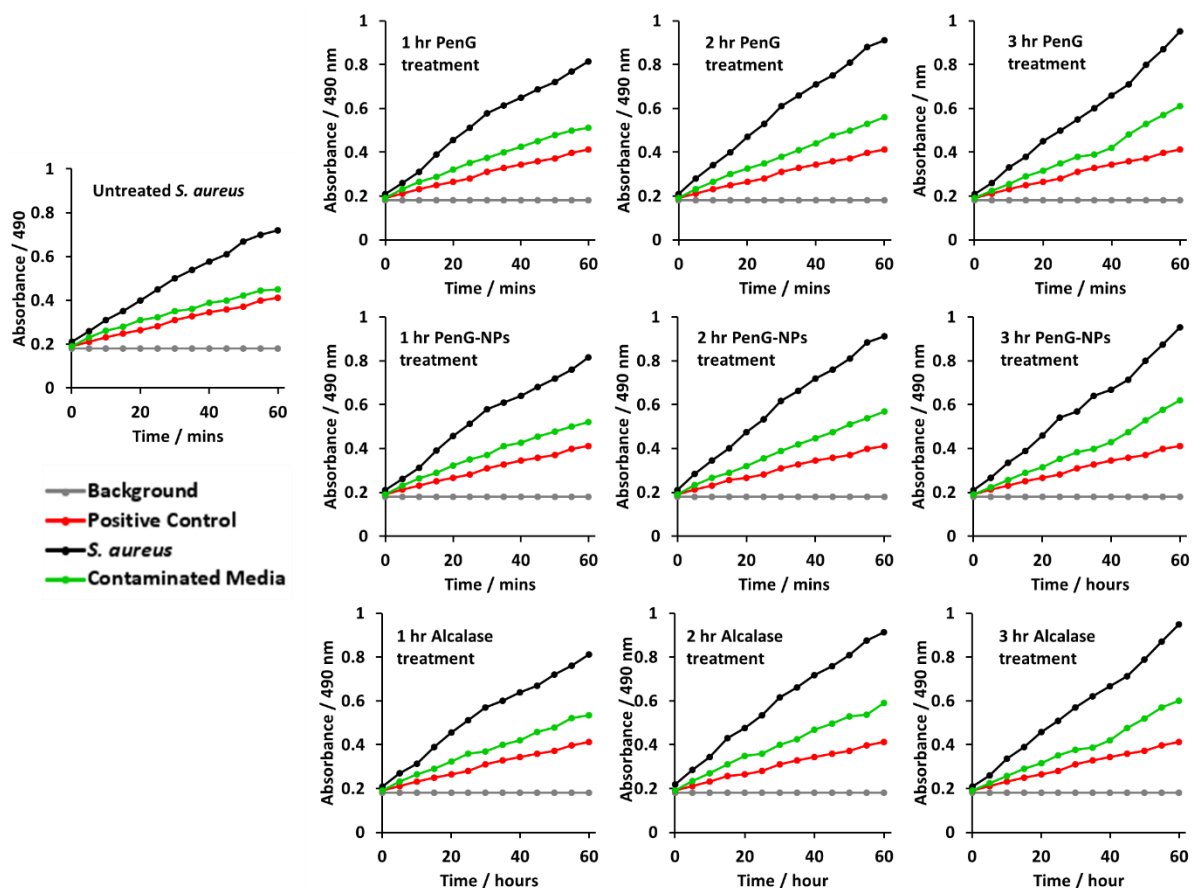


Figure 4.25. Comparison of beta lactamase activity of *S. aureus* after treatment with free PenG vs PenG-NPs over time. *S. aureus* samples were obtained after no treatment, or after treatment with either 0.1 wt% PenG or 0.25 wt% shellac-0.2 wt% P407-0.1 wt% PenG-0.2 wt% Alcalase (referred to as PenG-NPs) or 0.2 wt% Alcalase. *S. aureus* cells, contaminated (culture) media, a positive control and a background reading for the reaction mix were analysed. Note; there is no discernible difference in beta lactamase activity of *S. aureus* when treated with either free PenG, PenG-NPs (both 0.1 wt%) or 0.2 wt% Alcalase between 1 and 3 hours. Error bars are within the symbol size.

4.3.4 Effectiveness of 0.25 wt% shellac–0.2 wt% P407–0.1 wt% PenG/Oxa–0.2 wt% Alcalase NPs against biofilm-formed *S. aureus*

Next, an investigation into the effectiveness of the 0.1 wt% PenG/Oxa NPs on *S. aureus* biofilms was performed. Biofilms were grown in 96-well plates for 24 h, and then treated with free antibiotic and antibiotic-loaded shellac NPs for further 24 h. **Figure 4.26A and B** show the residual biofilm after staining the wells with Crystal Violet (CV). Compared to the control of an untreated biofilm, there was a ~90% biofilm reduction for both 0.1 wt% PenG-NPs and 0.1 wt% Oxa-NPs treatments. The treatment with 0.1 wt% free PenG showed no significant reduction in residual biofilm, due doubly to the resistance of *S. aureus* to this antibiotic and the protection a biofilm confers to exogenous treatments. 0.1 wt% free Oxa reduced the biofilm by ~50% compared to the growth control, significantly less the 90% achieved by the 0.1 wt% Oxa-NPs. The 0.25 wt% shellac and 0.2 wt% P407 showed only a negligible reduction in residual biofilm in the wells. The 0.2 wt% Alcalase reduced the biofilm to ~50% compared to the growth control, likely due to the protease activity degrading the EPS matrix protein structure. **Figure 4.27** shows images of the biofilm wells with the CV staining, there is a clear reduction in staining in the 0.1 wt% PenG/Oxa-NPs compared to the 0.1 wt% free antibiotics. **Figure 4.26C and D** show the biofilm mass after treatment, where the results corroborate the ones obtained with CV staining. Again, the 0.1 wt% PenG-NPs reduced the biofilm mass significantly (~1 mg compared to the ~3.4 mg untreated control). The free PenG showed only a marginal reduction of ~0.5 mg due to the resistance of *S. aureus*.

The 0.1 wt% Oxa-NPs reduced the biofilm mass to 0.3 mg, a significant improvement against 0.1 wt% free Oxa which reduced the mass to ~1.1 mg. The shellac, P407 and Alcalase showed a similar trend when measuring the biofilm mass to the biofilm stained with CV. **Figure 4.26E and F** measured the protein concentration of the biofilms after treatment. **Figure 4.27** shows the BCA calibration curve used to interpolate protein concentration in the samples. The 0.1 wt% PenG/Oxa-NP treatments reduced the protein concentration to ~150–100 $\mu\text{g mL}^{-1}$, respectively, significantly more than the ~800 $\mu\text{g mL}^{-1}$ for 0.1 wt% free PenG and 0.1 wt% ~400 $\mu\text{g mL}^{-1}$ for free Oxa. The 0.2 wt% Alcalase treatment alone was effective in reducing protein concentration (~500 $\mu\text{g mL}^{-1}$). A time and concentration-dependent examination of the free 0.1 wt% PenG/Oxa treatments vs. the 0.1 wt% PenG/Oxa-NPs was performed. **Figure 4.26G** shows that free PenG (at 0.1, 0.05 and 0.025 wt% concentrations) was no discernable effect at reducing the residual biofilm. In comparison, the PenG-NPs after 24 h had reduced the residual biofilm to ~20%. After 1 h the reduction was ~40% lower compared to no treatment indicating the antibiotic-loaded NPs are fast-acting on the biofilms. There was a very little difference between the 0.025 wt% and the 0.1 wt% stock NPs treatment. This reveals that the PenG-NPs remain potent at lower concentrations. **Figure 4.26H** shows the time and

concentration-dependent free Oxa vs. Oxa-NPs. There is a similar trend in the effectiveness of the Oxa-NPs (across 0.1, 0.05 and 0.025 wt% concentrations), with the residual biofilm being reduced by ~90% compared to no treatment after 24 h. The free Oxa showed a gradual reduction in residual biofilm over 24 h, culminating in a reduction of 20%, 50% and 60% in residual biofilm for the 0.1, 0.05 and 0.025 wt% free Oxa treatments.

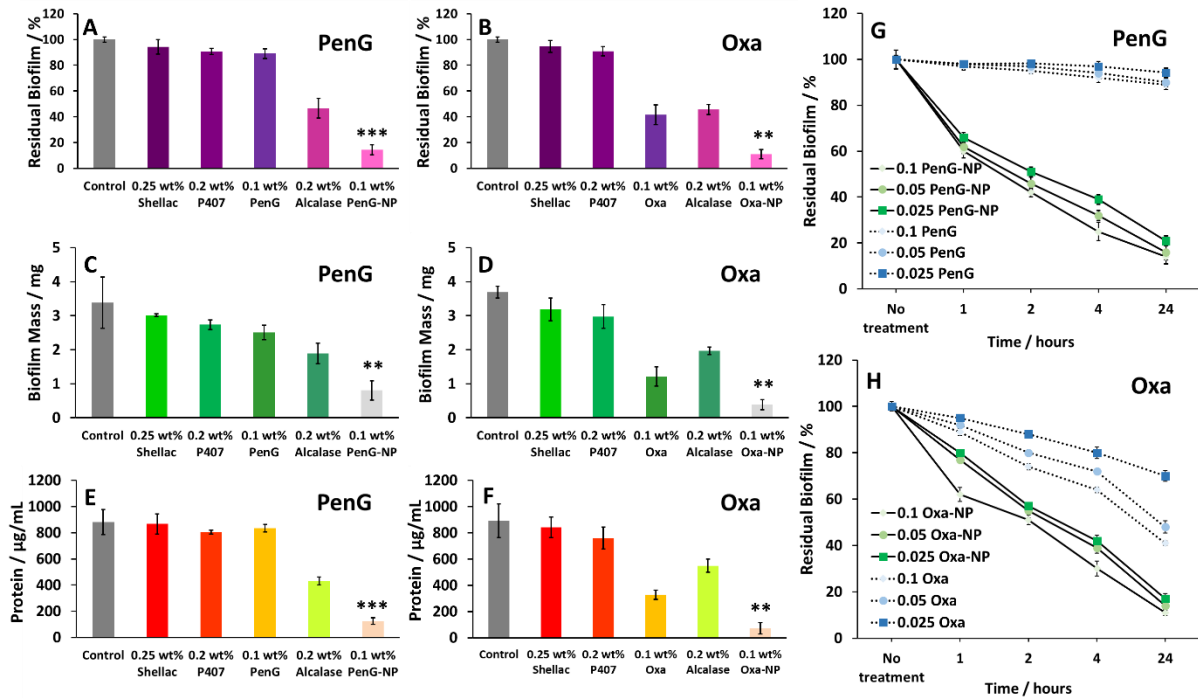


Figure 4.26. The effect of (A), (C) and (E) 0.25 wt% shellac–0.2 wt% P407–0.1 wt% PenG–0.2 wt% Alcalase and (B), (D), (F) 0.25 wt% shellac–0.2 wt% P407– 0.1 wt% Oxa–0.2 wt% Alcalase treatments on *S. aureus* biofilms after 24 h. Residual biofilm staining, biofilm mass and protein concentration respectively. 0.1 wt% PenG/Oxa-NP; 0.25 wt% shellac–0.2 wt% P407–0.1 wt% PenG/Oxa–0.2 wt% Alcalase. * $P < 0.05$, ** $P < 0.01$, *** $P < 0.001$ compared to the free antibiotic. **Table 4.5** shows the statistical analysis P-values. (G) Residual biofilm (CV staining) after treatment with shellac–P407–ABX formulations after 1, 2, 4 and 24 h treatment times. Treatments were made from a stock of 0.25 wt% shellac–0.2 wt% P407–0.1 wt% PenG–0.02 wt% Alcalase (referred as PenG-NP) or (H) 0.25 wt% shellac–0.2 wt% P407–0.1 wt% Oxa–0.02 wt% Alcalase (referred as Oxa-NP) and diluted 2-fold. All tests were performed in triplicates (N = 3 with \pm S.D.).

Table 4.5. Crystal Violet, dry mass weight and protein concentration statistical analysis between free PenG/Oxa and PenG/Oxa NPs. Data were expressed as average values \pm standard deviations of the mean. P-values of less than 0.05 were considered significant. All Student’s T-tests were performed in GraphPad v7.0.4.

Multiple Comparisons	P-value	Significance
PenG vs PenG-NPs (CV Staining)	0.00001824	***
Oxa vs Oxa NPs (CV Staining)	0.00326552	***
PenG vs PenG-NPs (Dry Mass Weight)	0.00113258	**
Oxa vs Oxa NPs (Dry Mass Weight)	0.00572886	**
PenG vs PenG-NPs (Protein Concentration)	0.0007	***
Oxa vs Oxa NPs (Protein Concentration)	0.00120271	**

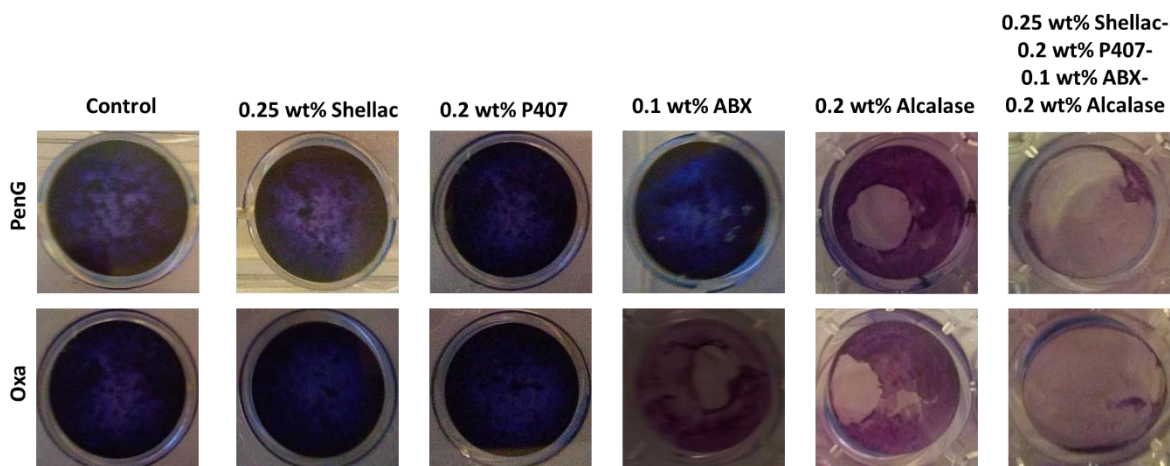


Figure 4.27. Photographs of *S. aureus* biofilms after CV staining and washing (before solubilisation in acetic acid).

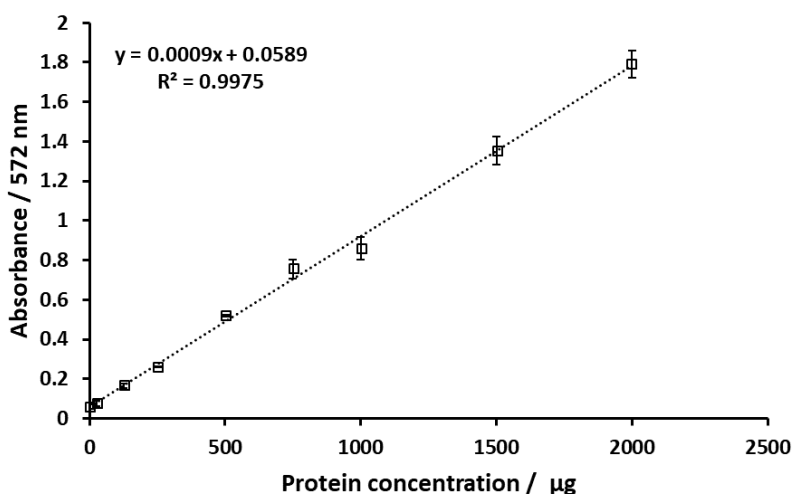


Figure 4.27. BCA (bicinchoninic acid assay) standard curve. N=3 with \pm S.D.

An investigation into the viability of the cells within the biofilm after 1, 6 and 24 h treatments was performed. **Figure 4.28A** shows the results after 1 h. The untreated control, 0.25 wt% shellac and 0.2 wt% P407 showed no reduction in cell viability, with all samples retaining $\sim 1 \times 10^9$ CFU per mL. The results were similar in the enumeration of the biofilm cells after 6 and 24 h, respectively. 0.1 wt% free PenG showed no reduction in viable cells, however, the 0.1 wt% free Oxa had reduced the cells to $\sim 1 \times 10^7$ CFU per mL. The 0.1 wt% PenG/Oxa-NPs showed a significant improvement compared to the free antibiotic, reducing the viable cells to $\sim 1 \times 10^6$ CFU per mL. **Figure 4.28B** shows the viable cells after 6 h of treatment. Both the 0.1 wt% PenG and Oxa-NPs reduced the viable cells to $\sim 1 \times 10^2$ CFU per mL. 0.1 wt% PenG remained unchanged compared to the untreated control, the 0.1 wt% free Oxa treatment has reduced the viable cells to $\sim 1 \times 10^5$ CFU per mL. The 0.2 wt% Alcalase

treatment had reduced the viable cells to $\sim 1 \times 10^6$ CFU per mL, likely due to the degradation of the biofilm by the protease releasing cells from biofilm. **Figure 4.28C** shows the viable cells after 24 h. There were no detectable cells in the 0.1 wt% PenG/Oxa-NP treatments, a significant reduction compared to $\sim 1 \times 10^9$ CFU per mL for the 0.1 wt% free PenG and $\sim 1 \times 10^4$ CFU per mL for the free Oxa. After 24 h treatment with 0.2 wt% Alcalase the viable cells were reduced to $\sim 1 \times 10^5$ CFU per mL. These results indicate that both the 0.1 wt% PenG-NPs and the 0.1 wt% Oxa-NPs are significantly more effective than an equivalent concentration of the free antibiotic. Crucially, the 0.1 wt% PenG-NP being effective against a strain of *S. aureus* classified as resistant to PenG. **Figure 4.28D** shows fluorescence microscopy images of the biofilms stained with Acridine Orange (AO) after 24 h treatment. It is clear to see that there is a much-decreased concentration in cells in the PenG/Oxa-NP treatment compared to the control, 0.25 wt% shellac and 0.2 wt% P407 treatments. The 0.1 wt% free PenG remains relatively unchanged compared to the untreated sample, with 0.1 wt% free Oxa and 0.2 wt% Alcalase reducing the AO staining by $\sim 50\%$. **Figure 4.29** shows the percentage of AO orange staining per sample.

The treatment/biofilm growth media was also examined. It is known that cells within biofilms are able to disperse during a biofilms natural formation (Richards & Melander, 2009). **Figure 4.30** shows the number of viable cells after 24 h treatments as described in **Figure 4.28A**. The untreated control and 0.25 wt% shellac contained $\sim 1 \times 10^4$ CFU per mL, much lower than the $\sim 1 \times 10^9$ CFU per mL than found in the biofilms. Biofilms treated with 0.2 wt% and 0.2 wt% Alcalase had fewer cells, $\sim 1 \times 10^3$ CFU per mL, likely due to the moderate cytotoxic nature of these compounds. 0.1 wt% PenG treatment produced $\sim 1 \times 10^4$ CFU per mL due to the resistance of *S. aureus* to this antibiotic. Treatment with 0.1 wt% free Oxa treatment showed no viable cells in the media. No viable cells were also found in the treatment media of biofilms treated with 0.1 wt% PenG/Oxa-NPs. These results mirror the CFU counts of planktonic cells shown in **4.20A**. This indicated that the ABX-NP treatments are able to effectively kill cells within a biofilm and planktonic cells outside. It is worth noting that metabolically inactive persister cells are known to be present in biofilms (Lewis, 2007). These cells are very difficult to culture and highly tolerant to antibiotics which target a metabolic mechanism, such as beta-lactam antibiotics. Therefore, it is possible that some cells survived treatment but were not detected during enumeration.

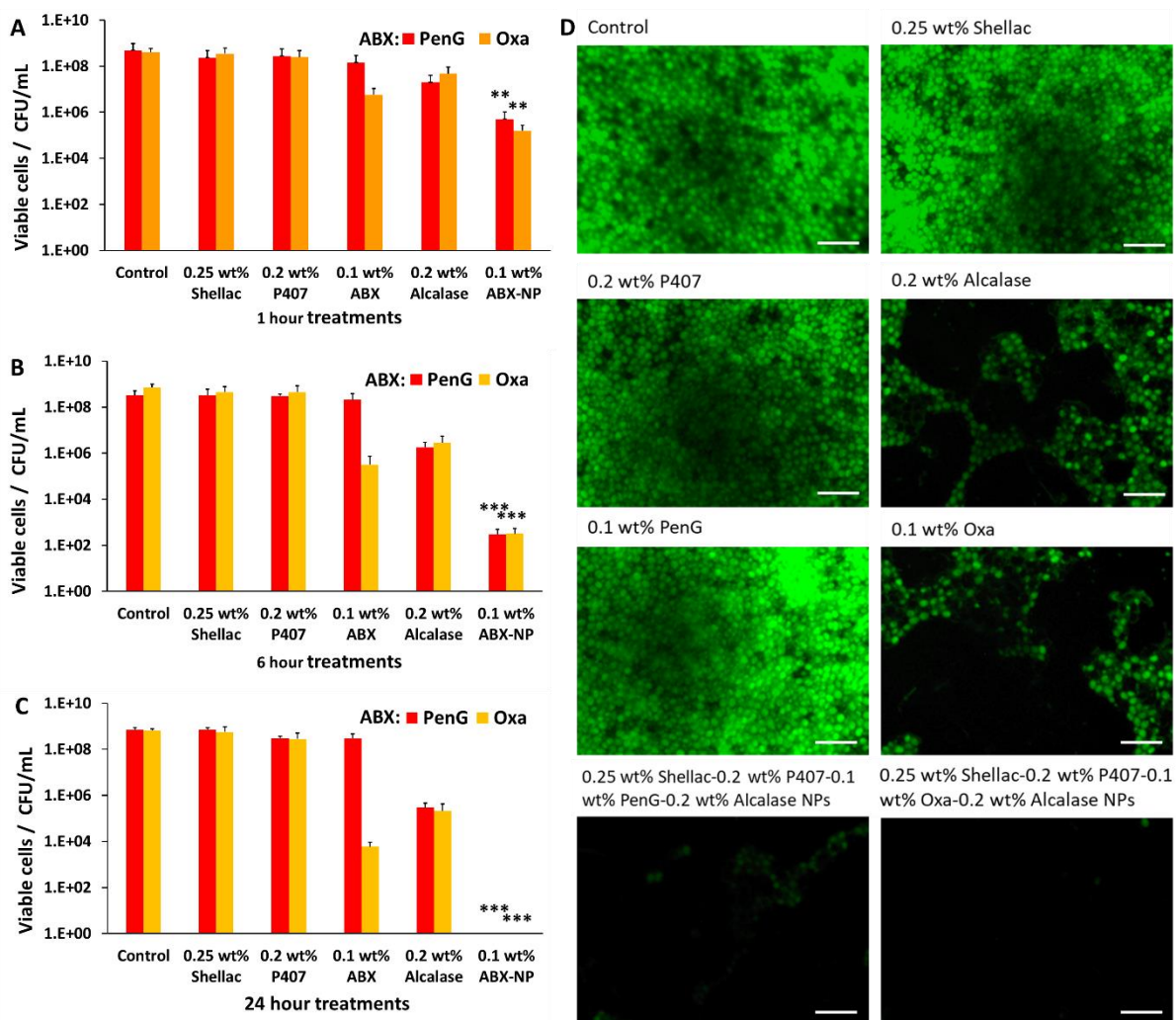


Figure 4.28. 24 h grown *S. aureus* biofilm cellular viability after anti-biofilm treatments. CFU per mL of colony biofilms after timed exposure after (A) 1 hour, (B) 6 hours and (C) 24 hours. Post-treatment, the colony biofilms were glass bead beaten in 1 mL of MHB with serial dilutions. 0.1 wt% ABX = NP; 0.25 wt% shellac–0.2 wt% P407–0.1 wt% PenG/Oxa–0.2 wt% Alcalase. The agar drop plate method was used to elucidate the CFU per mL. N = 3 with \pm S.D. * P < 0.05, ** P < 0.01, *** P < 0.001 compared to the free antibiotic. **Table 4.6** shows the statistical analysis P-values. (D) Representative fluorescent images of *S. aureus* biofilm stained with Acridine Orange after 24 h of treatment. The white inset bar represents 5 mm.

Table 4.6. *S. aureus* biofilm viability statistical analysis after 1, 6 and 24 hour treatments, comparing free PenG/Oxa and PenG/Oxa NPs. Data were expressed as average values \pm standard deviations of the mean. P-values of less than 0.05 were considered significant. All Student's T-tests were performed in GraphPad v7.0.4.

Multiple Comparisons	P-value	Significance
PenG vs PenG-NPs (1 hour)	0.00108547	**
Oxa vs Oxa NPs (1 hour)	0.00120226	**
PenG vs PenG-NPs (6 hours)	0.00096656	***
Oxa vs Oxa NPs (6 hours)	0.00263979	***
PenG vs PenG-NPs (24 hours)	0.00037384	***
Oxa vs Oxa NPs (24 hours)	0.00044592	***

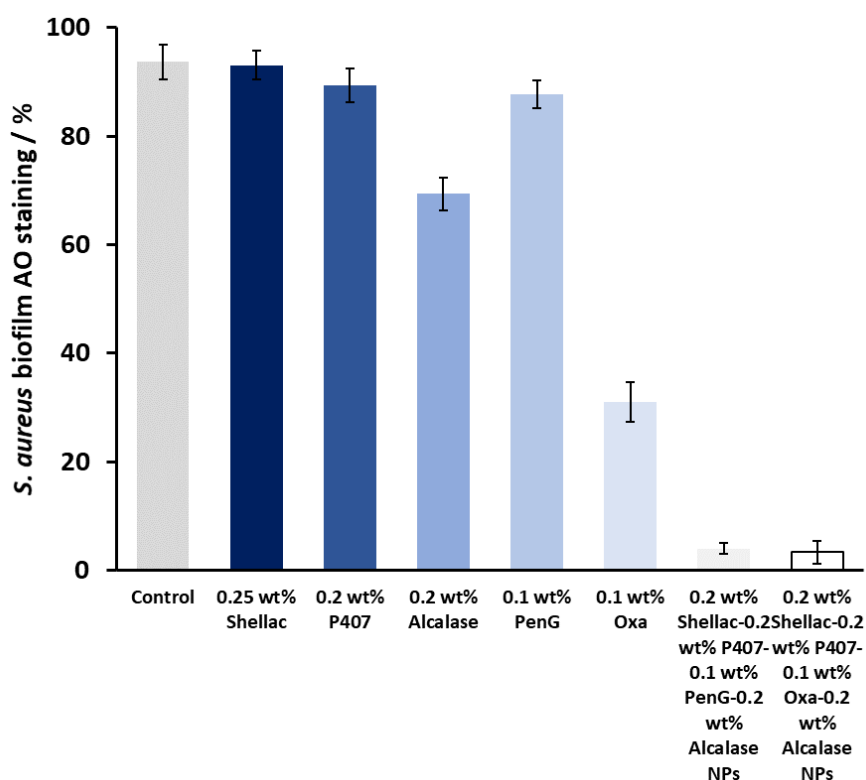


Figure 4.29. Quantification of AO staining of *S. aureus* biofilms treated for 24 hours. The % of biofilm stained with OA was quantified using ImageJ v1.52d.

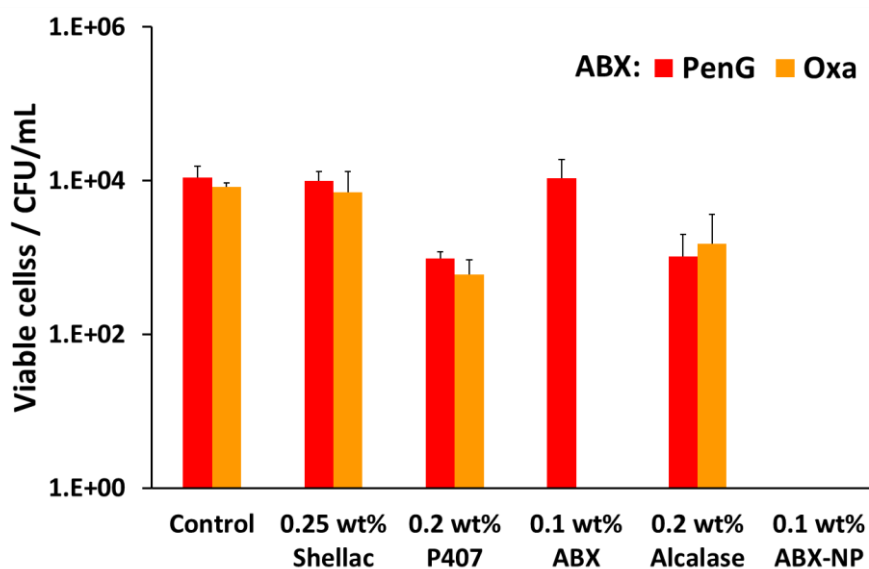


Figure 4.30. 24 hour grown *S. aureus* biofilm cellular viability after anti-biofilm treatments. CFU/mL of treatment media after 24 hours. Post-treatment 1 mL of the treatment media was serially diluted. The agar drop plate method was used to elucidate the CFU/mL. N=3 with \pm S.D.

4.3.5 The structure of biofilm-formed *S. aureus* when treated with 0.25 wt% shellac–0.2 wt% P407–0.1 wt% PenG/Oxa–0.2 wt% Alcalase NPs

To understand the structure of the biofilm after treatment a confocal laser scanning microscope (CLSM) was used to image *S. aureus* biofilms stained with AO. **Figure 4.31** shows images of *S. aureus* after 1 h and 24 h treatments as administered in **Figure 4.28**. The images show that 0.25 wt% and 0.1 wt% PenG had very little effect on the structure or thickness of the biofilms compared to the control, which was untreated. 0.2 wt% P407 and 0.2 wt% Alcalase treatments showed some reduction in biofilm thickness, more notably after 24 h of treatment. The structure appears less dense particularly on the surface of the biofilm. 0.1 wt% PenG had very little effect on the *S. aureus* PenG resistant biofilm, which agrees with the CV staining and the CFU viability counts. 0.1 wt% Oxa showed a slightly decreased thickness and less dense structure after 24 h of treatment. The 0.1 wt% PenG/Oxa-NPs showed a much-improved reduction in biofilm mass in comparison to the antibiotics alone at equivalent concentrations. There appear to be patches of completely cleared biofilm indicating the NPs are able to degrade the biofilm and reveal the cells within. The NPs showed most reduction after 24 h, confirming the CFU viability counts in **Figure 4.28**. Crucially, the PenG-NPs were effective against a species with PenG resistance.

To further corroborate the CLSM 3D images, the membrane biofilm was cryosectioned into 10 µm slices, and an examination of the thickness and structure of the EPS matrix with concanavalin A (ConA) dye under brightfield and fluorescent microscopy performed. Samples were treated for 24 h before examination. **Figure 4.31A** shows the biofilm lateral structure and **Figure 4.32B** shows the thickness of the sectioned biofilms measured across 3 standardised sections of the image. The sections show a densely packed biofilm, in the control (untreated) and 0.25 wt% shellac sections (57 µm and 59 µm, respectively). The thickness is reduced when treated with 0.2 wt% P407 and 0.2 wt% Alcalase (40 µm and 38 µm) which is consistent with the CLSM results. 0.1 wt% PenG showed very little change from the untreated control and 0.25 wt% shellac treatment, with a thickness of 55 µm. Treatment with 0.1 wt% Oxa reduced the mass to 40 µm. The samples treated with 0.1 wt% PenG/Oxa-NPs showed a completely cleared biofilm with no ConA staining detected. This agrees with CFU viability count results in **figure 4.28**. The reduction is also consistent with the much-reduced biofilm mass seen in **Figure 4.31** using CLSM. The biofilm remnants still visible in the 3D image is likely due to the differences in visualisation techniques, 3D visualisation vs. 2D cryo-sectioned lateral fluorescent imaging. However, both **Figure 4.31** and **4.32A** both provide visual support to the CFU viability counts and provide evidence the PenG/Oxa-NPs are much more effective biofilm clearing treatments than equivalent concentration of the free antibiotic. This provides evidence that formulations based on NP-encapsulated antibiotics with targeted delivery could be a useful tool in repurposing old antibiotics.

This option is becoming increasingly attractive in the antibiotic resistance era (Farha & Brown, 2019; Brown & Wright, 2016).

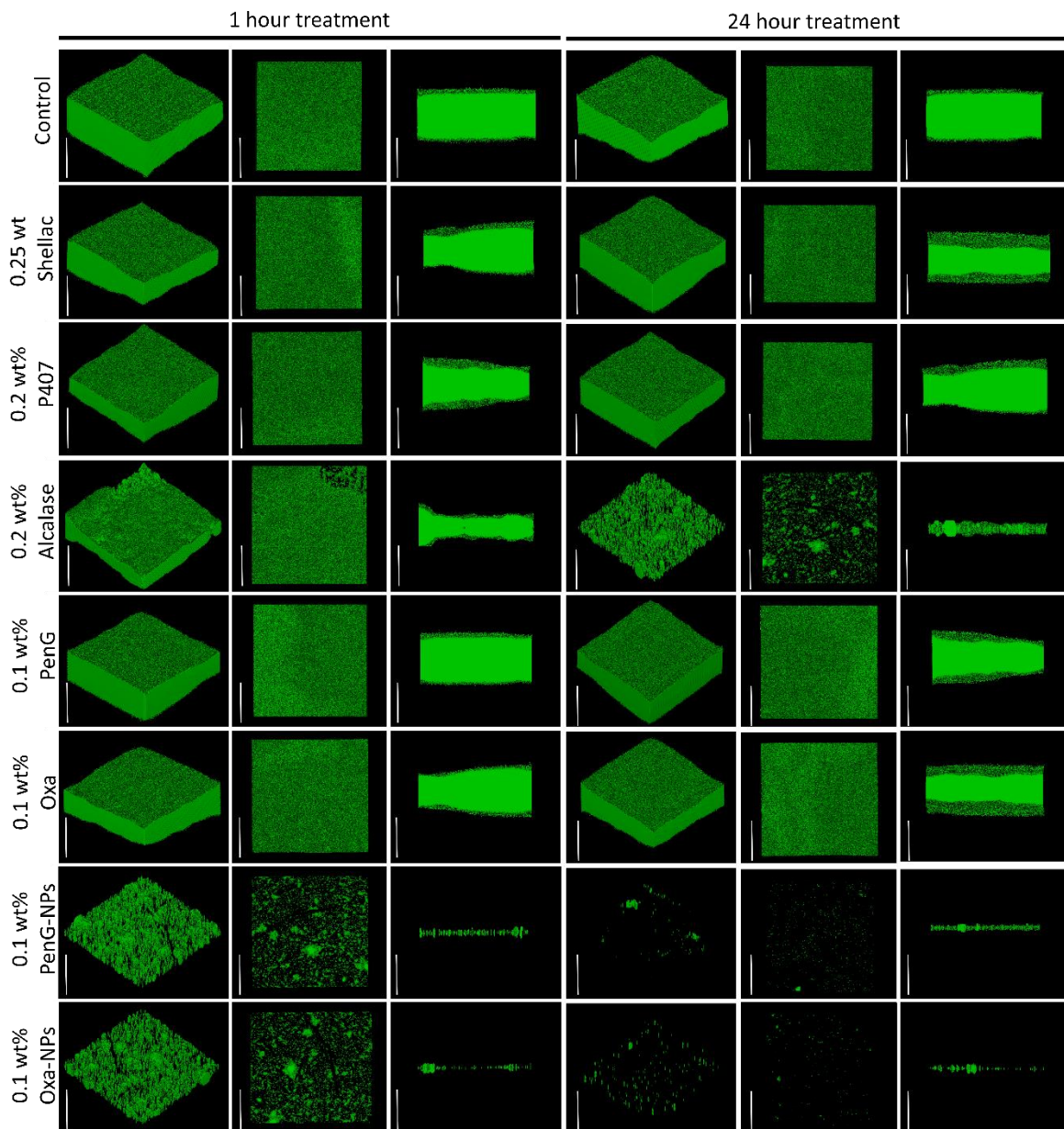


Figure 4.31. Confocal laser scanning microscopy. *S. aureus* 24 h grown biofilms treated for 1 or 24 h with various treatments. Biofilms were stained with 0.2 wt% Acridine Orange for 5 mins in darkness before gently washing away. The white inset bar represents 50 μm. 0.1 wt% PenG-NP and 0.1 wt% OxaNP refers to 0.25 wt% shellac–0.2 wt% P407–0.1 wt% PenG–0.2 wt% Alcalase NPs and 0.25 wt% shellac–0.2 wt% P407–0.1 wt% Oxa–0.2 wt% Alcalase NPs. Confocal laser scanning microscopy images (CLSM) were obtained with a Carl Zeiss LSM 710 confocal microscope with Z-series images taken in 1 mm slices.

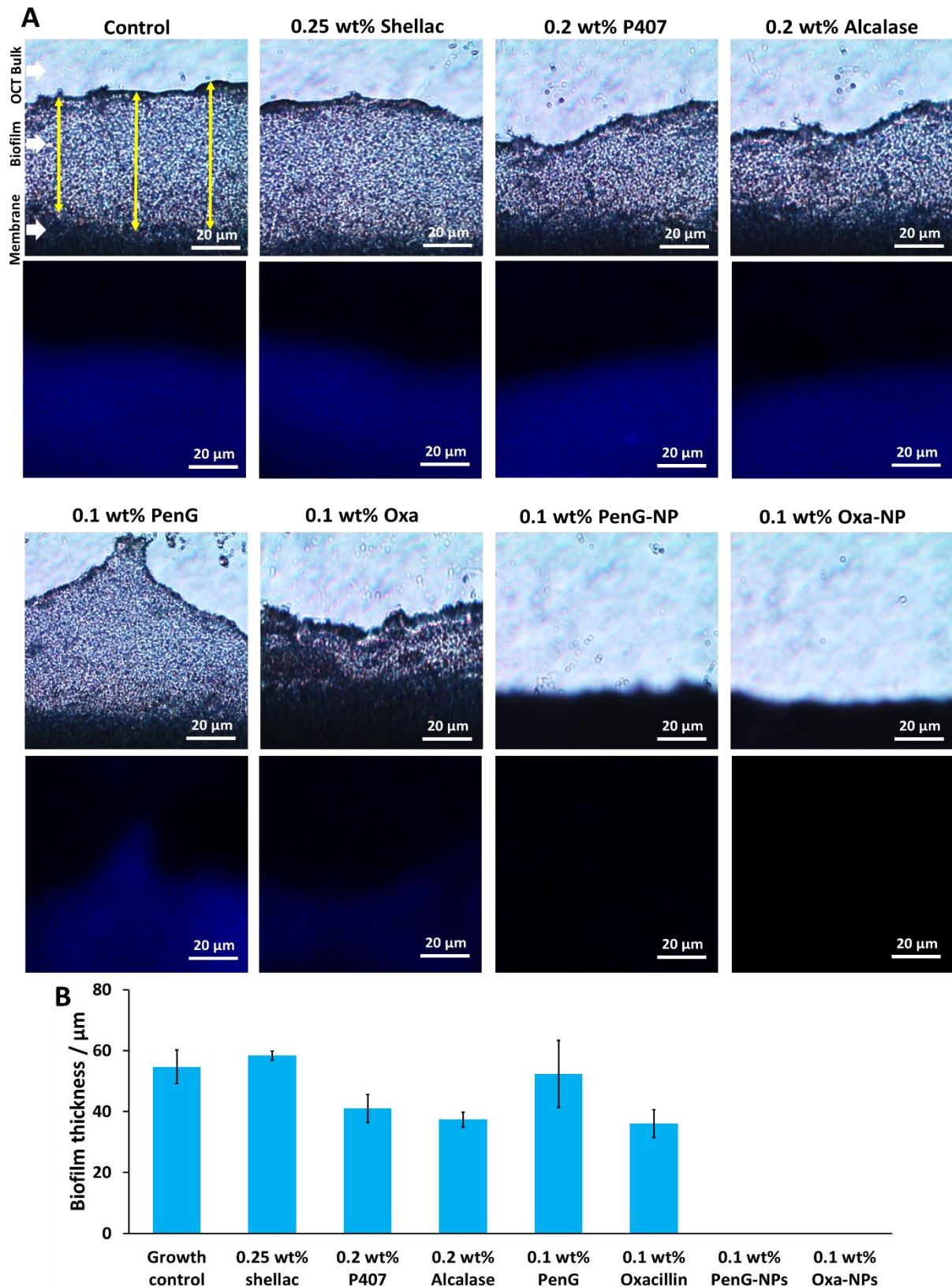


Figure 4.32. (A) Cryostat lateral 10 mm sliced images of *S. aureus* biofilms after 24 h treatments. Images were taken a 200 magnification. **(B)** Biofilm thickness measured over three locations (illustrated with yellow arrows) in Image J v1.52a. 0.1 wt% PenG-NPs and 0.1 wt% Oxa-NPs refers to 0.25 wt% shellac–0.2 wt% P407–0.1 wt% PenG–0.2 wt% Alcalase NPs and 0.25 wt% shellac–0.2 wt% P407–0.1 wt% Oxa–0.2 wt% Alcalase NPs.

4.3.6 Human cell cytotoxicity when treated with 0.25 wt% shellac–0.2 wt% P407–0.1 wt% PenG/Oxa–0.2 wt% Alcalase NPs

A preliminary human cell cytotoxicity experiment was performed on HaCaT and HEP G2 cells to investigate if the shellac, P407, free Alcalase, free antibiotic, and PenG/Oxa-NPs were toxic to human cells. HaCaT cells were chosen as they are a good proxy for studying human keratinocytes, a cell type which would be exposed to treatment in topical applications. HEP G2 were chosen as they are a good proxy for studying the effects of xenobiotics. **Figure 4.33A and B** shows that 0.25 wt% shellac had only a marginal reduction in cell viability over 1, 6- and 24-hour time points. 0.2 wt% P407 showed a slightly decreased viability, particularly after 24-hour treatment. This is to be expected of a surfactant which is known to be cytotoxic due to its ability to destroy the plasma membrane of cells. Interestingly, 0.25 wt% shellac-0.2 wt% P407 showed only a marginal reduction in viability in both the HaCaT and HEP G2 cells. This is likely due to the absorption of the P407 onto the shellac NP reducing the ability of the P407 to damage the cells. 0.2 wt% Alcalase showed again only a small reduction in viability over 1, 6- and 24-hour time points. 0.1 wt% free PenG/Oxa demonstrated only a small cytotoxic effect. This is to be expected as antibiotic supplementation of cell culture media is routinely used, particularly PenG, and is generally considered safe to use.

A similar result was observed with the 0.1 wt% PenG/Oxa-NP treatments indicating that concentrating of antibiotic into a NP centre had little effect on cell toxicity. The data shows that the PenG/Oxa-NPs had very little impact on cell viability in both HaCaT and HEP G2 cells, providing evidence they may be suitable for in vivo treatment topically on infected chronic wounds. **Figure 4.34A and B** showed the cytotoxicity of PenG-NPs and Oxa-NPs on HaCaT and HEP G2 cells as a function of concentration dependence after 24 hours of treatment. Dilutions of the NPs were made into serialised PBS. The results of the 0.1 wt% PenG/OxaNPs for both the HaCaT and HEP G2 cells are the same as revealed in **Figure 4.33A and B**. As the concentration is reduced the viability of the cells is shown to increase slightly, gradually improving towards the control of no treatment. This provides further evidence that the 0.1 wt% PenG/Oxa-NPs are only slightly toxic to mammalian cells over 24 hours.

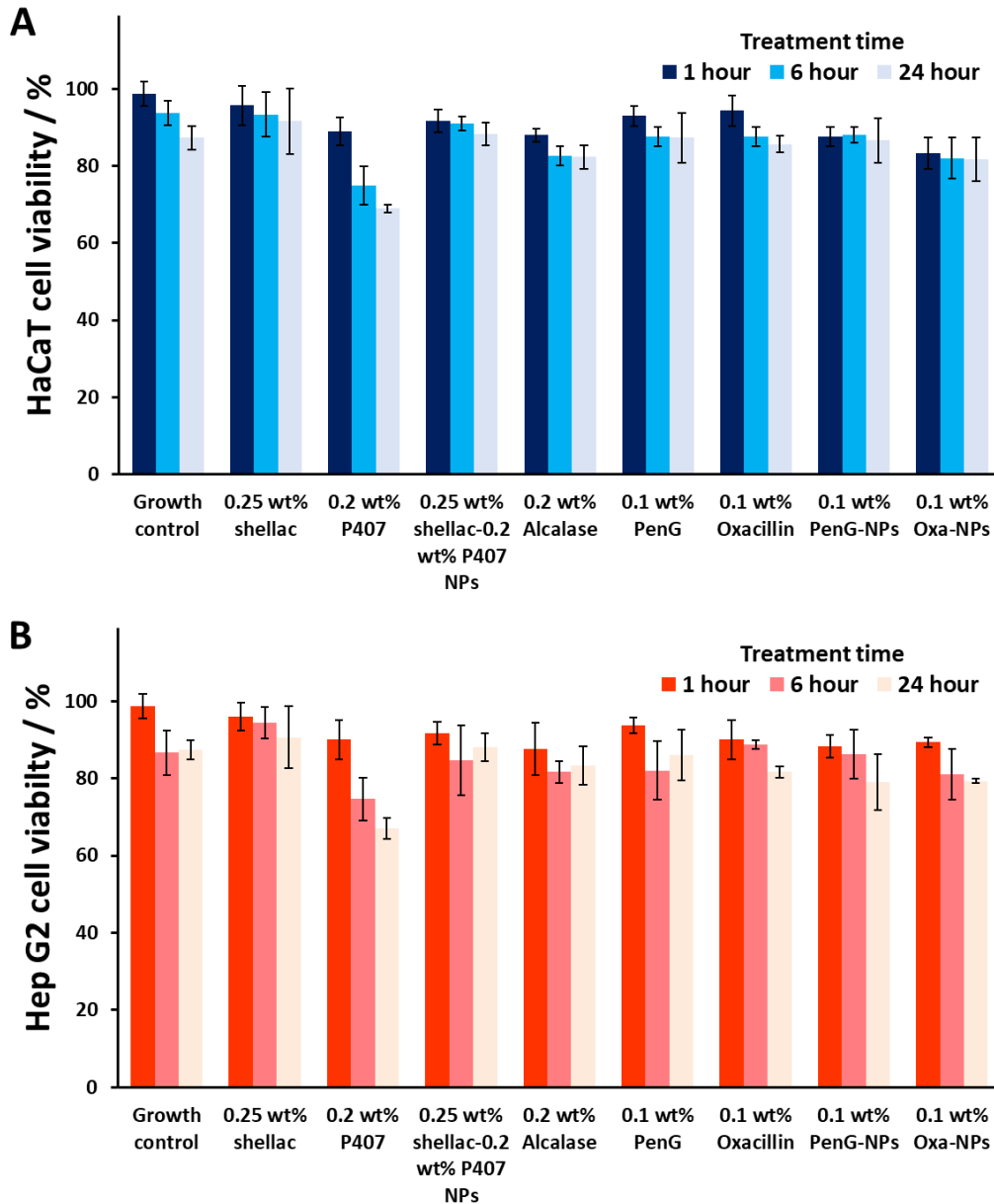


Figure 4.33. (A) HaCaT and **(B)** Hep 2G viability after treatment with 0.25 wt% shellac-0.2 wt% P407-0.1 wt% PenG/Oxa-0.2 wt% Alcalase NPs compared to 0.1 wt% free PenG/Oxa. NP components treated at the same concentration as the NP formulation were also tested. Cells were seeded at 1×10^4 and incubated for 24 hours at 37 °C in 5% CO₂ atmosphere (2 wt% FBS). The medium was then removed and replaced with treatment infused media under the same conditions. Viability counts were performed at 1, 6, and 24 hours. 0.1 wt% PenG-NP and 0.1 wt% Oxa-NP refers to 0.25 wt% shellac-0.2 wt% P407-0.1 wt% PenG-0.2 wt% Alcalase NPs and 0.25 wt% shellac-0.2 wt% P407-0.1 wt% Oxa-0.2 wt% Alcalase NPs. N=3 with \pm S.D.

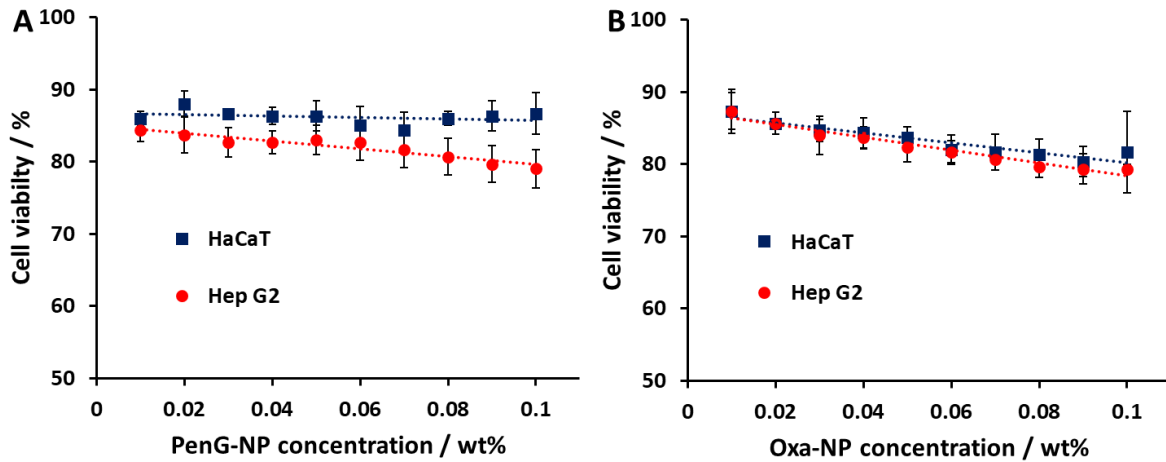


Figure 4.34. HaCaT and Hep 2G viability after treatment with decreasing concentrations of free **(A)** PenG-NPs and **(B)** Oxa-NPs. Cells were seeded at 1×10^4 and incubated for 24 hours at 37 °C in 5% CO₂ atmosphere (2 wt% FBS). The medium was then removed and replaced with treatment infused media under the same conditions. Viability counts were performed at 24 hours. 0.1 wt% PenG-NP and 0.1 wt% Oxa-NP refers to 0.25 wt% shellac-0.2 wt% P407-0.1 wt% PenG-0.2 wt% Alcalase NPs and 0.25 wt% shellac-0.2 wt% P407-0.1 wt% Oxa-0.2 wt% Alcalase NPs. N=3 with \pm S.D.

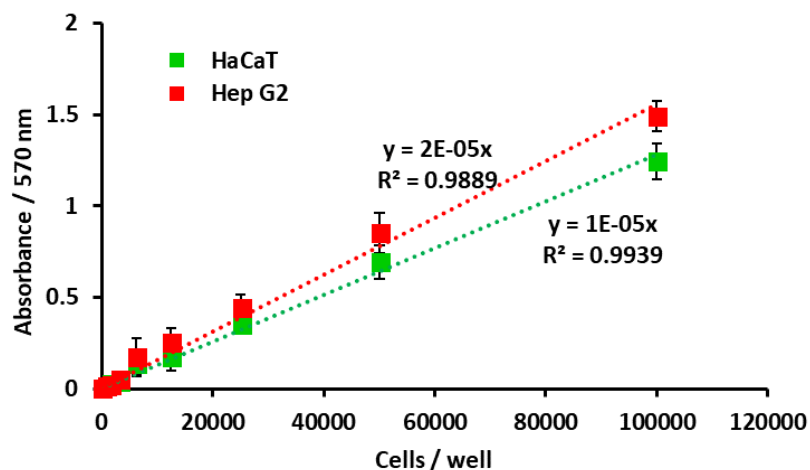


Figure 4.35. Calibration curve of HaCaT and Hep G2 cells. Various cell concentrations were seeded in DMEM (HaCaT) and EMEM (Hep 2G) medium and absorption values obtained at 570 nm. These data were used to calculate the number of cells in treatment / untreated wells. N=3 with \pm S.D.

4.4 Conclusions

In summary, this chapter shows the developed an innovative nanocarrier system with a protease coating which can overcome an antibiotic-resistant pathogen in both planktonic and biofilm form. A demonstration of the effectiveness of Penicillin G and oxacillin encapsulated in shellac NPs against a strain of *S. aureus* verified as Penicillin G resistant was performed. The functionalisation of the NPs with a coating of the cationic protease Alcalase creates a dual application NPs which allows the degradation of the biofilms and electrostatic adhesion to the anionic bacterial cell wall. The attachment of the antibiotic-loaded NPs to the bacterial cells allows a highly localised continuous release of concentrated antibiotic on the bacteria cell wall which is much higher than an equivalent concentration of the free antibiotic. Note that the Alcalase coating allows the antibiotic-packed nanocarriers to reach the bacterial cells which are “deeply buried” in the biofilm matrix. This novel method of bacteria-targeting active NPs with an additional anti-biofilm function offers an important opportunity to revive the usefulness of antibiotics considered obsolete (*i.e.* Penicillin G) and target biofilm embedded bacteria which are particularly prevalent in chronic wounds. It is concluded that Alcalase-coated and PenG/Oxa-loaded shellac NPs are an effective and safe method of clearing antibiotic resistant biofilms, and propose this could be an alternative approach to topical biofilm treatments, particularly in chronic wounds. It is suggested that further experimental investigation into the application of these NPs on biofilm-infected chronic wounds is required, and could provide a new therapeutic approach for treating antibiotic resistant biofilms.

4.5 Reference

- Al-Awady M.J., Weldrick P.J., Hardman M.J., Greenway G.M., Paunov V.N. (2018) Amplified antimicrobial action of chlorhexidine encapsulated in PDAC-functionalized acrylate copolymer nanogel carriers. *Mater. Chem. Front.*, 2, 2032–2044.
- Al-Awady, M., Fauchet, A., Greenway, G. & Paunov, V. (2017) Enhanced antimicrobial effect of berberine in nanogel carriers with cationic surface functionality. *J Mater Chem B*, 5(38), 7885–7897.
- Al-Awady, M., Greenway, G. & Paunov, V. (2015) Nanotoxicity of polyelectrolyte-functionalized titania nanoparticles towards microalgae and yeast: role of the particle concentration, size and surface charge. *RSC Advances*, 5(46), 37044–37059.
- Al-Obaidy S.S., Halbus A.F., Greenway G.M., Paunov V.N. (2019a) Boosting the antimicrobial action of vancomycin formulated in shellac nanoparticles of dual-surface functionality. *J. Mater. Chem. B.*, 7, 3119–3133.
- Al-Obaidy, S., Greenway, G. & Paunov, V. (2019b) Dual-functionalised shellac nanocarriers give a super-boost of the antimicrobial action of berberine. *Nanoscale Advances*, 1(2), 858–872.
- ATCC Genome Portal. (2020) <https://www.ncbi.nlm.nih.gov/pmc/articles/PMC154455/>. [Accessed 05/08/20]
- Ba, X., Harrison, E. M., Lovering, A. L., Gleadall, N., Zadoks, R., Parkhill, J., Peacock, S. J., Holden, M. T., Paterson, G. K., & Holmes, M. A. (2015). Old Drugs To Treat Resistant Bugs: Methicillin-Resistant *Staphylococcus aureus* Isolates with *mecC* Are Susceptible to a Combination of Penicillin and Clavulanic Acid. *Antimicrobial agents and chemotherapy*, 59(12), 7396–7404.
- Bæk, K. T., Gründling, A., Mogensen, R. G., Thøgersen, L., Petersen, A., Paulander, W., & Frees, D. (2014). β -Lactam resistance in methicillin-resistant *Staphylococcus aureus* USA300 is increased by inactivation of the ClpXP protease. *Antimicrobial agents and chemotherapy*, 58(8), 4593–4603.
- Baidamshina, D. R., Trizna, E. Y., Holyavka, M. G., Bogachev, M. I., Artyukhov, V. G., Akhatova, F. S., Rozhina, E. V., Fakhrullin, R. F., & Kayumov, A. R. (2017). Targeting microbial biofilms using Ficin, a nonspecific plant protease. *Scientific reports*, 7, 46068.
- Blackledge, M. S., Worthington, R. J., & Melander, C. (2013). Biologically inspired strategies for combating bacterial biofilms. *Current opinion in pharmacology*, 13(5), 699–706.
- Brown, E. D., & Wright, G. D. (2016). Antibacterial drug discovery in the resistance era. *Nature*, 529(7586), 336–343.
- Creech, C. B., Al-Zubeidi, D. N., & Fritz, S. A. (2015). Prevention of Recurrent Staphylococcal Skin Infections. *Infectious disease clinics of North America*, 29(3), 429–464.
- Din, F., Aman, W., Ullah, I., Qureshi, O., Mustapha, O., Shafique, S. & Zeb, A. (2017) Effective use of nanocarriers as drug delivery systems for the treatment of selected tumors. *International Journal of Nanomedicine*, Volume 12, 7291-7309.
- EUCAST Breakpoint Tables v 10.0. (2020) http://www.eucast.org/clinical_breakpoints/. [Accessed 05/08/20]
- Farha, M. A., & Brown, E. D. (2019). Drug repurposing for antimicrobial discovery. *Nature microbiology*, 4(4), 565–577.
- Gebreyohannes, G., Nyerere, A., Bii, C., & Sbhata, D. B. (2019). Challenges of intervention, treatment, and antibiotic resistance of biofilm-forming microorganisms. *Heliyon*, 5(8), e02192.
- Goetghebeur, M., Landry, P. A., Han, D., & Vicente, C. (2007). Methicillin-resistant *Staphylococcus aureus*: A public health issue with economic consequences. *The Canadian journal of infectious diseases & medical microbiology = Journal canadien des maladies infectieuses et de la microbiologie medicale*, 18(1), 27–34.
- Halbus A.F., Horozov T.S., Paunov V.N. (2019c) Self-grafting copper oxide nanoparticles show a strong enhancement of their anti-algal and anti-yeast action. *Nanoscale Adv.*, 1, 2323–2336.
- Halbus, A. F., Horozov, T. S., & Paunov, V. N. (2019a). Strongly Enhanced Antibacterial Action of Copper Oxide Nanoparticles with Boronic Acid Surface Functionality. *ACS applied materials & interfaces*, 11(13), 12232–12243.
- Halbus, A. F., Horozov, T. S., & Paunov, V. N. (2019b). Controlling the Antimicrobial Action of Surface Modified Magnesium Hydroxide Nanoparticles. *Biomimetics (Basel, Switzerland)*, 4(2), 1-20.

- Irazoki, O., Hernandez, S. B., & Cava, F. (2019). Peptidoglycan Muropeptides: Release, Perception, and Functions as Signaling Molecules. *Frontiers in microbiology*, *10*, 1-10.
- Jahangirian, H., Lemraski, E. G., Webster, T. J., Rafiee-Moghaddam, R., & Abdollahi, Y. (2017). A review of drug delivery systems based on nanotechnology and green chemistry: green nanomedicine. *International journal of nanomedicine*, *12*, 2957–2978.
- Kapoor, G., Saigal, S. & Elongavan, A. (2017) Action and resistance mechanisms of antibiotics: A guide for clinicians. *Journal of Anaesthesiology Clinical Pharmacology*, *33*(3), 300.
- Knudsen, G. M., Fromberg, A., Ng, Y., & Gram, L. (2016). Sublethal Concentrations of Antibiotics Cause Shift to Anaerobic Metabolism in *Listeria monocytogenes* and Induce Phenotypes Linked to Antibiotic Tolerance. *Frontiers in microbiology*, *7*, 1091.
- Kumari, A., Singla, R., Guliani, A., & Yadav, S. K. (2014). Nanoencapsulation for drug delivery. *EXCLI journal*, *13*, 265–286.
- Leroy, C., Delbarre, C., Ghillebaert, F., Compere, C. & Combes, D. (2008) Effects of commercial enzymes on the adhesion of a marine biofilm-forming bacterium. *Biofouling*, *24*(1), 11-22.
- Lewis K. (2007). Persister cells, dormancy and infectious disease. *Nature reviews. Microbiology*, *5*(1), 48–56.
- Limoli, D. H., Jones, C. J., & Wozniak, D. J. (2015). Bacterial Extracellular Polysaccharides in Biofilm Formation and Function. *Microbiology spectrum*, *3*(3), 10.1128/microbiolspec.MB-0011-2014.
- Lister, J. L., & Horswill, A. R. (2014). Staphylococcus aureus biofilms: recent developments in biofilm dispersal. *Frontiers in cellular and infection microbiology*, *4*, 178.
- Llarrull, L. I., Fisher, J. F., & Mobashery, S. (2009). Molecular basis and phenotype of methicillin resistance in *Staphylococcus aureus* and insights into new beta-lactams that meet the challenge. *Antimicrobial agents and chemotherapy*, *53*(10), 4051–4063.
- Lobanovska, M., & Pilla, G. (2017). Penicillin's Discovery and Antibiotic Resistance: Lessons for the Future?. *The Yale journal of biology and medicine*, *90*(1), 135–145.
- Lowy F. D. (2003). Antimicrobial resistance: the example of *Staphylococcus aureus*. *The Journal of clinical investigation*, *111*(9), 1265–1273.
- Markowska, K., Grudniak, A. M., & Wolska, K. I. (2013). Silver nanoparticles as an alternative strategy against bacterial biofilms. *Acta biochimica Polonica*, *60*(4), 523–530.
- Melander, R. J., & Melander, C. (2015). Innovative strategies for combating biofilm-based infections. *Advances in experimental medicine and biology*, *831*, 69–91.
- Mihelič, M., Vlahoviček-Kahlina, K., Renko, M., Mesnage, S., Doberšek, A., Taler-Verčič, A., Jakas, A., & Turk, D. (2017). The mechanism behind the selection of two different cleavage sites in NAG-NAM polymers. *IUCr*, *4*(Pt 2), 185–198.
- Mitrofanova, O., Mardanov, A., Evtugyn, V., Bogomolnaya, L. & Sharipova, M. (2017) Effects of Bacillus Serine Proteases on the Bacterial Biofilms. *BioMed Research International*, 2017, 1-10.
- Munita, J. M., & Arias, C. A. (2016). Mechanisms of Antibiotic Resistance. *Microbiology spectrum*, *4*(2), 10.1128/microbiolspec.VMBF-0016-2015.
- Newase, S. & Bankar, A. (2017) Synthesis of bio-inspired Ag–Au nanocomposite and its anti-biofilm efficacy. *Bulletin of Materials Science*, *40*(1), 157-162.
- Richards, J. J., & Melander, C. (2009). Controlling bacterial biofilms. *ChemBiochem : a European journal of chemical biology*, *10*(14), 2287–2294.
- Richter, A. P., Bharti, B., Armstrong, H. B., Brown, J. S., Plemmons, D., Paunov, V. N., Stoyanov, S. D., & Velev, O. D. (2016). Synthesis and Characterization of Biodegradable Lignin Nanoparticles with Tunable Surface Properties. *Langmuir: the ACS journal of surfaces and colloids*, *32*(25), 6468–6477.
- Sharma, D., Misba, L., & Khan, A. U. (2019). Antibiotics versus biofilm: an emerging battleground in microbial communities. *Antimicrobial resistance and infection control*, *8*, 76.

- Singh, R., Kumar, M., Mittal, A., & Mehta, P. K. (2016). Microbial enzymes: industrial progress in 21st century. 3 *Biotech*, 6(2), 174.
- Singh, S., Singh, S. K., Chowdhury, I., & Singh, R. (2017). Understanding the Mechanism of Bacterial Biofilms Resistance to Antimicrobial Agents. *The open microbiology journal*, 11, 53–62.
- Smith, A. M., Feldman, C., Massidda, O., McCarthy, K., Ndiweni, D., & Klugman, K. P. (2005). Altered PBP 2A and its role in the development of penicillin, cefotaxime, and ceftriaxone resistance in a clinical isolate of *Streptococcus pneumoniae*. *Antimicrobial agents and chemotherapy*, 49(5), 2002–2007.
- Soares, G. M., Figueiredo, L. C., Faveri, M., Cortelli, S. C., Duarte, P. M., & Feres, M. (2012). Mechanisms of action of systemic antibiotics used in periodontal treatment and mechanisms of bacterial resistance to these drugs. *Journal of applied oral science : revista FOB*, 20(3), 295–309.
- Sun, D., Jeannot, K., Xiao, Y., & Knapp, C. W. (2019). Editorial: Horizontal Gene Transfer Mediated Bacterial Antibiotic Resistance. *Frontiers in microbiology*, 10, 1933.
- Verderosa, A. D., Totsika, M., & Fairfull-Smith, K. E. (2019). Bacterial Biofilm Eradication Agents: A Current Review. *Frontiers in chemistry*, 7, 824.
- Weldrick P.J., Iveson S., Hardman M.J., Paunov V.N. (2019a) Breathing new life into old antibiotics: Overcoming antibacterial resistance by antibiotic-loaded nanogel carriers with cationic surface functionality. *Nanoscale*, 11, 10472–10485.
- Weldrick, P. J., Hardman, M. J., & Paunov, V. N. (2019b). Enhanced Clearing of Wound-Related Pathogenic Bacterial Biofilms Using Protease-Functionalized Antibiotic Nanocarriers. *ACS applied materials & interfaces*, 11(47), 43902–43919.
- WHO (2014) Antimicrobial Resistance and Surveillance Report 2014, https://apps.who.int/iris/bitstream/handle/10665/112642/9789241564748_eng.pdf;jsessionid=67D9BD148E9C9EFC44EB1D2F3B4C32C3?sequence=1.
- Wilkinson, H. N., Iveson, S., Catherall, P., & Hardman, M. J. (2018). A Novel Silver Bioactive Glass Elicits Antimicrobial Efficacy Against *Pseudomonas aeruginosa* and *Staphylococcus aureus* in an *ex Vivo* Skin Wound Biofilm Model. *Frontiers in microbiology*, 9, 1450.
- Worthington, R. J., & Melander, C. (2013a). Overcoming resistance to β -lactam antibiotics. *The Journal of organic chemistry*, 78(9), 4207–4213.
- Worthington, R. J., & Melander, C. (2013b). Combination approaches to combat multidrug-resistant bacteria. *Trends in biotechnology*, 31(3), 177–184.
- Yadav, A. K., Espaillet, A., & Cava, F. (2018). Bacterial Strategies to Preserve Cell Wall Integrity Against Environmental Threats. *Frontiers in microbiology*, 9, 2064.
- Yilmaz, Ç., & Özcengiz, G. (2017). Antibiotics: Pharmacokinetics, toxicity, resistance and multidrug efflux pumps. *Biochemical pharmacology*, 133, 43–62.
- Yu, X., Trase, I., Ren, M., Duval, K., Guo, X., & Chen, Z. (2016). Design of Nanoparticle-Based Carriers for Targeted Drug Delivery. *Journal of nanomaterials*, 2016, 1087250.

5.0 Chapter 5

Enhanced removal of fungal biofilms by protease-functionalised amphotericin B nanocarriers

Weldrick, P. J., Hardman, M. J., & Paunov, V. N. (2021). Super-Enhanced Removal of Fungal Biofilms by Protease - Functionalized Amphotericin B Nanocarriers. *Adv. Nanobiomed. Res.*, 1, 2000027. Reproduced by permission of Wiley-VCH GmbH. Attribution 4.0 International (CC BY 4.0). <https://creativecommons.org/licenses/by/4.0/>. Minor changes made to presentation of the material. Conceptualisation, V.N.P. All experiments were performed by P.J.W under V.N.P. supervision. P.J.W prepared the figures and wrote the manuscript, V.N.P and M.J.H. co-edited the manuscript. All authors have given approval to the final version of the manuscript.

A strong enhancement in the antifungal activity of amphotericin B (AmpB) encapsulated into shellac nanoparticles (NPs) surface functionalised with protease is reported. These AmpB-loaded shellac NPs are fabricated by pH-induced nucleation of aqueous solutions of shellac and AmpB in the presence of Poloxamer 407 (P407) as a steric stabiliser. The AmpB-loaded shellac NPs are surface coated with the cationic protease Alcalase 2.4L FG. The performance of the AmpB-encapsulated NPs against *Candida albicans* is evaluated. The AmpB-loaded shellac NPs show a remarkable boost of their antifungal action compared to free AmpB when applied to *C. albicans* in both planktonic and biofilm forms. The surface functionalisation with a cationic protease allows the NPs to adhere to the fungal cell walls, delivering AmpB directly to their membranes. Additionally, the hydrolysing activity of the protease coating degrades the biofilm matrix, thus increasing the effectiveness of the encapsulated AmpB compared to free AmpB at the same concentration. The protease-coated AmpB-loaded shellac NPs show no greater toxicity to human adult keratinocyte cells (HaCaT) compared to the free AmpB. These AmpB nanocarriers demonstrate increased efficacy against *C. albicans* and can be potentially used to treat fungal biofilm infection in the clinic, for example, in recalcitrant chronic wounds.

5.1 Introduction

Amphotericin B (AmpB) is a polyene antifungal agent used to treat serious and systemic fungal infections, including mucormycosis, cryptococcal meningitis, and certain aspergillosis and candidiasis (Warnock, 1991; Keane et al., 2018). Although effective, it can have serious and life-threatening side effects, including nausea, fever, cardiac inflammation, organ failure (hepatotoxicity/nephrotoxicity), and anaphylaxis (Balkovec et al., 2014). AmpB is typically administered intravenously as lipid, liposomal, and deoxycholate formulations (Hamill, 2013; Stone et al., 2016), where it has shown remarkable resilience to the development of resistance by fungal species (Vincent et al., 2018; Ksiezopolska & Gabaldón, 2018).- AmpB binds to a component of fungal cells called ergosterol, resulting in the formation of pores, and subsequent leaking of monovalent ions and ultimately cell death (Mesa-Arango et al., 2012). This mode of action favourably targets ergosterols found only in fungal cell membranes compared to mammalian cell cholesterol due to the increased affinity of AmpB to ergosterol (Neumann et al., 2010). AmpB remains the gold standard for treating fungal infected wounds, including *Candida albicans* (Grela et al., 2019).- However, additional research on enhancing efficacy and simultaneously reducing patient side effects is required (Faustino & Pinheiro, 2020).- Due to the low solubility of AmpB in water, it is usually administered as a liposomal or gel formulation to allow higher concentrations to be used intravenously (Takemoto et al., 2006; Ganeshpurkar et al., 2014). This approach does not guarantee AmpB will reach the site of infection in a wound (Akers et al., 2015). Another approach is to apply AmpB topically, therefore circumventing systemic cytotoxicity (Sanchez et al., 2014; Uppuluri et al., 2011). To date, these approaches have not been able to show reduced mammalian cell toxicity.

C. albicans is a pathogenic yeast and a highly prevalent biofilm-forming fungi, found in human tissue infections (e.g., chronic wounds) and colonising indwelling medical devices (Gulati & Nobile, 2016).- It resides naturally as part of healthy gut flora, in the gastrointestinal tract and orally, and is considered commensal; however, it is pathogenic for immune-compromised patients undergoing antibiotic therapy (Cauchie et al., 2017).- Human infection is termed “candidiasis” and is prevalent, particularly amongst women, where systemic infection is often associated with high mortality rates (up to 40%) (Pfaller & Diekema, 2007).- *C. albicans* is part of a cohort of fungal species, including *Candida tropicalis*, *Candida glabrata*, and *Candida parapsilosis*, which represents an estimated 90% of all cases of candidiasis in humans (Pfaller et al., 2014).- For this reason, *C. albicans* is often used as a proxy for all *Candida* species in the laboratory (Morad et al., 2018).- *Candida auris*, first discovered in 2009, is an emerging cause of candidiasis, and a known biofilm-producing pathogen (Sears & Schwartz, 2017).- *C. auris* infections are of particular concern due to the high rate of resistance

to fluconazole and voriconazole, and its high mortality rate of 30% (Osei-Sekyere, 2019).- *C. auris* is also highly transmittable and able to colonise skin indefinitely, which coupled with its high pathogenicity and limited susceptibility to antifungal agents, with the exception of AmpB, makes the development of novel antifungal treatments highly important (Forsberg et al., 2019).

Biofilms are composed of an extracellular polymeric substance (EPS), containing a matrix of biopolymers such as lipids, exDNA, exopolysaccharides, and proteins (Desai et al., 2014). This structured matrix contains hydrated and hydrophobic regions and allows microbial communities to grow and adhere to a wide range of biotic and abiotic substances (Costa-Orlandi et al., 2017).- The EPS confers a protective quenching effect against antimicrobial agents, which are normally able to kill planktonic cells (Sharma et al., 2019).- Chronic wounds such as diabetic foot ulcers often contain fungal species (21.4%) that can live in multispecies biofilms, usually associated with increased healing times (Chellan et al., 2010).- Most current research on chronic wound therapies is focused on antibacterial treatments that can increase the fungal diversity in wounds. This emphasises the need for more advanced antifungal therapies, especially for biofilm-forming fungal infections (Kalan & Grice, 2018).- Au nanoparticles (NPs), silica NPs, CuONPs, and Mg(OH)₂ NPs have shown to be effective antimicrobial agents (Newase & Bankar, 2017; Markowska et al., 2013; Halbus et al., 2019a; Halbus et al., 2019b; Halbus et al., 2019c).-

Encapsulation of antibiotics in polyacrylic acid-based nanogels subsequently surface-functionalised with a cationic polyelectrolyte has been shown to increase the efficacy of the antibiotic against species that demonstrate antimicrobial resistance (Weldrick et al., 2019a; Al-Awady et al., 2018).- In addition, enzyme surface functionalisation of the nanocarriers has also shown good effect against biofilm-dwelling bacteria (Weldrick et al., 2019b; Singh et al., 2016).- Bacterial proteases are used in their colonisation of new surfaces and may have an advantage in clearing biofilms as they can aid the detachment of the biofilm from a surface (Kostakioti et al., 2013; Kaplan, 2010). Gold NPs have also been functionalised with indolicidin (an antimicrobial peptide) and demonstrated effectiveness against *C. albicans* biofilms (de Alteriis et al., 2018).- Biofilm formation–preventative nitric oxide–releasing NPs have been used to cause *C. albicans* cell death by inducing apoptosis and reducing their metabolic activity (Ahmadi et al., 2016).- Poly(lactic-*co*-glycolic acid) (PLGA)-loaded AmpB combined with sonication has also been shown to be mildly effective against *C. albicans* biofilms (Yang et al., 2019).- Due to the increased clinical importance of fungal biofilms in chronic wounds and the very limited number of effective antifungal agents, there is a pressing need for the development of novel nanotechnologies that can increase the efficacy of existing treatments.

Shellac is a resin of insect origin and has numerous applications including lacquers, dental varnishes, and agricultural and pharmaceutical formulations (Tamburini et al., 2017; Nevin et al., 2009; Hoang-Dao et al., 2008; Limmatvapirat et al., 2008). It is composed of polar and nonpolar compounds such as lactones, anhydrides, and polyhydroxy acids- which dissolve well in basic aqueous solution but are insoluble in acidic media, forming a precipitate (Gardner & Whitmore, 1929; Badawy et al., 2001; Patel et al., 2013; Limmatvapirat et al., 2004). Colloidal shellac has been used as a drug coating, encapsulating silibinin, and protein with xanthan gum and chitosan used as stabilisers (Sun et al., 2017; Patel et al., 2011; Kraisit et al., 2013).

Here is reported a novel approach for clearing fungal biofilms based on Alcalase-functionalised shellac NPs that are loaded with AmpB, which show only minimal toxicity toward mammalian cells. This method allowed the encapsulation of AmpB into shellac NPs that were sterically stabilised using Poloxamer 407 (P407). P407 is a triblock copolymer consisting of a central block of polypropylene glycol, which is hydrophobic, and two-branched polyethylene glycol blocks, which are hydrophilic (Giuliano et al., 2018). P407 is used as a surface-active polymer, emulsifying and dispersal agent in pharmaceutical formulations (Pitto-Barry & Barry, 2014).

Figure 5.1 shows the process used to formulate the AmpB-encapsulated NPs coated with Alcalase 2.4L FG. AmpB was encapsulated based on the hydrophobic interactions between the drug and the shellac matrix. P407 was used to sterically stabilise the produced NPs. The NPs are then functionalised with a cationic protease (Alcalase 2.4 L FG) to promote a positive surface charge. In addition, the protease coating allows these NPs to digest glycoprotein-rich biofilms and reach the embedded fungal cells (Mitrofanova et al., 2017). The AmpB is slowly released from the NPs and is able to be localised on the *C. albicans* cell membrane after the Alcalase has partially decomposed the biofilm EPS. **Figure 5.2** outlines the chemical components of the shellac NP–AmpB formulation. An investigation the action of Alcalase-coated AmpB-loaded shellac NPs against *C. albicans* in both planktonic and biofilm form is performed, and compared their effectiveness against the formulations of equivalent concentrations of free AmpB. Additionally, the cytotoxicity of these NPs is compared to free AmpB on human keratinocytes.

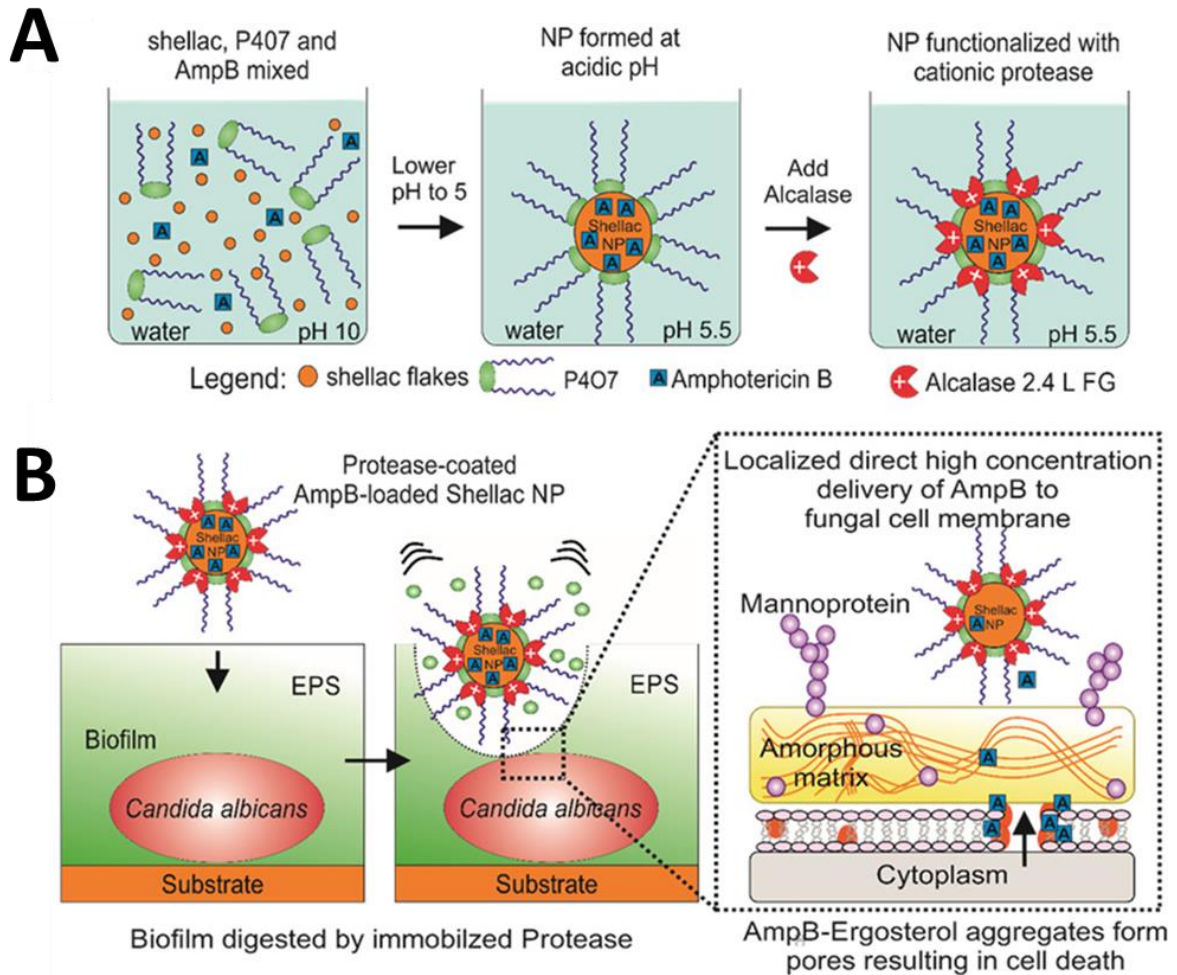
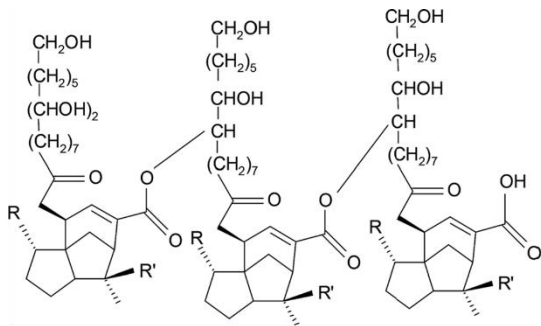
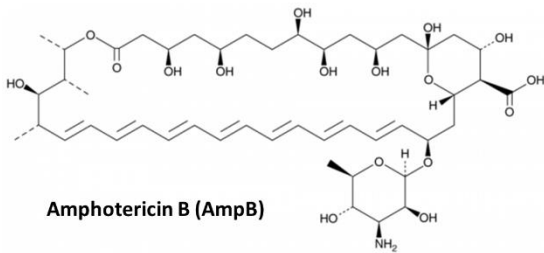


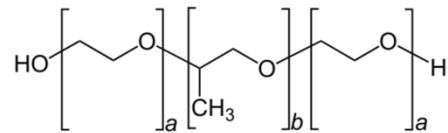
Figure 5.1. (A) Schematic for the synthesis of protease-functionalised shellac nanocarriers for AmpB. The AmpB-loaded shellac NPs are sterically stabilised with P407 and have cationic surface functionality achieved by coating with the cationic protease Alcalase 2.4L FG. **(B)** Diagram of the mechanism of action for AmpB-loaded shellac–Alcalase-functionalised NPs.



Shellac (SSB® Aquagold ammonia salt)
 $R=CHO/COOH, R'=CH_2OH/CH_3$



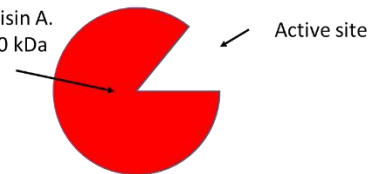
Amphotericin B (AmpB)



Poloxamer 407 (P407)

Triblock copolymer; central hydrophobic block of (b) polypropylene glycol and two hydrophilic blocks of (a) polyethylene glycol.
 Block lengths; a = ~101 and b = ~56.

Primarily subtilisin A.
 Typical MW ~30 kDa



Alcalase 2.4 L FG.

Serine endo-peptidase
 Isoelectric point ~pH 9. Cationic below pH 9.

Figure 5.2. Individual components and molecular structures of materials used in the preparation of shellac-P407-AmpB-Alcalase nanoparticles.

5.2 Materials and Methods

5.2.1 Materials

The shellac formulation was kindly provided as a gift by Stroeever Schellack Bremen (SSB) and is commercially available as SSB AquaGold, an aqueous solution of ammonium shellac salt (25 wt%). P407 (>99%) and AmpB solution were purchased from Sigma-Aldrich, UK. Amphotericin B was provided at 250 $\mu\text{g mL}^{-1}$ in deionised water, 0.1 μm filtered, and had the following components aimed to improve its solubility: sodium deoxycholate, sodium chloride, and sodium phosphate. Alcalase 2.4 L FG, EC number 3.4.21.62, was kindly provided as a sample by Novozymes, Denmark. Alcalase 2.4 L FG is a serine endopeptidase (mainly subtilisin A), which performs stereoselective hydrolysis of amino esters and selective esters. Alcalase also efficiently hydrolyses amino esters, which include heterocyclic amino esters. Optimal conditions for usage are 30–65 °C and pH 7–9. Its enzymatic activity was 2.4 au A g^{-1} . The protein concentration of Alcalase 2.4 L FG was 55 mg mL^{-1} , determined by a NanoDrop Lite Spectrophotometer (Thermo Scientific, U.K.). *C. albicans* (Robin) Berkhout (ATCC MYA-2876) was purchased by American Type Culture Collection (ATCC) and used in this study. *C. albicans* stock was streaked onto Sabouraud agar plates containing 4 wt% dextrose, 1 wt% peptone, and 2 wt% agar dissolved in deionised water. Overnight cultures (O/N) were grown in YPD media containing 1 wt% yeast extract, 2 wt% peptone, and 2 wt% dextrose dissolved in deionised water. Agar was provided by Melford (UK), Dextrose (analytic grade) by Fisher (UK), yeast extract by Sigma-Aldrich (UK), and peptone by Oxoid (UK). A Pierce BCA protein assay kit was used to determine protein concentration. CV, dye content, $\geq 90\%$ was provided by Sigma-Aldrich (UK), FDA (98%) by Fluka (UK), and propidium iodide (PI) by AbD Serotec (UK). HaCaT cells were obtained from AddexBio, T0020001. Dulbecco's modified Eagle's medium (DMEM) and foetal bovine serum (FBS) were obtained from Gibco (UK), L-glutamine and trypsin ethylenediaminetetraacetic acid (EDTA) from BioWhittaker (UK). Trypan Blue solution (0.4% phosphate buffered saline) was supplied by HyClone (GE Healthcare Sciences, UK). A 3-(4,5-dimethylthiazol-2-yl)-2,5-diphenyltetrazolium bromide (MTT) colorimetric survival and proliferation kit (Millipore Corp., USA) was used for HaCaT cell viability experiments. 2,3-Bis-(2-methoxy-4-nitro-5-sulfophenyl)-2H-tetrazolium-5-carboxanilide (XTT) was provided by Abcam (UK) and crystalline menadione by Sigma-Aldrich (UK). Roswell Park Memorial Institute media (RPMI-1640) without sodium bicarbonate was purchased from Gibco (UK). Acetonitrile and glacial acetic acid was provided by Fisher Scientific (UK), and DMSO by Sigma-Aldrich (UK). Deionised water purified by reverse osmosis and ion exchange with a Milli-Q water system (Millipore, UK) was used in all experiments. Its surface tension was 71.9 mN m^{-1} at 25 °C, with measured resistivity higher than 18 $\text{M}\Omega \text{ cm}^{-1}$. The consumable plasticware used in the study was purchased from Sarstedt (UK), Thermo Scientific (UK), or CytoOne (UK), unless otherwise stated.

5.2.2 Preparation of AmpB-loaded P407-stabilised shellac NPs

A stock solution of 25 wt% shellac-ammonia salt was diluted to 0.2 wt% and made up to a volume 50 mL in deionised water; the pH was then raised to 10 using droplets of 0.25 M NaOH. P407 and AmpB were added at various concentrations and mixed for 5 min. Afterward, the pH was reduced to 5.5 using 0.25 M HCl to allow the components to precipitate into NPs. The final concentration of 0.2 wt% shellac–0.25 wt% P407–0.02 wt% AmpB NPs was used as a stock preparation and for further experimentation.

5.2.3 Enzyme surface functionalisation of the 0.2 wt% shellac–0.25 wt% P407–0.02 wt% AmpB NPs

The stock NPs formulation was surface-functionalised with Alcalase 2.4L FG to create a coating of immobilised protease on the P407 corona of the NPs. The stock solution of Alcalase 2.4L FG was diluted in deionised water to 0.2 wt% to a volume of 50 mL and sonicated for 15 min to prevent aggregation. A total of 25 mL of this solution was added to 25 mL of AmpB-loaded P407-stabilised shellac NPs dispersion and mixed for 30 min at pH 5.5 to allow an effective coating of the NPs with the cationic protease. Afterward the mixture was centrifuged at 8000 *g* for 30 min to pelletise the NPs. The supernatant was retained for spectroscopic analysis. The pellet was redispersed into 25 mL of deionised water buffered to pH 5.5 (acetate buffer), yielding a stock dispersion of 0.2 wt% shellac–0.25 wt% P407–0.02 wt% AmpB–0.2 wt% Alcalase NPs, which were used further for NPs characterisation and antifungal experimentation.

5.2.4 Shellac NP hydrodynamic diameter, zeta potential, and SEM/TEM characterisation

Particle size distribution and zeta potential were measured using Malvern Zetasizer Nano ZS. The refractive index (RI) of shellac was found to be 1.512 as measured by an Abbe 60 refractometer, and this index and absorbance of 1.000 was used for all measurements. Measurements were repeated three times at 25 °C using a quartz cuvette and data represented as the mean. The size of the NPs was examined by SEM and TEM. For this purpose, a droplet of the 0.2 wt% shellac–0.25 wt% P407–0.02 wt% AmpB–0.2 wt% Alcalase NPs dispersion was placed onto a glass slide cover slip and left to evaporate overnight. The sample was then coated with ≈2 nm of gold and imaged using a Zeiss Evo-60 SEM (Germany) at a variable pressure 100 μm aperture at 40 Pa, electron high tension (EHT) 20 kV, probe current 100 pA. TEM photograph acquisition of 0.2 wt% shellac-0.25 wt% P407-0.02 wt% AmpB-0.2 wt% Alcalase NPs; Nanoparticles were prepared and redispersed in deionised water at pH 6. A droplet of the suspended sample was pipetted onto carbon-coated copper grids (EM Solutions, UK) and allowed to adhere for 2 min. The grid was quickly rinsed with deionised water and negatively stained with 1 wt% aqueous uranyl acetate. This was quickly rinsed with deionised water and allowed

to dry in air. The sample was then imaged with a Gatan Ultrascan 4000 digital camera attached to a Jeol 2010 TEM 2010 electron microscope running at 120 kV.

5.2.5 Surface tension measurements of AmpB solutions at various concentrations

A KRÜSS Force Tensiometer K100 was used to take measurements of the surface tension of AmpB solutions in deionised water. All measurements were taken at 25 °C. AmpB did not significantly change the density of water at the highest concentration of 0.02 wt%, so a density of 0.998 g cm⁻³ was used in all measurements. An Anton Paar DMA 35N density meter was used to obtain the mass density values of the mixtures. A Wilhelmy platinum plate method was used to obtain the surface tension measurements. The measuring time was 600 s with an immersion depth of 2 mm. Data acquisition was linear with a standard deviation less than 0.1 mN m⁻¹.

5.2.6 Encapsulation efficiency and release kinetics of AmpB from the shellac NPs

The encapsulation efficiency of AmpB (formulated as 0.02 wt% AmpB in 0.25 wt% shellac–0.2 wt% P407 NPs) was examined as a function of pH and AmpB concentration. The pH adjustments were made using drops of 0.25 M HCl or 0.25 M NaOH. The NPs were centrifuged for 30 min at 8500 *g* to pelletise, leaving the supernatant with unencapsulated AmpB. The absorbance of the supernatant was measured using a spectrophotometer to determine encapsulation efficiency and compared to a standard curve of AmpB to calculate the AmpB retained in the NP pellet. The supernatant sample and standard curve samples were read at 330 nm, pH 5.5, and room temperature. Release kinetics were also performed as a function of pH and temperature over 24 h using the same formulation. The release percentages of the temperature experiments were performed at pH 7, buffered with morpholinepropanesulfonic acid (MOPS). For both experiments, 10 mL of the 0.25 wt% shellac–0.2 wt% P407–0.02 wt% AmpB NPs formulation was placed in to a 10–12 kDa MWKO dialysis bag. The dialysis bag was placed into 250 mL of the specific buffered deionised water and specific temperature. Aliquots (1 mL) were taken at specific time points on the absorbance of the aliquot equated into the concentration of AmpB in the buffer using a standard calibration curve. Absorbance was measured at 330 nm.

Elemental analysis of the NP pellet was performed using a CHN analyser (Carlo Erba 1108). The pellet was washed with deionised water three times and dried overnight at 60 °C to remove any remaining water. This was compared with samples of dried individual components of the NPs (shellac, P407, and AmpB).

HPLC chromatograms of 0.2 wt% shellac, 0.25 wt% P407, 0.2 wt% shellac–0.25 wt% P407–0.02 AmpB NPs, and 0.02 wt% AmpB (at various concentrations). All samples were dissolved in DMSO. The NPs sample was pelletised prior to dilution in DMSO and sonicated for 5 min before injection to ensure

all components were thoroughly mixed. A total of 20 μL of each sample was injected into a 5 μm C18 column (Phenomenex, UK) and pumped at 1300 psi, 1 mL min^{-1} . The mobile phase was acetonitrile–water–acetic acid (44:51:5 v/v). UV absorbance at 400 nm was used for sample detection (Perkin-Elmer 785A UV/VIS Detector, UK). The AmpB linear calibration curve was created at concentrations between 0 and 0.02 wt%. The peak area was measured using Azur software.

5.2.7 FTIR, UV–Vis spectroscopy, and XRD studies

FTIR spectra were taken of shellac, P407, 0.25 wt% shellac–0.2 wt% P407 NPs, free AmpB, and 0.25 wt% shellac–0.2 wt% P407–0.02 wt% AmpB NPs. Samples were prepared by removing water using a silica gel desiccant in a vacuum chamber for 1 day, then dried at 60 $^{\circ}\text{C}$ for 2 days. The spectra were measured between 4000 and 600 cm^{-1} using PIKE ATR diamond settings. A spectrum was obtained with a blank of just air to reduce transmittance interference with the samples. UV–Vis absorbance of 0.25 wt% shellac, 0.2 wt% P407, 0.00016 wt% AmpB, and 0.25 wt% shellac–0.2 wt% P407–0.00016 wt% AmpB NPs formulation. Measurements were taken at pH 5.5 (acetate buffer) between 200 and 500 nm using a multiplate spectrophotometer (FLUOstar Omega, UK). A reduced concentration of AmpB was used because of the strong Lambda max absorbance reading.

XRD was performed of shellac, P407, AmpB, and 0.2 wt% shellac–0.25 wt% P407–0.02 wt% AmpB NPs. Samples were prepared by removing water using a silica gel desiccant in a vacuum chamber for 1 day, then dried at 60 $^{\circ}\text{C}$ for 2 days. The crystal forms of the samples were detected using an X-ray diffractometer (Malvern Empyrean PANalytical, UK). The current and voltage using Cu K α radiation were 30 mA and 40 kV, respectively. The angular range was scanned from 5 $^{\circ}$ to 80 $^{\circ}$ of 2 θ , with a step size of 0.02 $^{\circ}$ at a rate of 5 $^{\circ} \text{min}^{-1}$.

5.2.8 Time-kill assays for planktonic *C. albicans*

As working stocks, 0.02 wt% AmpB and 0.2 wt% shellac–0.25 wt% P407–0.02 wt% AmpB–0.2 wt% Alcalase NPs were created. Twofold dilutions of these stocks were prepared. A colony of *C. albicans* was taken from the streak plate and incubated O/N at 37 $^{\circ}\text{C}$ with constant shaking in 10 mL of YPD media (pH 6.5 \pm 0.2). The inoculate concentration was adjusted to 0.5 McFarland Standard by diluting with 0.85 w/v% sterile saline and measuring the optical density at 530 nm until a reading of 0.08–0.12 was obtained. The suspension was diluted 1:150 into 10 mL of YPD media, yielding a working concentration of $\approx 1 \times 10^6$ CFU mL^{-1} . The effect of treatments with 0.02 wt% AmpB and 0.2 wt% shellac–0.25 wt% P407–0.02 wt% AmpB–0.2 wt% Alcalase NPs (and individual NP components) was determined over time (0 to 180 min). 10 mL of each treatment was added to 10 mL of 1×10^6 CFU mL^{-1} *C. albicans* incubated at 37 $^{\circ}\text{C}$ with shaking. At 30 min intervals, 0.1 mL of samples was extracted from the shaking treatment sample tubes and added to 0.9 mL of Dey-Engley

Neutralising Broth. A total of 0.1 mL of aliquots from each serial dilution tube was enumerated onto Sabouraud agar plates overnight at 37 °C to determine CFUs per mL. The time-kill assay was repeated in three independent experiments.

5.2.9 Preparation of *C. albicans* biofilms

A single colony of *C. albicans* was removed from a Sabouraud plate using a plastic loop and inoculated into 10 mL of YPD medium. This was incubated overnight (O/N) for 12–16 h at 150 rpm shaking at 37 °C. The cells were harvested from the O/N culture by centrifugation into a pellet at $3000 \times g$ for 5 min. Afterward, the supernatant was discarded and the pellet washed with sterile PBS using a vortex for 30 s. The cells were pelleted again at $3000 \times g$ and resuspended in 20 mL of RPMI 1640 media prewarmed to 37 °C. RPMI media was supplemented with 1% L-glutamine and buffered to pH 6 using 165 mM of citrate buffer (0.1 M, pH 6). This is referred to as just “RPMI 1640.” *C. albicans* biofilm formation was poor at >7 pH. A 1:100 and 1:1000 fold dilution was prepared in fresh RPMI 1640 and cell density was counted using a haemocytometer. A 10 mL cell suspension of 1×10^5 cells mL⁻¹ was prepared in fresh RPMI 1640 media. This is the optimum cell density to promote biofilm formation; too low or too high cell concentration will interfere with the quorum-sensing mechanism.

From the 1×10^5 cell mL⁻¹ media 100 µL was pipetted into a flat-bottomed tissue culture–treated 96-well plate. Plates were incubated for 24, 48, and 72 h at either 30 or 37 °C in static conditions. After the allotted time period the media was aspirated away by pipetting from the side of the well to reduce potential damage from the pipette tip. The biofilms were washed three times using 300 µL of sterile PBS to remove any detached planktonic cells (leaving only sessile cells behind).

5.2.10 CV staining, biofilm weight, and biofilm protein concentration after treatments

Samples of *C. albicans* biofilms grown for 24 h at 37 °C were treated with 0.2 wt% shellac–0.25 wt% P407–0.02 wt% AmpB–0.2 wt% Alcalase NPs and their individual components for a further 24 h. Three 96-well plate techniques were used to assess biofilm degradation after treatment, CV staining of the biofilm mass, dry biofilm mass weight, and protein concentration. Biofilms were prepared as described previously. A total of 100 µL of the stock treatment was added to the wells at pH 6 and incubated at 37 °C for 24 h. Afterward the treatment was aspirated away and the plate washed twice by submersion in deionised water. The plate was gently shaken to remove water and left to air dry for 15 min in an inverted position. For CV staining, 125 µL of 0.1 wt% aqueous CV solution was added to each well and incubated at room temperature for 15 min. The plates were then again washed by water submersion to remove excess dye and then left to air dry for 2 h. Acetic acid (30 wt%) was used to solubilise the CV and 100 µL of this solution was transferred to a new plate and the

absorbance read at 570 nm. The readings were blanked against 30 wt% acetic acid and the results compared to normalised controls. For biofilm dry mass measurements, the treatment was again aspirated away. The plates were then left to dry overnight at 60 °C. After drying, the plate was weighed on a balance and the weight subtracted from the empty plate weight to give a measurement of the dry mass biofilm remaining. A protein assay kit (Pierce, USA) was used to determine sample protein content. The treatment was aspirated away and the biofilm was washed three times in deionised water. The biofilm was scrapped from the wells and placed into a glass test tube with 1 mL of deionised water. The mixture was sonicated in a water bath for 30 min and then vortexed with glass beads for 2 min to completely disperse the biofilm. A total of 25 µL of the sample was placed into a 96-well plate and 200 µL of the protein concentration determination working reagent (reagent A: reagent A 50:1) was added to the wells and incubated for 30 min at 37 °C with constant shaking. Absorbance was measured at 572 nm. Results were compared to a calibration curve of fixed protein concentrations prepared as per manufacturer's instructions. All tests were performed in triplicates ($N = 3 \pm \text{S.D.}$).

5.2.11 Measuring *C. albicans* biofilm metabolic activity using XTT colorimetric assay

The XTT solution was prepared by adding 1 µL of stock menadione (10 mM menadione in 100% acetone) to 10 mL of the XTT reagent. The XTT assay is based on the principle that viable cells/metabolically active cells can reduce a tetrazolium salt (XTT) into a water-soluble orange formazan compound. The intensity of the orange is increased by higher concentrations of metabolically active cells, and therefore can be used to quantify viable cells. Biofilms were grown and treated in the same manner as mentioned previously. After treatment the medium was removed and the samples washed in deionised water and air dried for 15 min. A total of 100 µL of the XTT/menadione solution was added to each well containing a biofilm, and to blank wells as negative controls. The plates were then covered in aluminium foil and incubated in darkness for 2 h at 37 °C. After incubation, 80 µL was removed and placed into a fresh 96-well plate and read at 490 nm. Absorbance readings were subtracted from the blank well reading, which had no sample inside. Results were normalised and compared to a positive growth control, which received no treatment. All tests were performed in triplicates ($N = 3$ with $\pm \text{S.D.}$).

5.2.12 Measuring HaCaT metabolic activity using MTT colorimetric assay

HaCaT cells were cultured in a T75 flask using DMEM supplemented with 10% FBS and 1% L-glutamine under humidified conditions at 37 °C, 5% CO₂. When a confluence of 80% was achieved, determined by visualisation with an optical microscope, passaging was performed to ensure that the cells remained in the exponential phase for experimentation. Passaging was performed by removing spent media, washing in Dulbecco's phosphate-buffered saline (DPBS), and incubating with 1× trypsin

EDTA at 37 °C 5% CO₂ for 5 min until the cells were detached in suspension. The trypsin EDTA was then neutralised with a 1:1 volumetric ratio of fresh DMEM and gently centrifuged at 400 *g* for 4 min, the supernatant was aspirated, and the pellet was resuspended in DMEM (supplemented as mentioned previously) at a 1:6 ratio and transferred into a fresh T75 flask. Surplus cells used for experimentation were diluted in fresh DMEM, supplemented with 2% FBS and 1% L-glutamine, seeded at 5×10^4 in 100 μ L of media, placed into a 96-well plate, and incubated for 24 h at 37 °C 5% CO₂. The medium was then removed, and the cells were replaced with 100 μ L of treatment-infused DPBS (DPBS was used to approximate physiological pH and so DMEM peptones did not interfere with the Alcalase protease activity). Treatments were the same as mentioned previously and performed for 24 h. A colorimetric (MTT) cell survival and proliferation assay kit was used to measure cell viability (similar tetrazolium dye to XTT). The treatment culture was aspirated away, and the cells washed for 2 min with fresh DPBS. Fresh DMEM (100 μ L) was added, after which 100 μ L of MTT reagent was added. This was incubated in the same conditions for 2 h until intracellular purple formazan crystals were visible under a light microscope. After 2 h, 100 μ L of the colour development reagent in isopropanol with 0.04 M HCl was added for 1 h, allowing the cells to lyse and the formazan crystal to be solubilised to a homogenous blue solution. The absorbance of the blue solution was read at 570 nm on a plate reader and subtracted from a blank of media only. These data were calculated into cell count data via interpolation from the standard curve (absorbance values from a fixed number of cells in media (see **Figure 4.35 – chapter 4**). The data was represented as viability percentage of the control which was normalised to 100%. ($N = 3 \pm$ S.D).

5.2.13 SEM imaging of planktonic *C. albicans* and *C. albicans* biofilms

Planktonic *C. albicans* samples were imaged after 24 h of treatment. The cells were centrifuged for 5 min at 4000 *g* to remove debris and residual NPs. The cells were redispersed into 1 mL of 1 wt% glutaraldehyde PBS buffer solution for 1 h at room temperature. After fixation, the cells were washed three times gently with deionised water to remove excess glutaraldehyde. The samples were then dehydrated in 50%/70%/90% and absolute ethanol solutions for 30 min per each ethanol concentration. The absolute ethanol was dried using liquid CO₂ at its critical point using an E3000 critical point dryer (Quorum Technologies, UK) and then coated in a 6 nm gold layer. Samples were imaged with a variable pressure 100 μ m aperture at 40 Pa, EHT 20 kV, probe current 100 pA. Images were captured with the Zeiss smartSEM software (Zeiss Evo-60 SEM, Germany). Biofilm samples for FDA, PI, and SEM imaging were prepared onto 7 mm circular glass cover slips placed inside a 24-well plate. Treatments were for 24 h and in the same conditions as mentioned previously. After treatment the coverslips were removed and fixed with 1 wt% glutaraldehyde PBS buffer solution for 1 h at room temperature in the same manner as planktonic cells. Ethanol dehydration, gold coating, and imaging

were as described previously. For FDA and PI staining fluorescent images were performed on *C. albicans* biofilms treated in 96-well plate. Biofilms were grown for 24 h, medium replaced, and subsequently incubated for another 24 h with the treatment-supplemented medium. After treatment the wells were washed thrice with deionised water and incubated with 100 μ L of deionised water infused fluorescent label dyes that distinguish between live and dead cells. Stock dye solutions were made as follows: live stain FDA 5 mg in 1 mL acetone, dead stain propidium iodide (PI) 2 mg in 1 mL PBS. Stock solutions were diluted into staining solutions in deionised water at 1.5 μ L FDA stock per 1 mL water, 10 μ L PI stock per 1 mL water. Samples were incubated for 5 min at room temperature in darkness. The stain was then removed and the sample washed with deionised water and air dried for 15 min. The FITC and TRITC filters were used during microscopy.

4.2.15 Statistical analysis

Data were expressed as average values \pm standard deviations of the mean. P-Values of less than 0.05 were considered significant. All One-Way ANOVAs, Tukey's post-test and Student T-tests statistical analysis were performed in GraphPad v7.0.4.

5.3 Results and discussion

5.3.1 Preparation, encapsulation efficiency, and release kinetics of AmpB-loaded shellac NPs

Figure 5.3A and B shows particle size and zeta potential distributions of 0.25 wt% shellac NPs precipitated at pH 5.5 in the presence of 0.2 wt% P407. The average hydrodynamic diameter was 63 nm with a zeta potential of -28 mV. The size and zeta potential of the P407-coated shellac NPs were investigated as a function of pH. **Figure 5.3C and D** shows that in the pH range of 4–8 there is only a negligible variation in the particle size; the NPs all measured between 62 and 64 nm, consistent with sterically stabilised NPs. The zeta potential of the NPs remained negative throughout this pH range. Shellac contains residual -COOH groups on the NPs' surface that deprotonate in aqueous solutions, yielding a negative zeta potential. The P407 coating was used to sterically stabilise the NPs. The likely reason shellac NPs do not dissolve above pH 7 (like shellac alone) but at higher pH is that the NPs' cores are made of a mixture of shellac and the hydrophobic poly(propylene oxide) (PPO)-chains of the P407, which has different solubility properties than pure shellac.

Figure 5.3E and F shows the particle size distribution and zeta potential of 0.25 wt% shellac NPs precipitated at various concentrations of P407 (0.01–0.6 wt%). The NPs' size plateaus to ≈ 63 nm for P407 concentrations higher than 0.2 wt%. The zeta potential remains negative throughout the various P407 concentrations but is reduced to -14 and -12 mV at concentrations of 0.4 and 0.6 wt%, respectively. This is likely due to the offsetting of the shear plane position by the surface layer of poly(ethylene oxide) (PEO) chains from the P407, which is covering the negative surface charge from the shellac -COO^- groups. The reduced zeta potential of the higher concentrations of P407 would likely reduce the coating efficiency of the shellac NPs with the cationic protease Alcalase 2.4L FG. Therefore, a ratio of 0.25 wt% shellac to 0.2 wt% P407 was chosen to give the NPs an optimum size of 63 nm and zeta potential of -28 mV.

The scanning electron microscopy (SEM) image in **Figure 5.3G** shows the spherical morphology of the 0.25 wt% shellac NPs coated with 0.2 wt% P407 NPs, confirming a size range of ≈ 60 – 70 nm after the coating of the sample with gold. An investigation into the encapsulation of AmpB in the P407-stabilised shellac NPs by mixing AmpB with the shellac solution and P407 at pH 10 was explored. It was envisaged that AmpB's hydrophobic nature would promote its encapsulation into the shellac cores of the NPs as they were precipitated upon pH change from 10 to 4. As very little is known about the aggregation behaviour of AmpB, the surface tension of AmpB solutions of various concentrations (0–0.02 wt%) in deionised water was measured to check for potential AmpB micelle formation, which would be detrimental for its encapsulation into the shellac NPs.

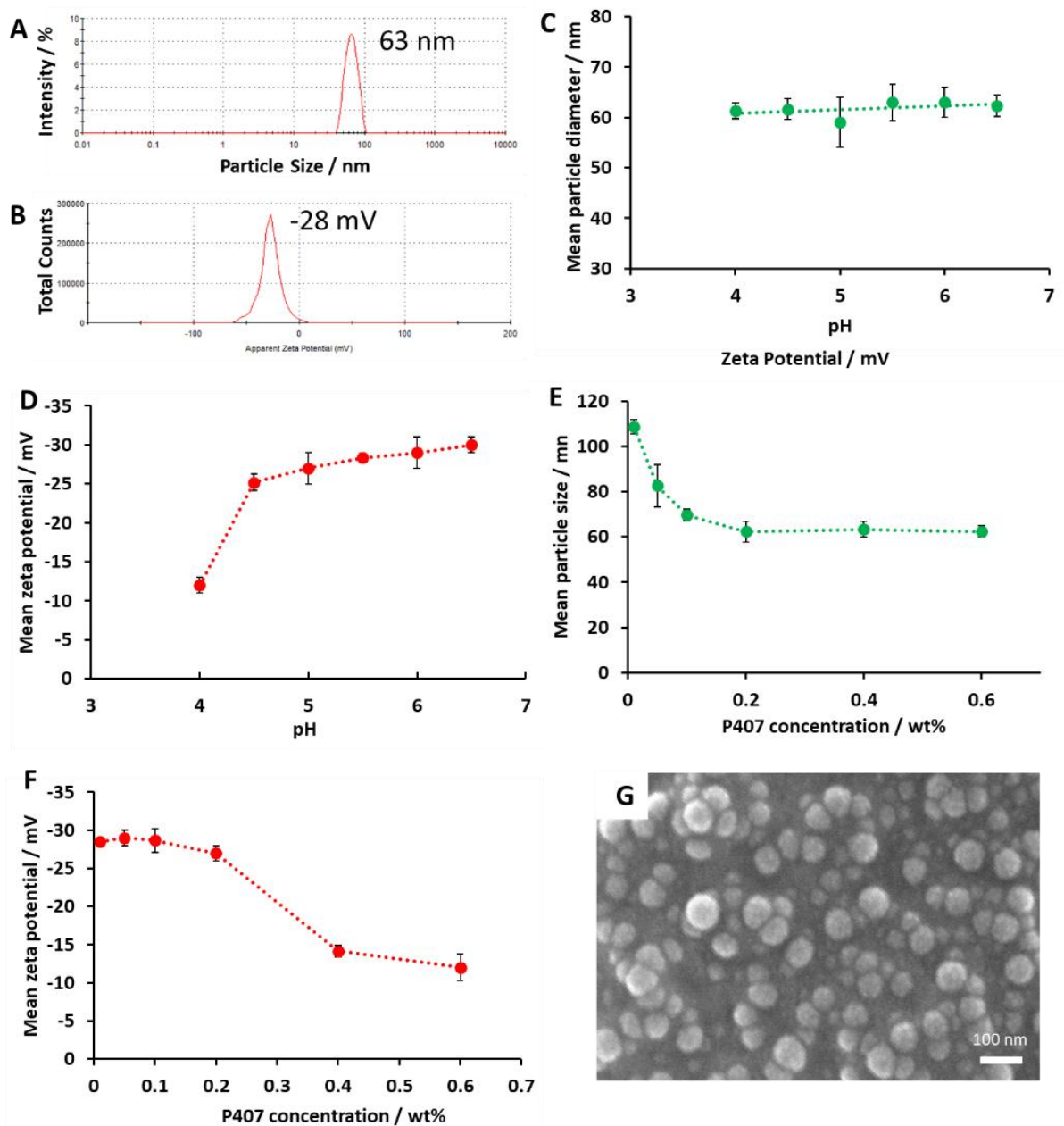


Figure 5.3. (A) Hydrodynamic diameter and (B) zeta potential distribution of 0.2 wt% P407–stabilised 0.25 wt% shellac NPs. Measurements were taken at pH 5.5, 25 °C, RI 1.516, Abs 1.000. (C) The mean particle hydrodynamic diameter and (D) zeta potential of 0.25 wt% shellac stabilised with 0.2 wt% P407 NPs measured between pH 4 and 8. (E) The mean particle hydrodynamic diameter and (F) zeta potential of 0.25 wt% shellac NPs with varied concentrations of P407. Measurements were taken at pH 6, 25 °C, RI 1.516, Abs 1.000. Each value represents a triple replicate with \pm S.D. (G) SEM image of 0.2 wt% P407–coated 0.25 wt% shellac NPs loaded with 0.00016 wt% AmpB. A droplet of the NPs suspension was placed onto a carbon adhesive disc and left to evaporate overnight. The sample was then coated with a 2 nm layer of gold and imaged by SEM.

Figure 5.4 shows that the surface tension is only reduced slightly from ≈ 72 to ≈ 71 mN m^{-1} with 0.02 wt% AmpB added. **Figure 5.5** shows the AmpB in solution with its characteristic pale green colour. The lack of plateauing indicates that the AmpB CMC is at higher concentrations than the target 0.02 wt%, revealing that AmpB is likely in the form of a monomers when mixed with the shellac and P407 at pH 10. **Figure 5.6A and B** shows that the shellac NP size and zeta potential remained largely constant upon increasing the AmpB concentration, starting from 0.00125 wt% up to 0.02 wt%. The particle size remained ≈ 63 – 64 nm throughout the addition of AmpB. The zeta potential was stable at -28 to -26 mV in the same AmpB concentration range.

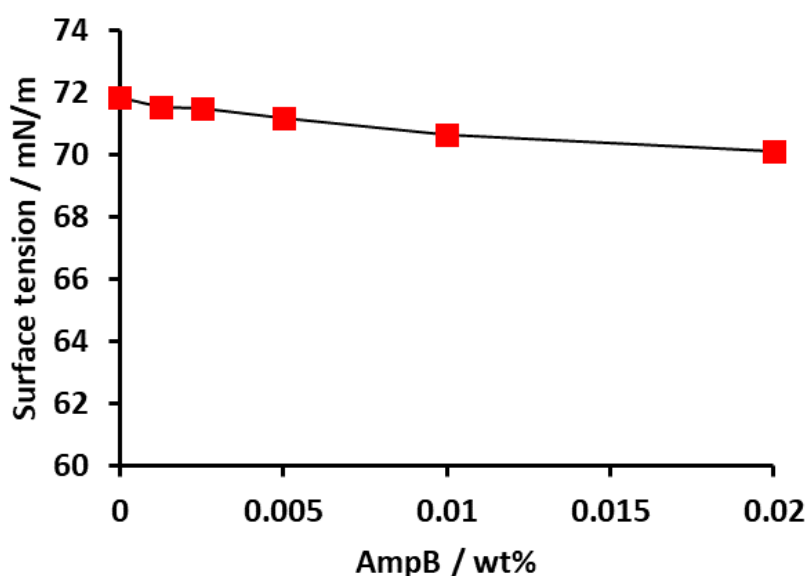


Figure 5.4. Dependence of surface tension on concentration in Amphotericin B aqueous solution. A KRUSS Force Tensiometer K100 was used to take the measurements. 0 wt% Amphotericin B is deionised water. All measurements were taken at 25°C. Amphotericin B did not significantly change the density of water at the highest concentration of 0.02 wt% so a density of 0.998 g/cm^3 was used in all measurements. An Anton Pear DMA 35N density meter was used to obtain values of the mixtures. A Wilhelmy platinum plate method was used to obtain the surface tension measurements. The measuring time was 600 s with an immersion depth of 2 mm. Data acquisition was linear with a standard deviation of < 0.1 mN/m . Error bars are within the symbol size.



Figure 5.5. Photographs of AmpB at concentrations ranging from 0 to 0.02 wt% (left to right). Dilutions were made in deionised water.

The encapsulation efficiency was examined as a function of pH and AmpB concentration. The solution of 0.25 wt% shellac, 0.2 wt% P407, and 0.02 wt% AmpB at pH 10 was subjected to pH change between 4 and 6.5 using 0.25 M HCl and 0.25 M NaOH. The NPs were centrifuged, pelletised, and the supernatant retained for analysis. Any remaining AmpB in the supernatant was considered nonencapsulated. The supernatant was adjusted to pH 5.5 and compared to a calibration curve of fixed concentrations of AmpB in solution at pH 5.5 (**Figure 5.7**). **Figure 5.6C** showed that there was very little difference in the AmpB encapsulation efficiency between pH 4 and 6.5 with all samples achieving an encapsulation efficiency of $\approx 77\%$. **Figure 5.6D** shows that the concentration of AmpB did not alter the encapsulation efficiency, with concentrations between 0.00125 and 0.02 wt% all yielding $\approx 77\%$ encapsulation. This indicated that a high concentration of 0.02 wt% AmpB can be effectively encapsulated into 0.25–0.2 wt% shellac P407 NPs. The encapsulation efficiency was indirectly calculated by measuring the absorbance value of the sample supernatant. To corroborate the results, a direct measurement of the AmpB retained within the NPs was performed by discarding the supernatant and dissolving the NPs completely in dimethyl sulfoxide (DMSO). DMSO was chosen as it can dissolve all components of the NPs. This mixture was then analysed by high performance liquid chromatography (HPLC) (**Figure 5.8**). The HPLC results show that $\approx 86\%$ of the AmpB mixed with 0.25 wt% shellac and 0.2 wt% P407 was successfully encapsulated within the precipitated NPs (at pH 4). This was determined by comparing the area of the peak obtained from NP formulations created with a range of 0–0.02 wt% AmpB to a calibration curve of fixed concentrations of AmpB. The HPLC data also show that the vast majority of the AmpB was successfully encapsulated within the P407-stabilised shellac NPs.

The release kinetics of the AmpB from the 0.25 wt% shellac NPs stabilised with 0.2 wt% P407 was investigated as a function of pH and temperature over time. **Figure 5.6E** shows that pH (5.5, 7, and 7.5) did not affect the release of AmpB over 24 h. Approximately 50% of the AmpB had diffused away from the NPs after 5 h, increasing to 60–70% after 24 h. **Figure 5.6F** shows that different temperatures (23, 30, 37 °C) showed a similar trend; however, at 37 °C the release occurred in a greater quantity compared to 23 and 30 °C (80% compared to 60%).

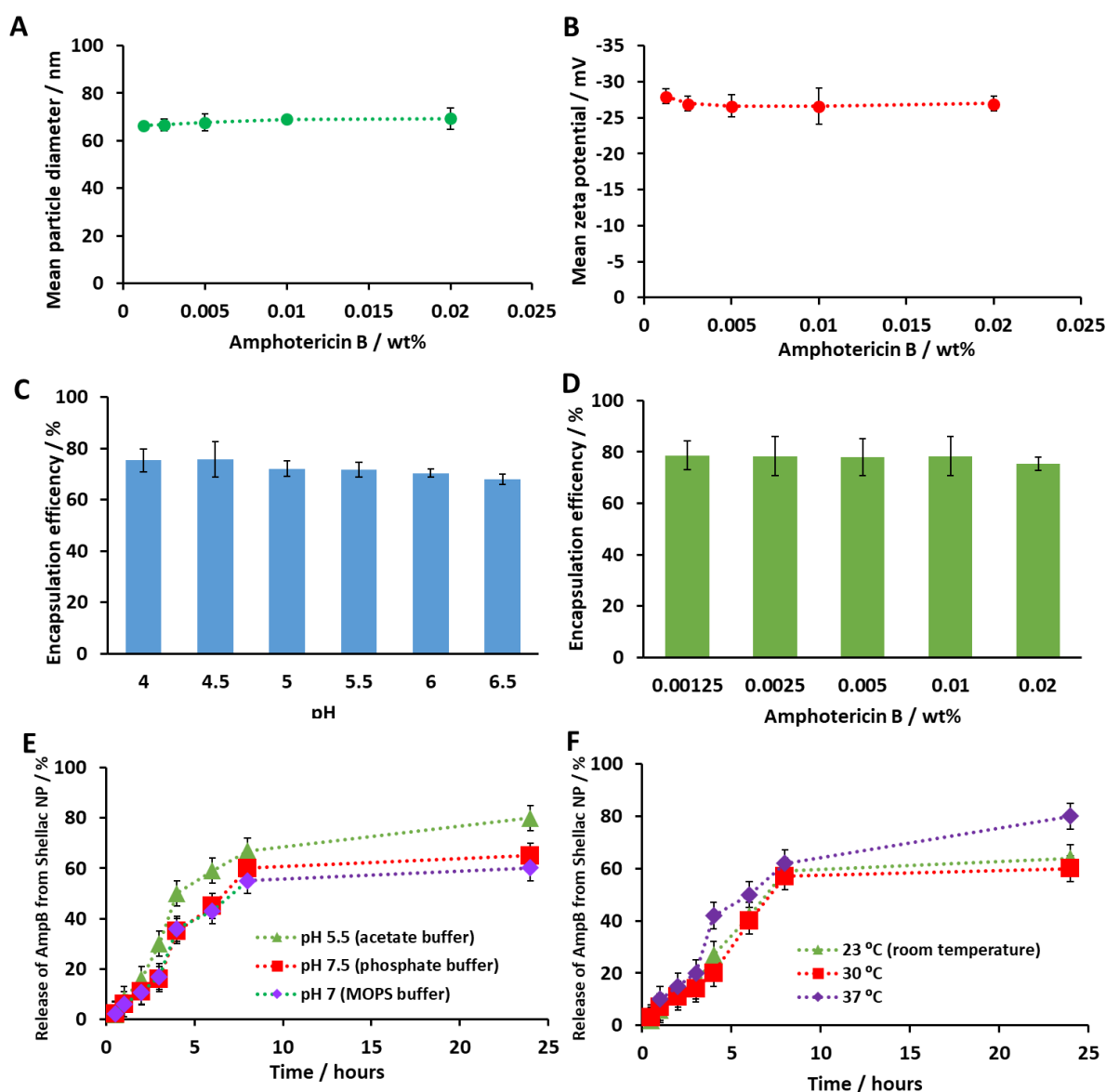


Figure 5.6. (A) Hydrodynamic diameter and (B) zeta potential of 0.25 wt% shellac NPs stabilised with 0.2 wt% P407 at different concentrations of AmpB. Measurements were taken at pH 6, 25 °C, RI 1.516, Abs 1.000 using a Malvern Zetasizer Nano ZS. Each value represents a triple replicate with \pm SD. (C) Encapsulation efficiency of 0.02 wt% AmpB into 0.2 wt% P407–0.25 wt% shellac NPs at different pH (4–6.5). (D) Encapsulation efficiency of varied concentrations of AmpB into 0.2 wt% P407–0.25 wt% shellac NPs at pH 4. pH adjustments were made using drops of 0.25 M HCl or 0.25 M NaOH. The NPs were centrifuged for 30 min at 8500 g to pelletise, leaving the supernatant with nonencapsulated AmpB. (E) Percentage of released AmpB from 0.25 wt% shellac–0.2 wt% P407–0.02 wt% AmpB NPs as a function of pH. (F) The release percentage of AmpB from 0.25 wt% shellac–0.2 wt% P407–0.02 wt% AmpB NPs as a function of temperature. The release percentage versus temperature experiments were performed at pH 7, buffered with MOPS.

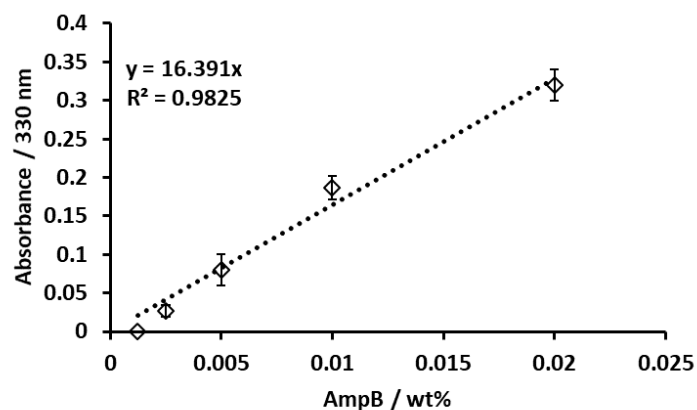


Figure 5.7. The standard calibration curve of different AmpB concentrations measured at 330 nm (0 to 0.02 wt% AmpB). Measurements were taken at room temperature and pH 5.5.

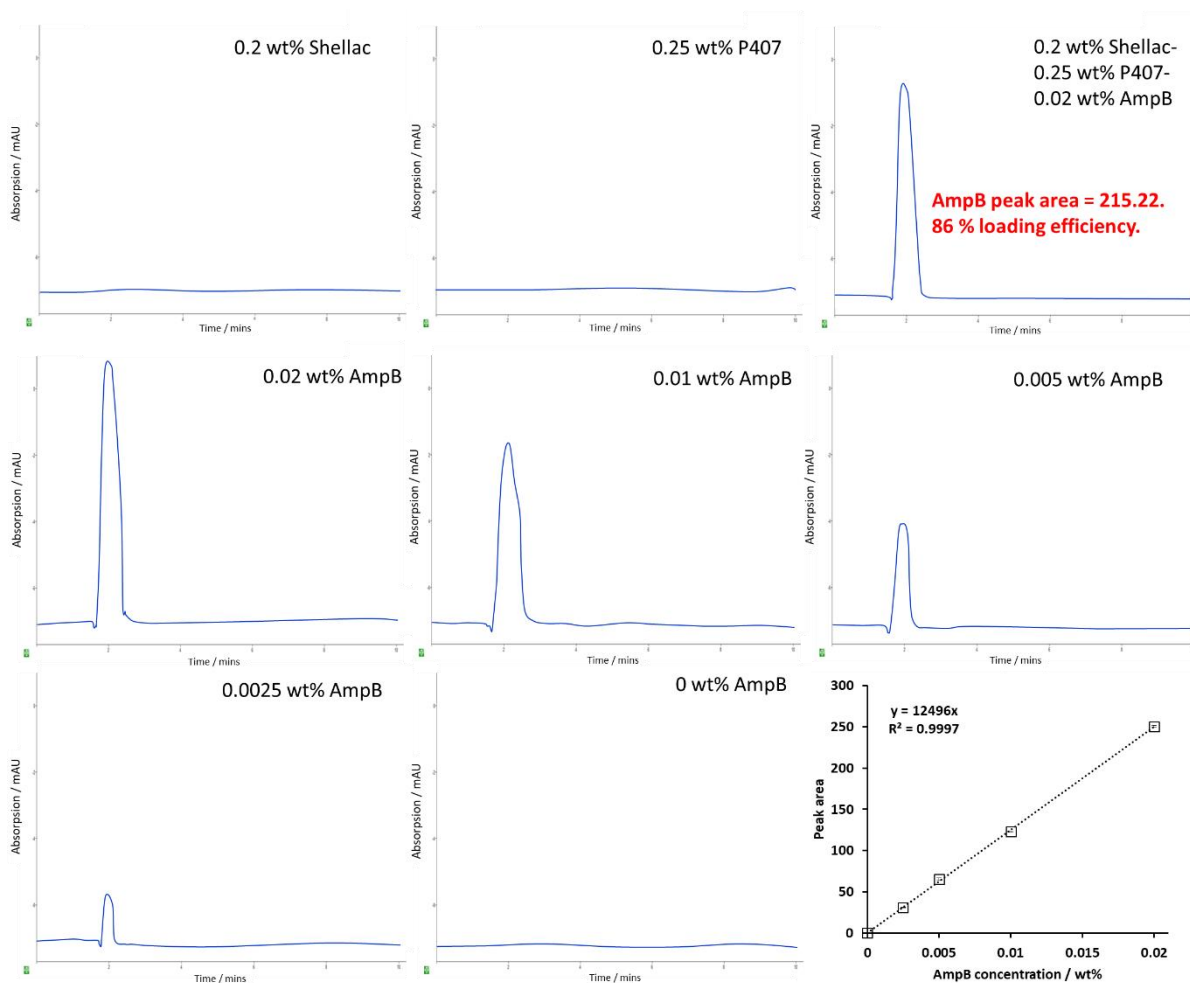


Figure 5.8. HPLC chromatograms of 0.2 wt% Shellac, 0.25 wt% P407, 0.2 wt% Shellac-0.25 wt% P407-0.02 AmpB NPs, and 0.02 wt% AmpB (at various concentrations). All samples were dissolved in DMSO. The NP sample was pelleted prior to dilution in DMSO and sonicated for 5 min before injection to ensure all components were thoroughly mixed. 20 μ L of each sample was injected into a 5 μ m C₁₈ column (Phenomenex, UK) and pumped at 1300 psi, 1 mL/min. The mobile phase was acetonitrile-water-acetic acid (44:51:5 v/v). UV absorbance at 400 nm was used for sample detection (Perkin-Elmer 785 A UV/VIS Detector, UK). The AmpB linear calibration curve was created between 0 and 0.02 wt%. The peak area was measured using Azur software.

5.3.2 Surface functionalisation of P407-stabilised AmpB-loaded shellac NPs with a cationic protease

The functionalisation of the 0.2 wt% P407–stabilised 0.02 wt% AmpB–loaded 0.25 wt% shellac NPs was done by coating with a cationic protease, Alcalase 2.4L FG. **Figure 5.9A and B** shows the NP size distribution and zeta potential after coating with different concentrations of Alcalase. The particle hydrodynamic diameter increased between 8 and 10 nm, which is consistent with the molecular size of this protease as observed with transmission electron microscopy (TEM) (**Figure 5.9F**). The NPs size did not increase beyond 74 nm at a concentration of 0.1 wt% Alcalase, indicating that the particle surface had been saturated. The zeta potential of the NPs flipped from negative to positive when a concentration of 0.1 wt% Alcalase was used, yielding NPs with a zeta potential of +5 mV. At 0.2 wt%, the charge of the particles is $\approx +15$ mV, increasing to +20 mV at 0.6 wt%. The combination of 0.2 wt% P407–stabilised 0.25 wt% shellac NPs loaded with 0.02 wt% AmpB and coated with 0.2 wt% Alcalase was chosen as the optimal formulation for experimentation as it yielded NPs with a size and zeta potential of 74 nm and +20 mV, respectively (**Figure 5.9C and D**). **Figure 5.9G and H** shows TEM images of the uncoated and coated NPs. The TEM image in the range of the Alcalase-coated NPs shows that they are ≈ 8 –10 nm larger in diameter, with a rougher and more textured surface indicating the presence of Alcalase upon the surface. This is consistent with the data obtained through dynamic light scattering. Next, an investigation into the stability of the Alcalase coating over time by monitoring the shellac NPs' zeta potential was carried out. **Figure 5.9E** shows that the positive charge was retained for 24 h at 0.2, 0.4, and 0.6 wt% Alcalase coating on 0.25 wt% shellac NPs stabilised with 0.2 wt% P407 and loaded with 0.02 wt% AmpB. For each coating concentration, there was a difference of less than 8 mV after 24 h. This indicated the Alcalase coating is stable and is retained electrostatically on the shellac NPs with minimal change of their surface charge.

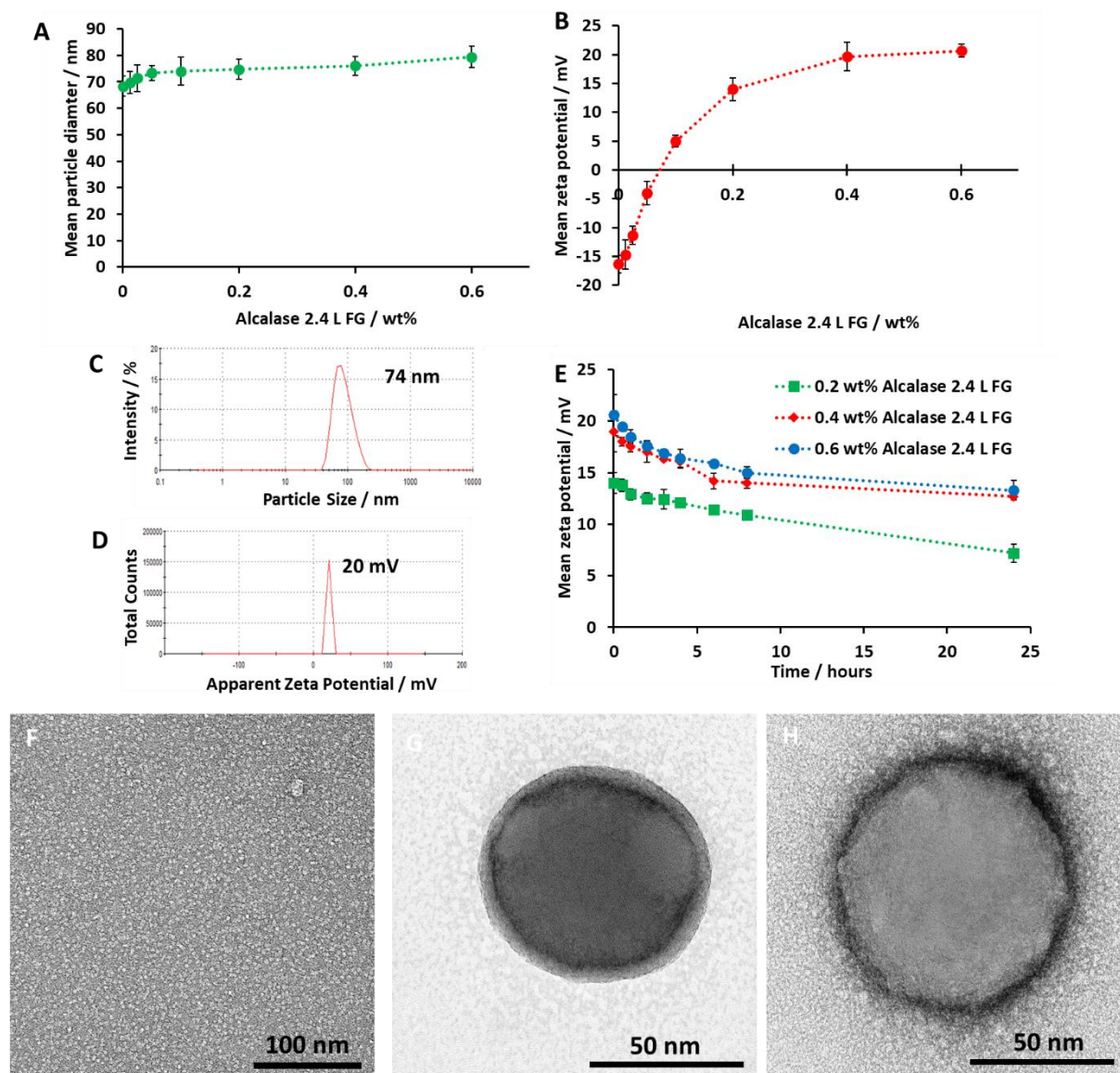


Figure 5.9. (A) The mean hydrodynamic diameter and (B) zeta potential of 0.2 wt% P407–0.02 wt% AmpB–0.25 wt% shellac NPs coated with various concentrations of Alcalase 2.4 L FG. (C) The hydrodynamic diameter and (D) zeta potential distributions of 0.2 wt% P407–0.02 wt% AmpB–0.25 wt% shellac NPs coated with 0.4 wt% Alcalase 2.4 L FG. Measurements were taken after centrifugation and washing of the coated NPs. Measurements were taken at pH 5, 25 °C, RI 1.516, Abs 1.000 using a Malvern Zetasizer Nano ZS. Each value represents a triple replicate with \pm S.D. (E) The zeta potential of 0.25 wt% shellac–0.2 wt% P407–0.02 wt% AmpB NPs coated with different concentrations of Alcalase 2.4 L FG (0.2, 0.4, 0.6 wt%). After coating with Alcalase 2.4 L FG, the NPs were centrifuged at 8000 g and the pellet washed three times in deionised water. The pellet was redispersed into deionised water adjusted to pH 5 using 0.25 M HCl. Zeta potential measurements were taken at different time points up to 24 h to investigate the stability of the Alcalase coating. TEM photographs of (F) 0.2 wt% Alcalase 2.4 L FG, (G) 0.2 wt% P407–0.02 wt% AmpB–0.25 wt% shellac NPs and (H) 0.2 wt% Alcalase–0.2 wt% P407–0.02 wt% AmpB–0.25 wt% shellac NPs.

5.3.4 Characterisation of shellac–AmpB–Alcalase NPs (UV–Vis, fourier transform infrared (FTIR), X-ray powder diffraction (XRD), and carbon, hydrogen and nitrogen elemental analysis (CHN))

The AmpB-formulated shellac NPs were characterised using UV–vis, FTIR, XRD, and CHN elemental analysis to further understand their physical parameters and to provide additional evidence that AmpB was successfully retained and encapsulated within them. **Figure 5.10** shows the UV–vis spectra of 0.2 wt% P407–0.00016 wt% AmpB–0.25 wt% shellac NPs and their individual constituents. Measurements were taken in an aqueous solution buffered to pH 5.5 with acetate buffer between 200 and 500 nm. The shellac (black line) showed small peaks at 300 and 400 nm with very low absorbance after. The P407 (orange line) showed very low absorbance with no specific peak detected. The AmpB (purple line) was measured at 0.00016 wt% as at higher concentrations the peak absorbance was beyond the limit of the detector. AmpB shows peaks at 340, 360, and 405 nm. The NPs sample (green line) closely followed the spectral pattern of the shellac but with small peaks at 340, 365, and 405 nm. These peaks are close to the peaks obtained from AmpB alone, indicating that AmpB has been encapsulated within the shellac NPs.

Figure 5.11 shows the FTIR spectra of shellac, P407, AmpB, 0.2 wt% P407–0.25 wt% shellac NPs, and 0.2 wt% P407–0.02 wt% AmpB–0.25 wt% shellac NPs. The non-loaded shellac NPs show a high degree of peaks in the range 1600–1000 cm^{-1} due to the presence of C-O bonds within both compounds. The peak at 1100 cm^{-1} is particularly strong with P407 due to the $\text{CH}_2\text{-O-CH}_2$ ether groups. This peak is also shown in the 0.25 wt% shellac–0.2 wt% P407 spectra, but with a smaller peak. This is likely due to the central hydrophobic polypropylene glycol block adsorption on the shellac NP surface. The AmpB shows a broad peak at 3300 cm^{-1} from O-H stretching, a peak at 1700 cm^{-1} due to C=O stretching, and a peak at 1100 cm^{-1} due to the C-O-C ether bond present within the compound. The 0.2 wt% P407–0.02 wt% AmpB–0.25 wt% shellac NP sample showed a pattern with commonalities to the individual shellac, P407, and AmpB samples. The peak at 1700 cm^{-1} is well defined and is likely attributed to the AmpB entrapped within the NPs. This wavenumber is not present on the P407 spectrum and is only a shoulder of multiple peaks from the shellac between 1650 and 1100 cm^{-1} . The complexity of the shellac chemical structure makes multiple unique peaks from the AmpB difficult to detect. However, in conjunction with the UV–vis data, there is strong evidence the AmpB has been successfully encapsulated within the NPs.

To corroborate the results from FTIR, an XRD analysis of shellac, P407, AmpB, and 0.2 wt% P407–0.02 wt% AmpB–0.25 wt% shellac NPs was performed (**Figure 5.12**). The shellac sample showed a broad undefined peak from a 15 to 25-degree angle. The P407 had two large peaks at 19 and 25 degrees, which dominated the pattern. AmpB showed a peak at 9 and 26 degrees. Interestingly

when the NP sample was examined, a combination of the peaks of the individual components were found, mirroring the trend from FTIR analysis. The concentration of AmpB within the NPs was much lower than the P407 and shellac components, meaning the peaks associated with AmpB are much smaller than the peaks associated with shellac and P407. However, in the NPs sample, a small peak appears at 9 degrees and another at 26 degrees, indicating that AmpB has been successfully encapsulated within the shellac–P407 NPs.

Next, the elemental ratios of carbon, hydrogen, and nitrogen in the 0.2 wt% P407–0.002 wt% AmpB–0.25 wt% shellac NPs was examined, and compared to the elemental ratios of the individual components (**Table 5.1**). AmpB has a carbon content of 57.52%, hydrogen 6.11%, and nitrogen 3.65%. Shellac shows a nitrogen content of 0.71%, which is contamination of the ammonium salt of the original shellac is provided in. In the NPs sample, the nitrogen content has increased to 0.94%, which is attributed to the nitrogen atom in the AmpB chemical structure. However, due to the residual NH_4^+ constituent in the shellac matrix, the percentage of AmpB in the NPs cannot be quantitatively determined, but indicates the presence of AmpB in the sample.

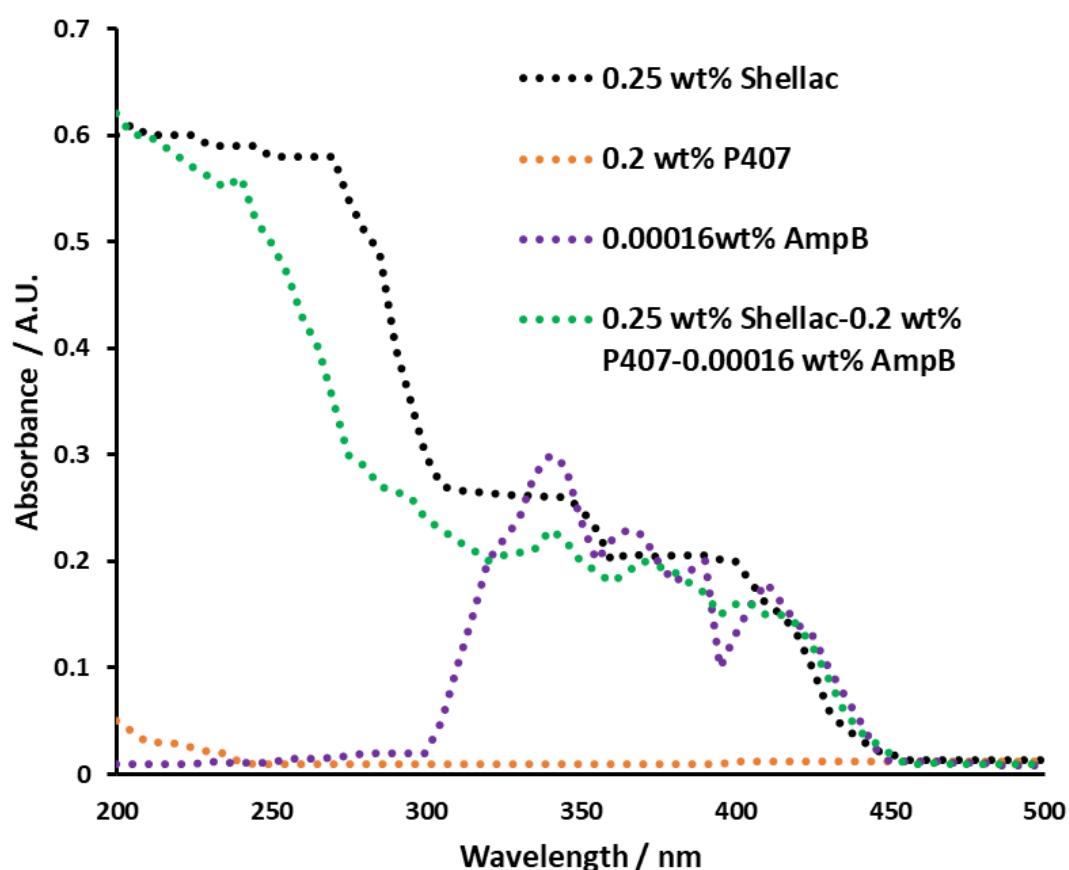


Figure 5.10. UV-Vis absorption of 0.25 wt% shellac, 0.2 wt% P407, 0.00016 wt% AmpB and 0.25 wt% shellac-0.2 wt% P407-0.00016 wt% AmpB nanoparticles. Measurements were taken at pH 5.5 (acetate buffer) between 200 and 500 nm using a spectrophotometer.

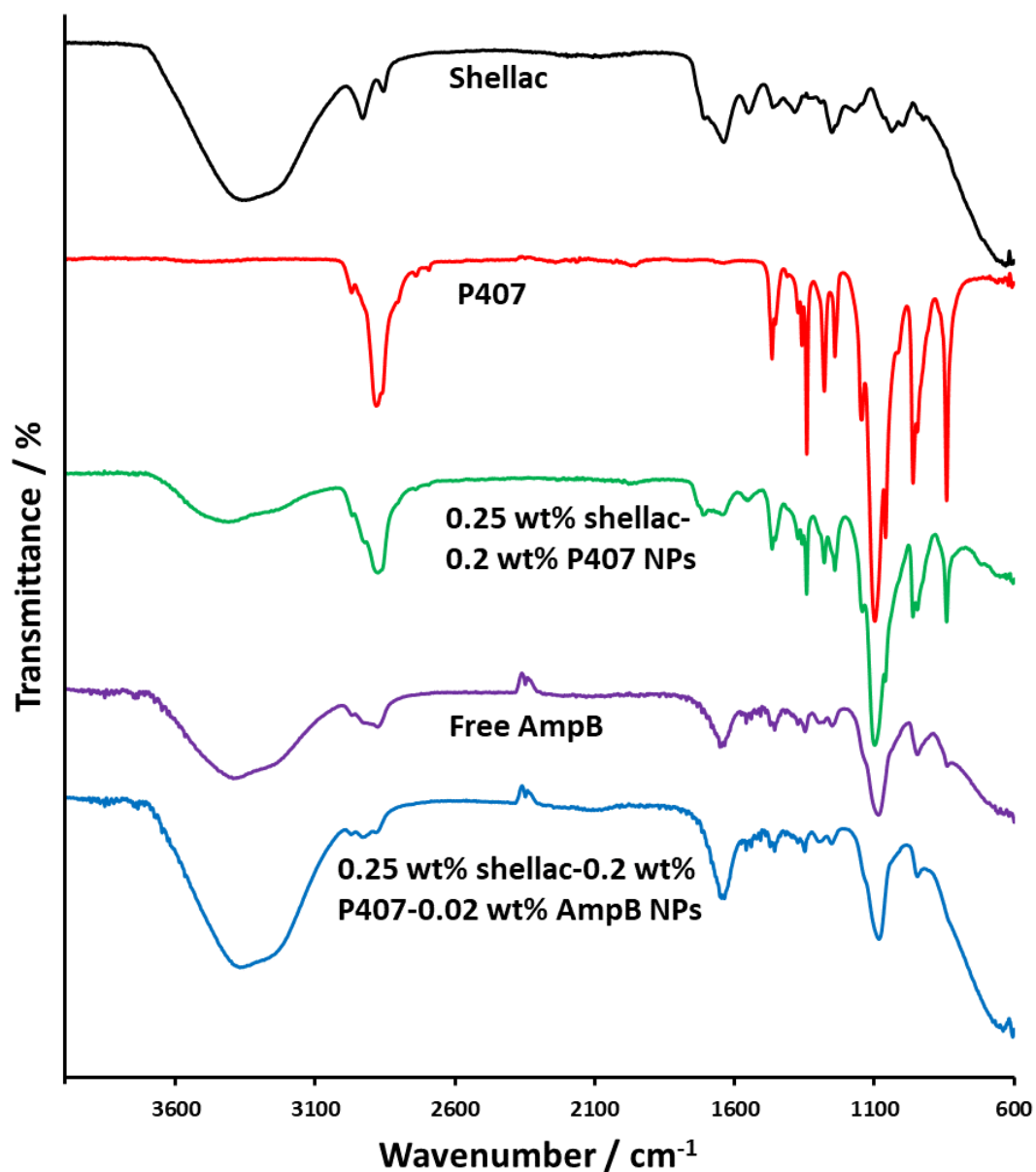


Figure 5.11. Fourier transform infra-red (FTIR) spectra of Shellac, P407, 0.25 wt% Shellac-0.2 wt% P407 NPs, free AmpB, and 0.25 wt% Shellac-0.2 wt% P407-0.02 wt% AmpB NPs formulation. Samples were prepared by removing water using a Silica gel desiccant by in vacuum chamber for 1 day, then dried at 60°C for 2 days. The spectra was measured between 4000-600 cm⁻¹ using PIKE ATR diamond settings. A spectra was obtained with a blank of just air to reduce transmittance interference with the samples.

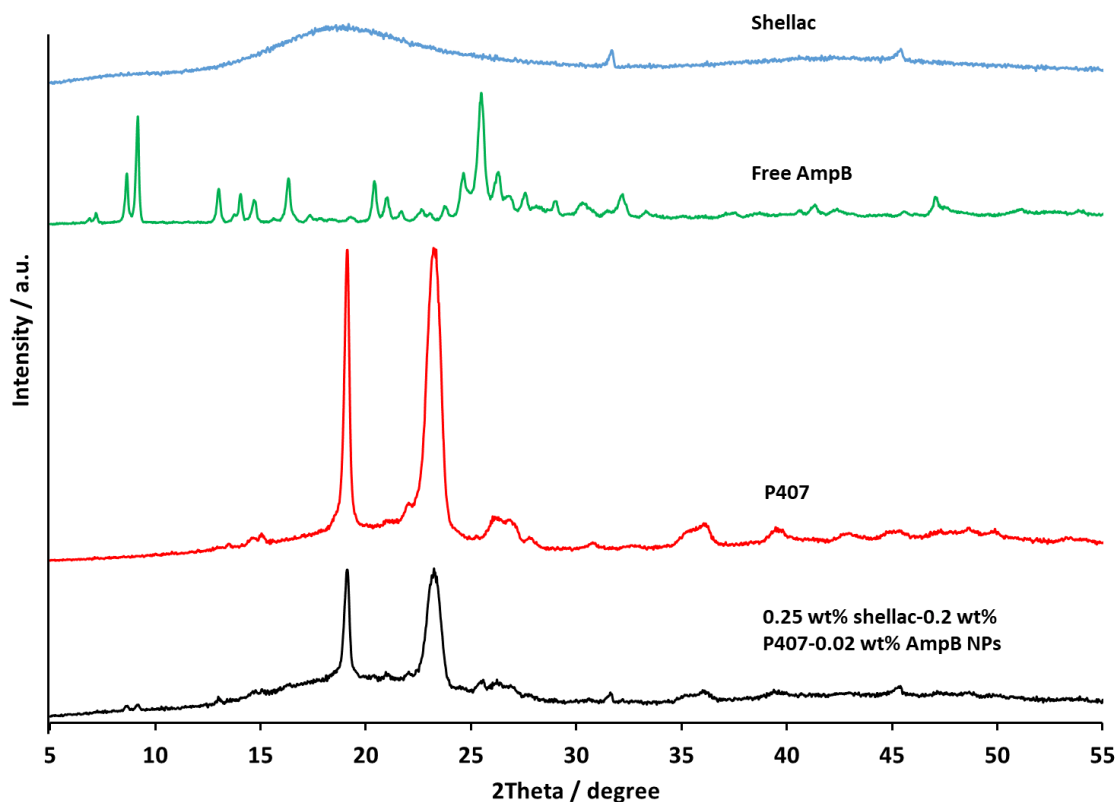


Figure 5.12. X-ray powder diffraction of Shellac, P407, AmpB and 0.25 wt% Shellac-0.2 wt% P407-0.02 wt% AmpB NPs. Samples were prepared by removing water using a silica gel desiccant by in vacuum chamber for 1 day, then dried at 60°C for 2 days. The crystal forms of the samples were detected using an X-ray diffractometer (Malvern Empryean PANalytical, UK). The current and voltage using Cu K α radiation were 30 mA and 40 kV, respectively. The angular range was scanned from 5° to 80° of 2 θ , with a step size of 0.02° at a rate of 5°/min.

Table 5.1. Elemental analysis of 0.2 wt% Shellac-0.25 wt% P407-0.02 wt% Amphotericin B NPs, and the individual components. The Amphotericin B content in the nanoparticle is calculated based on the nitrogen content of Amphotericin B.

Element	Shellac*	P407	Amphotericin B**	0.2 wt% Shellac-0.25 wt% P407-0.02 wt% Amphotericin B
C	39.90	55.54	57.52	57.65
H	9.06	10.96	6.11	9.64
N	0.71	-	3.65	0.94
% Amphotericin B content in Shellac NPs				15.18%

*Shellac - 586.7 g/mol - C₃₀H₅₀O₁₁, **Amphotericin B - 924.079 g/mol - C₄₇H₇₃NO₁₇

Calculation;

0.94-0.71=0.23 (This accounts for the N content of the Shellac sample which must the ammonium salt)

$$(0.23/14) \times 924.079 = 15.18$$

5.3.5 Antimicrobial time-kill assay for Alcalase-coated AmpB-loaded shellac NPs against planktonic *C. albicans*

The formulation of 0.2 wt% Alcalase–0.2 wt% P407–0.02 wt% AmpB–0.25 wt% shellac NPs was chosen as the working stock formulation for antifungal testing. *C. albicans* was cultured on Sabouraud agar plate (**Figure 5.13**) and grown overnight in yeast–peptone–dextrose (YPD) media (pH 6.5 ± 0.2) with constant shaking to create an exponentially grown planktonic culture. A time-kill assay was used to compare the effectiveness of the nanocarrier-formulated AmpB compared to the equivalent concentration of free AmpB. **Figure 5.14** shows that at an initial concentration of 0.02 wt% AmpB there is no difference between the nanocarrier-formulated AmpB and the free AmpB. After 60 min there were no detectable viable cells after enumeration. The 0.2 wt% Alcalase–0.2 wt% P407–0.25 wt% shellac NPs alone had only a mild effect on the *C. albicans* growth after 180 min, with the P407 showing a twofold drop in cell numbers. The formulation of 0.02 wt% AmpB (free) alone was extremely cytotoxic, so it is unsurprising that it was extremely effective at killing the *C. albicans*. An investigation into the effect of lower concentrations of the nanocarrier-formulated AmpB compared to free AmpB was performed. The treatments were performed in treatment-infused YPD media (pH 6.5 ± 0.2). **Figure 5.15A** shows that after twofold dilutions of the stock AmpB–NP formulation and free AmpB there was a significant difference in the performance of these treatments. 0.00125 wt% AmpB formulated in the Alcalase-functionalised nanocarrier killed the *C. albicans* 30 min earlier than the same concentration of free AmpB. At 0.0003 wt% AmpB encapsulated in the nanocarrier, this difference was improved further, with *C. albicans* being killed 1 h earlier. At 0.0002 wt% AmpB and 0.00008 wt% AmpB, both in Alcalase-coated nanocarriers after 180 min, there was a threefold and fourfold difference in the *C. albicans* cell concentration compared to an equivalent amount of free AmpB, respectively. This indicates that the AmpB formulated in the Alcalase-coated NPs is significantly more effective at killing *C. albicans* than AmpB alone. **Figure 5.15B** shows an SEM image of planktonic *C. albicans* after 180 min of no treatment (growth control). For comparison, **Figure 5.15C–E** shows *C. albicans* after 180 min of treatment with 0.02 wt% AmpB in NPs, where significant morphological differences can be seen compared to the untreated cells. The NPs themselves can also be observed on the surface on the cells where they deliver directly a high concentration of AmpB.

This localised highly concentrated release of AmpB is what likely increases the efficacy of the AmpB–NPs when compared to treatment with free AmpB. A further investigation into the zeta potential of planktonic *C. albicans* was carried out, it showed that the cells have a negative zeta potential across a pH range of 4–8 (**Figure 5.16**). This electrostatic attraction between the cationic shellac NPs (facilitated by the surface coating of Alcalase) and the anionic surface of the *C. albicans* cells leads to the accumulation of the NPs on the outer cell wall.

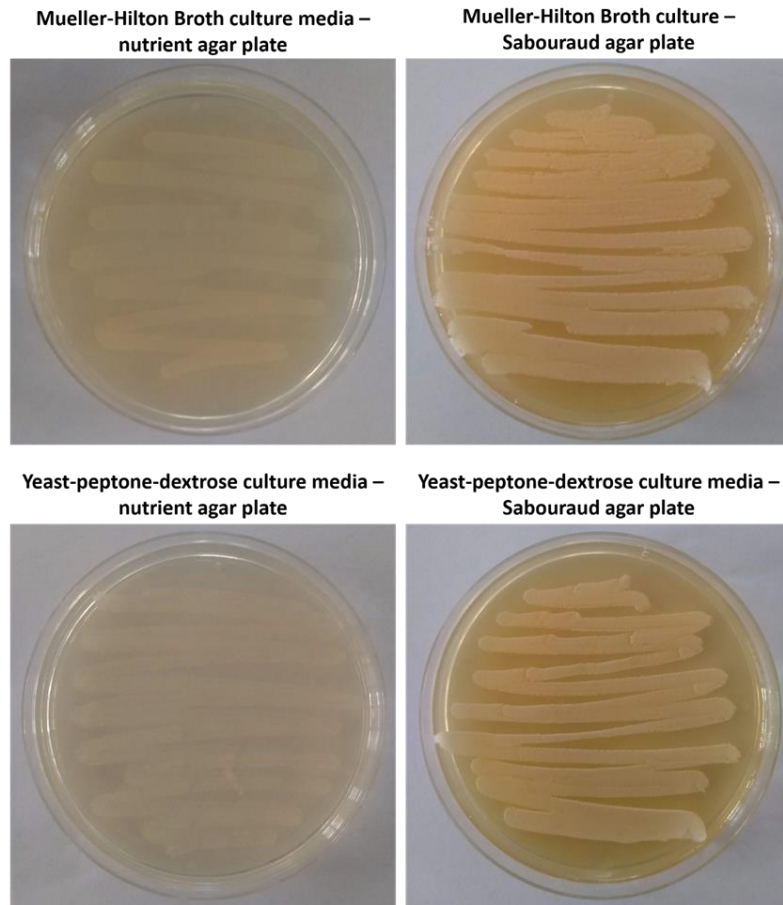


Figure 5.13. *C. albicans* cultured overnight in either Mueller-Hilton Broth or Yeast-peptone-dextrose media, the streaked onto either Nutrient agar plates or Sabouraud agar plates. All medias work well showing creamy white colonies. Yeast-peptone-dextrose culture media and Sabouraud agar plates will be used as this is convention in *C. albicans* experiments.

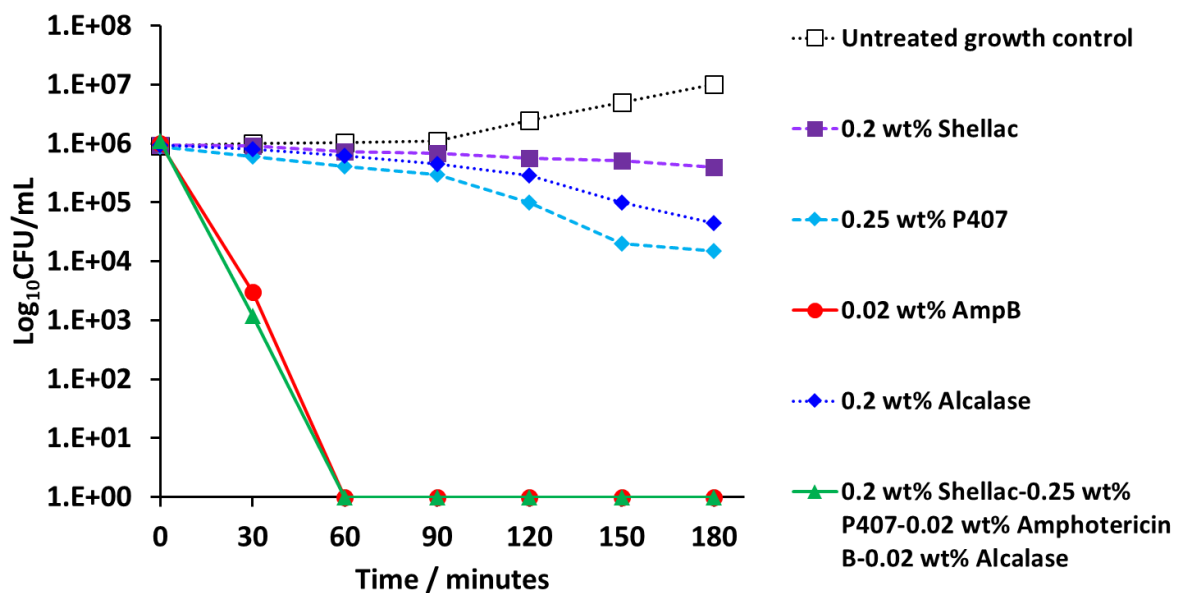


Figure 5.14. Time kill assay against planktonic *C. albicans*. 0.02 wt% Amphotericin and 0.2 wt% Shellac-0.25 wt% P407-0.02 wt% AmpB-0.2 wt% Alcalase NPs were compared, all other components of the NP were tested as controls. N=3.

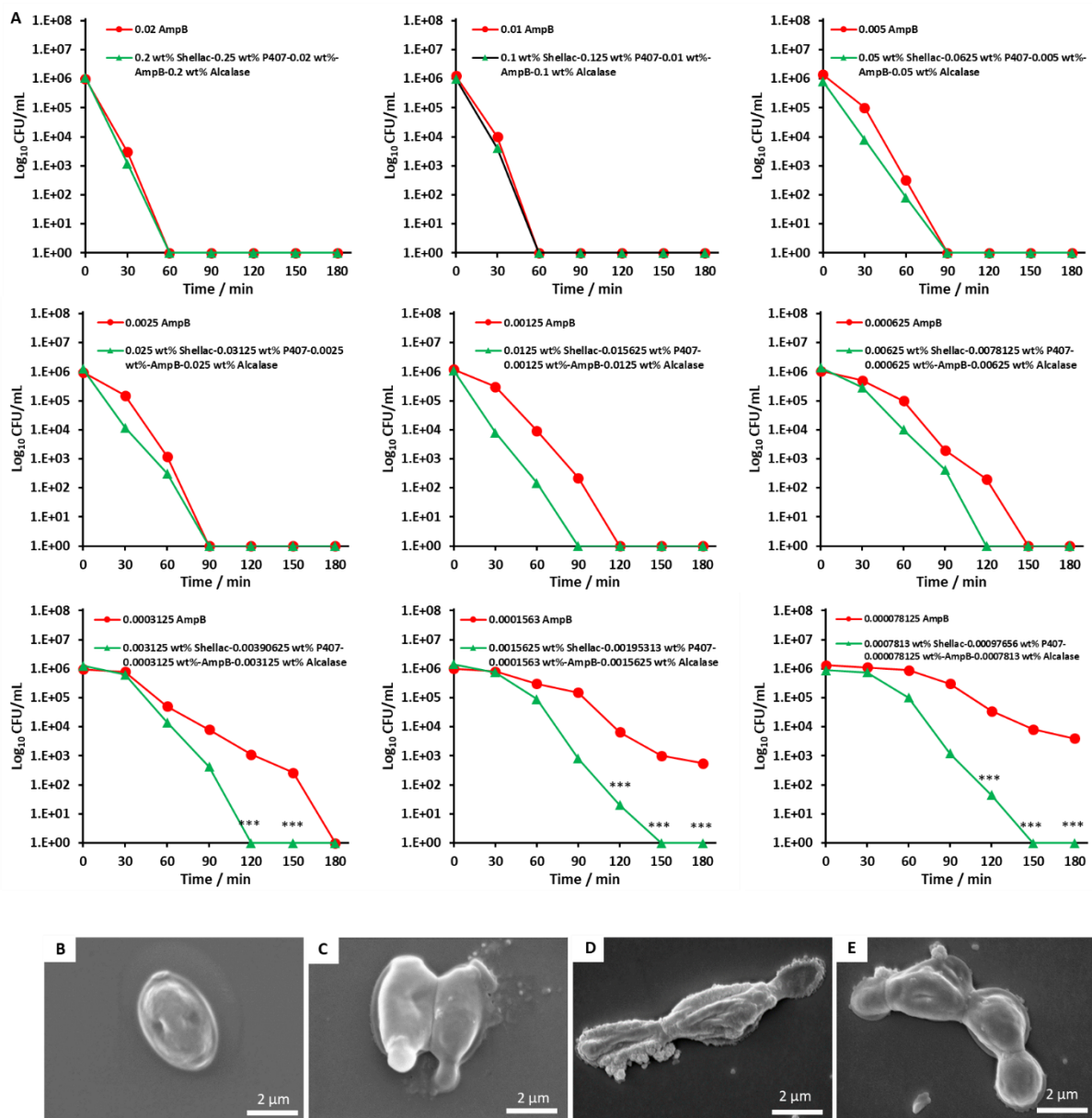


Figure 5.15. (A) Time-kill assay against planktonic *C. albicans*. 0.02 wt% AmpB and 0.2 wt% Alcalase–0.2 wt% P407–0.02 wt% AmpB–0.25 wt% shellac NPs were created as working stocks. Twofold dilutions of these stocks were prepared ($N = 3$). **(B)** SEM photographs of planktonic *C. albicans* after no treatment. **(C–E)** Images of *C. albicans* after incubation with 0.2 wt% P407–0.02 wt% AmpB–0.25 wt% shellac NP treatment applied for 180 min. $N = 3 \pm \text{SD} < 0.05$ is considered significant. $*P < 0.05$, $**P < 0.01$, $***P < 0.001$ compared to the case of free AmpB. All One-Way ANOVAs and Tukey’s post-test statistical analysis were performed in GraphPad v7.0.4. The statistical analysis data are shown in **Table 5.2**.

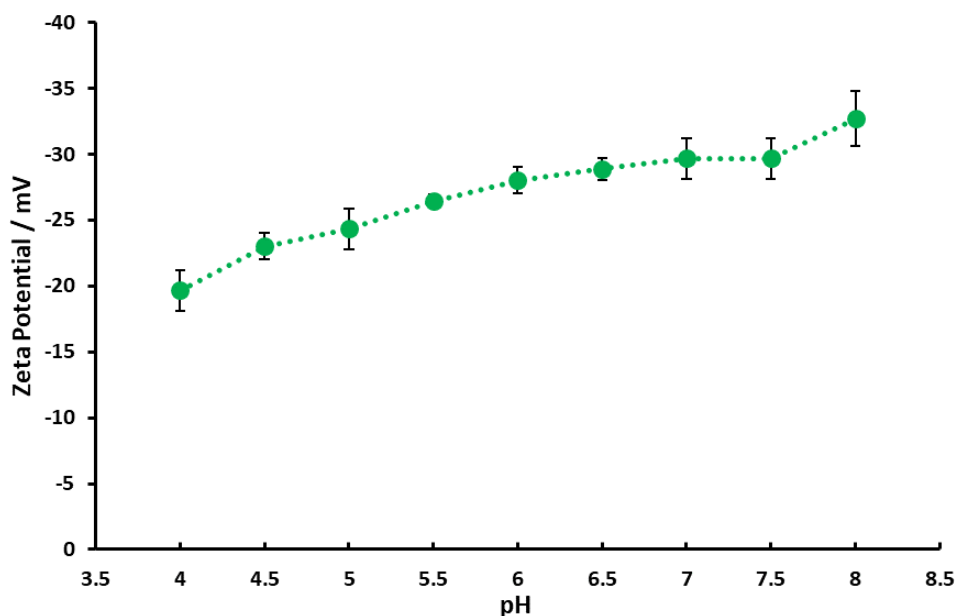


Figure 5.16. The zeta potential of *C. albicans* at various pH. A single colony from a steak plate was incubated YPD media overnight at 37 °C with constant shaking. The *C. albicans* suspension was centrifuged for 10 min at 5000 *g*. The supernatant was discarded, and the pellet was washed twice with deionised water. The pellet was resuspended in 45 mL of deionised water. 1 mL of this suspension was placed in a quartz cuvette and zeta potential was measured using the Dipstick probe and Malvern Zetasizer nano ZS. The refractive index was 1.333 and the absorption was 1.000. *N* = 3 with \pm S.D.

Table 5.2. Time-Kill assay statistical analysis between free AmpB and equivalent concentrations of shellac-P407-Alcalase encapsulated AmpB. Data were expressed as average values \pm standard deviations of the mean. P-values of less than 0.05 were considered significant. *N*=3 with \pm S.D for statistical analysis. All Student's T-tests were performed in GraphPad v7.0.4.

Time / sec	Multiple Comparison	P-value	Significance
120	0.0003125 wt% AmpB vs	<0.0001	***
150	0.003125 wt% Shellac-0.00390625 wt% P407-0.0003125 wt%-	<0.0001	***
180	AmpB-0.003125 wt% Alcalase NPs	N/A	N/A
120	0.0001563 wt% AmpB vs	<0.0001	***
150	0.0015625 wt% Shellac-0.00195313 wt% P407-0.0001563 wt%-	<0.0001	***
180	AmpB-0.0015625 wt% Alcalase NPs	<0.0001	***
120	0.000078125 wt% AmpB vs	<0.0001	***
150	0.0007813 wt% Shellac-0.00097656 wt% P407-0.000078125	<0.0001	***
180	wt%-AmpB-0.0007813 wt% Alcalase	<0.0001	***

< 0.05 is considered significant. **P*<0.05, ***P*<0.01, ****P*<0.001.

5.3.6 Antibiofilm action of Alcalase-coated AmpB-loaded shellac NPs against *C. albicans*

With the encouraging results obtained by treating planktonic cells with AmpB-loaded shellac NPs, it was necessary to investigate the effect the NPs have on *C. albicans* grown as a biofilm. A simple 96-well plate technique to grow biofilms was used (Pierce et al., 2008). The stock treatments were added to the wells at pH 6 and incubated at 37 °C for 24 h. Three techniques were used to examine the effectiveness of the AmpB–NPs and their individual components. **Figure 5.17A** shows residual biofilm staining using crystal violet (CV). CV can stain both dead and viable cells and also the components of the biofilm matrix, allowing it to effectively quantify the biofilm mass. Compared to the growth control, there was a 5–10% reduction of biofilm mass when treated for 24 h with 0.25 wt% shellac NPs and 0.2 wt% P407. Alcalase (0.2 wt%) treatment was able to reduce the biofilm mass by 50% of the control, likely due to the protease hydrolysing the matrix and allowing chunks of biofilm to be removed. Compared to the control, 0.02 wt% free AmpB reduced the biofilm mass by 70%. However, the 0.02 wt% AmpB–loaded shellac NPs reduced the biofilm mass by 92% compared to the control. This is due to the Alcalase coating on the NPs being able to degrade the biofilm, allowing them to locally deliver high AmpB concentration to the embedded cells. **Figure 5.18**, Supporting Information, shows images of the biofilm within the plate wells after CV staining and subsequent removal of excess stain. The growth control, 0.25 wt% shellac and 0.2 wt% P407, showed a very similar purple stain. The 0.02 wt% free AmpB, 0.2 wt% free Alcalase, and 0.02 wt% AmpB–NPs showed a reduced intensity of biofilm staining, with the AmpB–NPs showing the least staining. **Figure 5.17B**, which displays the dry weight of the biofilm before and after treatments on separate 96-well plates, shows a similar trend to the CV biomass staining. Again, the 0.02 AmpB–loaded shellac NP formulation showed the greatest reduction in biofilm weight compared to the control (a difference of 2.5 mg in weight compared to the control plate). This was significantly different from the 0.02 wt% free AmpB plate by ≈ 1.5 mg. Next, in **Figure 5.17C**, an investigation between the protein concentration of the treated biofilms was compared to the control was performed.

After 24 h of treatment, the biofilm was thoroughly scraped from the wells and vortex glass bead beaten to disintegrate any remaining biofilm matrix. The protein content of the biofilms was compared to a standard of fixed concentrations of protein using a commercially available kit (**Figure 5.19**). In the protein content results, the 0.02 wt% AmpB-loaded NPs reduced the protein content to $190 \mu\text{g mL}^{-1}$ compared to the growth control, which contained $\approx 1150 \mu\text{g mL}^{-1}$. The Amp-loaded NPs performed significantly better than the free AmpB, having $\approx 300 \mu\text{g mL}^{-1}$ less protein. Interestingly the free 0.2 wt% Alcalase also performed very well, reducing the protein content to $\approx 300 \mu\text{g mL}^{-1}$. This is in contrast to the CV and dry weight biofilm assay results, which show the Alcalase was not as effective at biofilm degradation as the 0.02 wt% free AmpB. This is likely due to the Alcalase being able to

significantly reduce the protein content by not necessarily reducing the biofilm mass by the same amount.

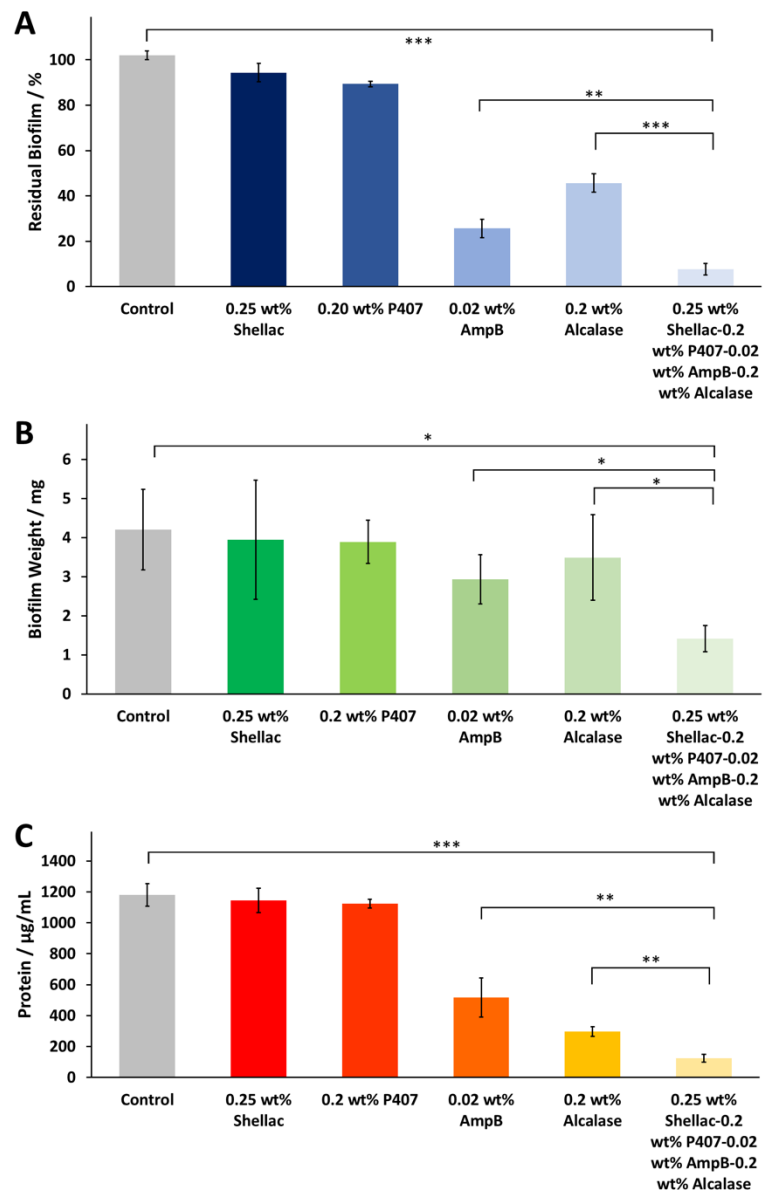


Figure 5.17. (A) The effect of Alcalase-coated AmpB-loaded shellac NP treatments on *C. albicans* biofilms after 24 h. *C. albicans* cells were cultured in YPD media for 24 h to allow biofilm formation. Afterward, the media were removed and replaced with treatments in deionised water at pH 6. Posttreatment 1% CV was used to stain the biofilms. Absorbance readings at 570 nm were taken by solubilising the CV in 30% acetic acid. Treatments were compared to the normalised control. (B) Dry mass of 24 h treated *C. albicans* biofilms on 24-well plates. *C. albicans* were cultured in YPD media for 24 h to allow biofilm formation; the media were removed and replaced with treatments in deionised water at pH 6. Posttreatment, the media were aspirated away and the plates left to dry overnight at 60 °C. After drying the plate was weighed and compared to the empty plate weight to determine the dry mass of the biofilm remaining. (C) Protein concentration of *C. albicans* biofilms after 24 h of treatment. A protein assay kit (Pierce, USA) was used to determine sample protein content. Absorbance was measured at 572 nm. $N = 3 \pm SD < 0.05$ is considered significant. * $P < 0.05$, ** $P < 0.01$, *** $P < 0.001$. All Student's *t*-tests were performed in GraphPad v7.0.4. The statistical analysis is shown in Table 5.3.

Table 5.3. Biofilm degradation statistical analysis between biofilm growth controls, 0.02 wt% AmpB, 0.2 wt% Alcalase and 0.2 wt% Shellac-0.25 wt% P407-0.02 wt% Amphotericin B-0.02 wt% Alcalase. Data were expressed as average values \pm standard deviations of the mean. P-values of less than 0.05 were considered significant. N=3 with \pm S.D for statistical analysis. All Student's T-tests were performed in GraphPad v7.0.4.

Biofilm reduction assay	Multiple Comparison	P-value	Significance
Crystal Violet staining	Control vs 0.2 wt% Shellac-0.25 wt% P407-0.02 wt% Amphotericin B-0.02 wt% Alcalase NPs	<0.0001	***
	0.02 wt% Amphotericin B vs 0.2 wt% Shellac-0.25 wt% P407-0.02 wt% Amphotericin B-0.02 wt% Alcalase NPs	0.0028	**
	0.02 wt% Alcalase vs 0.2 wt% Shellac-0.25 wt% P407-0.02 wt% Amphotericin B-0.02 wt% Alcalase NPs	0.0002	***
Biofilm weight	Control vs 0.2 wt% Shellac-0.25 wt% P407-0.02 wt% Amphotericin B-0.02 wt% Alcalase NPs	0.0111	*
	0.02 wt% Amphotericin B vs 0.2 wt% Shellac-0.25 wt% P407-0.02 wt% Amphotericin B-0.02 wt% Alcalase NPs	0.0215	*
	0.02 wt% Alcalase vs 0.2 wt% Shellac-0.25 wt% P407-0.02 wt% Amphotericin B-0.02 wt% Alcalase NPs	0.0349	*
Biofilm protein content	Control vs 0.2 wt% Shellac-0.25 wt% P407-0.02 wt% Amphotericin B-0.02 wt% Alcalase NPs	<0.0001	***
	0.02 wt% Amphotericin B vs 0.2 wt% Shellac-0.25 wt% P407-0.02 wt% Amphotericin B-0.02 wt% Alcalase NPs	0.0062	**
	0.02 wt% Alcalase vs 0.2 wt% Shellac-0.25 wt% P407-0.02 wt% Amphotericin B-0.02 wt% Alcalase NPs	0.0015	**

< 0.05 is considered significant. *P<0.05, **P<0.01, ***P<0.001.

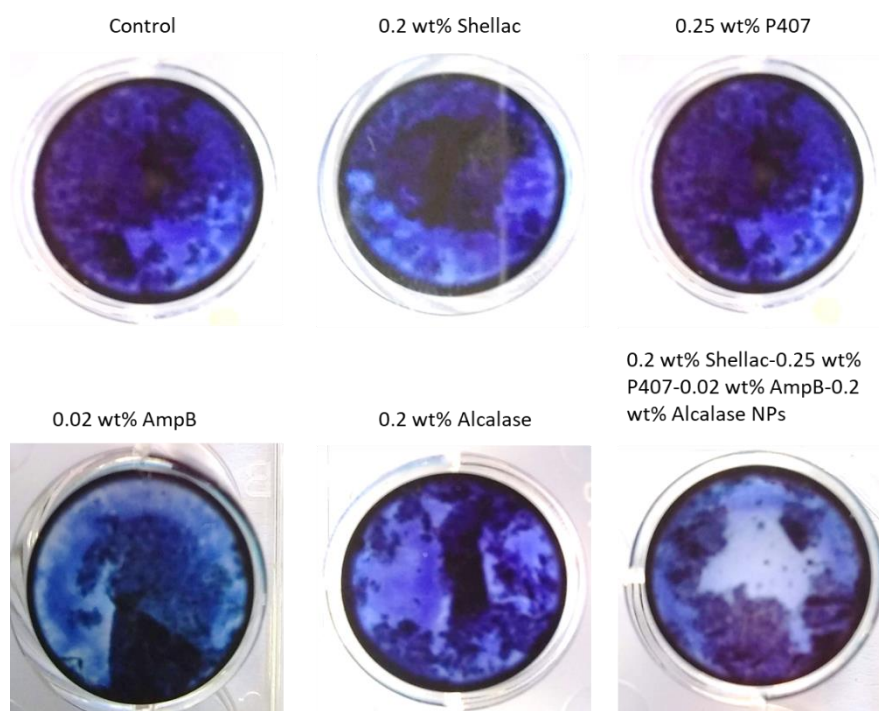


Figure 5.18. Photographs of *C. albicans* biofilms after CV staining and washing (before solubilisation in acetic acid).

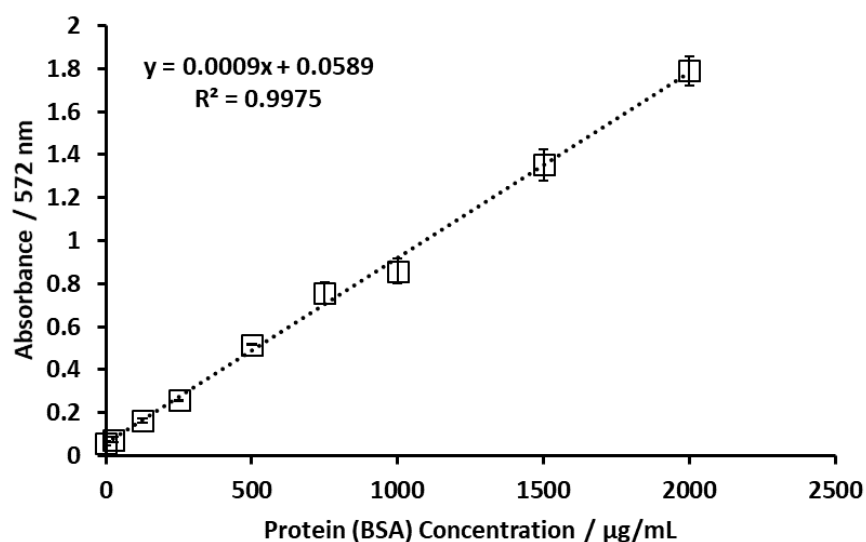


Figure 5.19. BCA (bicinchoninic acid assay) standard curve. N=3 with \pm S.D.

The cellular viability of the *C. albicans* biofilm after the same treatments was also examined. Before treatment testing, the biofilms were grown for 24, 48, and 72 h and at 30 and 37 °C to test how the XTT cell proliferation kit absorbance reading would be affected by different biofilm growth conditions. **Figure 5.20** shows that 37 °C increased the cell concentration compared to 30 °C across all growth time points. In addition, as expected, a biofilm that was able to mature for longer resulted in an increased absorbance reading. It was decided to utilise a biofilm grown for 24 h and 37 °C as the growth control absorbance reading was \approx 1au and this parameter allowed the results to be compared more effectively to the previous biofilm treatment data. **Figure 5.21A** shows that 0.02 wt% AmpB-loaded NPs reduced cellular viability to 7% compared to the growth control after 24 h. The 0.02 wt% AmpB-loaded NPs performed much better than 0.2 wt% Alcalase and 0.02 wt% AmpB, which conferred a reduction of 40% and 50%, respectively. This correlates with the previous biofilm staining, dry weight, and protein content results. In **Figure 5.21B** a further investigation into the effect of 0.02 wt% AmpB-loaded NPs and free AmpB on *C. albicans* biofilm cellular viability after twofold stock dilutions was performed.

As expected, the reduced treatment concentration increased the viability of the biofilm. However, even after large 32-fold and 64-fold dilutions, the AmpB-NP treatment was still highly effective in reducing biofilm viability to 25% and 35%, respectively. This indicates that AmpB-loaded NPs are highly potent and effective even at very low concentrations. Imaging of the biofilms was utilised to elucidate how the AmpB-NP treatment was altering the biofilm structural integrity or appearance (**Figure 5.22**). Using fluorescein diacetate (FDA)/PI live/dead staining, it was shown that

the viability of the cells is reduced in the 0.02 wt% AmpB and 0.2 wt% Alcalase biofilms, in which much less green fluorescing cells are visible. The 0.25 wt% shellac–0.2 wt% P407 NPs show very little difference in viable cells in comparison to the growth control.

The treatment of 0.02 wt% AmpB–loaded shellac NPs (without Alcalase) and 0.02 wt% AmpB–loaded shellac NPs (with Alcalase coating) shows there is a much greater reduction in viable cells compared to the control. This pattern is largely mirrored with the dead cell assay with PI staining. The 0.02 wt% AmpB–loaded NPs (without Alcalase) show a large concentration of dead cells; however, the 0.02 wt% AmpB–loaded NPs (with Alcalase coating) showed fewer dead cells. This is likely due to the Alcalase-coated NPs being able to physically detach large sections of the biofilm, leaving fewer cells to be stained. SEM images of the biofilms support this conclusion. In the 0.02 wt% AmpB–loaded NPs (with Alcalase coating), the biofilm was extremely sparsely distributed. The SEM images for the growth control, 0.25 wt% shellac–0.2 wt% P407 NPs, showed that the biofilm was intact. The treatments that involve Alcalase showed that large sections of the biofilm had been removed, indicating that the Alcalase coating is vital in the effective degradation.

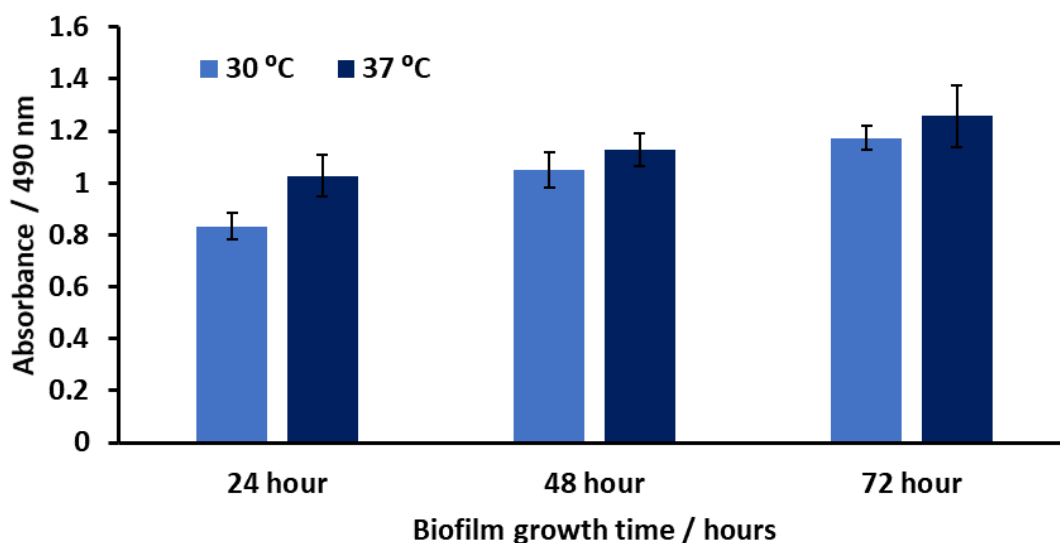


Figure 5.20. Colorimetric readings from XTT-reduction assays of *C. albicans* biofilms formed over 3 days and at either 30°C or 37°C. Biofilms were grown in RPMI media as described below. The results are presented as means ($n = 3$) with \pm S.D.

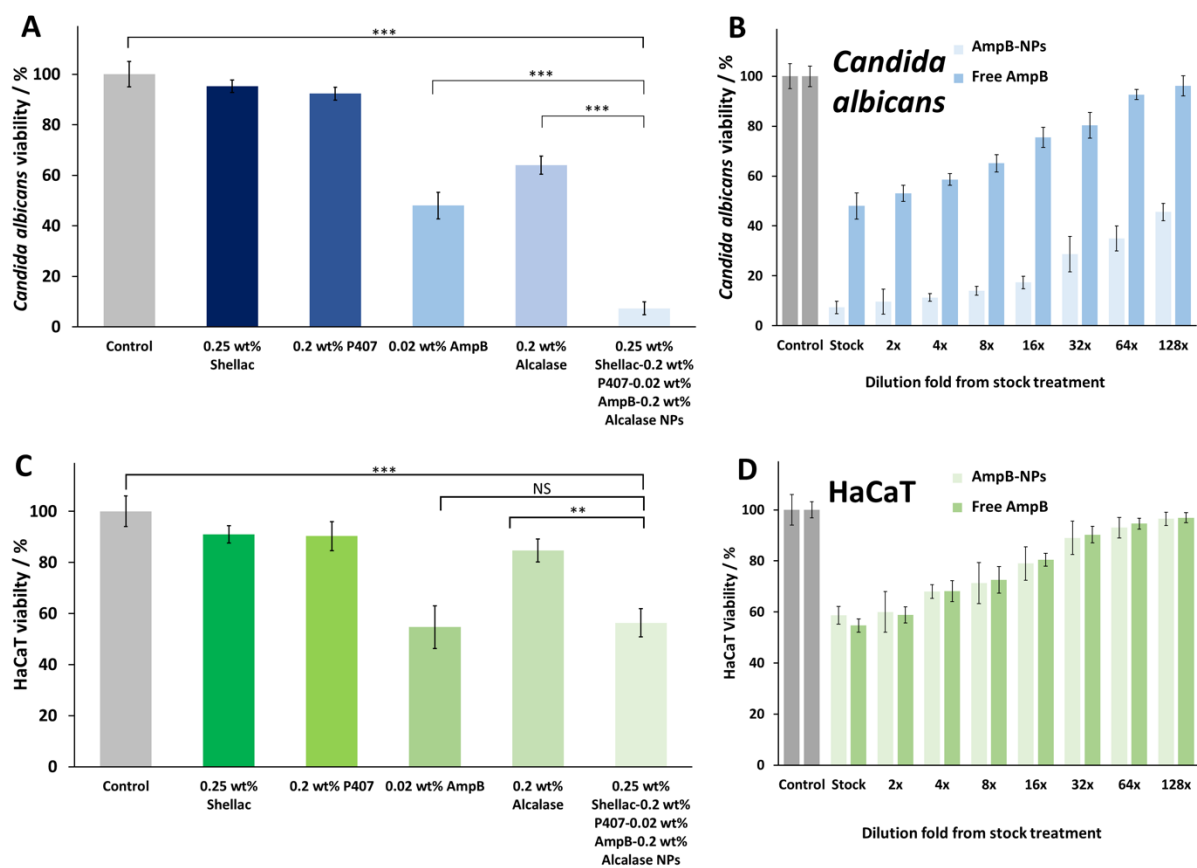


Figure 5.21. (A) Metabolic activity of *C. albicans* biofilms after 24 h treatment with 0.2 wt% shellac–0.25 wt% P407–0.02 wt% AmpB–0.2 wt% Alcalase NPs and various NP components. **(B)** Concentration dependence of 0.2 wt% shellac–0.25 wt% P407–0.02 wt% AmpB–0.2 wt% Alcalase NPs and 0.02 wt% free AmpB. Data shows *C. albicans* viability after 24 h treatment with twofold dilutions of the stock NP treatment. Data were normalised from XTT-reduction assay of sessile biofilm cells in 96-well microtiter plates. Colorimetric data were read at 490 nm. **(C)** HaCaT cell viability after comparative treatment with 0.2 wt% shellac–0.25 wt% P407–0.02 wt% AmpB–0.2 wt% Alcalase NPs and their constituent components after 24 h. **(D)** Concentration dependence of 0.2 wt% shellac–0.25 wt% P407–0.02 wt% AmpB–0.2 wt% Alcalase NPs and 0.02 wt% free AmpB. Data shows HaCaT viability after 24 h treatment with twofold dilutions of the stock NP treatment. An MTT metabolic cellular viability assay was used to determine the influence of the treatment on viable cells. $N = 3 \pm SD$, $p < 0.05$ is considered significant. * $p < 0.05$, ** $p < 0.01$, *** $p < 0.001$, NS = not significant. All Student's *t*-tests were performed in GraphPad v7.0.4. The statistical analysis is shown in **Table 5.4**.

Table 5.4. Viability assay statistical analysis between biofilm growth controls, 0.02 wt% AmpB, 0.2 wt% Alcalase and 0.2 wt% Shellac-0.25 wt% P407-0.02 wt% Amphotericin B-0.02 wt% Alcalase. Data were expressed as average values \pm standard deviations of the mean. P-values of less than 0.05 were considered significant. N=3 with \pm S.D for statistical analysis. All Student's T-tests were performed in GraphPad v7.0.4.

Viability assay	Multiple Comparison	P-value	Significance
XXT Candida viability assay	Control vs 0.2 wt% Shellac-0.25 wt% P407-0.02 wt% Amphotericin B-0.02 wt% Alcalase NPs	<0.0001	***
	0.02 wt% Amphotericin B vs 0.2 wt% Shellac-0.25 wt% P407-0.02 wt% Amphotericin B-0.02 wt% Alcalase NPs	0.0002	***
	0.02 wt% Alcalase vs 0.2 wt% Shellac-0.25 wt% P407-0.02 wt% Amphotericin B-0.02 wt% Alcalase NPs	<0.0001	***
MTT HaCaT viability assay	Control vs 0.2 wt% Shellac-0.25 wt% P407-0.02 wt% Amphotericin B-0.02 wt% Alcalase NPs	0.0008	***
	0.02 wt% Amphotericin B vs 0.2 wt% Shellac-0.25 wt% P407-0.02 wt% Amphotericin B-0.02 wt% Alcalase NPs	0.7878	Not significant
	0.02 wt% Alcalase vs 0.2 wt% Shellac-0.25 wt% P407-0.02 wt% Amphotericin B-0.02 wt% Alcalase NPs	0.0023	**

< 0.05 is considered significant. *P<0.05, **P<0.01, ***P<0.001

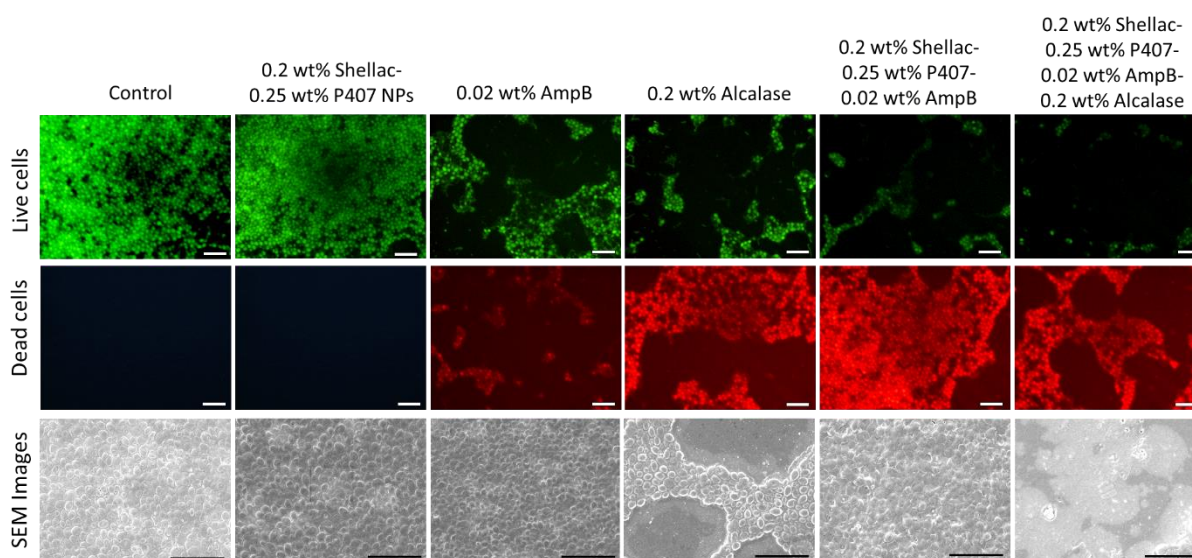


Figure 5.22. Representative fluorescence microscopy images of *C. albicans* biofilms on 96-well plate. Biofilms were grown for 24 h, medium replaced, and subsequently incubated for another 24 h with the treatment-supplemented medium. After treatment the wells were washed thrice with deionised water and incubated with 100 μ L of deionised water infused with fluorescent label dyes that distinguish between live and dead cells. The bottom row shows SEM images of *C. albicans* biofilms after treatment with 0.2 wt% shellac–0.25 wt% P407–0.02 wt% AmpB–0.2 wt% Alcalase and individual components. All samples were prepared for SEM imaging by drying and coated with an \approx 6 nm gold layer. Samples were imaged using a Carl Zeiss Evo-60 (Germany) with a variable pressure 100 μ m aperture at 40 Pa. EHT was 20 kV with a probe current of 100 pA. Images were captured with the Zeiss SmartSEM software. White and black scale bars are 10 μ m.

5.3.7 HaCaT cell cytotoxicity of shellac–AmpB–Alcalase NPs

Next, an investigation into the toxicity of the 0.02 wt% AmpB–loaded NPs when used to treat HaCaT cells was examined. HaCaT cells were chosen because they are an appropriate proxy for studying cell cytotoxicity of human keratinocytes. *C. albicans* biofilms can be a serious problem with chronic wound infection and so an investigation into how this treatment affects the surrounding human skin cells. **Figure 5.21A** shows that 0.25 wt% shellac and 0.2 wt% P407 NPs had only a negligible effect on HaCaT viability. The high concentration of 0.02 wt% free AmpB reduced the viability of the cells by 40% after 24 h treatment; however, there was no significant difference in HaCaT cells viability when treated with 0.02 wt% AmpB–loaded NPs, indicating the formulation of AmpB into the NPs does not increase the toxicity compared to free AmpB. Most interestingly, **Figure 5.21D** shows the effect that twofold dilutions of the 0.02 wt% AmpB–loaded NPs treatment and free AmpB had on the HaCaT cells viability.

Similarly to the treatments on *C. albicans* biofilms, as the dilutions of the treatment were increased, the viability of the HaCaT cells was also increasing, culminating in a HaCaT cell viability of only 5% less than the control at 32 times treatment dilution. When comparing to the same treatment concentrations of *C. albicans* biofilms (**Figure 5.21B**), it is clear that at the 0.02 wt% AmpB–loaded NPs dilutions are much more effective at the *C. albicans* biofilm cellular viability reduction than the HaCaT cell viability reduction. At 16 times treatment dilution, the HaCaTs have a viability of 75%, whereas the *C. albicans* biofilm viability is 18%. This trend continues. At 32 times treatment dilution, the HaCaTs have a viability of 89% and the biofilm-based cells had only 27% viability. There is an “early time window” where the AmpB–NPs show a negligible effect on HaCaT viability but remain potentially effective against established *C. albicans* biofilms. This shows that in a wound biofilm treatment context the 0.02 wt% AmpB–loaded NPs would be much more effective at clearing the biofilm than harming the resident human cells, and importantly would outperform equivalent concentrations of free AmpB. This could allow for a lower concentration of AmpB to be administered overall, which is an important factor is considering the toxicity dangers AmpB is associated with. Normal skin has a pH of ≈ 5.6 – 6.4 , a result of secretion of organic acids produced by keratinocytes (Kruse et al., 2015).

Chronic wounds are often infected with microorganisms, and the presence of necrotic tissue and reduced blood supply, impairing an immune response, are a leading cause of this (Zhao et al., 2013). Biofilm formation is extremely common in chronic wounds, including *Candida* species (Kalan & Grice, 2018; Dowd et al., 2008). This calls for the need for novel treatments with increased efficacy. Chronic wounds tend to have a basic pH, ranging from 7.15 to 8.9 (Gethin, 2007). However, *Candida* species have an optimal growth at pH between 7 and 8 and in this range are most prevalent in chronic wounds (Jones et al., 2015). These data show that 0.02 wt% AmpB–loaded

NPs are cationic and sterically stable within this pH range, and can electrostatically bind to *C. albicans*, which has a negative zeta potential in these conditions. This provides evidence that 0.02 wt% AmpB-loaded NPs would be useful for *Candida* infection treatments in the context of chronic wounds.

To further demonstrate the effect of free AmpB and AmpB-NPs on *C. albicans* and HaCaT cells, a comparison of the effect of the stock 0.02 wt% free AmpB was measured against a 128× dilution of 0.02 wt% AmpB-NPs. **Figure 5.23** shows these concentrations have a very similar effect on reducing *C. albicans* biofilm viability, with the 128× dilution of 0.02 wt% AmpB-NPs reducing viability to 45%, and 0.02 wt% free AmpB to 48%. This indicates that the 128× diluted AmpB-NPs treatment is much more potent than free AmpB. This is due to the ability of the AmpB-NPs formulation to degrade the *C. albicans* biofilms and electrostatically attach the cells. Interestingly, when comparing the effect of the stock 0.02 wt% free AmpB against a 128× dilution of 0.02 wt% AmpB-NPs on HaCaT cells, there is large difference in the cellular viability. The stock of 0.02 wt% free AmpB reduces the viability of the HaCaT cells to 54% and the 128× dilution of 0.02 wt% AmpB-NPs has a negligible effect on HaCaT viability, reducing it to 96%. This provides evidence that a formulated NP encapsulation of AmpB can have a similar effect on *C. albicans* biofilm viability at a lower concentration than free AmpB (128× dilution), while simultaneously having a limited cytotoxic effect on HaCaT cells. This could potentially aid wound healing by providing a potent antifungal treatment that has a lower overall concentration of the active agent AmpB. Resulting in a lower toxic effect on HaCaT cells, a proxy for keratinocytes, which are vital in wound healing.

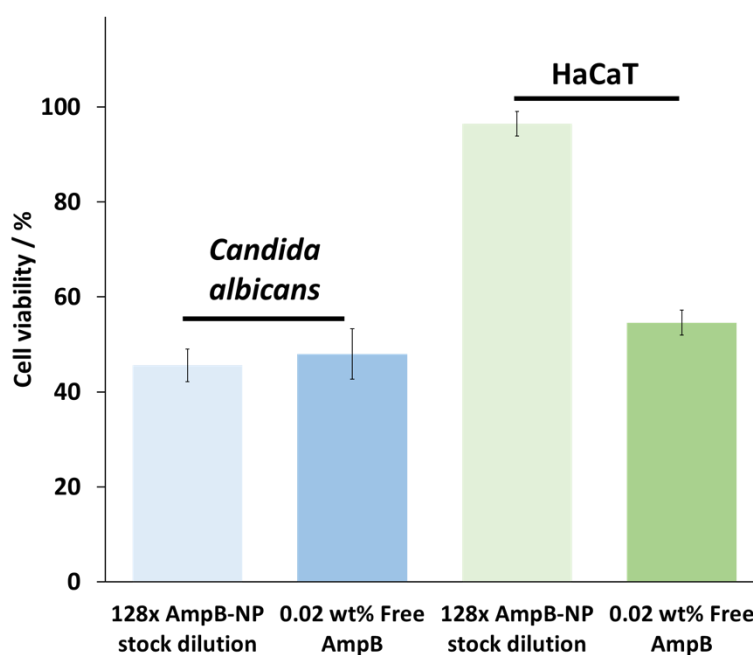


Figure 5.23. Comparison between free AmpB and AmpB-NPs on *C. albicans* (biofilm) cellular viability and HaCaT viability after 24 h treatments. The 128× AmpB-NP treatment was diluted 128× from a stock of 0.25 wt% shellac-0.2 wt% P407-0.02 wt% AmpB-0.2 wt% Alcalase NP suspension. $N = 3 \pm S.D.$

5.4 Conclusions

These results confirm that AmpB-loaded shellac NPs functionalised with the protease Alcalase 2.4 L FG can effectively kill *C. albicans* in both planktonic and biofilm form. The shellac-based NPs were sterically stabilised using P407, allowing the hydrophobic AmpB to be encapsulated within them. Functionalisation of the NPs with a cationic protease allows the biofilm to be degraded and concentrated form of AmpB be delivered locally to the fungal cell membrane. AmpB-loaded NPs are more effective than equivalent concentrations of free AmpB, causing up to a sixfold reduction in fungal colony-forming units after 180 min. Against *C. albicans* formed within a biofilm, AmpB-loaded NPs were able to reduce the biofilm viability to around 7% compared to the growth control, a significant improvement on the free AmpB, which reduced the biofilm viability to 50%. Fluorescence microscopy and SEM images showed the AmpB-loaded NPs-treated samples had a much more reduced concentration of viable cells and structural damage observed on the biofilm surface. In addition, the AmpB-loaded NPs showed no increased toxicity toward human adult keratinocytes (HaCaTs), indicating that formulating AmpB into shellac NPs can increase its effectiveness but has no negative impact on human cell viability. This indicated that these AmpB-loaded NPs could be used therapeutically on external wounds infected with fungal biofilms.

5.5 Reference list

- Ahmadi, M. S., Lee, H. H., Sanchez, D. A., Friedman, A. J., Tar, M. T., Davies, K. P., Nosanchuk, J. D., & Martinez, L. R. (2016). Sustained Nitric Oxide-Releasing Nanoparticles Induce Cell Death in *Candida albicans* Yeast and Hyphal Cells, Preventing Biofilm Formation In Vitro and in a Rodent Central Venous Catheter Model. *Antimicrobial agents and chemotherapy*, *60*(4), 2185–2194.
- Akers, K., Rowan, M., Niece, K., Graybill, J., Mende, K., Chung, K. & Murray, C. (2015) Antifungal wound penetration of amphotericin and voriconazole in combat-related injuries: case report. *BMC Infectious Diseases*, *15*(1).
- Al-Awady, M., Weldrick, P., Hardman, M., Greenway, G. & Paunov, V. (2018) Amplified Antimicrobial Action Of Chlorhexidine Encapsulated In PDAC-Functionalized Acrylate Copolymer Nanogel Carriers. *Mater. Chem. Front.*, *2*, 2032–2044.
- Badawy, S. I., Gawronski, A. J., & Alvarez, F. J. (2001). Application of sorption--desorption moisture transfer modeling to the study of chemical stability of a moisture sensitive drug product in different packaging configurations. *International journal of pharmaceuticals*, *223*(1-2), 1–13.
- Balkovec, J. M., Hughes, D. L., Masurekar, P. S., Sable, C. A., Schwartz, R. E., & Singh, S. B. (2014). Discovery and development of first in class antifungal caspofungin (CANCIDAS®)--a case study. *Natural product reports*, *31*(1), 15–34.
- Cauchie, M., Desmet, S., & Lagrou, K. (2017). *Candida* and its dual lifestyle as a commensal and a pathogen. *Research in microbiology*, *168*(9-10), 802–810.
- Chellan, G., Shivaprakash, S., Karimassery Ramaiyar, S., Varma, A. K., Varma, N., Thekkeparambil Sukumaran, M., Rohinivilasam Vasukutty, J., Bal, A., & Kumar, H. (2010). Spectrum and prevalence of fungi infecting deep tissues of lower-limb wounds in patients with type 2 diabetes. *Journal of clinical microbiology*, *48*(6), 2097–2102.
- Costa-Orlandi, C. B., Sardi, J., Pitangui, N. S., de Oliveira, H. C., Scorzoni, L., Galeane, M. C., Medina-Alarcón, K. P., Melo, W., Marcelino, M. Y., Braz, J. D., Fusco-Almeida, A. M., & Mendes-Giannini, M. (2017). Fungal Biofilms and Polymicrobial Diseases. *Journal of fungi (Basel, Switzerland)*, *3*(2), 22.
- de Alteriis, E., Maselli, V., Falanga, A., Galdiero, S., Di Lella, F. M., Gesuele, R., Guida, M., & Galdiero, E. (2018). Efficiency of gold nanoparticles coated with the antimicrobial peptide indolicidin against biofilm formation and development of *Candida* spp. clinical isolates. *Infection and drug resistance*, *11*, 915–925.
- Desai, J. V., Mitchell, A. P., & Andes, D. R. (2014). Fungal biofilms, drug resistance, and recurrent infection. *Cold Spring Harbor perspectives in medicine*, *4*(10), a019729.
- Dowd, S. E., Sun, Y., Secor, P. R., Rhoads, D. D., Wolcott, B. M., James, G. A., & Wolcott, R. D. (2008). Survey of bacterial diversity in chronic wounds using pyrosequencing, DGGE, and full ribosome shotgun sequencing. *BMC microbiology*, *8*, 43.
- Faustino, C., & Pinheiro, L. (2020). Lipid Systems for the Delivery of Amphotericin B in Antifungal Therapy. *Pharmaceutics*, *12*(1), 29.
- Forsberg, K., Woodworth, K., Walters, M., Berkow, E. L., Jackson, B., Chiller, T., & Vallabhaneni, S. (2019). *Candida auris*: The recent emergence of a multidrug-resistant fungal pathogen. *Medical mycology*, *57*(1), 1–12.
- Ganeshpurkar, A., Vaishya, P., Jain, S., Pandey, V., Bansal, D., & Dubey, N. (2014). Delivery of Amphotericin B for Effective Treatment of *Candida Albicans* Induced Dermal Mycosis in Rats via Emulgel System: Formulation and Evaluation. *Indian journal of dermatology*, *59*(4), 369–374.
- Gardner, W., & Whitmore, W. (1929) Nature and Constitution of Shellac I—Preliminary Investigation of the Action of Organic Solvents. *Ind. Eng. Chem.*, *21*, 226.
- Gethin, G. (2007) The significance of surface pH in chronic wounds. *Wounds UK*, *3*, 52.
- Giuliano, E., Paolino, D., Fresta, M., & Cosco, D. (2018). Mucosal Applications of Poloxamer 407-Based Hydrogels: An Overview. *Pharmaceutics*, *10*(3), 159.
- Grela, E., Zdybicka-Barabas, A., Pawlikowska-Pawlega, B., Cytrynska, M., Wlodarczyk, M., Grudzinski, W., Luchowski, R., & Gruszecki, W. I. (2019). Modes of the antibiotic activity of amphotericin B against *Candida albicans*. *Scientific reports*, *9*(1), 17029.

- Gulati, M., & Nobile, C. J. (2016). *Candida albicans* biofilms: development, regulation, and molecular mechanisms. *Microbes and infection*, 18(5), 310–321.
- Halbus, A. F., Horozov, T. S., & Paunov, V. N. (2019a). "Ghost" Silica Nanoparticles of "Host"-Inherited Antibacterial Action. *ACS applied materials & interfaces*, 11(42), 38519–38530.
- Halbus, A. F., Horozov, T. S., & Paunov, V. N. (2019c). Controlling the Antimicrobial Action of Surface Modified Magnesium Hydroxide Nanoparticles. *Biomimetics (Basel, Switzerland)*, 4(2), 41.
- Halbus, A., Horozov, T. & Paunov, V. (2019b) Self-Grafting Copper Oxide Nanoparticles Show A Strong Enhancement Of Their AntiAlgal And Anti-Yeast Action. *Nanoscale Adv.*, 1, 2323–2336.
- Hamill R. J. (2013). Amphotericin B formulations: a comparative review of efficacy and toxicity. *Drugs*, 73(9), 919–934.
- Hoang-Dao, B. T., Hoang-Tu, H., Tran-Hung, L., Camps, J., Koubi, G., & About, I. (2008). Evaluation of a natural resin-based new material (Shellac F) as a potential desensitizing agent. *Dental materials : official publication of the Academy of Dental Materials*, 24(7), 1001–1007.
- Jones, E. M., Cochrane, C. A., & Percival, S. L. (2015). The Effect of pH on the Extracellular Matrix and Biofilms. *Advances in wound care*, 4(7), 431–439.
- Kalan, L., & Grice, E. A. (2018). Fungi in the Wound Microbiome. *Advances in wound care*, 7(7), 247–255.
- Kaplan J. B. (2010). Biofilm dispersal: mechanisms, clinical implications, and potential therapeutic uses. *Journal of dental research*, 89(3), 205–218.
- Keane, S., Geoghegan, P., Pova, P., Nseir, S., Rodriguez, A., & Martin-Loeches, I. (2018). Systematic review on the first line treatment of amphotericin B in critically ill adults with candidemia or invasive candidiasis. *Expert review of anti-infective therapy*, 16(11), 839–847.
- Kostakioti, M., Hadjifrangiskou, M., & Hultgren, S. J. (2013). Bacterial biofilms: development, dispersal, and therapeutic strategies in the dawn of the postantibiotic era. *Cold Spring Harbor perspectives in medicine*, 3(4), a010306.
- Kraisit, P., Limmatvapirat, S., Nunthanid, J., Sriamornsak, P., & Luangtana-anan, M. (2013). Nanoparticle formation by using shellac and chitosan for a protein delivery system. *Pharmaceutical development and technology*, 18(3), 686–693.
- Kruse, C. R., Nuutila, K., Lee, C. C., Kiwanuka, E., Singh, M., Caterson, E. J., Eriksson, E., & Sørensen, J. A. (2015). The external microenvironment of healing skin wounds. *Wound repair and regeneration : official publication of the Wound Healing Society [and] the European Tissue Repair Society*, 23(4), 456–464.
- Ksiezopolska, E., & Gabaldón, T. (2018). Evolutionary Emergence of Drug Resistance in *Candida* Opportunistic Pathogens. *Genes*, 9(9), 461.
- Limmatvapirat, S., Limmatvapirat, C., Luangtana-Anan, M., Nunthanid, J., Oguchi, T., Tozuka, Y., Yamamoto, K., & Puttipatkhachorn, S. (2004). Modification of physicochemical and mechanical properties of shellac by partial hydrolysis. *International journal of pharmaceutics*, 278(1), 41–49.
- Limmatvapirat, S., Panchapornpon, D., Limmatvapirat, C., Nunthanid, J., Luangtanaanan, M., & Puttipatkhachorn, S. (2008) Development of New Shellac Based pH Responsive Polymer for Biomedical Applications. *Eur. J. Pharm. Biopharm*, 70, 335.
- Markowska, K., Grudniak, A. & Wolska, K. (2013) Silver Nanoparticles As An Alternative Strategy Against Bacterial Biofilms. *Acta Biochim. Pol.*, 60, 523–530.
- Mesa-Arango, A. C., Scorzoni, L., & Zaragoza, O. (2012). It only takes one to do many jobs: Amphotericin B as antifungal and immunomodulatory drug. *Frontiers in microbiology*, 3, 286.
- Mitrofanova, O., Mardanova, A., Evtugyn, V., Bogomolnaya, L. & Sharipova, M. (2017) Effects Of Bacillus Serine Proteases On The Bacterial Biofilms. *BioMed Res. Int.*, 2017,1–10.
- Morad, H., Wild, A. M., Wiehr, S., Davies, G., Maurer, A., Pichler, B. J., & Thornton, C. R. (2018). Pre-clinical Imaging of Invasive Candidiasis Using ImmunoPET/MR. *Frontiers in microbiology*, 9, 1996.
- Neumann, A., Baginski, M., & Czub, J. (2010). How do sterols determine the antifungal activity of amphotericin B? Free energy of binding between the drug and its membrane targets. *Journal of the American Chemical Society*, 132(51), 18266–18272.

- Nevin, A., Comelli, D., Valentini, G., & Cubeddu, R. (2009). Total synchronous fluorescence spectroscopy combined with multivariate analysis: method for the classification of selected resins, oils, and protein-based media used in paintings. *Analytical chemistry*, 81(5), 1784–1791.
- Newase, S. & Bankar, A. (2017) Synthesis Of Bio-Inspired Ag–Au Nanocomposite And Its Anti-Biofilm Efficacy. *Bull. Mater. Sci.*, 40, 157–162.
- Osei-Sekyere, J. (2019). Candida auris: A systematic review and meta-analysis of current updates on an emerging multidrug-resistant pathogen. *MicrobiologyOpen*, 8(8), e00901.
- Patel, A., Heussen, P., Hazekamp, J. & Velikov, K. (2011) Stabilisation and controlled release of silibinin from pH responsive shellac colloidal particles. *Soft Matter*, 7(18), 8549.
- Patel, A., Schatteman, D., Vos, W. & Dewettinck, K. (2013) Shellac as a natural material to structure a liquid oil-based thermo reversible soft matter system. *RSC Advances*, 3(16), 5324.
- Pfaller, M. A., & Diekema, D. J. (2007). Epidemiology of invasive candidiasis: a persistent public health problem. *Clinical microbiology reviews*, 20(1), 133–163.
- Pfaller, M. A., Andes, D. R., Diekema, D. J., Horn, D. L., Reboli, A. C., Rotstein, C., Franks, B., & Azie, N. E. (2014). Epidemiology and outcomes of invasive candidiasis due to non-albicans species of *Candida* in 2,496 patients: data from the Prospective Antifungal Therapy (PATH) registry 2004-2008. *PLoS one*, 9(7), e101510.
- Pierce, C. G., Uppuluri, P., Tristan, A. R., Wormley, F. L., Jr, Mowat, E., Ramage, G., & Lopez-Ribot, J. L. (2008). A simple and reproducible 96-well plate-based method for the formation of fungal biofilms and its application to antifungal susceptibility testing. *Nature protocols*, 3(9), 1494–1500.
- Pitto-Barry, A. & Barry, N. (2014) Pluronic® block-copolymers in medicine: from chemical and biological versatility to rationalisation and clinical advances. *Polym Chem*, 5(10), 3291-3297.
- Sanchez, D. A., Schairer, D., Tuckman-Vernon, C., Chouake, J., Kutner, A., Makdisi, J., Friedman, J. M., Nosanchuk, J. D., & Friedman, A. J. (2014). Amphotericin B releasing nanoparticle topical treatment of *Candida* spp. in the setting of a burn wound. *Nanomedicine : nanotechnology, biology, and medicine*, 10(1), 269–277.
- Sears, D., & Schwartz, B. S. (2017). *Candida auris*: An emerging multidrug-resistant pathogen. *International journal of infectious diseases : IJID : official publication of the International Society for Infectious Diseases*, 63, 95–98.
- Sharma, D., Misba, L., & Khan, A. U. (2019). Antibiotics versus biofilm: an emerging battleground in microbial communities. *Antimicrobial resistance and infection control*, 8, 76.
- Singh, R., Kumar, M., Mittal, A. & Mehta, P. (2016) Microbial Enzymes: Industrial Progress In 21st Century. *3 Biotech*, 6, 174.
- Stone, N. R., Bicanic, T., Salim, R., & Hope, W. (2016). Liposomal Amphotericin B (AmBisome®): A Review of the Pharmacokinetics, Pharmacodynamics, Clinical Experience and Future Directions. *Drugs*, 76(4), 485–500.
- Sun, C., Xu, C., Mao, L., Wang, D., Yang, J., & Gao, Y. (2017). Preparation, characterization and stability of curcumin-loaded zein-shellac composite colloidal particles. *Food chemistry*, 228, 656–667.
- Takemoto, K., Yamamoto, Y., & Ueda, Y. (2006). Evaluation of antifungal pharmacodynamic characteristics of AmBisome against *Candida albicans*. *Microbiology and immunology*, 50(8), 579–586.
- Tamburini, D., Dyer, J., & Bonaduce, I. (2017). The characterisation of shellac resin by flow injection and liquid chromatography coupled with electrospray ionisation and mass spectrometry. *Scientific reports*, 7(1), 14784.
- Uppuluri, P., Srinivasan, A., Ramasubramanian, A., & Lopez-Ribot, J. L. (2011). Effects of fluconazole, amphotericin B, and caspofungin on *Candida albicans* biofilms under conditions of flow and on biofilm dispersion. *Antimicrobial agents and chemotherapy*, 55(7), 3591–3593.
- Vincent, B., Lancaster, A., Scherz-Shouval, R., Whitesell, L. & Lindquist, S. (2013) Fitness Trade-offs Restrict the Evolution of Resistance to Amphotericin B. *PLoS Biology*, 11(10), e1001692.
- Warnock, D. (1991) Amphotericin B: an introduction, *J. Antimicrobial Chemotherapy*, 28, 27-38.

Weldrick, P. J., Hardman, M. J., & Paunov, V. N. (2019b). Enhanced Clearing of Wound-Related Pathogenic Bacterial Biofilms Using Protease-Functionalized Antibiotic Nanocarriers. *ACS applied materials & interfaces*, *11*(47), 43902–43919.

Weldrick, P. J., Iveson, S., Hardman, M. J. & Paunov, V. N. (2019a) Breathing New Life Into Old Antibiotics: Overcoming Antibacterial Resistance By Antibiotic-Loaded Nanogel Carriers With Cationic Surface Functionality. *Nanoscale*, *11*, 10472–10485.

Yang, M., Du, K., Hou, Y., Xie, S., Dong, Y., Li, D., & Du, Y. (2019). Synergistic Antifungal Effect of Amphotericin B-Loaded Poly(Lactic-Co-Glycolic Acid) Nanoparticles and Ultrasound against *Candida albicans* Biofilms. *Antimicrobial agents and chemotherapy*, *63*(4), e02022-18.

Zhao, G., Usui, M. L., Lippman, S. I., James, G. A., Stewart, P. S., Fleckman, P., & Olerud, J. E. (2013). Biofilms and Inflammation in Chronic Wounds. *Advances in wound care*, *2*(7), 389–399.

6.0 CHAPTER 6

6.1 Summary of thesis

Multidrug-resistant pathogens are prevalent in chronic wounds. There is an urgent need to develop novel antimicrobials and formulation strategies to overcome antibiotic resistance and provide a safe alternative to traditional antibiotics. A confounding factor is biofilms, which are prevalent in chronic wounds and once formed, are very hard to remove, which is associated with poor outcomes and high mortality rates. Biofilms are comprised of surface-attached bacteria embedded in an extracellular polymeric substance (EPS) matrix, which confers increased antibiotic resistance and host immune evasion. Therefore, disruption of this matrix is essential to tackle the biofilm-embedded bacteria. The research presented in this thesis explores if polymeric NPs can be used to encapsulate and deliver concentrated antibiotics by subsequent functionalisation of the NP with a cationic coating agent to kill antibiotic-resistant pathogenic planktonic and biofilm-formed bacteria and fungi.

Chapter 2 shows the development of a novel surface functionalised nanocarrier for tetracycline and lincomycin by using lightly cross-linked polyacrylic acid-based nanogels (Carbopol Aqua SF1) coated with a biocompatible cationic polyelectrolyte (bPEI). It is shown that this approach significantly enhanced the antimicrobial action against a range of wound isolated pathogens. Crucially, the bPEI surface coated nanogel with encapsulated antibiotics had an enhanced effect on several bacterial species which were validated to be resistant to either tetracycline or lincomycin. This enhanced antibiotic efficacy is likely due to favourable electrostatic attraction between the positively charged bPEI-coated antibiotic-loaded nanogel particles and the negatively charged bacterial cell wall. This is mediated by the attachment of the nanocarrier particles which then locally release the encapsulated antibiotic in much higher local concentrations than the free antibiotic at the same overall concentration. The results also show that the cytotoxicity of the antibiotics loaded in these nanocarriers on human keratinocyte cells is practically negligible in the range of concentrations which kill both resistant and susceptible bacteria. Antimicrobial resistance is a growing clinical epidemic. This novel method for bacteria-targeted topical antibiotic applications offers an important new opportunity to extend the clinically useful life-span of existing antibiotics, using inexpensive materials, while reducing future bacterial antibiotic resistance.

Chapter 3 advances the nanogel nanocarrier by surface functionalisation with the protease, Alcalase 2.4 L FG. The aim was to prove that functionalisation with the protease could degrade biofilms and allow an increased effect of the antibiotic encapsulated within the NP to in a more complex bacterial phenotype. These results confirm that protease Alcalase 2.4 L FG can disrupt the bacterial biofilm EPS matrix and reduce its biomass. The surface functionalisation of Carbopol Aqua SF1

nanogels with this enzyme further boosts this effect on six wound biofilm associated pathogens reducing the biomass 6-fold compared to untreated biofilms. The efficacy of the Alcalase-coated Carbopol nanogel particles was confirmed using fluorescence, atomic force, and scanning electron microscopy. Additionally, the application of Alcalase–Carbopol nanogels in a co-treatment with ciprofloxacin resulted in a 3-log reduction in viable cell counts compared to using of an equivalent concentration of ciprofloxacin alone. When ciprofloxacin was encapsulated within Alcalase-functionalised Carbopol nanogel at equivalent concentrations to the free ciprofloxacin, there was a very significant further boost to the effectiveness of the antibiotic in this dual-functionalised nanocarrier. These dual purpose Alcalase-coated antibiotic-loaded nanogel particles provided effective treatment against *S. aureus* biofilms, with no detectable CFU after 6 and 24 h treatment times. The Alcalase–Carbopol nanogels also showed negligible cytotoxicity and apoptosis-inducing influence toward adult human keratinocytes. It is concluded that the Alcalase-coated and ciprofloxacin-loaded Carbopol nanogel carriers are very effective and apparently safe antibiofilm formulation, which could provide an alternative approach to the treatment of external wound biofilms. This suggested that further investigation of the practical administration of Alcalase-coated Carbopol nanogels loaded with antibiotics on biofilm-infected wounds is required, where these nanogels could provide an advantageous tool for therapeutic antibiofilm treatments and fight against antimicrobial resistance.

Chapter 4 aimed to combine the efforts of utilising concentrated antibiotics into a polymeric NP (chapter 2) and the active surface functionalisation, using Alcalase 2.4 L FG (chapter 3) and prove if this could be effective against an antibiotic-resistant biofilm-formed pathogen. The antimicrobial susceptibility profile of *Staphylococcus aureus* was analysed and found to be resistant to penicillin G. It so was chosen as the pathogen to test the efficacy of the antibiotic encapsulated, protease functionalised NPs. Pathogens of this nature often result in dire outcomes for patients and are very difficult to treat, for example, in infected chronic wounds. This chapter shows the developed an innovative nanocarrier system with a protease coating which can overcome an antibiotic-resistant pathogen in both planktonic and biofilm form. A demonstration of the effectiveness of Penicillin G and oxacillin encapsulated in shellac NPs against a strain of *S. aureus* verified as Penicillin G resistant was performed. The functionalisation of the NPs with a coating of the cationic protease Alcalase creates a dual application NPs which allows the degradation of the biofilms and electrostatic adhesion to the anionic bacterial cell wall. The attachment of the antibiotic-loaded NPs to the bacterial cells allows a highly localised continuous release of concentrated antibiotic on the bacteria cell wall which is much higher than an equivalent concentration of the free antibiotic. Note that the Alcalase coating allows the antibiotic-packed nanocarriers to reach the bacterial cells which are “deeply buried” in the biofilm

matrix. This novel method of bacteria-targeting active NPs with an additional anti-biofilm function offers an important opportunity to revive the usefulness of antibiotics considered obsolete (*i.e.* Penicillin G) and target biofilm embedded bacteria which are particularly prevalent in chronic wounds. It is concluded that Alcalase-coated and PenG/Oxa-loaded shellac NPs are an effective and safe method of clearing antibiotic resistant biofilms, and propose this could be an alternative approach to topical biofilm treatments, particularly in chronic wounds. It is suggested that further experimental investigation into the application of these NPs on biofilm-infected chronic wounds is required, and could provide a new therapeutic approach for treating antibiotic resistant biofilms.

Chapter 5 aimed to prove antibiotic encapsulated NPs, surface functionalised with a protease could also be used against fungal pathogens, broadening their therapeutic potential. Further emphasise on the reduced toxicity of NPs, by way of reducing the overall concentration of the active agent encapsulated whilst simultaneously maintaining the anti-biofilm effect is explored. These results confirm that AmpB-loaded shellac NPs functionalised with the protease Alcalase 2.4 L FG can effectively kill *C. albicans* in both planktonic and biofilm form. The shellac-based NPs were sterically stabilised using P407, allowing the hydrophobic AmpB to be encapsulated within them. Functionalisation of the NPs with a cationic protease allows the biofilm to be degraded and concentrated form of AmpB be delivered locally to the fungal cell membrane. AmpB-loaded NPs are more effective than equivalent concentrations of free AmpB, causing up to a sixfold reduction in fungal colony-forming units after 180 min. Against *C. albicans* formed within a biofilm, AmpB-loaded NPs were able to reduce the biofilm viability to around 7% compared to the growth control, a significant improvement on the free AmpB, which reduced the biofilm viability to 50%. Fluorescence microscopy and SEM images showed the AmpB-loaded NPs-treated samples had a much more reduced concentration of viable cells and structural damage observed on the biofilm surface. In addition, the AmpB-loaded NPs showed no increased toxicity toward human adult keratinocytes (HaCaTs), indicating that formulating AmpB into shellac NPs can increase its effectiveness but has no negative impact on human cell viability. This indicated that these AmpB-loaded NPs could be used therapeutically on external wounds infected with fungal biofilms.

6.2 Future work

The advancement of the therapeutic potential of the polymeric NPs revealed in this thesis would require evaluation of a more realistic skin model. To this end, preliminary work has begun using a 3D biofilm/human keratinocyte clusteroids co-culture platform to investigate if these NP types can effectively clear the biofilm, whilst reducing any collateral damage to simple skin analogue (Celik et al., 2019; Wang et al., 2021). The results so far have been promising and demonstrate that co-culture models can be exploited as a novel platform for testing the biofilm-eliminating efficiency of various NPs formulations emulating skin and wound infections and could have broader applicability to replace animal models in similar experiments.

Additionally, experiments to investigate the antimicrobial properties of these NPs could be performed in an *ex vivo* Porcine Wound Biofilm Model. Tissue studies have been indicated as more adequate than *in vitro* models for testing the significance of clinical treatments as they provide the opportunity for bacteria to interact with host tissues (Davis et al., 2008; Roberts et al., 2015). *Ex vivo* porcine wound models have been used previously and provide a close physiological comparison to human wound tissue for use with clinically relevant bacteria (Meyer et al., 1978; Gjødsbøl et al., 2006; Wilkinson et al., 2016).

In vivo models will provide a further level of relevance, allowing the contribution of host factors such as ischemia and necrosis on biofilm to be assessed (Phillips et al., 2011). However, as animal studies are expensive, time-consuming, and technically demanding, *ex vivo* tissue models could allow easier control of experimental variables and assessment of outcomes (Progulske-Fox et al., 2013). It is also important to move away from animal studies. It is immoral to cause unnecessary pain and suffering for scientific knowledge, which is ultimately likely not to correlate closely to human outcomes (Akhtar et al., 2015; Levy, 2012; Ferdowsian & Beck, 2011).

An *ex vivo* human wound model could be used for providing an ethical alternative to nonhuman *in vivo* studies and reduced risk vs invasive clinical studies (Ansell et al., 2012). Although *ex vivo* human wound models cannot fully recapitulate the complexities of the *in vivo* healing environment (Zhou et al., 2018), they could be used to reveal how wound healing would be affected by pathogen infection and subsequent NP treatments, with useful histological and viability data potentially obtained, as well as wound healing biomarker response, such as keratin 6 (Wilkinson et al., 2020; Mansbridge & Knapp, 1987; Wong & Coulombe, 2003). A key advantage of *ex vivo* human wound models is that they retain native human skin structure and bypass cross-species differences that can hinder nonhuman *in vivo* wound studies interpretation. A limitation of the encouraging

results shown in this thesis the lack of understanding of how these NPs would perform in a more complex *ex vivo* environment, making further study in this area a good priority.

Additionally, a comparison of how antibiotic-encapsulated hydrogel NPs compare to the currently used antiseptic treatments (cetrimide, benzalkonium chloride and PVP-I) presently used in wound healing has recently been investigated (Weldrick et al., 2021). The data reveals these can provide a more significant effect against *S. aureus* biofilms compared to equivalent and therapeutic concentrations of these antiseptic formulations. Further investigation into how the antibiotic-encapsulated NPs, discussed in this thesis, perform against other antiseptics in a more complex model could be investigated.

6.3 Reference list

- Akhtar A. (2015). The flaws and human harms of animal experimentation. *Cambridge quarterly of healthcare ethics : CQ : the international journal of healthcare ethics committees*, 24(4), 407–419. <https://doi.org/10.1017/S0963180115000079>
- Ansell, D. M., Holden, K. A., & Hardman, M. J. (2012). Animal models of wound repair: Are they cutting it?. *Experimental dermatology*, 21(8), 581–585.
- Celik, S., Dominici, S. R., Filby, B. W., Das, A., Madden, L. A., & Paunov, V. N. (2019). Fabrication of Human Keratinocyte Cell Clusters for Skin Graft Applications by Templating Water-in-Water Pickering Emulsions. *Biomimetics (Basel, Switzerland)*, 4(3), 50.
- Davis, S. C., Ricotti, C., Cazzaniga, A., Welsh, E., Eaglstein, W. H., & Mertz, P. M. (2008). Microscopic and physiologic evidence for biofilm-associated wound colonization in vivo. *Wound repair and regeneration : official publication of the Wound Healing Society [and] the European Tissue Repair Society*, 16(1), 23–29.
- Ferdowsian, H. R., & Beck, N. (2011). Ethical and scientific considerations regarding animal testing and research. *PLoS one*, 6(9), e24059. <https://doi.org/10.1371/journal.pone.0024059>
- Gjødsbøl, K., Christensen, J. J., Karlsmark, T., Jørgensen, B., Klein, B. M., & Krogh, K. A. (2006). Multiple bacterial species reside in chronic wounds: a longitudinal study. *International wound journal*, 3(3), 225–231.
- Levy N. (2012). The use of animal as models: ethical considerations. *International journal of stroke : official journal of the International Stroke Society*, 7(5), 440–442.
- Mansbridge, J. N., & Knapp, A. M. (1987). Changes in keratinocyte maturation during wound healing. *The Journal of investigative dermatology*, 89(3), 253–263.
- Meyer, W., Schwarz, R., & Neurand, K. (1978). The skin of domestic mammals as a model for the human skin, with special reference to the domestic pig. *Current problems in dermatology*, 7, 39–52.
- Phillips, P., Yang, Q., Gibson, D., & Schultz, G. (2011) Assessing the bioburden in poorly healing wounds. *Wounds International*, 2, 17–19.
- Progulske-Fox, A., Jin, S., Antonelli, P., & Schultz, G. S. (2013). Development of a novel ex vivo porcine skin explant model for the assessment of mature bacterial biofilms. *Wound repair and regeneration : official publication of the Wound Healing Society [and] the European Tissue Repair Society*, 21(5), 704–714.
- Roberts, A. E., Kragh, K. N., Bjarnsholt, T., & Diggle, S. P. (2015). The Limitations of In Vitro Experimentation in Understanding Biofilms and Chronic Infection. *Journal of molecular biology*, 427(23), 3646–3661.
- Wang, A., Weldrick, P. J., Madden, L. A., & Paunov, V. N., (2021) A Biofilm-Infected 3D Human Cell Co-culture Platform to Replace Animal Models in Testing Antimicrobial Nanotechnologies. *Applied Materials & Interfaces*, in peer review.
- Weldrick, P. J., San, S., & Paunov, V. N. (2021) Advanced Alcalase-Coated Clindamycin-Loaded Carbopol Nano-gels for Removal of Persistent Bacterial Biofilms. *ACS Appl. Nano Mater.*, *Advanced Article*, DOI: 10.1021/acsanm.0c02810.
- Wilkinson, H. N., Longhorne, F. L., Roberts, E. R., Brownhill, V. R., & Hardman, M. J. (2020). Cellular benefits of single-use negative pressure wound therapy demonstrated in a novel ex vivo human skin wound model. *Wound repair and regeneration : official publication of the Wound Healing Society [and] the European Tissue Repair Society*, 10.1111/wrr.12888. Advance online publication.
- Wilkinson, H. N., McBain, A. J., Stephenson, C., & Hardman, M. J. (2016). Comparing the Effectiveness of Polymer Debriding Devices Using a Porcine Wound Biofilm Model. *Advances in wound care*, 5(11), 475–485.
- Wong, P., & Coulombe, P. A. (2003). Loss of keratin 6 (K6) proteins reveals a function for intermediate filaments during wound repair. *The Journal of cell biology*, 163(2), 327–337.
- Zhou, L., Zhang, X., Paus, R., & Lu, Z. (2018). The renaissance of human skin organ culture: A critical reappraisal. *Differentiation; research in biological diversity*, 104, 22–35.